Vol. 59 SEPTEMBER, 1955 No. 9

THE JOURNAL OF PHYSICAL CHEMISTRY

(Registered in U. S. Patent Office)

29th NATIONAL COLLOID SYMPOSIUM, HOUSTON, TEXAS, JUNE 20–22, 1955

THE JOURNAL OF PHYSICAL CHEMISTRY

(Registered in U. S. Patent Office)

Published monthly by the American Chemical Society at 20th and Northampton Sts., Easton, Pa.

Entered as second-class matter at the Post Office at Easton, Pennsylvania.

The *Journal of Physical Chemistry* is devoted to the publication of selected symposia in the broad field of physical chemistry and to other contributed papers.

Manuscripts originating in the British Isles, Europe and Africa should be sent to F. C. Tompkins, The Faraday Society, 6 Gray's Inn Square, London W. C. 1, England.

Manuscripts originating elsewhere should be sent to W. Albert Noyes, Jr., Department of Chemistry, University of Rochester, Rochester 3, N. Y.

Correspondence regarding accepted copy, proofs and reprints should be directed to Assistant Editor, Allen D. Bliss, Department of Chemistry, Simmons College, 300 The Fenway, Boston 15, Mass.

Business Office: Alden H. Emery, Executive Secretary, American Chemical Society, 1155 Sixteenth St., N. W., Washington 6, D. C.

Advertising Office: Reinhold Publishing Corporation, 430 Park Avenue, New York 22, N. Y.

Articles must be submitted in duplicate, typed and double spaced. They should have at the beginning a brief Abstract, in no case exceeding 300 words. Original drawings should accompany the manuscript. Lettering at the sides of graphs (black on white or blue) may be pencilled in, and will be typeset. Figures and tables should be held to a minimum consistent with adequate presentation of information. Photographs will not be printed on glossy paper except by special arrangement. All footnotes and references to the literature should be numbered consecutively and placed in the manuscript at the proper places. Initials of authors referred to in citations should be given. Nomenclature should conform to that used in *Chemical Abstracts*, mathematical characters marked for italic, Greek letters carefully made or annotated, and subscripts and superscripts clearly shown. Articles should be written as briefly as possible consistent with clarity and should avoid historical background unnecessary for specialists.

Symposium papers should be sent in all cases to Secretaries of Divisions sponsoring the symposium, who will be responsible for their transmittal to the Editor. The Secretary of the Division by agreement with the Editor will specify a time after which symposium papers cannot be accepted. The Editor reserves the right to refuse to publish symposium articles, for valid scientific reasons. Each symposium paper may not exceed four printed pages (about sixteen double spaced typewritten pages) in length except by prior arrangement with the Editor.

Remittances and orders for subscriptions and for single copies, notices of changes of address and new professional connections, and claims for missing numbers should be sent to the American Chemical Society, 1155 Sixteenth St., N. W., Washington 6, D. C. Changes of address for the *Journal of Physical Chemistry* must be received on or before the 30th of the preceding month.

Claims for missing numbers will not be allowed (1) if received more than sixty days from date of issue (because of delivery hazards, no claims can be honored from subscribers in Central Europe, Asia, or Pacific Islands other than Hawaii), (2) if loss was due to failure of notice of change of address to be received before the date specified in the preceding paragraph, or (3) if the reason for the claim is "missing from files."

Subscription Rates: to members of the American Chemical Society, $8.00 for 1 year, $15.00 for 2 years, $22.00 for 3 years; to non-members, $10.00 for 1 year, $18.00 for 2 years, $26.00 for 3 years. Postage free to countries in the Pan American Union; Canada, $0.40; all other countries, $1.20. $12.50 per volume, foreign postage $1.20, Canadian postage $0.40; special rates for A.C.S. members supplied on request. Single copies, current volume, $1.00; foreign postage, $0.15; Canadian postage $0.05. Back issue rates (starting with Vol. 56): $15.00 per volume, foreign postage $1.20, Canadian, $0.40; $1.50 per issue, foreign postage $0.15, Canadian postage $0.05.

The American Chemical Society and the Editors of the *Journal of Physical Chemistry* assume no responsibility for the statements and opinions advanced by contributors to THIS JOURNAL.

The American Chemical Society also publishes *Journal of the American Chemical Society*, *Chemical Abstracts*, *Industrial and Engineering Chemistry*, *Chemical and Engineering News*, *Analytical Chemistry*, and *Journal of Agricultural and Food Chemistry*. Rates on request.

(*Continued from first page of cover*)

THE JOURNAL OF
PHYSICAL CHEMISTRY

VOLUME 59 SEPTEMBER 20, 1955 NUMBER 9

THE THERMAL DECOMPOSITION OF GERMANE. I. KINETICS

BY KENZI TAMARU, MICHEL BOUDART AND HUGH TAYLOR
Frick Chemical Laboratory, Princeton University, Princeton, N. J.

Received February 25, 1955

The kinetics of decomposition of germane have been studied by a static method. The reaction rate is dependent only on the partial pressure of germane, being independent of that of hydrogen. The reaction is apparently first order at higher pressures, decreasing to zero order at low pressures of germane. The experimental results can be explained by assuming concurrent first- and zero-order reactions with activation energies of 51.4 and 41.2 kcal., respectively. By changing the specific surface area of the reaction vessel it was concluded that the zero-order reaction occurs on the deposited germanium surface, while the first-order reaction is homogeneous. For the surface reaction it is concluded that the germanium surface is covered by adsorbed molecules, radicals and atoms decomposing at the measured rate. Oxygen affects the decomposition process markedly. Contamination with oxygen accelerates the zero-order process and lowers the activation energy to 38.2 kcal. The oxygen appears to remain at the germanium surface even with subsequent germane deposition. Arsine accelerates the rate of germane decomposition on germanium surfaces although arsine itself is decomposed extremely slowly on germanium surfaces at 302°, much more slowly than on antimony or arsenic surfaces.

The thermal decomposition of germane to yield germanium films and molecular hydrogen occurs slowly below 280° but measurably rapidly at somewhat higher temperatures. During the decomposition the surface of germanium is constantly renewed by fresh deposition. The reaction therefore offers the possibility of kinetic studies on clean elemental surfaces. It offers also the possibility of studying the influence of contaminants, for example, oxygen and arsenic on such films. There is thus the possibility of correlating catalytic action with the known effects of foreign elements on the electrical properties of germanium.

Hogness and Johnson[1] studied the kinetics of the decomposition of germane in 1932. They found rates proportional to the one-third power of the germane pressure at higher temperatures with an inhibition by hydrogen in a lower temperature range. They developed an equation for their kinetics based upon the Langmuir adsorption theory which assumed a three-point contact between germane molecules and the germanium surface.

We decided to restudy the reaction with the extremely pure germanium now available as source of the germane, and to examine the effect of foreign elements deliberately introduced to the germanium.

Experimental

The decomposition of germane was studied by a static method. Since hydrogen is the only gaseous constituent resulting from the decomposition, the rate of the reaction was followed by observing the total pressure of the system which, on completion of decomposition, was twice the initial pressure. From the total pressure one may readily calculate the pressure of the undecomposed hydride and the pressure of the hydrogen resulting from the decomposition.

Apparatus.—A cylindrical Pyrex glass vessel, which had been carefully cleaned, was used for the reaction vessel. The inside diameter of the vessel was 2.7 cm. and its volume was 67 cc. The temperature of the reaction vessel was controlled satisfactorily using vapor baths of mercury, diphenylamine or acenaphthene under various constant pressures. The reaction vessel was attached to a mercury manometer by means of capillary tubing and during the reaction its pressure was followed by the manometer, keeping the volume constant. Between the reaction vessel and the manometer, a solid carbon dioxide trap was used to prevent the entry of vapor of mercury, grease or other impurities.

Before the reactant was introduced into the reaction vessel a vacuum of less than 10^{-4} mm. was obtained by means of a mercury diffusion pump backed up by a Cenco Hy-Vac oil pump.

Preparation of Germane.—Germane was prepared from germanium dioxide.[2] First $GeCl_4$ was obtained by boiling GeO_2 with pure concentrated HCl.[3] $GeCl_4$ (b.p. 86.5°) was separated from concentrated HCl by means of a sepa-

(1) T. R. Hogness and W. C. Johnson, *J. Am. Chem. Soc.*, **54**, 3583 (1932).

(2) This oxide was obtained from the Bell Telephone Laboratories. It was essentially free from the following impurities which were probably present in the materials of Hogness: traces of As, Si, and Sn, possibly totaling 0.33%. There might have been bare traces of Al Ag, Ca, Cr, Cu, Fe, Ga, Mg, Mn, Na, Pb.

(3) This HCl was obtained by distilling "chemically pure" HCl, of which the maximum impurities are: free Cl, 0.0000; sulfites, 0.00008; sulfates, 0.00008; hy. met. (as Pb) 0.0001; Fe, 0.00001; As, 0.000001; NH_4, 0.0003; residue on ignition, 0.0004%.

ratory funnel and was distilled again, taking the distillates between 86 and 88°. In a nitrogen atmosphere, $GeCl_4$ was dropped into a solution of $LiAlH_4$[4] in ethylene glycol–dimethyl ether which had been cooled by liquid nitrogen. The reaction vessel was allowed to warm up slowly. The germane produced was caught in a liquid nitrogen trap after passing through ascarite to remove HCl. The hydride was purified by distilling several times between solid carbon dioxide and liquid nitrogen.

Experimental Results

Decomposition of Germane at 302°.—Germane was decomposed at 302° at various initial pressures. The reaction proceeded with good reproducibility from the first experiment on the glass vessel. The results are shown in Fig. 1. All the curves in Fig. 1 are superimposable at corresponding pressures of germane, which shows that the rate of the decomposition is only dependent upon the partial pressure of germane, being independent of hydrogen.

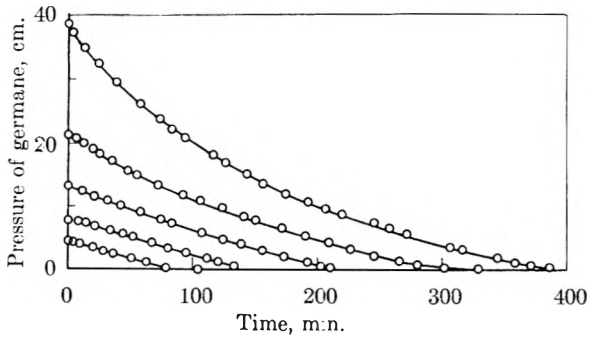

Fig. 1.—GeH_4 decomposition at 302°.

Effect of Temperature upon the Reaction Rate.—The kinetics of the decomposition was studied at various temperatures, which are shown in Figs. 2 and 3. Here also the reaction rates were only dependent upon the partial pressure of germane.

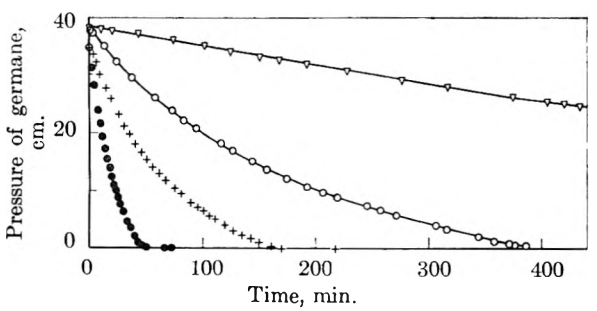

Fig. 2.—GeH_4 decomposition at various temperatures: ▽, 278°; ○, 302°; +, 314°; ●, 330°.

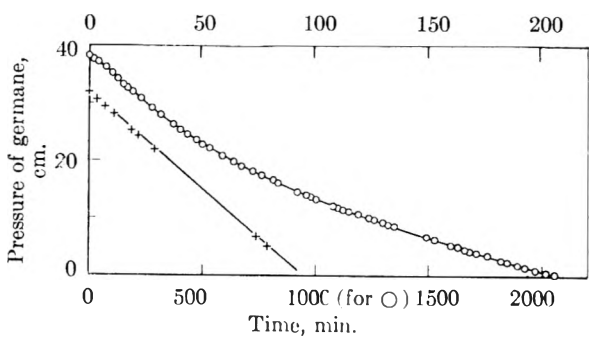

Fig. 3.—GeH_4 decomposition at 278°: ○, in open vessel (bottom legend); +, in vessel filled with glass wool (top legend).

(4) This hydride was obtained from Metal Hydrides, Incorporated.

Theoretical.—The experimental results showed that the decomposition was apparently first order at higher pressures, but the order decreased to zero with decreasing pressure. This suggested that two kinds of reactions, both first and zero order, are taking place simultaneously, with the former predominant at higher pressure while the latter predominates at lower pressure. Thus, the following equation was assumed

$$-\frac{dp}{dt} = k_0 + k_1 p \qquad (1)$$

where k_0 and k_1 are the velocity constants of the zero- and the first-order reactions, respectively. On integration

$$\frac{p + k_0/k_1}{p_0 + k_0/k_1} = e^{-k_1 t} \qquad (2)$$

where p_0 is the initial pressure. Figures 4 and 5 show the applicability of equation 2 to the observed data, where the results of the decomposition at 330 and 302° are shown, taking k_0 and k_1 as 0.248 cm./min., 0.0403 min.$^{-1}$ for the experiment at 330°, and 0.0296 cm./min., and 0.00510 min.$^{-1}$ for that at 302°, respectively. Table I shows the calculated values of k_0 and k_1 for experiments at four different temperatures and the dependence of the reaction rate constants upon temperature is shown in Fig. 6. Applying Arrhenius' equation, and the method of least squares, activation energies of 41.9 and 51.4 kcal./mole were obtained for the zero- and the first-order reactions, respectively.

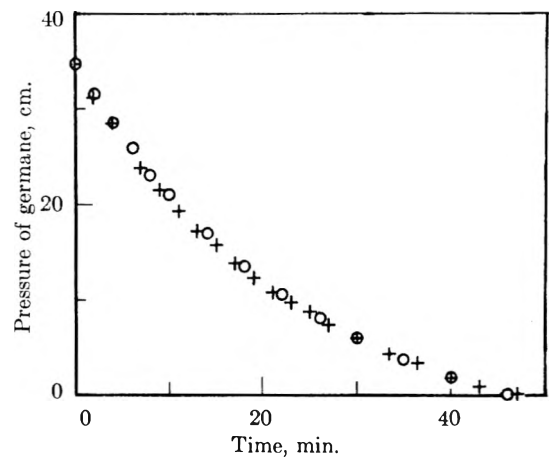

Fig. 4.—GeH_4 decomposition at 330°: +, observed; ⊙, calculated.

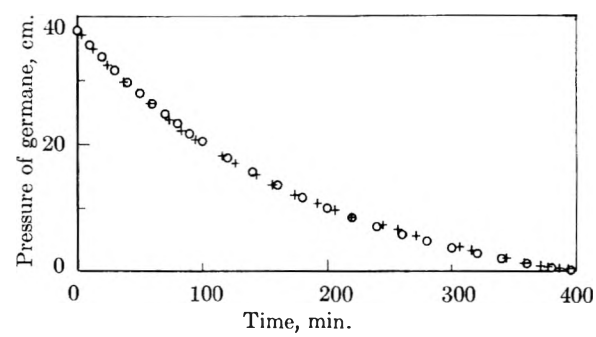

Fig. 5.—GeH_4 decomposition at 302°: +, observed; ⊙, calculated.

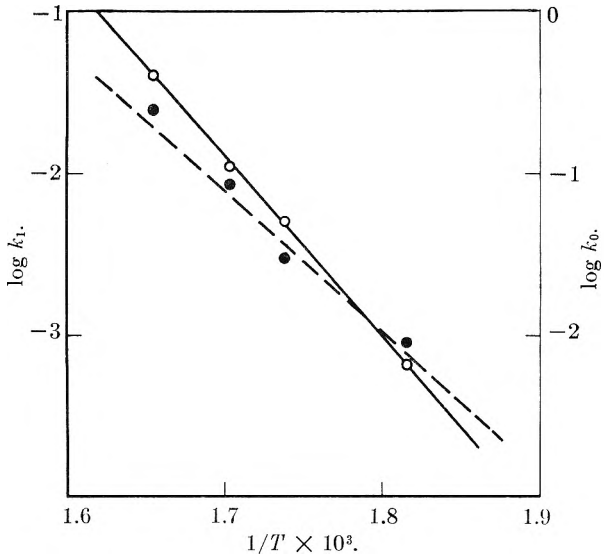

Fig. 6.—Dependence of GeH_4 decomposition rate upon temperature: ○ = k_1; ● = k_0.

TABLE I

THE REACTION VELOCITY CONSTANTS (k_0 AND k_1) AT FOUR DIFFERENT TEMPERATURES

T, °C.	k_0, cm./min.	k_1, min.$^{-1}$
330	0.248	0.0403
314	.0864	.0111
302	.0296	.00510
278	.00908	.000658

Effect of the Specific Surface Area of the Reaction Vessel.—The specific surface area of the reaction vessel was changed to study its effect upon the reaction velocity, by varying the shape of the reaction vessel or putting pieces of glass tubing or glass wool into it. The results are shown in Fig. 7, where the surface area-volume ratios are 1.6, *ca.* 4, *ca.* 4, and more than 7.5 cm.$^{-1}$ for the curves I, II, III and IV, respectively, and curve V was obtained by putting glass wool in the reaction vessel. It can be seen that as the surface area–volume ratio increases, the zero-order reaction becomes more predominant until, at sufficiently high ratios, the zero-order reaction is alone important.

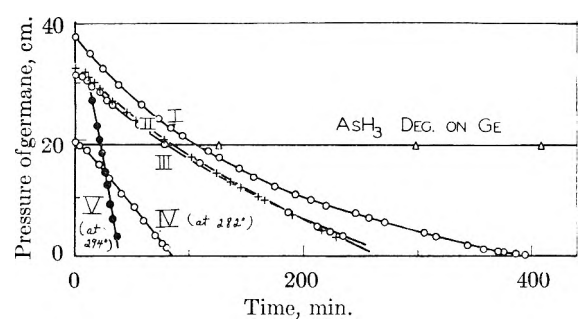

Fig. 7.—GeH_4 decomposition in various reaction vessels at 302°.

With glass wool in the reaction vessel, germane was decomposed at different temperatures, and the temperature coefficient of the zero-order rate as shown in Fig. 8, yields an activation energy of 41.2 kcal./mole. This value agrees well with the activation energy for the zero-order reaction in

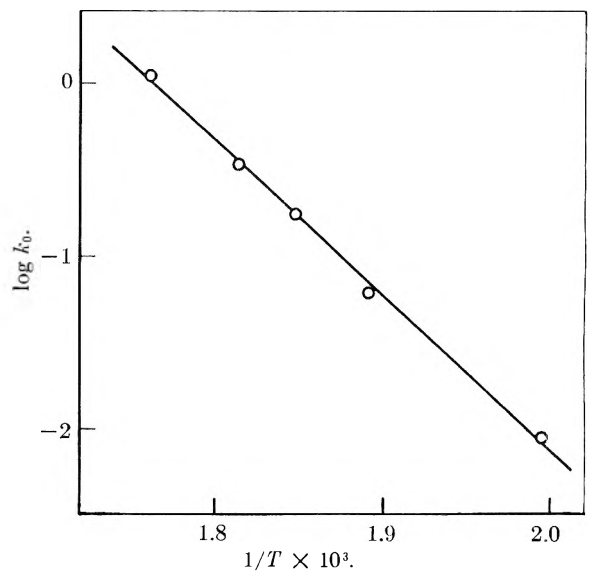

Fig. 8.—GeH_4 decomposition rates on Ge at various temperatures.

Fig. 6. The kinetics at 278° are shown as the zero-order line in Fig. 3.

These facts suggest that the zero-order reaction takes place on the germanium surface, while the first-order reaction is a homogeneous gas reaction.

Effect of Oxygen upon the Germane Decomposition.—When 1 cm. of oxygen was put into the reaction vessel before germane was introduced, it changed the decomposition rate quite remarkably. The oxygen caused an explosive reaction with germane, and the remaining germane decomposed as a zero-order reaction at a much faster rate than usual, shown by the crosses in Fig. 9, in com-

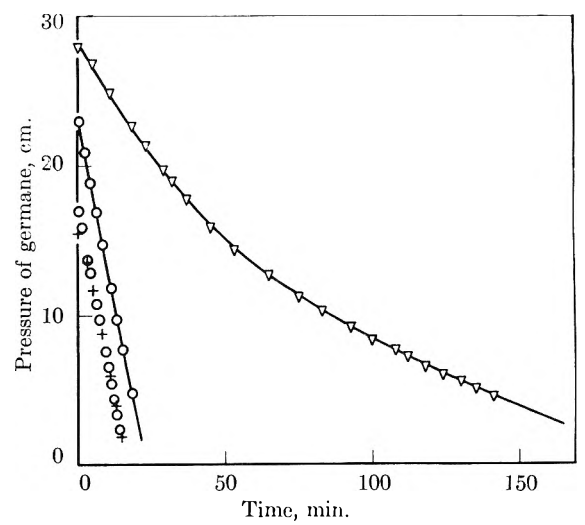

Fig. 9.—Effect of oxygen upon GeH_4 decomposition at 312°: ▽, without oxygen; ○, oxygen contaminated surface; +, additional oxygen.

parison with the triangles for rates on a clean germanium surface. After the reaction, the reaction vessel was evacuated and pure germane was introduced. This also showed reproducible zero-order reactions as shown by the circles in Fig. 9. With this vessel germane decompositions were repeated without oxgyen and the decompositions were quite

reproducible zero-order reactions, as shown in Figs. 9 and 10. When oxygen was again added, the reaction rate increased a bit.

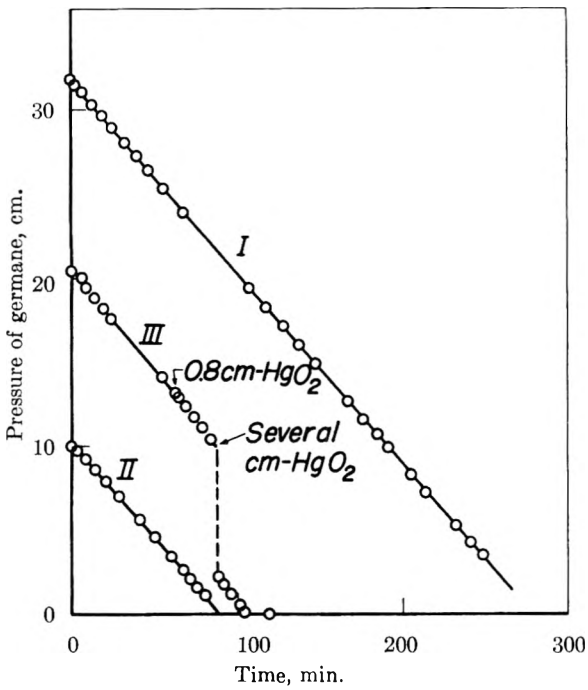

Fig. 10.—GeH_4 decomposition on the oxygen contaminated Ge surface at 278°.

The effect of temperature on the reaction on an oxygen-contaminated surface is shown in Fig. 11, from which an activation energy of 38.2 kcal./mole is obtained. This value is smaller than that of the reaction on the clean germanium surface.

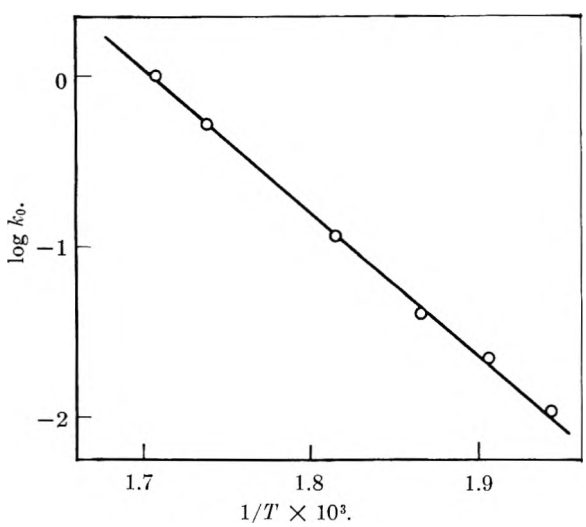

Fig. 11.—GeH_4 decomposition on the oxygen contaminated Ge surface at various temperatures.

The effect of a small amount of oxygen was studied, putting 1/10 mm. oxygen in a new vessel. This is shown by the curve I in Fig. 12. Curve II in Fig. 12 was obtained by putting 2/10 mm. oxygen into the vessel. The rates of the first- and the zero-order reactions, that is, k_1 and k_0, in this case, are:

	k_1, min.$^{-1}$	k_0, cm./min.
On the clean germanium	0.0115	0.0606
Curve I	.0118	.108
Curve II	.0102	.172

The data show the increase of the heterogeneous reaction rates and almost constant homogeneous reaction rates.

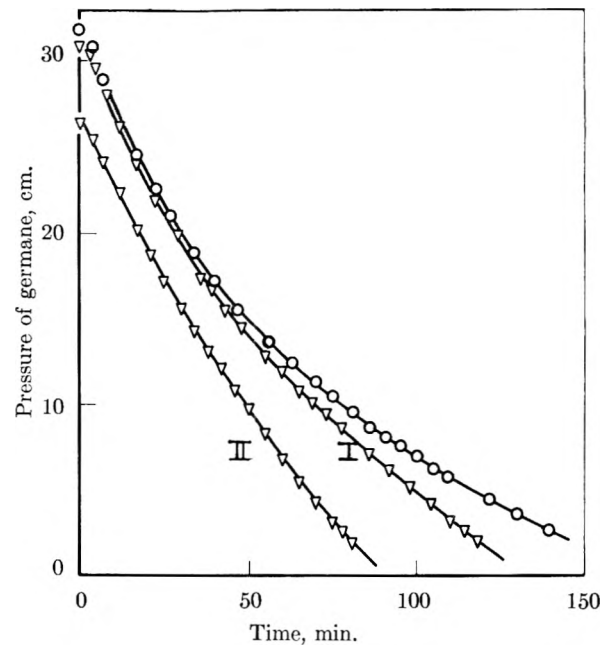

Fig. 12.—Effect of small amounts of oxygen on GeH_4 decomposition at 312°: ▽, with increasing amounts of oxygen I and II.

To make sure that part of the zero-order reaction in Fig. 1 is not due to an extremely small amount of air left in the reaction vessel, a new reaction vessel was flushed with oxygen-free nitrogen and was evacuated very carefully. The same result was obtained as in Fig. 1. Even when the vessel was flushed with oxygen, before it was evacuated, the result was quite the same.

Effect of Arsine upon the Germane Decomposition.—When a small amount of arsine was mixed with the germane, the decomposition of germane was slightly affected. The over-all reaction order was decreased probably due to a faster zero-order reaction and slower first-order reaction.

When arsine was introduced into a reaction vessel which is covered by germanium film, it decomposed extremely slowly at 302° as shown in Fig. 7.[5]

Germane–arsine mixtures were decomposed in a reaction vessel with glass wool and the heterogeneous decomposition rate of germane in presence of arsine was measured. The data, shown in Table II, indicate that germane, when mixed with arsine, decomposes a little faster than germane alone. The activation energy for the reaction was roughly estimated from Table II. It shows almost the same, or slightly lower, activation energy than with pure germane.

(5) It is interesting to note that arsine decomposes fairly rapidly on antimony surfaces at 278°, decomposes more slowly on arsenic surfaces, and the slowest on germanium surfaces.

TABLE II

EFFECT OF ARSINE ON THE GERMANE DECOMPOSITION

The reaction rate is in cm./min.

Temp., °C.	0% AsH_3	4.6% AsH_3	10.2% AsH_3	12% AsH_3
228	0.0088	0.0117		
255	.0620	.0825		
267	.160	.156	0.216	
			.217	
278	.339	.363		0.523 (280°)
294	1.105			

Discussion

Reaction Mechanism.—The fact that the catalytic decomposition of germane is a zero-order reaction suggests that the surface of the germanium is almost covered by adsorbed molecules, radicals or atoms. In this case, according to the statistical mechanical treatment of rate processes, the rate of the reaction can be expressed as[6]

$$v = G\frac{kT}{h}e^{-E/RT} \qquad (3)$$

where G is the number of sites per unit surface area and E is the activation energy of the reaction. The observed value of E is equal to 41.2 kcal./mole and thus the calculated reaction rate from equation 3 is equal to 1.0×10^{13} molecules per second per unit surface area. This assumes that the number of sites G is equal to 10^{15} which is the number of germanium atoms on unit surface area.

On the other hand the observed reaction rate at 302° is equal to 5.2×10^{13} molecules per second per unit surface area, assuming that the surface is smooth. The observed and calculated values agree fairly well, if the roughness of the surface is taken into consideration.

It seems to be most likely that the germanium surface is almost covered by GeH_x radicals or chemisorbed hydrogen during the reaction, and the desorption of the latter measures the rate of the over-all reaction.

As to the effect of oxygen upon the germane decomposition, the good reproducibility of the germane decomposition on the oxygen-contaminated surface suggests that the oxygen always stays on the germanium surface, migrating through the deposited germanium to the surface. The increase of the reaction rate by oxygen contamination (k_0 is about 17 times larger at 302°) is due to the lower activation energy of the reaction, as the 3.0 kcal./mole decrease of the activation energy corresponds to a 14 times faster reaction rate.

This increase in reaction rate due to oxygen contamination of the germanium surface is in marked contrast to the inhibitory action of oxygen on iron synthetic ammonia catalysts in ammonia synthesis and decomposition.

Acknowledgment.—The preceding work was carried out with the assistance of a post-doctoral fellowship kindly provided by the Shell Fellowship Committee of the Shell Companies Foundation, Inc. It also forms part of a program on Solid State Properties and Catalytic Activity supported by the Office of Naval Research N6onr-27018. For this support we wish to express our appreciation and thanks.

(6) *Cf.* S. Glasstone, *et al.*, "The Theory of Rate Processes," McGraw-Hill Book Co., 1941, p. 376; or, replacing T with $T_m e^{1-T/T_m}$, $v = Ge\,kT_m/h\,e^{-E_{obs.}/RT}$, where T_m is the median of the temperature range.

DISCUSSION

MAX BENDER.—You made reference to "absorbed" oxygen on the deposing germanium not being covered by the Ge that further is deposited. Rather it stays on top as the germanium film increases in thickness, *i.e.*, bubbles through. Would you expect that the hydrogen still associated with the germanium film, also does the same as the film builds up?

THE THERMAL DECOMPOSITION OF GERMANE. II. MECHANISM

BY P. J. FENSHAM, K. TAMARU, M. BOUDART AND HUGH TAYLOR

Frick Chemical Laboratory, Princeton University, Princeton, N. J.

Received February 25, 1955

The hydrogen–deuterium exchange reaction does not proceed at a measurable rate on a germanium film in a temperature range where germane decomposes readily. Similarly, when germanium hydride is decomposed in the presence of an excess of deuterium, no hydrogen deuteride can be detected in the reaction product. On the contrary, when mixtures of germanium hydride and germanium deuteride are decomposed together, abundant quantities of hydrogen deuteride are produced although no mixing takes place between germanes. Thus it appears that dissociative chemisorption of gaseous hydrogen molecules on a germanium surface is immeasurably slow as compared to the rate of desorption of hydrogen from a similar germanium surface covered with freely interacting fragments of partially decomposed germane. These observations impose definite limitations to the possible modes of decomposition of germane, both homogeneous and heterogeneous.

The thorough kinetic investigation of the thermal cracking of germane described in the first part of this series,[1] was preceded by an exploratory kinetic study supplemented by experiments involving light and heavy hydrogen and their exchange under conditions pertinent to a clarification of the mechanism of germane decomposition.

The kinetic work was carried out in two cylindrical reaction vessels surrounded by a jacket of boiling mercury similar to that used by Hogness and Johnson.[2] A large number of decompositions of germane were carried out between 270 and 350° the initial pressure of germane being varied between about 5 and 2 cm.

Because of the restricted pressure range within which the reactions could be followed manometrically, a kinetic analysis of the data did not lead to any firm conclusion. In the light of the more complete work that followed, the trends which were found are now understandable. Thus it appeared that most runs could be fitted approximately by expressions of the kind $-dp/dt = kp^n$ with various fractional values for n $(0 < n < 1)$, p being the pressure of undecomposed germane at time t. The value of n increased with temperature, being near zero at the lower temperatures and approaching unity at the higher temperatures.

In terms of the interpretation proposed in the first paper,[1] this means that even in the lower pressure range, both homogeneous and heterogeneous components of the decomposition operate simultaneously. The zero-order heterogeneous component becomes more important at low temperatures while the first-order homogeneous component is quite noticeable at higher temperatures. The relative activation energies of both processes explain this shift.

Apart from the pressure range, the experimental conditions of this work compare favorably with those of the later work. Thus the results of the mechanism studies which will be reported in this paper, must be considered as having been obtained in the best conditions of gas and film purity of the more complete kinetic investigation.

Experimental

Preparation of Gases.—Pure germanium dioxide was supplied by the Bell Telephone Laboratories. Spectrographic analysis revealed only faint traces of calcium, magnesium and copper.

For some of the preliminary experiments, germanium hydride was prepared after the method of Kraus and Carney.[3] This involved the reaction of magnesium germanide with a solution of ammonium bromide in liquid ammonia. The magnesium germanide was prepared by reducing the oxide with purified hydrogen at 700° and then fusing the germanium with the appropriate amount of magnesium in an atmosphere of hydrogen. The germanium hydride was collected over water, dried by passing over calcium chloride and phosphorus pentoxide. It was finally purified by fractional distillation, using isopentane-baths. This method of separation and purification of the various germanes is described by Corey, Laubengayer and Dennis.[4] The yield which was produced by this method was disappointing and other methods were tried. Finally, it was decided to use the reaction between lithium aluminum hydride and germanium tetrachloride. Germanium tetrachloride was prepared by the action of hydrochloric acid on the germanium dioxide.[5] The germanium tetrachloride was distilled into a flask containing a solution of the hydride in ether (pure dry) which was cooled with liquid nitrogen. Previously the whole system had been evacuated after being flushed out several times with hydrogen to remove any traces of oxygen. The mixture was then allowed to warm slowly to room temperature and a steady stream of gas was evolved and collected by liquefaction in an adjacent tube. This mixture of germanes and ether was separated by distillation from an ethyl alcohol bath at −112° and finally the hydrides were separated as described above.

The pure germanium hydride was stored in a large bulb at pressures up to 0.5 atm. In this way the gas could be kept in quite stable conditions for several months. The yields were reasonably satisfactory and corresponded to 25–35% of the germanium tetrachloride which had been used.

Germanium deuteride was prepared in an exactly analogous fashion using lithium aluminum deuteride (supplied with A.E.C. approval by Metal Hydrides, Inc.).

The hydrogen and deuterium which were employed in the various experiments on the mechanism of the decomposition reaction were prepared by the total decomposition of samples of pure germanium hydride and germanium deuteride, respectively. In this way there was no danger of introducing further impurities into the reaction system.

The absence of any appreciable traces of higher hydrides in the germanium hydride was shown by pressure studies of the total decomposition of samples of the gas. Within the experimental error of the manometer (±0.5 mm.), one volume of the hydride gave two volumes of hydrogen, as would be expected from the pure hydride.

Hydrogen–Deuterium Exchange on the Germanium Film.—As an important factor in elucidating the mechanism of the reaction, it was important to establish whether exchange occurred between hydrogen and deuterium in the presence of a germanium film. The following experiment was carried out in the first reaction vessel after a number of decompositions had been completed so that its inner wall was covered with a considerable film of germanium.

The reaction vessel was evacuated and the temperature raised by means of a tube furnace. This produced a

(1) K. Tamaru, M. Boudart and H. Taylor, THIS JOURNAL, **59**, 801 (1955).

(2) T. R. Hogness and W. C. Johnson, *J. Am. Chem. Soc.*, **54**, 3583 (1932).

(3) C. A. Kraus and E. S. Carney, *ibid.*, **56**, 765 (1934).

(4) R. B. Corey, A. W. Laubengayer and L. M. Dennis, *ibid.*, **47**, 112 (1925).

(5) L. S. Foster, J. W. Drenan and A. F. Williston, *ibid.*, **64**, 3042 (1942).

gradient along the reaction vessel from 300 to 320°. An analyzed mixture of hydrogen (6 cm.) and deuterium (6 cm.) was then introduced into the reaction vessel. After 15 minutes a sample was withdrawn for mass spectroscopic analysis and a final sample was taken after one hour. The analyses showed that there was no appearance of HD during the experiment. The experiment was repeated with different proportions of hydrogen (2 cm.) and deuterium (6 cm.) with an exactly similar result. It can, therefore, be concluded that there is no appreciable exchange between hydrogen and deuterium on a germanium film between 300 and 320°.

Decomposition of Germanium Hydride and Germanium Deuteride.—A mixture of GeH_4 (17.5 mm.) and GeD_4 (23.0 mm.) was prepared and analyzed with the mass spectrometer. This mixture was then admitted to the reaction vessel. This experiment and the others described in this section were carried out in the second reaction vessel after a number of simple decompositions had already occurred in it, so that the inside surface was covered with a coherent film of germanium. The temperature of the reaction vessel was 273°, and after one hour at this temperature no apparent decomposition had occurred. A sample of the gas mixture was withdrawn for analysis. The temperature was then raised to 305° and the decomposition commenced. When the fraction of the mixture which had decomposed was 0.3, another sample of the partially decomposed mixture was withdrawn for analysis. Decomposition was then allowed to continue to completion when an analysis of the final products was made.

This experiment was repeated with another mixture, GeH_4 (22 mm.) and GeD_4 (17 mm.), using a decomposition temperature of 322°. The results are given in Table I.

TABLE I

MASS NUMBER PROPORTIONS DURING THE EXPERIMENTS

Mass no.	Initial mixtures 1st expt.	Initial mixtures 2nd expt.	Mixtures after 1 hr. at 273° 1st expt.	Mixtures after 1 hr. at 273° 2nd expt.	Mixtures after 30% reacn. 1st expt.	Mixtures after 30% reacn. 2nd expt.	Products after complete reacn. 1st expt.	Products after complete reacn. 2nd expt.
70	1.0	1.0	1.0	1.0	1.0	1.0	1.0	
71	0.2	0.4	0.2	0.4	0.2	0.4		
72	2.5	3.1	2.4	3.0	2.2	3.0		
73	1.5	2.4	1.6	2.4	1.5	2.3		
74	5.0	5.2	6.5	5.4	6.0	5.1		
75	2.0	3.4	2.0	3.5	2.3	3.3		
76	6.3	6.0	6.4	5.9	6.6	5.9		
77	2.6	3.2	2.6	3.4	3.0	3.5		
78	5.3	3.3	5.3	3.5	5.5	3.7		
79	1.2	0.9	1.5	1.0	1.8	1.2		
80	3.2	1.7	3.2	1.6	3.0	1.7		
81	..	?	0.1	0.05	0.2	0.1		
82	1.0	0.3	0.6	0.3	0.4	0.3		
83	..	..	?	..	..	..		
84	0.2	..	0.1	..	0.05	..		
2					1.0	1.1	3.5	6.8
3					2.1	10.3	12.1	20
4					2.3	3.3	13.6	3.5

The mass spectrometer gave quantitative analyses for masses in the vicinity of mass number 70, and the proportions are all given in the table with respect to mass number 70 as unity. It is clear that little if any rearrangement occurs in the proportions of the hydride–deuteride mixture during the experiment. For mass numbers below 10, the instrument gave only qualitative results; but it is clear from the table that there was a considerable production of hydrogen deuteride during the decomposition along with hydrogen and deuterium.

Decomposition of Germanium Hydride and Deuterium.—A mixture of GeH_4 (25 mm.) and D_2 (52 mm.) was prepared and analyzed with the mass spectrometer. This mixture was then admitted to the second reaction vessel after the experiments which have just been described. The temperature of the previously evacuated reaction vessel was 325°. As soon as the gas had reached equilibrium temperature, a sample was withdrawn for analysis. Decomposition was then allowed to proceed and the pressure changes followed in the normal manner. When decomposition was complete, a sample of the product gases was analyzed for masses 2, 3 and 4. The results of this experiment are given in Table II.

TABLE II

HYDROGEN–DEUTERIUM ANALYSES FOR DECOMPOSITION OF $GeH_4 + D_2$

Mass no.	$D_2 + GeH_4$ at 25°	$D_2 + GeH_4$ at 325° and beginning of reacn.	$D_2 + GeH_4$ after 10% reacn.	Products after complete reacn.
2	0.7	0.4	3.3	20
3	..	..	..	..
4	4.2	2.7	3.4	5.3

It is clear from the data that there is no production of mass 3 during this experiment.

Discussion

The lack of formation of hydrogen deuteride in the direct exchange experiments as well as during the decomposition of germanium hydride in the presence of deuterium demonstrates that the rate of dissociative chemisorption of molecular hydrogen on our germanium surfaces is too slow to be measurable even above 300°. While contamination of the film between the time of its preparation and the direct exchange experiments cannot be ruled out entirely, it appears unlikely since both light and heavy hydrogen were produced in an earlier decomposition of germane and must be quite pure. Contamination is even more improbable during the decomposition of germanium hydride in the presence of deuterium. Indeed, it has been shown[1] that traces of oxygen profoundly affect the rate of decomposition of germane on germanium.

On the other hand, the abundant formation of hydrogen deuteride during the simultaneous decomposition of germanium hydride and deuteride, leads to the conclusion that the surface of germanium is covered to a certain extent, during decomposition, with radicals formed by the dissociative chemisorption of germane. The radicals must diffuse sufficiently freely along the surface and exchange their hydrogen readily, with possibly simultaneous desorption of hydrogen molecules. This mobility is also suggested by the smooth mirror-like appearance of the films obtained under the conditions of this work and of the preceding one. If mobility were restricted appreciably, uneven porous films might be obtained as also suggested by the fact that germanium does not sinter until heated to its melting point.[6] The germanium hydrides on the surface while exchanging their hydrogen mutually, may not exchange with hydrogen molecules striking them from the gas phase, as also shown by the lack of HD in the products of decomposition of GeH_4 in the presence of D_2.

These considerations exclude the following mechanism of germane decomposition on germanium (the subscript a stands for adsorbed):

$$GeH_4 \longrightarrow GeH_{2(a)} + H_2 \quad (1)$$

$$GeH_{2(a)} \longrightarrow Ge_{(a)} + H_2 \quad (2)$$

However, it is interesting to observe that a step similar to (1) suggests itself strongly for the homogeneous decomposition. Indeed, at the tempera-

(6) G. A. Geach, "Progress in Metal Physics," Vol. IV, Interscience Publishers, New York, N. Y., 1953, p. 174.

tures and pressures of the isotopic experiments, homogeneous decomposition, as revealed in the preceding paper, must have been taking place. But if the opening step of this gas phase decomposition were

$$GeH_4 \longrightarrow GeH_3 + H$$

one would expect it to be followed, in the presence of deuterium, by

$$H + D_2 \longrightarrow HD + D$$

a reaction with a low activation energy.[7] The latter is, however, excluded by the isotopic experiments. Thus we are led to propose the following initiating step for the homogeneous decomposition of germane

$$GeH_4 \longrightarrow GeH_2 + H_2$$

The subsequent fate of the GeH_2 radical is not known. It may diffuse to the walls where it is further decomposed. At any rate, it must be unreactive toward hydrogen. If the backward recombination step

$$GeH_2 + H_2 + M \longrightarrow GeH_4 + M$$

were important, it could again lead to isotope mixing in the presence of deuterium.

The mode of decomposition here suggested must be contrasted with the chain mechanism generally accepted[8] for the homogeneous pyrolysis of methane. Here, accumulation of energy into the bending and stretching modes of the tetrahedral germane molecule may lead predominantly to a splitting off of a hydrogen molecule. That several degrees of freedom are involved in this unimolecular decomposition is also indicated by the rate constants reported in the preceding work.[1] The data give a frequency factor equal to 2×10^{15} sec.$^{-1}$, a value suggesting a complex mode of dissociation. Finally, the exchange data show that no appreciable isotopic mixing of light and heavy germane takes place, either in the gas phase, or at the surface

$$GeH_4 + GeD_4 \longrightarrow GeH_xD_y$$

For the surface reaction itself, the opening step might very well be

$$GeH_4 \longrightarrow GeH_{2(a)} + H_2 \qquad (1)$$

by analogy with the homogeneous process. There is however no indication favoring this process rather than

$$GeH_4 \longrightarrow GeH_{3(a)} + H_{(a)} \qquad (3)$$

As mentioned earlier, if (1) is the opening step, the adsorbed radical GeH_2 must dissociate further, in order to account for the exchange data, according to the expression

$$GeH_{2(a)} \longrightarrow GeH_{(a)} + H_{(a)} \qquad (4)$$

Then we must admit the presence on the germanium surface, during decomposition, of adsorbed hydrogen atoms, represented by $GeH_{(a)}$ or $H_{(a)}$ without any further distinction between these two symbols.

Since the surface rate does not depend on the pressure of germane, the possible initiating steps (1) or (3) are ruled out as rate-determining steps. The rate controlling step must be either the surface dissociation of an adsorbed fragment GeH_x (x = 3 or 2) or the desorption of hydrogen from the surface. A decision between these two alternatives is not possible without further assumptions. The independence of the rate from germane pressure indicates that the adsorbed radical, the decomposition of which determines the rate, or the adsorbed hydrogen atoms, as the case may be, cover the surface fully. This is also indicated by the absence of mixing of heavy and light germanes during the decomposition: the equilibrium for the equilibrated steps preceding the rate controlling process must be overwhelmingly on the side of the rate controlling radical. Once a germane molecule has been chemisorbed, its chance of ever getting back to the gas phase is negligibly small.

Acknowledgment.—The assistance of Dr. K. E. Hayes in the mass spectrometric analyses is gratefully acknowledged. The preceding work was carried out with the assistance of a post-doctoral fellowship kindly provided by the Shell Fellowship Committee of the Shell Companies Foundation, Inc. It also forms part of a program on Solid State Properties and Catalytic Activity supported by the Office of Naval Research N6onr-27018. For this support we wish to express our appreciation and thanks.

(7) K. H. Geib and P. Harteck, *Z. physik. Chem.*, Bodenstein Festband, 849 (1931).

(8) E. W. R. Steacie, "Atoms and Free Radical Reactions," Reinhold Publ. Corp., New York, N. Y., 1954, p. 128.

SURFACE STRAIN IN OXIDE CATALYSTS—ALUMINA

BY E. B. CORNELIUS, T. H. MILLIKEN, G. A. MILLS AND A. G. OBLAD

Houdry Process Corporation, Marcus Hook, Pa.

Received February 25, 1955

The reversible adsorption of water by γ-alumina has been determined in the temperature range of 32 to 538° and water vapor pressures of 0.05 to 300 mm. An important preliminary step in the measurements was the pretreatment of the sample at 538° and 0.05 mm. water pressure *in situ* prior to making the measurements. Differential isosteric heats of hydration–dehydration have been calculated from the experimental results. The values obtained vary from 10 kcal./mole water adsorbed at 3 wt. % water adsorption level to over 105 kcal./mole at about 0.1 wt. % water adsorption level. The heterogeneity of the surface is interpreted on the basis of distortions of the normal crystalline lattice which must result from the removal of surface hydroxyl groups. The surface is apparently in a highly strained condition as a result of dehydration at 538°. Such highly strained surfaces are capable of activating many kinds of molecules and can function as catalytic centers for a number of reactions such as hydrogen–deuterium exchange and ethylene hydrogenation. Non-reducible oxides, therefore, have as one kind of catalytic activity that induced by dehydration–strain defects.

Introduction

The surface of a solid material is in an unusual crystallographic situation due to the requirements for termination of the solid structure. In solid, non-reducible oxides, the requirements of lowest energy lead to a surface ordinarily consisting of oxide ions rather than less polarizable metal ions. Furthermore, it is most significant that in order to satisfy chemical valences, many of the bivalent surface oxide ions have univalent hydrogen attached to them. When such oxides are evacuated at elevated temperatures, it is possible to remove at least a part of this hydrogen in the form of water. Even for high area oxides, it is usually possible to achieve a significant degree of such dehydration without an appreciable loss of surface area by sintering. Such dehydration is accomplished by the reaction between two surface MOH groups to form MOM and water. In the early stages of dehydration, it is the immediately neighboring MOH groups which can form MOM readily. As dehydration proceeds, the remaining surface MOH groups are not situated close enough to form MOM with normal crystallographic distances and, consequently, lattice distortion occurs. Therefore, more strenuous dehydration conditions are required to remove water and greater and greater energies of dehydration are required. Extensive dehydration of oxides is believed to produce a solid with a high energy surface strain condition. Further, it is proposed that such highly strained surfaces can function as catalytic centers under certain conditions. This paper is concerned with the measurement of the reversible sorption of water by a sample of γ-alumina at temperatures up to 538°, and calculation of isosteric heats of sorption. In addition, data are presented for the catalytic activation of molecular hydrogen by alumina as a function of degree of dehydration. These data are discussed in terms of their physical, chemical and catalytic significance. A brief consideration of the implication of dehydration in clay cracking catalysts has been given earlier.[1]

Experimental

The reversible water content of an activated alumina was measured at temperatures ranging from 32 to 538° and water vapor pressures from 0.05 mm. to as high as 300 mm. The γ-alumina, in the form of 4 mm. pellets, 1.35 g./cc. pellet density, produced by Harshaw Chemical Company, had been calcined above 565°. Surface area of the calcined pellets measured 76 m.²/g. by the BET method using nitrogen adsorbate, and remained substantially the same during the series of dehydration–hydration experiments.

A 75-g. sample of the activated alumina pellets was suspended in a perforated Vycor glass crucible by a fine platinum wire from an analytical balance. This apparatus is similar to that used in this Laboratory for quinoline chemisorption.[2] The crucible was carefully positioned inside a 50-mm. i.d. quartz tube surrounded by a nichrome wire-wound ceramic core furnace. Separate windings were provided to take care of end-losses, and the central winding was of sufficient length to provide a uniform temperature section adequate for both the crucible and a quartz chips air preheat zone below the crucible. Dry air or air of predetermined moisture content was passed at a controlled rate upwards through the preheat zone, past the perforated crucible and then drawn out through a tee in a 10-mm. i.d. tubing at the top, all substantially at atmospheric pressure. Dry "seal" air was introduced in a second tee above, to ensure against back diffusion of moisture from the atmosphere in the room. The air supply was partially dried by passing through fresh "Drierite" (calcium sulfate) towers, then further dried to as low as 0.05 mm. water vapor pressure in a "Dry ice"-chilled stainless steel "freeze-thaw" coil. This specially constructed coil was operated under air line pressure. It was designed to minimize ice-crystal carry-over by the simple expedient of chilling the air in a submerged section of the coil and reheating in an electrically heated upper section. Thus, the air is chilled, then thawed several times in succession. Two-stage constant temperature water bubbler saturators were used to provide air of desired moisture content. The "dewpoint" or "frost-point" of the air was checked periodically by noting the temperature at which dew or frost began to form in a Pyrex knock-out-trap tube plunged into a Dry Ice chilled acetone-bath. This method of determining the moisture content of the air was found to check the vapor pressure expected from a wet ice temperature two-stage bubbler within one degree centigrade. Where the higher vapor pressures were encountered, it was necessary to provide heated transfer lines to and from the apparatus to avoid condensation in the lines.

The precalcined sample of alumina was equilibrated at 538° in dried air, then subjected to air containing water at various vapor pressures, and at lower temperatures in a random sequence of steps as indicated by the adsorption data reported in Figs. 1A and 1B. In these figures, the sequence of experiments is indicated by the numbering of the data points. In order to provide a fixed basis for total "water" content of the alumina, a separate sample of the charge catalyst was taken to 1250° in a muffle type furnace, and this basis was subsequently checked by removing some of the 75-g. dehydration–hydration sample when conditions in the equipment approximated atmospheric conditions in the room. Thus, the water content data are based on 1250° ignited weight, though the sample itself was not taken any higher than 538° in the continuous weighing apparatus. In considering the data, it should be observed that the absolute water content of the sample calcined at 538° was

(1) T. H. Milliken, A. G. Oblad and G. A. Mills, "Use of Clays as Petroleum Cracking Catalysts," National Clay Conference, Berkeley, Cal., 1952.

(2) G. A. Mills, E. R. Boedeker and A. G. Oblad, *J. Am. Chem. Soc.*, **72**, 1554 (1950).

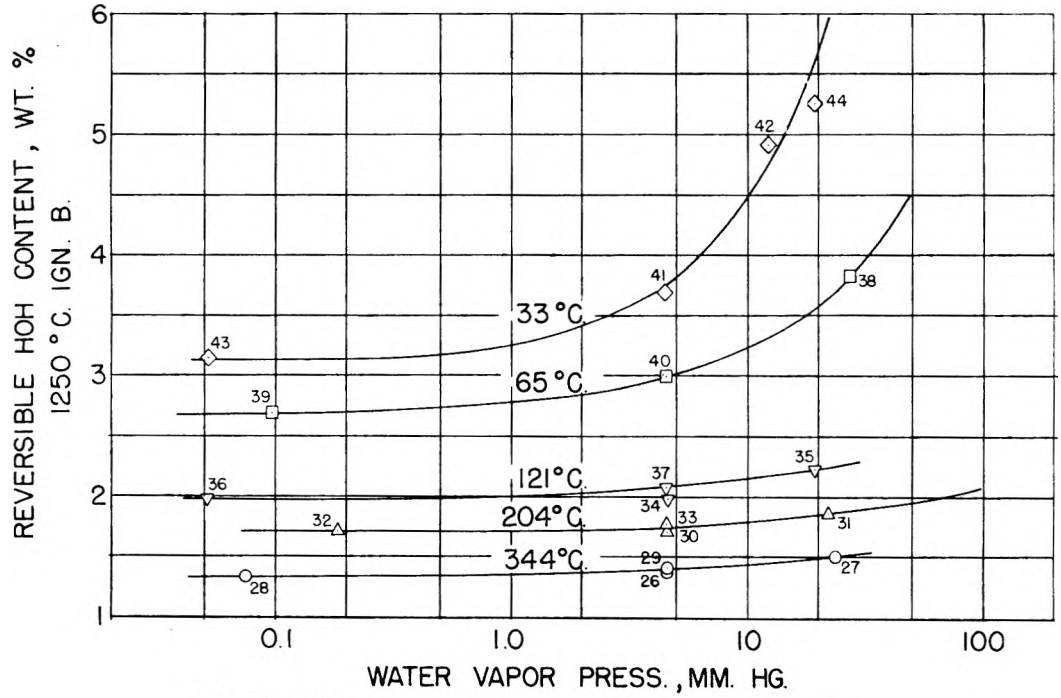

Fig. 1A.—Water vapor isotherms for a calcined alumina (33–344°).

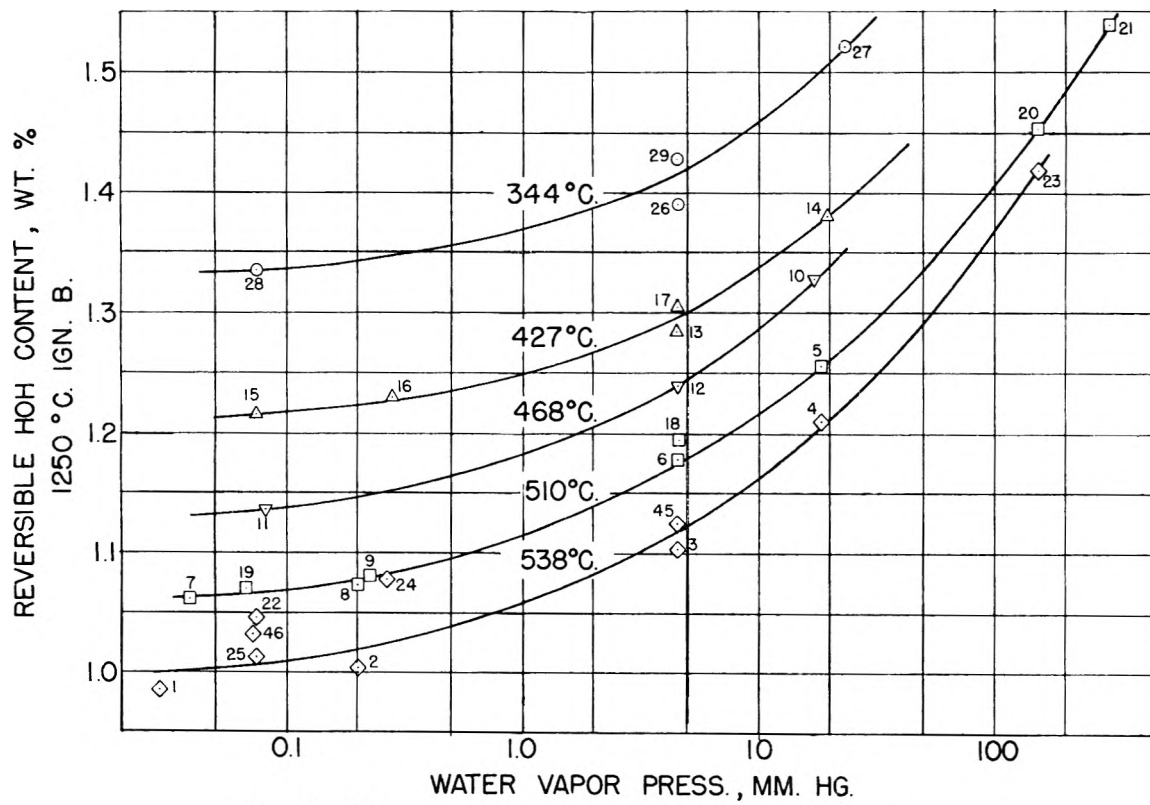

Fig. 1B.—Water vapor isotherms for a calcined alumina (344–538°).

found to be about 1.0% and water adsorption figures are obtained by subtracting this amount from the absolute water content. In general, it was found possible to return to the same weight for a given set of sorption conditions regardless of the path taken, although in some instances there appeared to be a slight hysteresis involved. However, the approach to equilibrium is slow, particularly for dehydration, so that the observed differences would be less if longer times were allowed. In the present work, the weights were arbitrarily considered to be at equilibrium when the weight change amounted to less than one milligram in one hour. As shown in Fig. 2, even this resulted in "equilibrium" approach times of 24 hours or more.

Discussion of Data

Many of the data were obtained at high temperatures under conditions of very low relative pressures, even above the critical temperature of water. Some idea of the range of alumina surface

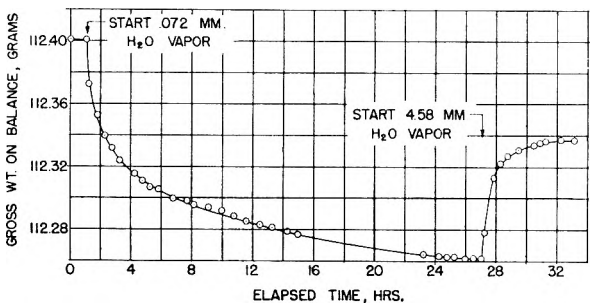

Fig. 2.—Typical approach to "equilibrium" weight (alumina sample weight ~ 75 g.) for 468° isotherm.

coverage involved in the present work is provided by Fig. 3. Water sorption at 35° from Fig. 1a and auxiliary data are plotted as a function of relative

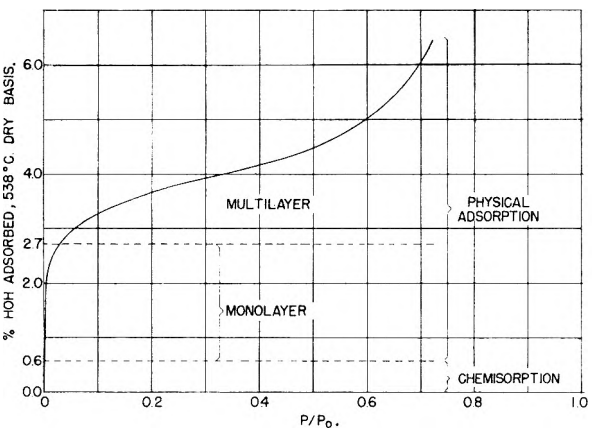

Fig. 3.—Sorption of water at 35° on alumina calcined at 538°.

pressure with the dry weight at 538° taken as the zero water adsorption basis. A determination of monolayer coverage according to the BET method gave a figure of 2.7% water adsorbed, corresponding to a surface area of 98 m.²/g., taking the water area as 10.8 Å.² per molecule. However, nitrogen adsorption data repeatedly gave a BET method area of 76 mg.²/g., using 16.4% Å.² as the area of the nitrogen molecule. The amount of water corresponding to a monolayer to cover 76 m.²/g. is 2.1%. Hence, the difference between 2.7 and 2.1, equals 0.6% water, can be considered to be chemisorbed water (HOH). Therefore, as shown in Fig. 3, water from 0 to 0.6% is designated as chemisorbed water; water above this amount is considered as physically sorbed water, from 0.6 to 2.7% essentially consisting of formation of a monolayer and above 2.7% formation of multilayers. Other instances of chemisorption followed by physical sorption are known, for example carbon monoxide on ammonia synthesis catalyst.[3] It is recognized that the division between chemical and physical sorption at 0.6% water is not exact and other ways of considering the data will provide a slightly different value. However, the range of chemi- and physical adsorption is consistent with the energies of sorption as will be discussed later.

From the isotherms of Fig. 1A and 1B, a graph of the reciprocal of the absolute temperature *versus* water vapor pressure for constant water content of the alumina has been drawn up as Fig. 4. From the slopes of these lines, the differential isosteric heat of sorption can be calculated for the various water content levels can be made, using the Clausius–Clapeyron equation

$$\log \frac{P_2}{P_1} = \frac{\lambda(T_2 - T_1)}{2.303R \times T_1 \times T_2}$$

where λ, the heat required to drive off a gram-mole of "water," is related to two vapor pressures P_1 and P_2, and the corresponding absolute temperatures T_1 and T_2.

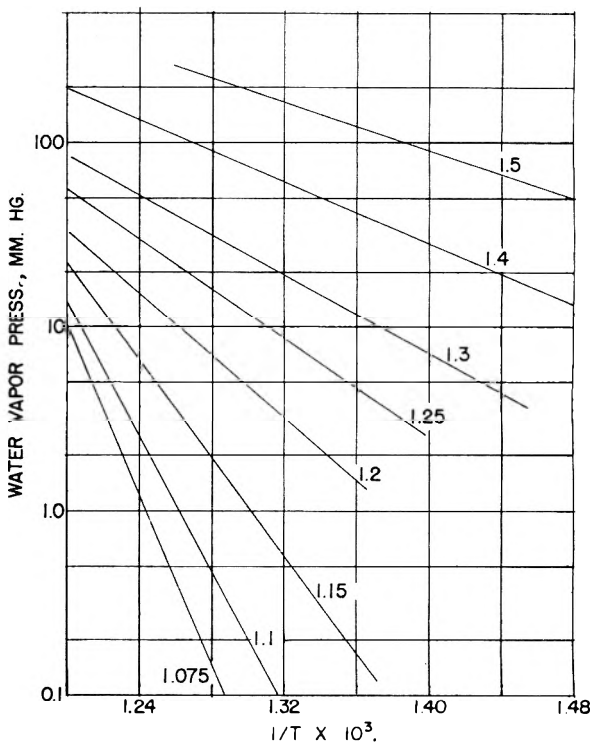

Fig. 4.—Calcined alumina hydration isosteres; parameter, % HOH on alumina, 1250°, ign. B.

Table I lists the isosteric heats of hydration–dehydration as a function of water content. The extremely high heats of adsorption evident at higher temperatures give some idea of the tre-

TABLE I

ISOSTERIC HEATS OF DEHYDRATION

"Water" pickup level on alumina, % wt., 1250° ign. B.	Isosteric heat of dehydration calcd. Clausius–Clapeyron eqn., kcal./g. mole	"Water" pickup level on alumina, % wt., 1250° ign. B.	Isosteric heat of dehydration calcd. Clausius-Clapeyron eqn. kcal./g. mole
1.075	105[a]	1.40	16
1.10	81[a]	1.50	15
1.15	60[a]	2.0	14
1.20	38	3.5	11
1.25	31	4.0	10
1.30	25		

[a] Figures given based on vapor pressures above ice; using vapor pressures above an extrapolated water curve below freezing, as recommended by R. M. Ilfeld,[4] these first three heats become 97, 73 and 57 kcal., respectively.

(3) P. H. Emmett and S. Brunauer, *J. Am. Chem. Soc.*, **59**, 1553 (1937).

(4) R. M. Ilfeld, *Anal. Chem.*, **23**, 1086 (1951).

mendous energies involved. These heats are also shown in graphical form in Fig. 5. It is apparent that at relatively high water contents, the differential isosteric heat of hydration is approximately 10 kcal./mole, equal to the heat of liquefaction. Below about 1.6% water, corresponding to 0.6% water adsorbed, the heat of adsorption increased rapidly, becoming greater than 100 kcal./mole, consistent with the idea, previously mentioned, that chemisorption is occurring. It is not known whether it is possible to obtain energies substantially higher than 100 kcal./mole.

Stowe[5] has measured the integral heat of wetting of activated alumina by liquid water. Values of about 3 kcal./mole of water were obtained for coverage of a monolayer from liquid water, which would correspond to 13 kcal./mole for adsorption from water vapor. This heat is low compared to values given in this paper for initial hydration because in Stowe's work the samples were not brought to and maintained at the same high degree of dehydration immediately before wetting. Due to the high energies involved, freshly dehydrated alumina surfaces are extremely hygroscopic, with a limited capacity, capable of removing water from P_2O_5 and other desiccants. It is significant that it is capable of effective drying even at high temperatures. High values for heats of sorption have been obtained in other systems. Values of 70 to 200 kcal./mole have been observed[6] for sorption of oxygen on carbon, and 162 kcal./g. atom[7] for oxygen on carbon.

Mills and Hindin[8] studied oxygen exchange between water and silica alumina. They found that there was a rapid exchange reaction between the water and surface hydroxyl. With progressive dehydration of the oxide, the amount of immediate oxygen exchange decreased, but only to a level which remained higher than the total hydroxyl content. It was proposed, therefore, that as more and more water was removed with increasing time and temperature of calcination, there was insufficient hydroxyl left to satisfy the normal valency of the metal ions present at the surface. It was suggested that such splitting out of water must leave the surface in a state of strain, that is, in a highly reactive condition, and that reaction with oxygen ions so involved accounts for the observed amount of rapid exchange.

Weyl[9] also has considered, in some detail, the energy of solid surfaces when subjected to a high degree of dehydration. He has found such surfaces capable of reacting with molecular oxygen or nitrogen. He has explained the high energy of such dehydrated surfaces as due to a strain derived from the circumstance that in order to split off water unusual crystallographic distances are involved.

In ionic structures, high energies may be achieved by displacement of ions relatively small distances. In referring to the surface or a site of strain, it seems clear that the strain will extend through a number of ions, both along the surface and beneath it. The energy released upon hydration will be a consequence of movement of a number of ions in a given area and not merely in a single bond shift. Such lattice energy would appear, therefore, to make possible very high energies for the hydration by a single molecule of water, greater than the amount to break a single chemical bond.

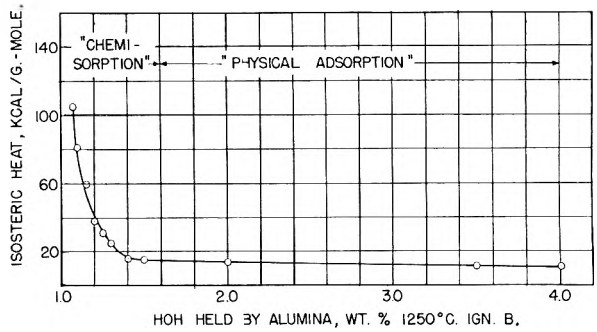

Fig. 5.—Isosteric heat of dehydration for a calcined alumina.

A highly reactive surface due to dehydration should be considered in the light of a number of chemical and so-called physical phenomena. For example, Cook, Pack and Oblad[10] have pointed out that surface strain can account for adsorbate–adsorbent attachment in the first layer of multimolecular films particularly in the low pressure region of the type II isotherm.

Highly dehydrated surfaces are capable of reacting with certain compounds to relieve such strain. Reaction with water at low temperature is an example. However, in other instances where under the temperature conditions a stable product is not formed, it is believed that these highly strained surfaces are important as catalytic centers[11] for example, for the activation of molecular hydrogen and hydrocarbons such as ethylene. This appears to be due to the ability of the surface to chemically activate molecular hydrogen in a reversible manner. Since catalysis is observed, the chemisorption of hydrogen and certain hydrocarbons is reversible to a certain extent even at low temperatures. The hydrogenation of ethylene is catalyzed by dehydrated alumina.[12,13] Part of the requirements then for this type of catalytic action are that the surface strain can react chemically with the molecules to be activated in a reversible manner and that neither reactants nor products form stable compounds with the surface.

Table II summarizes data obtained for the exchange reaction between hydrogen and deuterium. The first column referring to work of Holm and Blue,[12] indicates that when alumina is calcined from 400–650°, a remarkable increase in catalytic activity is achieved. Likewise, as shown in the second column for exchange carried out at −78°, Hindin[13] has observed a substantial increase in

(5) V. M. Stowe, THIS JOURNAL, **56**, 484 (1952).

(6) W. E. Garner, "The Adsorption of Gases by Solids," Faraday Society, 1932, p. 261.

(7) I. Langmuir and D. S. Villars, *J. Am. Chem. Soc.*, **53**, 486 (1931).

(8) G. A. Mills and S. G. Hindin, *ibid.*, **72**, 5549 (1950).

(9) W. A. Weyl, Trans., *N. Y. Acad. Sci.*, [II] **12**, 245 (1950); "A New Approach to Surface Chemistry and Heterogeneous Catalysis," Pennsylvania State College, Mineral Industries, no. 57, 118 pp. (1951); W. A. Weyl and T. Forland, *Ind. Eng. Chem.*, **42**, 257 (1950).

(10) M. A. Cook, D. H. Pack and A. G. Oblad, *J. Chem. Phys.*, **19**, 367 (1951).

(11) M. A. Cook and A. G. Oblad, *Ind. Eng. Chem.*, **45**, 1456 (1953).

(12) J. C. F. Holm and R. W. Blue, *ibid.*, **43**, 501 (1951).

(13) S. G. Hindin, Houdry Process Corp., unpublished results.

TABLE II

EFFECT OF WATER ON H_2–D_2 CATALYTIC EXCHANGE ACTIVITY OF ALUMINA

Ref.	12[a]		13[b]	
Temp. of H_2–D_2 exchange, °C.	200		−78	
	°C.	Rate	°C.	Rate
Calcination temp., °C.	400	0.62	450	0.25
vs. relative exchange	500	19.9	550	2.4
rate	650	200	650	3.2
			Wt.%	Rate
Calcined, then water	Atm.	Low	0	2.4
added, wt. % *vs.*	exposure	rate	.024	1.6
relative exchange			.048	0.9
rate			.085	0.2
Calcined and cooled in O_2	Same activity as H_2 calcined		Same activity as evacuated	

[a] J. C. F. Holm and R. W. Blue. Alumina of high purity prepared by precipitation from aluminum nitrate with ammonium hydroxide, dried and calcined at 400°. Calcinations of alumina before H_2–D_2 exchange experiments were in purified hydrogen except for effect of O_2 experiment.

[b] S. G. Hindin. Pure alumina prepared from aluminum isopropoxide, hydrolyzed, dried and calcined 560°; Fe_2O_3 0.003%, Na_2O 0.03%. Surface area 300 m.²/g., H_2O of constitution 1.8 and 0.98 and 0.37 after 450 and 550°, 650° evacuations for about 64 hours, as determined by D_2 exchange at 400°. Calcination of alumina before H_2–D_2 exchange experiments was under high vacuum. Rates given are for initial (15 second) activity—longer times give less activity. Water added to 550° calcined sample.

activity on progressive dehydration of a sample of alumina to 650°, when such tests are made for short reaction times. Additional experiments were carried out to add back either water or oxygen to the highly calcined alumina. It was found that very small amounts of water inactivated the catalyst for hydrogen–deuterium exchange. In contrast, oxygen did not change the activity when compared to either a hydrogen-calcined or an evacuated-calcined alumina. It has been reported[14] that alumina can be an oxygen deficient or "N" type semiconductor. The possibility that the catalytic activation of molecular hydrogen was achieved by a reduction center in the alumina, appears to be refuted by these data. It appears that it is a dehydration center and not a reduction center which is catalytically active.

The activity of chromia for hydrogen–deuterium exchange has been investigated in detail by Voltz and Weller.[15] For this oxide, a more active catalyst was produced when a stabilized sample was heated in hydrogen rather than oxygen, prior to measurement of catalytic properties. However, small amounts of water inactivated the chromia in either the oxidized or reduced conditions. In the case of chromia, it would appear that two types of defects or strains—a reduction and a dehydration type—are responsible for catalytic activity.

DISCUSSION

MAX BENDER.—This question involves the semantics of the term "chemisorption" as used in the paper. Request is made to give the basis on which the adsorptions were considered to have changed from chemisorption to physical adsorption.

G. A. MILLS.—A twofold basis was used. First, the chemisorbed water was calculated to be the additional amount of water needed to form a monolayer, when compared to adsorption of a nitrogen monolayer, p. 812. Second, the point of chemisorption was selected as the position at which the energy of sorption increases rapidly, Fig. 4. These methods give values considered to be in good agreement. While the transition from physical to chemical sorption undoubtedly covers a range, this range is believed sufficiently small here, that a fairly clear division can be made between the water sorbed "physically" and "chemically."

(14) W. Hartman, *Z. Physik*, **102**, 709 (1936).

(15) S. E. Voltz and S. Weller, *J. Am. Chem. Soc.*, **75**, 5231 (1953); **76**, 4695 (1954).

THE CATALYTIC OXIDATION OF CARBON MONOXIDE BY NITROUS OXIDE ON CARBON SURFACES[1]

BY R. NELSON SMITH AND JOHN MOOI

Chemistry Department, Pomona College, Claremont, Calif.

Received February 25, 1955

The catalytic oxidation of CO by N_2O on "ashless" carbon black and "ashless" charcoal surfaces has been studied over the temperature range of 300–500°. The reaction mixtures were circulated continuously over the carbon. All of the results can be explained on the assumption that CO is relatively strongly adsorbed and N_2O is relatively weakly adsorbed on a few active sites where the reaction takes place. Application of the Langmuir equation to this mechanism yields a mathematical rate expression which corresponds to the experimental rate over the full course of the reaction, regardless of whether the surface has been H_2-treated or possesses surface oxygen complexes. The surface oxygen complexes, formed by N_2O oxidation of the carbon, tend to poison the carbon surface, but this may be reduced to a minimum with an excess of CO in the gas mixture. It appears that the surface oxygen complexes do not in any way act as intermediates in the reaction.

This study was undertaken to discover whether carbon–oxygen surface complexes play the same role in reactions involving N_2O as they do in the reactions involving H_2O.[2] It seemed worthwhile also because of the interesting questions posed by the previous work of Strickland-Constable.[3,4]

Experimental

Two types of carbon were used in this study: one a black and the other a charcoal.

Graphon.—A partially graphitized carbon black (supplied through the courtesy of the Godfrey L. Cabot Co.) was made by heating Spheron Grade 6 (a medium processing channel black) to approximately 3000° in an electric furnace. The surface area is about 80 sq. m. per g. and its ash content is about 0.02%.

Su-60.—A sugar charcoal of extremely low ash content was prepared, starting with Confectioners AA sugar furnished through the courtesy of the California and Hawaiian Sugar Refining Corporation. This sugar was used because it had an ash content of 0.0008%. 25-gram samples of this sucrose were placed in porcelain evaporating dishes and carbonized at 400° in a muffle furnace lined with aluminum foil. This took about 30 min. Several batches of carbonized sugar were combined in a single evaporating dish and heated in a muffle furnace (with no Al foil) at 800° for about 30 min. Thirty grams of this sugar carbon was put into a platinum boat, heated in a stream of N_2 to 900°, then subjected at 900° to the steam from 100 ml. of water for a period of 30 min., followed by cooling in a stream of N_2. This process yielded 12 g. of activated carbon, denoted as Su-60 because of the 60% weight loss on activation. The BET surface area of Su-60 is 1020 sq. m. per g., using ethyl chloride, and its ash content is less than 0.005%.

Nitrous Oxide.—Obtained from the American Medical Gas Co. and used from the cylinder without further purification. Precautions were taken to prevent contamination on removal from the cylinder. The analytical method used in this study showed this gas to be pure N_2O.

Carbon Monoxide.—Obtained by dropping powdered, outgassed sodium formate onto outgassed concentrated H_2SO_4 in an evacuated system. The CO so produced was passed through a Dry Ice trap before storing in a Pyrex reservoir. The analytical method used in this study showed the gas to be pure CO.

Analytical Methods.—Gas samples were analyzed for CO, CO_2, N_2O and N_2 (by difference) by the micromethods of the Blacet–Leighton apparatus (Arthur H. Thomas Co.). CO_2 was determined by a KOH bead[5]; CO by a Ag_2O bead[6] held to the platinum holder with Kronig cement; N_2O by combustion with excess H_2.[7] Initial reaction mixtures were analyzed only after vigorous and turbulent mixing. Reaction mixtures were analyzed by removing samples from the circulating system with a Toepler pump. The samples were removed shortly after passing through the heated carbon bed, and since there was no dead space in the circulating system these samples were representative of the gas which had passed through the carbon bed immediately prior to sampling.

Reaction System.—In addition to the mechanical and diffusion vacuum pumps, the essential parts of the reaction system were reservoirs for CO and N_2O, a gas buret, a Toepler pump and the circulating system. The circulating system consisted of a sample tube, manometer and pump, and for most experiments a soda-lime tube. It was connected to the remainder of the system by a three-way vacuum-sealed precision-ground stopcock. This was the only stopcock involved in the circulating system. The circulation was accomplished by a modified all-glass Puddington[8] pump. The rate of circulation was about 300 cc. per min. A manometer, for measuring pressure changes during the course of the reaction, was connected to one arm of the 3-way stopcock. The dead space in the manometer was about 1 cc. The volume of the circulating system was 570 cc. Because of the slightly fluctuating pressures caused by the circulating pump, it was necessary to stop the pump briefly for each pressure measurement. The carbon samples were contained in a clear quartz tube which was connected to the rest of the system with quartz-to-Pyrex graded seals. The samples were retained in the quartz tube with Refrasil, silica wool from the H. I. Thompson Co. Usually as the CO_2 was produced it was removed with a soda-lime tube sealed into the system a short distance from the point at which the gases emerged from the carbon bed. The soda-lime was retained between coarse sintered disks and outgassed at 250° with an electric heater. It has been demonstrated that this method may be used in the quantitative microanalysis of gases at very low pressures.[9] To obtain a satisfactorily high vacuum it was necessary to outgas the circulating system for several hours (usually overnight) before each run. The furnace surrounding the silica reaction tube was controlled to about ± 5°, though in most cases the fluctuations were not that large. In order to H_2-treat the samples, H_2 was admitted to the circulation system after it had been evacuated and the sample heated to 1000°. When the H_2 had circulated for about 15 minutes it was pumped out and replaced by fresh H_2. After the third quantity of H_2 had been pumped out, the carbon sample was allowed to cool slowly and pumping was continued until the next run was begun. The circulation pump was also operated continuously during all outgassing operations.

Results

The general features of the N_2O oxidation of CC are described in the section which follows. The quantitative features are illustrated by the representative curves shown in Figs. 1–6. In each

(1) This is a progress report of work done under Contract N8onr 54700 with the Office of Naval Research.

(2) R. N. Smith, C. Pierce and C. D. Joel, THIS JOURNAL, **58**, 298 (1954).

(3) D. G. Madley and R. F. Strickland-Constable, *Trans. Faraday Soc.*, **49**, 1312 (1953).

(4) R. F. Strickland-Constable, *ibid.*, **34**, 1374 (1938).

(5) F. E. Blacet and P. A. Leighton, *Ind. Eng. Chem., Anal. Ed.*, **3**, 266 (1931).

(6) F. E. Blacet, G. D. McDonald and P. A. Leighton, *ibid.*, **5**, 272 (1933).

(7) F. E. Blacet and D. H. Volman, *ibid.*, **9**, 44 (1937).

(8) J. E. Puddington, *Anal. Chem.*, **17**, 592 (1945).

(9) C. H. Prescott, Jr., and J. Morrison, *Ind. Eng. Chem., Anal. Ed.*, **11**, 230 (1939).

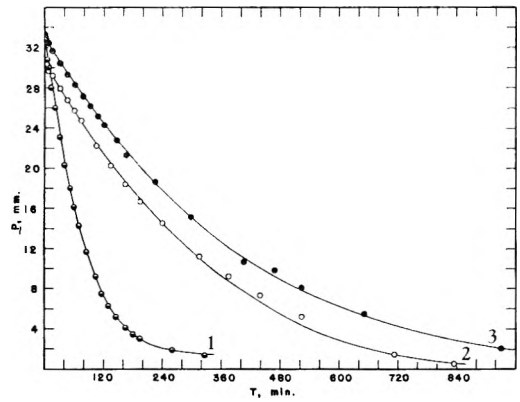

Fig. 1.—Reaction on Su-60 at 300°. See Table I for conditions. Initial pressures are (1) 62.8 mm., (2) 90.8 mm., (3) 93.3 mm.

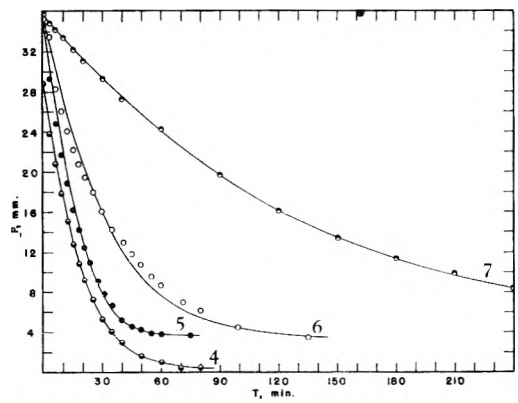

Fig. 2.—Reaction on Su-60 at 400°. See Table I for conditions. Initial pressures are (4) 58.8 mm., (5) 94.6 mm., (6) 97.5 mm., (7) 95.8 mm.

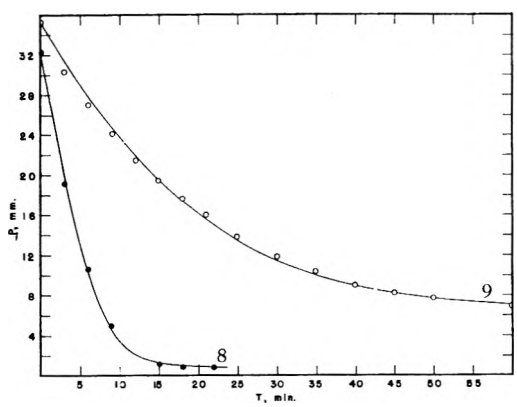

Fig. 3.—Reaction on Su-60 at 500°. See Table I for conditions. Initial pressures are (8) 95.3 mm., (9) 62.3 mm.

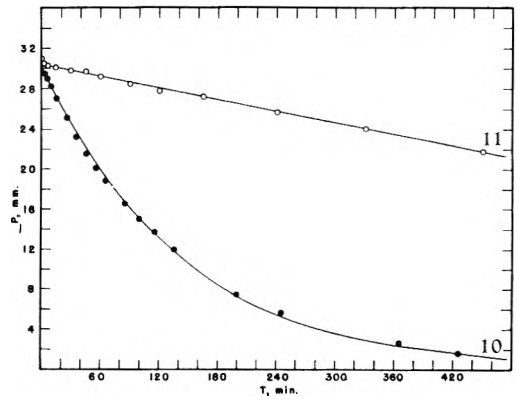

Fig. 4.—Reaction on Graphon at 300°. See Table I for conditions. Initial pressures are (10) 60.5 mm., (11) 61.0 mm.

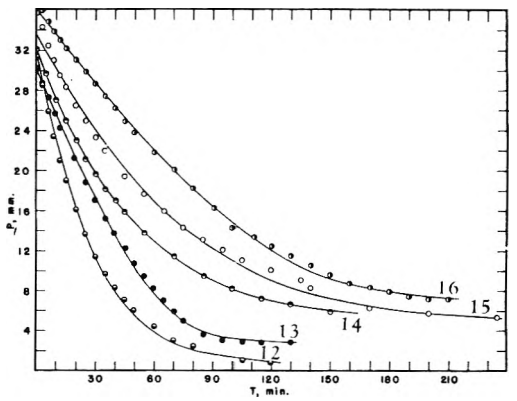

Fig. 5.—Reaction on Graphon at 400°. See Table I for conditions. Initial pressures are (12) 61.6 mm., (13) 82.3 mm., (14) 54.0 mm., (15) 61.8 mm., (16) 94.0 mm.

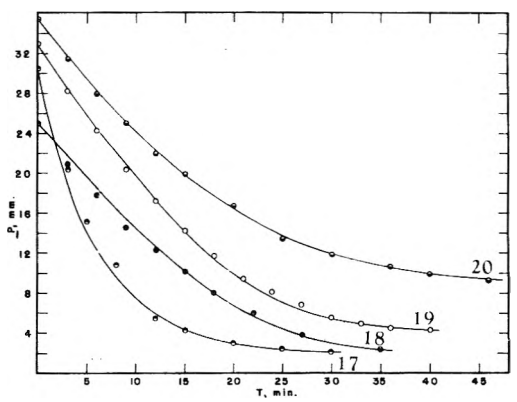

Fig. 6.—Reaction on Graphon at 500°. See Table I for conditions. Initial pressures are (17) 56.5 mm., (18) 75.0 mm., (19) 83.0 mm., (20) 55.5 mm.

figure the points are experimental, but the curves have been calculated in the manner described in a later section. In order to show Figs. 1–6 as compactly as possible the pressure values are arbitrary, though the units are mm. Each reaction actually starts at the pressure indicated in the caption. This method of plotting does not affect the *slope* of the curve, hence the reaction rates are satisfactorily compared in this way.

The Competing Reactions: 1.—N_2O oxidizes carbon surfaces to give N_2 and CO_2. In a series of experiments it was found that the oxygen content of the CO_2 produced was less than that contained in the N_2O which was used. The difference is held on the surface as oxygen complexes. N_2O oxidizes a freshly H_2-treated surface more rapidly than a surface containing oxygen complexes.

2.—CO oxidation is also much more rapid on a freshly H_2-treated surface than on one which has been allowed to accumulate surface oxides. Compare curves 1 and 3, 5 and 7, 8 and 9, 10 and 11, 12 and 15, 17 and 20.

3.—At 300° N_2O will not oxidize a Graphon surface, even after H_2 treatment. In one experiment

there was no change in pressure after 26 hours, and analysis showed the gas to be pure N_2O with no trace of N_2. This same surface at 300° catalyzed the oxidation of CO by N_2O (see curve 10).

4.—At 300° N_2O will oxidize Su-60 with a H_2-treated surface. In one experiment N_2O at an initial pressure of 44 mm. was circulated over the charcoal for 26 hours. Analysis showed 3.4% was converted to N_2 and that some surface oxides were formed. After outgassing at the same temperature, a fresh sample of N_2O would not undergo decomposition on this surface. In 14 hours there was no change in pressure and no N_2 in the gas. This same surface which contained oxygen catalyzed the oxidation of CO by N_2O (see curves 2 and 3).

5.—CO oxidation which occurs on a H_2-treated surface with an excess of N_2O is accompanied by the simultaneous oxidation of the surface by N_2O to give CO_2 and surface oxygen complexes. The oxygen content of the gases (CO, CO_2 and N_2O) during and at the end of the reaction is less than the oxygen content of the original N_2O gas. Also the rate, compared to that for mixtures containing equal or excess CO, is slowed during the course of the reaction as the surface oxides are formed. Under these conditions no great amount of N_2O is actually used in the carbon oxidation reaction; the main effect, other than CO oxidation, is the poisoning of sites useful for the CO oxidation.

6.—CO oxidation which occurs on a H_2-treated surface with mixtures containing as much CO as N_2O, or more, is accompanied by very little oxidation of the surface by N_2O. This is shown by pumping off the completed reaction mixture and adding a new gas mixture, which then proceeds to react at essentially the same rate as the first. See curves 2 and 3, 4 and 5, 14 and 15, 18 and 20. After many repetitions the reaction does proceed more slowly, presumably due to the formation of surface oxides.

7.—The rate of CO oxidation is zero order with respect to CO when there is as much CO as N_2O, or more. A mixture which contains initially twice as much CO as N_2O (and which at the end of the reaction contains infinitely more CO than N_2O) proceeds at the same rate as an equimolar mixture containing the same initial pressure of N_2O. See curves 4 and 5, 18 and 20. With an initial excess of N_2O the rate must inevitably become dependent on the CO concentration. As the CO approaches complete oxidation the rate approaches a first-order dependence on the CO concentration. This is best shown in the discussion of the mathematical treatment of the data. These effects of CO concentration on the rate of CO oxidation are the same whether the surface is H_2-treated or contains an oxygen complex.

8.—The rate of CO oxidation with respect to N_2O varies between zero order (at high pressure) and almost first order (at low pressure). This is true whether the reaction occurs on a H_2-treated surface or on an oxygen-complex surface, though the magnitude of the rates differs considerably. This is best shown in the later discussion of the mathematical treatment of the data.

9.—CO oxidation also occurs in an empty silica tube at 400–600° under the circulating conditions used in this study. However, the rate of the reaction under these conditions is about 1/1000 as fast as with the carbon samples used.

Reaction of CO with Surface Oxygen Complexes: 10.—When CO is added to a surface which possesses large amounts of oxygen complex, a change in pressure is noted (the CO_2 is absorbed by soda-lime) but the rate is very slow and CO uses only a small fraction of the total amount of oxygen available on the surface.

11.—When a reaction mixture containing an excess of CO is passed over a surface containing oxygen complexes, a little more CO is used than is equivalent to the initial amount of N_2O.

12.—When a mixture is added to a surface whose oxygen complexes have been treated previously with an excess of CO at the same temperature, the initial (first 5–10 min.) rate of reaction is a little more rapid than on the same surface which has had no CO treatment. This also indicates a small, slow reaction of CO with the oxygen complexes (see curve 15).

13.—Points 8–10 above indicate that CO oxidation is not the result of CO reacting with the oxygen complexes formed by N_2O, because the rate of CO oxidation is much faster than the rate of reaction of CO with surface complexes. These points supplement point 3, *i.e.*, the CO oxidation will occur on a carbon surface which will not cause any decomposition of N_2O whatever.

The Active Sites (see also points 2, 3 and 4): **14.**—The difference between the oxygen content of the gaseous reaction products (CO_2, N_2O, N_2) and the original N_2O when N_2O is passed over a freshly H_2-treated surface is the amount of oxygen held by the surface complexes. The total surface area divided by the cross-sectional area of a carbon atom (about 4.3 Å.^{2}) gives the number of carbon atoms in the surface. These calculations for Su-60 show that *at the most* there is one oxygen atom fixed on the surface for every 300 carbon atoms. For Graphon there is *at the most* one oxygen atom for every 500 carbon atoms. To get this much oxygen attached to the surface, the carbon must be exposed to N_2O for periods of time which are large compared to the time required for a N_2O–CO mixture to react completely.

15.—On Su-60 these surface oxides decrease the rate of CO oxidation to about $^1/_6$ of that observed on a H_2-treated surface, hence about $^6/_6$ of the active sites occur on less than 0.3% of the surface. On Graphon the surface oxides decrease the rate of CO oxidation to about $^1/_2$ of that observed on a H_2-treated surface, hence about $^1/_2$ of the active sites occur on less than 0.2% of the surface. See curves 1 and 3, 5 and 7, 8 and 9, 12 and 14, 17 and 20. On Graphon at 300° the surface oxides (formed by N_2O at higher temperatures) have an even more pronounced effect. See curves 10 and 11.

16.—If the difference in areas is taken into consideration, the initial rates of CO oxidation are essentially the same on both samples at 400° and at 500°, thus indicating that the number of active sites

per unit surface area is essentially the same for both the Graphon and the Su-60.

17.—Five-sixths of the active sites on Su-60 and $^1/_2$ of the active sites on Graphon must be carbon atoms. The remaining $^1/_6$ sites on Su-60 may be among the carbon atoms in 99.7% of the surface, among the oxygen complex sites in 0.3% of the surface, or on the trace of ash present. In the case of Graphon at 300° all of the sites must be carbon atoms (or perhaps ash) for at this temperature no surface oxide formation occurs. At 400 and 500° oxygen complex sites may be effective for CO oxidation.

18.—Active sites are created on the Graphon surface over a long period of time as the result of repeated oxidations by N_2O (at 400–500°) followed by H_2-treatment at 1000°. After nine treatments of this type the surface caused a slow pressure change of 1.14×10^{-3} mm./min. at 100°. A fresh Graphon sample will not catalyze the CO oxidation at 100° (no detectable change after 17 hours). At 300°, six treatments increased the initial reaction rate by a factor of 20. At 400°, four treatments caused a fourfold increase in the initial reaction rate. No such activating effect was observed for the Su-60. The results published here are for activated Graphon surfaces which do not seem to undergo any appreciable change with further H_2-treatment alternating with N_2O oxidation.

The Reaction Mechanism.—The following reaction steps are suggested to account for the experimental facts just described.

$$\begin{aligned} CO + C^* &= CO(C^*) && (1)\\ N_2O + CO(C^*) &= N_2 + CO_2 + C^* && (2)\\ N_2O + C^* &= N_2 + (C^*O) && (3)\\ N_2O + (C^*O) &= N_2 + CO_2 && (4) \end{aligned}$$

C* represents an active site (carbon atom); (C*O) represents a carbon–oxygen surface complex; CO(C*) represents CO physically adsorbed on an active site. Since the oxidation of CO is zero order with respect to CO (when there is as much CO as N_2O, or more) it must be that these active sites are saturated with CO. That this is a physical adsorption and not a chemisorption is shown by the fact that it is a reversible adsorption, and that not until temperatures exceed 700° is there any exchange of C atoms between CO (or CO_2) and carbon atoms of the lattice.[10] The production of CO_2 is determined primarily by the rate at which N_2O reacts with the CO-saturated sites (step 2) and the rate at which the active sites are removed by oxidation with N_2O (step 3). As long as there is as much CO as N_2O, or more, step 3 plays a minor and unimportant role. Also, if the carbon has been previously treated with N_2O so that there is little, if any, tendency for further reaction of N_2O with carbon, then again step 3 will play no significant role during the course of CO oxidation. In the last case, the reaction would be slower because there would be fewer C* sites available. Step 3 is important if the reaction mixture contains an excess of N_2O, for during the course of the oxidation the C* sites will be continually removed and the reaction will become increasingly slow. That production of CO_2 is not significantly affected under any conditions by step 4 has been shown by separate experiments with pure N_2O. These show that the rate of production of CO_2 by steps 3 and 4 is very slow compared to the oxidation of CO under the same conditions.

In deriving a rate expression from this mechanism, steps 3 and 4 will be neglected as being unimportant in the removal of N_2O. Step 3, however, is important with an excess of N_2O, for the rate of removal of C* has an effect on the number of sites available for CO oxidation in step 2. If the rate of CO oxidation is assumed to be proportional to the fraction of the surface (active sites) which contains N_2O and CO, then application of the Langmuir equation in the classical manner gives

$$-\frac{dP_{N_2O}}{dt} = \kappa\theta_{N_2O}\theta_{CO} = \frac{\kappa k P_{N_2O}}{1 + kP_{N_2O}} \times \frac{k'P_{CO}}{1 + k'P_{CO}} \quad (5)$$

if k_3 is the rate constant for the reaction in step 3, the rate at which active sites will be used up will be given by

$$-\frac{dC^*}{dt} = k_3\theta_{N_2O} = \frac{k_3 k P_{N_2O}}{1 + kP_{N_2O}} \quad (6)$$

and the general rate expression becomes

$$-\frac{dP_{N_2O}}{dt} = \frac{\kappa k P_{N_2O}}{1 + kP_{N_2O}} \times \frac{k'P_{CO}}{1 + k'P_{CO}} - \frac{k_3 k P_{N_2O}}{1 + kP_{N_2O}}$$

$$-\frac{dP_{N_2O}}{dt} = \frac{kP_{N_2O}}{1 + kP_{N_2O}}\left[\frac{\kappa k'P_{CO}}{1 + k'P_{CO}} - k_3\right] \quad (7)$$

For all those reaction mixtures which contain as much CO as N_2O, or more, the reaction is zero order with respect to CO indicating that $k'P_{CO}$ is large compared to 1. For these conditions, then

$$\frac{\kappa k'P_{CO}}{1 + k'P_{CO}} - k_3 = \kappa - k_3$$

With these assumptions for mixtures containing as much CO as N_2O, or more, equation 7 becomes

$$-\frac{dP_{N_2O}}{dt} = \frac{(\kappa - k_3)kP_{N_2O}}{1 + kP_{N_2O}} = \frac{KP_{N_2O}}{1 + kP_{N_2O}} \quad (8)$$

On integration, equation 8 becomes

$$\ln P_{N_2O} + kP_{N_2O} = -Kt + K' \quad (9)$$

where K' is an integration constant. (9) may be rearranged to

$$t = A - BP_{N_2O} - C \log P_{N_2O} \quad (10)$$

In most of the rate experiments involving N_2O and CO, the CO_2 was removed as formed; thus at any given time the total pressure $P = P_{N_2O} + P_{N_2} + P_{CO}$. If the nitrogen produced by steps 3 and 4 is assumed to be negligible compared to that produced in 2, then $P_{N_2} + P_{CO} = P_b$, the initial pressure of CO, and $P_{N_2} + P_{N_2O} = P_a$, the initial pressure of N_2O. It follows also that $P_{N_2O} = P - P_b$ and $P_{CO} = P - P_a$. Equation 10 can be rearranged with these relations to

$$t = A - B(P - P_b) - C \log (P - P_b) \quad (11)$$

Equation 11 is well-suited for the evaluation of the constants A, B and C ($K = 2.3/C$ and $k = BK$) for reaction mixtures that contain an initial CO:N_2O of one or more. For this purpose experimental values are taken for P at $t = 0$, t at $P = P_b + 1$, and a pair of values for P and t about midway between the other two pairs. To simplify the evaluation of constants, P_b was chosen to be the

(10) F. Brown, *Trans. Faraday Soc.*, **48**, 1005 (1952).

TABLE I

RATE CONSTANTS USED IN EQUATIONS 8 AND 12 FOR THE REACTION MIXTURES SHOWN IN FIGS. 1–6

Curve no.	Type of carbon	Type of surface[a]	Temp., °C.	Initial N_2O/CO	K	k	K'	k'
1	Su-60	HT	300	1	0.01815	0.02065		
2	Su-60	SOC	300	2	.00332[d]	.0125[d]	0.0669	0.0602
3	Su-60	SOC	300	0.5	.00332	.0125		
4	Su-60	HT	400	1	.0748	.02075		
5	Su-60	HT[b]	400	0.5	.1105	.0481		
6	Su-60	HT	400	2	.0748[d]	.02075[d]	.0256	.0254
7	Su-60	SOC	400	0.5	.01095	.0156		
8	Su-60	HT	500	0.5	.415	.0578		
9	Su-60	SOC	500	1	.0755	.0217		
10	Graphon	HT	300	1	.00815	.00725		
12	Graphon	HT	400	1	.0426	.01055		
13	Graphon	SOC	400	2	.0229[d]	.0070[d]	.1178	.2740
14	Graphon	SOC	400	1	.0229	.0070		
15	Graphon	SOC[c]	400	1	.0200	.0204		
16	Graphon	SOC	400	0.5	.0359	.106		
17	Graphon	HT	500	1	.1720	.0048		
18	Graphon	SOC	500	0.5	.1860	.1183		
19	Graphon	SOC	500	2	.1860[d]	.1183[d]	.1593	.113
20	Graphon	SOC	500	1	.1045	.0443		

[a] HT means H_2-treated; SOC means surface oxygen complex. [b] Used previously by reaction mixture of curve 4. [c] Surface oxygen complex was treated with CO prior to this run. [d] Value assumed to be the same as that obtained on similar surface at same temperature, but without an excess of N_2O.

final pressure of the reaction mixture, even though this might have been a small fraction of a mm. different from the initial pressure of CO (because of reaction steps 3 and 4).

When the initial reaction mixture contains a $CO:N_2O$ ratio of less than one the reaction rate is determined by equation 7, and the evaluation of constants is considerably more difficult. Under these conditions it is assumed that k_3 is small compared to the remainder of the factor which involves P_{CO}. This assumption is probably valid until near the end of the reaction where P_{CO} is very small and the excess N_2O may easily remove sites by step 3. With these assumptions, equation 7 becomes

$$-\frac{dP_{N_2O}}{dt} = \frac{KP_{N_2O}}{1 + kP_{N_2O}} \times \frac{K'P_{CO}}{1 + k'P_{CO}} \qquad (12)$$

When N_2O is in large excess, it has been found that the over-all rate of the reaction may be expressed by an equation of the form of equation 11, using $P - P_a$ instead of $P - P_b$. In other words

$$-\frac{dP_{N_2O}}{dt} = -\frac{dP_{CO}}{dt} = \frac{K''P_{CO}}{1 \times k''P_{CO}} \qquad (13)$$

K'' and k'' may be found in the same way that constants for equation 11 were found. Combining equations 12 and 13

$$\frac{KP_{N_2O}}{1 + kP_{N_2O}} \times \frac{K'P_{CO}}{1 + k'P_{CO}} = \frac{K''P_{CO}}{1 + k''P_{CO}} \qquad (14)$$

K and k are obtained from equation 11 for the same type of surface (H_2-treated or oxygen complex) but in a separate experiment using as much CO as N_2O, or more. P_{N_2O} and P_{CO} may be calculated from the composition of the original mixture and the total pressure at time t. With the values of K, K'', k, k'' and experimental pressures at two different times during the course of the reaction, it is possible to calculate K' and k'. As a check, the values of K', k', K and K are substituted into equation 12 and values of $-dP_{N_2O}/dt$ are calculated for the full course of the reaction and compared with those found by equation 13 using only values of K'' and k''. The agreement is usually very good.

How well these rate expressions fit the experimental data is shown by all the curves in Figs. 1–6. In all of these figures the points are experimental but the curves are calculated from the rate expressions just discussed using the constants summarized in Table I.

It will be noted that although the form of the rate expression is correct throughout the entire course of the reaction for a given reaction mixture, the magnitudes of the constants vary appreciably from one run to the next even though the same type of surface is used. The difficulty in obtaining reproducible results has been experienced by others and is caused by the extreme difficulty in repeatedly preparing a carbon surface with the same number of active sites. Strickland-Constable deliberately oxidized his surface with N_2O for long periods of time for he found that this gave a virtually reproducible surface even though it greatly reduced its activity.

The reaction mechanism of equations 1 to 4 and the application of Langmuir equations in the classical manner for heterogeneous gas phase reactions simply and satisfactorily explains all of the experimental data obtained in this study. There remain, however, two large discrepancies between the results of this study and those of Strickland-Constable.[3] Strickland-Constable found that the oxidation of CO by N_2O was first order with respect to CO and zero order with respect to N_2O. To explain his data he postulated the rapid formation of a "labile oxide" intermediate by the reaction

$$N_2O + C = \text{"labile oxide"} + N_2$$

followed by

$$\text{"labile oxide"} + CO = CO_2$$

The "labile oxide" was assumed to be part of the "missing oxygen" in each case. The "missing oxygen" was calculated as the difference between the oxygen content of the original gas and the gas during the course of the reaction; 0.05% of the reaction mixture was removed for each analysis. The "missing oxygen" was found to reach a constant concentration soon after the reaction started, and the constant amount increased in proportion to the square root of the initial N_2O pressure; it could also be completely pumped off as CO_2 at the end of the reaction without raising the temperature. Both of these points suggest a reversible process. On the other hand, CO_2 was not appreciably adsorbed nor did it have any effect on the rate of the reaction when added with the reactants. These two points suggest an irreversible process. A possible alternative explanation of the "missing oxygen" may lie in Strickland-Constable's reaction system. He used a 12-g. sample of charcoal that had a surface area of 856 sq. m. per g., and this was held in a 500-ml. silica reaction bulb. During the course of the reaction negligibly small samples were withdrawn for analysis, after pushing them back three times to insure that they were representative. It is not clear how large a volume was pushed back and forth for mixing. In such a static system involving a heterogeneous reaction which undergoes no pressure change it is necessary for fresh reactants to diffuse into the bulk of the charcoal while the products diffuse out of the bulk of the solid into the free gas volume. Under these conditions with a large charcoal sample possessing a large surface area in a fine-pored solid it is quite possible that diffusion rates play an important role in determining the observed rate of the reaction. And unless a very large volume were withdrawn and pushed back and forth before withdrawing samples for analysis it is unlikely that the concentration gradients set up within the bulk of the charcoal would be greatly disturbed. This would also offer a reasonable explanation for the fact that all of the "missing oxygen" can be pumped off as CO_2 at the same temperature, and for the fact that the amount of "missing oxygen" increases with increasing pressure. The constancy of the amount of "missing oxygen" which occurs soon after the reaction begins would be achieved when equilibrium concentration gradients had been established.

Strickland-Constable finds the rate of reaction is zero order with respect to N_2O and first order with respect to CO, while the experiments reported here show essentially zero order with respect to CO and zero-to-first order with respect to N_2O. It seems unlikely that diffusion effects can explain this difference. One possible explanation may lie in the different samples used. The principal difference here is ash content. Strickland-Constable's charcoal contained 1.8% ash while Graphon contains 0.02% and Su-60 less than 0.005%. This 1.8% is a far greater fraction of the charcoal than that actually involved in the reaction. Strickland-Constable states that "a commercial activated charcoal as such was used for this research rather than an artificially de-ashed charcoal, since the de-ashing process reduces the activity by a large factor, and it was feared that the chemically active surface would be too small to measure." He also states that "to show that CO was oxidized by N_2O on the charcoal and not on the mineral matter it contains, tests were made in which a mixture of N_2O and CO was added to a coconut charcoal which had been de-ashed (ash content, 0.04%)." With this last experiment he found a reaction half-life of 19.6 minutes at 412°, though on the high-ash sample it would have been 3.2 min. at this temperature. The slower rates on Graphon and Su-60 could not be ascribed to the de-ashing process itself, since they were made in such a way as to eliminate the need for de-ashing. All of these statements seem to indicate that the mineral matter does indeed play an important part and perhaps these sites are more active or more numerous than certain favored carbon atoms, especially on a surface which had been reduced in activity by repeated N_2O oxidation (13 times or more) to render it reproducible. Under these circumstances the mineral matter may have been the *only* sites effective in the CO oxidation. On these mineral matter sites the relative adsorbabilities of N_2O and CO could be just the reverse of that for Graphon and Su-60. Even so, the mechanism and rate expression suggested in this paper should be just as applicable to the mineral matter sites, the only change being

$$N_2O + M^* = N_2O(M^*) \qquad (1')$$

$$CO + N_2O(M^*) = CO_2 + N_2 + M^* \qquad (2')$$

In terms of the rate expression, one would say that k is now larger than k'.

It would appear that N_2O and H_2O are quite dissimilar in their behavior with carbon. The carbon–oxygen surface complexes are important intermediates in reactions involving water, whereas in the case of N_2O the complexes are actually poisons and do not appear to act as reaction intermediates.

THE ROLE OF HYDROGEN IN RANEY NICKEL CATALYST

BY HILTON A. SMITH, ANDREW J. CHADWELL, JR., AND S. S. KIRSLIS

Contribution No. 134 from the University of Tennessee, Department of Chemistry, Knoxville, Tenn.

Received February 25, 1955

The hydrogen content of Raney nickel has been found by direct analysis to vary between one-half and one atom of hydrogen per atom of nickel. The activity of a sample of this catalyst has been shown to be proportional to its hydrogen content. The surface area decreases linearly with loss of hydrogen until about 70% is removed; then it decreases more rapidly. If the hydrogen is released rapidly, heat is evolved which results in an explosion of the catalyst. The best explanation for these phenomena appears to be based on the assumption that the hydrogen is in the form of atoms attached to the nickel in a metastable state. If desorption of the hydrogen is rapid, the highly exothermic recombination of the hydrogen atoms becomes explosive.

In the reaction of nickel-aluminum alloy to form Raney nickel catalyst, a considerable amount of hydrogen is formed. The amount and character of the hydrogen in the catalyst has been the subject of some controversy. Raney[1] describes the catalytic material as a hydride of the formula NiH_2. Bougault and co-workers[2] also concluded from analytical experiments that this catalyst was a hydride or mixture of hydrides. Vandael[3] measured the quantity of hydrogen liberated from the hot leaching bath, and also claims that Raney nickel is a hydride of formula NiH_2. Difference methods such as those used by these workers may be subject to considerable error.

Freidlin and Ziminova[4] found that one gram of Raney nickel contained 95.3 ml. of hydrogen. This corresponds approximately to the formula Ni_2H. The catalyst lost its activity when all of the hydrogen was removed. These authors do not consider the catalyst to be a hydride, but rather skeletal nickel promoted with hydrogen. They consider that part of the hydrogen is adsorbed and part dissolved.[5] Furthermore, it is difficult to replace the dissolved hydrogen during a hydrogenation reaction.[6] These workers postulate that the loss of activity of the catalyst under the usual hydrogenation conditions is caused by destruction of active sites due to dehydrogenation and blocking.[7] Aubry[8] also states that the activity of Raney nickel is due to adsorbed and absorbed hydrogen, and that the catalyst behaves as a reversible electrode to hydrogen. In the *p*H range from 5 to 14, Raney nickel follows potential changes in the same manner as a hydrogen electrode.[9]

The influence of a number of factors in the preparation have been studied by Adkins and coworkers, who designate a series of catalysts of different activity depending on the particular conditions used.[10] It has been claimed[11] that the various conditions of preparation have little influence on the activity of Raney nickel as a catalyst in the hydrogenation of *d*-limonene. In the procedure of making these tests, the alcohol under which the catalyst was stored was evaporated from the catalyst under vacuum after which the *d*-limonene was added. Lieber and Morritz[12] suggest that with the probable loss of hydrogen under these conditions, it is doubtful that the more active types of Raney nickel were being investigated.

In view of the many controversies concerning the hydrogen in this catalyst, it was decided to determine by a direct method the hydrogen content of Raney nickel. In addition, the activity of this catalyst toward the hydrogenation of benzene and its ability to adsorb palmitic acid[13] were determined as a function of its hydrogen content.

Experimental

Raney nickel alloy was the commercial product, reported to have the following analysis: Ni, 51.06; Al, 48.19; Si, Fe and Cu combined, 0.75. The alloy was converted into Raney nickel catalyst by treatment with sodium hydroxide according to the directions of Adkins and Billica,[10c] except that 60 grams of alloy was treated with 300 g. of alkali in 1000 ml. of water instead of 125 g. of alloy with a solution of 160 g. of alkali in 600 ml. of water. In addition, hydrogen was bubbled through the wash water for 10–15 min. prior to its use, but no excess hydrogen was maintained over the mechanical washer. The use of a hydrogen atmosphere in the washing process made no difference in the activity of the catalyst toward the hydrogenation of benzene. The catalyst was stored in a refrigerator under absolute ethanol, and all measurements were made within 72 hours from the time of preparation of the catalyst sample.

A C.P. grade of benzene was purified by fractionation in a five-foot helix-packed column. Eastman Kodak Co., white-label palmitic acid was used for adsorption studies.

The total hydrogen content of the nickel catalyst was determined as follows: A sample of Raney nickel was placed into one arm of a tared, U-shaped vessel. The vessel was then cooled to −80° and the arm sealed off. The cold vessel was then attached to the hydrogen collecting system by means of a ball joint. A coarse fritted glass disk sealed between the catalyst and the joint prevented loss of nickel particles. The vacuum line led through a cold trap (−80°) which could be by-passed after all of the alcohol was condensed, through a mercury diffusion pump, followed by a cold trap, and then through a sealed "Cenco Pressovac" pump which discharged the hydrogen into a gas buret. The whole system was carefully tested for leaks. It was necessary to start the diffusion and mechanical pumps for

(1) M. Raney, *Ind. Eng. Chem.*, **32**, 1199 (1940).

(2) J. Bougault, E. Cattelain and P. Chabrier, *Bull. soc. chim. France*, [5] **5**, 1699 (1938).

(3) C. Vandael, *Ind. Chim. Belg.*, **17**, 581 (1952).

(4) L. K. Freidlin and N. I. Ziminova, *Doklady Akad. Nauk S.S.S.R.*, **74**, 955 (1950); *Izvest. Akad. Nauk S.S.S.R., Otdel Khim. Nauk*, 659 (1950).

(5) L. K. Freidlin and N. I. Ziminova, *ibid.*, 145 (1951).

(6) L. K. Freidlin and K. G. Rudneva, *Doklady Akad. Nauk S.S.S.R.*, **81**, 59 (1951).

(7) L. K. Freidlin and K. G. Rudneva, *Izvest. Akad. Nauk S.S.S.R., Otdel Khim. Nauk*, 1111 (1953).

(8) J. Aubry, *Bull. soc. chim.*, [5] **5**, 1333 (1938).

(9) A. Travers and J. Aubry, *Atti X^e congr. intern. chim.*, **2**, 546 (1938).

(10) (a) A. Pavlic and H. Adkins, *J. Am. Chem. Soc.*, **68**, 1471 (1946); (b) **69**, 3039 (1947); (c) H. Adkins and H. Billica, *ibid.*, **70**, 695 (1948); (d) H. Adkins and H. Billica, *Org. Syntheses*, **29**, 24 (1949); (e) H. Adkins and G. Krsek, *J. Am. Chem. Soc.*, **70**, 412 (1948).

(11) H. A. Smith, W. C. Bedoit, Jr., and J. F. Fuzek, *ibid.*, **71**, 3769 (1949).

(12) E. Lieber and F. L. Morritz in "Advances in Catalysis," Vol. V, Academic Press Inc., New York, N. Y., 1953, p. 419.

(13) H. A. Smith and J. F. Fuzek, *J. Am. Chem. Soc.*, **68**, 229 (1946).

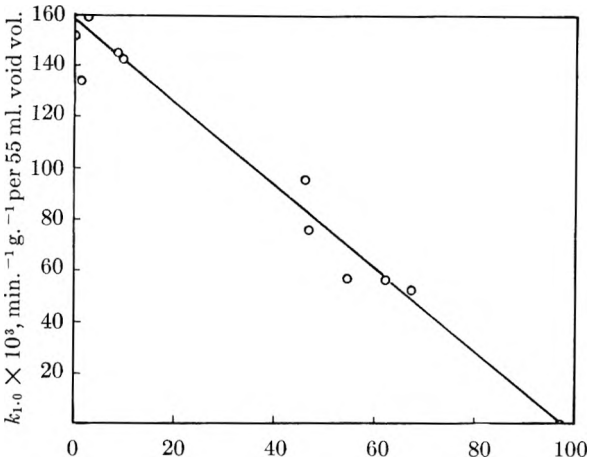

Fig. 1.—Catalytic activity of Raney nickel catalyst for the hydrogenation of benzene at 80° as a function of hydrogen content of the nickel.

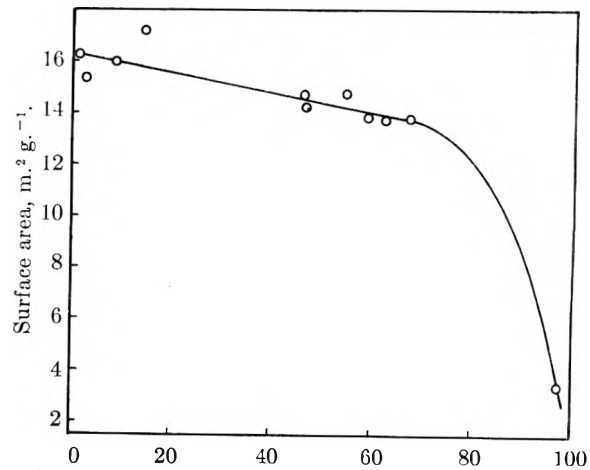

Fig. 2.—Surface area of Raney nickel catalyst as a function of hydrogen content.

several hours before each run in order to attain temperature equilibrium. The usefulness of this system was verified by attaching a calibrated bulb of hydrogen and comparing the volume collected with that known to have been present. The results always checked within 0.5%.

The catalyst bulb was opened to the system and thoroughly evacuated. The cooling bath around the bulb was then removed, and the alcohol allowed to distil from the bulb to the cold trap. No hydrogen was evolved until the alcohol had been removed. At this point, the cold trap bypass was opened, and the catalyst heated with a Bunsen burner. Hydrogen was evolved with increasing rapidity until the catalyst virtually exploded.[14] At this point, heat was produced so rapidly that the nickel attained red heat even though the outside of the glass bulb was relatively cool. Heating was continued for 15 minutes, and the volume of evolved hydrogen recorded. The vessel was then allowed to cool and a stopcock between the ball joint and glass frit closed. The catalyst bulb was removed and weighed. Next, dry oxygen was carefully admitted to the catalyst vessel, and a stream of oxygen subsequently led over the nickel. The bulb was carefully heated in the presence of oxygen until the entire sample was converted to the oxide. Excess oxygen was led through a tared absorption tube containing anhydrous magnesium perchlorate. When the highly exothermic reaction had subsided, the vessel was heated with the full flame of a Bunsen burner. The amount of moisture formed in the combustion process was determined gravimetrically.

When it was desired to remove only part of the hydrogen from a catalyst sample, a similar procedure was followed; an evacuating and filling apparatus similar to that previously described[13] was employed. A sample was placed in the adsorption-type bulb which was then attached to the vacuum system. The bulb was cooled to −80° and degassed. It was then warmed to room temperature, the alcohol removed, and the desired amount of hydrogen collected. The bulb could be immersed in warm water to speed up hydrogen evolution. However if the temperature was raised above 100°, the catalyst would "explode." Evolution of hydrogen was stopped by cooling the bulb to −80°, and the catalyst covered with alcohol before admitting atmospheric pressure. A sample of the nickel was withdrawn for catalytic activity measurements.

The aluminum content of the Raney nickel was determined by the method of Willard and Tang.[15]

The adsorption of palmitic acid on the nickel samples was measured by methods previously described.[11,13] Reaction rate constants were determined for the hydrogenation of benzene. The kinetics of this reaction show first-order dependence on hydrogen pressure. Quantities of catalyst used ranged from 0.2 to 0.3 g., initial pressures were around 1000 p.s.i. and 10 ml. of benzene was employed in a bomb of 65 ml. total void. The shaking rate (46 cycles per minute) was such that the rate of the reaction was a linear function of catalyst weight.

(14) Mr. Raney (ref. 1) reports that the catalyst which has been dried under acetone will decompose with a flash when warmed gently.

(15) H. H. Willard and N. K. Tang, *Ind. Eng. Chem., Anal. Ed.*, **9**, 357 (1937).

Results

The amount of hydrogen obtained from various samples of catalyst all prepared in the same manner showed considerable variation. Values ranged from 92 to 157 standard milliliters per gram of catalyst. The moisture collected after oxidation of four different catalyst samples from which the hydrogen had been removed by pumping was equivalent to 1.4, 1.3, 1.3 and 0.4% of total hydrogen. Three analyses for total aluminum in the catalyst showed 11.5 ± 0.3% as Al or 21.8 ± 0.6% as Al_2O_3.

The catalytic activity of a sample of the nickel as a function of its hydrogen content is shown in Fig. 1, while the influence of hydrogen in the catalyst on the adsorption of palmitic acid is given by Fig. 2.

Discussion

The amounts of hydrogen found on the various catalyst preparations corresponded to atomic ratios of hydrogen to nickel between one-half and one. In no case was there any indication that a hydride of the formula NiH_2 was present. The variation in the hydrogen associated with different catalyst preparations is in line with the concept of adsorbed hydrogen as suggested by Freidlin[7] and by Aubry.[8] The amount of hydrogen in Raney nickel catalyst which can be made to react with readily reducible organic compounds[4] is comparable to the amounts reported here.

The activity of any given catalyst varies linearly with the amount of hydrogen associated with the nickel. This is readily seen from Fig. 1. The loss of activity of the catalyst when all of the hydrogen is removed was also noted by Freidlin and Ziminova.[4] The small amounts of hydrogen remaining after pumping at high temperatures were apparently trapped in the catalyst pores, perhaps by alumina formed during the catalyst preparation.

Figure 2 shows that the surface area as determined by palmitic acid adsorption is a linear func-

tion of hydrogen content until some 70% of the hydrogen is removed. This may well explain the parallelism between surface area and activity of a catalyst as previously reported.[11] The catalyst is known to loose hydrogen slowly on standing. After 70% hydrogen evolution, the ability of the catalyst to adsorb palmitic acid decreases rapidly. When all of the hydrogen has been removed, the surface area of the catalyst is about one-fifth of its original value.

The total aluminum content found for the catalyst studied is compatible with that reported by Ipatieff and Pines[16] who found that W-6 nickel contained 12.72% total aluminum. However, their statement that the catalyst contained 21.13% aluminum oxide has been challenged by Watt and Parker.[17] These authors also find some 12 to 13% total aluminum in W-6 nickel, but state that the maximum present as the oxide does not exceed 1%.

(16) V. N. Ipatieff and H. Pines, *J. Am. Chem. Soc.*, **72**, 5320 (1950).
(17) G. W. Watt and S. G. Parker, *ibid.*, **74**, 1103 (1952).

No attempt was made in this research to determine the manner of combination of the aluminum.

The evidence presented here may be explained by the concept that Raney catalyst is a form of nickel promoted by adsorbed hydrogen. This hydrogen is evidently in the form of atoms attached to the nickel in a metastable state. If this is to be considered a hydride, its composition is rather indefinite. The hydrogen atoms are slowly desorbed on standing. This process may be accelerated by pumping although the hydrogen evolution is still rather slow. The process may be greatly accelerated by increasing the temperature. In fact, the desorption may be so rapid that the highly exothermic recombination of the hydrogen atoms becomes explosive. The catalytic activity of the nickel toward the hydrogenation of benzene is proportional to its hydrogen content.

Acknowledgment.—The authors are grateful to the Office of Ordnance Research, United States Army, for the sponsorship of this research.

EFFECT OF INTRA-PARTICLE DIFFUSION ON THE KINETICS OF CATALYTIC DEHYDROGENATION OF CYCLOHEXANE

BY P. B. WEISZ AND E. W. SWEGLER

Contribution from Socony-Vacuum Laboratories, A Division of Socony-Vacuum Oil Co., Inc. Research and Development Department, Paulsboro, N. J.

Received February 25, 1955

The effect of intra-particle diffusion rates on the product distribution and reaction rates during catalytic conversion by consecutive reaction steps in a porous catalyst particle is demonstrated. The reaction cyclohexane → cyclohexene → benzene on chromia–alumina catalyst was studied in a differential reactor. The ratio of cyclohexene to benzene is shown to depend on catalyst particle size. Derivation of the ratio of the two successive reaction velocity constants must include the effect of finite diffusive residence time. When this is done, consistent results are obtained for all particle sizes. Criteria for the detectability of reaction intermediates are also given.

Introduction

Diffusion transport rates of reactants within porous catalyst particles can markedly affect the kinetic interpretation of observed reaction rates and product distribution when more than a single one-step reaction proceeds. Wheeler[1] has mathematically examined a number of such cases. For the case of successive reactions *via* an intermediate compound, we will discuss simple criteria which allow estimates to be made whether diffusion phenomena will influence the observed product distribution, and for the detectability of reaction intermediates. For the dehydrogenation of cyclohexane to benzene over chromia–alumina catalyst, Herington and Rideal[2] have presented evidence for the successive dehydrogenation via cyclohexene. For this reaction an experimental study demonstrates the dependence of detected cyclohexene concentration on intra-particle diffusion parameters (particle size and diffusivity), which is found to be in excellent agreement with theoretical prediction.

Theoretical Principles

Competition of Reaction Velocity and Diffusive Escape of Reaction Intermediate.—When, in a porous catalyst particle, a reaction A → C proceeds by way of an intermediary product B, the over-all kinetics may be influenced by diffusion transport rates of A into, and B and C out, of the particle

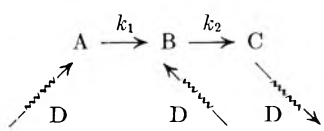

(1)

where ~~→ D symbolizes the rate of diffusive transport in the catalyst solid.

Molecules within the catalyst particle have a finite diffusive residence time whose magnitude is $\tau_D = \bar{X}^2/D_{eff}$, where $\bar{X}$ is a length parameter and D_{eff} the effective diffusivity in the pore structure. Assuming catalyst particles to be near spherical, with radius R, $\bar{X} \approx {}^1/_5\, R$, since one-half of the molecules will be within a depth equal to 0.207 R. The reaction rate decay constant τ_R has the magnitude of the reciprocal first-order rate constant, $1/k$ (referred to unit volume—strictly speaking of *pore* volume—of catalyst).

With these concepts it becomes clear that (a) no effect of diffusive transport on the observed concentration of B and C will exist when $\tau_D \ll \tau_R$; observed product concentrations are relatable directly to rate constants. (b) the product distribution, B/C, will be influenced by particle size (R) and diffusivity (D_{eff}), when $\tau_D \sim \tau_R$. (c) an intermediate species, B, will not be detectable, although it may truly exist, if $\tau_D \gg \tau_R$.

Detectability of an Existing Intermediate.—For the case where $\tau_D > \tau_R$, the ratio of the external concentration of the intermediate, B, to that of the product C, will be

$$B/C \approx e^{-k_2\tau_D}\,;\ \tau_D \approx \frac{1}{25}\frac{R^2}{D_{eff}} \qquad (2)$$

When for B/C the analytical limits of detection for the species B relative to C are used, this equation defines the magnitude of the rate constant k_2 above which the existence of the intermediate cannot be experimentally established.

Relation of Observed Production Rate of Intermediate Species, Rate Constants and Diffusion Parameters.—Assuming the two reaction steps in the scheme (1) above to follow first-order laws, we find

$$-\frac{dB}{dA} = \left\{\frac{1}{m-1} - \frac{B_0}{A_0}\left\{\frac{\varphi\sqrt{m}\coth(\varphi\sqrt{m}) - 1}{\varphi\coth\varphi - 1} - \frac{1}{m-1}\right\};\ m = k_2/k_1;\ \varphi = R\sqrt{\frac{k_1}{D_{eff}}} \qquad (3)$$

The solution relates the ratio dB/dA of the rate of emanation from the catalyst particle of product B to the total rate of reaction, the ratio of the concentrations B_0/A_0 of intermediate and primary reactant at the particle boundary, the ratio of the rate constants $m = k_2/k_1$, and the diffusion modulus φ which characterizes the degree of the diffusion effect of the primary reaction velocity $(-dA/dt)$.

The manner of derivation has already been discussed by Wheeler[1] for the case of cylindrical geometry. The above formula applies to spherical particles[3a] and neglects gas flow effects resulting from molar volume change during reaction. Although molar volume increase accompanies the dehydrogenation of cyclohexane the assumption is justified in the following work since the pore structure of the catalyst used is such that all diffusion is of the Knudsen type.[3]

(1) A. Wheeler, *Advances in Catalysis*, **3**, 250 (1951).

(2) E. F. G. Herington and E. K. Rideal, *Proc. Royal Soc. (London)*, **A190**, 289 (1947).

(3) P. B. Weisz and C. D. Prater, *Advances in Catalysis*, **6**, (1954): (a) p. 176 (erratum: in formula (30) "cosh" should read "coth.") (b) p. 154–157.

Experimental

Materials.—Phillips Pure Grade cyclohexane was further purified by passing through silica gel. The product was compared mass spectrometrically with a Bureau of Standards sample stated to be 99.96 mole % pure. It had less if any benzene, 0.04 mole % C_6H_{10} with respect to the standard, and better than 99.9% purity.

The catalyst was a sample of co-gelled chromia–alumina spherical bead catalyst, containing 20% Cr_2O_3 by weight, having a surface area of 180 $m^2/g.$ (BET), and a particle density of 1.56 g./cc. Three sizes were selected: beads of 0.310 cm. and 0.184 cm. radius, and particles of approximately 0.050 cm. radius, obtained by crushing and sizing through #16 on #20 screens.

Apparatus.—The apparatus was identical to that described by Weisz and Prater.[3b] A special reactor chamber design was used and is shown in Fig. 1. Differential reactor conditions were used, *i.e.*, very low conversion (about 1% or less), and the reactor chamber design was intended to result in highly turbulent flow to achieve "stirring" in the small reaction zone. In this way, the concentrations of reactant and products at the boundaries of all catalyst particles within the contact zone could be expected to be the same and known from the analysis of the product samples.

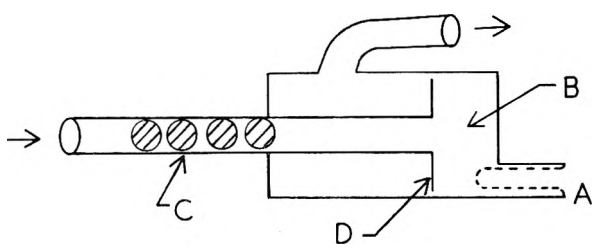

Fig. 1.—Reactor tube, with catalyst chamber.

Catalyst was introduced into the chamber B through the thermocouple well opening A. The well was then put in place and the ring seal made at A. The spacing between the rim of the glass plate D and the chamber walls was sufficiently small to retain the catalyst. The glass beads C were used to insure adequate preheating of the reactant.

Besides the thermocouple in the well, touching the catalyst, two others were attached to the outside of the catalyst chamber at opposite sides. All three couples (iron–constantan, #30 wire) gave the same temperature, within 0.5°, during all runs. Temperature variation was held within ±0.2° by use of a low heat capacity, cylindrical furnace, controlled by a thermel operated, high-sensitivity electronic relay. The controlling thermel junctions were located next to the furnace windings.

Starting Procedure.—Initial studies of the catalyst had shown that, for the dehydrogenation of cyclohexane, a reproducible activity, virtually constant for over one hour, could be obtained by evacuating the catalyst for three hours or more at 510°, 10^{-5} mm. Thus, with this constant activity, and with the fixed reactant concentration, the effect of variation in catalyst bead diameter on total reaction rate could be determined reliably. Therefore, prior to each run, after installing the catalyst sample, the above catalyst treatment was used. The rest of the apparatus was evacuated at the same time. The system was then closed off from the pumps and argon admitted to the apparatus to a pressure slightly greater than one atmosphere. With all parts of the system at operating temperatures, cyclohexane was admitted from the reservoir after opening the system to the atmosphere. Circulation of reactant began immediately.

Rate Measurements.—The rate of hydrogen production was measured by closing the system off from the atmosphere and observing the rate of pressure rise with and without a calibrated volume in the system. Periodically, weighed samples, accumulated over a short, measured time interval, of the condensed reactant and product vapors were taken. Measurements were continued over a 60–70 minute run time. The reaction temperature was 478.5°.

Analysis of Products.—Mass spectrometer analyses of samples of the gas stream showed the gas produced to be essentially 100% hydrogen.

The liquid samples were analyzed by the mass spectrometer. The only observed products were benzene and cyclohexene. Ultraviolet spectrophotometer analysis showed traces of other material. The latter material imparted fluorescence to the liquid samples. Since it was not detected by the mass spectrometer, a high molecular weight, greater than 200, was indicated. It was removable by silica gel, indicating unsaturation. A sample of liquid product was subjected to an azeotropic distillation to remove benzene. The ultraviolet absorption spectrum of the remaining sample indicated the presence of a polynuclear aromatic.

Results

Rates of reaction of cyclohexane $(-dA/dt)$ were determined from the rates of formation of all products. Total hydrogen production rate was determined from the pressure-rise data by the relation

$$\dot{n} = \frac{\dot{P}_S \dot{P}_{S+B} V_B}{(\dot{P}_S - \dot{P}_{S+B}) R T_B}$$

where

$\dot{n}$ = rate of production of H_2 in moles/unit time
$\dot{P}_S$ = rate of pressure rise in system
$\dot{P}_{S+B}$ = rate of pressure rise in system with calibrated bulb included
V_B = volume of bulb
T_B = temperature of bulb

Production rates of benzene and cyclohexene were obtained by direct observation of these products. Of the total cyclohexane rate, that part corresponding to the formation of the unknown aromatic and of the solid polymer remaining on the catalyst was determined from the additional hydrogen production rate not accounted for by cyclohexene and benzene production. For this purpose, a C/H ratio of unity was assumed for the unknown aromatic and the polymer. This is a fair assumption for a high-boiling aromatic, as well as the type of carbonaceous deposit observed. Only 7–15% of the total hydrogen rate is accounted for by these products. Therefore, an error in C/H ratio of as much as 25% would cause only a 2–5% error in the total cyclohexane rate.

Rates of Cyclohexene and Benzene Formation.—These rates were obtained directly from the mass spectrometer values for the liquid sample concentrations and the rates of sample accumulation in each case.

The Ratio B_0/A_0.—The ratio of the gas phase concentrations of cyclohexene and cyclohexane was obtained directly from the liquid sample analyses, with a small correction for the dilution by hydrogen which occurs in the reactor.

Summary of Measurements.—Complete results for one run are shown in Table I to indicate the level of conversion obtained (approximately 1%) and to demonstrate the near-constancy of the rates.

TABLE I

Run D-6, R_3 = 0.310 cm., 1.434 g. catalyst

Time (min.)	C_6H_6, mole %	C_6H_{10}, mole %	$\frac{dH_2}{dt}^a$	$\frac{dB}{dt}^a$	$\frac{dC}{dt}^a$	$\frac{dA}{dt}^a$
20.8	0.63	0.32	9.7	1.16	2.29	4.0
39.0	.66	.31	10.4	1.11	2.37	4.2
50.3	.68	.31	10.6	1.11	2.44	4.3
60.7	.68	.32	10.8	1.11	2.36	4.3
70.2	.68	.31	10.8	1.11	2.43	4.3

[a] Rate units are mole/min./g. × 10^5.

Table II gives total rates of reaction of cyclohexane ($-dA/dt$) *vs.* time for the other two runs. Table III shows average total rate of reaction of cyclohexane ($-dA/dt$), average rates of formation of cyclohexene (dB/dt) and benzene (dC/dt), B_0/A_0, and the ratios dB/dA and dB/dC, all *vs.* bead size.

TABLE II

Time (min.)	D-7 (R_2 = 0.184 cm.)[a]	D-8 (R_1 = 0.050 cm.)[a]
20	5.6 (1.579 g. catalyst)	9.2 (0.740 g. catalyst)
30	5.7	8.9
40	5.7	8.8
50	5.8	8.7
60	5.8	8.7

[a] $-dA/dt$ (mole/min./g. $\times 10^5$).

TABLE III

	$\frac{-dA}{dt}$[a]	$\frac{dB}{dt}$[a]	$\frac{dC}{dt}$[a]	$\frac{dB}{dC}$	$\frac{B_0}{A_0}$	$\frac{dB}{dA}$
R_3 = 0.310 cm.	4.2	1.11	2.4	0.46	0.0032	0.26
R_2 = 0.184 cm.	5.7	1.81	3.1	.58	.0054	.32
R_1 = 0.050 cm.	8.8	5.4	2.8	1.9	.0082	.61

[a] All rates in mole/min./g. $\times 10^5$.

The probable percentage error in total rate of reaction of cyclohexane is estimated to be about $\pm 4\%$. That for B_0/A_0 is $\pm 5\%$, and for dB/dA, about $\pm 6\%$, due primarily to the probable errors in the mass spectrometer results.

Discussion

Observed Rate of Production of Cyclohexene Intermediate, Particle Size Dependence.—The results concerning the observed ratio of the rate of production of the intermediate cyclohexene to that of benzene (column 4, Table III) show a clear dependence on particle size. For the smallest particles nearly twice as much net production of the intermediate was achieved as compared to the normal end product.

Determination of Kinetic Constants and Agreement with Theory.—The experimental procedure allowed the measurement of the over-all rate of reaction and of production of each component, and of the concentration ratio of B_0/A_0 at the boundary of the catalyst particles. Therefore, for the use of formula 3, B_0/A_0 and $-dB/dA$ are obtained from measurement, while $m = k_2/k_1$ and φ are unknown.

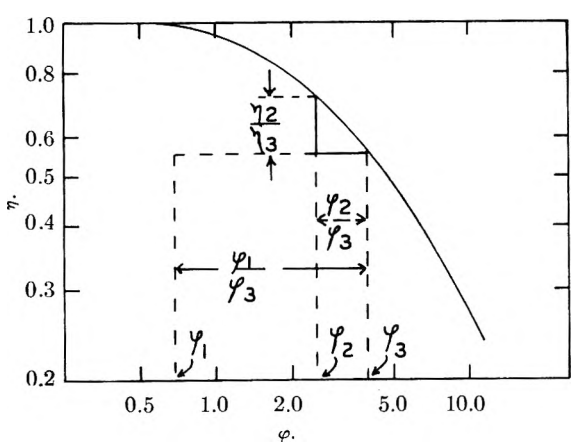

Fig. 2.—Functional relationship between η and φ, with method of obtaining φ's from measured η and φ ratios for different catalyst bead sizes.

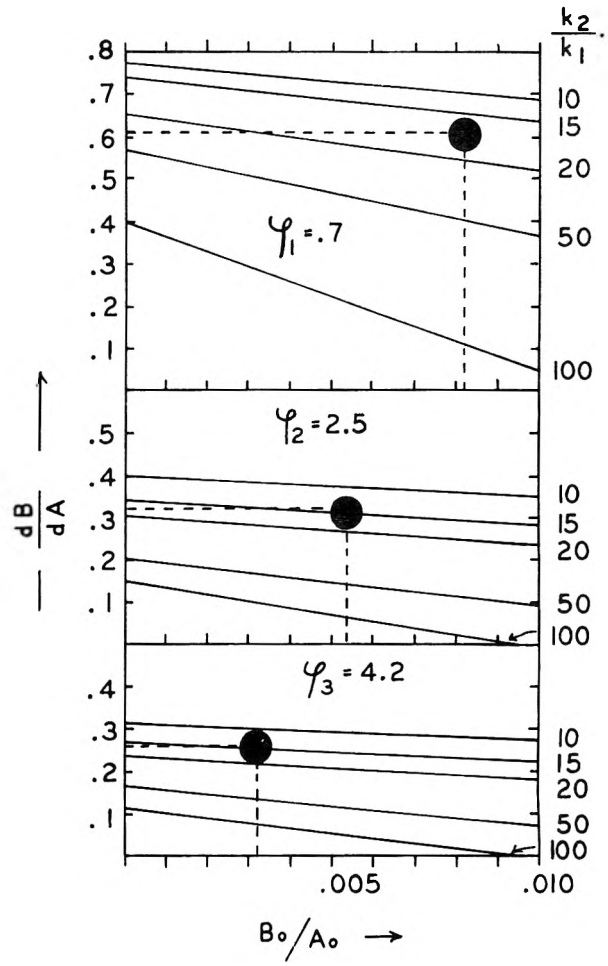

Fig. 3.—Graphical solutions of equation 3 for the measured values of φ.

The diffusion modulus φ is obtained from the variation of the over-all reaction rate for a known change in particle size, by the "triangle method" described by Weisz and Prater.[3] Use is made of the known functional relationship of the utilization factor η, defined by the first-order relationship of the primary reaction rate

$$-\frac{dA}{dt} = k_1 A_0 \eta \qquad (4)$$

and the diffusion modulus φ for spherical particles, as shown by the drawn out curve in Fig. 2. For the two measurements in which the particle sizes R_2 and R_3 were used, $\varphi_2/\varphi_3 = R_2/R_3$; and the ratio η_2/η_3 is found from the rate measurements as $\eta_2/\eta_3 = (dA_2/dt)/(dA_3/dt)$ (in view of (4)). Fitting the values of $\varphi_2/\varphi_3 = 0.59$ and $\eta_2/\eta_3 = 1.36$ on the double logarithmic plot in Fig. 2, φ_2 and φ_3 become determined. φ_1 is accordingly found from these by multiplication by the size ratio $\varphi_1/\varphi_3 = R_1/R_3 = 0.16$.

Accordingly, we find $\varphi_3 = 4.2$, $\varphi_2 = 2.5$, $\varphi_1 = 0.68$.

The rate constants ratio k_2/k_1 can now be found from the equation 3, with the measured values of B_0/A_0, $-dB/dA$, and φ for any one particle size. We can test the adequacy of the theoretical treatment by comparing the results of all three particle sizes. In Fig. 3 are plotted the functional rela-

tionships for $-dB/dA$ *vs.* B_0/A_0 for the three φ-values (particle sizes) used, with k_2/k_1 as the independent parameter. The measured values (dotted lines) yield the solutions

From particle size	k_2/k_1
$R_1 = 0.05$	16
$R_2 = 0.18$	13
$R_3 = 0.31$	14

The results of all three experiments are seen to give consistent solutions. The values of experimental errors lead us to estimate the probable error of each k_2/k_1 to be about ± 3. From the three measurements, we conclude that $k_2/k_1 = 14 \pm 2$.

In contrast to the above complete solution, a determination of the ratio of the kinetic constants without regard to the intra-particle diffusion effect, according to the simple solution

$$-\frac{dB}{dA} = 1 - \frac{k_1}{k_1}\frac{B_0}{A_0}$$

would have resulted in $k_2/k_1 = 50$, 125, 230, respectively, for the three experiments in order of increasing particle size, *i.e.*, in values which are much too large and inconsistent among the three cases.

The rate constants k_1 and k_2 are obtained from (4). The smallest particle size gives the simplest solution, since $\eta = 1.0$. With $A_0 = 1.55 \times 10^{-5}$ m./cc. (atmospheric pressure, $T = 478.5°$, cyclohexane) $dA/dt = 8.8 \times 10^{-5}$ m./min./g., and the particle density of 1.56 g./cc., we obtain for the primary rate constant referred to unit catalyst volume

$$k_1 = 0.15 \text{ sec.}^{-1}; \; k_2 = 2.1 \text{ sec.}^{-1}$$

The latter follows from the previously determined ratio.

The catalyst particle diffusivity, D_{eff}, can now be obtained from any of the three (particle size) sets of data.

$$\varphi_1 = 0.7 = R\sqrt{\frac{k_1}{D_{eff}}} = 0.50\sqrt{\frac{0.15}{D_{eff}}}$$

gives $D_{eff} = 0.8 \times 10^{-3}$ cm.^{2}/sec.

Diffusive Residence Time and Detectability of Intermediate.—The average diffusive residence time of a molecule within a catalyst particle of the medium size $R_2 = 0.18$ cm. calculates to $\tau_D = 1/25\ (R^2/D_{eff}) = 1.6$ sec. Comparison with the reaction rate decay constant $\tau_{R_2} = 1/k_2 \backsimeq 0.48$ sec. demonstrates how the above-described criteria predict a heavy diffusion effect on the rate of production of intermediate.

Using the criterion, formula (2), with the minimum detectable concentration of an *unknown* intermediate c_x—such as cyclohexadiene—taken as 1/50 of that of benzene c_c, we find, with $\tau_D \backsimeq 1/25\ (R^2/D_{eff}) = 0.13$ sec., for the smallest particle size R_3, that it would not have been detected if its reaction rate constant was $k_x \geqq 30$.

ACIDITY AND POLYMERIZATION ACTIVITY OF SOLID ACID CATALYSTS

BY O. JOHNSON

Shell Development Company, Emeryville, California

Received February 25, 1955

A method has been developed for the determination of the acidity of solid surfaces which consists of the titration of the solid suspended in benzene with *n*-butylamine, using *p*-dimethylaminoazobenzene as the indicator. This basic indicator forms a red color on acidic solids, and the end-point of the titration is the disappearance of the red color. It is shown by comparison with solid acids whose acid strength is known in aqueous solution that the amine titration method determines acids comparable in strength to those with a dissociation constant of 10^{-6} or higher in an aqueous solution. Propylene polymerization by acidic catalysts was used to study the correlation of acidity and catalytic activity. The propylene polymerization reaction at 200° was found to follow the equation $dx/dt = k(a - x)/(1 + bx)$, corresponding to a first-order reaction retarded by products (a = initial pressure of propylene, x = pressure drop in time t). The catalysts used were a series of alumina–silica catalysts prepared by the interaction of one silica gel with measured amounts of alumina sol. There was found to be a linear relation between the acidity of these alumina–silica catalysts and the propylene polymerization rate. It is concluded that the amine titration adequately measures acid sites on the solid catalyst which are important for polymerization of propylene at 200°. It is also shown that for a given number of acid sites the polymerization activity markedly increases with acid strength.

The understanding of the acidic nature of a solid surface is of great importance in the study of acidic catalysts for cracking, polymerization, alkylation and isomerization reactions. It is generally agreed that catalysts for these reactions are solid acids; it remains to be shown both the total number of acid sites on the solid surface and their acid strength.

Several methods for the determination of number of acid sites have been used for alumina–silica catalysts.[1] They include titration in aqueous solution with standard alkali, evolution of CO_2 from Na_2CO_3 solution, hydrolysis of sucrose, evolution of CH_4 from Zerewitinoff reagent, adsorption of quinoline vapor[2] and adsorption of NH_3 at elevated temperatures. The acidity determinations which are carried out in aqueous solution give acidity values which probably include all the surface hydroxyl groups. In principle the adsorption of basic gases at elevated temperatures should give accurate values for numbers of acid sites; actually such measurements are difficult to interpret because of very strong physical adsorption by solids such as alumina–silica catalysts.

The method which will be presented here falls between the extremes of aqueous titration and gas adsorption. It involves the titration of the solid acid with an organic base with benzene as the solvent and *p*-dimethylaminoazobenzene as the indicator to determine the end-point.

Acidity of Solid Surfaces by Amine Titration.—G. N. Lewis first reported the titration of a solid acid using an indicator dye to determine the end-point. He showed that $AlCl_3$ suspended in CCl_4 could be titrated with an amine solution using crystal violet as an indicator. This suggested that solid acid catalysts could be titrated in the same way. Crystal violet did not give an acidic color on alumina–silica catalyst so other basic indicators were tried. Indicators with low pK values were chosen since it is desired to titrate strong acids on the solid surface.

In the titration of a solid acid the basic indicator forms a colored compound with the acid sites on the surface; upon addition of the titrating base, which must be a stronger base than the indicator, the indicator base is displaced by the titrating base, and the color disappears or changes. Since the pK of the indicator is the factor determining the level of acid strength[3] of the acid sites which are titrated, all of the indicators in Table I were tried.

TABLE I

DATA ON INDICATORS USED FOR AMINE TITRATION OF SOLID ACIDS

Indicator	pK	Color change (base–acid)
p-Ethoxychrysoidin	5	Yellow-red
Aminoazoxylene	3.5	Yellow-red
p-Dimethylaminoazobenzene	3.3	Yellow-red
2-Amino-5-azotoluene	2.0	Yellow-red
Benzeneazodiphenylamine	1.5	Yellow-purple
4-Dimethylamino-azo-1-naphthalene	1.2	Yellow-purple
Crystal violet	0.8	Blue-yellow

All the indicators except crystal violet gave acid colors when added to alumina–silica and to acid salts such as $KHSO_4$, but did not give acid colors on pure silica gel or pure alumina. Thus, it appeared probable that the indicators were in the proper pK range for titration of acid catalysts. Since no appreciable difference in total acidities was found when different indicators were used, *p*-dimethylaminoazobenzene (butter-yellow) was chosen for further study because it gave the most distinct end-point.

Benzene, CCl_4 and isoöctane all appeared satisfactory as solvents for the titration; benzene was chosen because it is readily available in dry anhydrous form. Basic solvents such as ether, acetone or alkyl acetates are not suitable.

Several organic bases of differing basic strength were tested for the titration of solid acids. Trimethylamine ($k = 7.4 \times 10^{-5}$) gave satisfactory titrations, but the titrating solution required frequent standardization due to volatility of trimethylamine. Aniline ($k = 4.6 \times 10^{-10}$) and quinoline ($k = 1 \times 10^{-9}$) both gave dark products on some catalysts which interfered with the observation of a color change; they also required use of the indicators which are weaker bases than

(1) See the review articles by M. W. Tamele, *Faraday Soc. Discs.*, **8**, 270 (1950); T. Milliken, G. A. Mills and A. G. Oblad, *ibid.*, **8**, 279 (1950).

(2) G. A. Mills, E. R. Boedeker and A. G. Oblad, *J. Am. Chem. Soc.*, **72**, 1559 (1950).

(3) C. Walling, *ibid.*, **72**, 1164 (1950).

butter-yellow. Benzylamine ($k = 2 \times 10^{-5}$) and *n*-butylamine ($k = 4 \times 10^{-4}$) gave completely satisfactory results. *n*-Butylamine was chosen for use as the titrating base and was used in all subsequent experiments.

The following titration technique was developed and has been used in carrying out the titrations of a large number of solid acids. The catalyst sample is 0.1 g. of 100–200 mesh powder which has been dried for 2 hours at 500°. It is placed in a 10-ml. stoppered bottle, and 5 ml. of dry benzene containing 0.2 mg. of *p*-dimethylaminoazobenzene per 100 ml. is added. The yellow dye reacts with the solid to form the red acidic form of the indicator. Then the base, 0.1 *N* *n*-butylamine in benzene, is added dropwise from a calibrated pipet. The neutralization is followed by noting the gradual disappearance of the red color of the solid particle. The end-point, which is quite sharp, is taken as the point at which all the red color disappears. A 2–3 day period is allowed for the titration since gradual addition of amine will minimize adsorption of the amine on non-acidic portions of the surface. In order to ensure that no excess amine is present on the solid at the end-point, a drop of 0.05 *N* trichloroacetic acid in benzene is added. A reappearance of the red color indicates that no appreciable excess of amine was present. Small overtitrations can be corrected for by subtracting the amount of trichloroacetic acid required to restore the red color. This correction can only be used if small amounts of trichloroacetic acid (<0.2 ml. of 0.5 *N* solution) are involved since there is a slow reaction between trichloroacetic acid and the alumina–silica surface.

Titrations of dark colored solids can be carried out by addition of a small known amount of a white solid acid. The end-point of the titration is taken when the color change is observed on the white solid, and a correction is made for the amount of butylamine used for the added white material.

The reactions involved in an amine titration are

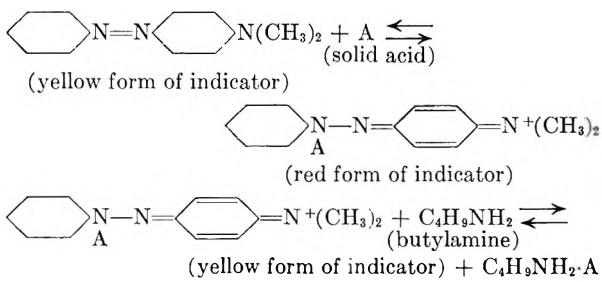

Acidities as low as 0.01 meq./g. can be determined by the amine titration method, and with ordinary care to keep materials dry the technique outlined gives results for acidity which are reproducible to ±5%. Catalysts should be titrated immediately after drying since adsorption of moisture leads to low values for acidity.

Several known acids mounted on silica gel were used as standards to determine whether the amine titration of a solid acid was quantitative. It was also expected that such titrations would show the strength of acid titrated by the indicator *p*-dimethylaminoazobenzene. The acidic solids were mounted on 500° dried silica gel by impregnation with aqueous solutions of the solids. All materials were then dried at 200° for 4 hours. Table II gives the expected acidity values and the data obtained by amine titration. For the first six acids a definite number of protons appeared to be titrated. On the average there appears to be a tendency toward high results by the amine titration method for these six acids. The last two gave no acid color with *p*-dimethylaminoazobenzene. Only 10–20% of the acidity of $KHAsO_4$ and potassium acid phthalates were titrated; these appear to be intermediate cases where varying acid strength on the solid surface may be involved. (Since both protons of phthalic acid are titrated, the potassium ion probably causes a lower acid strength in the case of the acid phthalate.) Thus, it appears that an acid with a dissociation constant of 10^{-6} in aqueous solution is the weakest acid that is titrated by the amine method. The agreement in the case of the standard acids of higher acidity is considered to be sufficiently good to conclude that the amine titration gives quantitative results for acids stronger than phthalic acid.

TABLE II

ACIDITY VALUES FOR STANDARD ACIDS MOUNTED ON SILICA GEL

Acid	Acidity, meq./g.	Acidity by amine titration, meq./g.	No. of H^+ titrated	Aqueous dissociation constant of last H^+ titrated
Toluenesulfonic	0.85	1.0	1	$\sim 10^{-1}$
$NaHSO_4$	2.7	2.6	1	2×10^{-2}
Silicotungstic	1.35	1.36	4	$\sim 10^{-1}$
Salicylic	0.4	0.5	1	1×10^{-3}
Oxalic (100° dried)	1.4	1.3	2	5×10^{-5}
Phthalic	0.9	0.8	2	3×10^{-6}
KH_2AsO_4	1.0	0.2	..	4×10^{-6}
Potassium acid phthalate	1.8	0.2	..	3×10^{-6}
KH_2PO_4	..	0.0	0	2×10^{-7}
K_2HAsO_4	..	0.0	0	6×10^{-10}

A further indication of the limiting value of acid strength titrated is the fact that the indicator benzeneazodiphenylamine ($pK = 1.5$) no longer gives the acid color on potassium acid phthalate. It is of interest that the apparent acid strength of the solid acid appears to be about 3 pK units higher than when the same material is dissolved in aqueous solution.

Amine titrations have been carried out for a number of acid catalysts. A series of alumina–silica catalysts with a wide range of alumina content has been titrated by the amine method and also used in propylene polymerization tests. This series of catalysts was prepared by the interaction of a very pure silica gel prepared at *p*H 3 with measured amounts of an alumina sol. The alumina sol was freshly prepared from aluminum chloride and ammonium hydroxide; the precipitate was thoroughly washed and then peptized in water. The alumina–silica gels formed when the 2 components were mixed were washed further and dried at 120°. The data in Table III include acidities obtained by amine titration after drying the catalysts at 200 and 500°. It is of interest that in spite of the increase in Al_2O_3 content for Catalyst G, both its acidity and polymerization activity are lower than for F.

Also included in the table is a magnesia–silica catalyst, which is alkaline toward indicators in aqueous solution, but which can be titrated by the amine method.

Correlation of Acidity and Propylene Polymerization Activity.—A simple reaction which proceeds without side reactions is desirable for testing the correlation of catalytic activity with acidities

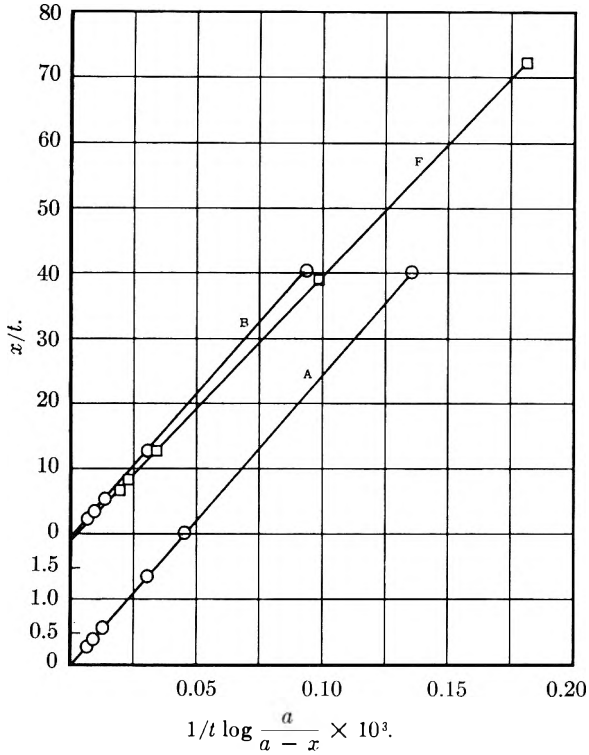

Fig. 1.—Relation of x/t and $1/t \log a/(a-x)$, for propylene polymerization of alumina–silica catalysts at 200°.

obtained by amine titration. The polymerization of propylene at 200° was found to be a catalytic reaction well suited to this purpose.

TABLE III

ACIDITY AND PROPYLENE POLYMERIZATION RATES FOR ACIDIC CATALYSTS

Catalyst	Al_2O_3, %	Surface area, m.²/g.	Acidity, meq./g. 200° Dried	Acidity, meq./g. 500° Dried	Propylene polymerization rate $k \times 10^3$, min.$^{-1}$
SiO_2 base	0.001	788	0	0	0
Alumina–silica					
A	0.12	722	0.09	0.05	0.3
B	0.32	699	.21	.10	1.2
C	1.04	695	.30	.22	1.9
D	2.05	622	.41	.26	2.4
E	3.56	622	.47	.31	3.0
F	10.3	545	.58	.35	3.4
G	25.1	450	.45	.32	2.8
Commercial[a]	10	525	.37	.45	2.3
Magnesia–silica					
Commercial[b]	(30% MgO)	555	..	.41	.2

[a] Cracking catalyst (American Cyanamid). [b] Cracking catalyst (Davison).

The polymerization of propylene was followed in an all glass system of 75-ml. volume by noting the pressure drop with a mercury manometer. The reaction vessel was kept at 200°, and an initial propylene pressure of 193 mm. was used. A 0.1 g. sample of 14–28 mesh catalyst was taken for the test and dehydrated one hour at 200° before use.

It was found that the equation $dx/dt = k(a - x)/(1 + bx)$ held for the polymerization reaction

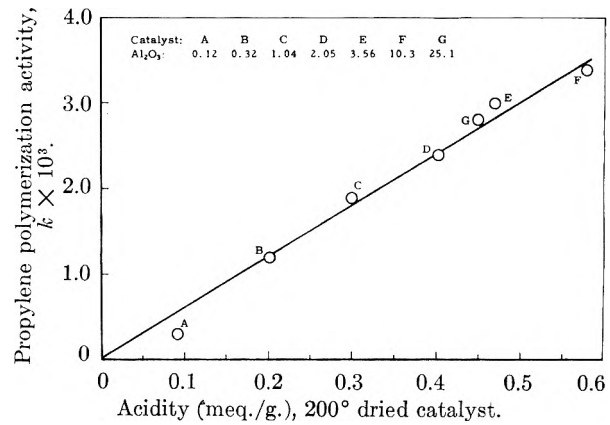

Fig. 2.—Dependence of propylene polymerization activity at 200° on acidity for a series of alumina–silica catalysts.

for a large number of acid catalysts. This represents a reaction of first order in the partial pressure of the reacting gas and inhibited by a strongly adsorbed product. In the equation a is the initial propylene pressure, and x the observed pressure drop in the system at the time t. Values of k are found[4] by plotting x/t *vs.* $1/t \log a(a - x)$; the straight line has a slope $(a + 1/b)$ and the intercept is $(-k/b)$. The data for catalysts A, B and F are tabulated in Table IV and plotted in Fig. 1.

TABLE IV

PROPYLENE POLYMERIZATION DATA FOR ALUMINA-SILICA CATALYSTS

Catalyst	t (min.)	x (mm.)	$\log \frac{a}{a-x}$	$\frac{1}{t} \log \frac{a}{a-x}$	$\frac{x}{t}$
	0	0	....	....	...
A	1/4	1.5	0.0034	0.0136	6
	1	4	.0091	.0091	4
(a = 193)	5	10	.0231	.0046	2
	9	14	.0327	.0036	1.56
	15	18.5	.0438	.0029	1.23
B	0	0	....	....	...
	1/4	10	0.0230	0.0920	40
(a = 194)	1	13	.0301	.0301	13
	5	26	.0625	.0125	5.2
	10	35	.0864	.0086	3.5
	16	43	.1088	.0069	2.6
F	0	0	....	....	...
	1/2	36	0.0902	0.1804	72
(a = 192)	1	39	.0986	.0986	39
	4	51	.1341	.0335	12.7
	7	58	.1562	.0223	8.3
	9	62.5	.1710	.0190	6.9

The polymerization rates found for several acid catalysts were given in Table III. The linear relation between acidity for 200° dried catalysts and propylene polymerization rate found for the alumina-silica catalysts is shown in Fig. 2. Such a simple relation can be taken as support that the amine titration method adequately measures the acid sites which are significant for propylene polymerization at 200°.

It should be emphasized that such a direct correlation of acidity and activity is to be expected only when the distribution of acid strength of the

(4) C. N. Hinshelwood and C. R. Prichard, *J. Chem. Soc.*, **127**, 327 (1925).

acids on the catalysts is the same; this is undoubtedly the case for the alumina–silica catalysts chosen since they have similar chemical and physical properties. It has been shown[1] that the relation of acidity and activity for cracking of isopropylbenzene at 500° is more complex. An approximately linear relation has also been shown between acidity by quinoline adsorption and cracking of a gas oil.[2]

Acid Strength of Solid Acids and Propylene Polymerization Rate.—In correlating polymerization rate and total acidity of alumina–silica it was assumed that the distribution of acid strength was the same for all of these materials. In studying other types of alumina–silica and other solid acids it becomes of great importance to know more about the acid strength involved.

A maximum value for the acid strength of alumina–silica catalyst is indicated by absence of an acidic color with the indicator crystal violet (pK = 0.8). However, the yellow acid color may be completely masked by the more intense blue color of adsorbed crystal violet. A more reliable indication is the observation[3] that *p*-nitrobenzeneazo-(*p'*-nitro)-diphenylamine (pK = 0.43) develops its acid color on alumina–silica catalyst. This means there are acids on alumina–silica with an acid strength corresponding to a pK of 0.43.

A dye-transfer method has been developed for obtaining relative acid strengths of solids which all give an acid color with *p*-dimethylaminobenzene. It consists of observing the transfer of the dye from one solid to another more acidic solid when they are both suspended in benzene. The dye in benzene is put on dried granules of one solid, the colored granules are washed thoroughly with benzene to remove excess dye, and then a powdered form of the solid acid to be compared is added. It is assumed that after equilibrium is reached the amounts of dye found on each solid will be related to their acid strengths in that the stronger acid will contain most of the dye. The transfer experiment may require several days, and moisture on the catalyst leads to an observation of low relative acid strength.

Relative acid strengths obtained by this method are listed in Table V for catalysts dried at 200°. The order of acid strengths is in agreement with the order known for their aqueous solutions for the very strong and very weak acids. The greater acid strength shown by H_3PO_4 as compared to toluenesulfonic acid probably results from differences between acids mounted on silica gel and their aqueous solutions.

From the position of alumina–silica catalysts in relation to other acids, it is indicated that the strongest acids on alumina–silica have a pK of approximately 2. This value is a considerably lower acid strength than expected from the observed acid color with *p*-nitrobenzeneazo-(*p'*-nitro)-diphenylamine (pK = 0.43).

A further indication of acid strength can be obtained by comparing propylene polymerization rates for a series of solid acids of the same total acidity. The data for several such materials are arranged in order of decreasing polymerization rate in Table VI. For the known acids, this order is the same as the order of decreasing acid strengths. The observed activity of alumina–silica catalyst indicates that its acid strength is between that of perchloric acid and silicotungstic acid, again a considerably higher acid strength than that obtained by the dye-transfer method.

TABLE V

RELATIVE ACID STRENGTH BY DYE TRANSFER METHOD

Order of decreasing acid strength (as mounted on silica gel dried at 500°)	Dissociation constant, aq. soln., first H^+
$HClO_4$ (100° dried)	.....
Silicotungstic acid	$\sim 10^{-1}$
H_3PO_4	1×10^{-2}
Toluenesulfonic acid	$\sim 10^{-1}$
Arsenic acid	5×10^{-3}
$KHSO_4$	2×10^{-2}
Iodic acid	2×10^{-1}
Alumina–silica catalysts	.....
Oxalic acid	3.8×10^{-2}
Phthalic acid	1.3×10^{-3}
Zirconia–silica catalysts	.....
KH_2AsO_4	4×10^{-5}
Potassium acid phthalate	3×10^{-6}
Boric acid	10^{-10}

TABLE VI

DEPENDENCE OF PROPYLENE POLYMERIZATION RATE ON ACID STRENGTH

Acid	Propylene polymerization $k \times 10^3$, min.$^{-1}$	Acidity, meq./g.
Perchloric acid[a]	5.0	0.16
Alumina–silica catalyst	2.4	.4
Silicotungstic acid	1.5	.4
$KHSO_4$	0.6	.4
Magnesia–silica catalyst	0.2	.4
Oxalic acid[a]	0	.7
Phthalic acid[a]	0	.8

[a] Polymerization test carried out at 150°.

These conclusions can only be qualitative since it will be seen that although acidity is determined for oxalic and phthalic acid, they are inactive for propylene polymerization at 150°. If there are such weak acids included in the 0.4 meq./g. titrated for the alumina–silica catalyst, it would increase its relative acid-strength position in Table VI.

The very large increase in polymerization rate with increase in acid strength as shown in Table VI demonstrates the importance of having quantitative data on acid strength of solid acids in addition to the data presented here on total number of acid sites as obtained by amine titration.

DISCUSSION

G. A. MILLS.—Catalysts A, B and C were found by the butylamine titration method to show more acidity than expected theoretically for one equivalent per Al atom. Is this experimental inaccuracy or greater acidity than shown by the above formula?

O. JOHNSON.—Although errors due to physical adsorption of the amine on the catalyst surface would be greater for samples containing the low amounts of alumina, it is believed that these data are correct to plus or minus 5%. It is possible that butylamine can coördinate successively with the two protons of a water molecule attached to an aluminum

ion in the catalyst surface, as in the model of an acid site proposed by M. W. Tamele (ref. 1).

G. A. MILLS.—Quinoline chemisorption studies have shown only about one-tenth the acidity values of those reported by the butylamine titration procedure indicating a range of acid strengths for SiO_2-Al_2O_3, as indeed is discussed by the Author. Yet it is stated that "no appreciable difference in total acidities was found when different indicators were used." How is this accounted for? Is it a consequence of the long times used in the titrations, as is the case with sodium hydroxide?

O. JOHNSON.—The low values of acidity obtained by quinoline chemisorption may be due to the large size of the quinoline molecule and to the higher temperature used as well as to the effect of acid strength proposed by Dr. Mills. Recent work in our laboratories has established that there is a range of acid strengths on acid catalysts, but the present data in the pK range of 1.5 to 5 did not show this effect.

The long time used in the titration simply assures that equilibrium is reached and does not represent an irreversible reaction with the catalyst as in the case of sodium hydroxide.

MAGNETIC SUSCEPTIBILITY STUDIES IN THE DUAL HYDROUS OXIDE SYSTEM: $NiO-Al_2O_3$

BY W. O. MILLIGAN AND JAMES T. RICHARDSON[1]

The Rice Institute, Houston, Texas

Received February 25, 1955

A comprehensive investigation of the magnetic susceptibility of the system: $NiO-Al_2O_3$, has been conducted on 105 samples, prepared at every 5 mole %, and heat-treated at temperature levels of 300, 400, 500, 600 and 700°. The magnetic measurements were made at room temperature. The resulting susceptibility–composition curve for the 300° temperature level exhibits three regions of interest. In region (a) from 100–80 mole % NiO, the susceptibility curve drops rapidly as the alumina content increases; in region (b) the curve exhibits a broad maximum at a composition of 60 to 80 mole % NiO; and in region (c) the susceptibility increases regularly as the amount of alumina is increased. The following somewhat speculative explanation is offered. In region (a), the initial higher susceptibility of the pure NiO is attributed to the decreased magnetic interaction, resulting from a decrease in the number of next nearest magnetic neighbors, as a consequence of the very small crystallite size, and the plate-like morphology of the aggregates of crystallites. In region (b), the maximum in the susceptibility curve results from the existence of a marked change in the structure of the alumina gel, previously known from X-ray studies to occur in the zone of mutual protection against crystallization. Such zones are likewise detectable in numerous multiple hydrous oxide systems by means of X-ray and electron diffraction studies (amorphous-like zone), and adsorption measurements (enhance differential and integral isoteric heats of adsorption and enhanced specific adsorptive capacity). In region (c) the regularly increasing magnetic susceptibility results from the increase in degree of dispersion of the NiO within the alumina gel structure. At higher temperatures of heat-treatment, the susceptibility of the NiO increases regularly throughout the entire composition range. Here the composition zone of mutual protection has narrowed or vanished. At the low concentrations of nickel, the susceptibility curves and the magnetic moments for NiO increase toward a limiting value of 3.2 bohr magnetons in accordance with the previous work of Selwood.

Introduction

In a previous report[2] from this Laboratory, it was found that dual hydrous oxide gels in the system $NiO-Al_2O_3$ exhibit a mutual protective action against crystallization. The observed composition zone of mutual protection occurred at about 50–70 mole % nickelous oxide, in samples heat-treated at a temperature of 500°. The zone of protection narrows and finally vanishes as the temperature of heat-treatment is increased, as do multiple zones of protection which have been observed in numerous other multiple hydrous oxide systems.[3] At the 1000° temperature level, X-ray evidence demonstrated the formation of nickel spinel, $NiO \cdot Al_2O_3$.

The magnetic properties of the system $NiO-Al_2O_3$ have been studied recently by Selwood and Hill[4] in the region of low nickel oxide concentrations. The paramagnetism of the nickel increased markedly when small amounts of nickel oxide were dispersed over a large excess of alumina. Current investigations[5] in this Laboratory show that very small crystals of pure nickel oxide, prepared by the controlled thermal decomposition of hydrous nickelous hydroxide, do not exhibit an antiferromagnetic Néel point at 250°, as do massive crystals previously studied by others.

Traces of sodium, or possibly silica, irreversibly adsorbed at the time of precipitation of the gel, stabilize the cubic, paramagnetic form of NiO, whereas the unstabilized oxide is antiferromagnetic and rhombohedral below the Néel point (about 250°).

Inasmuch as Selwood's careful investigations did not include the high concentration range of nickel oxide, and in view of our results obtained for highly dispersed nickel oxide free of alumina, it was considered desirable to extend our previous magnetic studies to the entire system $NiO-Al_2O_3$. It is the purpose of this paper to report the results of a systematic magnetic susceptibility investigation of this system for samples heat-treated at several temperature levels.

Experimental

Preparation of Samples.—Dual hydrous oxide gels were prepared by precipitation from varying volumes of 0.5 M nickelous nitrate and 0.5 M (with respect to Al_2O_3) aluminum nitrate solutions, using as the precipitant an amount of 3.77 M sodium hydroxide solution (carbonate-free) such that the final pH value was 7.50. The required amounts of alkali were determined by preliminary titration on aliquots of the metal ion solution mixtures. The compositions of the gels were adjusted to give a series of twenty-one hydrous oxide gels at every 5 mole %.

The gels were washed with distilled water by decantation in five-gallon containers, followed by ten washings in a

(1) Humble Oil & Refining Co. Fellow at The Rice Institute, 1952–1955.

(2) W. O. Milligan and L. Merten, THIS JOURNAL, **50**, 465 (1946).

(3) W. O. Milligan, *ibid.*, **55**, 497 (1951).

(4) P. W. Selwood and F. N. Hill, *J. Am. Chem. Soc.*, **71**, 2522 (1949).

(5) W. O. Milligan and James T. Richardson, to be published.

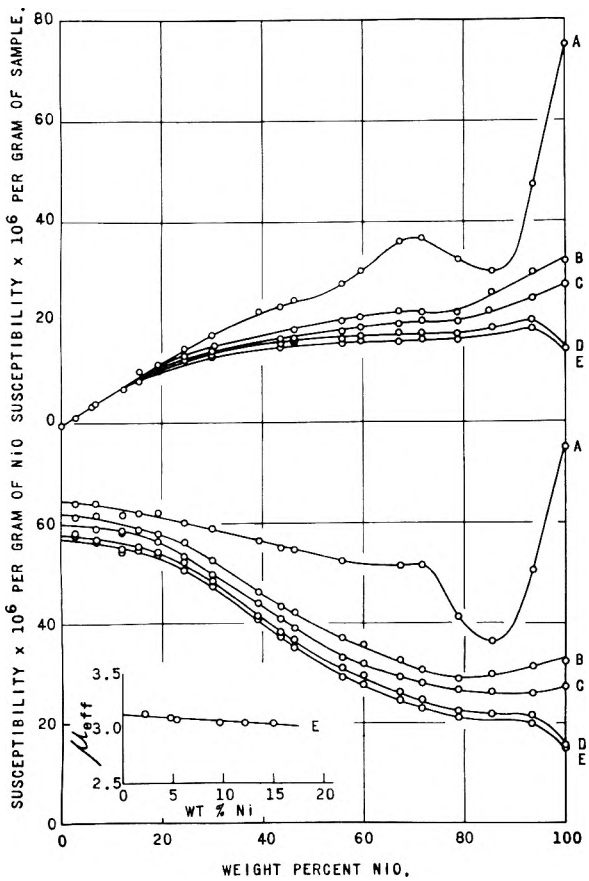

Fig. 1.—Upper portion, magnetic susceptibilities per gram of dry sample as a function of composition; lower portion, magnetic susceptibility per gram of NiO as a function of composition. Samples heat treated at A, 300°; B, 400°; C, 500°; D, 600°; E, 700°. Inset, magnetic moment of nickel ion as a function of low nickel concentration.

centrifuge, until the supernatant liquid was free of nitrate ions. The samples were filtered, air-dried and ground to a uniform powder.

Separate portions of the air-dried samples were heated for two hours in a stream of dry nitrogen at 300, 400, 500, 600 and 700°. These samples were then allowed to come to equilibrium with the moisture in the atmosphere, in order that the subsequent transfers could be made without detectable loss or gain of adsorbed water.

The series of twenty-one gels heated at 500° was analyzed for nickel content, using the standard gravimetric dimethylglyoxime method. The water content was determined from the loss in weight on prolonged ignition to constant weight at 1000°. The alumina content was determined by difference, and the mole % of NiO and Al_2O_3 were calculated on the dry basis. The series of gels derived from the original air-dried gels at the remaining four temperatures of heat-treatment were analyzed for water content, as just described, but the mole ratios of NiO to Al_2O_3 were assumed to be independent of the temperature of heat-treatment.

Magnetic Susceptibility Measurements.—Magnetic susceptibility measurements were conducted in an apparatus already described,[6] employing techniques reported elsewhere.[5] The samples were loaded into the magnetic apparatus concurrently with the weighing of the aliquots for chemical analysis, in order that the water contents of the samples would be accurately known. The measured magnetic susceptibilities were converted to a basis of one gram of dry sample, assuming that the diamagnetic susceptibilities of adsorbed water, alumina and the diamagnetic contribution of the nickel were all additive. These data are presented in the upper portion of Fig. 1. In the lower portion of Fig. 1, there is given an interpretation of the data, in which the susceptibility of the NiO alone is calculated on the assumption that the susceptibility of the alumina is independent of the concentration.

In the inset in the lower portion of Fig. 1, there is given the magnetic moment in bohr magnetons of the nickel ion as a function of concentration. The magnetic moment, μ_{eff}, was computed for concentrations of nickel below 15 weight %, from the relationship

$$\mu_{eff} = 2.83\sqrt{\chi_m T}$$

where χ_m is the molar susceptibility, and T is the absolute temperature. This expression is assumed to be valid at the low concentrations, where the nickel ions are sufficiently dispersed so that the ideal Curie law holds, in accordance with the views of Selwood.[4]

X-Ray Diffraction Patterns.—X-Ray diffraction patterns were obtained for many of the samples, employing standard powder methods. These results will not be reported in detail here, inasmuch as they agree with previous work in this Laboratory.[2]

Discussion

It will be noted in the lower portion of Fig. 1, where the magnetic susceptibility of the nickel oxide is plotted as a function of composition, that the curve corresponding to the 300° heat-treatment level exhibits three regions of interest. In the first region at high concentrations of nickel oxide, the susceptibility decreases rapidly as the amount of alumina in the gels increases. In previous work[5] the high susceptibility of the pure nickel oxide was attributed to extremely small size of the crystallites, and to the plate-like morphology of the aggregates (secondary particle) of the crystallites. The effect of reduction in crystal size and the morphology of the aggregates on the ratio of specific surface to specific volume (and hence the average number of next nearest magnetic neighbors) on the magnetic interaction is detailed elsewhere.[5] The observed reduction in the susceptibility as a consequence of the addition of alumina could be explained on the basis of an increase in crystal size, or to change in the plate-like morphology. X-Ray diffraction studies show that the addition of small amounts of alumina retards the development of the original hexagonal nickelous hydroxide plates, and the samples of gels containing alumina consist of spheroidal particles. Detailed X-ray diffraction, electron diffraction and electron microscopic studies have not been made on the structure and morphology of the original air-dried hydrous oxides or hydroxides, but it is evident that the plate-like form of the nickelous hydroxide is modified. As a hypothesis, on the basis of the presently known information, the reduction of the susceptibility of the nickel oxide on addition of alumina is attributed to change in the morphology of the original nickelous hydroxide, which is reflected in the samples heat-treated at 300°, so as to give spheroidal aggregates, rather than plate-like aggregates. Inasmuch as the size of the crystallites in the pure NiO at a heat-treatment level of 300° is of the order of 50–100 Å., one would expect little further reduction in size as the alumina is added.

The second region of interest is the maximum in the susceptibility curve in the composition range 60 to 80 mole % nickel oxide. This composition region corresponds to the zone of mutual protection already reported[2] for the system, wherein the samples are essentially amorphous to

(6) W. O. Milligan and H. B. Whitehurst, *Rev. Sci. Instr.*, **23**, 618 (1952).

X-rays. The maximum in the susceptibility curve for NiO in this composition region is considered to reflect the enhanced dispersion of the NiO within the gel structure of the alumina.

In the third region of interest, the susceptibility of the NiO increases in a regular manner, because of the increasing dispersion as the amount of alumina increases. This regular change would have continued toward the higher concentrations of NiO, had not the zone of protection occurred, wherein the properties of the alumina gels were markedly changed.

The one or more zones of mutual protection encountered in numerous multiple hydrous oxide systems were first detected by X-ray diffraction methods.[3] In 1948 it was predicted[7] that such zones of protection may correspond to regions of maximum surface, and which, therefore, may exhibit enhanced adsorptive and other surface properties. Enhanced differential and integral isoteric heats of adsorption,[8] enhanced specific adsorptive capacity[8] and a marked increase in the number of crystallites per aggregate[9,10] have been found in the zones of mutual protection occurring in the system $BeO-In_2O_3$. In view of these results, it is not surprising that magnetic susceptibility measurements can detect in a zone of protection an enhanced dispersion of NiO in alumina, the increased dispersion making the Ni ions more magnetically dilute, thereby decreasing the average number of next nearest magnetic neighbors, and thus the magnetic interaction.

In the samples heat-treated at successively higher temperatures, the zone of mutual protection as indicated by X-ray studies[2] narrows and vanishes, and inspection of Fig. 1 shows that the magnetic susceptibility of the NiO does not show any irregularity in this region.

In an earlier investigation,[2] X-ray diffraction patterns established the existence of a definite nickel spinel, $NiO \cdot Al_2O_3$, after heat-treatment of the original air-dried gel at 1000°, the new crystalline phase not being detectable at lower heat-treatments. It was considered possible that magnetic susceptibility measurements might be able to detect the formation or incipient formation of the spinel at lower temperatures of heat-treatment. However, no indication has been found of any irregularity in the susceptibility at a mole ratio of NiO to Al_2O_3 of unity.

In the inset of Fig. 1, for very low nickel concentrations, the magnetic moment approaches a limiting value of 3.2 bohr magnetons. These results agree almost exactly with the previous results of Selwood,[4] and hence will not be discussed in detail here.

We are grateful to the Humble Oil & Refining Company for making possible this investigation by establishing a fellowship program at The Rice Institute, and for making available facilities for the magnetic measurements and for chemical analyses. We wish to thank Dr. Charles F. Squire and Dr. L. W. Vernon for helpful discussions.

(7) H. B. Weiser, W. O. Milligan and G. A. Mills, THIS JOURNAL, **52**, 942 (1948).

(8) W. O. Milligan and C. R. Adams, *ibid.*, **57**, 885 (1953).

(9) C. R. Adams and W. O. Milligan, *ibid.*, **58**, 219 (1954).

(10) C. R. Adams and W. O. Milligan, *ibid.*, **58**, 817 (1954).

ANGULAR DEPENDENCE LIGHT SCATTERING STUDIES OF THE AGING OF PRECIPITATES

BY C. K. SLOAN

Contribution No. 370 from the Chemical Department, Experimental Station, E. I. du Pont de Nemours and Co., Inc., Wilmington, Delaware

Received February 25, 1955

Two typical precipitation processes have been studied by observing the rate of change of intensity of scattered light over the entire angular range from about 70° down to 0°. Such angular dependence light scattering data provide a more complete characterization of the dimensional changes involved in the precipitation process than is obtainable from measurements limited either to the 90° range (nephelometry or tyndallometry) or to the 0° range (extinction turbidimetry). The rapid changes in dimensions occurring during the first few seconds in the growth of barium sulfate precipitated under dilute conditions have been studied by recording the change in scattering intensity at several fixed angles. The initial rapid growth is complete within about one minute, after which relatively slow Ostwald ripening occurs. Complete angular scanning of the scattered light during this slow aging period shows that small dimensions are being replaced by larger dimensions, indicating continued particle growth. Unless the suspension is agitated, there is an even greater increase in small-angle scattering, resulting from formation of a loose flocculated structure. It is suggested that measurement of the intensity of scattered light at about 10° might improve the analytical procedure for determination of sulfate concentration inasmuch as scattering at this angle is least affected by changes occurring during aging. In studies of the alum precipitate used in water clarification, determination of the intensity of scattered light at an angle of about 0.5° from the unscattered beam appears to be most useful in studying the effect of agitation and precipitant concentration in formation of the desired stable floc condition.

The object of the present paper is to illustrate how the mechanism of the precipitation process and subsequent aging can be studied by angular-dependence light-scattering methods. Other techniques that have been employed in the past for studying such processes include measurement of the turbidity of the system by use of either extinction turbidimetry (measuring transmission) or nephelometry or tyndallometry (measuring the intensity of scattered light perpendicular to the transmitted beam). These one-point methods are at a particular disadvantage in the study of the polydisperse systems encountered under most conditions of precipitation. Even for monodisperse systems, particle size determination is dependent on a knowledge of concentration and refractive index factors. The extinction turbidimetry method has the further disadvantage that the angular cone of light used in measurement of transmission usually is so large that it includes a considerable amount of scattered light.

In previous studies[1] in this Laboratory, it has been shown how angular dependence light scattering data characterize disperse systems with respect to the size and size distribution of scattering particles having radii in the range of 0.1 to 100 μ, using plots of log $I\theta^2$ (intensity times angle squared) as a function of log θ for angles from 0.1 to 100°. The method is relatively independent of concentration and refractive index. The high resolution light scattering instrument described by Aughey and Baum[2] is particularly helpful for measuring scattered light at angles less than 30° from the unscattered beam in order to characterize dimensions larger than about 1 μ.

Previous angular dependence light scattering work in the field of turbidimetry has included dissymmetry measurements taken at two angles symmetrical with respect to 90°. This dissymmetry technique is most suitable for characterizing particles in the range of 0.1 μ, whereas the Aughey–Baum instrument is most useful in the 0.5–50 μ size range more commonly encountered in usual precipitate dispersions. Another angular dependence technique for measuring particle size by light scattering is the use of the Higher Order Tyndall Spectra phenomenon originally observed by Young.[3,4] This technique has been used by LaMer[5,6] and co-workers for determination of particle size and for studying the growth of colloidal particles. However, the Higher Order Tyndall Spectra technique is not generally useful in the study of precipitation because most dispersions of such systems are not sufficiently monodisperse. A comprehensive review of the general theory and practice of turbidimetry has been made by West.[7]

In our work angular dependence light scattering has been used to study the formation and aging of (1) the barium sulfate precipitate and (2) the alum precipitate used in the clarification of turbid water. The barium sulfate system has been a favorite one for colloidal studies inasmuch as its character can be varied widely by changing the conditions of precipitation. In his books on "Inorganic Colloid Chemistry," Weiser[8] includes a comprehensive chapter on the physical character of precipitated barium sulfate. A more recent study of the aging of barium sulfate precipitates using electron microscope techniques has been made by Suito and Takiyama.[9] The alum precipitate that finds ex-

(1) (a) C. K. Sloan, "Angular-Dependence Light Scattering. I," in press; (b) C. K. Sloan, II, in press; (c) C. H. Arrington, Jr., III, in press; (d) C. H. Arrington, Jr., IV, in press; (e) C. G. Wortz, V, in press.

(2) W. H. Aughey and F. J. Baum, *J. Opt. Soc. Amer.*, **44**, 833 (1954).

(3) T. Young, Chapter on "Remarks on Measurement of Minute Particles, Especially Blood and Pus" in "Introduction to Medical Literature" as included in "Miscellaneous Works-Thomas Young," edited by George Peacock, Vol. I, John Murray, London, 1855, pp. 343–358.

(4) R. W. Wood, "Physical Optics," The Macmillan Co., New York, N. Y., 1911, p. 241.

(5) V. K. LaMer, THIS JOURNAL, **52**, 65 (1948).

(6) I. Johnson and V. K. LaMer, *J. Am. Chem. Soc.*, **69**, 1184 (1947).

(7) W. West, "Physical Methods of Organic Chemistry," edited by Weissberger, 2nd Edition, Vol. II, Interscience Publishers, Inc., New York, N. Y., 1949, pp. 1448–1490.

(8) H. B. Weiser, "Inorganic Colloid Chemistry," Vol. III, John Wiley and Sons, New York N. Y., 1938, "Colloidal Salts," Chapter II.

(9) E. Suito and K. Takiyama, *Bull. Chem. Soc. Japan*, **27**, 121 (1954).

tensive use in clarification of water was chosen for these aging studies because of the known fact that the rate of agitation markedly affects the rate of coagulation of this precipitate.

Effect of Agitation in the Aging of the Barium Sulfate Precipitate Used in Nephelometry.—Our initial study showed how agitation prevents flocculation of the barium sulfate suspension commonly used in nephelometry. The procedure used in preparation of the suspension follows:

Add 3 mg. of sulfate (using a dilute solution of sulfuric acid) to a 100-ml. flask. Dilute to 70 ml. with distilled water. Add 10 ml. of a solution containing 64 g. of sodium chloride and 20 ml. of concentrated hydrochloric acid per liter. Add 10 ml. of a 3/1 mixture by volume of glycerol/water. Add 1 g. of barium chloride ($BaCl_2 \cdot 2H_2O$) in the form of crystals. Dilute to 100 ml. with distilled water. This procedure gives a finely dispersed suspension of the type suitable for nephelometric measurements of sulfate.

In accordance with nephelometry practice, the barium sulfate precipitate was allowed to age 30 minutes before measurement. A complete angular scan of the light scattering was then made in accordance with the experimental procedure previously described[1b] using a 1-cm. cell, and the data were plotted on log $I\theta^2$/log θ paper. General rules for interpretation of these curves in terms of size and size distribution have been given.[1a,b]

The curve for this sample aged 30 minutes is shown in Fig. 1. The pronounced peak at 30°

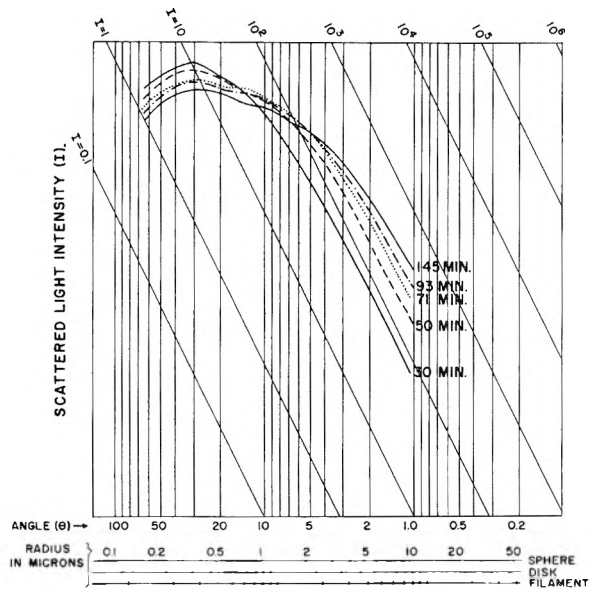

Fig. 1.—Aging of barium sulfate precipitated by barium chloride crystals—no stirring.

indicates that considerable scattering is coming from particles having a radius of about 0.3 μ. The gradual decrease in intensity at angles greater than about 5° indicates presence of some larger material, up to about 0.8 μ in size. The curve shows the finely divided character of this precipitate that makes it suitable for nephelometric determination. Its particle size is definitely smaller than that of a typical sample of blanc fixe that gave a scattering curve[1b] showing that most of the scattering was caused by 0.8 μ material.

Twenty minutes later the same sample was rerun to determine whether any change in particle dimensions had occurred. In order to minimize the possibility of sedimentation, the cell was inverted once between each run. Care was taken to avoid agitation during this inversion by ensuring that there was no free air space in the cell. The curve obtained for this 50-minute aged sample (Fig. 1) clearly shows that the dispersion has changed. Scattering at the 30° peak has decreased indicating a decrease in the 0.3 μ scattering component. In contrast, there is a relative increase in the intensity of the scattered light in the neighborhood of 10°, indicating a marked increase in scattering from particles having a radius of about 1 μ. The parallel character of the 30-minute and 50-minute curves below about 5° indicates that the additional aging has produced no appreciable increase in particles having a radius above the 1 μ range. The other curves representing the same sample aged for longer times show a progressive change in dimensions of the scattering component, indicating apparent disappearance of 0.3 μ particles and appearance of particles of larger dimensions. During the first part of the aging process, the greatest change appears to be in formation of material in the 1 μ size range, as indicated by the course of the curve at 10°. Later in the aging process, the curves at smaller angles (5 to 1°) indicate the appearance of larger dimensions of the order of 2 to 10 microns radius. A further change from small particles to larger particles is shown by a progressive decrease in scattering at 30° and a corresponding increase in scattering at 1°.

Much more information about the aging process can be obtained by such consideration of the changes in scattering at the several angle positions than from the change in transmission (*i.e.*, unscattered light at 0°). Change in transmission simply represents the net difference between the gain in intensity of scattered light over one part of the angular range and the loss in intensity of scattered light over the remainder of the angular range. Thus, the sample aged 200 minutes showed a transmission of 60.7%, an increase of 6.0% over that for the 30-minute sample. This indicates a net loss in total scattering. The decrease in scattering intensity at the larger angles produced by conversion of small particles into larger ones is greater than the accompanying increase in scattering intensity at small angles.

A subsequent experiment indicated that most of the apparent increase in dimensions of the scattering particles in the systems of Fig. 1 was caused by formation of a relatively loose flocculate structure rather than by formation of larger crystals or aggregates. Thus, it was shown that a period of vigorous shaking just before each angular scanning measurement effectively prevented most of the change in scattering intensity. This effect of agitation in maintenance of a deflocculated condition is shown by the curves of Fig. 2. The initial or 30-minute run gives the same type of curve as that for the initial sample of Fig. 1. The subsequent runs with shaken samples, however, show that the changes at 30° and at 1° are much less than in the unshaken systems. There is a slight, but progressive change in intensity at these two

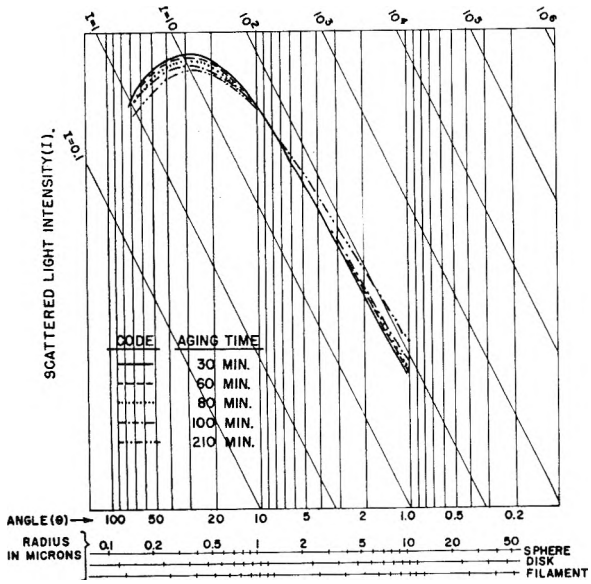

Fig. 2.—Aging of barium sulfate precipitated by barium chloride crystals—intermittent stirring.

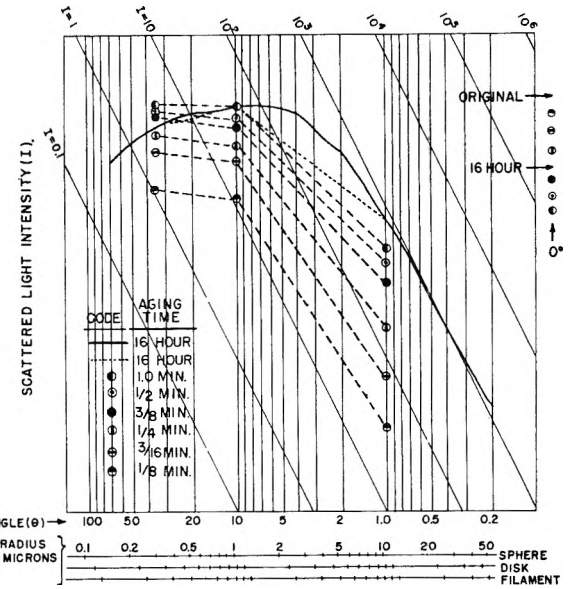

Fig. 3.—Aging of barium sulfate precipitated by barium chloride solution—continuous stirring.

selected angles, indicating that a few larger particles are being formed in spite of the vigorous shaking.

It is suggested that determination of sulfate concentration by measurement of scattering intensity at about 10° might give an analytical procedure that is less affected by the aging factor that is more troublesome at the 0 and 90° points commonly used. This is an example of the value of angular dependence light scattering in studying the mechanism of the precipitation process.

Early Stages in Growth of the Barium Sulfate Precipitate.—The earlier stage of the process was studied by conducting the precipitation in a 2-cm. cell in the light-scattering instrument. In order to make "zero" time more definite, the barium chloride crystal precipitant was replaced by a solution containing 1 g. of barium chloride in 10 ml. of water. Glycerol was omitted in order to avoid any protective action. Continuous vigorous mechanical stirring was used in order to obtain rapid mixing and also to prevent sedimentation.

The solid curve of Fig. 3 shows the angular dependence light scattering behavior of the suspension after very long aging (16 hours). The scattering peak is a broad one, extending from about 5° to about 40°, and indicates a wide range of sizes up to about 3.0 μ radius. This includes the 0.3 and 1.0 μ peaks shown in Fig. 1. Comparison with the curves of Fig. 2 shows that the suspensions prepared by the modified precipitation procedure have considerable larger material (*i.e.*, in the 1.0 to 2.5 μ radius range). The course of the scattering curve at 1° in Fig. 3 is more nearly parallel to the constant intensity lines of the diagram than is the case in Fig. 1. This indicates that the vigorous stirring employed in the experiments of Fig. 3 is effective in preventing formation of large flocculates. The course of the curve between 2 and 5° indicates presence of particles having radii up to 2.5 to 3 μ. Electron micrographs show that the crystals consist of uniform crosses 5 to 6 μ in length that have an internal structure with smaller dimensions that account for the scattering at larger angles. There is no evidence of small separate crystals. The crystal habit is similar to that shown in pictures of barium sulfate crystals published by Fischer.[10]

Figures 3, 4 and 5 show the informative data that can be obtained concerning dimensional changes in the precipitated particles during the first few seconds of growth and during subsequent long aging periods.

The points connected by broken lines in Fig. 3 illustrate the course of precipitation during the early stages. These data show the action during the first minute when most of the change occurs. Inasmuch as several minutes are ordinarily required to make a complete angular scan, the method was modified to observe the rapid change. The photomultiplier tube was set at a fixed angle, such as 1°. The precipitating solution was added rapidly, the door of the light-scattering instrument was closed, and the change in intensity of light at this angle was plotted directly by the recorder pen as a function of time rather than of angle. Tests made by addition of soluble dye to water in the cell indicated that the stirring used in these experiments was vigorous enough to give complete mixing within 4 seconds. Corresponding precipitations were subsequently made with the photomultiplier tube set at 10, 35 and 0°. Although observations at three angles are insufficient for drawing a complete scattering curve for each of the short intervals, the points of Fig. 3 connected by broken lines clearly show the course of the precipitation during the first minute. The first points (at one-eighth minute) indicate presence of small particles about 0.4 μ in radius. The line connecting the 10 and 35° points is nearly horizontal, indicating that the maximum in the scattering curve probably would come at an intermediate point (about 20°). At this early stage in the precipitation, there is not much evidence of larger particles, indicated by the fact that the line

(10) R. B. Fischer, *Anal. Chem.*, **23**, 1668 (1951), Fig. 1B.

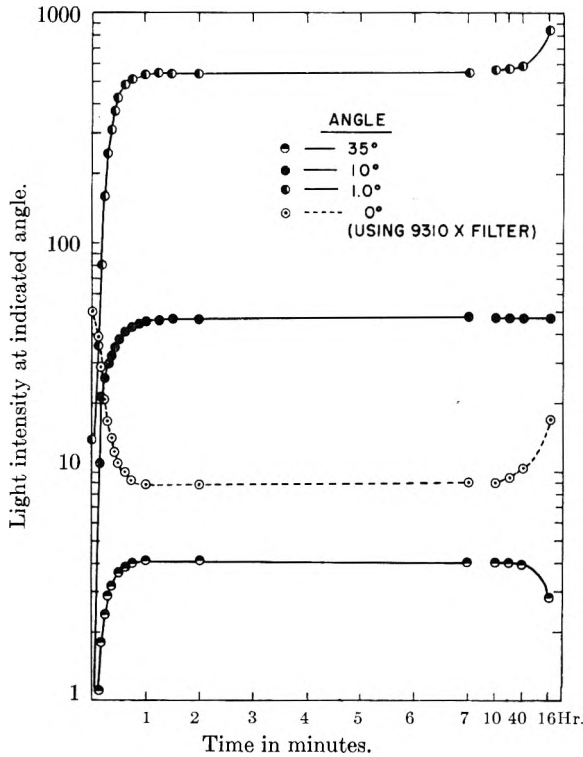

Fig. 4.—Aging of barium sulfate precipitate—change in intensity of light at fixed angles.

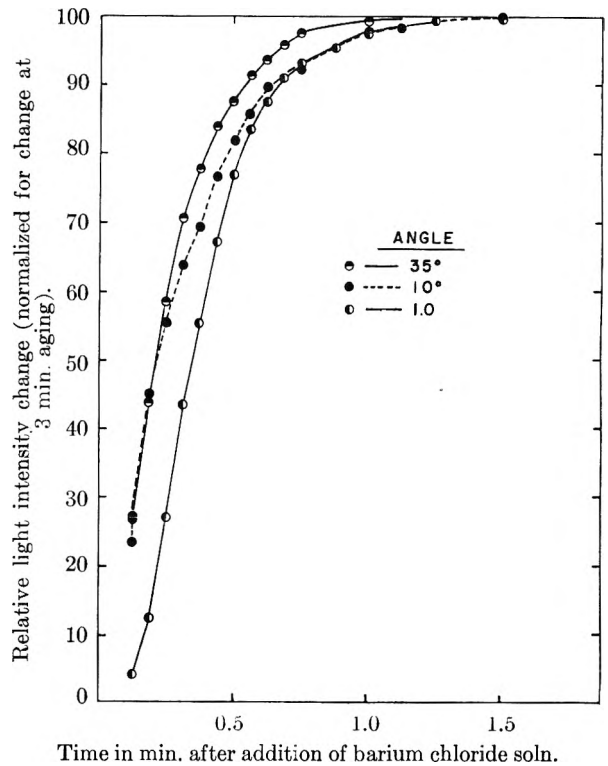

Fig. 5.—Early stage in growth of barium sulfate precipitate—relative rates of change in intensity of scattered light at three different angles.

joining the 10 and 1° scattering points is nearly parallel to the constant intensity lines. However, larger particles are formed in the first minute, as indicated by the change in slope of the lines connecting the successive corresponding 10 and 1° points.

Compared to this initial high rate of change, subsequent change in the scattering character of the suspension is much less while aging from one minute to 16 hours. During this later slower aging process, scattering intensity continues to increase at 1° but shows a decrease at 35°. The indicated shift to larger particle dimensions shown by the 35, 10 and 1° points of the 16-hour curve is confirmed by the complete curve that has a broad maximum extending over the 5 to 10° range.

There is no change in the intensity of scattering at 10° during the period from one minute to 16 hours of aging. This again confirms the value of the use of 10° scattering for measuring concentration in this system. At the right margin of Fig. 3, corresponding points are shown illustrating how the transmission (measured as 0° unscattered light) decreases during the early growth of the precipitate and then increases during the slow aging period.

Figure 4 contains a semilogarithmic plot showing more specifically the manner in which scattering at the three angles changes as a function of time. A plot is also included for the change in unscattered light at 0°. During the initial period of rapid change, points are included at intervals of $^1/_{16}$ of a minute. This method of plotting clearly shows that most of the initial change is complete within one minute. After the 7-minute point, the abscissa scale is compressed to show the changes occurring during longer aging periods. The scattering at 35° turns downward, indicating disappearance of small particles on long aging; whereas the scattering at 1° turns upward, indicating appearance of more large particles. Scattering at 10° remains constant. The transmission of the sample, as measured by the unscattered light at 0°, turns upward, showing that the decrease in scattering at the larger angles more than balances the increase in scattering at the smaller angles represented by the 1° curve.

These data for the changes occurring during the first minute of precipitation are plotted in another manner in Fig. 5 to emphasize the relative differences in the scattering behavior at the three angles. In each case, the scattering change has been normalized for that occurring for the respective 3-minute aging, at which time the initial stage of the precipitation can be considered essentially complete. For the first quarter-minute, the curves for the scattering at 35° and at 10° are practically identical whereas there is a greater lag in the 1° curve during this same period. This shows that the scattering at 10° during the earliest stage of precipitation is being controlled by precipitation of small particles that are also responsible for scattering at 35°. After the first quarter minute of precipitation, the curve for the 10° scattering moves over to join the 1° scattering curve, showing that the scattering at this intermediate angle is controlled after the first quarter minute by formation of the larger particles.

Similar experiments made by precipitation in the presence of glycerol showed that the final 16-hour suspension did not differ appreciably in light scat-

tering from the suspension prepared in the absence of glycerol. These experiments did not include tests of the effect of glycerol in the early stages of precipitation.

Aging of the Alum Precipitate Used in Water Clarification.—Figure 6 illustrates the use of the angular dependence light scattering method for studying the aging of the precipitate formed by addition of alum to Brandywine Creek raw water. Figure 6 includes scattering curves for raw water and for water one hour after treatment. In this aging study, the precipitate was formed by placing 200 ml. of raw water in a 2-cm. cell in the light scattering instrument and then adding 16 drops of a solution containing 6.8 g. of alum in 500 ml. of distilled water. Two types of gentle stirring were studied: namely, manual intermittent stirring and mechanical continuous stirring.

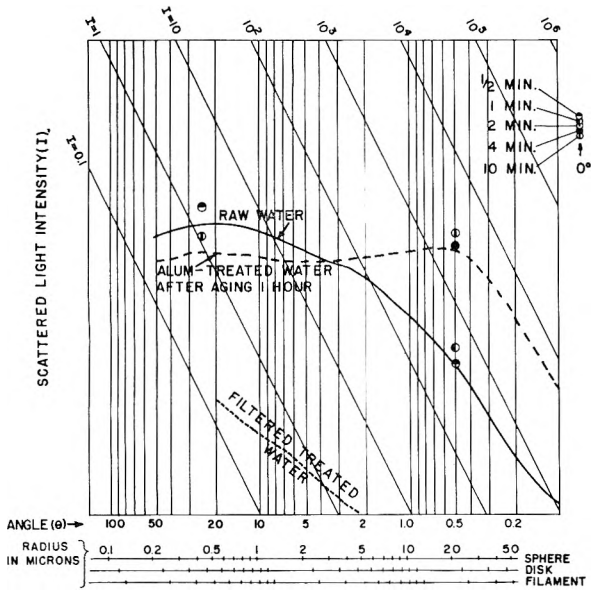

Fig. 6.—Aging of alum precipitate in raw river water—continuous stirring.

Figure 7 shows the stepwise change in scattering behavior obtained by the intermittent stirring method, the change in scattering with time being observed at fixed angles. Scattering intensity remained constant at each of the angles until the alum was introduced (point A), at which time the solution was stirred for about 3 seconds with a spatula. The scattering of the quiescent sample was then observed for several minutes, after which the suspension was again stirred for 3 seconds. The effects of these intermittent stirring operations were observed at the different angles over a period of about one hour for each experiment.

The change in intensity of scattered light is most prominent at the 0.5° angle. After addition of alum (point A) there is a slight rise in intensity of scattered light. This intensity soon levels out until the next stirring period (S), at which time there is a marked increase in intensity of scattered light. This stepwise change in scattered light induced by occasional, gentle stirring periods continued for about 45 minutes, after which it was observed that the flocculation was sufficiently advanced to produce sedimentation, with a decrease

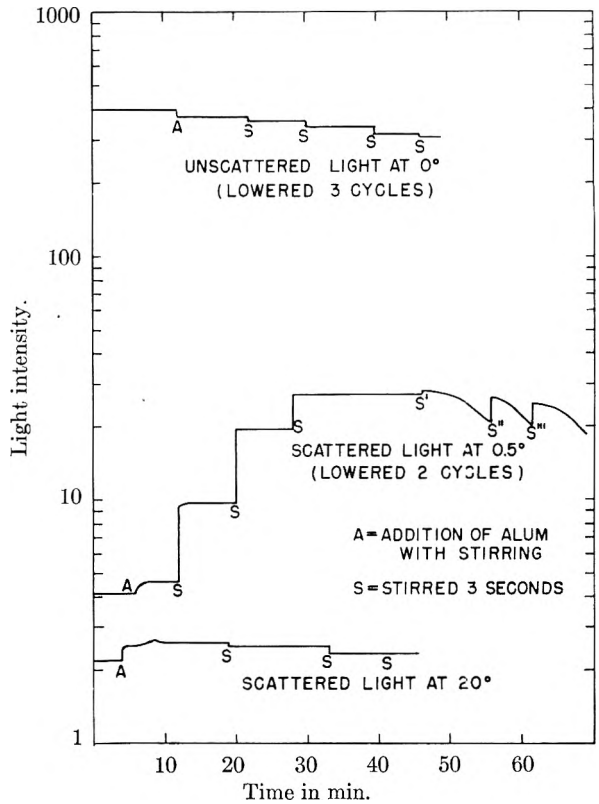

Fig. 7.—Aging of alum precipitate in raw river water—change in intensity of light at fixed angles—intermittent stirring.

in intensity of scattered light during the quiescent period. The first decrease is shown between the stirring points S′, S″. Subsequent stirrings (S″, S‴) break up and resuspend the precipitate.

At an angle of 20°, the first effect of alum addition is to increase the intensity of scattered light. However, in contrast to the behavior at 0.5°, the next stirring period produced a slight but sharply defined decrease in intensity of scattered light. The intensity remained constant during the next quiescent period but a further reduction occurred when the system was again stirred. It is clear from these 20° results that addition of alum first produces small particles that apparently grow to larger dimensions as flocculation occurs. This later formation of larger flocs is shown most strikingly by the changes in scattering at 0.5°.

The third curve represents the transmission or unscattered light measured at 0°. A stepwise decrease in unscattered light occurs, showing that the increase in scattered light at small angles as represented by the 0.5° curve more than balances the decrease in the scattered light at larger angles as represented by the 20° curve.

Since the change in intensity of scattered light is influenced more by the periods of stirring than by the long quiescent intervals, these experiments were repeated using continuous mechanical stirring. The rate of stirring in these alum experiments was much less vigorous than that used in the barium sulfate experiments in order to minimize disintegration of the loose floc structure. Figure 8 shows the course of the light scattering at 0, 0.5, 20 and 25° using continuous stirring. Points at

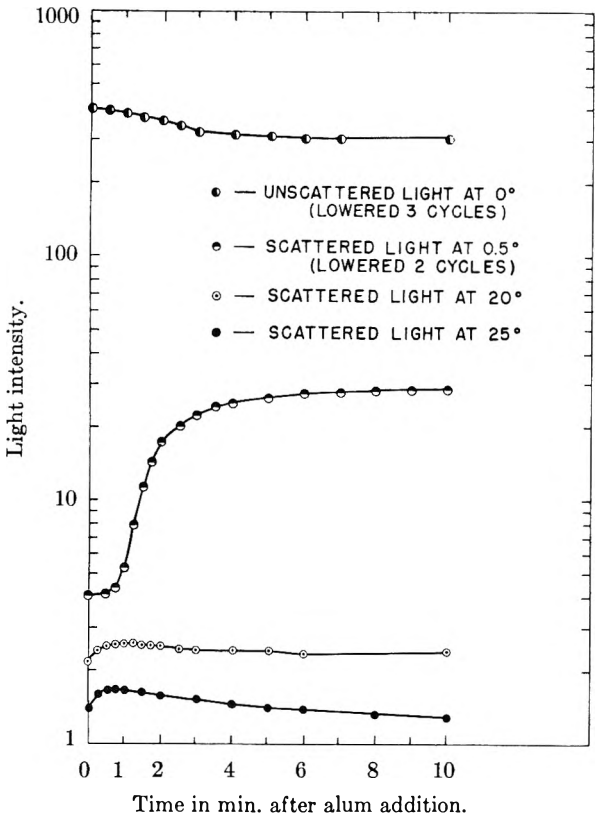

Fig. 8.—Aging of alum precipitate in raw river water—change in intensity of light at fixed angles—continuous stirring.

quarter-minute intervals are included for the first 2 minutes after alum addition. Scattering at 25° first increases, reaches a maximum at about a half minute, and then decreases. This behavior in scattering at the large angle represents first the appearance of small particles of alumina hydrate followed by their disappearance as larger particles during coagulation with the particles responsible for the turbidity of the raw water. An increase in scattered light occurs in this short time interval at 20°, but the subsequent decrease in scattering intensity is not as marked as it is at 25°.

The change in scattering at 0.5° is markedly different from what it is at the larger angles. Thus, there is very little change in the intensity of scattering at 0.5° for the first half minute, during which time formation of small particles is showing up as increased scattering at the larger angles. At about three quarters of a minute, at which time scattering at the larger angles has reached its peak and has begun to decrease because of conversion of the small particles to larger units, the scattering at 0.5° begins to show a marked increase. The rate of increase of scattering at 0.5° is greatest between one and two minutes aging. After this period, the scattered light at 0.5° levels off.

The fourth curve representing unscattered light at 0° shows a gradual decrease in intensity over a period of about 6 minutes. The transmission of the sample is lowered by the scattering at both large and small angles.

The broken curve in Fig. 6 shows the complete angular dependence scan for the treated water after aging about one hour. The effective maximum particle size of the flocs after this period of continuous stirring is about 15 μ radius. Such large flocs undergo a further increase in size when stirring is stopped, resulting in rapid sedimentation. A few of the points from Fig. 8 are included to show the effect of aging at the earlier periods. The line for the sample aged one hour appears to be slightly lower than the points representing scattering for the 10-minute sample at 0.5 and at 25°. This resulted from a continuation of the flocculation process with subsequent decrease in intensity of unscattered light. Finally, a third curve is included in Fig. 6 to show the scattering from the cell containing clarified water. This sample was obtained after sedimentation and filtration of the alum-treated flocculated water.

The course of scattering at small angles is of primary importance in this system inasmuch as it correlates directly with formation of the large flocculates required for clarification of the water by sedimentation and filtration. Measurement of scattering at or below 0.5° by the high-resolution instrument thus makes possible a differentiation between the light scattered by the flocs on the one hand and the unscattered light. This method provides a useful research tool in the study of the effect of precipitant and of agitation on the formation and stability of such flocculated systems.

Acknowledgment.—The assistance of Mrs. Janet P. Cordrey and Mr. Ernest M. Riley in the experimental phases of this study is acknowledged.

DISCUSSION

VICTOR K. LAMER (*Communicated*).—The statement "Another angular dependent technique for measuring particle size by light scattering is the use of the Higher Order Tyndall Spectra (H.O.T.S.) phenomenon originally observed by Young," is unfortunate. It is not only incorrect in fact, but it creates unnecessary confusion in understanding the complicated phenomena involved in the optics of small particles. The subject is of sufficient importance to merit clarification.

Thomas Young, the pioneer investigator of interference and diffraction, exposed blood corpuscles, which are normally of a uniform size of approximately 3.5 microns radius, as well as natural fibers of much larger size, to a beam of natural light. He observed colors in the diffraction rings of the transmitted beam at angles of observation, θ, confined to the near forward direction of propagation. Sinclair[11] has correctly designated such colors as *coronae* arising from the diffraction of the incident light at the perimeter of a disk or sphere. He used this angular dependence as a ready means of checking with simple equipment the size of lycopodium spores measured under the light microscope which shows them to be spheres of radii 15.0 ± 1.0 microns, all in good agreement with Young's estimate.

The angles and intensities of Young's diffraction rings have been computed[12] over the last century from simple formulas, or, more precisely, from the tables of Mascart and of Airy based on Babinet's principle. Only the order of diffraction, the angle and the wave length is necessary to calculate the size of the sphere, since the phenomenon is independent of m, the index of diffraction relative to the surrounding medium.[13]

(11) David Sinclair, *J. Opt. Soc. Am.*, **37**, 475 (1947); also in AEC Handbook on Aerosols, Washington, D.C., **50**, pp. 90 and 110.

(12) Humphreys, "Physics of the Air," McGraw-Hill Book Co., Inc., New York, N. Y., 3rd ed., 1940, Chap. 6.

(13) Van de Hulst, "Optics of Spherical Particles," Duwaer, Amsterdam, 1946, see pp. 3, Chaps. 2 and 3, particularly p. 16.

On the other hand, the Higher Order Tyndall Spectra represent light re-radiated by scattering from electric dipoles, quadrupoles, and higher multipoles, located within the particle, whose oscillations are induced by the electromagnetic field of the incident light. The individual wavelets from these internal scatters interact and interfere producing, on summation, an observed radiation from the surface of the sphere, the intensity of which is a more or less complicated function of λ, m and r. The observed radiation exhibits a dispersion in wave length over a range of angle extending from 0 to 180° (H.O.T.S.) and an analogous dispersion in polarization and phase angle[14] of the scattered light, dependent upon wave length and angle of observation. *The H.O.T.S. cannot be calculated from diffraction theory, but require the Mie theory of scattering for an accurate representation.*

We have resolved at least the first nine orders of H.O.T.S. (or polarization maxima)[14] which correspond to a range of particle size of 0.2 to 1.0 micron for $m = 1.5$. Rayleigh scattering is the zeroth order. In the case of Young's diffraction rings the practically useful range is restricted to about 3 microns as the lower limit and to 30 microns as an upper limit. Thus, we see that these two phenomena, distinguished in physical optics as scattering and diffraction, differ by a factor of about 10-fold in useful range of particle radius. If Thomas Young were the first to observe the H.O.T.S., then a most distinguished line of investigators, familiar with his work, missed an opportunity during the last century to propose the H.O.T.S. as a simple, convenient and rapid means of determining particle size in the important but more difficult range of 0.2 to 1.0 micron.

C. K. SLOAN.—The work of Thomas Young performed a century and a half ago with simple apparatus is still not sufficiently appreciated. In showing how the relative size of "minute" particles held close to the eye can be determined from the angular position of the diffraction ring surrounding an image of a candle flame, Young was observing a phenomenon that is more analogous to the Higher Order Tyndall Spectra than the latter is to the simple Tyndall beam phenomenon itself. I agree with Prof. LaMer that the size of particles above about 3 microns can be calculated from the angular position of Young's diffraction rings. It is generally known that the complicated Mie theory treatment approaches the simpler diffraction theory as particle size is increased. In papers presented at the A.C.S. meeting in Kansas City we showed this agreement graphically, using Mie theory data calculated by Sliepcevich, *et al.* These graphs also indicate our agreement with Prof. La Mer that, for smaller particles (*i.e.*, beginning at about 3 microns), the simpler Airy diffraction equation does not describe the scattering perfectly. However, we have emphasized that the difference between the curves obtained by the two theories is mainly one of difference in the magnitude of intensity rather than in the angular position of the first "red," that is determined by the part of the curve that includes the first rapid drop off and the minimum in intensity. This interference component of the diffraction component is thus very helpful in obtaining a close approximation of the size of the particle even in this range approaching the wave length of light. However, we agree with Prof. LaMer that the complete Mie theory (with consideration of the "m" factor) is necessary for determination of the *exact* angular position of the intensity minimum. Perhaps the difficulty in terminology could be resolved by using the term *Higher Order Tyndall Spectra* for the size range where m must be considered and *Ultra Higher Order Tyndall Spectra* for the larger particles that show the simpler diffraction behavior. In any case, the demarcation between the two phenomena will be uncertain.

Prof. LaMer mentions 30 microns as the upper limit of the Young diffraction method. I should like to point out that the method can be extended readily to much larger dimensions (*i.e.*, several hundred microns) by increasing the angular resolution by using a small point source. The phenomenon is readily photographed by replacing the eye of the eriometer by a camera focused on the point source.

C. M. SLIEPCEVICH.—The question raised by Dr. LaMer regarding the use of H.O.T.S. for determining particle sizes is essentially one of viewpoint and is of minor significance with respect to Dr. Sloan's paper. It would seem that Young demonstrated the feasibility of using the angular dependence of intensity despite the fact that he did not have access to subsequent developments in electromagnetic wave theory. His work was necessarily based upon Babinet's principle since Mie's theory was not yet available in his time.

(14) M. Kerker and V. K. LaMer, *J. Chem. Soc.*, **72**, 3516 (1950). References are given here to earlier work of LaMer and Sinclair on aerosols and work on sulfur hydrosols by various collaborators, published in *J. Colloid Science* (1946 on).

PARTICLE SIZE DISTRIBUTIONS FROM ANGULAR VARIATION OF INTENSITY OF FORWARD-SCATTERED LIGHT AT VERY SMALL ANGLES[1,2]

By J. H. Chin,[3] C. M. Sliepcevich[4] and M. Tribus[5]

Department of Chemical and Metallurgical Engineering, University of Michigan, Ann Arbor, Michigan

Received February 25, 1955

A mathematical basis of a method of determination of the size distribution in polydispersions based on the angular variation of the intensity of forward-scattered light is presented. An integral formula was first derived from the modified Bouguer–Beer[6] light transmission equation to enable the computation of the size distributions of particles, large in comparison with the wave-length of the incident light, from transmission measurements at various values of the forward-scattering half angle. The accuracy of the derived integral formula was checked graphically against typical distribution curves with good results. Three possible experimental techniques of applying the integral formula are discussed, a lens-pinhole, a moving pinhole, and a micro-densitometric method. In the latter two, the integral formula was modified so that the relative size distribution could be computed from measurements of the angular variation of the intensity of the forward-scattered light within a half angle of about three to four degrees.

Particle sizes in polydispersed systems can be determined by means of light transmission measurements combined with differential settling.[7] However, for steady-state flow systems and for systems undergoing changes other than gravity settling, *i.e.*, evaporation or agglomeration, this method presents difficulties which are amenable only to empirical approximation.[8] Since a technique based on light-scattering alone would circumvent these difficulties, a method based on the variation of the forward-scattering half angle was derived from the consideration of the modified Bouguer–Beer light transmission equation

$$\ln\left(\frac{F_0}{F}\right) = \frac{\pi t}{4}\int_0^\infty RK_t N D^2 \mathrm{d}D \qquad (1)$$

where

F_0 is the incident parallel flux, ergs/sec.

F is the flux after traversing a distance, t, through the dispersion and is picked up by the measuring system

K_t is the Mie theory total scattering coefficient and is a function of the particle diameter, D; the wave length of the incident light in the surrounding medium, λ; and the index of refraction of the particle relative to that of the surrounding medium, m

R is a factor allowing for the geometry of the optical system employed to measure the transmitted flux

N is the no. distribution function of the dispersion and is the no. of particles of average diameter D per unit volume of dispersion per unit range of particle diameter, or

$$\int N \,\mathrm{d}D = \sum_i n_i$$

where n_i is the no. of particles of size i per unit volume of dispersion.

For particles large in comparison with the wave length of the incident light and for a measuring system which has a small value of the forward-scattering half-angle θ, according to the diffraction theory the factor R may be obtained by the expression[7]

$$R = R(\alpha\theta) = (1/2)[1 + J_0^2(\alpha\theta) + J_1^2(\alpha\theta)] \qquad (2)$$

where α is $\pi D/\lambda$ and J_0 $(\alpha\theta)$ and J_1 $(\alpha\theta)$ are Bessel functions of the first kind and of orders zero and one, respectively.

For a given index of refraction of the particle and for a given wave length of the incident light, the total scattering coefficient K_t is a function of the particle diameter alone. Rather than using the distribution function $N(D)$, it is more convenient to define a distribution function in terms of α. Thus

$$N(D)\mathrm{d}D = N(\alpha)\mathrm{d}\alpha \qquad (3)$$

Equation 1 may thus be rewritten, for a given index of refraction m, and noting that $D = \lambda\alpha/\pi$

$$\frac{4\pi}{t\lambda^2}\ln\left(\frac{F_0}{F}\right) = \int_0^\infty R(\alpha\theta)K_t(\alpha)N(\alpha)\alpha^2\mathrm{d}\alpha \qquad (4)$$

Equation 4 is an integral equation. The Mellin transformation theorem[9] states that the quantity $K_t(\alpha)N(\alpha)\alpha^2$ in equation 4 may be calculated from an integral of the form

$$K_t(\alpha)N(\alpha)\alpha^2 = \int_0^\infty \frac{4\pi}{t\lambda^2}\ln\left(\frac{F_0}{F}\right)h(\alpha\theta)\mathrm{d}\theta \qquad (5)$$

where $h(\alpha\theta)$ is a kernel to be determined.

Development of Theoretical Equations.—The direct solution of the integral equation 4 is difficult. However, equation (4) may be changed to a new form by the process of differentiation with respect to θ and multiplication with a function of θ, thereby a solution may be obtained as follows.

Substituting for $R(\alpha\theta)$ as given by equation 2 and differentiating equation 4 with respect to θ, gives

$$\frac{-4\pi}{t\lambda^2}\frac{\mathrm{d}F}{F\mathrm{d}\theta} = \frac{1}{2}\int_0^\infty \frac{\mathrm{d}}{\mathrm{d}\theta}[1 + J_0^2(\alpha\theta) + J_1^2(\alpha\theta)]K_t(\alpha)N(\alpha)\alpha^2\mathrm{d}\alpha$$

By using the differentiation and recursion formulas for the Bessel functions, the above equation may be

(1) Presented before the twenty-ninth National Colloid Symposium which was held under the auspices of the Division of Colloid Chemistry of the American Chemical Society in Houston, Texas, June 20–22, 1955.

(2) This work was performed in partial fulfillment of the requirements for the Degree of Doctor of Philosophy in Chemical Engineering at the University of Michigan, Ann Arbor, Michigan.

(3) Graduate Fellow, Department of Chemical and Metallurgical Engineering, University of Michigan, Ann Arbor, Michigan.

(4) Department of Chemical Engineering, University of Oklahoma, Norman, Oklahoma.

(5) Department of Engineering, University of California, Los Angeles, California.

(6) The Bouguer–Beer transmission equation is sometimes called the Lambert–Beer law.

(7) R. O. Gumprecht and C. M. Sliepcevich, This Journal, **57**, 90 (1953).

(8) J. A. Consiglio, Ph.D. dissertation, University of Michigan, Ann Arbor, Michigan, 1953.

(9) I. N. Snedden, "Fourier Transforms," McGraw-Hill Book Co., Inc., New York, N. Y., 1951, p. 7.

simplified to

$$-\frac{4\pi}{t\lambda^2}\frac{dF}{Fd\theta} = -\int_0^\infty \frac{J_1^2(\alpha\theta)}{\theta} K_t(\alpha)N(\alpha)\alpha^2 d\alpha \quad (6)$$

Hence

$$\frac{4\pi}{t\lambda^2}\theta^2\frac{dF}{Fd\theta} = \int_0^\infty \theta J_1^2(\alpha\theta)K_t(\alpha)N(\alpha)\alpha^2 d\alpha \quad (7)$$

Differentiating equation 7 with respect to θ

$$\frac{4\pi}{t\lambda^2}\frac{d}{d\theta}\left(\theta^2\frac{dF}{Fd\theta}\right) = \int_0^\infty \frac{d}{d\theta}[\theta J_1^2(\alpha\theta)]K_t(\alpha)N(\alpha)\alpha^2 d\alpha \quad (8)$$

Titchmarsh[10] gives the formula

$$(fx) = -2\pi\int_0^\infty J_\nu(xu)Y_\nu(xu)u\,du \int_0^\infty \frac{d}{du}[uJ_\nu^2(tu)]tf(t)dt \quad (9)$$

where $Y_\nu(xu)$ is Bessel function of the second kind and of order ν. The above formula is true for $\nu \geqq 0$, if $tf(t)$ is integrable over $(0, \infty)$. Therefore, by letting $\nu = 1$, $x = \alpha$, $u = \theta$, $t = \alpha'$, and $f(x) = K_t(\alpha)N(\alpha)\alpha$

$$K_t(\alpha)N(\alpha)\alpha = -2\pi\int_0^\infty J_1(\alpha\theta)Y_1(\alpha\theta)\theta d\theta \int_0^\infty \frac{d}{d\theta}[\theta J_1^2(\alpha'\theta)]\alpha' K_t(\alpha')N(\alpha')\alpha' d\alpha' \quad (10)$$

Let

$$M(\theta) = \frac{4\pi}{t\lambda^2}\frac{d}{d\theta}\left(\theta^2\frac{dF}{Fd\theta}\right) \quad (11)$$

Then according to equations 8 and 10

$$K_t(\alpha)N(\alpha)\alpha = -2\pi\int_0^\infty M(\theta)J_1(\alpha\theta)Y_1(\alpha\theta)\theta d\theta \quad (12)$$

Hence

$$K_t(\alpha)N(\alpha)\alpha^2 = 2\pi\int_0^\infty M(\theta)[-J_1(\alpha\theta)Y_1(\alpha\theta)(\alpha\theta)]d\theta \quad (13)$$

$M(\theta)$ may be calculated from experimental data according to equation 11, *i.e.*, readings of the measured radiant flux F contained in cones of varying half-angle θ. Once $M(\theta)$ is obtained as a function of θ, $K_t(\alpha)N(\alpha)\alpha^2$ may be calculated from the integral formula 13 by inserting, one at a time, a series of values of α into the kernel $[-J_1(\alpha\theta)Y_1(\alpha\theta)(\alpha\theta)]$, graphically integrating the right-hand side of equation 13, and obtaining the value of $K_t(\alpha)N(\alpha)\alpha^2$ corresponding to the particular value of α used for the integration. From $K_t(\alpha)N(\alpha)\alpha^2$ the number distribution $N(D)$ may be easily computed. The feasibility of computing $K_t(\alpha)N(\alpha)\alpha^2$ from equation 13 was successfully tested with a typical distribution function, $K_t(\alpha)N(\alpha)\alpha^2 = A\alpha^3 e^{-(p\alpha)^2}$. With $p = 0.00884$, $A = 0.20$, and $\lambda = 5460$ Å., the distribution function $K_t(D)N(D)$ has a peak at $D = 14\,\mu$ and the corresponding weight concentration (specific gravity = 1) is approximately 3 grams per cubic meter. Figures 1, 2 and 3 show the distribution functions, $M(\theta)$, and the kernel $xJ_1(x)Y_1(x)$, respectively. The graphical integrations of equation 13 for two values of $\alpha(\alpha = 100$ and $\alpha = 200)$ are given in Figs. 4 and 5. The comparisons between the assumed and calculated values of $K_t(\alpha)N(\alpha)\alpha^2$ are

α	$K_t(\alpha)N(\alpha)\alpha^2$ From typical distribution function, $A\alpha^3e^{-(p\alpha)^2}$	$K_t(\alpha)N(\alpha)\alpha^2$ from eq. 13
100	91548	92200
200	70229	71800

(10) E. C. Titchmarsh, *Proc. London Math. Soc.*, **23**, XXIII (1925).

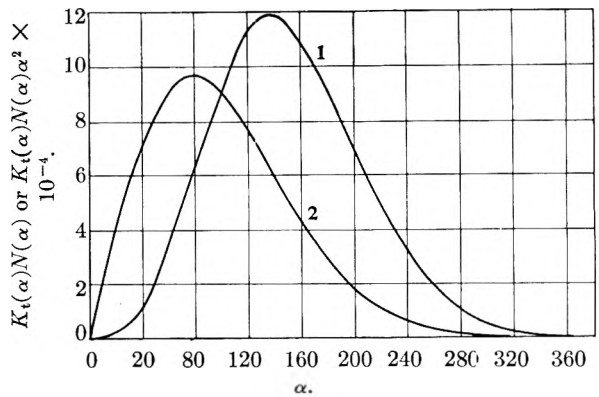

Fig. 1.—Typical particle distribution: 1, $K_t(\alpha)N(\alpha)\alpha^2 \times 10^{-4}$; 2, $K_t(\alpha)N(\alpha)$.

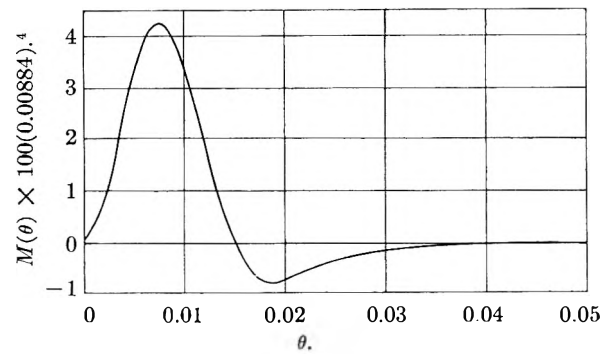

Fig. 2.—$M(\theta)$ for typical particle distribution.

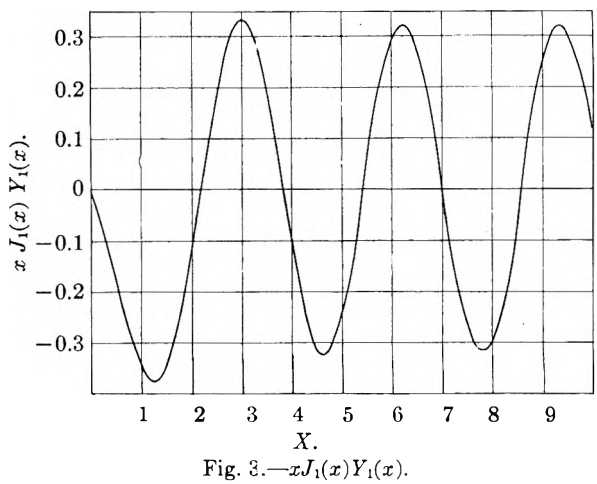

Fig. 3.—$xJ_1(x)Y_1(x)$.

Experimental Methods of Applying the Integral Formula.—To apply the integral formula, three possible experimental methods are considered.

(1) **Lens-Pinhole Method.**—The lens-pinhole optical system[7] is shown in Fig. 6. From the lens law

$$\frac{1}{S} + \frac{1}{S'} = \frac{1}{f} \quad (14)$$

where f is the focal length of the lens, S is the object distance of the particle, and S' is the image distance. By similar triangles

$$\frac{r}{S' - f} = \frac{h}{S'} \quad (15)$$

where r is the radius of the receiving pinhole and h is the radius of the receiving lens. From equations

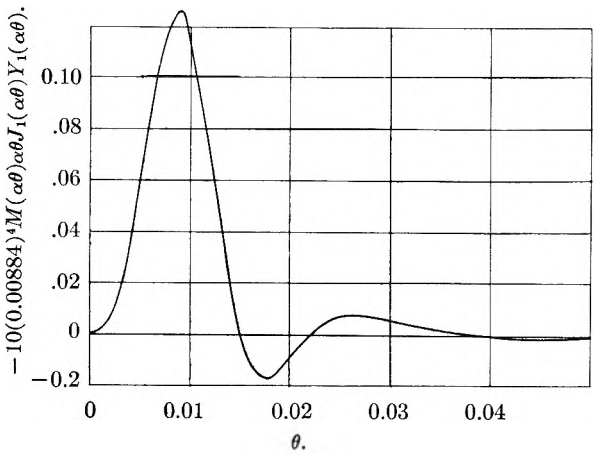

Fig. 4.—Graphical integration for typical particle distribution (α = 100).

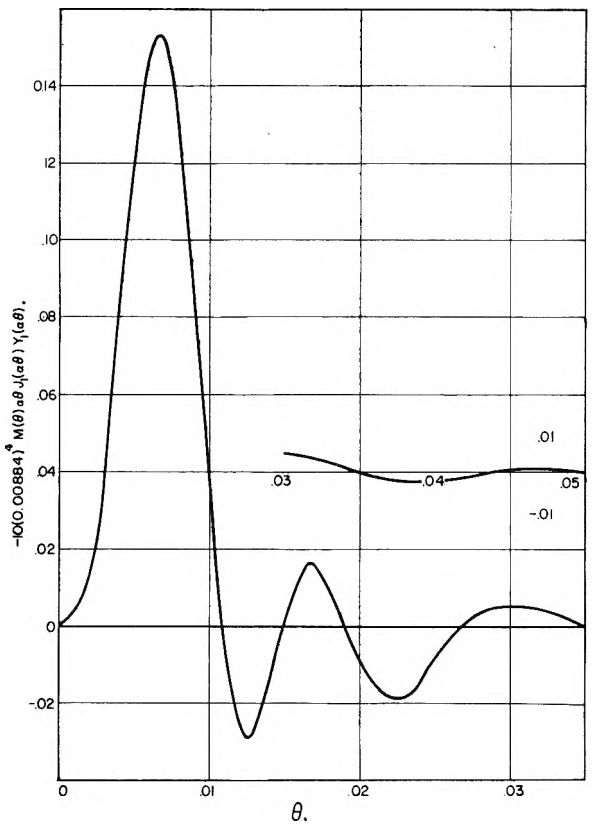

Fig. 5.—Graphical integration for typical particle distribution (α = 200).

14 and 15

$$\frac{1}{S} = \frac{1}{f} - \frac{1}{S'} = \frac{S' - f}{fS'} = \frac{r}{hf}$$

Therefore

$$\frac{h}{S} = \frac{r}{f} = \tan\theta \sim \theta \qquad (16)$$

for small θ. Consequently, if the light is scattered only once to the receiver, the half-angle θ is independent of the position of the particle in the light beam and is characterized only by the ratio of the radius of the receiving pinhole to the focal length of the receiving lens, according to equation 16. It is evident from Fig. 6 that as long as

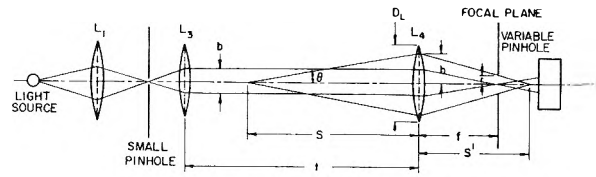

Fig. 6.—Lens-pinhole system.

$$\frac{\frac{1}{2}(D_L - b)}{t} \gtrless \frac{r}{f}$$

or

$$D_L \gtrless \frac{2tr}{f} + b \qquad (17)$$

the photocell will receive all the light with half-angle $\theta \gtrless r/f$. Here D_L is the diameter of the receiving lens, b is the diameter of the light beam, and t is the distance between the most remote particle to the receiving lens. The radiant flux which passes through the receiving pinhole is F. By varying the radius of the receiving pinhole, a series of F's with different half-angle θ, may be measured. $M(\theta)$ may then be computed from equation 11.

(2) **Moving Pinhole Method.**—If a moving tiny pinhole instead of a pinhole with varying aperture is used, the first differentiation step in computing $M(\theta)$ from equation 11 may be eliminated. From Fig. 7, the radiant flux received by the tiny pinhole with diameter a is given by

$$\mathfrak{F} = \frac{\frac{\pi}{4}a^2\Delta F}{\Delta(\pi r^2)} = \frac{a^2\Delta F}{8r\Delta r} \qquad (18)$$

From equation 16

$$r = f\theta \text{ and } a = f\phi \qquad (19)$$

Therefore

$$\mathfrak{F} = \frac{\phi^2}{8\theta}\frac{\Delta F}{\Delta\theta} \qquad (20)$$

If the moving pinhole is very small

$$\frac{\Delta F}{\Delta\theta} \sim \frac{dF}{d\theta}$$

Hence

$$\mathfrak{F} \sim \frac{\phi^2}{8\theta}\frac{dF}{d\theta} \qquad (21)$$

Using $\mathfrak{F}$, the first differentiation step in obtaining $M(\theta)$ according to equation 11 is eliminated.

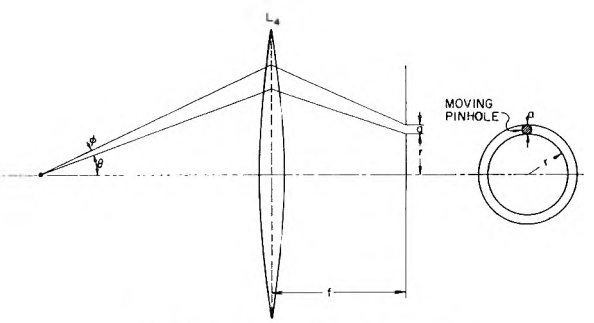

Fig. 7.—Moving pinhole system.

(3) **Micro-densitometric Method.**—If a piece of photographic film is placed on the focal plane of the receiving lens (Fig. 8) and a beam of parallel

monochromatic light is passed through the dispersion in front of the lens, the distribution of the blackness or density is somewhat like that given in Fig. 8b. The central peak density is the result of the parallel beam of light and the light scattered at $\theta = 0°$. The density outside the central peak is the result of the light scattered with forward half-angle θ. The densities on the photographic film may be measured by means of a micro-densitometer. If the film is calibrated, the relative illumination E on each position of the film may be determined. The relationship between the illumination E and the radiant flux F may be obtained as

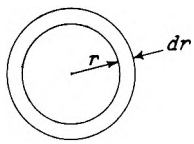

The radiant flux falling over a ring of radius r and width dr on the film is

$$dF = 2\pi r E dr \tag{22}$$

Therefore

$$E = \frac{1}{2\pi r}\frac{dF}{dr} = \frac{1}{2\pi f^2\theta}\frac{dF}{d\theta} \tag{23}$$

The total radiant flux over a circle with radius r is then

$$F = 2\pi\int_{\delta}^{r} E r dr + F_{\delta} \tag{24}$$

where F_{δ} is the flux falling on a very small circle of radius δ.

$M(\theta)$ may be computed using equations 11, 23, and 24.

It may be noted that the radiant flux $\mathfrak{F}$ in equation 21 may be converted into the illumination E by dividing $\mathfrak{F}$ by the area of the moving pinhole

$$\frac{\mathfrak{F}}{\frac{\pi a^2}{4}} \sim \frac{\phi^2}{8\frac{\pi a^2}{4}\theta}\frac{dF}{d\theta} = \frac{\phi^2}{2\pi f^2\phi^2\theta}\frac{dF}{d\theta} = \frac{1}{2\pi f^2\theta}\frac{dF}{d\theta} = E$$

Thus the micro-densitometric method and the moving pinhole method are equivalent. Greater accuracy is possible with these two methods than with the lens-pinhole method because as pointed out above one differentiation step is eliminated.

By combining equations 11 and 23, the following expression for $M(\theta)$ may be obtained.

$$M(\theta) = \frac{8\pi^2 f^2}{t\lambda^2}\frac{d}{d\theta}\left(\theta^3\frac{E}{F}\right) \tag{25}$$

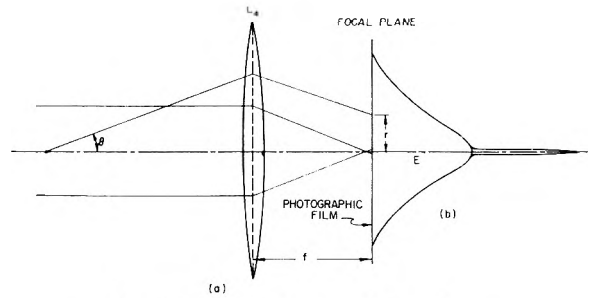

Fig. 8.—Micro-densitometric system.

For dilute dispersions, F increases very slowly while E changes rather rapidly with θ; therefore, as a very good approximation $M(\theta)$ may be written as

$$M(\theta) \sim \frac{8\pi^2 f^2}{t\lambda^2 F_{\delta}}\frac{d}{d\theta}(\theta^3 E) \tag{26}$$

If only the relative distribution of sizes is needed, the value of the constant $8\pi^2 f^2/t\lambda^2 F_{\delta}$ is immaterial. Since the integral method is derived using the principle of diffraction theory for which $K_t = 2$, equation 13 may then be written

$$N(\alpha)\alpha^2 = \frac{8\pi^3 f^2}{t\lambda^2 F_{\delta}}\int_0^{\infty}\frac{d}{d\theta}(\theta^3 E)\,[-J_1(\alpha\theta)Y_1(\alpha\theta)(\alpha\theta)]d\theta \tag{27}$$

If the diameter of the moving pinhole (assumed very small) is a, then

$$N(\alpha)\alpha^2 = \frac{32\pi^2 f^2}{t\lambda^2 a^2 F_{\delta}}\int_0^{\infty}\frac{d}{d\theta}(\theta^3\mathfrak{F})\,[-J_1(\alpha\theta)Y_1(\alpha\theta)(\alpha\theta)]d\theta \tag{28}$$

The relative distribution may then be obtained as

$$N(D)D^2 = C\int_0^{\infty}\frac{d}{d\theta}(\theta^3\mathfrak{F})\,[-J_1(\alpha\theta)Y_1(\alpha\theta)(\alpha\theta)]d\theta \tag{29}$$

where C is a proportionality constant. The flux $\mathfrak{F}$ measured by the moving pinhole as a function of θ is a measure of the angular variation of the intensity of the forward-scattered light.

The relative number distribution and volume distribution may be readily computed from the relative $N(D)D^2$ distribution curve. Thus the integral method provides a convenient means of determination of particle size distributions.

Acknowledgment.—The Eastman Kodak Company provided a Fellowship Grant for the year 1951–1952 and the Horace H. Rackham School of Graduate Studies of the University of Michigan provided the Horace H. Rackham Predoctoral Fellowship Grants for the years 1952–1954.

DETERMINATION OF PARTICLE SIZE DISTRIBUTIONS IN POLYDISPERSED SYSTEMS BY MEANS OF MEASUREMENTS OF ANGULAR VARIATION OF INTENSITY OF FORWARD-SCATTERED LIGHT AT VERY SMALL ANGLES[1,2]

By J. H. Chin,[3] C. M. Sliepcevich[4] and M. Tribus[5]

Department of Chemical and Metallurgical Engineering, University of Michigan, Ann Arbor, Michigan

Received February 25, 1955

An experimental technique for the determination of the particle size distributions in polydispersed systems, based on the angular variation of the intensity of forward-scattered light at very small angles, is described. The experimental apparatus consists of a monochromatic, parallel light source, a dispersion cell, a lens-moving-pinhole receiving unit and a photomultiplier-potentiometer measuring system. An example of an analysis of a polydispersion of glass spheres in water is given. Close agreement was obtained between the distributions obtained by the experimental technique and the distributions obtained by microscopic counting.

In the previous paper, an integral formula for computing the relative particle size distribution $N(D)D^2$ is derived. According to the integral formula, the distribution $N(D)D^2$ is given by

$$N(D)D^2 = C\int_0^\infty \frac{\mathrm{d}}{\mathrm{d}\theta}(\theta^3\mathfrak{F})\,[-J_1(\alpha\theta)Y_1(\alpha\theta)(\alpha\theta)]\mathrm{d}\theta \quad (1)$$

where

$N(D)$ is the no. distribution function of the dispersion and is the number of particles of av. diameter D per unit volume of dispersion per unit range of particle diameter, or $\int N\,\mathrm{d}D = \sum_i n_i$, where n_i is the number of particles of size i per unit volume of dispersion

C is a proportionality constant

θ is the forward-scattering half angle

$\mathfrak{F}$ is the radiant flux passing through a small pinhole moving on the focal plane of a receiving lens in front of which is placed the dispersion cell

α is the ratio of the particle circumference to the wave length of the incident light in the surrounding medium, or $\alpha = \pi D/\lambda$, where λ is the wave length of the incident light in the surrounding medium

$J_1(\alpha\theta)$ is Bessel function of the first kind and of order 1

$Y_1(\alpha\theta)$ is Bessel function of the second kind of order 1

For small angles, the half-angle θ is proportional to the radial distance, r, between the moving pinhole and the optical axis of the receiving lens

$$\theta = r/f \quad (2)$$

where f is the focal length of the receiving lens. The value of θ in the medium is less than that in air because of the difference in index of refraction. However, the value of α in the medium is increased by the same amount because of the shortening of the wave length of the incident light. Therefore, the product of α and θ is independent of the index of refraction of the medium and it is convenient to use the value of α and θ in air for the computation. If a traversing unit for moving the pinhole is designed in such a way that the focal plane of the lens is traversed by the turning of a screw, the radial distance r may be expressed as this turn number ν measured from the central position where the transmitted parallel light is focused. The quantities $\mathfrak{F}$, θ^3, $\theta^3\mathfrak{F}$, and $\mathrm{d}/\mathrm{d}\theta(\theta^3\mathfrak{F})$ may be expressed as a function of ν. For a given α, $-J_1(\alpha\theta)Y_1(\alpha\theta)(\alpha\theta)$ is also a function of ν. Equation 1 may then be rewritten as

$$N(D)D^2 = C\int_0^\infty \frac{\mathrm{d}}{\mathrm{d}\nu}(\theta^3\mathfrak{F})h(D,\nu)\mathrm{d}\nu \quad (3)$$

where

$$h(D,\nu) = -J_1(\alpha\theta)Y_1(\alpha\theta)(\alpha\theta) \quad (4)$$

noting that $D = \lambda\alpha/\pi$ and that ν is proportional to θ.

Experimental Work

The experimental apparatus consists of a collimated-source unit, a dispersion unit, and a receiving-measuring unit. A General Electric type C-H3 mercury lamp and a Wratten 77-A filter are used to obtain the monochromatic green light (λ 5460 Å.). The Wratten 77-A filter transmits 68% of the green line and a negligible percentage of the yellow lines. With a receiver of S-9 response, the net spectral purity of the green line is over 95%.

An effective point source is used to obtain a parallel beam of light. The parts are mounted on optical benches. The light sent out by the mercury lamp is condensed by a condensing lens onto a pinhole after passing through the Wratten 77-A filter. An iris diaphragm is placed behind the condensing lens to prevent the unwanted radiation from getting to the collimating lens. A shutter is placed just next to the pinhole, near which the smallest cross-section of the light cone is located. The pinhole is at the focal point of a collimating lens. The collimating lens is an achromatic, coated, telescope objective, 54 mm. in diameter and 508 mm. in focal length. A diaphragm is placed in front of the collimating lens to limit the diameter of the parallel beam. The inside of the collimated-source-unit enclosure is blackened to minimize reflections and scattering. A small blower is used to supply a stream of air to provide cooling for the lamp.

With a $^1/_{32}$-inch pinhole and a collimating lens of 508 mm. focal length, the divergence of the parallel beam is 2.68 minutes, according to equation 2.

The dispersion unit consists of a brass cell and a variable-speed electric stirrer. The cell is provided with two plain-glass windows held in place by screws and rubber gaskets.

The camera is behind the dispersion cell. The camera body is a wood box painted flat-black inside. The front of the camera box is fitted with a lens holder with fine threads for focusing. The camera lens is an achromatic, coated, telescope objective, 83 mm. in diameter and 914 mm. in focal length. The quality of this lens is not excellent as several small bubbles are observed in the optical glass. There is no shutter in the camera, the shutter being placed

(1) Presented before the twenty-ninth National Colloid Symposium which was held under the auspices of the Division of Colloid Chemistry of the American Chemical Society in Houston, Texas, June 20–22, 1955.

(2) This work was performed in partial fulfillment of the requirements for the Degree of Doctor of Philosophy in Chemical Engineering at the University of Michigan.

(3) Graduate Fellow, Department of Chemical and Metallurgical Engineering, University of Michigan, Ann Arbor, Michigan.

(4) Department of Chemical Engineering, University of Oklahoma, Norman, Oklahoma.

(5) Department of Engineering, University of California, Los Angeles, California.

at the source unit. The apparatus is placed in a dark room and the experiments are carried out in complete darkness.

The radiation is collected by a Du Mont 6291 photomultiplier. The Du Mont 6291 is a ten-stage, head-on type multiplier phototube with S-9 spectral response. The multiplier phototube is operated by a Furst Electronics Model 710 PR, 300 to 1500-volt variable negative power supply. The circuit diagram for the photomultiplier is shown in Fig. 1. Two 45-volt "B" batteries are used in series to provide the potential difference between dynode No. 10 and the anode. The anode current is determined by measuring the potential drop across a 5100-ohm resistor in the anode circuit with a potentiometer. Precision resistors of low temperature coefficients are used in the multiplier circuit to minimize temperature effects during measurement. The voltage drop between the cathode and the first dynode is made twice as large as that between dynodes to better the collection efficiency and to obtain higher multiplication on the first dynode. A 20-megohm and a 500-ohm resistor in series are used across the cathode and dynode No. 10 so that the cathode supply voltage can be determined more accurately by measuring the potential across the 500-ohm resistor with a potentiometer.

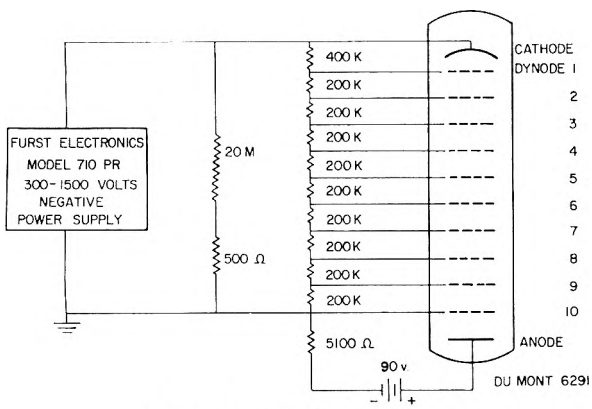

Fig. 1.—Photomultiplier circuit.

The Du Mont 6291 tube, facing against a $^3/_{16}$-inch pinhole to limit the receiving area, is mounted in a traversing unit which traverses vertically on the focal plane of the camera lens. The traversing unit is designed in such a way that it can move the multiplier either continuously or in small steps of $^1/_{96}$ of an inch by the turning of a large knurled-head screw. Each turn of the knurled-head screw corresponds to $^1/_{24}$ of an inch or a value of θ about 4 minutes for a camera lens of 914 mm. focal length. A feeler is provided so that each step ($^1/_4$ turn) may be felt in the dark and the position of the multiplier tube may be determined.

In order to test the validity of the theoretical method, a polydispersion of glass spheres (diameter from 2 to 40 μ) in water, having a known distribution as obtained from microscopic counting, was used. The polydispersion was prepared by mixing several narrow-cut dispersions which were obtained from Pyrex glass bead samples prepared by Gumprecht.[6]

The light source was regulated by means of a manual-adjust rheostat and a constant-voltage Sola transformer. The multiple reflection effect between the dispersion cell and the camera lens may be eliminated by tilting the cell slightly with respect to the camera lens. In order to correct for the effect of dust particles on the optical parts and in the distilled water, it was necessary to traverse the focal plane of the camera lens and record the readings for both distilled water and the dispersion. A definite procedure of experiment was followed. First, the dispersion cell was cleaned and the cell windows were aligned parallel to each other. After the optical parts were cleaned with a camel hair brush, the cell was aligned in front of the camera lens. Then the focal plane was traversed with distilled water in the cell, the electric stirrer being turned on. Readings were obtained intermittently as a function of the number of turns on the knurled-head screw by remotely opening the shutter at the source unit through a solenoid. The multiplier was then idled for about one hour to allow the recovery of possible changes of sensitivity from prolonged operation. Then a weighed sample of the glass bead dispersion was added to the distilled water to obtain the desired concentration. The dispersion cell was maintained at the same position as before. The stirrer was turned on and the focal plane was traversed again as before. The gain was adjusted by increasing the cathode supply voltage at suitable turn numbers so that the signals could be measured conveniently by means of a potentiometer. To obtain relative values for the readings, at suitable turn numbers, the readings were tied-in by measuring the signal both before and after the gain was changed.

The method of correction for dust particles on optical surfaces and in the distilled water is to subtract the reading for distilled water from that for the dispersion when the incident beam to the front window of the dispersion cell is of the same illumination for both traversings.

To compute the size distribution from the readings, a smooth curve was drawn through the data points for the dispersion and distilled water. The values at each turn of the knurled-head screw as read from the smooth curve were used for further computations. Because distribution curves are not in general smooth, the $\mathfrak{F}$-curves will be expected to have slight irregularities. These slight irregularities were disregarded because they are indistinguishable from experimental errors. The $\mathfrak{F}$-readings after multiplication by θ^3 are to be differentiated. The differentiation of a smoothed curve will give more representative results. Large irregularities, of course, should be handled differently. For instance, the $\mathfrak{F}$-curve for narrow-cut dispersions exhibits maxima and minima which can be easily distinguished from experimental irregularities. Figure 2 shows the net $\mathfrak{F}$-curves for two runs for the polydispersion.

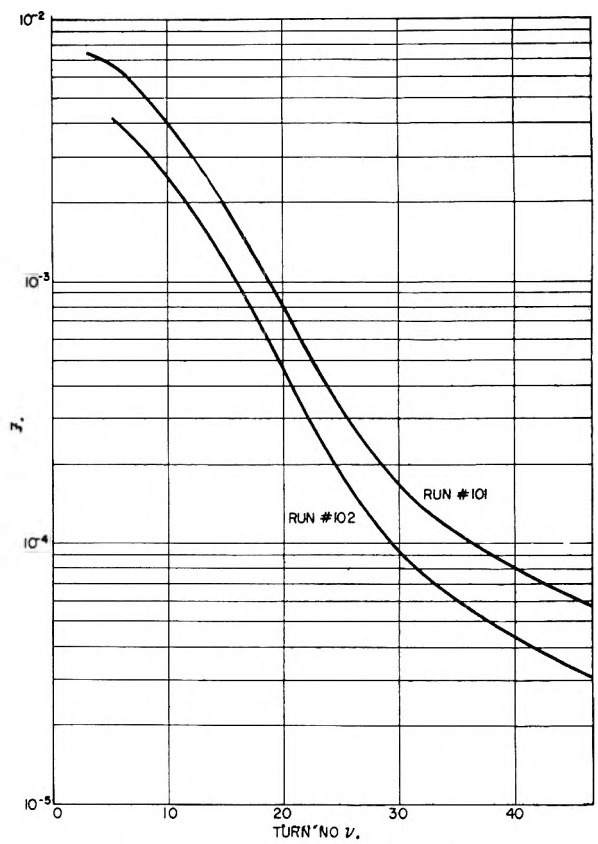

Fig. 2.—$\mathfrak{F}$-Curve for polydispersion.

The values of $d/d\nu\ (\theta^3\mathfrak{F})$ were obtained by differentiating the smoothed $\theta^3\mathfrak{F}$-curve. The slopes of the $\theta^3\mathfrak{F}$ *versus* ν curve were calculated by finding the average slope between successive points on the curve and calling it the slope at the mid-point values of ν between the corresponding pair of points on the curve. The slopes thus obtained were plotted against ν and were used for graphical integrations after

(6) R. O. Gumprecht and C. M. Sliepcevich, THIS JOURNAL, **57**, 90 (1953).

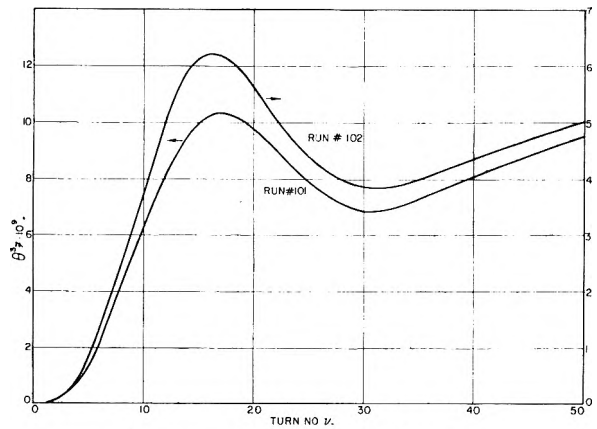

Fig. 3.—$\theta^3\mathfrak{F}$-Curve for polydispersion.

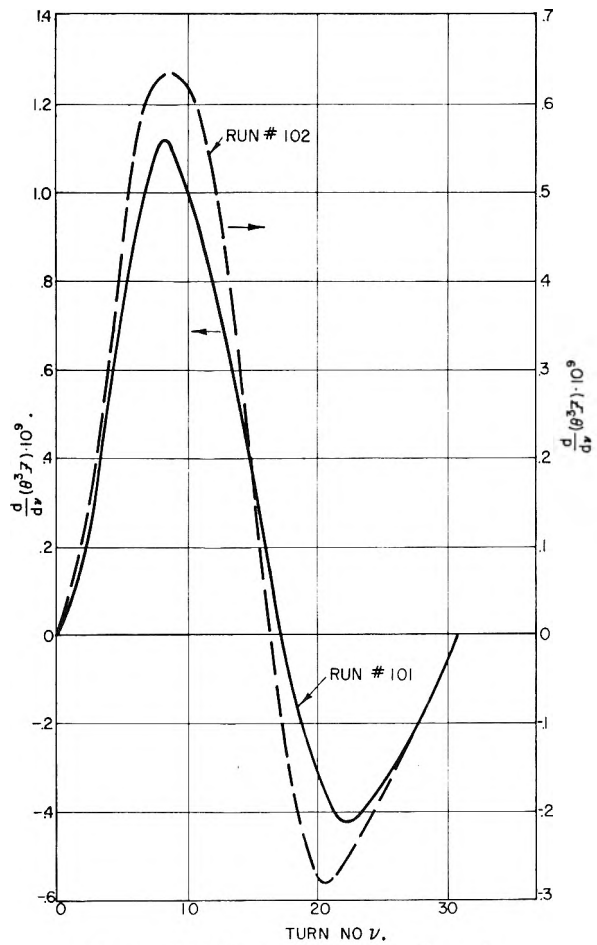

Fig. 4.—$\mathrm{d}/\mathrm{d}\nu(\theta^3\mathfrak{F})$-curve for polydispersion.

being multiplied by the factor $h(D,\nu)$. Figures 3 and 4 show the plot of $\theta^3\mathfrak{F}$, $\mathrm{d}/\mathrm{d}\nu\ (\theta^3\mathfrak{F})$ for the polydispersion.

For the polydispersion, only the first two loops, one positive and one negative, of $\mathrm{d}/\mathrm{d}\nu\ (\theta^3\mathfrak{F})$ were used for computation. For runs #101 and #102, the $\theta^3\mathfrak{F}$ *versus* ν curves exhibit a rather obvious maximum and a less obvious minimum and then an apparently constant or slightly decreasing positive slope up to $\nu = 50$, the last turn of the screw. This latter slope gives a positive loop of $\mathrm{d}/\mathrm{d}\nu\ (\theta^3\mathfrak{F})$ after the first negative loop. It is expected that $\mathrm{d}/\mathrm{d}\nu\ (\theta^3\mathfrak{F})$ has more oscillations before it approaches zero. In other words, $\mathrm{d}/\mathrm{d}\nu\ (\theta^3\mathfrak{F})$ oscillates about the ν-axis with decreasing amplitudes as ν increases. Theoretically, better results will be obtained if more loops of $\mathrm{d}/\mathrm{d}\nu\ (\theta^3\mathfrak{F})$ are used. However, for polydispersions in which the size ranges are not too narrow, the higher order loops of $\mathrm{d}/\mathrm{d}\nu(\theta^3\mathfrak{F})$ have very small

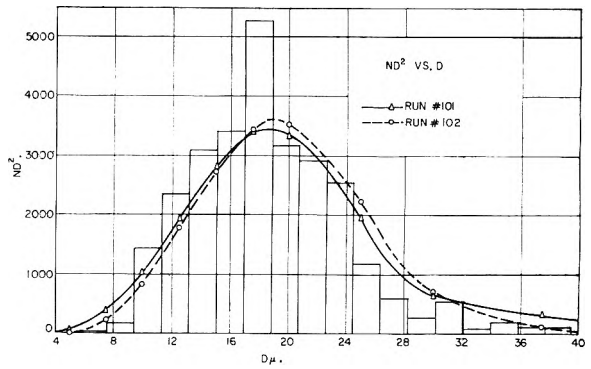

Fig. 5.—ND^2 *vs.* D for polydispersion.

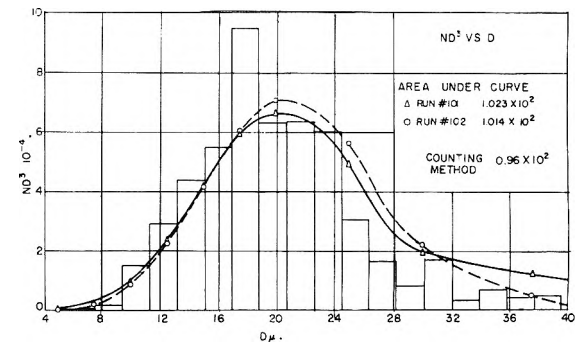

Fig. 6.—ND^3 *vs.* D for polydispersion.

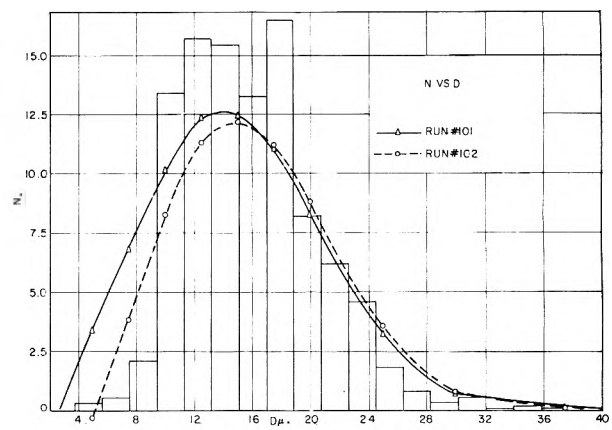

Fig. 7.—N *vs.* D for polydispersion.

amplitudes compared to that of the first two and may be neglected in the computation without introducing too much error. Furthermore, as will be explained later, the readings above ν in the order of 30 were not as accurate as for smaller ν because of limitations of the experimental apparatus. Consequently, it was necessary to use only the first two loops of $\mathrm{d}/\mathrm{d}\nu\ (\theta^3\mathfrak{F})$ for computation.

According to equation 3, the areas from graphical integrations are proportional to $N(D)D^2$. The relative $N(D)D^2$ *versus* D curves obtained were then compared with that computed from counting data, after being normalized to give the same area under both curves. This method of comparison was selected because it is the surface distribution which is of most importance in many applications. From the $N(D)D^2$ *versus* D curve, the $N(D)$ *versus* D and the $N(D)D^3$ *versus* D curves may easily be computed and compared with those obtained from counting data. Figures 5 to 7 show the comparisons. The specific surface (total particle surface per unit volume of particles, S_p) and the surface mean diameter ($D = 6/S_p$) of the polydispersion were also computed. Table I shows the comparisons.

The agreement for the distribution curves, the specific surface, and the surface mean diameter between the integral method and the counting method is rather good, con-

Table I

Comparison of Results of the Integral Method and Counting Method

Basis: (100) (1.885) counted particles; D in μ.

	$\int ND^2\,dD$	$\int ND^3\,dD$	Sp (cm.²/cm.³)	Ds	% deviation Sp	% deviation Ds
Counting	51660	965000	3215	18.68	0	0
Run #101	51660	1023000	3033	19.70	−5.66	+5.45
Run #102	51660	1014000	3058	19.65	−4.89	+5.20

sidering the possible errors in the counting method, especially near the toes of the distribution curve where only very few particles are counted. The close agreement of the results of runs #101 and #102, obtained for the same polydispersion but different concentrations, shows that the integral method is probably more accurate than the counting method.

The dark current and noise introduced an error of not greater than 5% over most of the distance traversed and only in large distances traversed the error might have been as high as 10 to 20%. The use of a finite pinhole introduced but a very small error because the photomultiplier readings were approximately linear over a distance of the diameter of the pinhole for most of the distance traversed.

Since $\alpha\theta$ appears as a product in the function $h(D,\nu)$ and θ is inversely proportional to the focal length of the lens, f, a positive error in f corresponds to a shift of the distribution curves toward larger diameters. Because the error in f was not more than 3%, the shift of the distribution curve was very small.

As to the counting method, the most serious possible error was due to the inadequate number of particles counted for the particles with diameters near the toes of the distribution curves. Unless a great number of particles are counted, an accurate statistical distribution cannot be obtained. Inaccurate focusing introduces errors, especially to the particles whose diameter occupies full divisions of the eyepiece micrometer of the microscope. A slight variation of focus may attribute the particle to either n or $n + 1$ division of the eyepiece micrometer, corresponding to a possible error of one size group or 1.885 μ in diameter. Again, this error may be compensated only if a great number of particles are counted. From the above considerations, it is reasonable to conclude that the integral method is more accurate than the counting method.

Summary

The experimental apparatus is satisfactory for this preliminary investigation although it is rather primitive in design. However, this investigation suggests the possibility that a commercial high-speed measuring and computing unit for the determination of particle size distributions in polydispersed systems may be designed according to this technique.

Acknowledgment.—The Eastman Kodak Company provided a Fellowship Grant for the year 1951–1952 and the Horace H. Rackham School of Graduate Studies of the University of Michigan provided the Horace H. Rackham Predoctoral Fellowship Grants for the years 1952–1954.

LIGHT TRANSMISSION MEASUREMENTS ON MULTIPLE-SCATTERING LATEX DISPERSIONS[1,2]

BY P. H. SCOTT, GEORGE C. CLARK AND C. M. SLIEPCEVICH[3]

Department of Chemical and Metallurgical Engineering, University of Michigan, Ann Arbor, Michigan

Received February 25, 1955

An experimental investigation was made of the transmission of light by a multiple-scattering dispersion of finite thickness but infinite lateral dimensions to evaluate the results of a theoretical analysis of this same problem by Chu and Churchill. The experimental investigation encompassed the following range of variables: (1) optical thicknesses, $n\sigma_T t$, from 0.630 to 11.0; (2) particle diameters, D, from 0.236 to 1.18 μ; (3) tangents of the azimuth angle, tan θ, from 0 to 12. All measurements were made with an incident wave length of approximately 6000 Å. in air. The dispersion consisted of water suspensions of polystyrene and polyvinyltoluene latexes which had a relative index of refraction of 1.20. Each latex consisted of very uniform particle diameters. In general, satisfactory agreement was observed between the experimental results and the theoretical predictions. The predicted effect of the parameters, optical thickness, tan θ, particle diameter, and wave length was verified. The values of the predicted power transmission through the particle bed varied from 45% below to 20% above the experimentally determined power transmission. The major discrepancies were observed at low values of tan θ where the theoretical results are from 20 to 45% low as was anticipated from assumptions made in the analysis. At high values of tan θ the agreement is generally better than 20%.

Introduction

An experimental study was made of the attenuation of light reaching the non-reflecting base of a dense particle dispersion of finite thickness but of infinite lateral dimensions from a point source located above the dispersion. The main purpose of this experimental work was to evaluate the accuracy of a theoretical study of this same problem which was presented in a previous paper.[4]

The experimental work consisted essentially of measuring the light power at points along the base of a particle dispersion of finite dimensions illuminated by a point source of known strength located outside the dispersion, as shown in Fig. 1. The

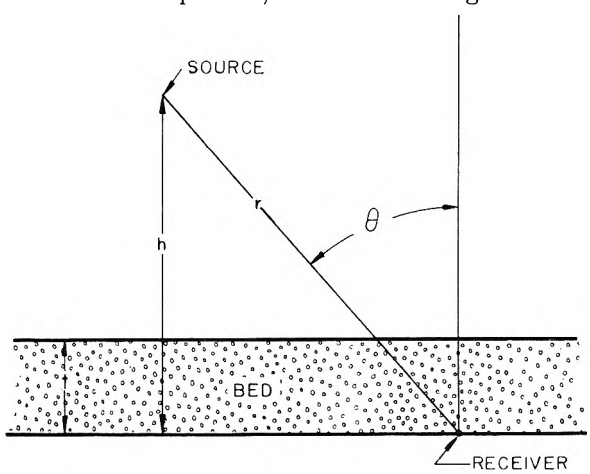

Fig. 1.—Illustration of experimental parameters.

important parameters used to describe the theoretical results are

$n\sigma_T t$, the optical thickness of the dispersion, where n is the number of particles per unit volume of the scattering dispersion, σ_T is the effective scattering cross section per particle, and t is the thickness of the particle bed

$\alpha = \pi D/\lambda$, the circumference of a particle divided by the wave length of the incident radiation

tan θ, the tangent of the azimuth angle or the angle between a line from the source to the point of observation and the normal to the base of the dispersion passing through the point of observation.

It was necessary to study experimentally the effect of each of these parameters in order to evaluate the theoretical results.

A comparison of the results of the experimental and theoretical studies of the monochromatic power interception function, $\bar{E}(\lambda)$, is presented graphically. This function is defined as the ratio of the monochromatic power striking the receiver after passing through the particle dispersion to the power that would strike a receiver of the same area but normal to the line from the source to the receiver when no particles are present in the bed (see Fig. 2).

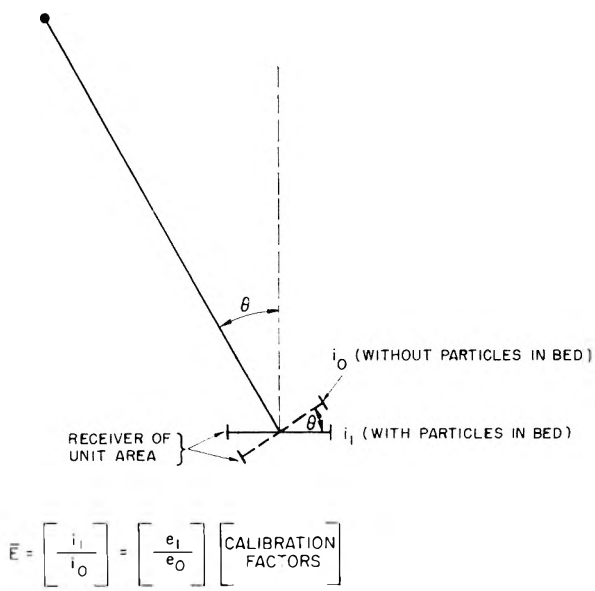

Fig. 2.—Geometric representation of the definition of the monochromatic intensity function, E.

Experimental Equipment and Procedure

The experimental equipment consisted of a rectangular tank, 46 inches long by 22 inches wide by 26 inches deep. The tank walls were constructed of 1/4-inch plate glass supported by an angle iron framework on an angle iron dolly. Glass was chosen as the material of construction because it

(1) Presented before the twenty-ninth National Colloid Symposium which was held under the auspices of the Division of Colloid Chemistry of the American Chemical Society in Houston, Texas, June 20–22, 1955.

(2) This paper reports work done through the Engineering Research Institute of the University of Michigan, under contract with the Chemical Corps, U. S. Army, Washington 25, D. C.

(3) Department of Chemical Engineering, University of Oklahoma, Norman, Oklahoma, since February, 1955.

(4) Chiao-Min Chu and S. W. Churchill, THIS JOURNAL, **59**, 855 (1955).

is structurally strong and inert to the water contained in the tank. In addition, the glass provided convenient observation ports. Since the bed consisted of an aqueous dispersion of latex particles, water was selected as the medium surrounding the bed and source in order to minimize the effects of reflection and refraction at the bed boundary.

In order to minimize reflections from the glass walls of the tank, it was necessary to make these boundaries light-absorbing. Because a permanent bond could not be obtained between various types of black paint and glass in the presence of water, false walls of 0.060-inch Lucite (painted black) were installed to provide light-absorbing boundaries.

The optical properties of the bed containing the particle dispersion must approximate those of a hypothetical bed of identical thickness and of infinite lateral dimensions. An examination of the boundary conditions of the ideal infinite bed establishes what must be attained or approximated in the laboratory model. At the surface of the bed nearest the source, all light incident from the source must enter the bed (to ensure uniform illumination of the bed independent of the angle of incidence), while no light scattered from the bed can be reflected or scattered back into the bed. All light incident on the surface farthest from the source must be absorbed or transmitted from the bed so that it is not reflected back into the dispersion.

In the laboratory model an absorbing boundary at the surface away from the source was obtained by coating this surface with flat black paint. However, the surface nearest the source had to be transparent to light from both sides of the boundary irrespective of the angle of incidence. In order to minimize reflection it was necessary to define the surface of the bed nearest the source with a glass plate and to require that the source operate in a water-bath in contact with this glass plate. Thus, the index of refraction was the same on each side of the bed boundary, with the result that the critical angle of total reflection approached 90°. The water bath was then bounded by a light-absorbing surface (Lucite, painted black).

The approximation of the laboratory model to an infinite bed will be complete if the containing walls are sufficiently removed from the point of measurement so as not to affect the measurement in any way. Assuming that any intensity, I_w, scattered, reflected, or absorbed at these walls obeys the *Bouger-Beer* transmission equation, the resultant intensity, I, at the point of measurement from the boundary disturbance can be expressed as $I = I_w e^{-n\sigma_T d}$, where d is the distance from the wall to the point of measurement and n and σ_T are, respectively, the number of particles per unit volume and the scattering cross-section per particle. It was arbitrarily stipulated that the product $n\sigma_T d$ be no smaller than 5, which gives $I = I_w e^{-5}$. The value of e^{-5} is 0.007. Thus, any wall effects should be negligible in the measurements. The edges of the bed were painted black to prevent appreciable reflection, thus minimizing any disturbance at the boundary.

The dimensions of the bed were established in the following manner. The minimum value of $n\sigma_T l$ to be used in the experiments was set at 0.5. Choosing a bed thickness of 1 inch gave $n\sigma_T = 0.5$. Since this value of $n\sigma_T$ was the minimum to be used and $n\sigma_T d$ must be not less than 5, d must be at least 10 inches. The minimum lateral dimension (2d) of a bed 1 inch thick must therefore be at least 20 inches. The actual internal dimensions of the bed are 32 by 24 by 1.15 inches. The location of the light receiver is at the intersection of the diagonals of a 20-inch square taken at one end of the rectangle.

Water suspensions of polystyrene and polyvinyltoluene latexes obtained through the courtesy of the Dow Chemical Company, served as the dispersions. Four different dispersions, each containing particles of very uniform diameters (less than 2% standard deviation from the mean) were available in sufficient quantity. The particle diameters of these dispersions were 0.236, 0.333, 0.514 and 1.18 μ. These dispersions were obtained in a very concentrated form and were diluted to the desired concentrations. Values of $n\sigma_T l$ were obtained by light transmission techniques.[5]

The light source consisted of a General Electric Neon 69 glow lamp mounted on a movable arm to permit location of the source at any position in the tank. This source was selected, after an extensive laboratory study of various types of light sources, to fulfill the following conditions: (a) The source must be physically small so as to approach a point source. (b) It should emit light over a very limited band of wave lengths, *i.e.*, it should be nearly monochromatic. (c) It should radiate uniformly over the solid angle subtended by a cone having a half-angle of 35° in order to illuminate indiscriminately the entire boundary of the particle bed. (d) The source must be capable of operation under water.

The receiver consisted of a Dumont 6291 head-on type photomultiplier tube mounted in a magnetically shielded housing on the side of the tank bounding the bed. The receiver housing was extended through the glass wall of the tank by means of an O-ring seal and was bolted to the tank frame.

The electrical system consisted of a high-voltage, phototube power supply, a control and instrument panel, a powerstat and batteries for the light source—all mounted on a 6-foot-by-19-inch standard relay rack. All electrical measurements were made on a Leeds and Northrup Precision Portable Potentiometer.

The following calibrations were made after the experimental equipment was properly aligned and adjusted: (a) The direct proportionality of the output signal of the photomultiplier to the amount of light incident on the photocathode was established by a $1/r^2$ calibration. (b) The relationship between the output signal and the angle of incidence of light on the photocathode was established. This relationship, termed the acceptance function, was used in the reduction of the data. (c) The signal due to light reflected from the walls of the tank and scattered by dust particles in the water was determined by measuring the output of the receiver when it was shielded from direct illumination only.

Once the calibrations were completed, a series of measurements of the signal output voltages of the receiver was made as a function of the position of the light source with respect to the bed. These measurements were made with water in the bed and with latex dispersions of several concentrations for each of the four particle diameters, 0.236, 0.333, 0.514 and 1.18 μ. In all these experimental runs the receiver remained fixed in the base plane of the particle bed while the source position was varied.

The experimental data were expressed in terms of the monochromatic power interception function, $\bar{E}(\lambda)$, as defined above. Nineteen cases were studied experimentally in the range of variables: $n\sigma_T l$ (0.6–11.0), α (1.68–8.33), $\tan\theta$ (0–12).

A comparison between the experimental and theoretical values of the monochromatic power interception function, $\bar{E}(\lambda)$, is presented graphically in Figs. 3 through 10 for the four different values of α and the extremes in particle concentrations for each α, except for $\alpha = 8.33$. In this case measurements made on two more concentrated dispersions were not considered reliable because of agglomeration. Nine other intermediate concentrations for the various alphas were investigated but are not presented here. The solid line on these plots represents the value of $\bar{E}(\lambda)$ predicted theoretically by the six-flux method. The points shown on the plots were obtained experimentally.

Figures 3 through 10 show a dashed curve labeled "Experimental (Maximum Correction)," which lies above the experimental curve at large values of $\tan\theta$. In the experimental equipment the dispersion was separated from the tank by plate glass. Since the index of refraction of the material on both sides of the glass is the same, and since the glass plate is relatively thin, the path of the light is not materially affected. The surface of the glass, however, reflects light back into the water-bath, and the fraction of the light reflected is a function of the angle of incidence. In the six-flux analysis for a fixed position of the point source, the incident power per unit area at the surface of the bed varied only with the square of the distance from the source (*i.e.*, $E_0 = P_s/4\pi r_1^2$, where P_s is the source strength and r_1 is the distance from the source to any point on the surface of the dispersion). However, in the experimental work the reflection from the water–glass interface caused the incident power falling on the dispersion to be also a function of the angle of incidence. Therefore, the boundary conditions in the experimental and theoretical cases are not the same. The variation with the angle of incidence is more pronounced at high values of $\tan\theta$ because of the high reflection and resulting low transmission. It is impossible to make an

(5) R. O. Gumprecht and C. M. Sliepcevich, This Journal, **57**, 90 (1953).

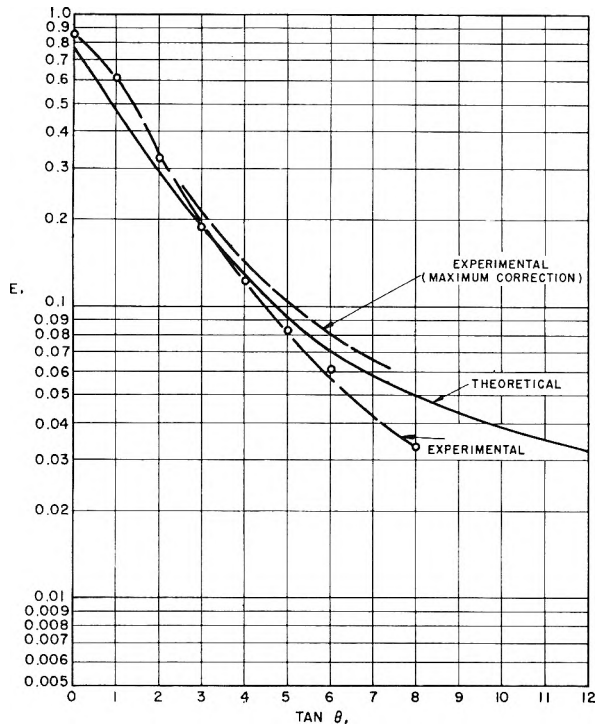

Fig. 3.—Comparison of the theoretical and experimental results at $\alpha = 1.68$, $n\sigma_T l = 1.03$.

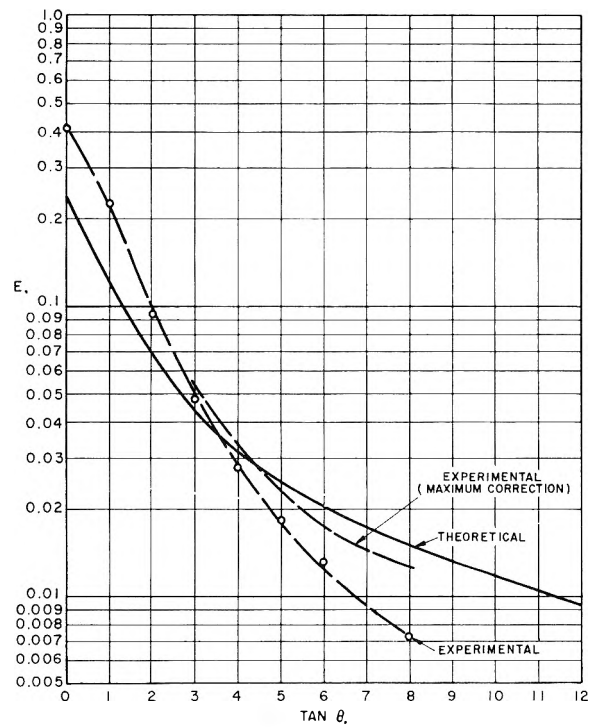

Fig. 4.—Comparison of the theoretical and experimental results at $\alpha = 1.68$, $n\sigma_T l = 11$.

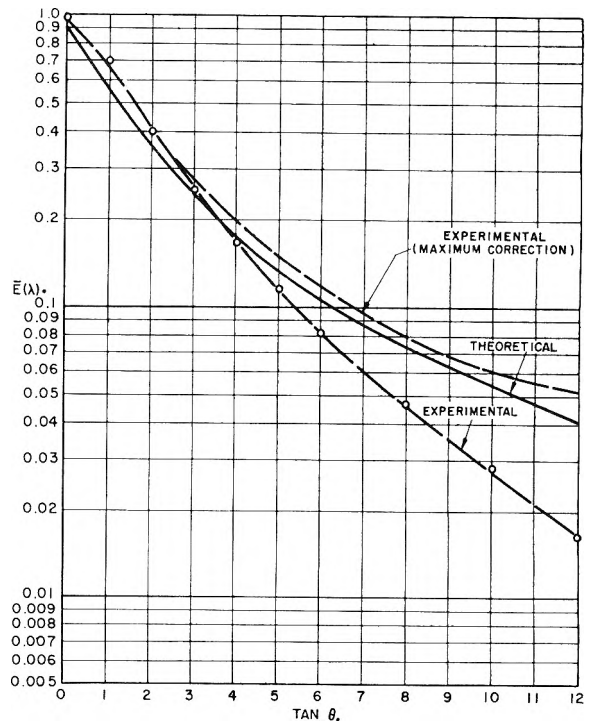

Fig. 5.—Comparison of the theoretical and experimental results at $\alpha = 2.36$, $n\sigma_T l = 0.630$.

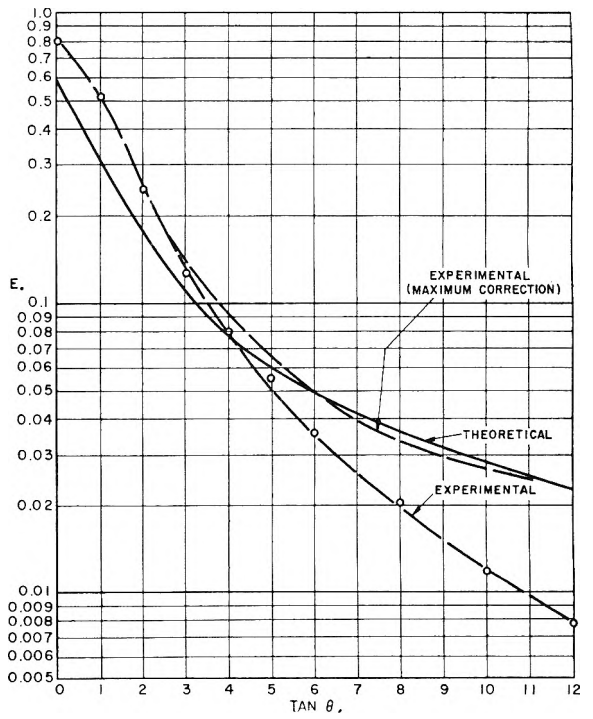

Fig. 6.—Comparison of the theoretical and experimental results at $\alpha = 2.36$, $n\sigma_T l = 3.66$.

exact correction for this effect since the light which the receiver intercepts with the dispersion present comes from a large area on the surface of the dispersion.

Because the light entering the laboratory dispersion from a point source is distributed over the entire surface of the glass boundary, the effect of boundary reflection on the collection of the scattered light by the receiver depends on two factors: (a) the fraction of light transmitted through the glass boundary at a point and (b) the fraction of light transmitted through the boundary at that point which is then scattered into the receiver. Both factors (a) and (b) are functions of the position on the boundary. Theoretically, at least, it is possible to determine a mean fraction of transmission for the entire boundary, weighted with respect to factor (b). From the transmission characteristics of the boundary calculated by Snell's law, this mean fraction of transmission may also be represented by an effective angle of incidence, *i.e.*, the angle at which the fraction of transmission has the calculated mean value. This effective angle, θ_e, is a function of θ and also depends on the optical properties and dimensions of the dispersion, but obviously

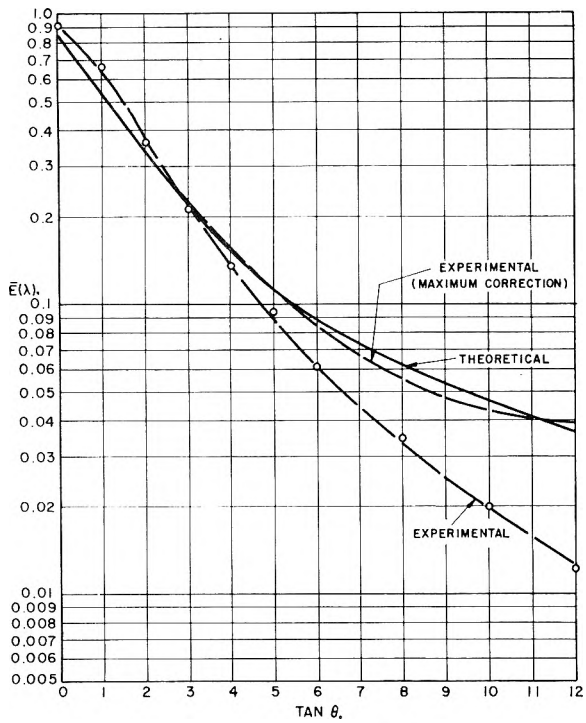

Fig. 7.—Comparison of the theoretical and experimental results at $\alpha = 3.64$, $n\sigma_T l = 1.54$.

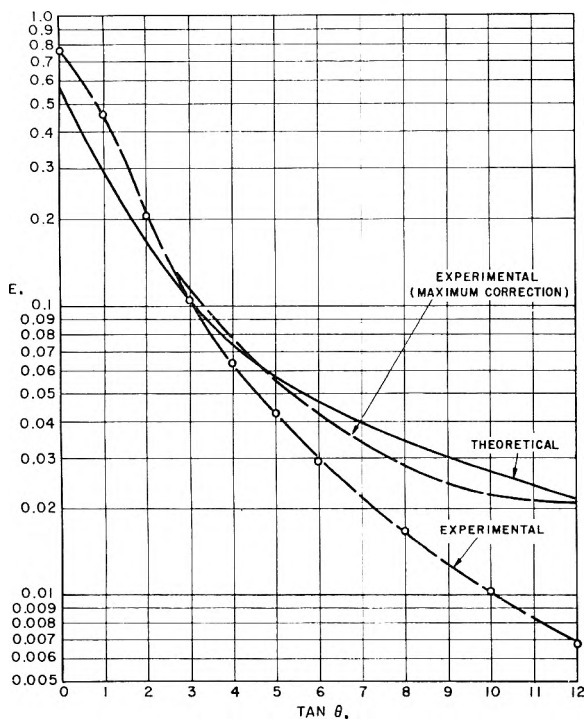

Fig. 8.—Comparison of the theoretical and experimental results at $\alpha = 3.64$, $n\sigma_T l = 6.75$.

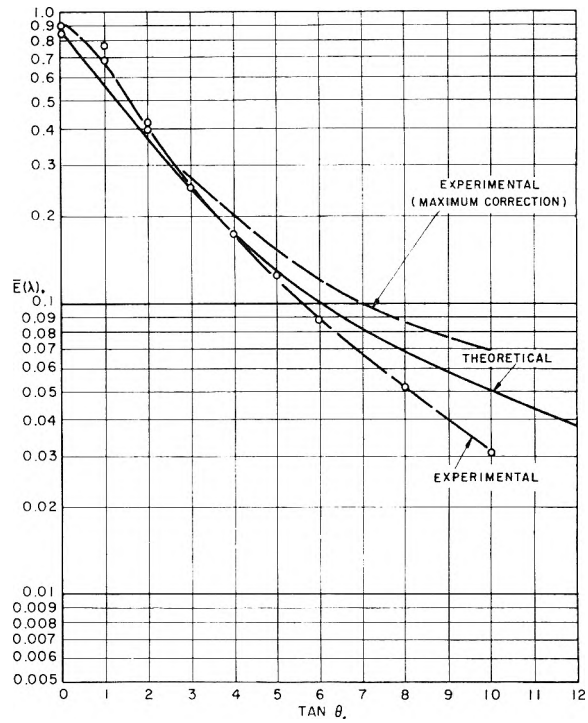

Fig. 9.—Comparison of the theoretical and experimental results at $\alpha = 8.33$, $n\sigma_T l = 1.30$.

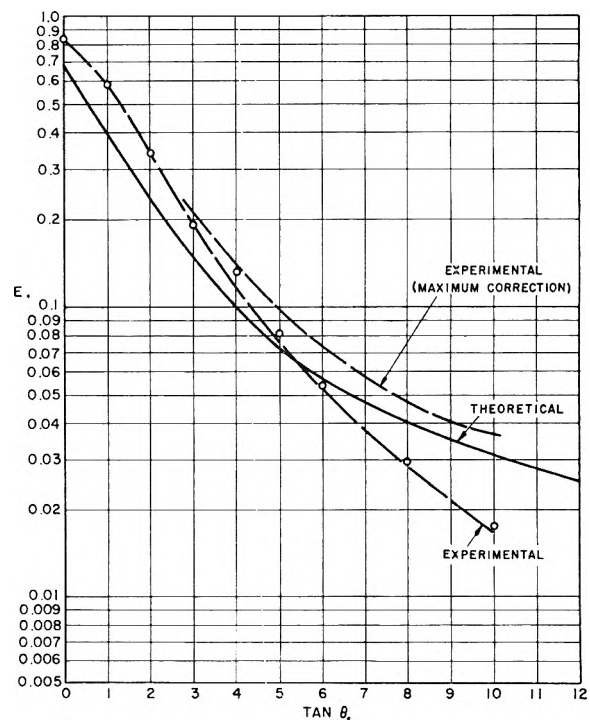

Fig. 10.—Comparison of the theoretical and experimental results at $\alpha = 8.33$, $n\sigma_T l = 4.01$.

it must be between θ and θ' as shown in Fig. 11. For the range of variables considered in the experimental study, θ_e always lies nearer to θ' than to θ. The angles θ, θ' and θ_e are illustrated in Fig. 12.

The experimental curves plotted in Figs. 3 through 10 were calculated from the data using values of the boundary transmission at the angle θ, while the curves labeled "experimental (maximum correction)" were calculated from the data using values of the boundary transmission at the angle θ'. These corrected curves are a more accurate representation of the data than the uncorrected curves.

The glass boundary also reflects some scattered light from the dispersion back into the dispersion. While this back reflection may be considered in effect as an increase in incident light, it is too small in magnitude to compensate for the loss of incident light from the source due to reflection at the glass boundary since the back-scattered light is always less than the incident light and is, moreover distributed. A small amount of light is also reflected into the bed from the receiver surface and the absorbing boundary. All these reflections tend to make the experimental value higher than the theoretical prediction. It is impossible to correct for

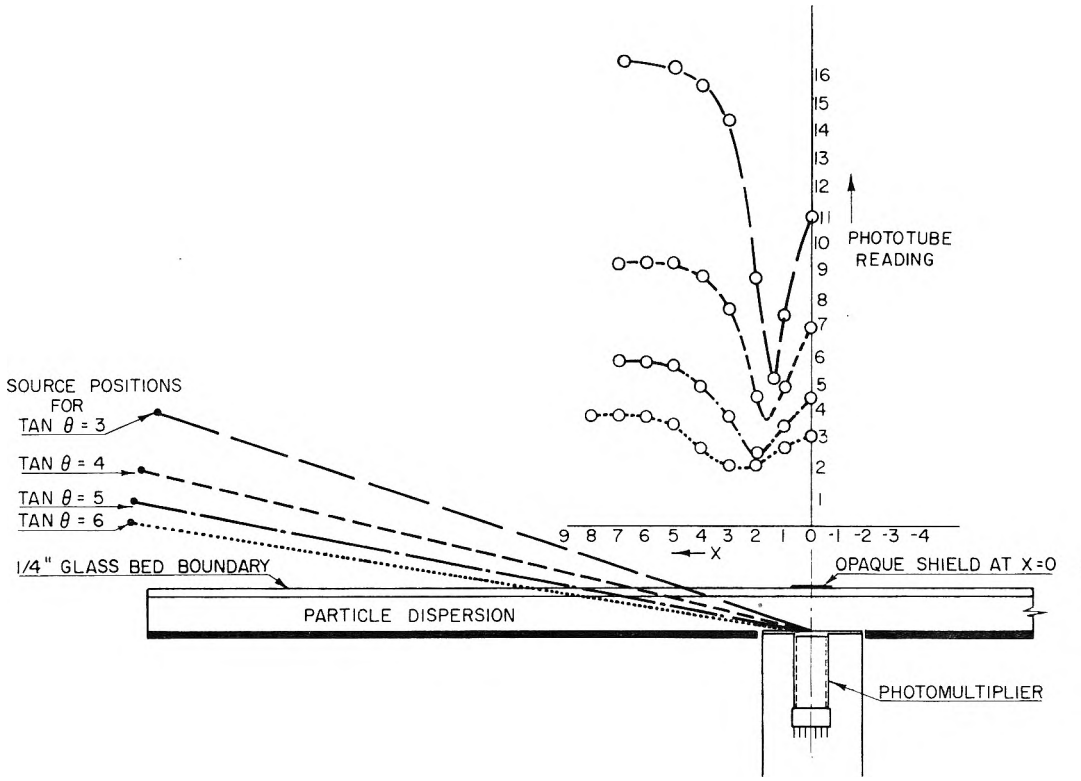

Fig. 11.—Power on photocathode as a function of X, the distance from the center of the opaque shield to the phototube normal.

any of these effects without a prior knowledge of the intensity distribution of the scattered light. However, these effects are small in comparison with the effect of the reflection of the incident light at the glass boundary and are therefore neglected.

In summary, there are five ways in which the experimental conditions differ from the conditions used in the theoretical investigation: (a) reflection of the incident light from the water-glass interface, (b) reflection of a portion of the scattered light back into the dispersion at the dispersion-glass interface, (c) reflection of light into the dispersion from the absorbing boundary of the dispersion, (d) reflection of light from the receiver back into the dispersion, and (e) reflection of light from the walls of the tank.

Condition (a) tends to make the experimental results low while the other four make them high for comparison with the theoretical. For the experimental conditions the effect of (a) is much greater than the combination of (b), (c) and (d) and, therefore, the experimental results would be expected to be low. Because of the difficulty in making corrections for the reflections in the bed, the experimental (maximum correction) curves include only the maximum correction for reflection of light directly from the source at the water–glass interface. Thus, the experimental results corresponding to the case considered theoretically must lie between the curves labeled experimental and experimental (maximum correction). The results of the experiments with an opaque shield at various positions along the boundary (see Fig. 11) indicate that the upper limit curves describe more nearly the physical situation treated theoretically. For this reason the upper limit curves were used for the evaluation of the accuracy of the theoretical results. In making this critical analysis, it is necessary to study not only the numerical magnitude of the theoretical values in relation to the experimental values but also the theoretical prediction of the effect of the various parameters. The accuracy of the theoretical prediction of the variation of $\bar{E}(\lambda)$ with tan θ can be observed by comparison of the theoretical curve with the experimental (maximum correction) curve. This comparison shows that the experimental and theoretical curves are essentially parallel at values of tan θ greater than 3.

The contribution to the receiver signal due to reflection from the tank walls is essentially constant and independent of the position of the source. Since, at high values of tan θ, the receiver signal due to direct light from the source was low, the per cent. contribution of wall reflection to the total receiver signal became correspondingly greater. The measurement of the wall reflection was somewhat uncertain in any case. Therefore, the experimental points at high values of tan θ are believed to be less accurate than those at low values of tan θ.

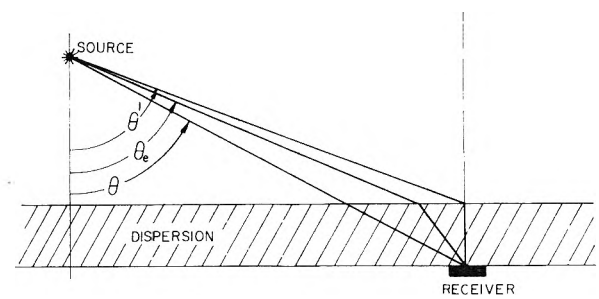

Fig. 12.—Geometric representation of the observed, effective, and maximum angles of incidence.

The accuracy of the theoretical variation of attenuation with optical thickness, $n\sigma_T t$, can be obtained most effectively by cross plotting both the experimental data and the theoretical values given in Figs. 3 through 10 as functions of $n\sigma_T t$, as shown in Fig. 13. The theoretical prediction of the effect of $n\sigma_T t$ is good for optical thicknesses greater than 1.0. At optical thicknesses below 1.0, the theoretical curve for $n\sigma_T t$ shows a greater effect on the attenuation than the experimental values indicate. The error in the theoretical values at low values of tan θ and $n\sigma_T t$ arises from the linearization of the differential equations and was anticipated.

The variation of $\bar{E}$ as a function of α can be observed from plots of $\bar{E}$ as a function of particle diameter at constant tan θ and $n\sigma_T t$. Such plots are not presented, but, in general,

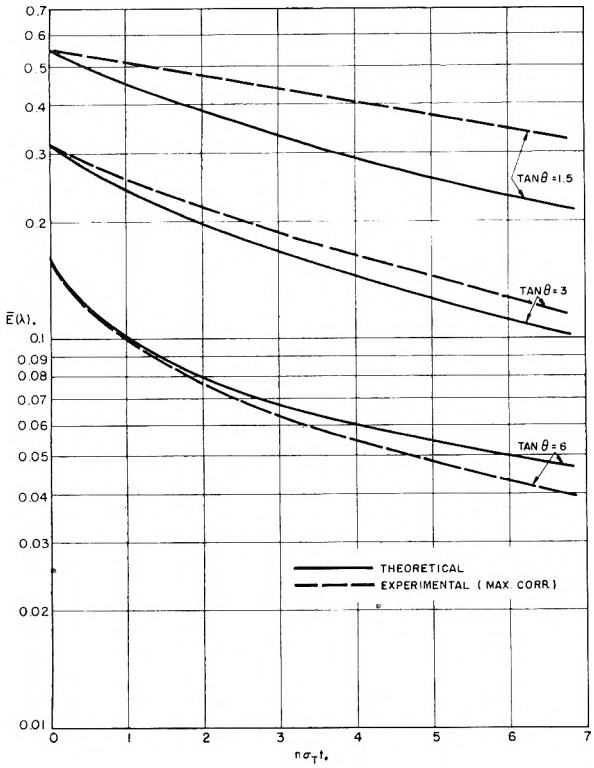

Fig. 13.—Comparison of the theoretical and experimental prediction of the effect of $n\sigma_T t$ on $\bar{E}$ for $\alpha = 3.64$.

the theoretical prediction agreed with the variation found experimentally. In the range of α considered, the transmission decreased with decreasing particle size.

Conclusion

A quantitative idea of the numerical magnitude of the difference between the theoretical prediction and the experimental results can be determined easily from Figs. 3 through 10. In general, the theoretical prediction of $\bar{E}$ is low at values of tan θ less than 3 and slightly high above tan $\theta = 3$. Below tan $\theta = 3$ the theoretical prediction is as much as 45% low and, generally, is low by 20–30%. Above tan $\theta = 3$ the agreement is much better and the experimental values range from about 20% below to about 20% above the theoretical prediction.

In general, the correlation between theory and experiment appears to justify the method of resolution of the continuous distribution of energy around a single particle into six components for this particular geometry.

Acknowledgment.—Professors S. W. Churchill and Chiao-Min Chu were of invaluable assistance throughout the course of this work. Dr. J. W. Vanderhoff of the Dow Chemical Company generously supplied the latex suspensions. Mr. Jin Chin of the University of Michigan measured the optical thickness of all the dispersions. Professor W. Heller and Mr. R. M. Tabibian of Wayne University, Detroit, Michigan, checked several of the measurements of optical thickness. Graduate students J. F. Shea, R. H. Boll and B. K. Larkin assisted in the experimental work. Dr. R. O. Gumprecht of General Electric Co., Hanford, Washington, and Mr. V. E. Kennedy, Jr., of Streeter–Amet Co., Chicago, Illinois, served as consultants.

NUMERICAL SOLUTION OF PROBLEMS IN MULTIPLE SCATTERING OF ELECTROMAGNETIC RADIATION[1,2]

BY CHIAO-MIN CHU[3] AND STUART W. CHURCHILL

Department of Chemical and Metallurgical Engineering, University of Michigan, Ann Arbor, Michigan

Received February 25, 1955

The steady-state scattering and absorption of electromagnetic radiation by dense dispersions of particles was investigated theoretically. The results should also have applicability in describing the behavior of thermal neutrons in dense material. Particular attention was given to dispersions of finite thickness and to anisotropic distribution of scattered energy characteristic of wave lengths less than the circumference of the particles. The objective was to find methods of solution suitable for numerical calculations. Existing analytical solutions of problems in multiple-scattering were found to be limited to isotropic scattering and/or dispersions of infinite extent. Approximate and numerical methods of solution proposed by previous investigators were evaluated with respect to accuracy and usability. A six-flux model was developed which reduces the general transport equation to a set of simple differential equations. Solutions suitable for numerical calculation can be obtained for most geometrical configurations of source and dispersion. An analytical solution is presented for an obliquely incident wave and a parallel-plane dispersion of finite thickness. Extension of the results to point and plane sources outside a dispersion is outlined. Degeneration of the six-flux model into a very simple two-flux model is also considered. The transmission through representative dispersions was calculated using the six-flux model, the simple two-flux model, and the diffusion equation, and the results are compared graphically.

Introduction

This paper presents the results of a theoretical investigation of the steady-state scattering of electromagnetic radiation by dense dispersions of uniformly sized particles. Point and plane sources, finite dispersions, and anisotropic distributions of radiation were considered. The objective of the work was to develop methods of solution suitable for the numerical calculation of radiant intensities at the boundaries and at interior points of a dispersion.

The interaction of electromagnetic radiation and single spherical particles is described by the Maxwell equations, and a series solution giving the angular distribution of scattered energy as well as the total amount of absorption and scattering has been presented by Mie.[4] The detailed calculations required for application of the Mie equations and the available values have been discussed by Gumprecht, *et al.*[5]

For thin dispersions of particles, such that the mean free path for radiation is large with respect to the dimensions of the dispersion, multiple scattering can be neglected and the scattering phenomena can be described by elementary mathematical application of the Mie results. For example, the transmission of scattered and unscattered radiation can be described with a simple modification of the Bouger–Beer law.[6]

For extensive dispersions, such that the mean free path for radiation is of the order of or less than the least dimension of the system, these simple expressions are inadequate. The importance of multiple scattering has been recognized in the transmission of stellar radiation, in thermal radiation through porous insulations, and in the transmission of light through fogs and colloidal suspensions.

The interaction of thermal neutrons with atomic nuclei results in similar phenomena, and most of the mathematical operations considered herein are applicable. The dependence of the interaction upon the velocity of the neutron and the mass of the nucleus is analogous to the dependence of the interaction of electromagnetic radiation upon the wave length and the particle diameter, but contrary to the invariant wave length characteristic of electromagnetic radiation, the neutron velocity decreases with interaction.

Analytical solutions of multiple-scattering problems are available and probably possible only for rather idealized conditions. Most attention in the literature has been given to isotropic scattering within dispersions of infinite extent, because such geometries are more tractable mathematically. In the present case, numerical solutions have been obtained for anisotropic scattering in dispersions having at least one finite dimension. The solutions are based on a new discrete-flux representation of scattering. The results are in the form of simple algebraic equations for six components of the flux at any position in the dispersion and require only the absorption cross section, the scattering cross section, and the angular distribution of single-scattered radiation from a particle. Degeneration of the six-flux solution to only two components gives results comparable to those obtained from classical diffusion theory and previously reported two-flux models.

Mathematical Formulation of Multiple Scattering.—The following variables are convenient for the mathematical expression of multiple scattering.

(1) The specific intensity, $i(\vec{R},\vec{\Omega})$, the energy intercepted per unit time by a unit area at $\vec{R}$, per unit steradian from the direction $\vec{\Omega}$ normal to the area, where $\vec{R}$ is the radial vector from the origin of the coördinate system and $\vec{\Omega}$ is a unit vector representing direction. In general $i(\vec{R}, \vec{\Omega})$ is a function of five variables, three for position and two for direction.

(1) Presented before the twenty-ninth National Colloid Symposium, held under the auspices of the Division of Colloid Chemistry of the American Chemical Society in Houston, Texas, June 20–22, 1955.

(2) This paper reports work done through the Engineering Research Institute of the University of Michigan, under contract with the Army Chemical Corps, Washington 25, D. C.

(3) Associate Professor of Electrical Engineering, Detroit Institute of Technology, Detroit, Michigan.

(4) Gustav Mie, *Ann. Physik*, **25**, 377 (1908).

(5) R. O. Gumprecht, N. L. Sung, J. H. Chin and C. M. Sliepcevich, *J. Opt. Soc. Am.*, **42**, 226 (1952).

(6) R. O. Gumprecht and C. M. Sliepcevich, THIS JOURNAL, **57**, 90 (1953).

(2) The number of particles per unit volume of the dispersion, N.

(3) The effective cross sections of a particle for scattering, σ_s, for absorption, σ_a, and for total interaction, $\sigma_t = \sigma_s + \sigma_a$. These cross sections are functions of the index of refraction, the dimensions of the particle, and the wave length of the radiation.

(4) The albedo for single scattering, $\omega = \sigma_s/\sigma_t$.

(5) The mean free paths, $\lambda_s = 1/N\sigma_s$, $\lambda_a = 1/N\sigma_a$ and $\lambda_t = 1/N\sigma_t$ for scattering, absorption and interception, respectively.

(6) The angular distribution function, for single scattering, $f_1(\vec{\Omega}, \vec{\Omega}')$, which gives the fraction of energy scattered from a beam with the direction, $\vec{\Omega}'$, into a unit steradian in the direction, $\vec{\Omega}$. It is a function of the index of refraction, the dimensions of the particle, and the wave length of the radiation. For spherical particles the angular distribution is symmetrical about the direction of the incident radiation and may be expressed in terms of a single angle, θ, measured from the incident direction, *i.e.*, $f_1(\vec{\Omega}, \vec{\Omega}')$, reduces to $f_1(\theta)$, as illustrated in Fig. 1(a).

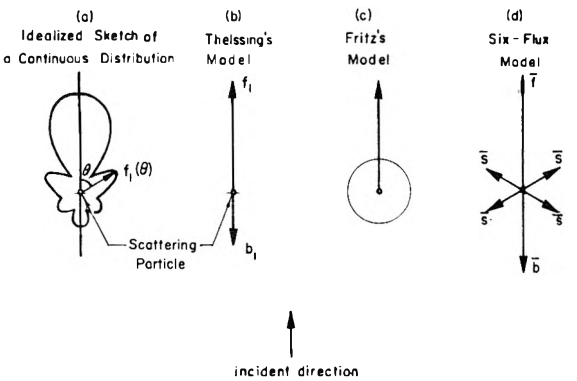

Fig. 1.—Angular distribution of radiation from a single scattering.

From an energy balance over a volume in the dispersion of unit cross section and length $dS_{\vec{\Omega}}$ along $\vec{\Omega}$, the following integro-differential equation, generally known as the transport equation, is obtained.

$$\frac{di(\vec{R},\vec{\Omega})}{dS_{\vec{\Omega}}} = -N\sigma_t i(\vec{R},\vec{\Omega}) + N\sigma_s \int_{\Omega'} i(\vec{R},\vec{\Omega}') f_1(\vec{\Omega},\vec{\Omega}')d\Omega' \quad (1)$$

net rate of increase of intensity in the direction $\vec{\Omega}$ | rate of decrease of intensity in the direction $\vec{\Omega}$ due to interception | rate of increase of intensity due to scattering into the direction $\vec{\Omega}$

The integral term in eq. 1 thus introduces the contribution of multiple scattering.

Previous Methods of Solution.—Exact solutions of the multiple-scattering problem have been discussed by Chandrasekhar,[7] Grosjean[8] and Case,[9] but the practical application of these integral solutions is limited to isotropic scattering and infinite dispersions. In principle, series solutions can be obtained by using quadrature,[10] spherical harmonics[11] or reiteration. However, analytical expressions can be obtained only for simple geometries and even in these cases the numerical calculations are exceedingly detailed.

The Monte Carlo method of numerical analysis has been suggested for neutron-scattering problems.[12] Exploratory calculations indicated that the computing requirements were excessive in comparison with numerical evaluation of the analytical solution obtained for a six-flux model of comparable accuracy.

Representation of the specific intensity by a two-term series of spherical harmonics permits reduction of the transport equation to the classical diffusion equation. The diffusion equation can be solved by elementary methods, but the results are of limited accuracy as noted by Glasstone and Edlund.[13]

If the angular distribution of radiation from a single scattering is represented by one or more components, the transport equation can be reformulated as a set of relatively simple differential equations, and analytical solutions may be possible. Theissing[14] formulated a two-flux model in which the scattered radiation was confined to the forward and backward direction, as illustrated in Fig. 1(b). Hartel's[15] approximate distribution for the kth scattered radiation was utilized, and energy balances were written for each individual order of scattering. Fritz[16] represented the radiation from a single scattering by a forward component and an isotropically distributed component as indicated in Fig. 1(c) and obtained a numerical solution by a stepwise procedure. The models of Theissing and Fritz should yield more accurate results than the diffusion equation.

A Six-flux Model.—Representation of the angular distribution of radiation scattered by a single particle by six discrete components and hence the specific intensity within a dense dispersion by six corresponding components should yield a more accurate description of scattering phenomena than the two-component representations of Thiessing and Fritz. The development of such a six-flux representation and the resulting solution of the transport equation for several scattering problems are outlined in the following paragraphs.

The angular distribution function for single scattering by spherical particles, $f_1(\theta)$, is represented by a forward-scattering component, $\bar{f}$, by a backward-scattering component, $\bar{b}$, and, because of symmetry, by four equal sidewise-scatter-

(7) S. Chandrasekhar, "Radiative Transfer," Oxford University Press, London, 1950.

(8) C. C. Grosjean, "The Exact Mathematical Theory of Multiple Scattering of Particles in an Infinite Medium," Verhandelingen af de Konicklike Vlaamse Acad. (Belgium), Jaargang XIII, No. 36, 1951.

(9) K. M. Case, F. de Hoffmann and G. Placzek, "Introduction to the Theory of Neutron Diffusion," Vol. I, Government Printing Office (1953), (Los Alamos Scientific Laboratory, Washington, D. C.)

(10) V. Kourganoff, "Basie Methods in Transfer Problems," Oxford University Press, London, 1952.

(11) J. C. Mark, "The Spherical Harmonic Method," Vols. I and II, Nat. Res. Coun. Can., CRT-340 and CRT-338 (June, 1947).

(12) "Monte Carlo Method," Government Printing Office (1951), (National Bureau of Standards Applied Mathematics Series, No. 12), Washington, D. C.

(13) S. Glasstone and M. C. Edlund, "Elements of Nuclear Reactor Theory," D. Van Nostrand Co., New York, N. Y., 1952.

(14) H. H. Theissing, *J. Opt. Soc.*, **40**, 232 (1950).

(15) W. Hartel, *Das Licht*, **40**, 141 (1940).

(16) S. Fritz, Ph.D. Thesis, M.I.T., 1953.

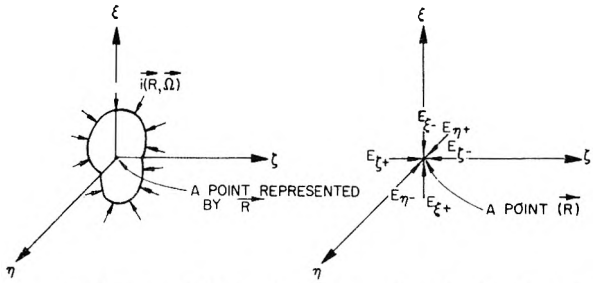

Fig. 2.—Representation of specific intensity by discrete components.

ing components, $\bar{s}$, as shown in Fig. 1(d). The division or resolution of the continuous distribution of scattered radiation into a finite number of discrete components, *i.e.*, the definition of $\bar{f}$, $\bar{b}$ and $\bar{s}$ in terms of $f_1(\theta)$, is obviously arbitrary and cannot be justified except from a practical standpoint. Although certain limitations, including convergence of the components to equality for an isotropic distribution ($f_1(\theta) = 1/4\pi$) and the conservation of energy, are imposed, the criterion for definition should be the accuracy of the over-all solution. Suggested definitions, having some physical significance are given below, but the results of the six-flux solutions are presented in general terms and are directly applicable if the components are defined in some alternate manner or if they are fitted experimentally.

The direct allotment of the energy passing through the six faces of a cube into the six corresponding normal directions satisfies the conservation and isotropy limitations, but appears to underrate the sidewise component for forward-peaked distributions, *i.e.*, the neglect of the forward inclination of part of the beam through the side-oriented face is insufficiently compensated for by the neglect of the sidewise inclination of the more intense beam through the forward-oriented face.

The direct vectorial resolution of energy, *i.e.*, by the cosine law, is non-conservative. However, the representation

$$\bar{f} = 2\pi \int_0^{\pi/2} f_1(\theta) \cos^2\theta \sin\theta \, d\theta \qquad (2)$$

$$\bar{b} = 2\pi \int_{\pi/2}^{\pi} f_1(\theta) \cos^2\theta \sin\theta \, d\theta \qquad (3)$$

$$\bar{s} = (1 - \bar{f} - \bar{b})/4 \qquad (4)$$

is conservative and degenerates to $\bar{f} = \bar{b} = \bar{s} = 1/6$ for an isotropic distribution. This representation, which is recommended in the absence of generous data for multiple-scattering problems, can be interpreted physically as the vectorial resolution of the momentum of the scattered photons.

The six discrete components of the specific intensity, $i(\vec{R}, \vec{\Omega})$, are chosen in the direction of, and opposite to, the direction of the three major axes of any orthogonal system of coördinates. However, the proper choice of the coördinate system may greatly affect the accuracy of the six-flux approximation. As a general rule, one of the axes should have the direction of the incident radiation, since the flux in that direction will generally be predominant. The remaining two axes should be chosen from consideration of the boundaries of the dispersion. The significance of the components of $i(\vec{R}, \vec{\Omega})$, illustrated in Fig. 2, is obvious; *i.e.*, if an elementary area, dA, is placed at the point R, perpendicular to the ξ axis, then the power received on the under side is $E_\xi + dA$ and that on the top side is $E_\xi - dA$. The four sidewise components, $E_{\zeta+}$, $E_{\zeta-}$, $E_{\eta+}$ and $E_{\eta-}$, are not necessarily equal although it may be possible to make two or four of them equal for certain symmetrical configurations of source and dispersion.

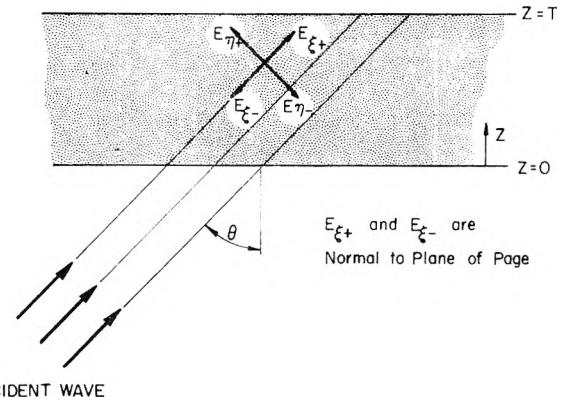

Fig. 3.—Six-flux representation for a plane-parallel dispersion and an obliquely-incident wave.

By introduction of the six components of the specific intensity and of the angular distribution function into the transport equation, or by writing an energy balance around an elementary volume, dV, of sides $d\xi$, $d\eta$ and $d\zeta$, the following set of differential equations is obtained

$$\frac{1}{N\sigma_t}\frac{d}{dV}[E_{\xi+} d\eta d\zeta] = -[1 - \omega\bar{f}]E_{\xi+} + \omega\bar{b}E_{\xi-} + \omega\bar{s}[E_{\eta+} + E_{\eta-} + E_{\zeta+} + E_{\zeta-}] \qquad (5)$$

$$-\frac{1}{N\sigma_t}\frac{d}{dV}[E_{\xi-} d\eta d\zeta] = -[1 - \omega\bar{f}]E_{\xi-} + \omega\bar{b}E_{\xi+} + \omega\bar{s}[E_{\eta+} + E_{\eta-} + E_{\zeta+} + E_{\zeta-}] \qquad (6)$$

$$\frac{1}{N\sigma_t}\frac{d}{dV}[E_{\eta+} d\xi d\zeta] = -[1 - \omega\bar{f}]E_{\eta+} + \omega\bar{b}E_{\eta-} + \omega\bar{s}[E_{\xi+} + E_{\xi-} + E_{\zeta+} + E_{\zeta-}] \qquad (7)$$

$$-\frac{1}{N\sigma_t}\frac{d}{dV}[E_{\eta-} d\xi d\zeta] = -[1 - \omega\bar{f}]E_{\eta-} + \omega\bar{b}E_{\eta+} + \omega\bar{s}[E_{\xi+} + E_{\xi-} + E_{\zeta+} + E_{\zeta-}] \qquad (8)$$

$$\frac{1}{N\sigma_t}\frac{d}{dV}[E_{\zeta+} d\eta d\xi] = -[1 - \omega\bar{f}]E_{\zeta+} + \omega\bar{b}E_{\zeta-} + \omega\bar{s}[E_{\xi+} + E_{\xi-} + E_{\eta+} + E_{\eta-}] \qquad (9)$$

$$-\frac{1}{N\sigma_t}\frac{d}{dV}[E_{\zeta-} d\eta d\xi] = -[1 - \omega\bar{f}]E_{\zeta-} + \omega\bar{b}E_{\zeta+} + \omega\bar{s}[E_{\xi+} + E_{\xi-} + E_{\eta+} + E_{\eta-}] \qquad (10)$$

The solution of equations 5 through 10 and approximation of the specific intensity, $i(\vec{R}, \vec{\Omega})$, from six components obtained will be considered for several geometries.

Parallel-plane Dispersion and an Obliquely-incident Parallel Wave.—For this configuration, which is illustrated in Fig. 3, the three principal axes may be chosen as follows: (i) ξ-axis, in the direction of the incident beam; (ii) η-axis, perpendicular to ξ-axis and in the plane of incidence (the plane of incident is determined by the direction of the inci-

dent, beam and the normal-to-the-plane boundary of the dispersion); and (iii) ζ-axis, perpendicular to the plane of incidence, and hence parallel to the boundary of the parallel-plane dispersion, so that in the (Z,θ) coördinate system

$$d\xi = \sec\theta\, dZ \tag{11}$$
$$d\eta = \csc\theta\, dZ \tag{12}$$
$$dV = \sec\theta \csc\theta (dZ)^2\, d\zeta \tag{13}$$

Substituting in equations 5 through 10, abbreviating the subscripts ξ_+, ξ_-, ζ_+, ζ_-, η_+ and η_- with 1, 2, 3, 4, 5 and 6, and noting from symmetry that $E_5 = E_6$, gives the following set of linear equations

$$\frac{dE_1}{dZ} = -C_1 \sec\theta\, E_1 + C_2 \sec\theta\, E_2 + C_3 \sec\theta\,(E_3 + E_4) \tag{14}$$

$$-\frac{dE_2}{dZ} = -C_1 \sec\theta\, E_2 + C_2 \sec\theta\, E_1 + C_3 \sec\theta\,(E_3 + E_4) \tag{15}$$

$$\frac{dE_3}{dZ} = -C_1 \csc\theta\, E_3 + C_2 \csc\theta\, E_3 + C_3 \csc\theta\,(E_1 + E_2) \tag{16}$$

$$-\frac{dE_4}{dZ} = -C_1 \csc\theta\, E_4 + C_2 \csc\theta\, E_3 + C_3 \csc\theta\,(E_1 + E_2) \tag{17}$$

and

$$E_5 = E_6 = \left(\frac{\omega\bar{s}}{1 - \omega\bar{f} - \omega\bar{b}}\right)(E_1 + E_2 + E_3 + E_4) \tag{18}$$

where

$$C_1 = \left(1 - \omega\bar{f} - \frac{2\omega^2\bar{s}^2}{1 - \omega\bar{f} - \omega\bar{b}}\right) N\sigma_t \tag{19}$$

$$C_2 = \left(\omega\bar{b} + \frac{2\omega^2\bar{s}^2}{1 - \omega\bar{f} - \omega\bar{b}}\right) N\sigma_t \tag{20}$$

$$C_3 = \left(\omega\bar{s} + \frac{2\omega^2\bar{s}^2}{1 - \omega\bar{f} - \omega\bar{b}}\right) N\sigma_t \tag{21}$$

A general solution can be obtained by classical methods. Since the differential equations are linear, all the components of the specific intensity can be expressed as linear combinations of $e^{p_1 Z}$, $e^{p_2 Z}$, $e^{p_3 Z}$ and $e^{p_4 Z}$, where the eigenvalues are

$$p_{1,2} = p_{3,4} = \left[\tfrac{1}{2}\left\{1 \pm \sqrt{1 - \sin^2 2\theta \left(\frac{(C_1 - C_2)^2 - 4C_3^2}{(C_1 - C_2)^2}\right)}\right\}\right]^{1/2} \sqrt{C_1^2 - C_2^2}\sec\theta\csc\theta \tag{22}$$

For the case of no absorption

$$p_{1,2} = \pm p = N\sigma_t \sqrt{(2\bar{b} + 4\bar{s})(3\bar{s})}\sec\theta\csc\theta \tag{23}$$
$$p_3 = p_4 = 0 \tag{24}$$

so that a linear term in Z must be included in the general solution.

For a source of unit power per unit area at one boundary and no entering power (corresponding to either complete absorption or escape) at the other boundary of a dispersion of thickness, T, the boundary conditions can be written

$$E_1 = 1 \text{ and } E_3 = 0 \text{ at } Z = 0$$
$$E_2 = E_4 = 0 \text{ at } Z = T$$

and the following particular solution is obtained

$$E_1 = \frac{A_{11}}{\Delta} e^{-p_1 Z} + \frac{A_{12}}{\Delta} e^{-p_1(T-Z)} + \frac{A_{13}}{\Delta} e^{-p_2 Z} + \frac{A_{14}}{\Delta} e^{-p_2(T-Z)} \tag{25}$$

$$E_2 = \frac{A_{21}}{\Delta} e^{-p_1 Z} + \frac{A_{22}}{\Delta} e^{-p_1(T-Z)} + \frac{A_{23}}{\Delta} e^{-p_2 Z} + \frac{A_{24}}{\Delta} e^{-p_2(T-Z)} \tag{26}$$

$$E_3 = \frac{A_{31}}{\Delta} e^{-p_1 Z} + \frac{A_{32}}{\Delta} e^{-p_1(T-Z)} + \frac{A_{33}}{\Delta} e^{-p_2 Z} + \frac{A_{34}}{\Delta} e^{-p_2(T-Z)} \tag{27}$$

$$E_4 = \frac{A_{41}}{\Delta} e^{-p_1 Z} + \frac{A_{42}}{\Delta} e^{-p_1(T-Z)} + \frac{A_{43}}{\Delta} e^{-p_2 Z} + \frac{A_{44}}{\Delta} e^{-p_2(T-Z)} \tag{28}$$

where

$$\Delta = (a_1b_3 - a_3b_1)^2 - (a_2b_3 - a_3b_2)^2 e^{-p_1 T} - (a_1b_4 - a_4b_1)^2 e^{-2p_2 T} + 2(a_1b_2 - a_2b_1)(a_3b_4 - a_4b_3)e^{-(p_1 + p_2)T} + (a_2b_4 - a_4b_2)^2 e^{-2(p_1 + p_2)T} \tag{29}$$

$$A_{11} = a_1b_3(a_1b_3 - a_3b_1) - a_1b_4(a_1b_4 - a_4b_1)e^{-2p_2 T} + a_1b_2(a_3b_4 - a_4b_3)e^{-(p_1 - p_2)T} \tag{30}$$

$$A_{21} = a_2b_3(a_1b_3 - a_3b_1) - a_2b_4(a_1b_4 - a_4b_1)e^{-2p_2 T} + a_2b_2(a_3b_4 - a_4b_3)e^{-(p_1 - p_2)T} \tag{31}$$

$$A_{31} = b_1b_3(a_1b_3 - a_3b_1) - b_1b_4(a_1b_4 - a_4b_1)e^{-2p_2 T} + b_1b_2(a_3b_4 - a_4b_3)e^{-(p_1 + p_2)T} \tag{32}$$

$$A_{41} = b_2b_3(a_1b_3 - a_3b_1) - b_2b_4(a_1b_4 - a_4b_1)e^{-2p_2 T} + b_2(a_3b_4 - a_4b_3)e^{-(p_1 + p_2)T} \tag{33}$$

$$A_{12} = -a_2b_3(a_2b_3 - a_3b_2)e^{-p_1 T} - a_2b_1(a_3b_4 - a_4b_3)e^{-p_2 T} + a_2b_4(a_2b_4 - a_4b_2)e^{-(p_1 + 2p_2)T} \tag{34}$$

$$A_{22} = -a_1b_3(a_2b_3 - a_3b_2)e^{-p_1 T} - a_1b_1(a_3b_4 - a_4b_3)e^{-p_2 T} + a_1b_4(a_2b_4 - a_4b_2)e^{-(p_1 + 2p_2)T} \tag{35}$$

$$A_{32} = -b_2b_3(a_2b_3 - a_3b_2)e^{-p_1 T} - b_2b_1(a_3b_4 - a_4b_3)e^{-p_2 T} + b_2b_4(a_2b_4 - a_4b_2)e^{-(p_1 + 2p_2)T} \tag{36}$$

$$A_{42} = -b_1b_3(a_2b_3 - a_3b_2)e^{-p_1 T} - b_1^2(a_3b_4 - a_4b_3)e^{-p_2 T} + b_1b_4(a_2b_4 - a_4b_2)e^{-(p_1 + 2p_2)T} \tag{37}$$

$$A_{13} = -a_3b_1(a_1b_3 - a_3b_1) + a_3b_2(a_2b_3 - a_3b_2)e^{-2p_1 T} + a_3b_4(a_1b_2 - a_2b_1)e^{-(p_1 + p_2)T} \tag{38}$$

$$A_{23} = -a_4b_1(a_1b_3 - a_3b_1) + a_4b_2(a_2b_3 - a_3b_2)e^{-2p_1 T} + a_4b_4(a_1b_2 - a_2b_1)e^{-(p_1 + p_2)T} \tag{39}$$

$$A_{33} = -b_3b_1(a_1b_3 - a_3b_1) + b_3b_2(a_2b_3 - a_3b_2)e^{-2p_1 T} + b_3b_4(a_1b_2 - a_2b_1)e^{-(p_1 + p_2)T} \tag{40}$$

$$A_{43} = -b_4b_1(a_1b_3 - a_3b_1) + b_4b_2(a_2b_3 - a_3b_2)e^{-2p_1 T} + b_4^2(a_1b_2 - a_2b_1)e^{-(p_1 + p_2)T} \tag{41}$$

$$A_{14} = -a_4b_3(a_1b_2 - a_2b_1)e^{-p_1 T} + a_3b_1(a_1b_4 - a_4b_1)e^{-p_2 T} - a_1b_2(a_2b_4 - a_4b_2)e^{-(2p_1 + p_2)T} \tag{42}$$

$$A_{24} = -a_3b_3(a_1b_2 - a_2b_1)e^{-p_1 T} + a_3b_1(a_1b_4 - a_4b_1)e^{-p_2 T} - a_1b_2(a_2b_4 - a_4b_2)e^{-(2p_1 + p_2)T} \tag{43}$$

$$A_{34} = -b_4b_3(a_1b_2 - a_2b_1)e^{-p_1 T} + b_4b_1(a_1b_4 - a_4b_1)e^{-p_2 T} - b_2b_2(a_2b_4 - a_4b_2)e^{-(2p_1 + p_2)T} \tag{44}$$

$$A_{44} = -b_3(a_1b_2 - a_2b_1)e^{-p_1 T} + b_3b_1(a_1b_4 - a_4b_1)e^{-p_2 T} - b_2b_2(a_2b_4 - a_4b_2)e^{-(2p_1 + p_2)T} \tag{45}$$

$$a_1 = \frac{(C_1 - C_2)\sec\theta + p_1}{(C_1 - C_2)\sec\theta} \tag{46}$$

$$a_2 = \frac{(C_1 - C_2)\sec\theta - p_1}{(C_1 - C_2)\sec\theta} \tag{47}$$

$$a_3 = \frac{(C_1 - C_2)\sec\theta + p_2}{(C_1 - C_2)\sec\theta} \tag{48}$$

$$a_4 = \frac{(C_1 - C_2)\sec\theta - p_2}{(C_1 - C_2)\sec\theta} \tag{49}$$

$$b_1 = \frac{(C_1^2 - C_2^2)\sec^2\theta - p_1^2}{2(C_1 - C_2)C_3\sec^2\theta} \frac{(C_1 - C_2)\csc\theta + p_1}{(C_1 - C_2)\csc\theta} \tag{50}$$

$$b_2 = \frac{(C_1^2 - C_2^2)\sec^2\theta - p_1^2}{2(C_1 - C_2)C_3\sec^2\theta} \frac{(C_1 - C_2)\csc\theta - p_1}{(C_1 - C_2)\csc\theta} \tag{51}$$

$$b_3 = \frac{(C_1^2 - C_2^2)\sec^2\theta - p_2^2}{2(C_1 - C_2)C_3\sec^2\theta} \frac{(C_1 - C_2)\csc\theta + p_2}{(C_1 - C_2)\csc\theta} \tag{52}$$

$$b_4 = \frac{(C_1^2 - C_2^2)\sec^2\theta - p_2^2}{2(C_1 - C_2)C_3\sec^2\theta}\,\frac{(C_1 - C_2)\csc\theta - p_2}{(C_1 - C_2)\csc\theta} \quad (53)$$

For no absorption, the corresponding solution is

$$E_1 = \frac{1}{\Delta}\{A_{11}e^{-p(T-Z)} + A_{12}e^{-p(Z)} + CA_{13}(Z) + [A_{14} - A_{13}\cos\theta]\} \quad (54)$$

$$E_2 = \frac{1}{\Delta}\{A_{21}e^{-p(T-Z)} + A_{22}e^{-p(Z)} + CA_{23}(Z) + [A_{24} + A_{23}\cos\theta]\} \quad (55)$$

$$E_3 = \frac{1}{\Delta}\{A_{31}e^{-p(T-Z)} + A_{32}e^{-p(Z)} + CA_{33}(Z) + [A_{34} - A_{33}\sin\theta]\} \quad (56)$$

$$E_4 = \frac{1}{\Delta}\{A_{41}e^{-p(T-Z)} + A_{42}e^{-p(Z)} + CA_{43}(Z) + [A_{44} + A_{43}\sin\theta]\} \quad (57)$$

$$E_5 = E_6 = \frac{1}{4}[E_1 + E_2 + E_3 + E_4] \quad (58)$$

where

$$A_{11} = \sin\theta(\sin\theta - u)A_1 \quad (59)$$

$$A_{21} = \sin\theta(\sin\theta + u)A_1 \quad (60)$$

$$A_{31} = -\cos\theta(\cos\theta - u)A_1 \quad (61)$$

$$A_{41} = -\cos\theta(\cos\theta + u)A_1 \quad (62)$$

$$A_{12} = \sin\theta(\sin\theta + u)A_2 \quad (63)$$

$$A_{22} = \sin\theta(\sin\theta - u)A_2 \quad (64)$$

$$A_{32} = -\cos\theta(\cos\theta + u)A_2 \quad (65)$$

$$A_{42} = -\cos\theta(\cos\theta - u)A_2 \quad (66)$$

$$A_{13} = A_{23} = A_{33} = A_{43} = A_3 \quad (67)$$

$$A_{14} = A_{24} = A_{34} = A_{44} = A_4 \quad (68)$$

$$\Delta = CT[\sin\theta(\sin\theta + u) + \cos\theta(\cos\theta + u)]^2 + 2[\sin\theta(\sin\theta + u) + \cos\theta(\cos\theta + u)][\sin^2\theta(\sin\theta + u) + \cos^2\theta(\cos\theta + u)] - 4u(\cos\theta - \sin\theta)^2\cos\theta\sin\theta\, e^{-pT} \quad (69)$$
$$- e^{-2pT}\{CT[\sin\theta(\sin\theta - u) + \cos\theta(\cos\theta - u)]^2 + 2[\sin\theta(\sin\theta - u) + \cos\theta(\cos\theta - u)][\sin^2\theta(\sin\theta - u) + \cos^2\theta(\cos\theta - u)]\}$$

$$A_1 = \cos\theta(\cos\theta + u)(\cos\theta - \sin\theta) - e^{-pT}CT[\sin\theta(\sin\theta - u) + \cos\theta(\cos\theta - u)] - e^{-pT}[2\sin^2\theta(\sin\theta - u) + \cos\theta(\cos\theta + \sin\theta)(\cos\theta - u)] \quad (70)$$

$$A_2 = CT[\sin\theta(\sin\theta + u) + \cos\theta(\cos\theta + u)] + 2\sin^2\theta(\sin\theta + u) + \cos\theta(\cos\theta + \sin\theta)(\cos\theta + u) - e^{-pT}\cos\theta(\cos\theta - u)(\cos\theta - \sin\theta) \quad (71)$$

$$A_3 = -\{\cos\theta(\cos\theta + u)[\sin\theta(\sin\theta + u) + \cos\theta(\cos\theta + u)] - e^{-pT}2u\sin\theta\cos\theta(\cos\theta - \sin\theta) - e^{-2pT}\cos\theta(\cos\theta - u)[\sin\theta(\sin\theta - u) + \cos\theta(\cos\theta - u)]\} \quad (72)$$

$$A_4 = CT\cos\theta(\cos\theta + u)[\sin\theta(\sin\theta + u) + \cos\theta(\cos\theta + u)] + \cos\theta(\cos\theta + u)[\sin^2\theta(\sin\theta + u) + \cos^2\theta(\cos\theta + u)] + e^{-pT}2u\sin^2\theta\cos\theta(\cos\theta - \sin\theta) - e^{-2pT}\cos\theta(\cos\theta - u)\{CT[\sin\theta(\sin\theta - u) + \cos\theta(\cos\theta - u)] + [\sin^2\theta(\sin\theta - u) + \cos^2\theta(\cos\theta - u)]\} \quad (73)$$

$$u = \sqrt{\frac{3\bar{s}}{2\bar{b} + 4\bar{s}}} \quad (74)$$

$$C = N\sigma_t(2\bar{b} + 4\bar{s}) \quad (75)$$

Although these solutions are composed of many terms, numerical calculations may be carried out by hand or on automatic computers. Some of the coefficients may involve the differences of large numbers, in which case an appropriate number of significant figures must be utilized.

Parallel-plane Dispersion and a Normally Incident Parallel Wave.—For this configuration, the ξ-axis is again chosen as the direction of incidence, but η and ζ may be any two mutually perpendicular axes in the plane parallel to the boundaries of the dispersion. Again abbreviating the subscripts, ξ_+, ξ_-, ζ_+, ζ_-, η_+ and η_-, with 1, 2, 3, 4, 5 and 6 $E_3 = E_4 = E_5 = E_6$ from symmetry and equations 5 to 10 degenerate to

$$\frac{1}{N\sigma_t}\frac{dE_1}{dZ} = -\left[1 - \omega\left(\bar{f} - \frac{4\omega\bar{s}^2}{1 - \omega\bar{f} - \omega\bar{b} - 2\omega\bar{s}}\right)\right]E_1 + \omega\left[\bar{b} + \frac{4\omega\bar{s}^3}{1 - \omega\bar{f} - \omega\bar{b} - 2\omega\bar{s}}\right]E_2 \quad (76)$$

$$-\frac{1}{N\sigma_t}\frac{dE_2}{dZ} = -\left[1 - \omega\left(\bar{f} - \frac{4\omega\bar{s}^2}{1 - \omega\bar{f} - \omega\bar{b} - 2\omega\bar{s}}\right)\right]E_2 + \omega\left[\bar{b} + \frac{4\omega\bar{s}^2}{1 - \omega\bar{f} - \omega\bar{b} - 2\omega\bar{s}}\right]E_1 \quad (77)$$

$$E_3 = E_4 = E_5 = E_6 = \frac{\omega\bar{s}}{1 - \omega\bar{f} - \omega\bar{b} - 2\omega\bar{s}}(E_1 + E_2) \quad (78)$$

Equations 76 and 77 are identical in form with equations 94 and 95 subsequently derived for a simple two-flux model, for which a solution is given.

Point Source Outside a Parallel-plane Dispersion.—If spherical coördinates (r, θ, ϕ), with the source at the origin are used to represent the position of any point in this configuration, the proper choice of the directions for the principal axes is

$\vec{\xi}$, in the direction of the incident direction, *i.e.*, in the direction of increasing r, so that $d\xi = dr$

$\vec{\eta}$, in the direction of increasing θ, so that $d\eta = rd\theta$

$\vec{\zeta}$, in the direction of increasing θ, so that $d\zeta = r\sin\theta d\phi$

as illustrated in Fig. 4.

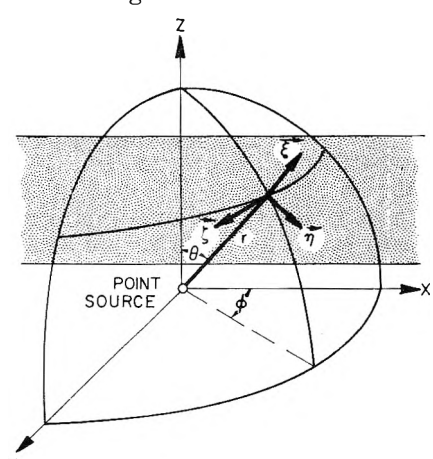

Fig. 4.—Six-flux representation in spherical coördinates for a point source outside a plane parallel dispersion.

Substituting the above coördinates in equations 5 through 10, using the same abbreviated subscripts, and expressing the components of the intensity in terms of the ratio of the power to the power in the absence of a dispersion, *i.e.*

$$\bar{E}_1 = 4\pi r^2 E_{\xi+} \quad (79)$$

$$\bar{E}_2 = 4\pi r^2 E_{\xi-} \quad (80)$$

$$\bar{E}_3 = 4\pi r^2 E_{\eta+} \quad (81)$$

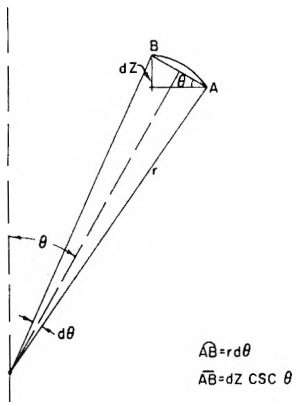

Fig. 5.—Approximation of an arc with the chord.

and taking into account axial symmetry, gives the following set of equations

$$\frac{\partial(\bar{E}_1 \sin\theta)}{N\sigma_t \partial r} + C_1\bar{E}_1 \sin\theta - C_2\bar{E}_2 \sin\theta = C_3[\bar{E}_3 \sin\theta + \bar{E}_4 \sin\theta] \quad (82)$$

$$\frac{\partial[\bar{E}_2 \sin\theta]}{N\sigma_t \partial r} + C_2\bar{E}_1 \sin\theta - C_1\bar{E}_2 \sin\theta = -C_3[\bar{E}_3 \sin\theta + \bar{E}_4 \sin\theta] \quad (83)$$

$$\frac{\partial[\bar{E}_3 \sin\theta]}{N\sigma_t r \partial\theta} - C_1\bar{E}_3 \sin\theta + C_2\bar{E}_4 \sin\theta = -C_3[\bar{E}_1 \sin\theta + \bar{E}_2 \sin\theta] \quad (84)$$

$$\frac{\partial[\bar{E}_4 \sin\theta]}{N\sigma_t r \partial\theta} - C_2\bar{E}_3 \sin\theta + C_1\bar{E}_4 \sin\theta = C_3[\bar{E}_1 \sin\theta + \bar{E}_2 \sin\theta] \quad (85)$$

$$\bar{E}_5 = \bar{E}_6 = \frac{\omega\bar{s}}{1 - \omega\bar{f} - \omega\bar{b}}[\bar{E}_1 + \bar{E}_2 + \bar{E}_3 + \bar{E}_4] \quad (86)$$

The above differential equations for $\bar{E}_1$, $\bar{E}_2$, $\bar{E}_3$ and $\bar{E}_4$ are non-linear and no analytical solution is apparent. Numerical solution by reiteration appears possible, but preliminary calculations indicate that a large number of reiterations are necessary. By introducing the approximate relationship

$$r\,d\theta = -\csc\theta\,dZ \quad (87)$$

and noting that

$$dr = \sec\theta\,dZ \quad (88)$$

equations 82 through 85 reduce to the identical form of the linear equations 14 through 17 which have been solved. The above approximation is geometrically equivalent to the representation of a differential length of a circular arc, $r\,d\theta$, by its subtended chord, or physically equivalent to considering any "ray" from the source as a differential portion of a plane wave at the same angle of incidence as indicated in Figs. 5 and 6. For dense dispersions and for large θ this approximation should be reasonable.

Solutions for plane sources can be derived by considering the plane source as an infinite series of point sources and integrating the point source solution.

Interpretation of the Six-flux Components.—The six components, E_1, E_2, E_3, E_4, E_5 and E_6 are by definition the forward and backward power per unit area in three appropriately chosen orthogonal directions. The expression of the distributed radiation, $i(\vec{R}, \vec{\Omega})$, and of the power intercepted by an arbitrarily oriented plane in terms of these

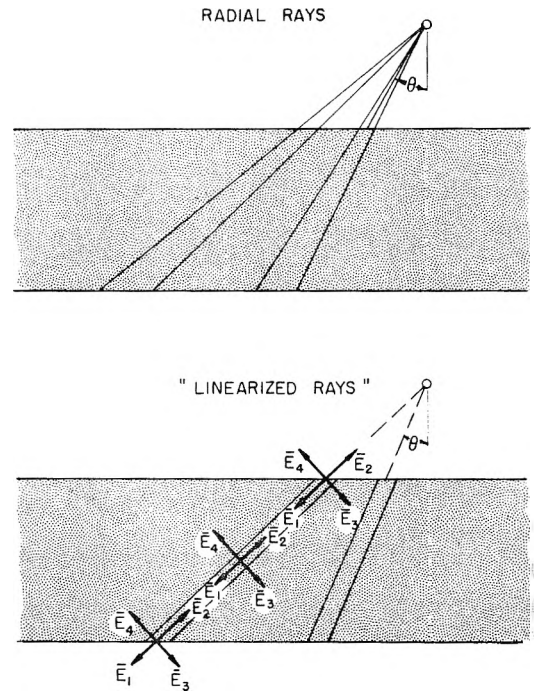

Fig. 6.—Physical illustration of approximation.

discrete components is necessarily an approximate and arbitrary process, as illustrated below for a plane parallel dispersion and an obliquely incident plane wave. This configuration is illustrated in Fig. 3 and solutions are given by equations 25 through 53 and equations 54 through 75.

Since $(E_1 - E_2)$, $(E_3 - E_4)$ and $(E_5 - E_6)$ are the components of the net power per unit area along the orthogonal axes, the net power per unit area through any arbitrarily oriented plane can be obtained directly by cosine resolution of the components. The net power per unit area crossing a plane parallel to the boundaries is then $(E_1 - E_2)$, $\cos\theta + (E_3 - E_4) \sin\theta$, and the power per unit area leaving the far boundary, where $E_2 = E_4 = 0$, is $E_1 \cos\theta + E_3 \sin\theta$. The net power crossing a plane of symmetry, *i.e.*, a plane perpendicular to the boundaries and containing the incident direction, is evidently zero, since $E_5 - E_6 = 0$.

The power intercepted by an arbitrarily oriented plane, cannot, in general, be obtained by cosine resolution. It is arbitrary but reasonable to assume that cosine resolution is a sufficient approximation for planes of symmetry, for planes parallel to the boundaries, and for their mutually normal planes. For other planes, the specific intensity must first be approximated and then integrated over the appropriate hemisphere.

The forward component, E_1, represents both scattered and unscattered radiation. The latter must be deleted before resolution. The distributed portion of E_1 is

$$E'_1 = E_1 - e^{-N\sigma_t S} \quad (89)$$

where S is the distance travelled in the dispersion by the unscattered radiation. The specific intensity can then be represented by a series of Legendre polynomials involving five arbitrary constants. Due to the discontinuity in the specific

intensity at the boundaries, separate expressions are advantageous for the specific intensity directed toward the boundary

$$i_+(\alpha,\beta) = b_0 + b_1P_1(\cos\alpha) + b_2P_1^1(\cos\alpha)\sin\beta + b_3P_2^2(\cos\alpha)\cos 2\beta \text{ for } \left(0 \le \alpha \le \frac{\pi}{2}\right) \quad (90)$$

and the specific intensity directed away from the far boundary

$$i_-(\alpha,\beta) = b_0' + b_1'P_1(\cos\alpha) + b_2'P_1^1(\cos\alpha)\sin\beta + b_3'P_2^2(\cos\alpha)\cos 2\beta \text{ for } \left(\frac{\pi}{2} \le \alpha \le \pi'\right) \quad (91)$$

where α is the azimuth angle with respect to the normal of the boundary and β is the bearing angle measured from the normal to the plane of symmetry. Continuity requires

$$b_0 = b_0'$$
$$b_2 = b_2'$$

and

$$b_3 = b_3'$$

The interception determined from cosine resolution for the three particular planes fixes the five arbitrary constants.

The distribution of the specific intensity obtained from equations 90 and 91 is of course not exact, and the resulting interception calculated for the coördinate directions will not exactly equal E_1, E_2, E_3, E_4, E_5 and E_6. However, numerical calculations for a variety of conditions indicate that the discrepancy is generally less than 10%.

The local absorption per unit volume equals $N\sigma_a$ times the integral of the specific intensity over 4π steradians. The total absorption can be obtained from an energy balance over the boundaries of the dispersion.

Degeneration to a Two-flux Model.—A very simple solution of multiple-scattering problems, useful for rough calculations and for bounding the six-flux solution, can be obtained as a degenerate case of the six-flux representation with the sidewise scattering component, $\bar{s}$, equated to zero.

The forward- and backward-scattering components for this two-flux representation are logically the same as those employed by Theissing for single-scattering and are defined as

$$f_1 = 2\pi\int_0^{\pi/2} f_1(\theta)\sin\theta\,d\theta \quad (92)$$

$$b_1 = 2\pi\int_{\pi/2}^{\pi} f_1(\theta)\sin\theta\,d\theta \quad (93)$$

The differential energy balances, which can either be written directly or obtained from equations 5 through 10 by noting that $E_{\eta+}$, $E_{\eta-}$, $E_{\xi+}$ and $E_{\xi-}$ must equal zero, are

$$\frac{dE_{\xi+}}{N\sigma_t d\xi} = -(1-\omega f_1)E_{\xi+} + \omega b_1 E_{\xi-} \quad (94)$$

$$\frac{dE_{\xi-}}{N\sigma_t d\xi} = -(1-\omega f_1)E_{\xi-} + \omega b_1 E_{\xi+} \quad (95)$$

Equations 94 and 95 can be solved readily for any of the geometrical configurations and boundary conditions previously considered for the six-flux model.

For a plane parallel dispersion, an obliquely incident plane wave, and the previous boundary conditions, the solutions are

(a) for appreciable absorption

$$E_+ = \frac{e^{-pZ\sec\theta} - G^2e^{-p(2T-Z)\sec\theta}}{1 - G^2e^{-2pT\sec\theta}} \quad (96)$$

$$E_- = G\,\frac{e^{-pT\sec\theta} - e^{-p(2T-Z)\sec\theta}}{1 - G^2e^{-2pT\sec\theta}} \quad (97)$$

(b) for no absorption

$$E_+ = \frac{1 + b_1N\sigma_s(T-Z)\sec\theta}{1 + b_1N\sigma_sT\sec\theta} \quad (98)$$

$$E_- = \frac{b_1N\sigma_s(T-Z)\sec\theta}{1 + b_1N\sigma_sT\sec\theta} \quad (99)$$

where

$$p = N\sigma_t\sqrt{(1-\omega f_1)^2 - \omega^2b_1^2} \quad (100)$$

$$G = \frac{N\sigma_t(1-\omega f_1+\omega b_1) - p}{N\sigma_t(1-\omega f_1+\omega b_1) + p} \quad (101)$$

Approximate solutions for a point source can be obtained by dividing the right side of equations 96, 97, 98 and 99 by $4\pi r^2$, as noted for the six-flux representation. This approximation has the physical consequence of confining the radiation to the radial direction.

The two-flux model is very similar to the diffusion model. However, the explicit representation of the forward and backward fluxes permits more direct specification of the boundary conditions and application of the results in many problems. The scattering components also have a more direct physical interpretation than the analogous diffusivity employed in the diffusion equation. Direct comparison of solutions obtained by the two methods for particular problems gives some indication of the relationship between the scattering components and the diffusivity. For plane-parallel symmetry and no absorption the solutions are identical if the diffusivity is chosen equal to $1/4N\sigma_sb_1$. For isotropic scattering the two-flux solution is identical to the diffusion solution with a linear extrapolation discussed by Glasstone and Edlund.[13]

As noted previously, the six-flux equations reduce to the same form as the two-flux equations for a normally incident wave and a plane-parallel dispersion. Comparison of equations 94 and 95 with equations 76 and 77, indicates that the equivalent two-flux components for the six-flux model are

$$f_1 = \bar{f} + \frac{4\omega\bar{f}^2}{1-\omega\bar{f}-\omega\bar{b}-2\omega\bar{s}} \quad (102)$$

$$b_1 = \bar{b} + \frac{4\omega\bar{s}^2}{1-\omega\bar{f}-\omega\bar{b}-2\omega\bar{s}} \quad (103)$$

which for no absorption reduce to

$$f_1 = \bar{f} + 2\bar{s} \quad (104)$$
$$b_1 = \bar{b} + 2\bar{s} \quad (105)$$

The models differ negligibly if $\bar{s}$ is small or if the distribution is nearly isotropic. For some strongly peaked distributions the results may differ appreciably. Physical reasoning indicates that with such distributions the two-flux model may be more accurate than the degenerate six-flux model for normally incident waves. This is due to the fact that in the degenerate six-flux model the side-scattered radiation is rescattered half forward and half backward, etc., although the actual radiation scattered in the sidewise direction has a strong

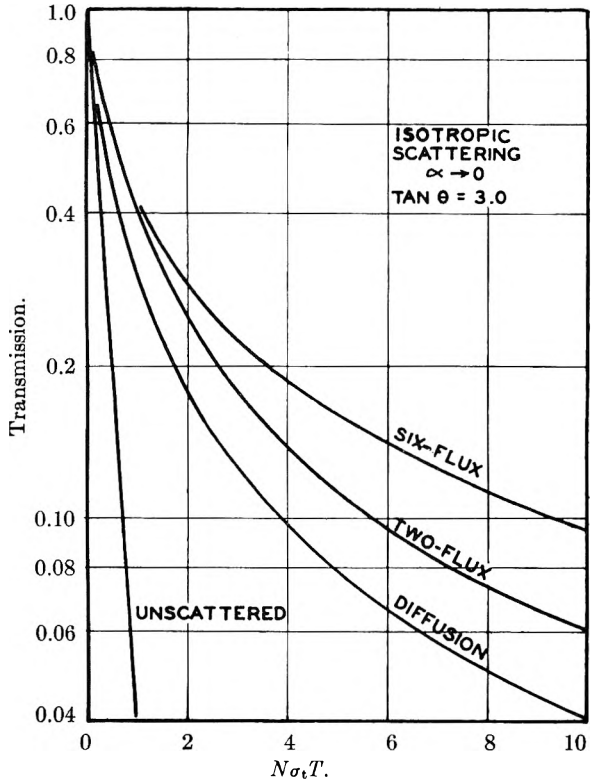

Fig. 7.—Calculated transmission through dispersions of different thickness.

forward tendency. For large angles of incidence, where the higher order scattering is not symmetrical about the incident direction, the six-flux solution should be the more accurate representation.

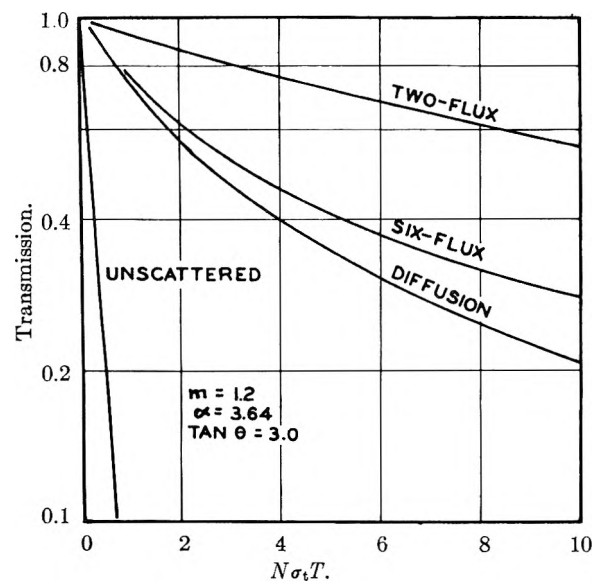

Fig. 8.—Calculated transmission through dispersions of different thickness.

Graphical Comparison of Various Models.—For comparative and illustrative purposes, the transmission of a plane wave through a parallel plane dispersion has been calculated for several representative conditions using the six-flux solution (equations 23 and 54 through 75), the two-flux solution equations (98 through 101). and diffusion

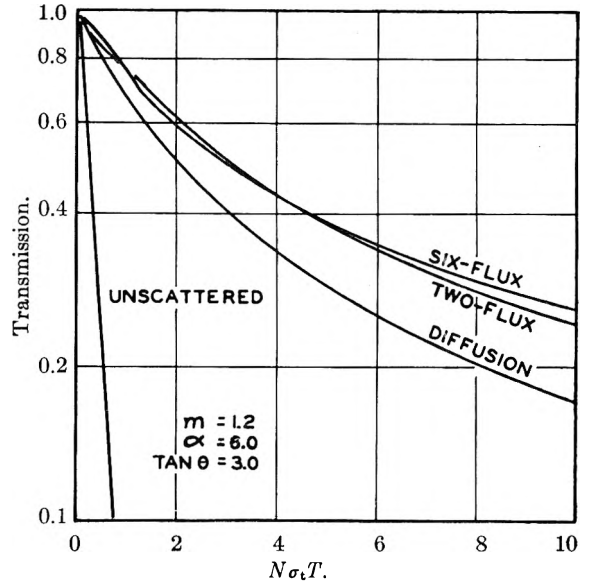

Fig. 9.—Calculated transmission through dispersions of different thickness.

theory. The transmission is defined as the power striking the far boundary divided by the power striking the same area in the absence of the dispersion.

In Fig. 7, the calculated transmission for an angle of incidence of arctan 3.0 and isotropic scattering is plotted *versus* $N\sigma_t T$, *i.e.*, the thickness of the dispersion in mean free paths. The transmission of unscattered radiation is also plotted to emphasize the effect of multiple scattering.

Similar plots were prepared for a dispersion of spherical particles of polystyrene latex in water having a relative index of refraction of 1.20. In Fig. 8, the results are presented for a circumference to wave length ratio, α, of 3.64, and in Fig. 9 for a ratio of 6.0. The characteristic scattering parameters, estimated from the Mie theory, are

α	$\bar{f}$	$\bar{b}$	$\bar{s}$	f_1	b_1
(Isotropic)	1/6	1/6	1/6	1/2	1/2
3.64	0.7645	0.0055	0.0575	0.975	0.025
6.00	.823	.047	.0325	.900	.100

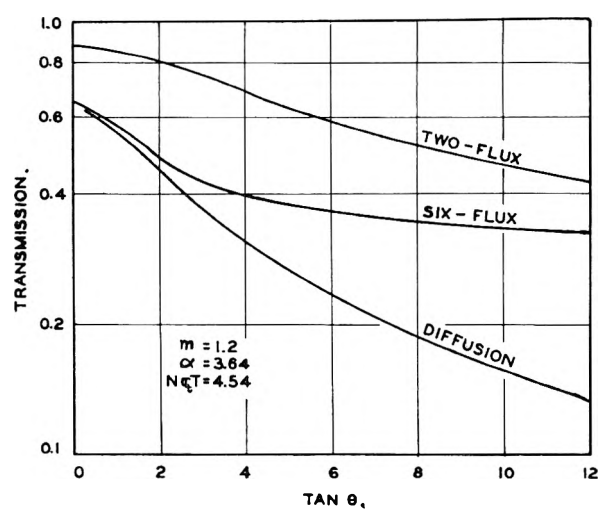

Fig. 10.—Calculated transmission for different angles of incidence.

The transmission is plotted as a function of the tangent of the angle of incidence in Fig. 10 for α equal to 3.64 and $N\sigma_t T$ equal to 4.54.

As anticipated from the previous discussion, the two-flux model generally predicts higher transmissions than the six-flux model for highly peaked distributions and lower transmissions for large angles of incidence and very dense dispersions. Diffusion theory appears to predict low values for the transmission for all the cases considered.

Conclusions

None of the previously proposed methods of solving problems in multiple scattering, except the diffusion representation, was found practical for numerical calculations with finite dispersions and anisotropic distributions.

The six-flux model developed in this paper permits an analytical solution for absorption and anisotropic scattering for most geometrical configurations of a dispersion and a plane or point source. The solutions are suitable for hand calculations for particular conditions or for machine calculation for an extended number of conditions. The six-flux representation is believed to be sufficiently accurate for most practical applications.

The very simple two-flux model obtained by degeneration of the six-flux model gives a first-order approximation for multiple scattering which is of comparable accuracy but easier to apply than the classical diffusion equations.

Acknowledgment.—Prof. C. M. Sliepcevich, now at the University of Oklahoma, Norman, Oklahoma, and Dr. R. O. Gumprecht, now with the General Electric Co., Hanford, Washington, initiated the work and provided invaluable assistance. Graduate students G. C. Clark and B. K. Larkin assisted in the calculations and programming.

THE TRANSMISSION OF LIGHT BY STABLE FOAMS[1]

BY SYDNEY ROSS AND M. J. CUTILLAS

Departments of Chemistry and Chemical Engineering, Rensselaer Polytechnic Institute, Troy, New York

Received February 25, 1955

The transmission of light by stable foams is measured throughout the transition of the foam from a collection of spherical bubbles separated by relatively thick layers of liquid (*kugelschaum*) to a system of polyhedral bubbles separated by thin, plane films (*polyederschaum*). It is found that the light transmitted by the former type of foam increases relatively rapidly with time in a way that is described by a linear I^2 *vs.* time plot. The latter type of foam appears only after most of the liquid has drained out of the films. Diffusion of gas, contained in smaller bubbles at higher pressures, into larger bubbles, at lower pressures, causes a spontaneous decrease of the specific interfacial area of the foam. A relatively slow increase in the intensity of transmitted light occurs during this process, and is described by a linear $\log (I_0/I - 1)$ *vs.* t plot. Since the function $(I_0/I - 1)$ is proportional to the specific interfacial area, these results confirm previous statements in the literature that the rate of decrease of interfacial area of stable foams is logarithmic. The technique described separates the effects of drainage of liquid in a foam, during which there is no change in the sizes of bubbles, from that of gas diffusion, which causes a decrease of interfacial surface area. Preliminary tests with low concentrations of two antifoaming agents show that they accelerate the former process and do not affect the latter process.

Introduction

The transmission of light by stable foams has been investigated experimentally and theoretically by Clark and Blackman.[2] For foams prepared from non-absorbing solutions a relation was deduced that enabled one to calculate the specific interface (sq. cm. of interface per cc. of foam) from the transmitted light. It is thereby possible to measure, with simple techniques, the variation of specific interface of foam with time, provided that the foam is sufficiently stable so that no rupture of the films occurs during the measurement.

In the present study the measurement of light transmission was commenced while the bubbles were still separated from each other by relatively thick liquid films. When observations are then continued long enough, it is known that two distinct phenomena occur, one after the other: at first the foam alters by drainage of liquid, the bubbles remaining of constant size; then, when the separating liquid films are thin, passage of gas takes place from smaller bubbles at higher pressures to larger bubbles at lower pressures. The latter occurrence was the only one investigated by Clark and Blackman, but it comes only gradually into existence as the first process nears its end. During the course of both processes, the transmission of light increases continuously; but since the physical occurrences are quite dissimilar, the mathematical description of each portion of the transmission curve should be based on different hypothetical models.

Materials and Methods. The solutions examined were similar to those described by Ross, Barth and Terenzi.[3] The foams were produced from 200 ml. of solution by the action of a Hamilton-Beach mixer for one minute. The transmission of light (λ 600 mμ) was measured with a Lumetron colorimeter (Model 402-E), operated as a direct-reading colorimeter. The operating procedure has been described elsewhere in detail.[3] The measurements were all made at room temperature, 24°.

Experimental Results

In Fig. 1 are reported the experimental results for light transmission calculated as "loss factor" (I_0/I), for solutions of Nacconol NRSF of 0.10 and 0.033%, and of 0.10% Nacconol NRSF containing (a) 0.02% (by volume) of tributyl phosphate and (b) 0.02% (by volume) of methylisobutyl-

(1) Presented at the 29th National Colloid Symposium, at The Rice Institute, Houston, Texas, on June 20–22, 1955.

(2) N. O. Clark and M. Blackman. *Trans. Faraday Soc.*, **44**, 7 (1948).

(3) S. Ross, B. Barth and J. F. Terenzi, THIS JOURNAL, **58**, 247 (1954).

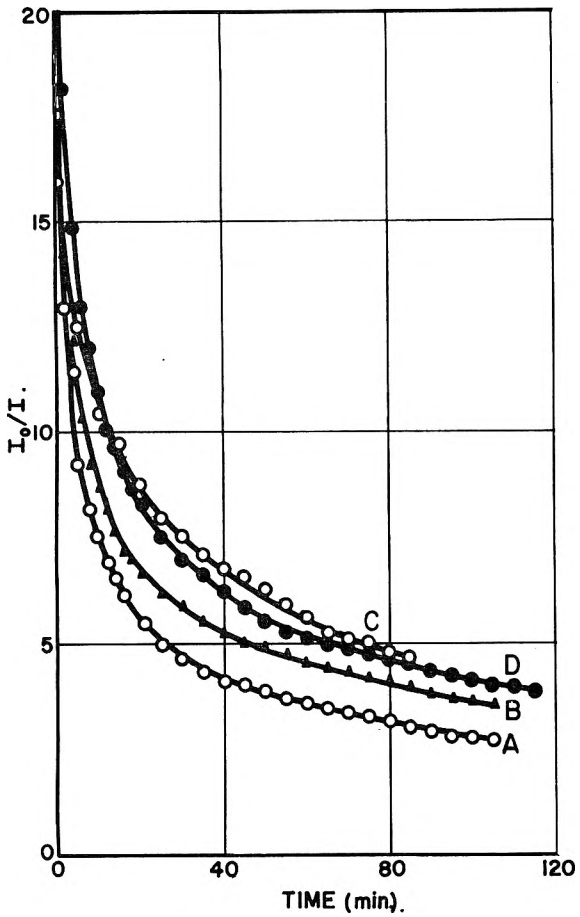

Fig. 1.—The variation with time of the loss factor, I_0/I for foams produced from aqueous solutions of 0.033% (C) and 0.10% (D) by weight of Nacconol NRSF; 0.10% Nacconol NRSF plus 0.02% tributyl phosphate (B); and 0.10% Nacconol NRSF plus 0.02% methylisobutylcarbinol (A).

carbinol. These agents are used as antifoams, and their effects on the foam characteristics of the Nacconol solution are sought. They are used at concentrations low enough to preclude their rupturing the films, but great enough to detect any effects that they might have on drainage rates or diffusion of gas through thin liquid films.

The effects of an increased bulk viscosity of the solution was determined by measuring foams made of 0.10% Nacconol NRSF containing approx. 1.0, 2.5 and 5.0% polyvinyl alcohol. The original experimental observations are not reported, but functions derived from them are included in Table I.

Discussion

The initial rapid increase of the light transmitted by a stable foam takes place during the first 30–40 minutes of observation (compare with 6–7 minutes for unstable foams[3]) after which the foam transmits light at a much slower rate of increase. The foam at the beginning of the observations is wet; the bubbles are spheres, separated from each other by thick layers of liquid: an hour later the foam bubbles are polyhedra, separated from one another by thin, plane liquid films. The two types of foam have been designated *kugelschaum* and *polyederschaum* by Manegold.[4] This is a convenient classification, since distinctly different spontaneous changes take place in each type of foam. In *kugelschaum* there is a gravitational outflow of liquid from the foam, during which the bubbles, without any change of size or shape, are brought closer together: in *polyederschaum* there is a spontaneous diffusion of gas between bubbles, during which the larger bubbles grow and the smaller ones shrink; the net result is a continuous decrease of the interfacial area of the foam.

(4) E. Manegold, "Schaum," Chemie und Technik Verlagsgesellschaft, Heidelberg, 1953, *passim*.

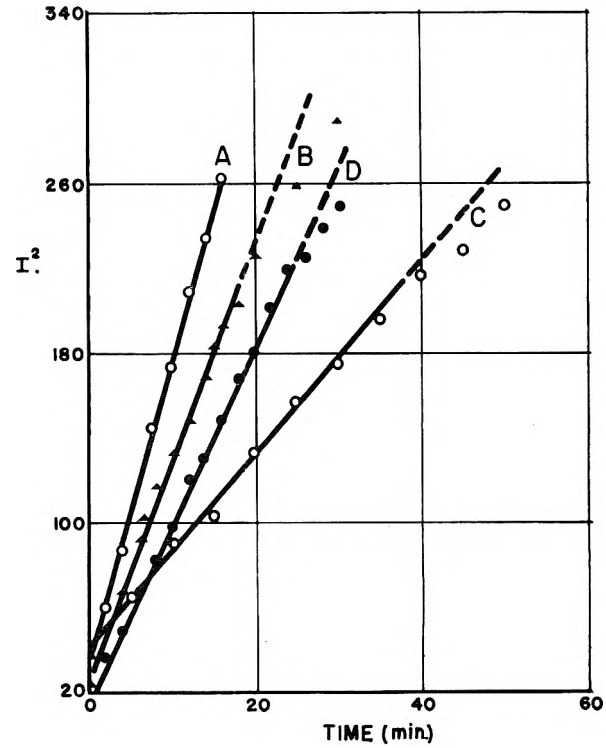

Fig. 2.—The variation of I^2 with time for the solutions A, B, C and D designated in the legend to Fig. 1.

1. Drainage of Liquid from Foam.—The only change that takes place in *kugelschaum* is the outflow of liquid. According to Ross,[5] the decrease of the volume of liquid in a foam with time is described by the equation

$$\frac{V_0}{V_t} = (1 + bt)^{1/2} \qquad (1)$$

where

V_0 = initial vol. of liq. in the foam
V_t = vol. of liq. in the foam after time t
b = constant, determined by the bubble size and the bulk viscosity of the liq.

The observations were plotted in the form I^2 *vs.* t, and found to yield the linear relation shown in Fig. 2. The plot is based on the assumption that, with the passage of time, the increase of the transmitted light is related in a regular way to the decrease of liquid contained in the foam. The relation between the transmitted light and the liquid content of the foam cannot be explained as caused merely by absorption of light in the bulk liquid, since the solutions are non-absorbent to visible light. The absorption of light in relatively thick liquid films is probably due to a progressive

(5) S. Ross, THIS JOURNAL, **47**, 266 (1943).

diffusion of the light toward an almost spherical distribution.

The effect of an increase in the bulk viscosity of the liquid would reduce the rate of liquid efflux from the foam, which could reasonably be expected to reduce in turn the rate at which the intensity of the transmitted light increases. Solutions of 0.10% Nacconol NRSF were thickened with varying concentrations of polyvinyl alcohol; the general trend of the results is certainly toward a decreased slope of the I^2 *vs.* t curves (Table I).

TABLE I

SLOPE OF I^2 *vs.* t CURVES (FOAM DRAINAGE) OF SOLUTIONS OF NACCONOL NRSF AND VARIOUS ADDITIVES

Solutions			Slope of I^2 *vs.* t curve (foam drainage)
Concn. Nacconol NRSF (% by wt.)	Additive	Concn. of additive (% by vol.)	
0.033	None	..	1.11
.10	None	..	1.43
.10	Tributyl phosphate	0.02	2.50
.10	Methylisobutylcarbinol	0.02	2.86
.10	Polyvinyl alcohol	*ca.* 1.0	1.57
.10	Polyvinyl alcohol	*ca.* 2.5	1.19
.10	Polyvinyl alcohol	*ca.* 5.0	0.96

The results of Table I indicate that the slope of the I^2 *vs.* t curve measures indirectly the rate of drainage of liquid from the films. The presence of small amounts, 0.02% by volume, of tributyl phosphate or of methylisobutylcarbinol, which, at concentrations greater than 0.02% are known to act as antifoaming agents in Nacconol NRSF solutions,[6] causes a pronounced increase in the rate of drainage. Although the agents are present in concentrations too low to affect the bulk viscosity of the liquid, it is known that the surface viscosity at the air–liquid interface can be greatly changed by small amounts of surface-active additives.[7] Changes in surface viscosity have, in turn, great effects on the drainage of liquid out of films and foams.[8]

Whether the increase in drainage rate caused by tributyl phosphate and methylisobutylcarbinol is the result of a decrease of surface viscosity (as seems probable), or is due to some other cause, the observation itself is a valuable clue to the mechanism of anti-foaming action. The potential of the method of light transmission for the investigation of antifoams should not be overlooked.

2. Decrease of Interfacial Area of Foam.—Clark[9] has made direct measurements by photomicrography of the specific interface of stable foams as a function of time, and found that his results could be described by the equation

$$S = S_0 e^{-\alpha t} \qquad (2)$$

where

S = specific surface at time t
S_0 = specific surface at time of initial measurement
α = a constant

As a less direct but more convenient alternative to photomicrography, the method of light transmission can be used to obtain the specific interface. The relation deduced by Clark and Blackman[2] is

$$S = k(I_0/I - 1) \qquad (3)$$

where

I_0/I = loss factor (see Fig. 1)

and

k = proportionality constant

In Fig. 3 some of the results of the present study are plotted as log $(I_0/I - 1)$ *vs.* t. There is complete agreement with the conditions of eqs. 2 and 3, which are restricted in their application to *polyederschaum*. It requires 40–60 minutes for the "wet" foams of the present study to become sufficiently dry that gas diffusion can be isolated from the effects of drainage.

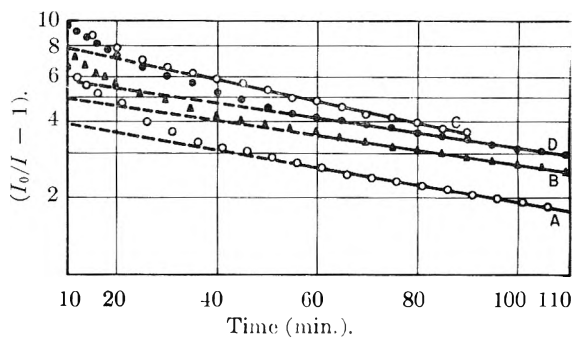

Fig. 3.—The variation of log $(I_0/I - 1)$ with time for the solutions A, B, C and D, designated in the legend to Fig. 1.

The observations reported in Fig. 1 are those from which the derived functions of Figs. 2 and 3 are calculated. The I^2 *vs.* t relation is linear for the first 20–40 minutes of the foam life; there is then a transition region where the change in the intensity of the transmitted light is compounded from both the effects of liquid drainage and gas diffusion; finally the liquid drainage becomes negligible, and the slow increase of transmitted light intensity is due solely to gas diffusion and its accompanying effect, namely, decrease of interfacial area. The last phase of the life of a stable foam is described by the logarithmic relation of eq. 2.

It is of interest in the study of antifoams to find that the linear portions of the curves of Fig. 3 are parallel for the 0.10% Nacconol NRSF solution, and for the same solution containing additives. Tributyl phosphate and methylisobutyl alcohol show their influence only in the first, or drainage, portion of the foam life. The concentrations of antifoam included in the Nacconol solution were deliberately less than required for good antifoaming action, since the rupture of liquid films was not desired during the measurements. At higher concentrations the effects disclosed here would, presumably, be more pronounced. There is evidence, from previous studies of these systems, that tributyl phosphate at higher concentrations continues

(6) S. Ross and G. J. Young, *Ind. Eng. Chem.*, **43**, 2520 (1951); S. Ross, A. F. Hughes, M. L. Kennedy and A. R. Mardoian, THIS JOURNAL, **57**, 684 (1953).

(7) A. G. Brown, W. C. Thuman and J. W. McBain, *J. Colloid Sci.*, **8**, 491 (1953).

(8) G. D. Miles, J. Ross and L. Shedlovsky, *J. Am. Oil Chemists' Soc.*, **27**, 268 (1950).

(9) N. O. Clark, "A Study of Mechanically Produced Foam for Combating Petrol Fires," D.S.I.R., Chemistry Research, Special Report No. 6, H.M.S.O., London, 1947, p. 106; N. O. Clark and M. Blackman, *Trans. Faraday Soc.*, **44**, 1 (1948).

to display no effects other than that of accelerating the drainage rate; whereas methylisobutylcarbinol at higher concentrations destroys the film-stabilizing action of the foaming agent. Part of the value of the light-transmission method is that it enables us to separate discrete functions of antifoaming agents, which show up as a complex of concomitant effects by the usual methods of measuring foam stability.

DISCUSSION

C. V. KING.—At first glance it may seem improbable that air can diffuse from small bubbles to large ones rapidly enough to make the former disappear in a few minutes. However, the following calculation indicates that the process is possible; perhaps the authors will check and comment further.

Assume a bubble 1.0 mm. in diameter, wall thickness 10^{-4} cm., surface energy of liquid 70 ergs/cm.^{2}, suspended in air at atmospheric pressure. The excess pressure in the bubble is $4\gamma/r$, or about 4 mm. of mercury. The diffusion rate through the wall may be approximated by the equation

$$dn/dt = DA\Delta C/\delta$$

where δ is the wall thickness. Using the diffusion coefficient $D = 6 \times 10^{-4}$ cm.^{2}/min., area $A = 3 \times 10^{-2}$ cm.^{2}, ΔC = volume solubility air per cm.^{3} water $\times$ fractional pressure difference $= 1.6 \times 10^{-4}$, the above equation gives

$$dn/dt = 3 \times 10^{-5} \text{ cm.}^3\text{/min.}$$

as the amount of air escaping from the bubble. Since the volume of the assumed bubble is 5×10^{-4} cm.^{3}, and dn/dt increases as the bubble gets smaller, the bubble would soon disappear if the wall did not get thicker.

SYDNEY ROSS.—We are grateful to Dr. C. V. King for his calculation, which as far as we are aware has not been made before, and which makes the explanation of gaseous diffusion from small to larger bubbles much more credible.

We must admit an error in our terminology in equating the *polyederschaum* of Manegold to a foam in which gaseous diffusion is still taking place. If *polyederschaum* is defined as the state where bubbles are separated by planar liquid films, there can exist no pressure differences between bubbles, and hence no diffusion of gas would take place across liquid films. At that stage there would no longer be any variation of the intensity of the transmitted light. The foams of the present investigation, therefore, are slowly tending toward *polyederschaum* but do not reach that point within the period of the measurements.

MAX BENDER.—Do you have any knowledge of the nature of the surface viscosity at the air–liquid interface of the Nacconol NRSF solutions?

SYDNEY ROSS.—We have measured the surface viscosity of Nacconol solutions, using the damping of a torsion-pendulum, in a manner similar to that described by Wilson and Ries at the First National Colloid Symposium in 1923. Unlike soap solutions, and some other commercial synthetic detergents, such as sodium lauryl sulfate, solutions of Nacconol NRSF do not show surface plasticity, but have Newtonian surface viscosity coefficients. The surface viscosity of a Nacconol solution is slightly greater than that of a pure water surface: when 0.02% tributyl phosphate is added, the surface viscosity coefficient is reduced to about that of pure water.

It is this reduction of the surface viscosity that is probably responsible for the increased rate of liquid drainage when tributyl phosphate is present.

AN INVESTIGATION OF THE EFFECTS OF WETTABILITY ON THE RECOVERY OF OIL BY WATER FLOODING

BY HARVEY T. KENNEDY, EDWARD O. BURJA AND ROBERT S. BOYKIN

Agricultural and Mechanical College of Texas, College Station, Texas

Received February 25, 1955

This paper presents data on the effect of the relative wetting properties of oil and brine toward reservoir rock from two standpoints. In the first method carried out with Woodbines and cores, the effect of the variation of wetting properties, without any control of the interfacial tension, was investigated. In the second, performed with cores of pure silica and consolidated by hydrated silicon tetrachloride, the interfacial tension was maintained constant while the wetting properties were varied. In both methods, wetting properties were controlled by the addition of surface active chemicals and wetting properties were measured by the sessile drop method. In the tests where the interfacial tension varied, a trend is evident in the data, indicating somewhat increased recoveries at low sessile drop ratios, although there is a large scattering of data. Where the interfacial tension was maintained constant, the data indicate a maximum recovery occurs at sessile drop ratios of about 0.5. This is the value at which the oil and brine have equal tendency to wet the rock.

Introduction

According to the most recent survey of the oil reserves of Texas only 25.6 billion barrels of the State's 79 billion barrels of proved oil in place can be recovered by normal production methods, supplemented by all known methods of secondary recovery. A portion of the huge unrecoverable remainder, 53.4 billion barrels, exists, no doubt, in reservoirs too tight to yield its contents at a commercial rate. The greater portion, however, will probably be retained because of capillary forces, resisting the displacement of oil, which scientists and technologists are as yet unable to control.

The mechanics of fluid flow and retention even in single phase in porous rock are too complicated for direct analysis, and would remain so even if the exact geometry of the pore spaces were known. Many attempts have been made to represent pore systems by idealized concepts. While some of these concepts are of value in giving a qualitative understanding of flow phenomena. none can be relied on to give a true indication of the effect of varying surface forces on the recovery of oil.

Up to this time the majority of published investigations have indicated that the presence of surface active agents in flood water will lead to an increase in recovery. The reason for this effect has usually been attributed to either a change in the oil–water interfacial tension or a change in the wettability of the sand or both; however, there has been no general agreement among the results published in the literature as to the specific effect of either property. The present work is an effort to improve this situation, since independent changes in these properties are possible with different chemicals.

Materials, Equipment and Procedure

Cores.—The cores used in the first part of this work, composed mainly of fine-grained silica, iron oxide particles and clay, were taken from a Woodbine Sandstone outcrop located near Arlington, Texas. They were cut from a large block into cores approximately two feet long and two inches in diameter. Core A had a pore volume of 517 cc., a porosity of 38.9%, an air permeability of 3370 md.* and a brine permeability of 3021 md. Core B had corresponding property values of 513 cc., 38.4%, 3700 and 2300 md. and Core C had values of 460 cc., 36.9%, 1410 and 466 md.

* The permeability of a porous medium, in darcies, is the number of ml. of fluid, of 1 centipoise viscosity, that will flow through a cube, 1 cm. on a side, in one second under a pressure differential of 1 atmosphere. A millidarcy is one thousandth of a darcy.

For the part of the work in which interfacial tensions were held constant, an artificial core, made from pure silica sand was used. The sieve analysis before consolidation was

passed 60 mesh and caught on 100 mesh	20%
passed 100 mesh and caught on 150 mesh	57%
passed 150 mesh and caught on 200 mesh	20%
passed 200 mesh	3%

The consolidation process involved the use of silicon tetrachloride which reacted with water in the core and precipitated out hydrated silica, which acts as the cementing material. First, the silica sand was placed in position inside a section of steel pipe and saturated with water. The water was then displaced to as low a residual as possible by flowing kerosene through the core. When the water was reduced to a minimum a solution of 5% by volume of silicon tetrachloride in kerosene was flowed through the core. The reaction zone moved down the core, and when the effluent from the core contained unreacted silicon tetrachloride and produced a white precipitate in water the reaction was complete.

Since the small amount of water remaining in the core after flushing by kerosene was distributed at the contact points between silica grains, the cementing material formed was deposited at these points. The permeability of the core before consolidation was 2.34 darcys* and was reduced to 1.16 darcys. The porosity of the consolidated core was 31.8% as determined by weighing the core before and after saturation with water.

Oil, Gas and Brine.—The oil used in these experiments was obtained from the East Texas oil field at atmospheric temperature and pressure and had not been subjected to any type of chemical treatment. The API gravity was 39.9°. To prepare the reservoir fluid for the flow test the oil was recombined with gas of composition similar to gas from the field. It contained the same mole per cent. of

TABLE I

CHEMICALS INVESTIGATED FOR THEIR EFFECT OF INTERFACIAL TENSION AND WETTABILITY

1.	Renex	Polyoxyethylene ester of mixed fatty and resin acids
2.	Sterox SE	Polyoxyethylene thioether
3.	Span 20	Sorbitan monolaurate
4.	NNO	Glycerol mannitan laurate
5.	G-1086	Polyoxyethylene sorbital hexaoleate
6.	Ethomid HT-60	N-Substituted hydrogenated tallow amide
7.	Arquad-2C	Dialkyl dimethylammonium chloride
8.	Petronate L	Petroleum sulfonate
9.	Antarox A-400	Polyglycol ether
10.	Ultrawet K	Probably alkylated aromatic hydrocarbon
11.	Pluronic L-64	A polyethylene glycol chain
12.	Brij 30	Polyoxyethylene lauryl alcohol
13.	Petronatel	Petroleum sulfonate

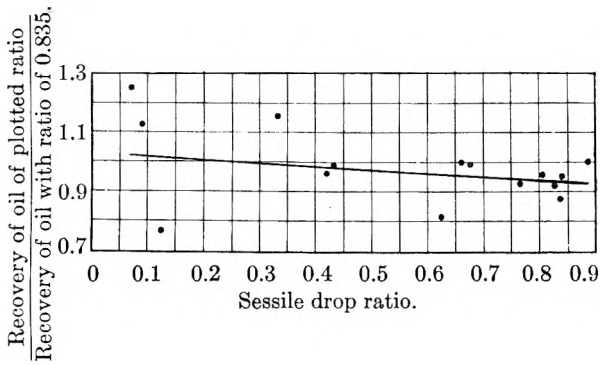

Fig. 1.—The effect of wettability on the recovery of East Texas crude oil by water flooding at 146° F. and 1000 p.s.i.g.

methane, ethane and propane plus as the actual gas produced.

The synthetic brine used in these tests was made up to duplicate the published composition of East Texas brine.

The chemicals used in this work are listed in Table I by number, commercial name and chemical type.

Wettability was determined by placing a small droplet of oil on the underside of a crystal of silica immersed in brine. When the droplet has spread to a constant shape, as determined by frequent measurements of its height and width, the ratio of these two quantities is called the sessile drop ratio. A ratio of unity indicates complete wetting by the brine, while one of 0.5 would indicate equal wetting of the surface by both oil and brine. A sessile drop ratio of zero would mean that oil had spread completely over the solid surface.

Precautions required in the sessile drop method include: 1, the surface must be clean, and an effective and reproducible cleaning method must be available; 2, droplets must be small enough to make distortion due to gravity negligible; 3, sufficient time of contact between the liquids and the solid, usually 24 hours or longer must be allowed for equilibrium to be attained.

A visual cell was filled with synthetic East Texas oil field brine or the brine containing a definite concentration of surface-active chemical. After careful cleaning, the crystal was immersed in the brine and a droplet of oil placed on its underside and measurements of its diameters made at intervals. With the cathetometer used it was possible to estimate diameters to 0.001 mm.

The crystals were cleaned by washing them twice in carbon tetrachloride and twice in acetone. They were scrubbed with a separate brush in each case. After being washed in these liquids they were held in a blue flame of a Meker burner for one minute. During all of these cleanings the crystals were not touched by hands.

Interfacial tension measurements were made at 100°F. and 500 p.s.i. by the pendant drop method. Since the time of formation, especially in the presence of chemicals, had an effect on the volume of the drop, only those drops requiring from one to two minutes to separate from the tip were measured.

A circulating system was used to saturate the core with oil and to distribute the surface active chemicals throughout the core. The procedure was substantially the same as described by Kennedy and Guerrero. Recoveries were determined by material balance on the fluids entering and leaving the core. All flow tests were made above the bubble point of the oil and the recoveries were considered complete after ten pore volumes of brine had flowed through the core.

Discussion of Results

The recoveries obtained by water flooding Woodbine cores, as a function of the sessile drop ratio of the oil in contact with brine, are shown in Table II and Fig. 1. Since the recoveries from different cores varied appreciably, the data are put on a common basis by plotting as ordinate the ratio of the recovery of oil for a given sessile drop ratio to the recovery of oil of sessile drop ratio 0.885, *i.e.*, oil containing no surface active chemical. The wide scattering of data, particularly at low sessile drop ratios, suggests that the wetting power alone is not the controlling factor in determining the recovery.

TABLE II

WATER FLOODING TESTS INVOLVING TWO PHASES, SYNTHETIC EAST TEXAS BRINE AND UNDER-SATURATED EAST TEXAS OIL AT 146°F. AND 1000 P.S.I.G. BUBBLE POINT −755 P.S.I.A.

Core used	Chem. used	P.p.m. in brine	P.p.m. in oil	% orig. oil sat.	% Resid. res. oil	Wetting ratio
A	None	0	0	72.5	18.0	0.885
A	None	0	0	75.6	20.4	.885
A	2	100	5500	71.7	22.2	.767
A	2	120	6500	68.7	21.4	.829
A	None	0	0	66.4	19.1	.885
A	2	0.5	20	67.4	17.2	.664
A	2	3	150	67.0	19.1	.806
A	2	0.02	1	68.3	19.6	.841
B	None	0	0	71.8	20.6	.885
B	3	10	130	68.8	19.3	.678
B	9	250	250	71.4	20.8	.431
B	11	75	50	73.1	30.4	.636
A	6	25	25	70.0	24.3	.837
C	None	0	0	73.3	42.3	.885
C	None	0	0	73.3	40.8	.885
C	12	0	300	74.8	43.5	.420
C	12	0	1000	70.2	34.8	.332
C	5	300	300	70.0	35.7	.0872
C	7	0	300	70.5	46.8	.1255
C	13	0	300	67.5	30.7	.0710

In tests where the interfacial tension was held constant, a value of 12 dynes was chosen as one at which a wide range of sessile drop ratios could be attained with the surface active chemicals available. Table III shows the compounds investigated, the concentrations in brine at which the above surface tension was realized, and the corresponding sessile drop ratio.

TABLE III

RESULTS OF WATER FLOOD TESTS

Chemical used	Concn. required to give 12 dynes/cm. interfacial tension, p.p.m.	Sessile drop ratio	Initial oil (% pore space)	Residual oil (% pore space)	Recovery % initial oil)
Renex	35	0.816	84.8	24.2	71.5
Sterox SE	115	.480	83.5	17.8	79.0
Span 20	440	.395	80.9	20.0	76.5
NNO	140	.862	85.2	23.2	72.9
G-1086	18	.213	84.4	20.6	75.7
Ethomid HT-60	18	.810	83.3	23.7	75.4
Arquad-2C	540	.150	85.5	21.9	73.5
Petronate L	625	.710	84.2	20.6	75.5
Antarox A-400	115	.775	82.8	21.9	73.5
Ultrawet K	560	.459	86.1	21.3	75.2
Mixture A	44	.290	85.8	19.0	77.8
Pluronic L-64	4	.820	..	..	..

The results of flood tests for oil–brine systems of constant interfacial tension (12 dynes per centimeter) and varying sessile drop ratios are also

shown in Table III and plotted in Fig. 2. It is seen that the extreme range of recoveries is from 71.5 to 79.0% of the initial oil in place, and that the best curve through the points shows a maximum near a sessile drop ratio of 0.5. It should be noted that at this ratio, in the absence of effects due to hysteresis, capillary forces might be expected to vanish and recoveries match those obtainable with miscible fluids, *i.e.*, they should approach 100%.

The curve shown in Fig. 2 shows the effect of the wetting of the rock at one value of the interfacial tension. On the basis of Fig. 1, which shows a favorable trend for lower sessile drop ratios, and the work of Kennedy and Guerrero,[7] which shows an adverse effect for lower interfacial tensions, it seems probable that curves similar to Fig. 2 at higher interfacial tensions would show higher recovery peaks.

Conclusions

The results of this investigation support the following conclusions as applied to the conditions under which the investigation was made: 1. When the sessile drop ratio is lowered by the addition of surface active chemicals, without regard to the interfacial tension between oil and brine, there is a trend of higher recoveries by waterflooding for lower ratios. 2. When the interfacial tension between oil and brine is maintained constant, the recovery is found to be a maximum at sessile drop ratios of about 0.5.

Acknowledgment.—The authors wish to acknowledge the financial support afforded by the Humble Oil and Refining Company, whose fellowship made this work possible.

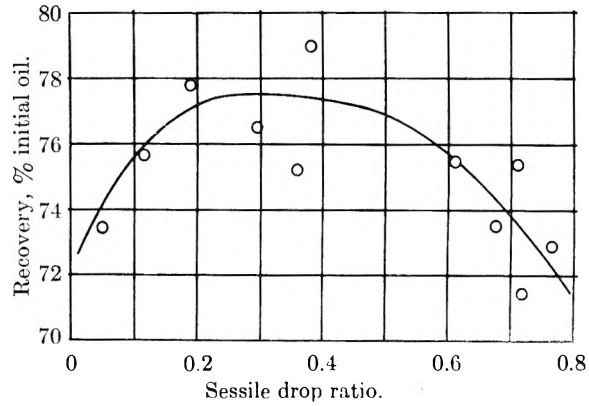

Fig. 2.—The effect of rock wettability on oil recovery.

(1) G. H. Fancher, R. L. Whiting and J. H. Cretsinger, "Oil Recovery of Texas," Texas Petroleum Research Committee, 1954.
(2) P. G. Nutting, *Ind. Eng. Chem.*, **17**, 1035 (1925).
(3) F. E. Bartell and F. L. Miller, *ibid.*, **20**, 738 (1928).
(4) F. E. Bartell and F. L. Miller, *ibid.*, **24**, 335 (1932).
(5) J. C. Calhoun, C. O. Stahl, F. W. Preston and R. F. Nielson, *Producers Monthly*, **15**, 16 (1951).
(6) P. L. Terwilliger and S. T. Yuster, **XI**, No. 1, 42 (1946).
(7) H. T. Kennedy and E. T. Guerrero, *Trans. AIME*, **41**, 201 (1954).

DISCUSSION

JOHN TREANOR SMITH.—Were the cores dried after flowing water through them and the air permeabilities remeasured to make certain that the changes were due to swelling of clays only rather than to migration of clays or a combination of both.

R. A. SALATHIEL.—What was the size of the cores used; and what was the pressure drop across the cores during the flooding?

H. T. KENNEDY.—Cores were about 1 foot long by 2" in diameter. Pressure drop was of the order of one p.s.i./foot, although this varied somewhat.

THE EFFECT OF VARIOUS MUD FILTRATES ON THE PERMEABILITY OF SANDSTONE CORES

BY HARVEY T. KENNEDY AND ROBERT A. PFILE

Agricultural and Mechanical College of Texas, College Station, Texas

Received February 25, 1955

This work describes the effects of distilled water, four salt solutions, a dilute caustic soda solution, and six drilling mud filtrates on the permeability of four cores taken from three drilling wells in Texas, Louisiana and Mississippi. In all cases the permeability to water solutions is substantially lower than the air permeability of the dried and cleaned cores. The greatest effect, attributed to the swelling effect of the intergranular clays in the cores, resulted from contact with alkaline solutions. Distilled water and solutions with low salt content showed the intermediate reduction of permeability, while salt solutions showed the least reduction. The susceptibility of cores to plugging effects of the same solution varied widely. There was no apparent relationship between the action of the different solutions and distilled water on the same core. The variation of the results is attributed to the different kind and amount of clay contained in the different cores.

Introduction

There is general agreement among members of the petroleum industry that the productive capacity of a well penetrating a clay-containing oil sand may be seriously impaired due to the swelling of the intergranular clays in the vicinity of the well bore as a result of the reaction between the clays and the invading drilling mud filtrates. The permeability reduction in the water-sensitive sands is generally attributed to the hydration of argillaceous or bentonitic materials in the sand which are located between the sand grains.

As early as 1911 two soil scientists, Green and Ampt,[1] reported decreases in permeability obtained by flowing water through clay materials. Their work consisted of determining permeabilities to water and air of loam, clay and sand soils; the characteristic feature of their results was the high ratio of the air permeability to the water permeability of the clay soils. They concluded that the water has the effect of swelling the colloidal matter in the clay soil and so constricting the capillary passages.

In recent times numerous investigators have observed reductions of permeability in sands from various locations and for several types of water solutions. The type of mud was found to be an important factor in actual drilling performance by Wade, who correlated mud type and loss of productive capacity in newly completed wells.

In regard to the question of permanence of water blocking, it should be noted that all investigators have found a reduction in the permeability to oil following the introduction of water into a water-sensitive sandstone; and all except Bertness have reported that part, at least, of the reduction is permanent. It should be mentioned that even if plugging is temporary, it might cause considerable loss in production, and possibly cause the passing by of valuable pays due to faulty drill-stem or perforation tests.

It has become common practice in recent years to use oil-base and emulsion-base muds to avoid formation plugging when drilling into sands which are known to be water-sensitive. Both muds have definite advantages over the water-base muds; the oil-base mud yields no aqueous filtrate while the emulsion-base mud cuts down the filter loss to a negligible amount. Both muds are considerably more expensive for the same weight when compared to common water-base muds; therefore the question arises whether or not a more economical mud can be found for use in areas where water-sensitive sands are encountered.

At this time there is no information available making it possible to predict the degree of plugging of a particular sand by a specific filtrate utilizing air and water permeability data. Nor is there available published information concerning the effects of various mud filtrates and solutions on water-sensitive sands from the southern and southwestern producing areas. In view of the fact that these areas are highly productive, it would appear that information of this type would be desirable. It is also noted that work published to date consisted of flowing various solutions through test plugs of the same sand taken at different locations, rather than through specimens that were substantially identical, as in the present work. In previous work, test plugs, not taken at different locations, were treated in order by different solutions—a procedure which might greatly change the indicated effects.

Description of Materials

Cores.—One group of cores used in this work was taken from a well in Adams County, Mississippi, at depths of 5319, 5320 and 5574 feet and were from the Wilcox sand. They had an average air permeability of 254 md. and an average distilled water permeability of 118 md. Another group came from a well in Iberia Parish, Louisiana, at depths of 15,827, 15,827.5, and 15,828 feet and represents the lower Burkeville member of the Miocene Age. These cores had an average air permeability of 67.1 md., and an average distilled water permeability of 50.2 md. The third group used was from a well in Midland County, Texas, at depths of 7181, 7184 and 7186 feet from the Upper Spraberry sand. They had an average air permeability of 1.78 md. and an average distilled water permeability of 0.80 md.

The plugs used for permeability tests were one-half inch cubes cut from the cores. Using a diamond edge cutting blade, discs one-half inch thick were cut from the core sample on a stratigraphic plane and then the discs were cut into one-half inch cubes as illustrated in Fig. 1. This method of cutting plugs was utilized in order to obtain nearly identical plugs for comparative permeability tests. Considering the Burkeville sand core from Louisiana from which three different discs were cut from a one-foot length of core, the average deviation of the air permeabilities within each of the three discs was 5.8, 5.5 and 4.4%, respectively, while the average deviation of the air permeability considering the three discs combined was 7.6%. Considering the Spraberry sand core from Texas from which three different discs were cut from five feet of core, the average deviation of the air permeabilities within each of the three discs was 3.5, 2.4 and 4.6%, respectively, while the average deviation of the air permeability considering the three discs

combined was 13%. No comparison of this type is made of the Wilcox sand core from Mississippi since the discs tested were separated by over 250 feet.

When plugs were cut, bedding planes were indicated to ensure that flow tests would be made parallel to them. After the cubical plugs were cut from the core samples, they were cleaned by extraction with carbon tetrachloride in a Soxhlet extractor for six or eight hours. Following extraction the plugs were oven-dried for at least 24 hours at a temperature of 200°F.

Muds.—Filtrates from muds taken from mud pits of four drilling wells in Texas were used in the test procedure. The muds used were

F-1 Native mud treated with Hydrotan, *p*H of filtrate 8.0, salt content 0.60%

F-2 Lime base mud with caustic, quebracho, starch and salt, *p*H of filtrate 11.9, salt content 0.36%

F-3 Native mud treated with caustic, quebracho and Kembreak, *p*H of filtrate 8.0, salt content 0.12%

F-4 Common water base mud, *p*H of filtrate 7.8, salt content 0.16%

The common laboratory tests were performed on the field mud samples prior to the extraction of the filtrate for permeability tests. These mud tests included weight, Marsh funnel viscosity, shearometer, sand content, gel strength and filtrate; the results are listed in Table I. Approximately one liter of filtrate was extracted from each mud sample using the Bariod filter press at 100 p.s.i. It was necessary to determine the viscosity of each filtrate for later use in permeability calculations; this was accomplished by using the Ubbelohde viscosimeter to determine the ratio of filtrate viscosity to water viscosity at test temperature.

TABLE I

PROPERTIES OF FIELD MUDS

Mud	Wt., lb./gal.	Marsh funnel, sec.	Shearometer, lb./100 sq. ft.	Sand content, %	Initial gel, g.	Final gel, g.	Filtrate rate, cc./30 min.
F-1	10.25	46	10	1.4	44	174	13.5
F-2	10	42	3	0.3	2	4	14.0
F-3	10.25	42	4.25	0.3	3	50	17.5
F-4	10	48	10	0.2	3	64	11.0

Two muds were mixed in the laboratory, Mud L-1 was a sodium silicate mud with a filtrate *p*H of 10.9. The sodium silicate mud was mixed by combining Grade D sodium silicate solution, distilled water, bentonite and salt. The rate of filtration was negligible using the Bariod filter press at 100 p.s.i. so the mud was centrifuged and the separated liquid then filtered through paper. Mud L-2 was an oil-emulsion mud prepared by adding 5% by volume of a commercial oil-emulsion concentrate to a high grade water-clay mud. The low content of oil-emulsion concentrate was employed to give a high filtrate on the Baroid filter press and thus avoid excessive filtration time.

Solutions.—Five solutions in distilled water were prepared in the laboratory to determine their effects on the cores. The solutions were filtered through paper after mixing in order to ensure a clear sample for permeability tests. The solutions were S-1 (1% NaCl), S-2 (5% NaCl), S-3 (15% NaCl), S-4 (10% NaCl plus 5% CaCl) and S-5 (0.01 normal NaOH, *p*H of 12.0).

Equipment and Procedure

After the test plugs had been cut, extracted, dried and measured with a micrometer, air permeability determinations were made on all plugs. The test plugs were inserted in a tapered rubber stopper prepared with a square hole; the rubber stopper was mounted under pressure in a lucite cylinder with a tapered bore—tests made with impermeable plugs showed that there was no by-passing of fluid using this core mounting procedure at any pressures used in subsequent permeability tests. Two regulators in series were used to maintain a fine control on the supply of dry air. A wet test meter in combination with a stopclock was used to measure the flow of air.

The normal procedure used in air permeability determination was to make three or four measurements of the flow rate at one pressure for each plug. On several plugs, selected at random, the flow rate was measured at several pressures for use in computing a factor for correction due to the slippage effect for each formation (Klinkenberg effect). The uncorrect air permeability of each plug was computed using the equation derived from Darcy's law for linear flow of compressible fluids.

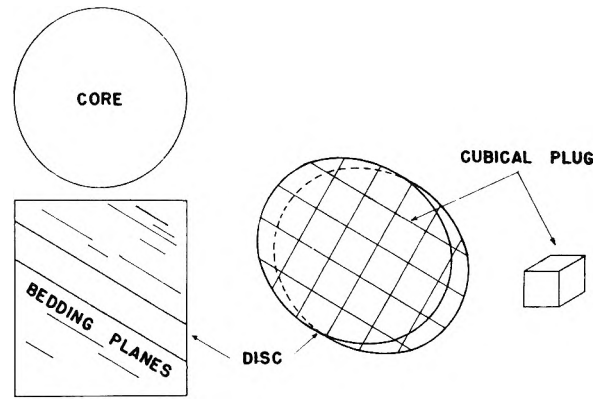

Fig. 1.—Method of obtaining cubical plugs from core samples.

Following the air permeability determinations, the plugs were again oven-dried, evacuated in a vacuum bottle and saturated with distilled water. The plugs remained in distilled water at least 24 hours to allow the swelling of clay to take place before permeability tests were made. Lucite and stainless steel materials were used throughout the liquid containing portions of the system to minimize contamination of the system due to corrosion. Air was first removed from the system with a vacuum pump and the saturated plug was introduced into the core mounting apparatus in such a way that no air would be trapped in the system. Pressure from the compressed air line was used to force distilled water through the plug. Fluid flow rates were measured with burets or small volume pipets and a stopclock. On several plugs, selected at random, flow was maintained for a period of 24 hours to ensure that the permeability was constant—an indication that the clay swelling within the plug, if any, was complete.

Following the distilled water tests, all plugs were again oven-dried. Then at least one plug from each formation was evacuated and saturated with one of the test solutions or filtrates. The permeabilities to solutions and filtrates were determined in a manner similar to the distilled water permeabilities. In some cases these permeabilities continued to decrease with flow after the plugs had been saturated for as long as three weeks. In such instances, the permeability was reported as that determined after 24 hours flow since in most cases it was negligible at that time.

Discussion of Results

The results of the tests are shown graphically in Figs. 2, 3, 4, 5 and 6, in which K_a, K_w, and K_f refer to the permeabilities measured with air, distilled water and the mud filtrate or solution.

Figures 2 and 3 show the effects of all the filtrates and solutions tested on the various sands as compared to the effects of water and of air, respectively. The bars representing the results of the Burkeville and Spraberry sands are average results for plugs from the three different depths. Since the plugs from different depths in the Wilcox formation exhibit different plugging tendencies, the Wilcox 5320′ plugs have been segregated from those taken at 5319′ and 5574′.

The variations in bar lengths in a group for each liquid tested indicate the variations in susceptibility to plugging of various formations. The variations appear more prominently in Fig. 2, where water permeability is used as the basis for comparison.

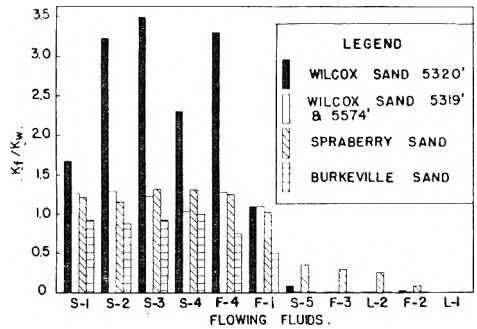

Fig. 2.—Variation of average K_f/K_w for various solutions and filtrates.

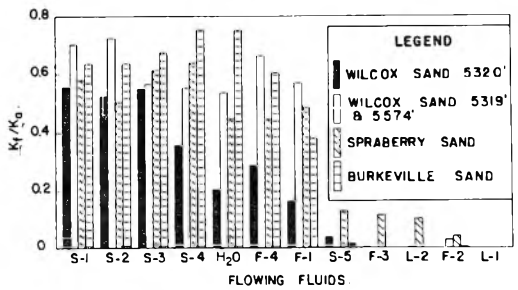

Fig. 3.—Variation of average K_f/K_a for various solutions and filtrates.

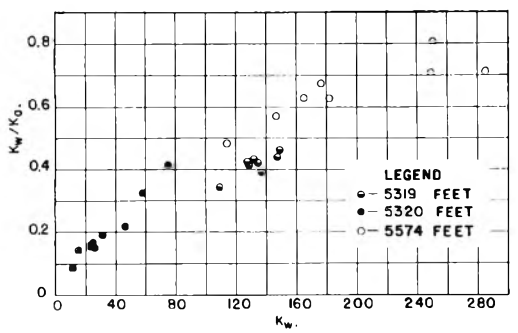

Fig. 4.—Permeabilities to water and air in the Wilcox sand.

The bar graph in Fig. 3 shows that, for all the aqueous solutions tested, K_f/K_a varies from 0.746 to zero; thus, for the cores tested, the permeability to these solutions is substantially lower than the corrected air permeability.

The permeabilities of the plugs to S-5, F-3, L-2 and F-2 are those measured after 24 hours of continuous liquid flow; at this time the permeability in each case was still slowly decreasing, but the tests were discontinued since the plugs had been saturated for at least three weeks prior to the permeability determination. The conspicuous magnitude of the bars representing the permeability of the Spraberry formation to these particular solutions is noteworthy. From the data obtained, it appears that the rate of decrease in permeability of the plugs to these particular solutions is a function of the volume of the solutions flowed through the plugs. Since the permeability of the Spraberry plugs is very much lower than the permeability of the other formations tested, the volume rate of flow of the solutions through the Spraberry plugs was considerably lower—consequently the permeability reduction after 24 hours flow of solutions S-5, F-3, L-2 and F-2 was

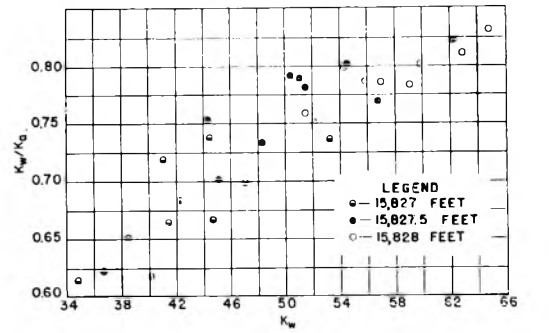

Fig. 5.—Permeabilities to water and air in the Burkeville sand.

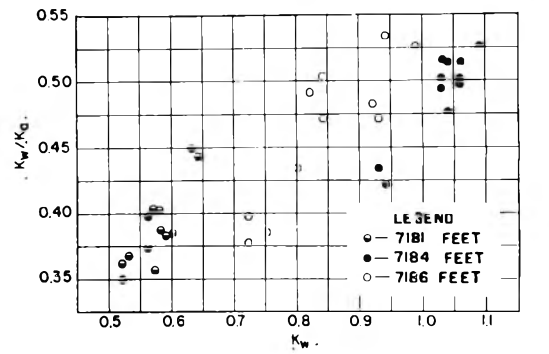

Fig. 6.—Permeabilities to water and air in the Spraberry sand.

considerably less than the permeability reduction in the other formations.

The solutions in Fig. 3 have been arranged in order of their increasing plugging effect on the average of the formations tested. Solutions S-1, S-2, S-3 and S-4 are brine solutions of various concentrations and compositions, but the bars indicate there is little difference in the plugging tendencies of the various brine solutions; the average permeability reductions by the four solutions ranged from 39 to 43%.

The average reduction in permeability by distilled water for all formations was 52%, but the lengths of the bars representing water permeability show the wide variation in plugging by water in the different formations tested; this probably is due to the various amounts of clay present in the different formations. While water reduces the air permeability of the Burkeville sand by only 25%, it reduces the permeability of the Wilcox 5320′ sand by as much as 80%. The average effect of water-base mud F-4 compares favorably with the effect of distilled water, the average reduction in permeability being 51%.

Highly alkaline solutions S-5, F-2 and L-1 caused a considerable reduction in the permeability and it is possible that the permeability would have been reduced to zero in all cases with these solutions had the tests been carried to completion. A dilute caustic soda solution reduced the permeability by 94%, a lime-base field mud filtrate reduced the permeability by 98%, and a sodium silicate mud filtrate completely plugged the sands tested.

The filtrate from the oil-emulsion mud prepared in the laboratory reduced the permeability by 94%. Though the permeability reduction by such

a filtrate is significant, it should be recalled that the laboratory mud was especially mixed to yield a relatively high filtrate loss (10 ml. in 30 minutes by API test). In the case of a carefully controlled field oil-emulsion mud, the filtrate invasion into the formation can be held to a minimum with the result that little of the formation would be affected.

Figures 4, 5 and 6 were plotted to show a significant trend in the data obtained. Water and air permeability results obtained from flow through several plugs from each core are plotted on separate graphs for each formation. With the results plotted as K_w/K_a *versus* K_w, a consistency is noted in all instances—there is a definite trend toward an increase in K_w/K_a with an increase in K_w when considering all plugs from a formation or when considering the plugs from within a particular disc. These three graphs can be interpreted as illustrating the effect of variation in the clay content of a rock. For each of the formations tested, where the permeability to water is comparatively low, the ratio K_w/K_a is comparatively low; where the permeability to water is comparatively high, the ratio K_w/K_a is comparatively high. In other words, where the clay content is comparatively high, the reduction in permeability is extensive upon the introduction of distilled water, whereas a much less pronounced permeability reduction results in flowing distilled water through a plug containing a lesser amount of clay.

Conclusions

1. The susceptibility of various cores to plugging by a specific aqueous solution varies widely, probably because of the variation of the nature and amount of the clay contained in the rock. For example, plugs from the Wilcox Sand at 5319′ and 5320′ are from the same formation and only one foot apart, yet show widely different susceptibility to plugging by various salt solutions.

2. For the cores tested, the permeability to all aqueous solutions is substantially lower than the permeability to air even after applying a correction for the slippage effect.

3. The greatest reduction in the permeability of all cores resulted from contact with alkaline filtrates and solutions. One filtrate from a lime-base mud with a *p*H of 11.9 reduced the average permeability of the cores tested by 98%, while a filtrate from a sodium silicate mud with a *p*H of 10.9 caused a reduction of 100%. A dilute caustic soda solution (0.01 *N*) reduced the average permeability by 94%.

4. A filtrate from an oil-emulsion mud, prepared in the laboratory to give a filtrate somewhat higher than normal (10 ml. in 30 minutes by API method), gave a reduction of 97%.

5. Two filtrates from field muds which had been subjected to considerable chemical treatment and with a *p*H of 8.0 and low salt content gave average reductions of 79%. Another field mud filtrate, with *p*H of 7 8 and low salt content, gave a reduction in permeability of 51%.

6. Three salt solutions, containing 1, 5 and 15% sodium chloride, reduced permeability on the average of 39, 41 and 42%, respectively. A 15% salt solution to which 5% calcium chloride had been added caused a reduction of 43%.

7. Distilled water reduced permeabilities on the average by 52%.

8. Considering results from any of the formations individually, there is a trend toward an increase in the ratio of the water to air permeability with an increase in the water permeability.

9. A new method of cutting plugs for comparative tests was developed, consisting of the preparation of numerous 0.5-inch cubes cut at a definite stratigraphic level. This method allows the obtaining of numerous plugs from a small volume of core which increases the probability of obtaining similar samples for comparative tests.

Acknowledgment.—The authors wish to acknowledge the financial support afforded by the Humble Oil and Refining Company, whose fellowship made this work possible. The cores and the field muds were also supplied by this company.

BIBLIOGRAPHY

(1) W. H. Green and G. A. Ampt, *J. Agr. Sci.*, **4**, 1 (1911).
(2) Fancher, Lewis and Barnes, Pennsylvania State Univ. Mineral Industries Experiment Station Bulletin 12, 1933, pp. 65–171.
(3) J. N. Breston and W. E. Johnson, *Producers Monthly*, **9**, 19 (1945).
(4) N. Johnston and C. M. Beeson, *AIME Transactions*, **160**, 43 (1945).
(5) T. F. Bates, R. M. Gruver and S. T. Yuster, *Producers Monthly*, **10**, 16 (1946).
(6) L. E. Miller, *ibid.*, **11**, 35 (1946).
(7) K. T. Miller, F. Morgan and M. Muskat, *ibid.*, **11**, 31 (1946).
(8) F. R. Wade, *Am. Petroleum Inst. Drilling Production Practice*, 186 (1947).
(9) W. F. Rogers, "Composition and Properties of Oil Well Drilling Fluids," Gulf Publishing Company, Houston, Texas, 1948, p. 11.
(10) T. J. Noak and R. F. Krueger, *World Oil*, **133**, 125ff (1951).
(11) T. A. Bertness, *Oil and Gas J.*, **52**, 58 (1953).

DISCUSSION

L. M. HERMES, JR.—What was the emulsifying agent in the emulsion mud whose filtrate was used in the permeability studies?

HARVEY T. KENNEDY.—It was a commercial compound sold for blending with oil and mud. Its trade name is not available.

V. N. BEDNARSKI.—To what do you attribute failure of Darcy's law in this case?—a decrease in the size of the pore or an increase in the viscosity of water in the pores.

HARVEY T. KENNEDY.—We do not consider that Darcy's law has failed, but merely that the coefficient K has changed due to the swelling of clays, with consequent decrease in size of pores.

STUDIES ON ION EXCHANGE RESINS. XIV. TITRATION, CAPACITY AND SWELLING OF METHACRYLIC ACID RESINS

BY HARRY P. GREGOR, MARY JANE HAMILTON,[1] JANE BECHER[2] AND FABIAN BERNSTEIN[3]

Contribution from the Department of Chemistry of the Polytechnic Institute of Brooklyn, New York

Received February 25, 1955

Titration curves of cross-linked polymethacrylic acid polymers are typical of those of polyacids. The polyacids are apparently weaker than their linear counterparts measured at the same salt concentration, reflecting the high Donnan concentration in the gel. When quaternary ammonium bases are used in place of alkali metal bases, there is a pronounced decrease in the average dissociation constant of the polyacids, which is presumed due to an increased chain potential resulting from the greater distance of closest approach with large gegenions. The swelling of the resins was larger with large gegenions, again indicative of a higher chain potential. Lithium and, to a lesser extent, sodium ions associate with the polyacid, as shown by swelling measurements.

The potentiometric titration of weak acid cation-exchange resins has been described by several investigators, namely, Gregor and Bregman,[4] Kunin and Berry,[5] Hale and Reichenberg,[6] and Katchalsky and Michaeli.[7] Swelling measurements on weak acid polyelectrolytes which have been made insoluble by either chemical cross-linking or by adsorption have been reported by Kuhn,[8] Kuhn and Hargitay,[9] Gregor[10] and others. A recent article by Katchalsky[11] presents an excellent review of the literature.

This contribution describes the behavior of carboxylic acid cation-exchange resin systems of different degrees of cross-linking when titrated with various bases and at varying ionic strengths. The *p*H of the solution phase, the absorptive capacities toward bases and the swelling of the resins were measured. Subsequent papers in this series will take up the selective uptake of one cationic species over another by the same resin systems.

Experimental

Preparation of Resins.—A series of methacrylic acid–divinylbenzene copolymers was prepared. The methacrylic acid monomer (Rohm and Haas Company) was a 90% aqueous solution; the divinylbenzene (DVB) mixture (Koppers) contained 40% divinylbenzene, 45% ethylvinylbenzene, and 15% diethylbenzene and other non-polymerizable materials. Monomer mixtures were weighed into 500-ml. round-bottomed flasks, benzoyl peroxide was added (1% by weight) and dissolved in the mixture by shaking. The contents of the flasks were then frozen in Dry Ice and the necks sealed.

The reactions were carried out to completion at 70° for 24 hours. Mixtures containing small amounts of DVB (< 5%) were homogeneous; systems containing more DVB were agitated constantly to prevent separation of phases. Each resin is referred to by its DVB content, as resin DVB 0.25, 0.5, etc., where the DVB number is the weight % of pure DVB of the total monomer mixture.

The solid resin mass was broken up, ground in a ball mill, and the particles conditioned by treatment with large excesses of 1 *M* hydrochloric acid and 1 *M* sodium hydroxide in alternate cycles.[12] After final regeneration with acid, the resins were rinsed with distilled water until the effluent gave no test for chloride ion and its *p*H was 4.5–6.0. The resin samples were air-dried until free flowing, screened and the −16 + 20 mesh fraction bottled for subsequent use. The moisture content was determined by drying to constant weight over P_2O_5. All data reported refer to one gram of dry hydrogen resin, and are called specific capacities, volumes, etc.

Rate of Uptake of Base.—In order to ensure equilibrium conditions in subsequent experiments, the rate of uptake of the potassium, tetramethylammonium, and tetraethylammonium hydroxides was measured. A measured excess (2–3 fold) of 0.05 *M* base was added to the hydrogen resin, the system stirred rapidly, and the concentration of base determined periodically. Throughout this investigation polyethylene vessels were used to avoid contamination from glass, and the systems were kept carbon dioxide free. Unless otherwise specified, the temperature was 24–26°.

For resins of DVB 2 or less, the half-times were in the range 5 to 15 minutes; equilibrium was reached within 12 hours. The rate of base absorption drops off sharply for the higher DVB resins; half-times of about 90 minutes were observed with DVB 9, 300–400 min. with DVB 16 and 24–200 hours with DVB 24. The longest half-times were for the tetraethylammonium base, the shortest for the potassium base. About 40 days were required for equilibrium of DVB 24 resin with tetraethylammonium hydroxide.

All of the data reported herein are equilibrium values; experiments were routinely continued for at least 1.5 times the period of time required to attain equilibrium. The rate of absorption follows the parabolic diffusion equation for the lower DVB resins. A later paper in this series will describe detailed rate experiments.

Titration and Determination of Capacity.—The acid resins were titrated with base as described by Gregor and Bregman.[4] At lower *p*H values (<10) the amount of base sorbed was equal to the amount added, with a minor correction applied where necessary for the base remaining in the solution phase. At higher concentrations of base and particularly at high neutral salt concentrations other methods were required because these resins swell on going from the acid to the base state,[10] absorbing water in the process and thereby concentrating the solution phase. This effect can be minimized by making appropriate corrections. Also, base in the form of non-exchange electrolyte enters the resin phase; this amount is small for all but those resins of low (<1%) DVB content.[13]

For the capacity determinations reported in this paper, the resin phase was freed of solution by centrifugation, and

(1) A portion of this work is abstracted from the thesis of Mary Jane Hamilton, submitted in partial fulfillment of the requirements for the degree of Master of Science in Chemistry, Polytechnic Institute of Brooklyn, June, 1950.

(2) A portion of this work is abstracted from the thesis of Jane Becher, submitted in partial fulfillment of the requirements for the degree of Master of Science in Chemistry, Polytechnic Institute of Brooklyn, June, 1950.

(3) A portion of this work is abstracted from the Dissertation of Fabian Bernstein, submitted in partial fulfillment of the requirements for the degree of Doctor of Philosophy in Chemistry, Polytechnic Institute of Brooklyn, February, 1952.

(4) H. P. Gregor and J. I. Bregman, *J. Am. Chem. Soc.*, **70**, 2370 (1948).

(5) R. Kunin and R. Berry, *Ind. Eng. Chem.*, **41**, 1269 (1949).

(6) D. K. Hale and D. Reichenberg, *Discs. Faraday Soc.*, **7**, 79 (1949).

(7) A. Katchalsky and I. Michaeli, *Bull. Research Council Israel*, **2**, 3 (1952).

(8) W. Kuhn, *Experientia*, **5**, 318 (1949).

(9) W. Kuhn and B. Hargitay, *Z. Elektrochem.*, **55**, 490 (1951).

(10) H. P. Gregor, *J. Am. Chem. Soc.*, **73**, 642 (1951).

(11) A. Katchalsky, "Polyelectrolyte Gels," from "Progress in Biophysics and Biophysical Chemistry," Vol. 4, Pergamon Press Ltd., London, 1954

(12) H. P. Gregor, J. I. Bregman, F. Gutoff, R. D. Boardley, D. E. Baldwin and C. G. Overberger, *J. Colloid Sci.*, **6**, 20 (1951).

(13) H. P. Gregor, F. Gutoff and J. I. Bregman, *ibid.*, **6**, 245 (1951).

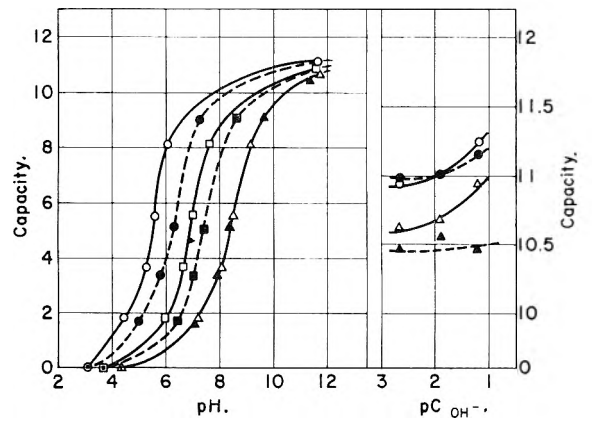

Fig. 1.—Titration of resin DVB 0.5 with sodium hydroxide in the presence of no salt (△), 0.01 M (□) and 1 M (○) sodium chloride, and with tetramethylammonium hydroxide in no salt (▲), 0.01 M (■), and 1 M (●) tetramethylammonium bromide. Data are given as capacity in millimoles of base sorbed per gram of dry hydrogen resin as a function of the pH of the solution phase. The capacity at high base concentrations is given as a function of the negative logarithm of the hydroxide concentration of the solution phase, determined by direct titration.

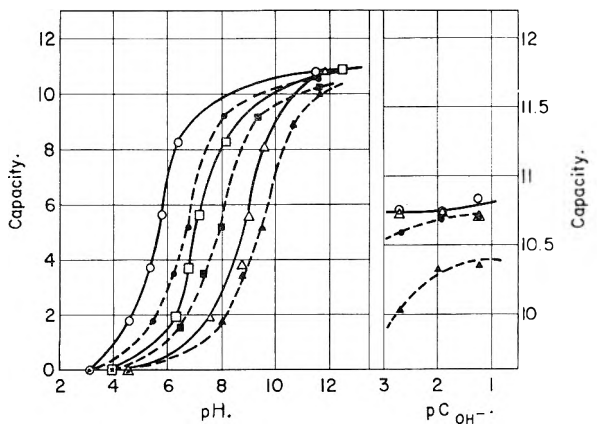

Fig. 2.—Titration of resin DVB 2 (see legend to Fig. 1).

its total base content determined by adding an excess of standard acid and back-titrating. The capacity determinations reported are accurate to within ±0.2% when dilute (< 0.05 M) solutions were used. At higher concentrations the error increases to about ±1%.

Potassium was determined by Flame Photometry; the average error in each determination was ±1%.

Titrations with sodium and with tetramethylammonium hydroxide in solutions of varying ionic strengths (as the corresponding chloride or bromide salts) for resins DVB 0.5, 2, 6 and 16 are shown in Figs. 1–4. The specific exchange capacities are given in millimoles per gram as a function of the pH of the equilibrating solution and of the negative logarithm of the hydroxide concentration.

Table I gives the specific absorptive capacity of different resins in dilute (0.03–0.06 M) solutions of various bases. The theoretical capacity was calculated from the composition of the monomer mixture, assuming complete conversion to the polymer.

Volume Determinations.—The specific external volume V_e of the resins was determined pycnometrically as described by Gregor, Gutoff and Bregman.[13] The specific wet weight W_e of the resin equilibrated with various solutions was determined by centrifugation. Since the particles are non-spherical, it was found necessary to centrifuge the higher cross-linked resins for 4 minutes; resins DVB 1 and 2 were centrifuged for 8 minutes. The centrifuge baskets were 100 mesh, which served to retain the relatively soft particles.

It was not possible to centrifuge the very low (0.5% and less) DVB resins because these were too soft and gelatinous in the salt state. Wet weights were determined by drawing

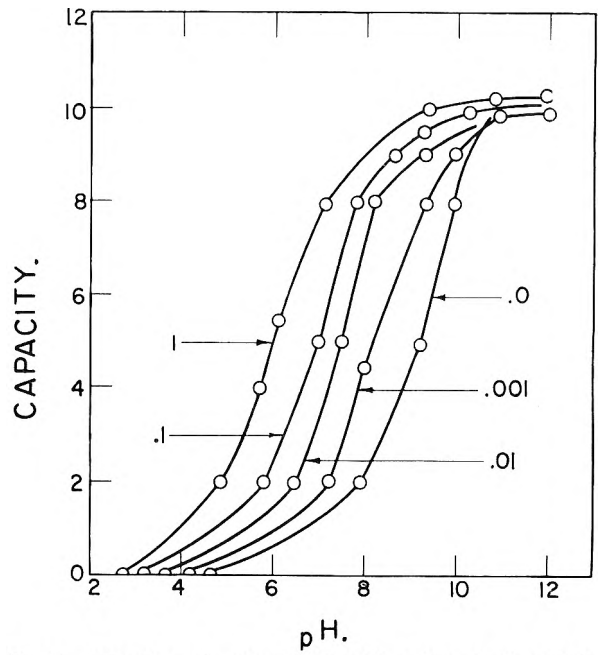

Fig. 3.—Titration of resin DVB 6 with sodium hydroxide in no salt, 0.001, 0.01, 0.1 and 1 M sodium chloride.

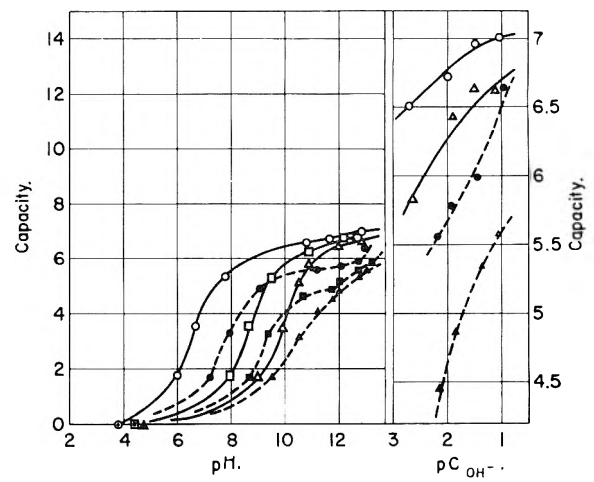

Fig. 4.—Titration of resin DVB 16 (see legend to Fig. 1).

air through a bed of resin to remove excess solution.[14] These values may be somewhat low, but the amount of water sorbed is so high as to make the absolute error small.

TABLE I

SPECIFIC CAPACITY OF RESINS IN DIFFERENT STATES

(Meq. absorbed at base concn. of 0.03–0.06 M)

DVB	Calcd.	Li^+	K^+	$(CH_3)_4N^+$	$(C_2H_5)_4N^+$
0.25	11.5	10.17	10.01	9.95	9.78
0.5	11.5		10.70		10.02
1	11.3	11.00	10.70	10.52	10.11
2	11.1	10.70	10.73	10.12	9.38
5	10.3		9.76		7.90
9	9.1		8.63	7.35	6.24
16	7.2	6.66	6.60	5.25	4.20
24	4.7	3.28	3.22	2.69	2.08

Table II summarizes experimental results of wet weight and volume determinations of various resins in the water-equilibrated hydrogen form and in dilute (0.03–0.06 M) solutions of lithium, potassium, tetramethyl- and tetraethyl-

(14) H. P. Gregor, K. M. Held and J. Bellin, *Anal. Chem.*, **23**, 620 (1951).

TABLE II

SPECIFIC WEIGHTS AND VOLUMES OF RESINS IN 0.03–0.06 *M* BASE SOLUTIONS

DVB	RCOOH W_e	RCOOH V_e	Li^+ W_e	Li^+ V_e	Li^+ m	K^+ W_e	K^+ V_e	K^+ m	Me_4N^+ W_e	Me_4N^+ V_e	Me_4N^+ m	Et_4N^+ W_e	Et_4N^+ V_e	Et_4N^+ m
0.25	14.87	14.62	33.48		0.31	34.16		0.31	36.44		0.29	49.44		0.21
.5						21.71		0.50						
1	2.88	2.62	8.57	8.06	1.47	10.10		1.23	11.80		1.05	15.88		0.75
2	2.42	2.17	5.01	4.53	2.71	5.31	4.58	2.75	6.77	6.46	2.01	9.90	9.55	1.22
9						4.06	3.45	3.16	3.94	3.65	3.07	4.44	4.14	2.37
16	1.31	1.12	2.38	2.04	4.99	2.90	2.42	3.95	2.65	2.40	4.15	3.49	3.25	2.16
24	1.12	0.99	1.62	1.39	5.44	1.80	1.50	4.72	1.73	1.56	5.00	1.76	1.59	4.24

ammonium hydroxides. The molality of the exchange cation, expressed as millimoles per gram of sorbed water, is also given. The swelled wet weights of various DVB resins in the hydrogen, potassium and tetraethylammonium states are shown graphically in Fig. 5.

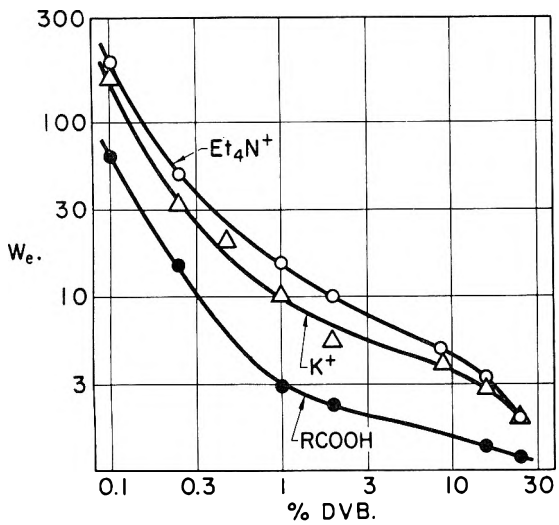

Fig. 5.—Specific wet weights of various DVB resins in the acid state and in dilute (0.03–0.06 *M*) solutions of potassium and tetraethylammonium hydroxide.

The swelling of a hydrogen form resin upon neutralization with various bases is shown in Fig. 6. Here 0.5-g. portions of resin DVB 6 in 100 ml. of water were neutralized with base. In these experiments, the approximate *p*H values at equilibrium were: 0 mmoles, *p*H 5; 2, *p*H 8; 4, *p*H 8.5; 6, *p*H 9.5; 8, *p*H 10; 10, *p*H 10.5. The V_e values are given at different apparent degrees of neutralization α, where α is the moles of base added divided by the total capacity of the resin toward *potassium* hydroxide.

Deswelling in Concentrated Base Solutions.—When a resin equilibrated with dilute base solutions is placed into more concentrated solutions, deswelling takes place.[13] Resin DVB 6 was treated with a large excess of potassium hydroxide solutions of different concentrations. After equilibration, the external volumes of the resin particles were determined pycnometrically. Then the centrifuged resin was placed in a small quantity of distilled water and the non-exchange base eluted and determined conductometrically. The concentration of base in this eluate was sufficiently high so that the extent of hydrolysis was small. Figure 7 shows a plot of the specific resin volume *vs.* the logarithm of the concentration of potassium hydroxide in the solution phase; the specific non-exchange base content also is given.

It was observed that in the highly swelled state (dilute base solutions) the resin was quite soft and crumbled easily. When deswelled in concentrated base solutions the gel particles were firm and as stable as in the relatively unswelled, hydrogen state.

The external volume of the resin in the dry hydrogen state was also determined using octane (which did not swell the resin) as pycnometric fluid. The specific volume as determined by this method was 0.802 ml./g.

Equilibration with Hydrochloric Acid.—Resin DVB 6 in the hydrogen form was equilibrated with hydrochloric acid solutions, following which W_e and V_e were determined and the hydrochloric acid present in the resin phase eluted and determined. The results are shown in Fig. 8. The external volume of the resin is almost constant up to hydrochloric acid concentrations of 1 *m* (molal); some deswelling takes place in 3 *m* solutions, which may be the result of a "salting out" of the polymer by the high electrolyte concentration.

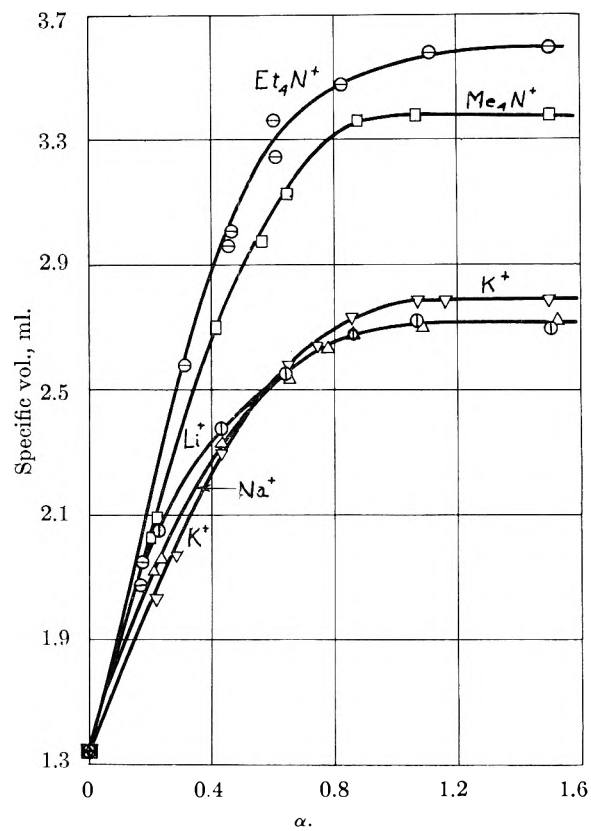

Fig. 6.—Specific volume V_e of resin DVB 6 as a function of α, the millimoles of base added divided by base capacity of the resin toward *potassium* hydroxide with the following bases: potassium (▽); sodium (△); lithium (Φ); tetramethylammonium (□); tetraethylammonium (⊖).

The molal concentration of hydrochloric acid in the resin phase was proportional to that in the solution phase, but less than the latter. For example, at a solution molality of 0.5 the molality in the resin phase was 0.3.

Discussion

In this contribution the qualitative aspects of the observed phenomena are discussed; later papers in this series will deal with quantitative calculations. Since we are dealing here with a cross-linked polyelectrolyte system, the data and theory of linear polyelectrolytes are particularly pertinent. The reader is referred to the excellent review

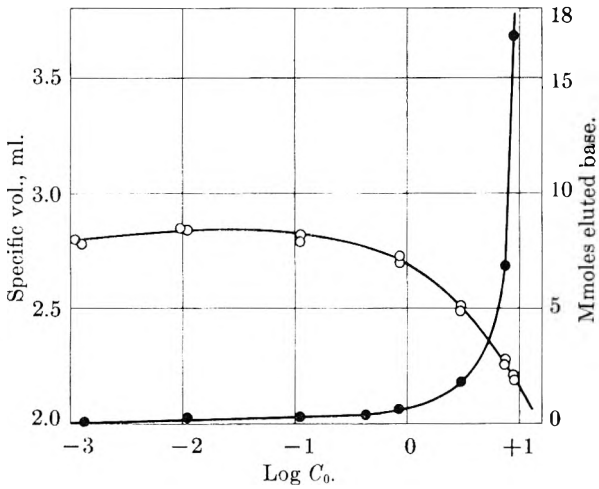

Fig. 7.—Specific volume (○) of resin DVB 6 as a function of the concentration of potassium hydroxide in the solution phase (C_0). The specific millimoles of sorbed diffusible base shown (●).

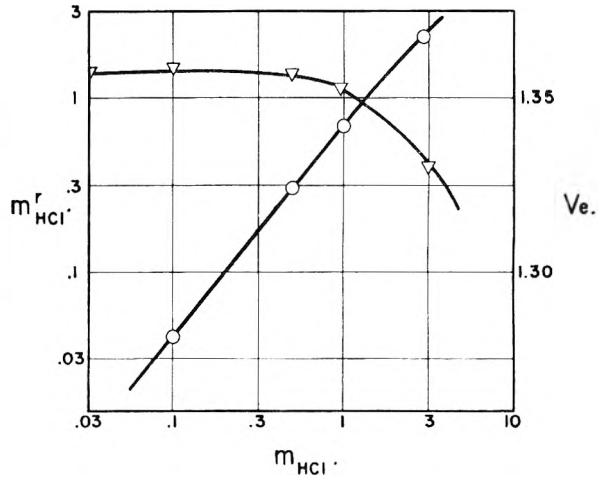

Fig. 8.—Specific volume of resin DVB 6 (▽) and molality of hydrochloric acid in the resin phase m^r_{HCl} (○) as a function of the molality of hydrochloric acid in the solution phase.

articles by Doty and Ehrlich,[15] Fuoss[16] and Katchalsky.[17]

A pictorial representation of the systems being considered is shown in Fig. 9. A ten-unit segment of a polyacid chain which is 20 and 80% neutralized by either potassium hydroxide or by a quaternary ammonium hydroxide is shown. The parallel situation which may prevail with the same polyacid with ten units between cross-links is also shown.

With the linear fragments, the chain unfolds and assumes a lower configurational entropy upon neutralization because of mutual repulsion by the negative charges formed there. If the gegenions are large and cannot approach the chain as closely as smaller ions the potential on the chain is greater. Accordingly, the dissociation constant of carboxyl groups on the chain is less with large than with small gegenions. An equivalent statement is that smaller gegenions which can approach closer to the chain are more efficient at shielding than are the larger gegenions.

When a cross-linked polyacid is titrated the same considerations would appear to apply. Because there are restrictive forces upon extensions of the chain and the degree of elongation is less, the concentration of negatively charged groups in a volume element is greater. Also, the average distance separating fixed and mobile charges would be greater with cross-linked than with linear polymers because the coiling of the chain prevents close approach of the gegenions. Other things being equal, one would expect a larger chain potential with cross-linked polyacids with a resulting smaller average dissociation constant.

When the cation of the base used in neutralization is large, the effects described above are expected to be stronger. In particular, coiling of the chain would make the close approach of large gegenions much less probable.

The principal effects observed in this contribution are as follows: (1) the titration curve of the resin acid is typical of those of polymeric acids; (2) as the size of the base cation is increased the resin acid apparently becomes weaker; (3) the base absorptive capacity of the resin is the same with small inorganic cations and significantly less with large gegenions; (4) the swelling of the resin is a function of both the size of the exchange cation and of specific interactions of exchange cations with the carboxyl groups of the resin.

The validity of the model of Fig. 9 for linear polyacids has been demonstrated by direct experiment of Gregor,[18] who found that the average dissociation constant of polyacrylic acid became successively smaller when titrated with bases in the following sequence: potassium > tetramethylammonium > tetraethylammonium > tetrabutylammonium. Further work on these systems will be reported upon later.[19] The titration curves were found to follow the Henderson–Hasselbalch equation $pH = pK_a - n \log (1 - \alpha)/\alpha$ where α is the degree of neutralization, n a constant and K_a the apparent or average ionization constant. The term α is defined as equivalents of base added per equivalent of polymer acid present when one is considering the titration of linear polyacids; the self-ionization of the polymer acid is neglected. When considering the behavior of cross-linked polyacids, α is the equivalents of base sorbed by the resin divided by the equivalents of resin acid present as determined by capacity measurements. Here self-ionization of the acid is neglected also.

The basic difference between the two α's is that with the linear polymer it is *assumed* that virtually all of the added base reacts with the acid. This is apparently true with alkali metal ions, but may not be the case with the quaternary bases. For example, the titration curve of polyacrylic acid with tetramethylammonium hydroxide does not show a break until $\alpha = 1.2$, while with tetrabutylammonium hydroxide no break is observed even up to $\alpha = 1.4$.[18] In the case of the cross-linked resins, however, α can be determined directly.

(15) P. Doty and G. Erhlich, *Ann. Rev. Phys. Chem.*, **3**, 81 (1952).
(16) R. M. Fuoss, *J. Polymer Sci.*, **12**, 185 (1954).
(17) A. Katchalsky, *ibid.*, **12**, 159 (1954).
(18) H. P. Gregor, L. B. Luttinger and E. M. Loebl, *J. Am. Chem. Soc.*, **76**, 5879 (1954).
(19) H. P. Gregor and M. Frederick, to be published.

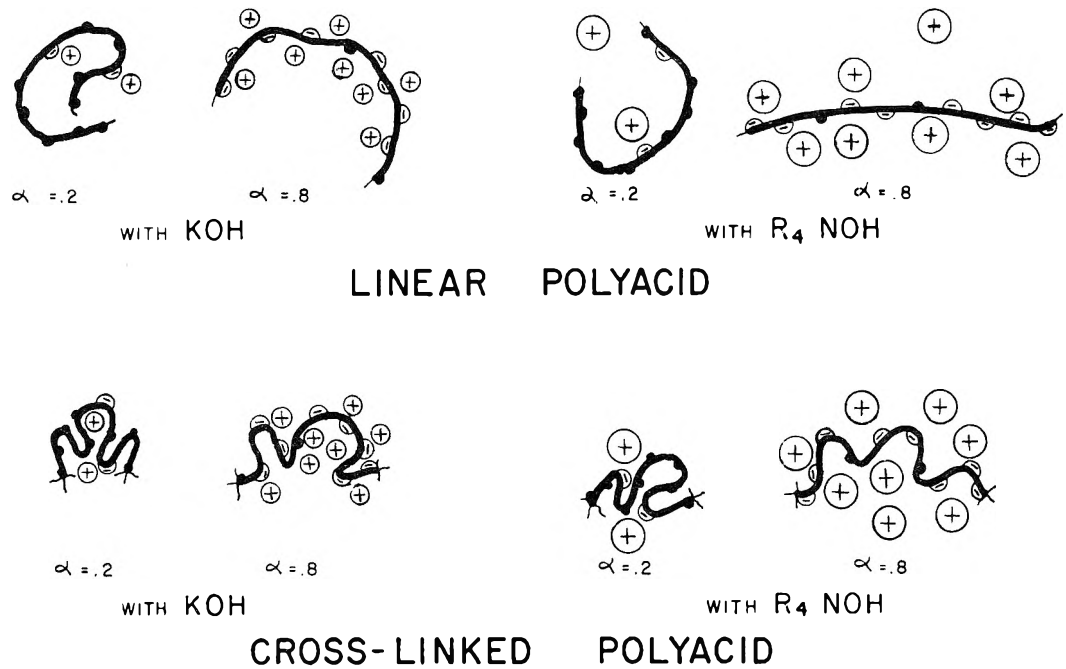

Fig. 9.—Model of a ten-unit segment of a linear and cross-linked polyacid. Undissociated carboxyl groups shown (●), ionized carboxylate groups shown (⊖). The polymer is 20 and 80% neutralized with bases having small and large cations.

When a cross-linked polyacid is titrated the *p*H which is measured is that of the solution phase in equilibrium with the polymer gel, whereas with the linear polyacid the *p*H of a homogeneous phase is measured. If one postulates that with soluble polymers the *p*H of the solution outside of the polymer coils is being measured, then measurements on the two systems are directly comparable. The polymer coil can be treated as a microscopic Gibbs–Donnan system; Kimball, Cutler and Samelson[20] and others have used this approach.

Measurements performed on the resin systems are free of errors due to potentials arising at polyelectrolyte solution–salt bridge junctions; these potentials give low *p*H values, according to Loosjes.[21]

A comparison of Figs. 1–4 shows that with resins DVB 0.5, 2 and 6 the sodium capacity apparently levels off at about *p*H 12 or 0.01 *M* base in both the absence and presence of salt. Certain significant differences are found to occur with resin DVB 0.5 which can be ascribed as being due to the sorption of non-exchange base by a resin having a low Donnan concentration from solutions which are relatively concentrated. Gregor, *et al.*,[13,22,23] have measured this sorption by different cross-linked polystyrenesulfonic acid systems. To demonstrate this effect, in Fig. 10 the molality of diffusible electrolyte (ammonium chloride) in the resin phase is shown plotted against the total cationic molality of the resin system in equilibrium with 0.01, 0.1, 1 and 5.7 *m* solutions of ammonium chloride. The strong divergence between the experimental curves and those calculated for ideal Donnan systems when the solution phase becomes dilute is due to the strong binding of gegenions by the polyion. These results are similar to those obtained with linear polymers by several authors,[16,17] in particular Wall[24] and Katchalsky and Michaeli.[7]

Resin DVB 0.5 sorbs more base from 0.1 *M* solutions than from 0.001 *M* solutions in the absence of salt. This is consistent with the data of Fig. 10. The increase in capacity on going from no salt to 1 *M* salt of about 3–5% is similarly due, at least in part, to the sorption of non-exchange electrolyte. The capacity toward tetramethylammonium hydroxide is significantly low in the absence of salt.

As regards base absorptive capacity, resin DVB 16 shows sharp differences in capacity toward sodium hydroxide in no salt and 1 *M* salt solutions; the capacities toward tetramethylammonium hydroxide are low and very much dependent on salt concentration as shown in Fig. 4.

The data of Figs. 1–4 were plotted as solution *p*H *vs.* log $(1 - \alpha)/\alpha$. The capacity of the resin was taken at the point where it apparently leveled off. Small errors in the capacity as taken do not affect the plots markedly. For resins DVB 0.5 and 2, the capacities were taken as 10.7 mmoles/g.; with resin DVB 16 it was 6.8 for sodium, 6.0 for tetramethylammonium. The Henderson–Hasselbalch plot is given in Fig. 11 for resin DVB 2; data for other resin systems gave similar straight lines. Table III lists values of pK_a and n for these and other systems.

An examination of Figs. 1, 2, 4 and 11 and Table III shows the significant apparent decrease in polyacid strength when large gegenions are in-

(20) G. E. Kimball, M. Cutler and H. Samelson, THIS JOURNAL, **56**, 57 (1952).

(21) R. Loosjes, Thesis, Utrecht, 1942.

(22) H. P. Gregor and M. H. Gottlieb, *J. Am. Chem. Soc.*, **75**, 3539 (1953).

(23) M. H. Gottlieb and H. P. Gregor, *ibid.*, **76**, 4639 (1954).

(24) J. R. Huizenga, P. F. Grieger and F. T. Wall, *ibid.*, **72**, 2636, 4228 (1950).

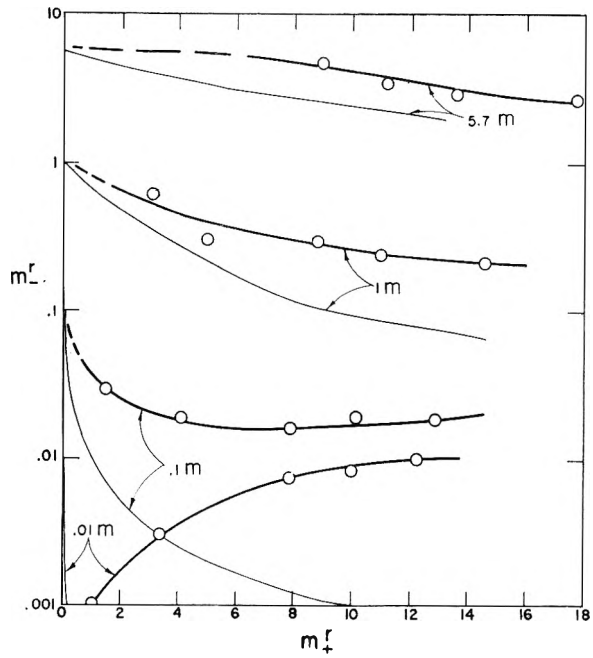

Fig. 10.—Molality of diffusible or non-exchange electrolyte (m_-^r) in various polystyrenesulfonate–DVB resin phases plotted against the total cationic molality of the resin (m_+^r), for resin systems in equilibrium with ammonium chloride solutions of different molalities.[13,22] Curves calculated for ideal systems are shown (——).

volved. The effects increase sharply with an increase in cross-linking, as would be expected from the model.

TABLE III

AVERAGE DISSOCIATION CONSTANT pK_a AND SLOPE n OF HENDERSON-HASSELBALCH PLOTS FOR LINEAR AND CROSS-LINKED POLYACRYLIC AND POLYMETHACRYLIC ACIDS

Polymer	DVB, %	Base	No salt pK_a	No salt n	0.01 M salt pK_a	0.01 M salt n	1 M salt pK_a	1 M salt n
PMA[a]	0	Na^+	7.2	2.0	6.6	1.7	5.2	1.2
(0.01 N)		Me_4N^+	7.3	2.2				
PMA	0.5	Na^+	8.5	1.5	7.0	1.4	5.6	1.3
		Me_4N^+	8.5	1.5	7.6	1.6	6.4	1.5
PMA	2	Na^+	8.9	1.8	7.2	1.8	6.9	1.7
		Me_4N^+	9.5	1.9	8.0	2.0	5.7	1.9
PMA	16	Na^+	9.8	1.7	8.7	1.6	6.7	1.5
		Me_4N^+	10.5	2.3	9.4	2.0	7.9	1.7
PAA[b]	0	K^+	6.4	2.2	6.0	2.3	4.7	1.5
(0.01 N)		Me_4N^+	6.5	2.3	6.2	2.5		
PAA	2	K^+	7.3	2.1	6.7	1.8	5.1	1.7

[a] Polymethacrylic acid. [b] Polyacrylic acid.

Examination of Table III shows that the resins are apparently always weaker than the corresponding linear polymer; the difference is greatest at low salt concentrations, smallest at high salt concentrations. It increases with cross-linking. This apparent difference is probably the result of the Donnan distribution. The molality of the carboxylate polyanion is very much higher in resin systems (see Table II) than in the linear polymer solutions (0.01 N in Table III), and consequently the ratio of "internal" to "external" phase cationic activities is very much higher in the resin systems. At the same "inside" hydrogen ion activity the measured "outside" pH will be higher for cross-linked than for linear polyacids, and thus the

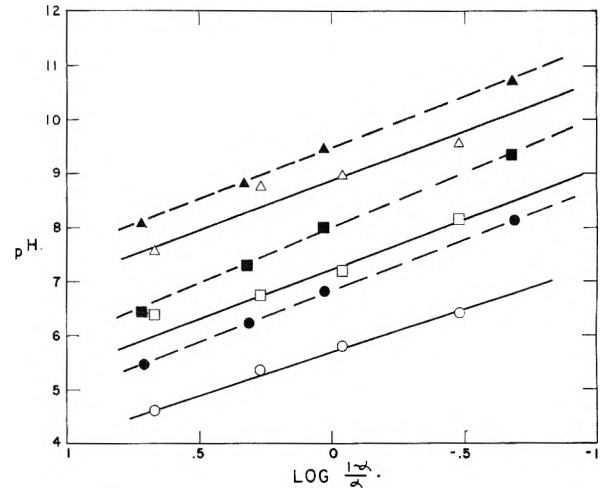

Fig. 11.—Modified Henderson–Hasselbalch plot for resin DVB 2 (see Fig. 2). Points are as follows: sodium hydroxide in no salt (△), 0.01 M (□) and 1 M (○) sodium chloride; tetramethylammonium hydroxide in no salt (▲), 0.01 M (■) and 1 M (●) tetramethylammonium bromide.

apparent dissociation constant will be lower. A simple calculation will show, however, that the model of a polyacid in a Donnan system does not suffice to explain differences in n; the configurational entropy of the chain probably is an important factor.

The actual absorptive capacities of the resins in 0.03–0.06 M base solutions are shown in Table I. The calculated capacities decrease at high DVB contents because of the weight per cent. of the inert cross-linking agent. The alkali metal hydroxides were taken up in equal amounts, and the capacity was lower toward the quaternary ammonium hydroxides. The relative capacities to potassium, tetramethylammonium and tetraethylammonium hydroxide by the various DVB resins were as follows: DVB 1, 1:0.98:0.95; DVB 9, 1:0.85:0.72; DVB 16, 1:0.80:0.64; DVB 24, 1:0.84:0.65. The relative decrease is the same for resins DVB 16 and 24; this is probably due in part to a smaller chain potential because of a lower density of carboxyl groups along the chain, and in part to the adsorption of the organic cations by the increasingly apolar polymer.[25]

The hydrogen form resins swell with the addition of base, attaining a more or less constant volume upon neutralization. Figure 6 shows the swelling of a DVB 6 resin upon the addition of potassium, sodium, lithium, tetramethylammonium and tetraethylammonium hydroxides. These data were obtained in the absence of neutral salt. It is noted from Fig. 6 that at $\alpha \leqq 0.5$ the potassium resin had a significantly smaller volume than did the sodium form of the resin, which was smaller in turn than the lithium form. However, there is a cross-over at about $\alpha = 0.7$ above which the potassium form of the resin has the largest volume while those of sodium and lithium resinates are smaller. These differences are the result of specific interactions between the carboxyl groups of the resin and the alkali metal ions. There is association or ion-pair formation between the lithium ion and car-

(25) H. P. Gregor and F. Bernstein, to be published.

boxyl groups; this occurs to a lesser extent with sodium and to a slight extent if at all with potassium. These interactions are postulated because of various experimental results. For example, the mean activity coefficients of the alkali metal acetates decrease in the series potassium > sodium > lithium; this series is the reverse of that with the chlorides. Also, the insolubility of dicarboxylic acids are in the sequence Li > Na > K. A discussion of the nature of these interactions may be found in Harned and Owen.[26] Certain chelates exhibit the same phenomenon, as has been described by Schwarzenbach[27] and Van Wazer.[28] Gregor[19] has shown these same effects with polyacrylic acid.

At low values of α these specific interactions are relatively weak because the polymer chain has a low charge. Under these circumstances, the smaller (hydrated) potassium ion gives a smaller resin volume. However, as the potential on the chain increases, appreciable association of sodium and lithium ions with the polymer chain is observed. The selective uptake of the various alkali metal ions by these resins bears out this point of view.[25]

The volume of the resin in the tetraethylammonium and tetramethylammonium states was significantly larger than in the alkali metal state due to the larger size of the gegenions.[10,13] Significantly, the polyacid was apparently neutralized with tetramethylammonium hydroxide as evidenced by a leveling-off of the curve at $\alpha = 1.1$ but not at $\alpha = 1.5$ in the case of the tetraethylammonium hydroxide. This swelling behavior confirms the titration curves discussed previously.

The swelling of polymethacrylic acids having different degrees of cross-linking in dilute (0.03–0.06 *M*) solutions of potassium and tetraethylammonium hydroxides were shown in Fig. 5. Curves for the same resin in the hydrogen form in distilled water were also shown. The considerable increase in volume with decrease in cross-linking is evident from Fig. 5. Resins have been prepared which contain 0.03% DVB which have wet weights of approximately 1000 g.[19]

It is particularly significant to note that the swelled volume of the tetraethylammonium resins was greater than that of the potassium resin even for very weakly cross-linked resins. At moderate (8–16% DVB) degrees of cross-linking, the large volume of the tetraethylammonium ion makes for a higher osmotic pressure and consequently a larger swelled volume when compared to the potassium resin.[13] With resin DVB 26 adsorption of the organic ion is such as to make the differences in volume negligible. However, resin DVB 0.25 which is approximately 0.31 *m* with respect to potassium and 0.21 *m* with respect to tetraethylammonium has a swelled weight of 34.1 g. in the potassium state and 49.4 g. in the tetraethylammonium state. At this low degree of cross-linking the osmotic pressure is negligible, and one would expect that the resin volumes would be approximately equal in the absence of other effects. However, here the large quaternary ammonium gegenion makes for a high chain potential and consequently a lower configurational entropy.

It is interesting to compare the swelling results obtained here with carboxyl resins of low degrees of cross-linking with data on similar polystyrenesulfonic acid resins.[13] A DVB 0.4 sulfonic acid resin had a specific wet weight of 42.8 g. and was 0.13 *m* to potassium; with tetraethylammonium the corresponding values were 33.9 g. and 0.21 *m*. The lower degree of swelling of the quaternary ammonium sulfonate resin is the result of adsorption of the large gegenion by the aromatic polyacid. Polymethacrylic and acrylic acids are more polar in nature and therefore adsorption is not significant. In the absence of osmotic pressure effects, the polystyrenesulfonate resins select the quaternary ammonium ions preferentially over potassium,[29] and the reverse is observed with polymethacrylic acid resins.[25]

Evidence for association between the polyacid and lithium ions may also be seen in Table II. The swelled volume of potassium form resins is consistently larger than that of lithium form resins, even with resin DVB 0.25 where osmotic pressure effects and differences in hydrated ionic sizes are not significant.

The deswelling of resin DVB 6 in concentrated base solutions shown in Fig. 7 is typical of the behavior of ion exchange resins.[13,23] From the amount of sorbed non-exchange base the mean activity coefficients of potassium hydroxide in the resin phase may be calculated.[13,22] It is of more interest to calculate the reduced mean activity coefficient, defined as the ratio of the mean activity coefficient of diffusible base in the resin phase divided by the mean activity coefficient in the solution phase. For resin DVB 6, values of the reduced mean activity coefficient at various solution concentrations are as follows: $\gamma'_{\pm} = 0.47$, 0.1 *M*; 0.74, 0.9 *M*; 1.35, 3 *M*; 1.29, 7.5 *M*. These results are similar to those obtained with sulfonic acid cation-exchange resins and quaternary ammonium anion exchange resins, where the reduced mean activity coefficient is low at low solution phase concentrations, and rises to about unity at high concentrations. Similar results have been obtained with linear polyacids.[11,17]

The sorption of hydrochloric acid by resin DVB 6 is quite different than in the case of base sorption, as expected. The molality of acid in the resin phase is about 0.6–0.7 that in the solution phase, reflecting probably hydration of the polymer.

This investigation was supported in part by the Office of Naval Research, and in part by a research grant RG-2934 from the Division of Research Grants of the National Institutes of Health, Public Health Service.

(26) H. S. Harned and B. B. Owen, "The Physical Chemistry of Electrolytic Solutions," Reinhold Publ. Corp., New York, N. Y., 1950.

(27) G. Schwarzenbach and H. Ackermann, *Helv. Chim. Acta*, **30**, 1798 (1947).

(28) J. R. Van Wazer and D. A. Campanella, *J. Am. Chem. Soc.*, **72**, 655 (1950).

(29) H. P. Gregor and J. I. Bregman, *J. Colloid Sci.*, **6**, 323 (1951).

DISCUSSION

MAX BENDER.—Would you, on a summary basis, relate the degree of swelling with the degree of cross-linking and the ions associated with the resins. The role of Donnan equilibrium in all this?

FABIAN BERNSTEIN.—The degree of swelling decreases with increase in cross-linking as shown in Fig. 5. In general, the greater the degree of hydration of the gegenion, the smaller the resin volume will be with weak acid resins (as opposed to strong acid resins). This is due to "ion pair" formation with the carboxyl group through a water molecule according to the "local hydrolysis" mechanism (see ref. 26). Where the cations are not hydrated, as with the quaternary ammonium ions, the swelled volume increases with the size of the gegenion. At low degrees of cross-linking, it is due to the ineffective shielding of the gegenions resulting in high chain potentials; at moderate degrees of cross-linking, the large size of the gegenions makes for a high osmotic pressure. Donnan effects will generally cause a decrease in swelling because of the additional shielding of the fixed charges on the chain by the additional diffusible gegenions.

SURFACE INTERACTION BETWEEN METALLIC NICKEL AND ETHYLENEDIAMINE SOLUTIONS

BY THOS. L. KEELEN AND ROBBIN C. ANDERSON

Department of Chemistry, University of Texas, Austin, Texas

Received February 25, 1955

Rates of solution have been measured for metallic nickel in basic solutions of ethylenediamine, diethylenetriamine and triethylenetetramine in water or methanol. Comparative rates show that the solution is not simply a result of decreased nickel ion concentration because of complex formation, but that it involves rather a surface reaction of the amines. It was found that appreciable reaction could occur in the absence of oxygen. Other results indicate that adsorption of both water and the amine are necessary for the surface reaction.

In recent years there has been increasing interest in the role of adsorption in the action of corrosion inhibitors, including chemisorption of inhibitor molecules by formation of coördinate covalent bonds with surface atoms of the metal.[1] Such bond formation is also of interest as a possible explanation for various cases in which the inhibitor can actually cause dissolution of the metal—cases which are usually explained on the basis of increased oxidation potential resulting from the decrease of concentration of metal ion by complex formation in solution. Corrosion of nickel has, for example, been found[2] to occur in concentrated ammonium hydroxide solutions which are aerated.

Preliminary tests with nickel and various complexing agents showed that the metal dissolves fairly readily in basic solutions of ethylenediamine. This was chosen as an example for study and diethylenetriamine and triethylenetetramine were included for purposes of comparison. The results of an investigation to obtain information on the adsorption and surface reactions occurring in this solution process are reported below.

Experimental

Materials.—The nickel used for these experiments was in the form of a powder supplied by the International Nickel Company. This powder was prepared by high temperature reduction of nickel carbonyl. Gravimetric analysis indicated that it was 99.67% nickel, with carbon as the most probable impurity. The average particle size was about 7 μ, and the surface area 0.72 m.^{2}/g.

The methanol was reported to be 99.85% pure. Analysis using the Karl Fischer reagent[3] showed 0.09% water. The alcohol was kept under air dried by anhydrous magnesium perchlorate.

The ethylenediamine (en) was obtained from Eastman Organic Chemicals and was purified by the method of Bromley and Luder.[4] The diethylenetriamine (dien) was purified by the method of Jonassen, LeBlanc and Rogan.[5] Technical grade triethylenetetramine (trien) was purified by recrystallization of the dihydrochloride from ethanol.

Procedure.—In general a weighed portion of nickel was placed in the amine solution in a glass-stoppered flask, and after a certain length of time a portion of the solution was withdrawn and the concentration of the nickel–amine complex determined spectrophotometrically, using a Beckman model DU spectrophotometer.

In methanol solution the absorption for the triethylenediamine nickel(II) ion showed a maximum at 550 mμ and followed Beer's law. There was no significant variation with temperature under the conditions used here.

The "*p*H" values reported in these results are readings obtained with a Beckman model G or H meter. They are useful for comparative purposes but not necessarily accurate on an absolute basis.

Adsorption measurements were made by exposing the nickel to an amine solution, then removing the solution and determining the loss of amine by titrating potentiometrically with standard hydrochloric acid.

One set of nickel samples were treated in the manner described by Zettlemoyer and Chessick[6] to remove adsorbed water vapor. This consists of degassing for 3 hours at 300° and 10^{-5} mm. Another set of nickel samples were treated with 0.2 *N* HCl in methanol to dissolve the nickel oxide. These were then washed repeatedly with methanol and degassed. This procedure was designed to remove the bulk of any surface oxide.

Results

With nickel and solutions of ethylenediamine in water or methanol, a lavender-colored solution was obtained. Traces of gas formed could be observed, and qualitative tests showed this to be hydrogen. The optimum *p*H was around 9.0. These are similar to the observations of Ponzio[7] on dimethylglyoxime solutions. Diethylenetriamine and triethylenetetramine also gave lavender solutions. In acid solutions, the ethylene-

(1) *Cf.* N. Hackerman and A. C. Makrides, *Ind. Eng. Chem.*, **46**, 523 (1954).

(2) R. J. McKay and R. Worthington, "Corrosion Resistance of Metals and Alloys," Reinhold Publ. Corp., New York, N. Y., 1936, p. 364.

(3) K. Fischer, *Z. angew. Chem.*, **48**, 394 (1935).

(4) W. H. Bromley and W. F. Luder, *J. Am. Chem. Soc.*, **66**, 107 (1944).

(5) H. B. Jonassen, R. B. LeBlanc and R. M. Rogan, *ibid.*, **72**, 4968 (1950).

(6) A. C. Zettlemoyer and J. J. Chessick, THIS JOURNAL, **58**, 242 (1954).

(7) G. Ponzio, *Gazz. chim. ital.*, **51**, [II] 213 (1921).

diamine had a small inhibitory effect on the nickel–acid reaction. With diethylenetriamine and triethylenetetramine the effect was greater; but all three showed less effect than quinoline, which has been used as a corrosion inhibitor.[8]

Some stirring was necessary to bring fresh solution into the bulk of the powder, but the effect of diffusion was not a major one. Stirring the solutions and powder vigorously and continuously did not increase the rate of reaction over that observed when the mixture was swirled in the flask every ten minutes.

Measurements at different temperatures with the ethylenediamine solutions showed a fourfold increase in rate over the range of 33–52°. (This would correspond to an apparent activation energy of roughly 14 kcal./mole.)

Effect of Complexing Agent.—To determine the effect of reduction in the nickel ion concentration in the solution because of complex formation, the rate of reaction was determined in solutions containing different complexing agents in concentrations such that the equilibrium nickel ion concentrations would be the same.

Solutions of en, dien, and trien in water were prepared such that their complexing tendencies for nickel ions (*i.e.*, the ratios of the complex ion concentration to the nickel ion concentration as determined from the equilibrium constants for formation of the complexes) were equal. The equilibrium constants used for ethylenediamine were determined by Carlson, McReynolds and Verhoek.[9] Those for diethylenetriamine were determined by Jonassen, LeBlanc and Rogan,[5] and those for triethylenetetramine by Jonassen and Meibohm.[10] Results are given in Table I.

TABLE I

EFFECT OF COMPLEXING AGENT AT EQUAL COMPLEXING TENDENCIES

*p*H 9.00, time contact = 5 days, vol. of soln. = 20.0 ml., complexing tendency = 1.6×10^{12}, wt. of nickel = 2.00 g.

Complexing agent	O.D. at 550 mμ	Concn. of complex, moles/l.	Concn. of Ni, moles/l.
En (0.100 *M*)	0.112	0.0148	0.0148
Dien (0.0098 *M*)	.032	.0042	.0042
Trien (0.122 *M*)	.090	.0049	.0096

Under these conditions the extent of reaction was greatest with the diamine, second greatest with tetramine, and least with the triamine. The approximate ratios of the amount of nickel reacted in 5 days was 3:2:1.

Effect of Oxygen.—It was found that in air the reaction was slower than under nitrogen, particularly when the solutions were agitated. Nickel samples which were precoated with oxide by heating in air and then placed in ethylenediamine solutions showed no appreciable dissolution. A nickel oxide sample, prepared by decomposition of nickel carbonate, dissolved extremely slowly in the ethylenediamine solutions.

(8) S. G. Clark, *Trans. Electrochem. Soc.*, **69**, 131 (1936).

(9) G. A. Carlson, J. P. McReynolds and F. H. Verhoek, *J. Am. Chem. Soc.*, **67**, 1334 (1945).

(10) H. B. Jonassen and A. W. Meibohm, THIS JOURNAL, **55**, 726 (1951).

MacGillavry, Singer and Rosenbaum[11] have reported successful removal of oxygen so that no reaction occurs with phosphoric acid. Their technique was used as a basis for further tests of the oxygen effect. With nickel wire, conditions were obtained in which only a trace of nickel dissolved in phosphoric acid in two weeks, but there was still appreciable reaction with the much more extensive surface of the nickel powder. There is, therefore, as usual no definite proof of the complete removal of oxygen. However, experiments were carried out under static conditions and using as atmosphere nitrogen or nitrogen–oxygen mixtures in varying proportions. These showed an increased rate in the presence of oxygen; but even in the carefully purified nitrogen, 0.072 mg. Ni/dm.^{2} were dissolved in 3 days in 0.13 *M* ethylenediamine solution and 0.173 mg. Ni/dm.^{2} in 0.5 *M* triethylenetetramine. They clearly indicate that a major part of the reaction does not require oxygen.

Effect of Water.—As in the case of oxygen, it was not practicable to be certain that all water was removed from any system. A series of tests were made with samples of nickel powder added under nitrogen to amine solutions in carefully-dried methanol to which water had been added. The results are summarized in Table II.

TABLE II

EFFECT OF WATER ON REACTION IN METHANOL

En concn. = 0.30 molar, vol. of soln. = 50 ml., wt. Ni = 10.00 g., time of contact = 3 days.

Vol. % water	O.D. at 550 mμ	Concn. of nickel, moles/l.	Vol. % water	O.D. at 550 mμ	Concn., of nickel moles/l.
0.00	0.016	0.0026	2.00	0.033	0.0054
0.10	.018	.0029	4.00	.035	.0057
0.40	.020	.0033	10.00	.026	.0043
1.00	.028	.0046			

The water has a definite effect on the reaction, with an optimum region around 3–4%. These results would not, however, exclude the possibility of some reaction involving the methanol.

Adsorption of Diamine.—Tests made on dilute solutions of ethylenediamine in methanol at intervals of one-half to one hour after addition of nickel powder indicated that some of the diamine was removed from solution, but no quantitative data could be obtained because of the reaction occurring.

Tests were then made with a benzene solution of the diamine. It was noted that when nickel powder was placed in benzene containing ethylenediamine, the powder appeared to agglomerate into coarser particles and to adhere to the surface of the glass container. The powder showed no such effects in pure benzene. Measurements of the amount of adsorption of the amine on the powder gave the curve shown in Fig. 1.

To test the effect of water on this adsorption, samples of nickel which had been treated as described above to remove adsorbed water were used. Other samples were treated with acid first, as noted above, to remove oxide layers as much as possible. The results, which are summarized in Table III, show a sharp decrease in adsorption.

(11) D. MacGillavry, J. J. Singer and J. H. Rosenbaum, *J. Chem. Phys.*, **19**, 1195 (1951).

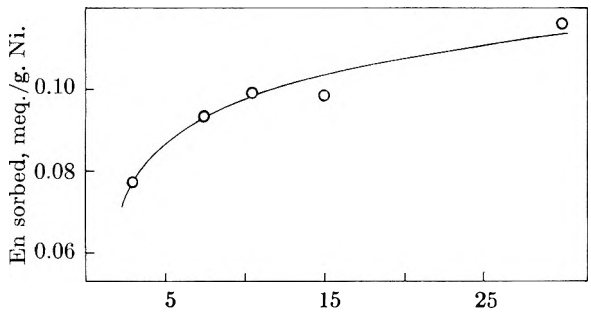

Fig. 1.

However, if these degassed samples were exposed to methanol vapor or water vapor before adding them to the solution, extensive adsorption was once again observed.

The last column of Table III shows the number of apparent layers adsorbed, based on an assumed area of 20 Å.^{2} per molecule.

Effect of Pretreatment on Reaction Rate.—Comparative rates of reaction were measured for ordinary nickel samples and for samples which had first been placed in benzene solution to adsorb diamine. The latter gave consistently higher results, *e.g.*, 2.17×10^{-3} mole/l. of nickel dissolved in 3.5 hr. as contrasted to 1.4×10^{-3} mole/l. without pretreatment. If the nickel samples were degassed and treated with acid (so that little adsorption could occur) the reaction occurring became almost negligible. Pretreatment with methanol or water vapor alone had no effect, but if this was followed by treatment with the benzene solution, the rate of reaction was again increased. Some typical results are shown in Table IV.

TABLE III

EFFECT OF PRETREATMENT OF NICKEL ON THE ADSORPTION OF ETHYLENEDIAMINE FROM BENZENE SOLUTIONS

Wt. Ni = 10.00 g., vol. of soln. = 50.0 ml.

Pretreatment	En concn., moles/l.	Meq. ads. / g. Ni	Layers (assuming 20 Å.^{2}/ molecule)
None	0.15	0.050	17
Degassed	.15	.009	3
HCl, then degassed	.050	.0034	1
HCl, then degassed	.005	.0025	1
HCl, then degassed and exposed to MeOH vapor	.050	.0392	13
HCl, then degassed and exposed to HOH vapor	.050	.0510	18

Effects of Amine Concentration and *p*H on Rate.—Comparative studies were made of the rate of reaction with a constant amount of nickel for solutions of various *p*H's and amine concentrations. Typical results are given in Figs. 2 and 3. (In water solution similar results were obtained except that all the *p*H curves seem to extrapolate to the origin.) By adding controlled amounts of hydrochloric acid, comparisons could also be made for systems containing effectively constant free amine or a constant concentration of the singly-charged onium ion. These gave results of the type shown in Fig. 4, indicating that both the free amine and the singly-charged ion affect the rate.

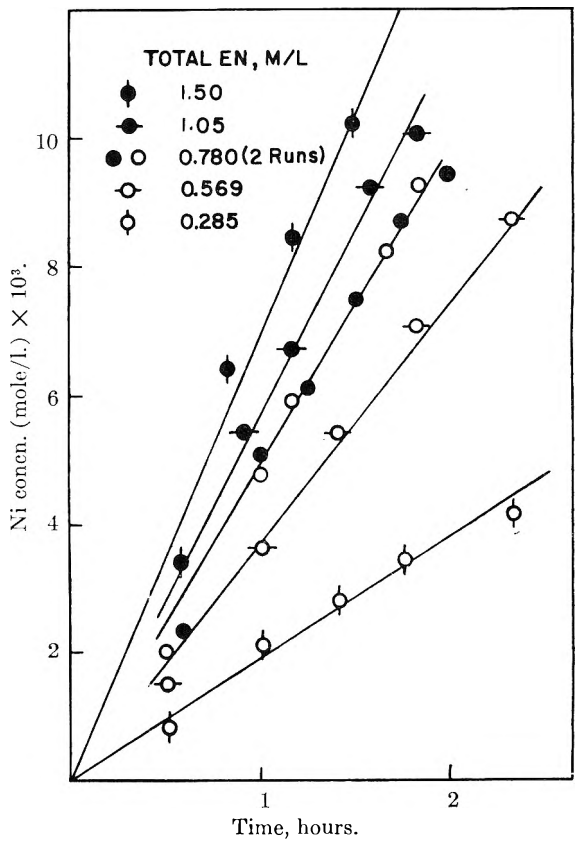

Fig. 2.

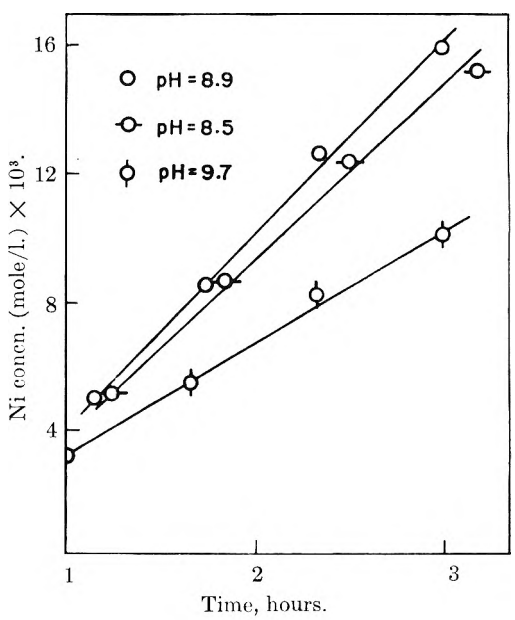

Fig. 3.

The apparent rate constants (including a constant factor for the nickel surface concentration) were in the range of 0.025 and 0.136, respectively.

In methanol, tests could not be run below *p*H 8.5, because of limited solubility of ethylenediamine dihydrochloride; but in water solution, where the reaction could be carried out at lower *p*H ranges, the rate falls off sharply to about *p*H 6, indicating that the doubly-charged ion is not effective in this

TABLE IV

EFFECTS OF PRETREATMENT ON REACTION

Pretreatment	Total time on contact with en soln.	Wt. Ni (grams)	Ni concn. in soln., moles/l.
MeOH at room temp. for 1 hr.	1 hr.	40	0.0043
MeOH at 60° for 3 hr.	1 hr.	40	.0043
None	1 hr.	40	.0041
Alcoholic HCl, degas, then benzene soln.	Benzene 4 hr. MeOH 15 min.	10	Neglig.
Alcoholic HCl, degas	MeOH 4 hr., 15 min.	10	0.0035
Alcoholic HCl, degas, MeOH vapor, benzene soln.	Benzene 4 hr. MeOH 15 min.	10	.0055
Alcoholic HCl, degas, MeOH vapor	MeOH 4 hr. 15 min.	10	.0046
Alcoholic HCl, degas, HOH vapor, benzene soln.	Benzene 4 hr. MeOH 15 min.	10	.0058
Alcoholic HCl, degas, HOH vapor	MeOH 4 hr. 15 min.	10	.0045

reaction. (It has been reported to have inhibitor properties by Swearingen and Schram.[12])

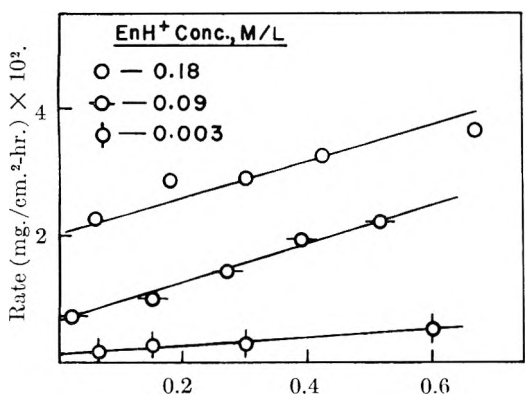

Fig. 4.

Discussion

Throughout all the tests there was close similarity in the reaction in water and in methanol. The results of the comparative tests made with the ethylenediamine, diethylenetriamine and triethylenetetramine at concentrations such that they should be equally effective in removing nickel ions from solution indicate that the dissolution is not simply a matter of a change in the oxidation–reduction potential because of changes in ionic activities. The order of reactivity is also such that the variations observed are not explainable on the basis of differences in rates of diffusion. The effects on the rate of reaction of pretreatment of the nickel samples further confirm that more than ionic activities in solution is involved.

The evolution of hydrogen in the course of reaction and the results obtained with varying concentrations of oxygen and with oxide-coated surfaces show that the reaction of particular interest here is not one involving oxygen. For most circumstances, water must be the oxidizing agent. Certain results—in particular the effectiveness of pretreatment with methanol vapor in causing adsorption and reaction—indicate, however, that the methanol molecule may also act as oxidizing agent.

There are no indications of a diffusion-controlled process and the adsorption processes involved are rapid, so the rate-determining step seems to be a surface reaction. The *p*H ranges, etc., are such that reaction of the nickel with water or methanol alone is not thermodynamically feasible. The lack of correlation with complexing tendencies for the nickel ion as noted above, and the effectiveness of pretreatment with both water vapor and diamine as contrasted to either alone, indicate that adsorption of the amine is an essential factor for the surface reaction in which nickel is oxidized to nickel ion. This would apparently involve formation of a chelate-type, surface complex between nickel and the amine.

The results indicate also that this surface reaction involves both water or methanol and the amine and that this is effectively a case of "coöperative and competitive" adsorption similar to certain of those reported by James and Vanselow.[13]

It is interesting to note that the necessity for the formation of a dual complex on the surface may reasonably explain the more rapid reaction with the singly-charged ion than with the diamine. The double linkage possible in adsorption of the latter could actually interfere with reaction. This is also suggested by the effect of pretreatment with diamine alone (Table IV) in decreasing markedly the rate of reaction.

The authors wish to acknowledge the assistance of Dr. Hung Li Wang in obtaining the information on particle sizes and surface area for the nickel powder. They also wish to acknowledge the support of part of this work by the Defense Research Laboratory, University of Texas, operating under Contract NOrd-9195 with the Bureau of Ordnance, U. S. Navy Department.

DISCUSSION

A. C. ZETTELMOYER.—Suppose the experiments were done with nickel which had some fresh oxide on the surface since it is very difficult to be aseptic with regard to oxygen. Recently we have shown that such a surface has chemisorbed oxygen which converts to nickel oxide on heat-treatment to 350°. Your nickel oxide samples which showed slower or no rate of dissolution may therefore not be the same oxide film you may have had on your nickel samples. At what temperature did you heat-treat the nickel in air and was it wet or dry air?

THOMAS L. KEELEN.—From the experiments carried out under conditions such that oxygen was quite accessible to the surface an actual decrease in the rate of dissolution was observed. No particular control of the temperature was made in the heat-treatment of the nickel and this was carried out under atmospheric conditions.

ROBERT D. VOLD—With respect to adsorption of ethylenediamine by the untreated nickel, is it not far more likely that the large amounts adsorbed are due to capillary condensation somewhere in the system rather than to the presence of thick multilayers over the surface?

THOMAS L. KEELEN.—Not according to surface area measurements and the actual change in the appearance of

(12) L. E. Swearingen and A. F. Schram, THIS JOURNAL, **55**, 180 (1951).

(13) T. H. James and W. Vanselow, THIS JOURNAL, **58**, 894 (1954).

the nickel powder. There actually appears to be something on the order of a separate phase formation.

W. FEITKNECHT.—How were the different kinds of nickel preheated; were they free of oxide? Is the normal potential of nickel in a solution of "en" such that water may be decomposed?

G. A. MILLS.—Has nickel from otherpre parational methods been tried (an extreme would be Raney nickel)? Is the solution of nickel more than a monolayer removal? Would you picture the electron transfer process as occurring at a different nickel atom from that being dissolved, where nickel dissolving may be complexed by OH and at an adjacent nickel atom H?

THOMAS L. KEELEN.—Three different nickel samples were tested and all showed the same general properties in the reaction system. No highly active sample such as Ranev nickel was tried, however. In general considerably more than a monolayer was removed from the nickel.

Yes, we picture the electron transfer occurring at different sites from those complexed by the amine.

A TRACER METHOD FOR DETERMINATION OF DEPOSITION OF CARBON ON COTTON

BY ACHYUT K. PHANSALKAR AND ROBERT D. VOLD

Contribution from the Department of Chemistry, University of Southern California

Received February 25, 1955

A method is described for labelling a dispersion of colloidal carbon with radiotracer Zr-Nb-95P, thus permitting direct determination of the amount adhering to a cotton strip dipped in the suspension. This method was used to determine deposition of carbon on cotton from solutions of sodium dodecyl sulfate, and the results compared with those calculated by the Kubelka–Munk equation from reflectance data. Under these experimental conditions the reflectance method was shown to give incorrect results, the difficulty being attributed to change of particle size distribution of the suspended carbon with changing concentration of detergent.

Introduction

The determination of the amount of soil on surfaces is of fundamental importance in studies of adhesion and of the stabilizing action of colloidal electrolytes as well as in investigation of the mechanism of detergent action. This is rather easily accomplished by a microscopic technique if extremely low concentrations of solid are involved[1,2] and by direct chemical analysis in the case of such soils as iron oxide or manganese dioxide.[3] However, in the practically important case of carbonaceous soil direct analysis is virtually impossible although recently a turbidimetric method has been successfully used for a graphitic soil on cotton.[4] Consequently most of the work on soil deposition and detergency has utilized the difference in reflectance of clean and soiled cloths as a measure of the amount of carbon remaining on the cotton[5–8] despite the fact that there are serious questions as to the validity of this procedure.[9–11]

This paper describes a radioactive tracer technique which we have found suitable for direct determination of the amount of carbon adhering to a cotton strip dipped in a suspension of the carbon in solutions of sodium dodecyl sulfate. The method developed has the advantage of adaptability to a variety of soils not determinable by chemical methods without causing any change in such variables as the particle size or surface area of the soil. Simultaneously, measurements were made of the reflectance of the cloth and of the degree of dispersion of the carbon in suspension in order to evaluate the applicability of the Kubelka–Munk equation[5] for converting reflectance readings into weight of soil present, and to account for the apparent difference in the concentration dependence of the protective action of the surfactant as judged by the reflectance and the analytical data.

Materials.—The same Sterling NS carbon (mean diameter 75 mμ), Duchess sheeting No. 150, and sodium dodecyl sulfate (SDS) were used as in previous work.[9] As already described, precautions were taken to ensure cleanliness of the surfaces, uniformity of carbon deposition on the cotton, and purity of the detergent.

Radio isotope Zr-Nb95P in oxalate solution (3.56 mc. per cc.) was used for labelling the carbon. This isotope emits β (0.39 and 1.0 mev.) and γ (0.73 and 0.92 mev.) radiations and has a half life of 65 days. Geiger–Muller counter GS4 of Technical Associates, Los Angeles, was used as a detector.

Technique.—It was first necessary to develop a method for fixing most of the activity on the carbon and demonstrating that changing the concentration of surfactant did not change the distribution of activity between carbon and solution. The stock solution of tracer as obtained was too active to be used directly and was diluted in all work in the ratio of 0.20 ml. stock tracer solution to a final volume of 10.00 ml. in 0.5 wt. % potassium oxalate solution. Simple stirring of tracer solution with a carbon suspension was unsatisfactory, 30% of the activity remaining in solution after the carbon was filtered off. However, making the solution slightly alkaline by addition of two drops of very dilute ammonia to the tracer resulted in much better retention of activity by the carbon, the filtered solution retaining about 1% of the initial activity. Presumably this results from more complete adsorption of the metal hydroxides on the surface of the carbon owing to their insolubility in water.

Addition of sodium dodecyl sulfate to the dispersion resulted in virtually no desorption of tracer from the carbon, the activity in the filtrate still being approximately 1% of the initial activity. In order to obtain reproducible results, however, it is necessary to stir the carbon suspension with the detergent *before* addition of the tracer solution, since

(1) R. C. Palmer and E. K. Rideal, *J. Chem. Soc.*, 573 (1939).
(2) A. von Buzagh, *Kolloid Z.*, **47**, 370 (1929); **51**, 105 (1930).
(3) P. H. Fall, THIS JOURNAL **31**, 801 (1927).
(4) J. C. Harris, M. R. Sullivan and L. E. Weeks, *Ind. Eng. Chem.*, **46**, 1942 (1954).
(5) P. Kubelka and F. Munk, *Z. tech. Physik*, **12**, 593 (1931).
(6) W. P. Utermohlen and E. L. Wallace, *Textile Research J.*, **17**, 670 (1947).
(7) O. C. Bacon and J. E. Smith, *Ind. Eng. Chem.*, **40**, 2361 (1948).
(8) J. Compton and W. J. Hart, *ibid.*, **43**, 1564 (1951).
(9) R. D. Vold and A. K. Phansalkar, *Rec. trav. chim. Pays Bas*, **74**, 41 (1955).
(10) I. Reich, F. D. Snell and L. Osipow, *Ind. Eng. Chem.*, **45**, 137 (1953).
(11) W. J. Hart and J. Compton, *Textile Research J.*, **23**, 418 (1953).

TABLE I

DISTRIBUTION OF ACTIVITY BETWEEN CARBON AND SOLUTION

Vol. of tracer, ml.	Carbon in suspension, wt. %	SDS initial concn., wt. %	Activity on carbon, counts/min.	Activity in supernatant liq., counts/min.	Activity in soln. / Activity on carbon
0.2	0.10	0.05	16,000	150	0.0094
.4	.20	0.05	33,000	325	.0098
.3	.30	.10	23,500	240	.0102
.4	.40	.20	34,000	320	.0094
.4	.50	.50	34,200	360	.0105

otherwise after deflocculation brought about by the SDS some carbon aggregates will be more active than others.

The following procedure for preparing the active carbon suspension, soiling the cotton, and determining the amount of carbon remaining on the cotton was shown to give reproducible results. Sufficient carbon was suspended in 100 ml. of distilled water to make a 0.25 or 0.50 wt. % suspension which was then stirred 1.5 minutes at 11,800 r.p.m. in a Waring Blendor to attain an initial dispersion. After addition of SDS in powdered form to give the desired concentration the suspension was stirred three minutes at 3000 r.p.m., the lower speed being necessary to avoid foaming. Sufficient tracer solution was then added [0.2 to 1.0 ml. with 0.02 ml. ammonia (one drop of 15 M in 100 ml. water)] to give about 600 counts per minute per mg. of carbon, and the suspension stirred for an additional two minutes at 3000 r.p.m.

In order to determine the amount of carbon on the cloth from measurement of the activity it is necessary to know the activity per mg. of carbon, and the activity per swatch of cloth due to adsorption of tracer by the cloth or absorption of tracer solution. The specific activity of the carbon was determined in each experiment by removing two portions of the initial labelled carbon suspension, each containing 1.5 to 2.0 mg. of carbon, and evaporating to dryness on weighed 1″ watch glasses on a hot plate. After reweighing the activity was determined with the counter.

Two identical strips of cotton cloth (2.5 × 3.7 cm., weighing about 125 ± 2 mg.) were then soiled by moving up and down vertically in the suspension for one minute (about 50 times).[9] The cloth was not absolutely rigid but no appreciable flexing was observed. Non-adherent carbon was removed by rinsing the strips for one minute in 100 ml. of distilled water using the same technique as in soiling.

The carbon suspension was then centrifuged 55 minutes at 4500 r.p.m. and the clear supernatant liquid separated. Frequently portions of this solution were withdrawn, evaporated to dryness on watch glasses, and the activity determined to check the constancy of distribution of activity between carbon and solution. Two cloth strips were then dipped first in this solution and then in rinse water as in the soiling technique in order to determine the activity picked up by the cloth from the solution in the absence of deposition of carbon. This constitutes a correction which must be subtracted from the total activity of the soiled cloths in order to determine the amount due to deposited carbon, but fortunately amounted only to about 1%.

The activity was determined by placing the cotton strips in a fixed position in lead containers about ¾ cm. below a Geiger tube suspended from the top of the container. The two samples were counted alternately for five or ten minutes each, thus reducing the number of background determinations needed, until a total of 18,000 to 20,000 counts had been reached (about a half hour for carbon samples and two to three hours for cloth samples). The background was generally small (9 to 15 counts/minute), and was subtracted from the total count determined for the sample.

Table I shows data illustrative of the effect of variation in the amount of carbon, the amount of detergent and the amount of tracer on the activity remaining in the supernatant solution after removal of carbon. It is clear that the technique used resulted in only about 1% of the total activity remaining in the solution irrespective of the amount of carbon and detergent in suspension within the range studied.

The weight of carbon present on each swatch of cloth is calculated by the relation $(C - D)/(B - E)A$ = mg. of carbon, where A is the weight of carbon from the small portion of the suspension evaporated on the watch glass and B its activity in counts/minute, C and D are, respectively, the counts per minute from swatches of cloth dipped in the carbon suspension and in the supernatant liquid, and E the counts per minute from the same volume of supernatant liquid used for the determination of B. Duplicate values determined in this way agreed within 1 to 2%.

Reflectance values of the soiled cloth pieces were measured with a Beckman spectrophotometer with a diffuse reflectance attachment, taking magnesium oxide as a standard (100%). The clean cloth gave a value of 84% in four layers for light of 600 mμ wave length. After suitable pretreatment[9] of the cloth, average values of reflectance agreeing to 0.5 to 0.7 unit were obtained with different samples, each measured in five or six different spots.

The objection might be raised that addition of the tracer modifies the surface of the carbon particles so that the adhesion behavior of the tagged and untagged particles would be different. This seems unlikely since the maximum concentration of metal tracer ions in the suspensions used was not greater than $3.6 \times 10^{-10} M$. Conclusive evidence that the procedure described gives reliable results is found in Fig. 2, where it is shown that the curve of reflectance *vs.* SDS concentration is the same within experimental error whether determined using tagged or natural carbon.

Numerical values proportional to the average size of the carbon aggregates in suspension were obtained as in previous work[9] by measuring the light absorption of the suspensions with a Klett photoelectric colorimeter. In the range of particle sizes involved here the intensity of the transmitted light decreases rapidly as the degree of dispersion increases. Accordingly, nearly constant readings as detergent concentration is increased show there is little change in the degree of dispersion of the carbon aggregates in that concentration range, while increasing numerical readings of light absorption indicate a marked decrease in the average size of the carbon aggregates. The results obtained for 0.50 and 0.25 wt. % carbon suspensions with varying concentration of SDS are shown in Fig. 3.

Results and Discussion

Typical data showing the amount of carbon actually adhering to cotton strips after immersion in carbon suspensions containing varying concentrations of sodium dodecyl sulfate are presented in Table II, together with reflectance readings on the same strips.

It is clear from Fig. 1 that the amount of carbon deposited on the cloth decreases very rapidly with the first small additions of detergent but that a limiting concentration is soon reached beyond which carbon deposition decreases only very slowly with further increase in detergent concentration. This concentration is much smaller than the critical micelle concentration, and appears to vary directly with the concentration of carbon in suspension.

Figure 2 shows that the reflectance of the soiled cloth first rises with increasing concentration of detergent and then falls. The maximum in the reflectance curve occurs at very nearly the same concentration at which the actual deposition of carbon as determined by the tracer method becomes nearly independent of further change in detergent concentration.

It is obvious from comparison of Figs. 1 and 2 that serious error can be made if the amount of

TABLE II

ANALYTICAL AND REFLECTANCE DATA ON CARBON DEPOSITION

Concn. of SDS, g./100 ml.	Amount of soil on cloth,[a] mg. 0.25% carbon suspension	Amount of soil on cloth,[a] mg. 0.50% carbon suspension	Reflectance of soiled cloth[a] 0.25% carbon suspension	Reflectance of soiled cloth[a] 0.50% carbon suspension
0.000	0.995	1.642	29.1	19.5
.001	.767	...	32.3	...
.010	.388	0.968	42.6	...
020	.198	.699	53.2	...
.024	.166	...	56.7	35.2
.030	.149	.551	51.5	40.9
.040	.142	.468	49.2	45.6
.050	.131	.397	46.4	49.4
.060	.123	.352	...	52.1
.070	...	...	...	47.5
.080	.116	...	...	...
.090	...	.312	...	45.8
.100	...	...	37.5	44.3
.120	...	...	34.9	...
.140	...	...	32.5	...
.150	...	...	...	35.5
.160	...	.305	...	...
.200	...	...	...	29.9
.250	...	.306	...	...

[a] Cloth swatches 2.5 × 3.7 cm.

carbon is taken to be simply related to the reflectance of the cloth, as in the Kubelka–Munk[5] and related equations.[6,7,10] However, under some circumstances good agreement has been obtained between analytically determined amounts of soil on cloth and values calculated from reflectance data. Thus, where a mixed graphitic soil was removed from cotton by washing, the amount remaining on the cloth was found to be the same as calculated by the Kubelka–Munk equation and as determined turbidimetrically after solution of the cloth.[4] Likewise Utermohlen and Wallace[6] working with iron oxide pigment found good correlation at medium levels of soiling between the results of reflectance measurements and chemical analysis of iron on the cloth.

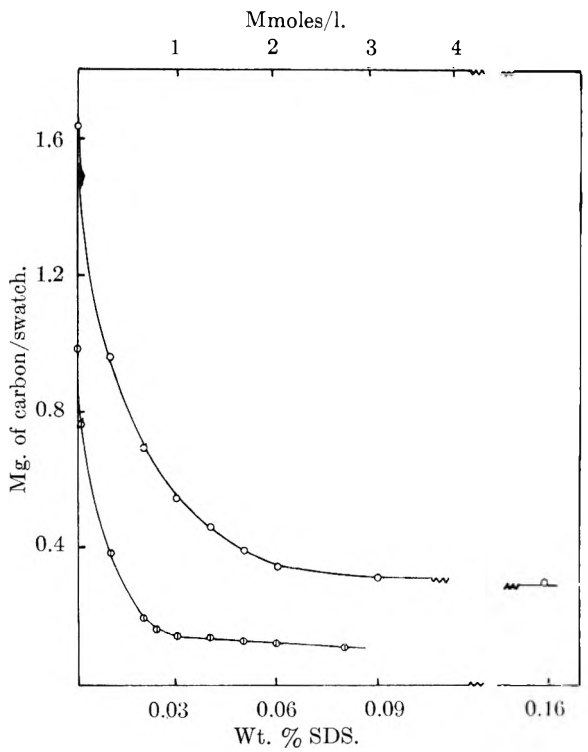

Fig. 1.—Weight of carbon deposited on cotton from sodium dodecyl sulfate solutions: ○, ⊙, respectively, 0.50 and 0.25%, carbon suspension.

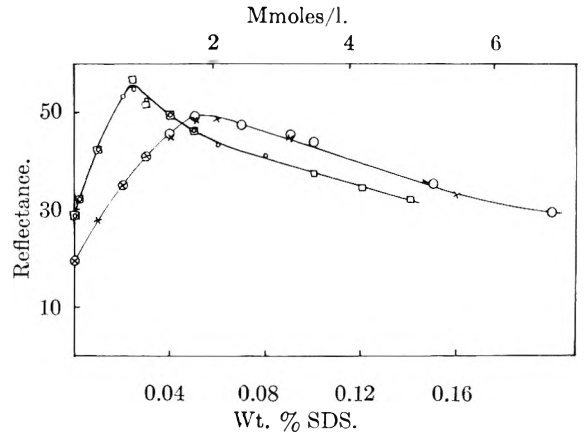

Fig. 2.—Reflectance of cotton dipped in carbon suspensions in sodium dodecyl sulfate: ○, X, respectively, plain and labeled carbon in 0.50% concn.; □, ○, respectively, plain and labeled carbon in 0.25% concn.

The explanation for the failure of the Kubelka–Munk equation to give correct values for the amount of carbon on the cloth in the present investigation is found in Fig. 3, which shows the effect of changing detergent concentration on the degree of dispersion of the suspended carbon. The apparent blackness as measured by the reflectance technique depends on both the quantity and the subdivision of the carbon deposited, the reflectance being lower for a given quantity of carbon the more finely it is dispersed. The first additions of SDS have little effect on the particle size distribution of the carbon but, as shown in Fig. 1, greatly decrease the amount adhering to the cloth, with the result that the reflectance increases. Presently, a concentration is reached such that the weight of carbon deposited decreases only slightly with further increase in concentration of detergent. However, with further increase in detergent concentration the average size of the suspended—and also presumptively of the deposited—carbon aggregates decreases markedly (Fig. 3), with the result that the reflectance decreases with increasing detergent concentration in this range even though the amount of carbon deposited is still decreasing slowly. A somewhat similar conclusion was reached by Hart and Compton[11] who concluded that the Kubelka–Munk equation frequently fails when applied to reflectance systems because of effects due to particle distribution, orientation and specific absorbence.

Hence it appears to be necessary to demonstrate that the size distribution of suspended carbonaceous soil is not changed over the concentration range of detergent used if it is to be possible to obtain correct values for the amounts deposited on cotton from measurement of the reflectance. The success of the Kubelka–Munk equation in some of the direct tests of its validity[4,6] may be due to limitation

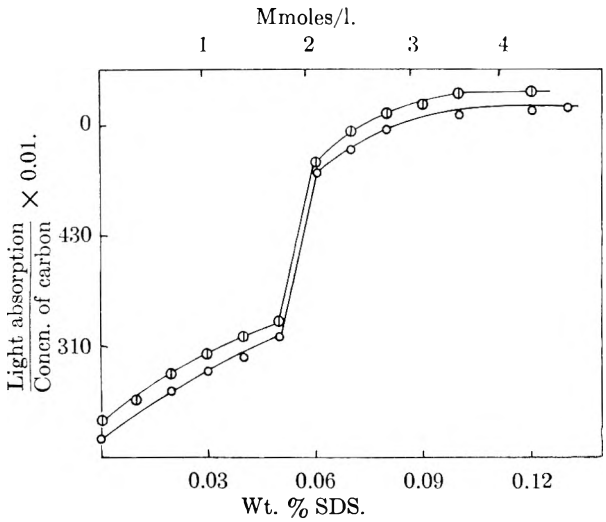

Fig. 3.—Effect of sodium dodecyl sulfate on size distribution of suspended carbon: ○, ①, respectively, 0.50 and 0.25% carbon suspension.

of the variation in detergent concentration to a range such that the size distribution of the suspended solid did not change appreciably. Since commercial preparations presumably containing large quantities of inorganic salts were used in previous work this is entirely possible, even though had single pure alkyl sulfates been used changes in particle size would have been expected on the basis of the present work.

In view of the ambiguities inherent in any reflectance method for determination of the amount of carbon remaining on cotton it seems desirable to calibrate such methods by a direct determination. This is easily done for soils such as manganese dioxide or iron oxide by chemical analysis for the metal content. A second general method involves removal of the soil from the cloth, followed by turbidimetric determination, and is applicable to solids such as carbon and clays or other siliceous particles. However, the technique is rather tedious, the results likely to be uncertain unless careful control of particle size is maintained during the turbidimetric determination, and the precision is rather poor.[4] A third possibility involves use of a tracer technique, tagging the soil so it can be measured directly on the cloth without the necessity for preliminary separation. This can be done by use of carbon black made from compounds containing the C_{14} isotope, by neutron irradiation of the soil sample in a nuclear reactor, or, as in the present technique, by addition of aged, mixed fission products to an aqueous suspension of the soil.

The irradiation method is not feasible for carbon. The preparation of carbon black containing C_{14} (according to the method of Snell)[12,13] suffers from the disadvantage that neither the porosity nor the particle size of the resultant carbon is known. Addition of tracer to a carbon suspension, as in the present method, has the advantage of permitting direct determination of the amount of carbon of previously known characteristics which adheres to a cotton surface. Thus it is possible to use the same carbon in deposition experiments which has already been characterized as to surface area, aggregate size distribution in dispersion, etc., and so to obtain a greater insight into the mechanism of the detergent process.[9]

The authors wish to thank Dr. Arthur W. Adamson for his suggestions during the development of this method.

DISCUSSION

A. C. ZETTLEMOYER.—It would be interesting to repeat the work with carbon blacks having different amounts of polar groups on the surface, or to start with Graphon and work with samples which have been oxidized to increasing extents.

1. If I understand correctly, there is an optimum concentration of surfactant in so far as *apparent* detergency is concerned.

2. Can you suggest what the effect of builders on your results would be?

ROBERT D. VOLD.—1. It must be remembered that the results in this paper refer only to protection against deposition of oil-free carbon rather than to detergency in general, which involves as the first step removal of deposited material. However, work in other laboratories has shown a general similarity in the results of the two types of experiments. Subject to this possible limitation it is certainly true that the present data show that the cloth will appear "dirtier" beyond an optimum concentration of surfactant even though the analytical data by the tracer method prove that the actual amount of soil deposited is remaining nearly constant or still decreasing slowly with increasing concentration of surfactant.

2. Although many possible explanations might be advanced for the effectiveness of polyphosphate builders, such as preferential adsorption at polar spots, alteration of the concentration dependence of the zeta potential at cloth and carbon surfaces, etc. I would not wish to attempt prediction without further experimental work.

MAX BENDER.—I raised questions on the zeta potential being of much influence in connection with the fall-off in C pick-up by the cotton as a function of surface active agent concentration.

ROBERT D. VOLD.—The initial rapid decrease in carbon deposition at low concentrations of detergent is probably due to two factors, the zeta potential on the carbon and on the cotton, and the extent of surface coverage of carbon by adsorbed detergent. Unpublished experiments in this laboratory show that the zeta potential on the carbon increases rapidly until the concentration of SDS reaches about 0.03%, and thereafter is nearly constant.

(12) F. D. Snell, personal communication, September, 1953.

(13) A. N. Campbell and E. A. Brown, *J. Am. Chem. Soc.*, **60**, 3055 (1938).

SURFACE OXIDATION OF MOLYBDENUM DISULFIDE[1]

BY SYDNEY ROSS AND ALAN SUSSMAN

Department of Chemistry, Rensselaer Polytechnic Institute, Troy, N. Y.

Received February 25, 1955

Samples of pulverized molybdenum disulfide of different specific surface areas were analyzed for surface oxidation by colorimetric determination of molybdic oxide, gravimetric sulfate and potentiometric surface acidity. The surface oxidation was found to be proportional to the surface area, and corresponded closely to the calculated oxidation of only the outermost molecular layer of the sulfide. There is evidence that the oxide layer protects the sulfide from further oxidation at room temperature, and greatly decreases the rate of further oxidation at 100°. Preliminary studies of oxidation rates of unprotected sulfide particles at 85–100° show significant increases caused by high relative humidity, finer degree of subdivision and greater ease of access of moist air to the particle surface. Oxidation of molybdenum disulfide below 450° has not hitherto been reported.

Introduction

In some applications molybdenum disulfide is most effective as a lubricant when finely dispersed in oil. It is found, however, that the stability of a dispersion of molybdenum disulfide in oil is affected by the extent of the surface oxidation of the particles. The instability is caused by flocculation of the primary particles. Ballou and Ross[2] showed that, whereas the non-oxidized surface is hydrophobic, oxidized surface tends to be hydrophilic. According to well-known principles of surface chemistry,[3] therefore, in an oil dispersion, the unoxidized, hydrophobic sulfide particles would not be flocculated; whereas the oxidized, hydrophilic particles would be flocculated.

Whatever the explanation of the effects may be, it is clearly of importance in a practical application to have a knowledge of the resistance to oxidation of powdered molybdenum disulfide. Uyeda,[4] using the diffraction of electrons from a freshly cleft surface of a single crystal of molybdenite, detected no oxidation below 440°: Godfrey and Nelson,[5] using X-ray diffraction, also failed to find any oxidation below 450°. Chemical methods are more sensitive, however, than these physical methods and Ballou and Ross[2] reported the presence of a water-soluble acid on the surface of pulverized molybdenum disulfide heated to 110°. The present contribution reports experiments at 85 and 100°, in which it is shown, by direct chemical analyses of the reaction products, that the rate of oxidation is measurable even at these relatively low temperatures. Calculations indicate that only the outermost layer of the crystal is oxidized.

Materials and Equipment

Molybdenum disulfide, obtained from the natural mineral *molybdenite*, is purified by the Climax Molybdenum Co., by a method described by Killeffer and Linz.[6] The purified material has an assay of 99% MoS_2. A sample was supplied by the Climax Molybdenum Co., as grade No. 3, and was found to have a nitrogen B.E.T. area of about 3 m.²/g. Other samples were prepared by the Micronizer Co., by pulverizing grade No. 3 in a Micronizer. The main pulverized product had a nitrogen B.E.T. area of about 10 m.²/g.; it was this sample that was used in the investigation by Ballou and Ross.[2] Two finer samples, with nitrogen B.E.T. areas of 14.2 and 17.0 m.²/g., respectively, were obtained by collecting the dust remaining after the removal of the principal ground product.

Molybdic acid C.P., 99% MoO_3 (Fisher Scientific Co.), was used as a standard for the colorimetric analysis. Sodium thiocyanate, stannous chloride and butyl acetate were all Fisher Scientific Company's C.P. grade. The butyl acetate was reused several times; after each use it was repurified by washing with water, with silver nitrate solution and then distilling.

The nitrogen B.E.T. surface areas were measured by K. Starr and E. V. Ballou of this laboratory, using the customary nitrogen adsorption apparatus.

Methods of Analysis and Procedure

(a) **Analysis of Oxide.**—The amount of oxide present on the surface of different samples of pulverized molybdenum sulfide was determined colorimetrically, essentially by the method described by Young.[7] The standard molybdenum solution was made from C.P. molybdic acid, dissolved in 1:1 ammonia and diluted to give a solution containing 0.100 mg. MoO_3 per ml. A calibration curve was determined by using different amounts of this solution, from which the colored quinquevalent molybdenum thiocyanate complex was produced and extracted with butyl acetate. The absorbances of the butyl acetate solutions were measured in quartz cells at λ 465 mμ against distilled water, using a Beckman Model B Spectrophotometer. The absorbence *vs.* concentration curve is a straight line. Samples of powdered sulfide were shaken in concd. ammonia and then separated by filtration; the filtrates were then diluted and analyzed in the same way as the standard molybdenum solution. Each analysis was done in duplicate or triplicate.

(b) **Analysis of Sulfate.**—The amount of soluble sulfate on the surface of the principal sample of pulverized molybdenum sulfide was determined by washing 2.500 g. of sample in distilled water; the solid was then separated by filtration and the amount of soluble sulfate determined gravimetrically by precipitation of barium sulfate. This analysis was done in duplicate.

(c) **Acid Number.**—Weighed amounts (about 0.50 g.) of each sample of molybdenum disulfide were mixed with distilled water, and the resulting slurry was titrated with standard NaOH solution, using a Beckman *p*H meter to follow the neutralization. The end-point was determined from a plot of volume added *vs.* *p*H.

(d) **Determination of Rate of Oxidation.**—The oxide originally present on the sample was first removed by rinsing several times with concd. ammonia. The damp sulfide was dried under vacuum, after which the lumps were readily disintegrated by shaking with glass beads in an atmosphere of nitrogen. The sample was not exposed to the atmosphere until the beginning of the oxidation run. To present fresh surface to the atmosphere the powder was tumbled continually inside a wide-mouth bottle, which was rotated about its longitudinal axis at 200 r.p.m. The bottle was mounted on a plate, connected by a shaft through the wall of the oven to a motor outside. One series of oxidations was under relatively dry conditions at 100°, with a drying

(1) Presented at the 29th National Colloid Symposium, at The Rice Institute, Houston, Texas, on June 20–22, 1955.

(2) E. V. Ballou and S. Ross, THIS JOURNAL, **57**, 653 (1953).

(3) See S. Ross and H. F. Schaeffer, *ibid.*, **58**, 865 (1954).

(4) R. Uyeda, *Proc. Phys. Math. Soc. Japan*, [3] **20**, 656 (1938).

(5) D. Godfrey and E. C. Nelson, "Oxidation Characteristics of Molybdenum Disulfide and Effect of Such Oxidation on its Role as a Solid Film Lubricant," N.A.C.A. Tech. Note No. 1882, Washington, D. C., 1949.

(6) D. H. Killeffer and Arthur Linz, "Molybdenum Compounds, Their Chemistry and Technology," Interscience Publishers, New York, N. Y., 1952, pp. 196–7.

(7) R. S. Young, "Industrial Inorganic Analysis," John Wiley and Sons, Inc., New York, N. Y., 1953, pp. 183–5.

agent present in trays inside the oven; another series was under humid, nearly saturated, conditions at 85°, with a tray of water, automatically replenished through a tube from an outside supply, inside the oven. Samples were withdrawn at measured intervals for analysis.

Experimental Results

The surface oxidation of pulverized samples of molybdenum disulfide of different degrees of fineness are reported in Table I. This table also contains the results of the sulfate analysis of the principal (10 m.²/g.) sample, and the surface acidity (acid number), calculated as millimoles of dibasic acid per gram of sulfide. Two sets of results for surface acidity are reported: the first contains those determined in this Laboratory in 1953 by R. Maier and A. Tarasewich; the other contains those for analyses repeated 20 months later in 1954.

TABLE I

ANALYSES OF OXIDATION PRODUCTS OF PULVERIZED MOLYBDENUM DISULFIDE

Surface area, m.²/g.	MoO_3 %	MoO_3 Mmoles/g.	Surface acid, mmoles/g. 1952	1954	Surface sulfate, mmoles/g.
2.8	...	...	0.0065	0.010	
3.25	0.088	0.0061	.0037	.0076	
10.0	3.0	.208	.486	.467	0.434
14.2	4.2	.29	.78	...	
17.0	4.6	.32	...	.91	

The rates of oxidation, under conditions of both high and low humidity at 85 and 100°, respectively, are reported graphically in Fig. 1 for the 14.2 sq. m./g. sample of molybdenum disulfide, and in Fig. 2 for the 10.0 sq. m./g. sample. Other differences in operating conditions are described in the legends of the diagrams. In Fig. 2 the oxidation curves start from 0% *additional* oxide: the amount of oxide present initially, which never could be reduced by the washing treatment below about 10% of the calculated monolayer oxidation, was subtracted from the subsequent analysis. Several different determinations, both at low and high humidities, gave reproducible curves when treated in this way. In Fig. 1 the total per cent. oxide is reported.

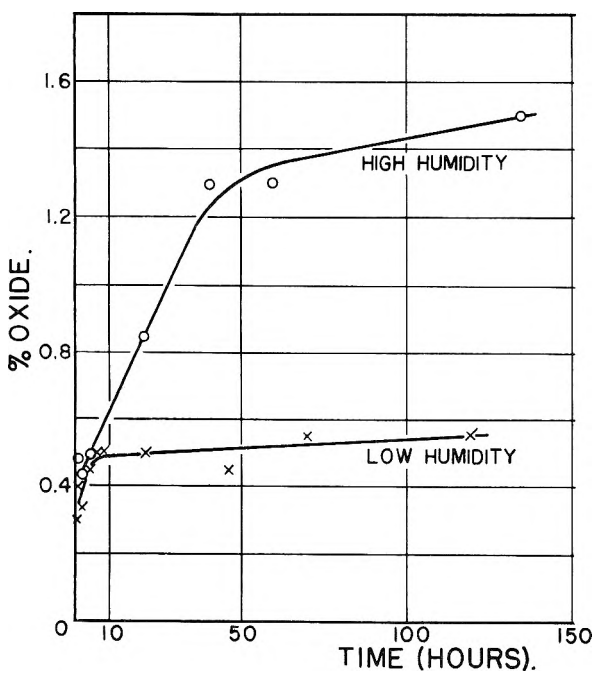

Fig. 1.—Rates of oxidation of pulverized molybdenum disulfide (14.2 m.²/g.) at 100° (low humidity) and 85° (high humidity). The lower curve was obtained from analyses of an undisturbed sample in an open dish; the upper curve from a sample constantly tumbled inside an open, wide-mouth bottle. The calculated oxidation of a monolayer is 3.92% MoO_3.

Discussion

1. Calculation of Oxide Produced by Monolayer Oxidation.—For the purpose of this calculation it is assumed that practically the entire under-

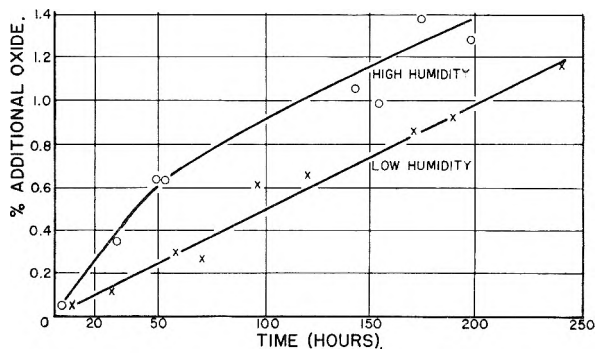

Fig. 2.—Rates of oxidation of pulverized molybdenum disulfide (10 m.²/g.) at 100° (low humidity) and 85° (high humidity). Both curves were obtained from analyses of samples constantly tumbled inside an open wide-mouth bottle. The calculated oxidation of a monolayer is 2.76 % MoO_3.

lying sulfide surface of the pulverized samples consists of the natural cleavage plane of molybdenite. These 0001 planes consist of stacks of sandwiches of hexagonal close packed sheets of molybdenum atoms (Fig. 3) between two similarly packed sheets of sulfur atoms; the outside layer is one of sulfur, since cleavage takes place between the adjacent sheets of sulfur atoms. We are to estimate how much MoO_3 would be produced per gram of sulfide when the outermost MoS_2 sandwich is oxidized. The reasoning is as follows:

(1) Referring to Fig. 3, there are $6(1/3) + 1 = 3$Mo atoms per hexagon.

(2) The Mo–Mo distance in the 0001 plane is 3.15 Å.[8]; therefore area of each hexagon = $2.60\text{-}(3.15)^2$ Å.²; therefore, area of each Mo atom = $2.60(3.15)^2/3 = 8.60$ Å.².

(3) Let Σ represent the surface area of each sample in sq. m./g., then the number of Mo atoms in the surface layer of sulfide is $\Sigma \times 10^{20}/8.60$.

(4) Considering that each Mo atom forms one MoO_3, the per cent. oxide is

$$\frac{\Sigma \times 10^{20} \times 143 \times 100}{8.60 \times 6.023 \times 10^{23}} = 0.276\Sigma$$

i.e.,

$$\% \text{ oxide as } MoO_3 = 0.276\Sigma \qquad (1)$$

2. Evidence of Protection of Sulfide from Oxidation below 85°.—In Table II the analytical results for the per cent. MoO_3 found in the pulverized samples are compared with the values calculated from equation 1.

The experimental results disclose that in nearly every sample analyzed, regardless of its surface area,

(8) R. W. G. Wyckoff, "Crystal Structures," Vol. 1, Interscience Publishers, Inc., New York N. Y., 1951, Chapter IV, Text p. 15.

TABLE II

COMPARISON OF ANALYSIS OF SURFACE OXIDE WITH CALCULATED MONOLAYER OXIDATION

Surface area of sample, m.²/g.	% surface MoO_3/g. MoS_2 Obsd.	Calcd.
3.25	0.088	0.86
10.0	3.0	2.76
14.2	4.2	3.92
17.0	4.6	4.69

the oxidation is close to that which would be obtained from oxidation of only the outermost layer of molybdenum sulfide. The coarsest sample, the original grade 3, is farther from the relation of equation 1 than any of the others; this is not unexpected since it is known that in the preparation of this material surface traces of the oil used in the flotation process of separation are present, which may seal off the surface from access by water vapor or oxygen. In the purification of grade 3 it is heated in air, ostensibly to volatilize the oil, and, as the present analysis shows, even this treatment does not produce much oxidation. The surface oxidation of the other samples did not necessarily take place at room temperature; it is probable that during the process of "micronizing," which is done under favorable conditions for oxidation, in a current of air, there is a local rise of temperature.

The resistance of the sample to further oxidation at relatively low temperatures can be deduced from their history. The pulverized products were received from the Micronizer Co., in April, 1951 (10 m.²/g.) and in February, 1952 (14.2 and 17.0 m.²/g.). Determinations of surface acidity done in this Laboratory in 1952 and repeated in 1954 are in good agreement, indicating that no further oxidation has taken place under laboratory conditions during 20 months. An even more stringent test of the protective ability of the oxide monolayer was to place these stable oxidized samples in the oven at 110° for several days. No further development of oxide was discovered, although samples from which the oxide had first been removed showed new oxide formation when tested in the same way. Had these experiments been given more time, the protection may have proved ineffective, since Ballou and Ross[2] reported a tenfold increase in surface acidity on heating at 110° for 45 days. The protection for shorter times at 110°, and almost indefinitely at room temperature, is nevertheless strongly indicated by the present evidence. The most conclusive argument for protection is the close correspondence of the experimental results of Table II to the calculated values. It is not probable, if oxidation is unhindered beyond the first molecular layer, that each sample, formed under different local conditions in the Micronizer, would oxidize by chance to an extent that bears so regular and simple a relation to monolayer oxidation.

It has not yet been found that a metal can be protected from oxidation by a single molecular layer of surface oxide: a coating of about 50 Å. is required.[9] In the oxidation of molybdenum disulfide both the sulfur and the molybdenum are oxidized, so that a mixture of oxidation products is produced at the surface, occupying more bulk than the sulfide layer that it replaces. An increase in volume is characteristic of protective layers.[9] Also it is possible that the underlying second layer is wholly or partially affected during oxidation, but it is not removed and analyzed by the present techniques.

(9) F. Seitz, "The Physics of Metals," McGraw-Hill Book Co., Inc., New York, N. Y., 1943, pp. 189–191.

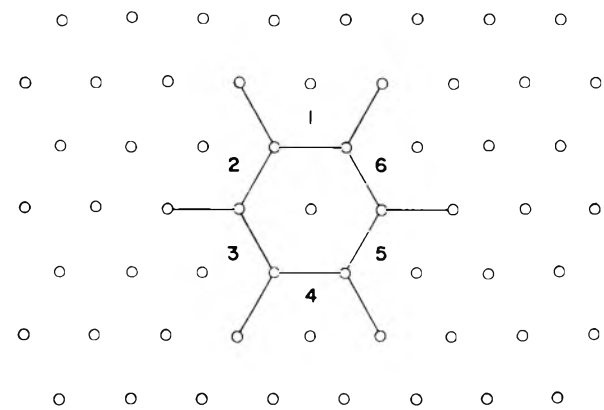

Fig. 3.—The principal cleavage (0001) plane of molybdenum disulfide, showing hexagonal, close-packed array of molybdenum atoms. Each atom at the vertex of the hexagon is shared by each of three hexagons.

3. Surface Acidity.—The surface oxidation reaction is described by the equation

$$2MoS_2 + 9O_2 + 4H_2O = 2MoO_3 + 4H_2SO_4$$

On one sample both the molybdenum trioxide and the sulfuric acid (as sulfate) were analyzed, and were found to be in the molar ratio of 0.434/0.208 = 0.208, close enough to the stoichiometric ratio of 2.00 to confirm the equation. The acid obtained on washing the pulverized sulfide includes more than the four equivalents of sulfuric acid yielded by oxidation of each mole of sulfide. This is shown in Table III, which lists the yield of surface acid in equivalents, calculated on the assumption that it is derived from the outermost molecular layer of the sulfide (an assumption that gave a good agreement for the yield of molybdic oxide).

TABLE III

SURFACE ACIDITY CALCULATED AS YIELD PER SURFACE MOLE OF MoS_2

Area of sulfide, m.²/g.	Surface acidity obsd. (equiv. acid/g. MoS_2)	Surface moles MoS_2 per g.[a]	Equiv. acid yield per surface mole MoS_2
10.0	0.477×10^{-3}	1.93×10^{-2}	5.0
14.2	0.78×10^{-3}	2.74×10^{-2}	5.7
17.0	0.91×10^{-3}	3.28×10^{-2}	5.5

[a] Calculated by the expression $\Sigma \times 10^{20}/(8.60 \times 6.023 \times 10^{23})$.

The yield of soluble acid is between 5.0 and 5.5 equivalents per mole of surface sulfide, which is greater than the four equivalents of sulfuric acid by between 1.0 and 1.5 equivalents, presumably because of the neutralization of variable amounts of molybdic acid.

Surface acidity is readily determined, and can be used as a method of estimating the amount of surface oxidation. An estimate of this sort was used by Ballou and Ross[2] in 1953, and now seems to have been justified. However, the presence and probable effects of sulfuric acid on the surface were not appreciated at that time.

4. Rate of Surface Oxidation.—Since the rate of oxidation of pulverized molybdenum disulfide has never been reported, it was considered worth the effort to determine it. The conditions that require control were not known at the start of the work; and the present studies of rates were not done under sufficiently controlled conditions to be more than preliminary. The results obtained give the order of magnitude of the oxidation rate, and show that at least three significant variables are relative humidity, particle size, and ease of access of moist air to the surfaces of the particles. A comparison of Figs. 1 and 2 shows that the rate of oxidation is increased by greater relative humidity and finer state of subdivision. It also shows that even after more than 100 hours at 100° the oxidation has not proceeded to as much as 50% of the calculated monolayer oxidation.

DISCUSSION

DONALD GRAHAM.—It would be interesting to compare the adsorbent properties of powdered molybdenum oxide with those of the oxide monolayer on molybdenum disulfide described in this paper.

THE PROPERTIES OF ASBESTOS. I. THE COLLOIDAL AND SURFACE CHEMISTRY OF CHRYSOTILE

BY FRED L. PUNDSACK

Contribution from the Johns-Manville Research Center, Manville, New Jersey

Received February 25, 1955

The composition of chrysotile asbestos is discussed and the potential nature of isomorphous substituents in the lattice of the mineral is pointed out. Differential thermal analysis and thermogravimetric dehydration data characteristic of chrysotile are presented, and interpretation is attempted. The wide variations in nitrogen adsorption surface area values for chrysotile are shown to be due in part, at least, to the inaccessibility of inter-fibril pores to nitrogen adsorption measurements. Similarities of certain aspects of the chemical behavior of chrysotile to that of magnesium hydroxide are shown to be compatible with the crystal structure of the mineral. An attempt is made to explain the variation in the stability of asbestos suspensions as a function of *p*H on the basis of partial dissociation of the chrysotile surface.

Asbestos is a general name applied to certain fibrous inorganic minerals. Chrysotile is the variety of asbestos most commonly encountered, although a number of species are known.[1] Chrysotile is a serpentine mineral with an idealized empirical formula of $3MgO{\cdot}2SiO_2{\cdot}2H_2O$, and it is found widely distributed although deposits of economic significance are relatively few. Fibers from different locations (*e.g.*, Canada, Arizona and Southern Rhodesia) are known to vary slightly in physical properties and chemical composition.

From a structural point of view[2-6] chrysotile is considered to be a silicate with a sheet structure which makes it the magnesium analog of the kaolin group.[7] The composition of the mineral may be represented on a unit cell basis as $Mg_6(OH)_8Si_4O_{10}$. Electron micrographs of the fibers have indicated that they may exist as hollow tubes several hundred ångströms in diameter.[8-10] Bates and his co-workers hypothesize that the tubes are formed as the result of the bending of the silica–magnesium hydroxide layers in order to relieve strain caused by differences in the dimensions of the intermeshing layers. This type of strain effect was predicted as early as 1930.[11] Recently Roy and Roy[12] have attempted to substantiate the tubular hypothesis by showing that isomorphous substitution of various cations for magnesium or silicon ions can relieve the strain in the chrysotile lattice and form flat plates similar to many clay mineral structures.

Despite the extensive work which has been carried out on a structural analysis of chrysotile, the substance has remained something of an enigma from a chemical point of view. The tendency of the mineral to vary slightly in composition depending upon its source necessitates a careful characterization of samples, and failure to do this makes it difficult to assess the value of some of the data in the literature. The work reported in this paper was undertaken in order to elucidate the properties of chrysotile from a major asbestos source in Quebec, Canada.

Experimental

Materials.—The sample of chrysotile fiber used in this investigation, unless otherwise indicated, was hand-picked from several blocks of fiber each about one inch thick and each with a mass of several hundred grams. The specimens were from the Danville area of Quebec, Canada and corresponded to a commercial No. 1 crude grade of fiber. The sample selected for use was examined under low power magnification to ensure a sample free of gross mineral impurities. The indices of refraction determined by an immersion method[13] were $N_x = 1.549$ and $N_z = 1.556$. X-Ray diffraction data from the sample showed satisfactory agreement with other standard chrysotile patterns. An analysis of a representative fiber sample is shown in Table I.

(1) Other asbestos minerals include actinolite, amosite, anthophyllite, crocidolite and tremolite. The latter is the variety generally used in Gooch crucibles.

(2) V. A. Fock and V. A. Kolpinsky, *J. Phys. U.S.S.R.*, **3**, 125 (1940).

(3) B. E. Warren and K. W. Hering, *Phys. Rev.*, **59**, 925 (1941).

(4) E. Aruja, *Mineralog. Mag.*, **27**, 65 (1944).

(5) E. J. W. Whittaker, *Acta Cryst.*, **6**, 747 (1953).

(6) J. Zussman, *Nature*, **172**, 126 (1953).

(7) G. W. Brindley, "X-Ray Identification and Crystal Structure of Clay Minerals," The Mineralogical Society, London, 1951.

(8) J. Hillier and J. Turkevich, *Anal. Chem.*, **21**, 475 (1949).

(9) T. F. Bates, L. B. Sand and J. F. Mink, *Science*, **111**, 512 (1950).

(10) W. Noll and H. Kircher, *Neues Jahrb. Mineral. Monatsh.*, 219 (1951).

(11) L. Pauling, *Proc. Nat. Acad. Sci. U.S.*, **16**, 578 (1930).

(12) D. M. Roy and R. Roy, *Am. Mineralogist*, **39**, 957 (1954).

(13) Indices of refraction were determined by C. S. Hurlbut, Jr., Department of Mineralogy and Petrography, Harvard University.

TABLE I

ANALYSIS OF CHRYSOTILE FROM DANVILLE AREA, QUEBEC, CANADA

Component	Weight %	Component	Weight %
MgO	42.50	Fe_2O_3	0.38
SiO_2	41.97	Al_2O_3	~0.10
H_2O[a]	13.56	K_2O	0.08
FeO	1.57	Others (*e.g.*, Cr_2O_3, TiO_2, CaO, NiO, Mn_2O_3)[b]	~0.10

[a] Ignition loss between 175–1100°. [b] Determined by spectrographic analysis.

The distilled water used in making up the chrysotile suspensions was boiled to remove carbon dioxide, and precautions were taken to protect it from atmospheric contamination during storage. The water treated in this way had a *p*H of 7.0 ± 0.1 and a specific resistance > 3×10^6 ohms. The hydrochloric acid and sodium hydroxide employed were of analytical reagent grade.

Differential Thermal Analysis and Thermobalance.—Differential thermal analysis (DTA) of the sample was made using a DTA apparatus with a Leeds and Northrup Speedomax controller-recorder[14] and a linear heating rate of 12.5° per minute. The equipment was checked periodically using the α-β quartz inversion as a reference point. A Chevenard thermobalance[15] operated at a heating rate of 8° per minute and utilizing about a one-gram sample was employed in obtaining a dynamic weight loss curve for chrysotile.

Surface Area Measurements.—Nitrogen adsorption areas were determined by the BET method.[16] It was found convenient to outgas the samples at 175° after a number of runs had been made which established the fact that for a given sample an outgassing temperature between 25° and at least 200° had very little effect on the surface area.

Turbidity Measurements.—These measurements were made using a Brice-Phoenix Light Scattering Photometer[17] to determine the ratio of the intensity of light scattered by the chrysotile suspensions at 90° (I_{90}) to the light transmitted at 0° (I_0). Blue light of approximately 436 mμ was used as the incident light source, and the turbidity τ was calculated from equation 1 where 0.12 is an instrument-refractive index constant, and F is the product of transmittances of neutral filters used in determining I_0.

$$\tau = \frac{0.12FI_{90}}{I_0} \qquad (1)$$

Experiments showed that reproducible suspensions could be prepared by placing 30.0 ± 0.1 mg. of pulverized fiber in 100 ml. of the desired solution in a graduated cylinder and inverting the mixture twenty times. The *p*H of the suspending medium was adjusted initially by adding either hydrochloric acid or sodium hydroxide. The chrysotile used in making up the suspensions was pulverized first in a Mikro-Samplmill and then was passed through a Laboratory Wiley Mill to complete the size reduction process.

After preparation of a suspension it was immediately placed in a semioctagonal dissymmetry cell, and the turbidity was determined as a function of time. Since the turbidity of the suspending medium was relatively low compared to the magnitude of the turbidities of the suspensions, no correction for solvent turbidity was made. This method was capable of yielding reproducible results, and the turbidity values obtained for any given suspension were related to the particle size distribution in the system. Although the turbidities of all suspensions were recorded continuously for at least one hour, it proved convenient to compare the quantity of finely divided material retained in each suspension by taking arbitrarily the turbidity at the end of 40 minutes as proportional to the amount of fines in suspension. This turbidity value in turn was considered to be a measure of the relative stability of the suspension since coagulation reduced the quantity of fines in suspension and dispersion increased the value when compared to a suspension in distilled water. The equivalent diameters of the particles retained in the suspension at any given moment can be calculated by using Stokes Law, but such a value has little real meaning in view of the extremely fibrous nature of the chrysotile particles.

Electrokinetic Observations.—Observations on the sign of the electrokinetic charge of the suspended particles were made with a Siedentopf-Zsigmondy type of ultramicroscope as supplied by the E. Leitz Co.[18] The ultramicroscope was fitted with a Mattson Cataphoresis cell attached to a continuously variable voltage supply of 0–400 volts.

***p*H Measurements.**—These were made with a Beckman Model G *p*H meter standardized from time to time against a buffer of *p*H 7.00 ± 0.02.

Results and Discussion

Sample Composition.—The analysis of the chrysotile sample indicates that with the exception of appreciable amounts of ferrous and ferric ions the substance is essentially a hydrated magnesium silicate containing slightly more water than would be expected on the basis of empirical composition. This analysis, it should be pointed out, is not characteristic necessarily of all chrysotiles. Studies in this and other laboratories tend to indicate that fibers from different localities vary somewhat in the quantity and type of minor constituents present. In view of the fact that the sample used in this study was essentially a pure mineral entity it seems reasonable to suppose that the ferrous and ferric ions are present as isomorphous substituents for magnesium. This view is strengthened by the fact that upon ignition above 500° the fibers assume a uniform reddish brown color due presumably to oxidation of iron(II) to iron(III).

Substitution of ferric ions for magnesium ions would result in an unbalanced lattice charge unless equivalent substitution of a lower valent cation for silicon(IV) also occurred (*e.g.*, Al(III)), or unless equivalent vacant cation sites existed in the lattice. The presence of excess anions in the structure might also maintain electrostatic neutrality, and the relatively high water content of the asbestos would tend to favor such an explanation. However, it is not certain that all the water shown in the analysis is present in the structure as hydroxyl groups. Thus on the basis of present evidence it has not been established which of the preceding factor or combination of factors is operative in maintaining lattice neutrality.

Thermal Analyses.—The DTA pattern for the chrysotile sample used in this investigation is shown in Fig. 1. It is characterized by a broad endothermic peak between about 650–720° with a peak maximum at 670°. A relatively sharp exothermic peak occurs between 790–810° with a peak height at 800°. This pattern agrees in general with the location of peaks reported for serpentine minerals.[19,20] However, thermal examination of over half a dozen different chrysotile samples in the course of this work indicates that varying ratios of endothermic to exothermic peak

(14) P. F. Kerr, J. L. Kulp and P. K. Hamilton, "Reference Clay Minerals, American Petroleum Institute Research Project 49," Report No. 3, API, 1949.

(15) C. Duval, "Inorganic Thermogravimetric Analysis," Elsevier Publishing Co., New York, N. Y., 1953.

(16) P. H. Emmett and T. Dewitt, *Ind. Eng. Chem., Anal. Ed.*, **13**, 28 (1941).

(17) B. A. Brice, M. Halwer and R. J. Speiser, *J. Optical Soc. Am.*, **40**, 768 (1950).

(18) J. W. McBain, "Colloid Science," D. C. Heath and Co., Boston, 1950.

(19) A. J. Kauffman, Jr., and E. D. Dilling, *Econ. Geol.*, **45**, 222 (1950).

(20) N. E. Efremov, *Compt. rend. acad. sci. U.R.S.S.*, **28**, 442 (1940).

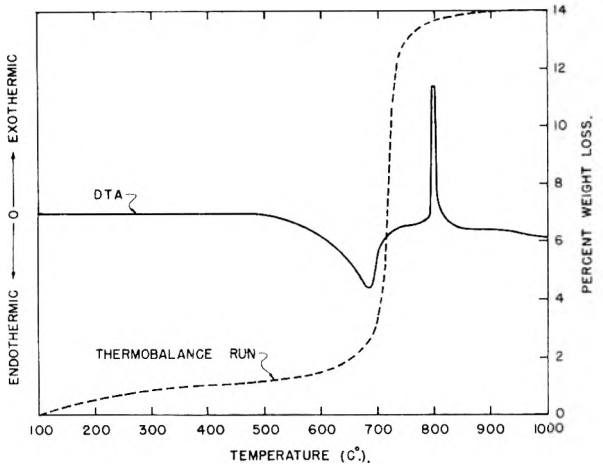

Fig. 1.—Differential thermal analysis (DTA) and dehydration characteristics of chrysotile.

heights and areas occur depending upon the source of the sample. The DTA curve shown in Fig. 1 is an example of a maximum exothermic/endothermic peak ratio. The endothermic peak at 670° corresponds to the stage of rapid weight loss shown in the dehydration curve in Fig. 1, and is associated with the loss of combined water from the chrysotile structure.[21] The peak at 800° occurs in a region in which the substance is slowly losing water. On the basis of X-ray evidence[22] this peak is believed to be associated with the formation of a forsterite phase, although some conversion to forsterite appears to occur prior to the exothermic reaction at 800°.[23]

Surface Area Variations.—In view of the fact that the surface of chrysotile is of primary importance in determining the behavior of the material in suspensions, an effort was made to resolve the differences in reported nitrogen adsorption surface areas.[24-26] These areas have ranged from 7 to 18 m.²/g. for samples outgassed at room temperature. In the present study it was observed that the surface area of chrysotile is affected greatly by the degree to which the macro to micro fiber bundles are spread apart or opened. Pulling fibers from a block of crude fiber with tweezers yielded a material with a surface area of from 4 to 12 m.²/g. depending upon how thoroughly the fibers were pulled apart. Opening the same fiber further by passing it through a Laboratory Wiley Mill gave a product with a surface area of more than 30 m.²/g., while surface areas in excess of 50 m.²/g. were obtained for fiber dispersed in a Waring Blendor with a dispersing agent of the type discussed by Novak.[27] It has been reported on the basis of small angle X-ray scattering that the fundamental fibrils of chrysotile are of the order of 200 Å. in diameter and are hexagonally close packed.[28] The fact that the surface area of chrysotile is dependent on the degree of fiber bundle openness indicates that the spaces between the close packed fibrils are not available completely for nitrogen adsorption. The reason for the inaccessibility of these interfibril pores is not known since it can be shown geometrically that the pores are large enough to admit nitrogen molecules. It is possible that due to discontinuities in the packing of the fibrils not all the inter-fibril pores open into the ends of the macro fiber bundles.

Suspension Properties.—From a chemical point of view chrysotile behaves in certain aspects as if it were magnesium hydroxide. This is not unexpected when one considers that the structure generally ascribed to the mineral[4] consists of fundamental layers made up in terms of a unit cell of O_6–Si_4–$O_4(OH)_2$–Mg_6–$(OH)_6$ planes. An example of the magnesium hydroxide-like behavior of chrysotile is the observation that the *p*H of a 0.5% suspension of finely divided chrysotile in water free of carbon dioxide is 10.33. This compares to a value of 10.37 determined for a suspension of magnesium hydroxide under the same experimental conditions and is in line with the value to be expected on the basis of the solubility product constant of magnesium hydroxide.[29] The chrysotile did exhibit a peculiar behavior, however, when the suspension was allowed to settle out for a 24-hour period. Under these conditions the clear supernatant liquid above the loosely settled fiber had a *p*H of 9.20. When the glass and calomel electrode tips were immersed in the loose fiber mass a *p*H of 9.87 was recorded. Withdrawing the electrodes into the clear supernatant liquid gave a reading of 9.20 again. Resuspending the fiber gave a *p*H > 10.0. The observation was reproducible with other chrysotile suspensions examined in this way. The phenomenon appears to be an unusual example of a gross and easily observable hydroxyl ion concentration gradient from a region relatively close to the chrysotile particles to a region which is apparently the bulk suspending medium. No experimental evidence is available at present concerning a corresponding magnesium ion concentration gradient.

When suspensions of pulverized chrysotile in distilled water free of dissolved carbon dioxide were examined with a slit ultramicroscope fitted with a cataphoresis cell, the chrysotile particles behaved as slightly negatively charged entities and migrated to the anode.[30] The dependence of the electrokinetic behavior on *p*H was investigated by measuring the turbidity of standardized chrysotile suspensions in solutions in which the *p*H had been previously adjusted by the addition of sodium hydroxide or hydrochloric acid. The sign of the particle charge in these suspensions was determined too. The data illustrated graphically in Fig. 2 indicate that the suspensions pass through an isoelectric point in the vicinity of *p*H 10.1. In more highly alkaline solu-

(21) Although the thermobalance curve was run at a slower heating rate than the DTA curve, subsequent experiments indicated that increasing the heating rate of the thermobalance run to 12.5° per minute shifted the dehydration curve to slightly higher temperatures but did not alter appreciably its relationship to the DTA curve.

(22) F. L. Pundsack and P. Greebler, to be published.

(23) W. Epprecht and E. Brandenberger, *Schweiz. mineralog. petrog. Mitt.*, **26**, 229 (1946).

(24) P. E. Bugge and R. H. Kerlogue, *Nature*, **158**, 28 (1946).

(25) B. Nagy and T. F. Bates, *Am. Mineralogist*, **37**, 1055 (1952).

(26) G. J. Young and F. H. Healey, THIS JOURNAL, **58**, 881 (1954).

(27) I. Novak, U. S. Patent 2,626,213 (Jan. 20, 1953).

(28) I. Fankuchen and M. Schneider, *J. Am. Chem. Soc.*, **66**, 500 (1944).

(29) J. W. Ryznar, J. Green and M. G. Winterstein, *Ind. Eng. Chem.*, **38**, 1057 (1946).

(30) It was found that relatively small concentrations of CO_2 in the water resulted in suspensions with positively charged particles.

tions the suspended particles are negative, and in acidic solutions the suspensions are positive. It is important to note that chrysotile reacts with strong acids to form eventually a hydrated silica residue. Therefore, the particles suspended in initially acid solutions are not chrysotile in the strict sense, but they represent instead intermediate reaction products of the acid and the fiber. This is reflected in the marked increase in the turbidity of the suspensions when the initial *p*H of the medium is less than 4.

A working hypothesis capable of accounting for the observed electrokinetic behavior of chrysotile can be constructed by regarding the surface of fundamental chrysotile fibers as a magnesium hydroxide layer on a silica substrate. In contact with relatively pure water the fiber surface dissociates partially until an equilibrium of the order of that attained by pure magnesium hydroxide is reached. Under these conditions a slight excess of hydroxyl ions appears to exist at the fiber surface which accounts for the observed negative zeta potential. Increasing the hydroxyl ion concentration of the suspending medium represses the dissociation of the fiber surface by a common ion effect, and it is inferred from the increase in the stability of these suspensions that an increase in the negative zeta potential also occurs due to increased excess hydroxyl ion concentration in the particle micelle. On the other hand when the suspending medium is acidic, the dissociation of the surface is more pronounced because of the interaction of surface hydroxyl groups with hydrogen ions. This reaction displaces the magnesium hydroxide-like equilibrium of the fiber. Probably the net result is to bring about an excess magnesium ion concentration at the surface of the fiber which gives the particle micelle a positive zeta potential. In relatively strong acid solutions the contribution of sorbed hydrogen ions to the micelle potential cannot be precluded. Since the normal fiber suspension is relatively close to the isoelectric point, the presence of carbon dioxide in the suspending medium makes it acidic enough to shift the suspension to the positive side of the isoelectric point under the experimental conditions employed in this investigation.

Acknowledgment.—The author wishes to thank Mr. George Reimschussel for his assistance in making many of the measurements reported here and Mr. Thomas Sopoci and Mr. Richard Wiley for their analysis of the chrysotile sample. Helpful discussions of certain aspects of this work with Dr. Paul Greebler are gratefully acknowledged.

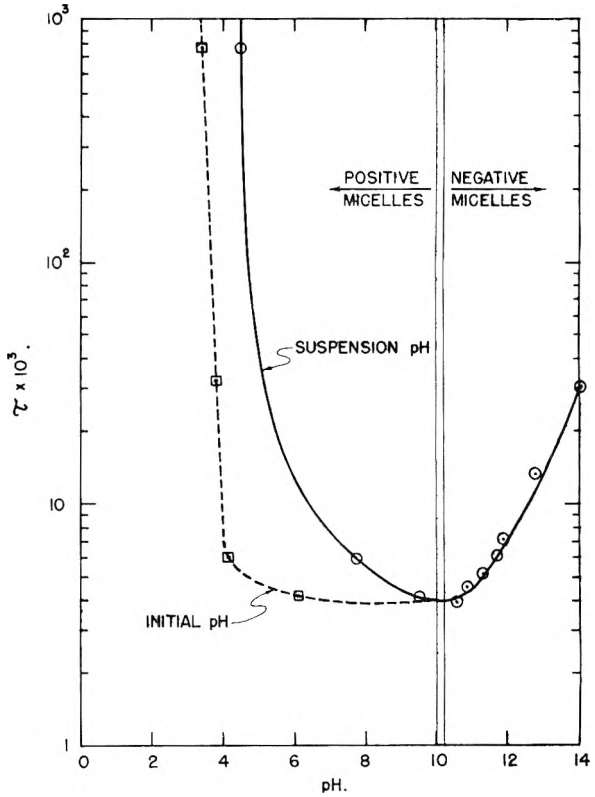

Fig. 2.—Turbidity at the end of 40 minutes of a standard chrysotile suspension as a function of *p*H. Initial *p*H of the suspending medium increased when fiber was added due to the basic interaction of chrysotile.

DISCUSSION

E. J. MILLER.—Do you feel that the present data on chrysotile are compatible with the hollow-tube structure postulated by Bates?

F. L. PUNDSACK.—The data presented in this paper do not prove or disprove the tubular structure hypothesized for chrysotile. However, on the basis of density measurements, which will be fully reported in a separate paper, it does not appear that chrysotile has a tubular structure. The density measurements are based on the premise that a hollow tube structure will possess considerable void volume when packed into bundles of fibers. In fact, based on dimensions which have been reported for the hypothesized tubes, the void volume to be expected for chrysotile fiber bundles is of the order of 20–30% of the total bundle volume. Such void volumes are not observed when unopened bundles of pure chrysotile fibers are sealed with paraffin to prevent the entry of liquid into any void volume present, and then the density is determined. Density measurements on these sealed blocks of fibers indicate a maximum void volume of about 6%. This is even less void volume than would be required for solid cylindrical fibers in hexagonal close-packing, and it is well below the values required by hollow tubes. The experimental void volumes which we have observed appear to be more compatible with distorted strips or ribbons of fiber rather than with hollow tubes.

CHARACTERIZATION OF PHYSICAL ADSORPTION SYSTEMS. III. THE SEPARATE EFFECTS OF PORE SIZE AND SURFACE ACIDITY UPON THE ADSORBENT CAPACITIES OF ACTIVATED CARBONS

BY DONALD GRAHAM

Contribution No. 179 from Jackson Laboratory
E. I. du Pont de Nemours and Co., Wilmington, Delaware

Received February 25, 1955

The effective adsorbent surface of an activated carbon is limited by pore screening and by the effects of impurities and substituent groups in the carbon surface. Of possible impurities and substituents, acid groups are among the most important. The effects of pores and surface acidity are separated and measured for a series of commercial carbon adsorbents using as adsorbates, cationic and anionic dyes sufficiently large in molecular dimensions to average out the effects of heterogeneity. The fraction of the total surface which adsorbs a cationic dye (methylene blue) is in most cases determined by pore screening alone. However, an anionic dye (metanil yellow) is repelled by acidic substituents on the carbon and finds a receptive surface smaller than that for methylene blue by an amount related to the surface acidity.

Introduction

Physical adsorption on a non-porous, essentially unsubstituted carbon surface (such as that of Graphon) is non-specific in that the entire surface is receptive to any adsorbate. The strength of the adsorption bond varies only with those factors which determine the van der Waals forces involved. Activated carbon, on the other hand, is porous and varies widely in purity and in the degree of substitution of its surface.

Pore screening in adsorption from aqueous solution has been repeatedly recognized and an attempt has been made to measure its effect.[1] For a particular adsorbate on a number of different activated carbons, adsorption capacity was plotted *vs.* the area of all pores with diameters larger than a selected value. That limiting diameter which gave the straightest line was considered the smallest which would admit the adsorbate molecules. Adsorbents were treated in groups which could include some in which other factors obscured the effect of pore size. Since any such effect would impose a further limit on adsorption capacity, the indicated limiting pore diameter would tend to err on the high side.

The pore size distribution of an activated carbon always limits its capacity for adsorbate molecules too large to enter the smallest pores. Substituent groups or impurities in the carbon surface may also limit adsorption if they repel or fail to attract the molecules of the adsorbate. In the characterization of an adsorbent, it is therefore desirable to select an adsorbate for which the capacity is measurably related to the surface concentration of the substituent or impurity under study.

Acidic groups produced by oxidation during or following activation, constitute an important class of substituents in the surfaces of porous activated carbons. It will be shown that these groups limit the capacity of the adsorbent for an acid (anionic) dye.

The present work illustrates a method for measuring separately the effects of pore size and acidic substitution, upon the fraction of the total carbon surface accessible to the first monolayer of cationic and anionic adsorbates. This method has been used in the study of over forty different carbon adsorbents. It has proven applicable to the majority of porous activated carbons, without serious interference from other factors. The method provides for the detection of such interference, when present, as illustrated later in this paper.

Some adsorbents, of course, require a different approach. An extreme example is found in the non-porous carbon black prepared by thermal decomposition of acetylene. Its surface substitution is largely hydrocarbon in character and its adsorbent properties are therefore very different from those of carbons activated by oxidation.

The adsorbates used in this study were two dyes of comparable molecular dimensions and opposite ionic character.

Methylene blue, a cationic (basic) dye

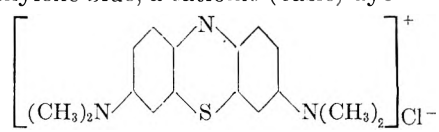

was selected for use in measuring the effect of pore screening alone. This dye when ionized in aqueous solution carries a positive charge. Any interaction with negative acidic groups in the carbon surface is therefore attractive and the quantity of dye adsorbed in the first monolayer may, in the absence of other factors, be considered a measure of the total physically accessible surface, or the surface limited by pore screening alone.

Metanil yellow, an anionic (acid) dye, was used in studying the effects of acidity of the carbon surface. As an anion, in aqueous solution it tends to be repelled by acidic groups on the carbon. Therefore, although subject to practically the same pore screening, it finds less receptive surface on an acidic carbon than does methylene blue.

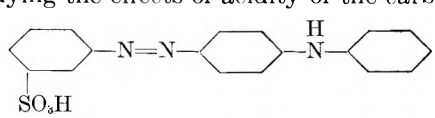

The molecular dimensions of these dyes are important. The molecules of both are approximately 18 Å. long, and 9 Å. wide. They are thus closely comparable with respect to pore screening. They are sufficiently large to average out most of the heterogeneity of the carbon surfaces and at the same time small enough for the anionic metanil yellow to

(1) A. J. Juhola, W. H. Matz and J. W. Zabor, paper presented April 1, 1951, before the Division of Sugar Chemistry at the 119th meeting of the American Chemical Society, Boston, Mass.

TABLE I

INORGANIC IMPURITIES OF CARBON ADSORBENTS

No.	Starting material	Sulfate ash, %	Sulfur, %	Phosphorus, %	Iron, %
Graphon	Spheron 6 (heat treated)	...	...	...	...
1	Wood	4.27	0.02	0.01	0.11
2	Black ash from paper mill liquor	3.06	1.60	0.02	0.06
3	Soft coal	22.70	1.40	0.09	1.32
4	Wood	1.80	0.40	0.65	0.02
4Δ	#4 (heat treated)	...	...	...	...
5	Lignite	15.70	0.61	0.03	0.14
6	Wood	2.47	0.40	0.007	0.03

TABLE II

SUMMARY OF ADSORPTION DATA

Carbon	Total surface area, m.²/g.	Methylene blue $(\frac{x}{m})_m$, g./g.	Methylene blue Accessible area, m.²/g.	Methylene blue Accessible area, % of total surface	Metanil yellow $(\frac{x}{m})_m$, g./g.	Metanil yellow Accessible area, m.²/g.	Metanil yellow Accessible area, % of total surface	Ratio of acc. areas metanil yellow / methylene blue	Acidity of carbon surface, meq./1000 m.²
Graphon	83.9	0.0265	83.9	100	0.0291	83.9	100	1.00	0
1	1120	.239	757	68	.250	721	64	0.95	.12
2	1130	.264	836	74	.218	629	56	.76	.45
3	1300	.288	912	70	.305	880	68	.97	.06
4	1300	.190	602	46	.114	329	25	.55	.94
4Δ	1300	.300	950	73	.250	721	55	.76	.80
5	600	.136	430	72	.112	323	54	.75	.70
6	580	.118	374	64	.102	294	51	.79	.60

be measurably sensitive to the effect of acidic surface substituents.

Materials and Methods

A. Adsorbates.—The methylene blue used was the Eastman Kodak Company Certified Grade. Analyses for nitrogen, chlorine and sulfate ash indicated a purity of about 99% and the dye was used on this basis.

The metanil yellow was repeatedly recrystallized from water until a small sample dried first at low temperature and finally at 140° showed a purity of at least 99.9% *vs.* a standard $TiCl_3$ solution. The product was then dried in the same way and bottled.

Both dyes were used as 0.100% solutions in distilled, deionized water. The solutions were made up by weight and checked for concentration by optical density measurements in the Cenco Photelometer. The molarity of the methylene blue solution was 0.00267 and the metanil yellow, 0.00266.

B. Adsorbents.—Six different, commercial, active carbons, recommended by their manufacturers for adsorption from aqueous solution, were studied. They are identified by numbers rather than trade names as the data may be applicable only to the specific samples used. Graphon was employed as the reference standard.

Inorganic impurities, iron, sulfur, nitrogen and phosphorus were determined by routine analytical methods. The results are given in Table I.

Total surface areas were obtained by application of the BET equation[2] to the nitrogen isotherm at −195.8° using 16.2 Å.² as the area of the nitrogen molecule. The results are listed with other adsorption data in Table II. Pore area distributions were determined by the Barrett, Joyner, Halenda method.[3] The results are plotted in Fig. 1.

C. Adsorption Equilibrium Measurements.—A temperature of 80° was used for the adsorption measurements to provide high diffusion rates. The equilibration time was determined by a series of measurements for each carbon extending from 0.5 to 100 hours. Graphon reached essentially complete equilibrium in about one hour but the porous activated carbons required 6 to 20 hours to approach their 100-hour values. The time for all runs was therefore fixed at 20 hours. This is consistent with earlier results on TiO_2[4] which showed up to 9 days required for equilibration at 25° but only 1 day at 60°.

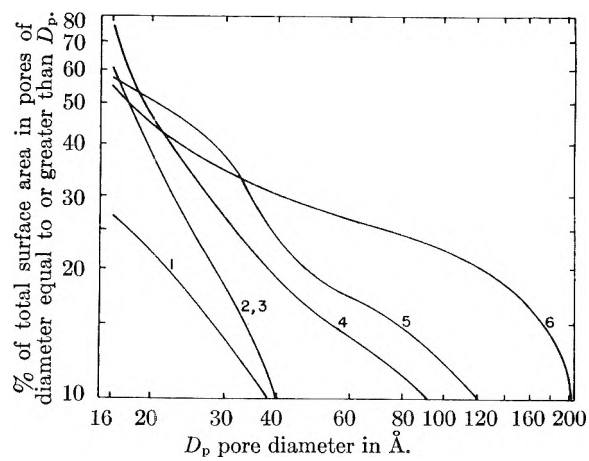

Fig. 1.—Pore area distributions.

The procedure employed was as follows: 50 ml. of a 0.100% dye solution was placed in a flask, heated to 80°, and a predetermined quantity of carbon added. The flask was closed, placed in a water-bath at 80° (±1.0°) and shaken gently with a reproducible rocking motion for 20 hours. The water-bath accommodated 21 samples and the usual charge comprised three checks for each of seven different points on an isotherm.

At completion of the run, the carbon was removed by filtration at 80° on a 5.5 cm. Whatman No. 5 paper under slight suction. A hot filter was used on a cold 500-ml. flask. (The usual centrifugal method proved poorly suited to some of the carbons used.) Filtration introduced no appreciable error in the metanil yellow data but it was necessary to apply a correction (which varied with concentration) to the methylene blue results. The final equilibrium concentration was determined by means of a Cenco Photelometer with an empirical calibration for each dye. The amount adsorbed per unit weight of carbon was calcu-

(2) S. Brunauer, P. H. Emmett and E. Teller, *J. Am. Chem. Soc.*, **60**, 309 (1938).

(3) (a) E. P. Barrett, L. G. Joyner and P. P. Halenda, *ibid.*, **73**, 373 (1951). (b) Measurements of pore area distributions were made at Juniata College by Dr. Raymond T. Davis, Jr., present address U. S. Steel Corporation, Pittsburgh, Pennsylvania.

(4) W. W. Ewing and F. W. J. Liu, *J. Colloid Sci.*, **8**, 204 (1953).

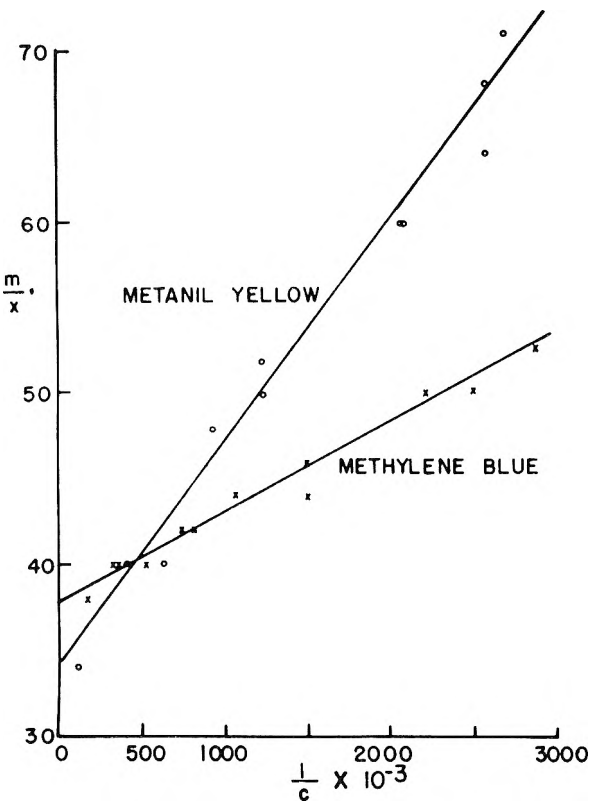

Fig. 2.—Reciprocal plots of 80° isotherms for the adsorption on graphon of methylene blue and metanil yellow from aqueous solution.

lated from the measured change in concentration and the weight of carbon used.

D. The Measurement of Surface Acidity.—The concentration of acidic substituent groups in the carbon surface was determined by titration. A quantity of carbon representing 1000 square meters of total surface was slurried in 50 ml. of 0.0100 *N* NaOH solution at 80° for 30 minutes. The slurry was then titrated back to the *p*H of 0.0100 *N* NaOH solution with 0.100 *N* NaOH solution. The results are listed in Table II in milliequivalents per 1000 square meters of surface (meq./1000 m.²).

Discussion of Results

A. Areas Occupied by Adsorbate Molecules.—Methylene blue and metanil yellow lying flat on a solid surface in a close packed monolayer would cover 160–180 sq. Å. per molecule (based on molecular dimensions). However, their multiple bonds to the adsorbent tend to limit mobility and to give a more random packing. The areas occupied by each molecule were therefore determined experimentally by adsorption on Graphon.

Determination of the content of a complete adsorbed monolayer is greatly simplified if the system can be treated as "ideal" (uniform sites and no interaction between adsorbed molecules). Graphon is exceptionally uniform and its adsorption of a wide variety of compounds is essentially free from evidence of heterogeneity. Also, effects of lateral interaction between adsorbed molecules are rarely observed in aqueous systems.

Under these "ideal" conditions, a plot of (m/x), the reciprocal of the amount adsorbed per unit mass of adsorbent, *vs.* $1/C$, the reciprocal of the corresponding equilibrium solution concentration for isothermal adsorption, is a straight line. The intercept $(m/x)_0$ at $1/C = 0$ is the reciprocal of $(x/m)_m$, the content of the filled monolayer per unit mass of adsorbent.

Such reciprocal plots of data representing the 80° adsorption isotherms of methylene blue and metanil yellow on Graphon (Fig. 2) are linear as expected. The intercepts (obtained by the method of least squares) gave values of $(x/m)_m$ of 0.0265 for methylene blue and 0.0291 for metanil yellow. These results in combination with the BET surface area of the Graphon, 83.9 m.²/g., gave values for the areas occupied by the individual molecules of 197 sq. Å. for methylene blue and 179 sq. Å. for metanil yellow.

B. Pore Screening and Accessible Surface Area.—Use of the "ideal" reciprocal plot to determine the content of a monolayer adsorbed on an activated carbon with a heterogeneous surface is made possible by proper selection of the adsorbate. We have found (in work to be reported separately) that much of the heterogeneity of carbon surfaces is of molecular dimensions and that its effects disappear when the adsorbate molecules are large enough to average out the discontinuities. Both of the dyes used in this investigation fill this requirement.

The isotherms for the adsorption of methylene blue and metanil yellow on the different activated carbon samples gave reciprocal plots comparable in linearity to those of Fig. 2. From the intercepts, values of $(x/m)_m$ were obtained as before. These, combined with the molecular areas, determined on Graphon, gave values for the surface of each activated carbon accessible to each of the two dyes, in square meters per gram (Table II). The difference between the total surface area of a carbon and that accessible to methylene blue is (unless otherwise noted) considered due to the action of pore screening. This premise is shown later to be consistent with experiment. The still smaller area accessible to metanil yellow involves the additional factor of carbon surface acidity which is also considered later.

C. Hindered Adsorption.—The surface areas accessible to methylene blue (Table II) are greater than the areas of pores with diameters exceeding 16 Å. (Fig. 1) except for Carbon No. 4. Since the accessible surface of Carbon No. 4 for methylene blue was only 46% of the total surface *vs.* 75% for pores of diameters exceeding 16 Å. (and since that accessible to metanil yellow was only 25% of the total) it was concluded that the surface carried substituent groups which hindered the adsorption of both dyes. A sample of Carbon No. 4 was therefore heated at 900° for 20 hours in an atmosphere of nitrogen and cooled to room temperature before contact with air. The product, Carbon No. 4Δ, was unchanged in total surface area but the surface areas accessible to both dyes were greatly increased. The nature of the chemical change in the carbon surface caused by the heat treatment has not yet been determined.

D. The Limiting Pore Diameter for Methylene Blue.—The pore area distributions of Fig. 1 involve the assumption of round, tubular pores. The nominal diameter of an irregular shaped pore (as

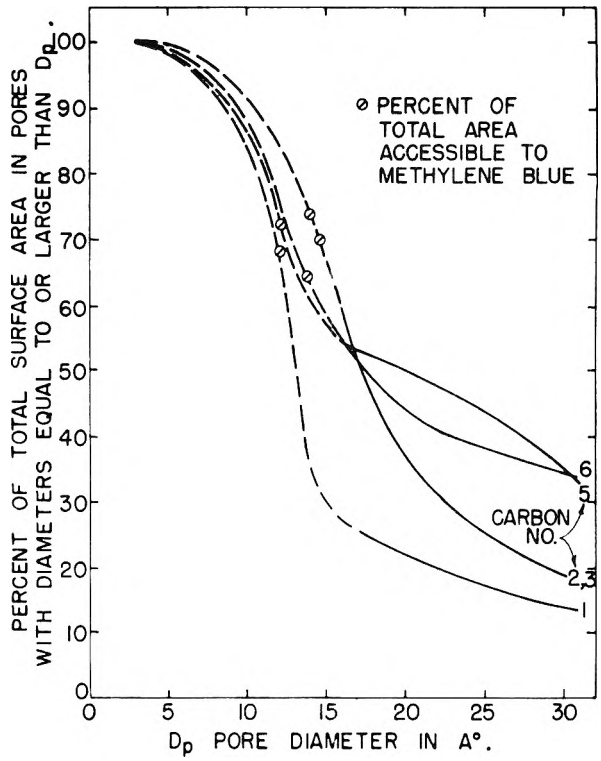

Fig. 3.—Extrapolated pore area distributions.

calculated by the Barrett, Joyner, Halenda method) is more representative of its average diameter than of its smallest. The nominal limiting diameter is therefore somewhat larger than that of the smallest round, tubular pore which can pass methylene blue molecules. At this point it can be stated that the nominal limiting pore diameter for methylene blue lies between 16 Å., shown in the preceding section to be too large, and 10 Å., the diameter of the smallest round pore that would freely pass the dye molecules. A simple average of these two values (13 Å.) might provide an acceptable approximation but it is useful to approach the solution in a different way, considering the different carbons individually.

The calculation of pore area distribution employs the Kelvin equation, which is of questioned validity for diameters below those of Fig. 1. Therefore, rather than extend the calculation to lower diameters, a simple extrapolation was used, based on two assumptions: (1) only a very small fraction of the total surface area is found in pores with diameters less than 10 Å. This is in agreement with all available data. (2) The total surface as measured by nitrogen adsorption includes no pores with diameters less than 4 Å. (approximately twice the diameter of the space occupied by a carbon atom in amorphous carbon). A nitrogen molecule would not be expected to enter a pore representing the absence of a single carbon atom. The extrapolation (excluding Carbons 4 and 4Δ) is shown in Fig. 3. The percentage of the total surface area of each carbon which is accessible for the adsorption of methylene blue (from Table II) is marked on the extrapolated curve for the same carbon in Fig. 3. The corresponding abscissa represents the nominal limiting

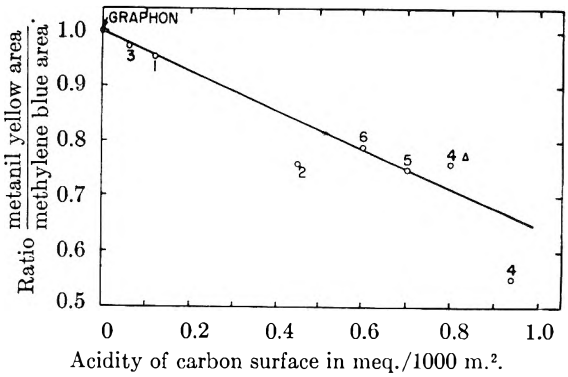

Fig. 4.—The effect of surface acidity upon the carbon surface area receptive to metanil yellow.

pore diameter for the adsorption of methylene blue by that carbon (and presumably also for metanil yellow).

Carbon No.	1	2	3	5	6	
Limiting D_p	12.0	14.0	14.6	12.2	13.7	Av. = 13.3 Å.

Part of the observed variation between the individual values is of course due to error but part may be real as the pore shape distribution may be expected to vary with the source and method of activation of the carbon. The over-all general agreement between the results from the different carbons confirms the earlier suggestion that, except for Carbon No. 4, pore screening is the principal factor limiting the surface accessible to methylene blue.

The average nominal limiting pore diameter of 13.3 Å. for methylene blue is in reasonable agreement with the 15.0 Å. value obtained from the very different approach of Juhola, *et al.*,[1] particularly since error in the latter value would tend to be on the high side.

E. The Effects of Surface Acidity.—For every activated carbon studied, the surface area accessible to the first adsorbed monolayer of metanil yellow is less than that for methylene blue. The observed differences vary widely. The molecular dimensions of the two dyes are closely similar and the observed differences in accessible surface area show no relation to the pore area distributions of the different carbons. The measurement of accessible areas is based on the premise that an unsubstituted, nonporous carbon surface (Graphon) is equally receptive to both. The observed differences are therefore ascribed to interactions of the adsorbate molecules with specific substituents in the carbon surfaces.

Acidic substitution of the carbon surfaces could explain the observed effect and a correlation was sought. The effect was measured as the fraction of the surface accessible to methylene blue which would also receive metanil yellow, or the ratio of the two accessible surface areas. A plot of this ratio against surface acidity (Fig. 4) was roughly linear. The data for Carbons 4 and 4Δ are not seriously out of line, indicating that the general hindrance noted in the single case of Carbon 4 is separate from the effect of acidic surface substitution.

These results indicate that acidic groups in the

carbon surface tend to reduce the capacity of a carbon adsorbent for metanil yellow, and probably for anionic adsorbates in general, roughly in proportion to the concentration of these groups in the surface.

Summary

(1) The areas occupied by individual molecules of methylene blue and metanil yellow in monolayers adsorbed on Graphon have been determined and used to measure the surface areas of activated carbons accessible to these molecules.

(2) The surface area of an activated carbon accessible to Methylene Blue is usually limited only by the size of the pores.

(3) In some cases, unidentified substituent groups, in the carbon surface, hinder the adsorption of either dye. In the single case observed, the effect was greatly reduced by heating in nitrogen at 900°.

(4) The nominal limiting pore diameter for methylene blue (and presumably also for metanil yellow) is approximately 13 Å.

(5) Acidic substituents in the carbon surface reduce the surface area accessible to the anionic adsorbate, metanil yellow, roughly in proportion to their concentration in the surface.

Acknowledgment.—The author wishes to thank Dr. F. C. Chromey of this Laboratory for assistance in the statistical treatment of experimental data.

THE EFFECT OF GASES ON THE CONTACT POTENTIALS OF EVAPORATED METAL FILMS

BY NORMAN HACKERMAN AND EMERSON H. LEE

Department of Chemistry, University of Texas, Austin 12, Texas

Received February 25, 1955

The effect with time of oxygen, nitrogen, water vapor and air on the contact potential differences between aged bulk platinum and evaporated metal films was studied by the vibrating condenser method. The metals used were aluminum, lead, nickel, chromium and iron. Both reversible and irreversible effects were observed. An explanation is offered based on sorption of the gases which provides either a dipole barrier or an ion barrier to the emission of electrons.

Introduction

If two unlike metals are brought into contact in air and then separated slightly, a static electrical potential difference exists between them. This potential difference is called the contact potential, or Volta potential difference. Contact potentials are a function of the electronic work functions of the two metals involved; the difference of the two work functions, in electron volts, is numerically equal to the contact potential difference, in volts.

The work function of a metal is changed by adsorbed gas films or chemical films[1]; therefore contact potentials can be used to study adsorption and reactions of a gas with a metal. This may be done by measuring the potentials between a freshly formed surface and an aged surface. Since the aged metal is relatively stable, any change in contact potentials is ascribable to a change in work function of the fresh metal surface as it adsorbs a gas or reacts with it.

The work functions of pure metals have been found to be anisotropic[2-4] and to vary with allotropic modifications.[5,6] Therefore crystal structure and orientation in metals affect contact potential measurements.

Methods for obtaining a bare metal surface include abrasion in air[7] or in a vacuum system,[8,9] cleavage of a metal crystal,[10] out-gassing of a pure metal in a vacuum,[11,12] and evaporation of metal films.[13] Use of evaporated films offers some advantages since occluded gases are boiled out prior to and during evaporation. The disadvantage in using metal films is that of correlating the properties of the films with those of bulk metals.[14,15] Two important factors to be considered are the effect of crystal orientation and film thickness on the work function of the films.

In this work, contact potentials between evaporated films and an aged platinum reference were measured in a vacuum system at room temperature as a function of time after evaporation. Potentials were measured by the vibrating condenser method.[16] The effects of air, oxygen, nitrogen and water vapor on evaporated films of aluminum, chromium, nickel, iron and lead were studied. The stability of the platinum reference was also studied for the experimental conditions used.

(1) R. Suhrman, *Z. Elektrochem.*, **56**, 351 (1952).
(2) R. Smoluchowski, *Phys. Rev.*, **60**, 661 (1941).
(3) S. T. Martin, *ibid.*, **56**, 947 (1939).
(4) P. A. Anderson, *ibid.*, **59**, 1034 (1941).
(5) A. Goetz, *ibid.*, **33**, 373 (1929).
(6) H. B. Wahlin, *ibid.*, **61**, 509 (1942).
(7) H. H. Uhlig, *J. Applied Phys.*, **22**, 1399 (1951).
(8) F. Fianda and E. Lange, *Z. Elektrochem.*, **55**, 237 (1951).
(9) J. Giuer and E. Lange, *Naturwissenschaften*, **40**, 506 (1953).
(10) F. B. Daniels and M. Y. Colby, *Phys. Rev.*, **52**, 1200 (1937).
(11) J. R. Anderson and A. E. Alexander, *Australian J. Ch.*, **6**, 109 (1953).
(12) C. W. Oatley, *Proc. Phys. Soc.*, **51**, 318 (1939).
(13) P. A. Anderson *Phys. Rev.*, **47**, 958 (1953); **49**, 320 (1936); **57**, 122 (1940); **76**, 388 (1949); R. Kh. Burstein, M. D. Surova and I. A. Zuidenman, *Zhur. Fiz. Khim.*, **24**, 214 (1950) [*C. A.*, **44**, 6743 (1950)]; E. W. J. Mitchell and J. W. Mitchell, *Proc. Roy. Soc. (London)*, **A210**, 70 (1952); I. Ogawa, T. Doke and I. Nakada, *Oyo Butsure*, **22**, 101 (1953) [*C. A.*, **47**, 10380 (1953)]; T. V. Kalish and R. Kh. Burstein, *Doklady Acad. Nauk SSSR.*, **81**, 1093 (1951) [*C. A.*, **46**, 3829 (1952)]; C. F. Ying and H. E. Farnsworth, *Phys. Rev.*, **85**, 485 (1952); Y. Yashiro, *Bull. Nagoya Inst. Technol.*, **3**, 333 (1951); J. C. P. Mignolet, *J. Chem. Phys.*, **20**, 341 (1952); *Disc. Faraday Soc.*, 185 (1950).
(14) J. A. Allen, *Rev. Pure App. Ch.*, **4**, 133 (1954). This is a comprehensive review on evaporated metal films.
(15) R. A. Sennett, T. A. McLaughlin and G. D. Scott, *Can. J. Phys.*, **30**, 370 (1952).
(16) W. A. Zisman, *Rev. Sci. Instr.*, **3**, 367 (1932).

Experimental

The vacuum system included a Megovac forepump and a two-stage oil-diffusion pump, employing Octoil as the pump fluid. The ultimate pumping pressure was about 7×10^{-7} mm.; the system could be pumped down readily to the 10^{-6} mm. range. With the vacuum system sealed off from the pumps, the pressure stayed in this range for several hours. The system contained a Pirani gage, a Phillips gage and a calibrated McLeod gage. All stopcocks and sources of mercury vapor were separated from the contact potential unit by two cold traps in series. These traps were usually maintained with liquid nitrogen, although the use of Dry Ice and alcohol instead did not noticeably affect the experimental results. A magnetically operated, dry, ground-glass joint was used to separate the contact potential unit from the cold traps when water vapor was admitted.

The contact potential unit was outgassed for several hours at 300° before each experiment. The system was then flushed several times with dry, oxygen-free nitrogen before pumping down.

A mercury cut-off opened and closed the system to the pumps; metering stopcocks were used to admit gases. Thus any number of samples could be quickly admitted and withdrawn from the system thereby providing a means for studying the reversibility of adsorption and contact potentials.

The contact potential unit is shown in Fig. 1. Metal-to-glass joints on each of the three necks of the flask were soft-soldered to the various units indicated. The metals were evaporated from tungsten or other filaments according to recommendations of other workers.[14] The metals were outgassed and a small amount was evaporated into the flask to provide some gettering action. However, pressures still rose to 1×10^{-4} to 5×10^{-3} mm., during subsequent evaporations; thus no completely bare metal surfaces were obtained. The metal vapor was directed downward by a glass tube and was condensed on microscope cover-glasses. These were outgassed at 300° for several hours in the contact potential unit before evaporation of the metal samples. Each cover-glass was coated on one edge with evaporated metal prior to installation. This gave good electrical contact with a brass spring clip which also held the cover-glasses in place. After evaporation, the cover-glass and support was moved under the platinum reference by means of an external magnet. The distance between the film and the reference was adjusted through a monel bellows, which supported the reference electrode, by a screw adjustment which compressed the bellows. Contact potential measurements began about one minute after evaporation of the films; the method of measurement was that described earlier,[17] except that an oscilloscope was used as the null indicator. Sensitivity of the measurements was ±3 mv.

Contact potentials were measured as the gases were admitted to the system. After each run the films were weighed by difference, and their thickness was estimated by the weight, area and density of the metal. The evaporated films were checked spectrographically for tungsten and other impurities. These data, along with data on the gases used, are shown in Table I.

Two non-transition metals, aluminum and lead, were studied for comparison with the transition metals, chromium, nickel and iron. The work functions of these metals are 3.38, 3.94, 4.38, 4.32 and 4.40 e.v., respectively.[18] The effects of air, oxygen and nitrogen were measured by exposing the freshly evaporated films to the gases at pressures of 0.03 to 0.05 mm. Water vapor was used at lower pressures, 5×10^{-4} to 3×10^{-3} mm., because of the difficulty in manipulating it in the vacuum system.

Results

Nitrogen had no permanent effect on the work function of the films. However, temporary changes were observed when nitrogen first entered the system, apparently because of the temperature drop of the gas when it was admitted. This reversibly increased the work function of the metals studied, and was apparently caused by temporary adsorption of the gas before it warmed to the temperature of the apparatus.

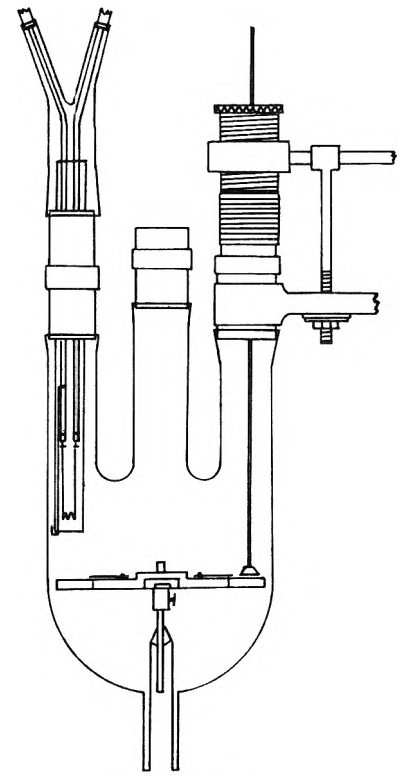

Fig. 1.

On standing in the evacuated system the work functions decreased continuously and irreversibly for several hours, undoubtedly the result of oxidation by adsorbed oxygen. After the films reached a stable potential, exposure to oxygen caused a reversible increase in work function, just as with nitrogen. The final potentials between oxidized films and platinum compared favorably with potentials found for abraded metals *vs.* platinum in air.[7]

The work functions of the transition metals increased when first exposed to oxygen, becoming greater than that of the platinum reference. The values remained at these noble levels until oxidation, with corresponding decreases in work function, took place. Aluminum and lead did not go through these "passive" states, instead the work functions steadily decreased until a stable potential was reached.

Water vapor had a noticeable effect only on the lead films.

The work functions of the platinum reference and other aged bulk metals were stable under the experimental conditions used, as shown in Fig. 2.

A small change in contact potential was observed when the distance between two unlike metal surfaces was varied as shown in Fig. 3. With like metals, the potential passed through zero at one point, and the potential–distance relation was essentially linear. This effect has been observed before with this type of apparatus.[7]

Some variation of potential was observed on rotating one metal surface a few degrees with respect to the other. There was also some effect

(17) L. Antes and N. Hackerman, *J. App. Phys.*, **22**, 1395 (1951).

(18) B. E. Conway, "Electrochemical Data," Elsevier Publishing Co., Houston, Texas, 1952, p. 31.

TABLE I

MATERIALS USED

Materia	Form	Original purity, %	Purification treatment	Spectrographic anal. of films approx. impurities
Oxygen	Commercial	99.5	Dried	....
Nitrogen	Commercial	99.5	Oxygen removed with vanadyl sulfate soln.; dried	....
Water	Distilled	..	Redistilled from alk. permanganate, boiled to remove gases	....
Aluminum	Wire	99.7	Outgassed before evaporation	Si, Fe, 0.10 Cu, trace; W, none
Iron	Wire	99.8	Outgassed before evaporation	Cr, Mg, Mn, Si, heavy trace; W, Al, Cu, Sn, trace
Chromium	Electro-deposited	...	Outgassed before evaporation	Fe, Cu, trace; W, none
Nickel	Wire	99	Outgassed before evaporation	Fe, Mn, Mg, Cu, 0.10; B, Cr, Ca, Ag, W, trace
Lead	Sheet	...	Outgassed before evaporation	Ni, Mn, Ag, 0.01; Cu, Fe, B, trace

because of change in amplitude of vibration. These variations were on the order of a few hundreths of a volt. No variation with frequency of vibration was observed.

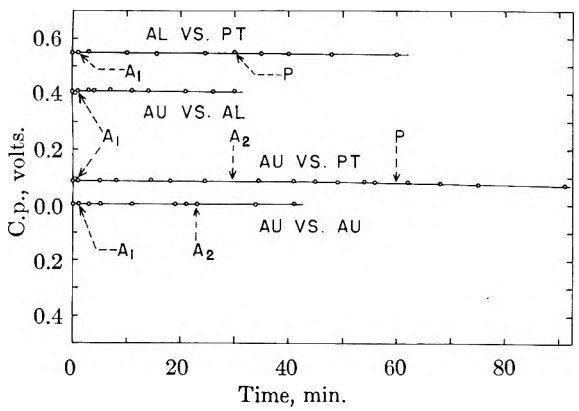

Fig. 2.—Effect of aging on the contact potential difference between the aged bulk metals shown. Air admitted to 0.04 mm. at A_1, to 0.10 mm. at A_2; system pumped at P.

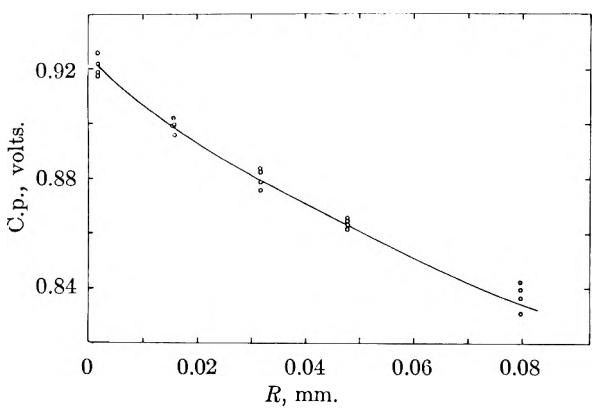

Fig. 3.—Effect of minimum distance of separation on the contact potential difference between bulk aluminum and brass.

These facts indicate that the measured contact potentials are in fact a difference between modified work functions. In these experiments the position and amplitude of vibration remained constant during any one run and therefore even the small effects mentioned above did not enter into the observed potential changes of the metal films with time.

Aluminum Films.—As shown in Fig. 4, nitrogen did not affect the initial potential trend, which was caused by oxidation of the aluminum film by residual oxygen in the vacuum system. The reversal of the potential changes due to nitrogen which became evident on the lightly oxidized film took place before the gas was pumped out, indicating that adsorption was caused by a temporary drop in temperature of the gas. Slower admission of the nitrogen through a capillary leak eliminated the cooling effect and the potential changes, as shown.

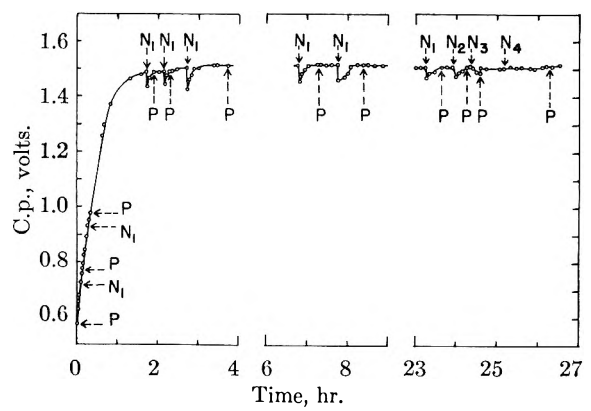

Fig. 4.—Contact potential difference between platinum reference and 300 Å. aluminum film. Nitrogen admitted instantaneously to 0.04 mm. at N_1; same but 1 minute for admission at N_2, same but 4 minutes at N_3, same but 50 minutes at N_4; system pumped at P.

Admission of air (or oxygen) to a fresh aluminum film gave the effects shown in Fig. 5. The peak values of potential were about the same after the films had been exposed to the atmosphere and pumped again. The reversible potential changes of the oxidized film are believed to be due to reversible, physical adsorption.

No correlation was found between film thicknesses of aluminum and contact potentials for

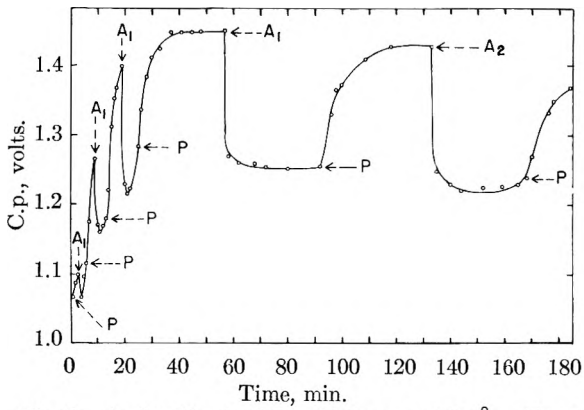

Fig. 5.—As for Fig. 4. Film thickness at 700 Å. Air admitted to 0.04 mm. at A_1, to 0.10 mm. at A_2; system pumped at P.

films thicker than about 250 Å. Data on several films are shown in Table II. Some of the differences seen resulted from the different ages of the films and some from the positional effects mentioned previously.

TABLE II

EVAPORATED ALUMINUM FILMS

Thickness, Å.	Final C.P.	Hr. elapsed	Thickness, Å.	Final C.P.	Hr. elapsed
280	1.514	24	792	1.484	7
620	1.400	24	1400	1.362	8
695	1.024	1	2130	1.301	3
710	1.424	2			

Chromium Films.—Chromium films exhibited fairly active, stable potentials until air or oxygen was admitted, then the potentials immediately dropped by a volt or more, as shown in Fig. 6. The effect of air on the potentials decreased continously as the film oxidized. The over-all potential changes involved an increase in the work function, although a decrease in work function took place during the subsequent oxidation process, as it did with aluminum.

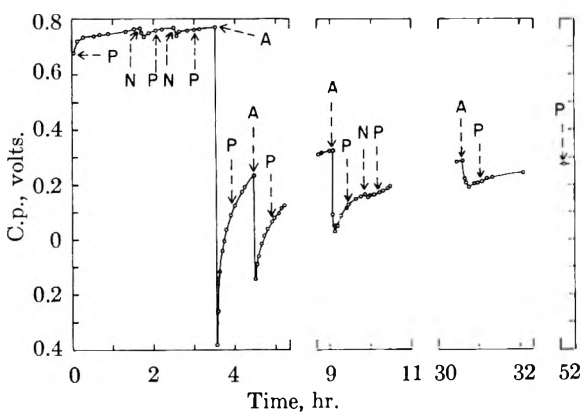

Fig. 6.—Contact potential difference between platinum reference and 250 Å. chromium film. Nitrogen to 0.04 mm. at N; air to 0.05 mm. at A; system pumped at P.

Nickel Films.—Nickel films reacted much as did chromium films (Fig. 7). The increase in work function due to physical adsorption and decrease for the oxidation process is opposite to that reported by Mignolet.[19] The drop in potential that occurred on pumping at 42 hours was not observed in other experiments.

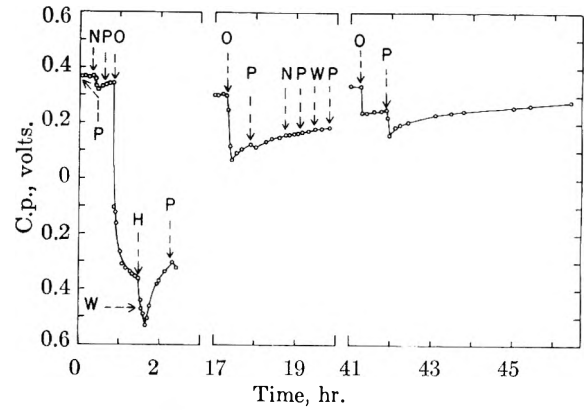

Fig. 7.—Contact potential difference between platinum reference and 250 Å. nickel film. Nitrogen to 0.05 mm. at N; oxygen to 0.06 mm. at O; water vapor to 0.001 mm. at W; cold traps warmed to −78° at H; system pumped at P.

Iron Films.—The initial potentials of the iron films were more noble than that of the platinum references, as shown in Figs. 8 and 9. Comparison with data on chromium and nickel indicates that the iron films were already partly covered with

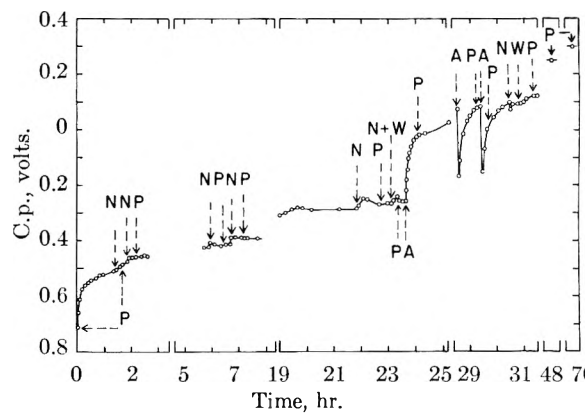

Fig. 8.—Contact potential difference between platinum reference and 250 A. iron film. Air to 0.04 mm. at A; nitrogen to 0.04 mm. at N; water vapor to 0.002 mm. at W; system pumped at P.

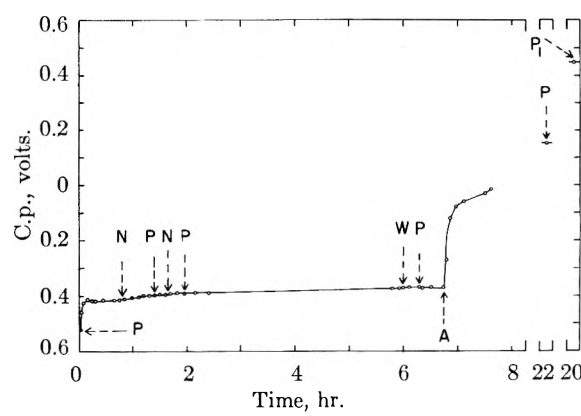

Fig. 9.—As for Fig. 8 except water vapor to 1×10^{-4} mm. at W and system pumped at P_1 after exposure to atmosphere.

(19) J. C. P. Mignolet, *Disc. Faraday Soc.*, **8**, 105, 326 (1950); *J. Chem. Phys.*, **20**, 341 (1952).

oxygen. Dushman[20] has shown that all types of iron contain significant amounts of dissolved oxygen; therefore the iron sample itself was a source of oxygen contamination.

The iron films differed from those of chromium and nickel in that the first addition of oxygen caused a rapid rise in potential. This indicated that the iron oxidized much more rapidly than the nickel and chromium. After the initial exposure to oxygen, the effect of this gas was reversible, and potential changes were in the same direction as with other metals.

Burstein, Surova and Zuidenman[21] also found that the work function of iron films decreased during the initial oxidation process. Subsequent heating of these films caused the work function to increase again as more massive oxidation took place. In the present work, the later increase in work function was not observed. At room temperature, the films showed an insignificant oxidation rate; the films retained a bright lustre in the vacuum system, and the work function approached a constant value.

Lead Films.—The lead films showed the general characteristics of the aluminum films; no passive states were observed. After the films were lightly oxidized, reversible adsorption was measurable as with other films, as shown in Fig. 10. Comparison of Figs. 10 and 11 shows that the combination of oxygen and water vapor quickly oxidized the lead. This is in agreement with the known properties of freshly distilled lead.[22]

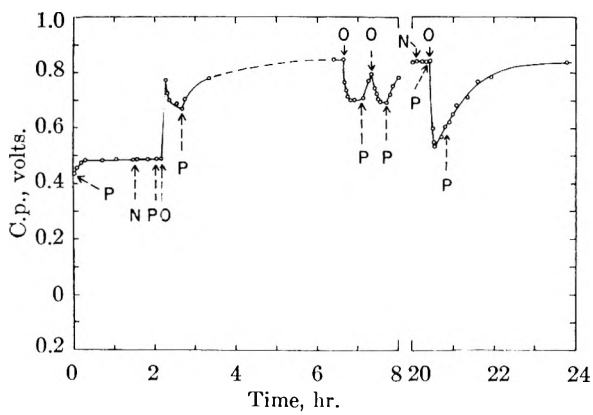

Fig. 10.—Contact potential difference between platinum reference and lead film. Nitrogen to 0.04 mm. at N; oxygen to 0.05 at O; system pumped at P.

Discussion

Zisman,[16] who introduced the vibrating condenser method, stated that measured potentials were independent of the position of the surfaces. However, Koenig[23] believes that compensation methods for measuring contact potentials are based on an unproved assumption. He states that there is no

(20) S. Dushman, "Vacuum Techniques," John Wiley and Sons, Inc., New York, N. Y., 1949.

(21) R. Kh. Burstein, M. D. Surova and I. A. Zuidenman, *Zhur. Fiz. Khim.*, **24**, 214 (1950) [*C. A.*, **44**, 6743 (1950)].

(22) J. N. Friend, Editor, "Textbook of Inorganic Chemistry," Vol. V, Chas. Griffin and Co., London, 1917, p. 379.

(23) F. O. Koenig, "A Thermodynamic Analysis of the Volta Effect," Comite International de Thermodynamique et de Cinetique Electrochemiques, Comptus Rendus de la III Reunion, 1951, p. 299.

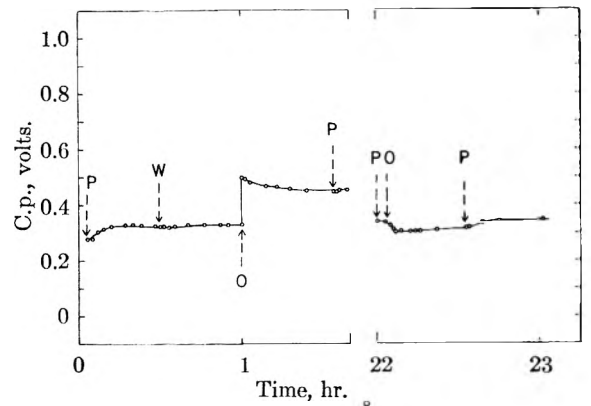

Fig. 11.—As for Fig. 10 except 500 Å. film and water vapor to 0.002 mm. at W.

phenomenological principle which requires the composition potential to be equal to the Volta potential.

The potential–distance variation found indicates that the vibrating condenser method is contingent on such a variation. It appears that it is this variation which produces the alternating signal received by the oscilloscope, and thus the null potential varies with the mean distance between the surfaces.

Contact potentials were detected with surface separations as large as one millimeter, but the potential–distance variations shown in Fig. 3 involved separations of only a few hundredths of a millimeter. This indicates that the electrons at the surface of one metal were in the potential field of two metals, rather than one. Such a field would modify the work function of each metal since the work function includes the distance from inside the metal to infinity. This appears to be the reason for the observed variation of potential with distance.

The data on bulk metals shows the feasibility of a noble metal reference. It is necessary to conclude that the bulk metals did not change in work function during adsorption of air, or to make the unlikely assumption that values for all the metals changed by the same amount.

Koyen found that adsorption of water vapor changed the work function of bulk platinum[24]; therefore there is some doubt about the use of a platinum reference with water vapor.

The range of potentials found with evaporated films shows that no measurements were made with a bare metal surface. The work function of oxidized platinum is 6.35 e.v.[12] Therefore the contact potential between a platinum reference and one of these bare metal films should be on the order of two to three volts, with the film at the more active potential.

The work functions of all the films decreased as oxidation took place. This phenomenon is not restricted to evaporated films.[8,10,25,26] An explanation for the various reported data is shown in Fig. 12. Using 4.4 and 6.3 e.v. as work functions of chromium[18] and oxidized platinum,[12] the contact

(24) S. Koyen, *J. Sci. Res. Inst.*, **47**, 172 (1953).

(25) F. L. Jones and C. G. Morgan, *Proc. Roy. Soc. (London)*, **A218**, 88 (1953).

(26) R. J. Cashman and W. S. Huxford, *Phys. Rev.*, **43**, 811 (1953).

potential between these two metals would be at point A, with a value of 1.9 volts. In this work initial potentials were measured at B (see Fig. 6), after the surface of the chromium was partly covered with oxygen. Admission of oxygen at C caused the potential to drop to D, where the film had a work function greater than that of the platinum reference. The relatively slow oxidation then decreased the work function of the film to E. More massive oxidation would presumably increase the work function in the direction of F. There are several regions of this curve over which an increase or decrease in work function is observed, depending on the quality of the vacuum system used and on experimental procedures.

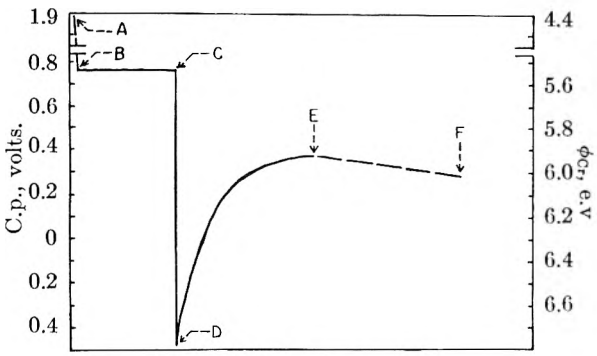

Fig. 12.—Schematic curve for contact potential *vs.* time for chromium; see text.

A similar analysis for aluminum (see Fig. 4) is shown in Fig. 13. Since aluminum is such an active getter of oxygen, it is probable that it was already in the process of oxidation when initial measurements were made at B. Data equivalent to the conditions at A and D of Fig. 12 were not observed in this case.

The noble potentials of chromium, nickel and iron caused by oxygen may be explained by a negative space charge at the metal surface induced by the adsorbed molecules. Such a charge would repel electrons in the metal and increase the effective work function. The space charge might be caused by polarization of the adsorbed molecules with the negative side out, by formation of an adsorbed complex with an excess negative charge, or by formation of negative ions. Since oxygen is ionized in forming oxides, it is suggested that the initially adsorbed oxygen on a bare metal becomes ionic in form, thus producing the observed noble potentials. Such ionization should be possible by virtue of the high electronegativity of oxygen, and the small energy barrier for electron emission at a bare metal surface. After the metal surfaces become lightly oxidized, electron emission becomes more difficult and ionization would be less likely. However, the adsorbed molecules could still be strongly polarized, and perhaps a few per cent. ionized on a statistical basis. This should increase the effective work function, but to a lesser extent than by a full layer of ions. This would explain the diminishing effect of adsorbed oxygen on the work function of the films as they aged (Figs. 6 and 7).

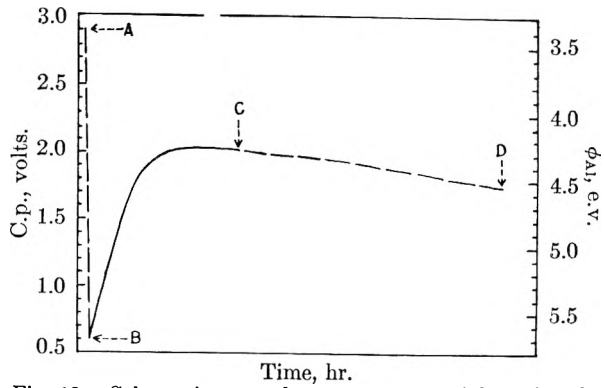

Fig. 13.—Schematic curve for contact potential *vs.* time for aluminum; see text.

Adsorbed molecules at this stage could form the no-bond-charge-transfer complex that has recently been described.[27-29] On such a basis, oxygen would be a Lewis acid and the metal a Lewis base. The adsorbed complex would be described by a linear combination of wave functions for a no-bond state and a dative state where an electron had been transferred from the metal to the oxygen. The increase in negative charge density just outside the metal should increase the work for emission of electrons from within. It should be noted, however, that Mignolet[28] used no-bond-charge-transfer states to explain a decrease in the work functions in the case of physical adsorption of inert gases.

The noble potentials of the transition metals that resulted from the initial oxygen adsorption were stable for a number of hours in the evacuated system. This may be attributed to the close-packed structure of these metals, which would prevent diffusion of oxygen inward, and the high cohesive energy, which would prevent movement of metal atoms outward. The comparatively small work function found initially for aluminum is attributable to ionization or polarization. This effect would be expected to diminish as the film oxidized, and therefore the work function should decrease as in Fig. 4. The aluminum films differed from the others in that they rapidly combined with the adsorbed oxygen, and therefore reached a stable potential rather quickly. These films showed little effect of aging after the first few hours. Boetcher and Haas[30] found that the oxide film on evaporated aluminum did not exceed 40 Å. even after two months. These phenomena result from the strong affinity of aluminum for oxygen, and to the high chemical stability of the resulting oxide.

The effects of oxygen on lead were similar to those on aluminum. Water vapor increased the oxidation rate of lead,[22] but apparently not for aluminum or for the other metals. At higher vapor pressures, an adsorbed film of water vapor probably increases oxidation rates of various metals through local cell reactions, as described in corrosion theory.

Nitrogen showed no permanent reaction with the

(27) R. S. Mulliken, *J. Am. Chem. Soc.*, **74**, 811 (1952).
(28) J. C. P. Mignolet, *J. Chem. Phys.*, **21**, 1298 (1953).
(29) F. A. Matsen, A. C. Makrides and N. Hackerman, *ibid.*, **22**, 1800 (1954).
(30) A. Boetcher and G. Haas, *Optik*, **6**, 299 (1950).

metals studied. At room temperature such a reaction is expected to be very slow and unable to compete with oxidation by residual oxidation in the system.

For oxides of iron, nickel or chromium which might be semiconductors the question arises as to whether or not the potential trends observed can be correlated with a change in semi-conductor type in the thin oxide film. There seems to be no answer to this question with contact potential data alone.

The studies with the three transition metals indicate that the transitory passive states found in electrochemical systems can be caused by an adsorbed layer of oxygen, and that this oxygen possibly is ionic in form.

The proposed ionic mechanism suggests that heterogeneous oxidation catalysts might operate by ionizing adsorbed oxygen. This would require that catalysts have properties similar to these evaporated films at the conditions where the catalysts are used. At the higher temperatures usually encountered in catalyst systems, the work function of the metals would be less, thus favoring the emission of electrons and the formation of adsorbed ions. Such a state should serve as a continuous source of active oxygen for the reaction. These studies indicate that the transition metals, because of their relative passivity in contact with oxygen, would be the most stable source of the proposed ions, and thus the best catalysts.

Acknowledgment.—The authors are grateful to the Office of Naval Research for their support of this work.

DISCUSSION

MAX BENDER.—In terms of your experimental approach using the measurement of contact potentials would you elaborate on the possibilities of distinguishing between chemisorption and physical adsorption.

NORMAN HACKERMAN.—Although not mentioned in this paper, one of the aims of this work was to distinguish between chemisorption and physical adsorption by means of contact potentials. It is believed that the initial adsorption of oxygen corresponded to a chemisorption process—for example from C to D in Fig. 12 However, the reversible potentials found with the lightly oxidized films are believed to be physical adsorption, or possibly in the border-line region between chemisorption and physical adsorption. This process is best shown in Fig. 5. In this case, the chemisorption process had apparently already taken place before potential measurements were started, as shown in Fig. 13.

ELECTROCHEMICAL METHOD FOR THE KINETIC STUDY OF FAST ADSORPTION PROCESSES[1]

BY TALIVALDIS BERZINS AND PAUL DELAHAY

Department of Chemistry, Louisiana State University, Baton Rouge, Louisiana

Received February 25, 1955

A theoretical analysis is made of the kinetics of adsorption of neutral organic substances on an electrode whose potential is a sinusoidal function of time of small amplitude (0.005 volt). The surface concentration of adsorbed substance is derived for simultaneous control by the kinetics of adsorption and by linear diffusion—in solution—of the substance adsorbed on the electrode. Conditions are derived under which either diffusion or adsorption or both processes control the over-all rate. Parameters characterizing the adsorption kinetics are deduced from the differential capacity of the double layer. Rates as high as those corresponding to the adsorption or desorption of a monolayer in 10^{-4} sec. could possibly be determined. The use of the "exchange rate" at equilibrium is suggested to characterize the kinetics of adsorption processes.

Little is known about the kinetics of adsorption of neutral organic molecules on metals. Equilibria for such processes can be studied, for example, by determining the distortion of the electrocapillary curve[2] or from the variation of the double layer capacity.[3] It is found in this manner that the amount of adsorbed substance depends on the potential of the metal, and that there is no adsorption at sufficiently cathodic and anodic potentials. Frumkin and Melik-Gaikazyan[4] developed a method for the kinetic study of adsorption which embodies these two characteristics of adsorption processes, namely, the variation of the double layer capacity and the influence of potential. The potential of the metal varies periodically with a small amplitude (0.005 volt) about a constant value, and the differential capacity of the double layer is measured at various frequencies.[5] Frumkin and Melik-Gaikazyan considered only the two limiting cases in which either diffusion or adsorption is rate determining. We treat here the general case in which both processes are taken into account simultaneously.

Variations of Surface Concentration

We assume that linear diffusion in solution is the sole mode of mass transfer of the substance adsorbed on the electrode. The concentration C of this substance is thus a solution of Fick's differential equation. As boundary condition we prescribe that the flux of adsorbed substance is equal to the rate of adsorption. Thus, one has per unit area for $t > 0$ and $x = 0$

$$d\Gamma/dt = D(\partial C/\partial x)_{x=0}$$

(1) Paper presented at the National Colloid Symposium in Houston on June 20–22, 1955.

(2) N. K. Adams, "The Physics and Chemistry of Surfaces," 3rd ed., Oxford University Press, London, 1941, p. 341.

(3) See for example D. C. Grahame, *Chem. Revs.*, **41**, 441 (1947).

(4) (a) A. Frumkin and V. I. Melik-Gaikazyan, *Doklady Akad. Nauk U.S.S.R.*, **77**, 855 (1951); (b) V. I. Melik-Gaikazyan, *J. Phys. Chem. U.S.S.R.*, **26**, 560 (1952). English translations available from D. C. Grahame of Amherst College.

(5) This method of electrolysis is also very valuable in the kinetic study of electrode processes (Ershler, Randles, Gerischer, Grahame and others). For a detailed review see P. Delahay "New Instrumental Methods in Electrochemistry—Theory, Instrumentation, and Applications to Analytical and Physical Chemistry," Interscience Publishers, New York, N. Y., 1954, pp. 146–178.

or

$$\Gamma = \Gamma_0 + \int_0^t D(\partial C/\partial x)_{x=0}dt \qquad (1)$$

where D is the diffusion coefficient of the adsorbed substance, x the distance from the electrode, t the time and Γ_0 and Γ are the amounts adsorbed at times $t = 0$ and t, respectively. The rate of adsorption is (Langmuir's isotherm)

$$d\Gamma/dt = k_a(\Gamma_m - \Gamma)C_{x=0} - k_d\Gamma \qquad (2)$$

where Γ_m is the maximum of Γ value for complete coverage, and the k's are rate constants characterizing the adsorption process. The k's are functions of the electrode potential, and we shall write

$$\left.\begin{aligned} k_a &= k^0_a \exp(\alpha E) \\ k_d &= k^0_d \exp(\beta E) \end{aligned}\right\} \qquad (3)$$

where the k^0's are the values of k for $E = 0$, and α and β have opposite signs. The potential E in (3) is expressed with respect to some reference electrode, the normal hydrogen electrode for example. There is some justification for equations 3 in the work of Butler,[6] who showed that the amount of substance adsorbed on the electrode at equilibrium varies exponentially with potential. This result undoubtedly represents a simplification of actual conditions, but it is nevertheless verified rather well by experiment. Since the amount adsorbed at equilibrium is an exponential function of E it is reasonable to assume that one or both rate constants in equation 3 are also exponential functions of E. We shall consider only a small departure from equilibrium as resulting from a variation of potential of a few millivolts, and it is then permissible to expand the exponentials and retain only the first two terms. The use of such linear relationships in the vicinity of equilibrium can also be justified, independently of Butler's treatment, on the basis of the thermodynamics of irreversible phenomena. Thus, the rate of a reaction in the immediate vicinity of equilibrium is proportional to the affinity of the reaction.[7] This amounts to linearizing a function for small increments of the variable.

Let us now assume that adsorption equilibrium is achieved at potential E_0 and that the potential is changed to a value E. The rate of adsorption at E can be written as

$$d\Gamma/dt = k^0_a(\Gamma_m - \Gamma)C_{x=0}\exp(\alpha E_e)\exp[\alpha(E - E_e)] - k^0_d\Gamma\exp(\beta E_e)\exp[\beta(E - E_e)] \qquad (4)$$

where $E - E_e$ is a certain function of time. Since $d\Gamma/dt = 0$ at equilibrium, one has

$$k^0_a(\Gamma_m - \Gamma_0)C_0\exp(\alpha E_e) = k^0_d\Gamma_0\exp(\beta E_e) = v_0 \qquad (5)$$

where Γ_0 and C_0 are the values of Γ and C at equilibrium, and v_0 is the common value of the rates of desorption at equilibrium.[8] By expanding the exponentials in (4) and retaining only the first two terms one obtains after dropping negligible terms

$$\frac{d\Gamma}{dt} = v_0\left[\frac{\Gamma_m(C_{x=0} - C_0) - (\Gamma C_{x=0} - \Gamma_0 C_0)}{(\Gamma_m - \Gamma_0)C_0} - \frac{\Gamma - \Gamma_0}{\Gamma_0} + (\alpha - \beta)(E - E_e)\right] \qquad (6)$$

Defining now the relative concentrations

$$\varphi = (C - C_0)/C_0 \qquad (7)$$

we obtain the boundary condition

$$DC_0\left(\frac{\partial\varphi}{\partial x}\right)_{x=0} = v_0\left\{\varphi_{x=0} + (\alpha - \beta)(E - E_e) - \frac{\Gamma_m DC_0}{(\Gamma_m - \Gamma_0)\Gamma_0}\int_0^t\left(\frac{\partial\varphi}{\partial x}\right)_{x=0}dt\right\} \qquad (8)$$

where $(E - E_e)$ is now assumed to be a sinusoidal function of time of the form $\epsilon \sin \omega t$ ($\omega = 2\pi f$, f being the frequency). Fick's equation as written for φ must be solved for condition (8) and for the initial condition $\varphi = 0$ for $t = 0$ with $x \geq 0$. One also has $\varphi \to 0$ for $t \geq 0$ and $x \to \infty$.

We are interested in the surface concentration Γ rather than in the concentration C or the relative concentration φ. In view of (1) we must therefore derive $\int_0^t(\partial C/\partial x)_{x=0}\,dt$ or $\int_0^t(\partial\varphi/\partial x)_{x=0}\,dt$ rather than C or φ. This derivation, which is given in Appendix, yields for the steady state

$$\Gamma - \Gamma_0 = \frac{(\alpha - \beta)\epsilon\sin(\omega t - \lambda)}{\left\{\left[\left(\frac{\omega}{2D}\right)^{1/2}\frac{1}{C_0} + \frac{\Gamma_m}{(\Gamma_m - \Gamma_0)\Gamma_0}\right]^2 + \left[\left(\frac{\omega}{2D}\right)^{1/2}\frac{1}{C_0} + \frac{\omega}{v_0}\right]^2\right\}^{1/2}} \qquad (9)$$

with

$$\lambda = \tan^{-1}\frac{\left(\frac{\omega}{2D}\right)^{1/2}\frac{v_0}{C_0} + \omega}{\left(\frac{\omega}{2D}\right)^{1/2}\frac{v_0}{C_0} + \frac{v_0\Gamma_m}{(\Gamma_m - \Gamma_0)\Gamma_0}} \qquad (10)$$

It follows from (9) that the surface concentration is a sinusoidal function of time out of phase by λ with respect to the voltage $\epsilon \sin \omega t$.

Condition of Balance of A.C. Bridge and Calculation of Kinetic Parameters

The differential capacity is determined with an a.c. bridge whose adjustable elements are a resistance R_s and a capacity C_s in series or parallel. We shall use the series circuit, and the condition of balance will be established on the assumption that the resistance of the cell is equal to zero. In practice it suffices to add the cell resistance to the resistance R_s calculated below.

The surface charge density q is a function of the potential E and the surface concentration Γ, and the current for the charge or discharge of the interphase is

$$i = \frac{dq}{dt} = \left(\frac{\partial q}{\partial E}\right)_\Gamma\frac{dE}{dt} + \left(\frac{\partial q}{\partial\Gamma}\right)_E\frac{d\Gamma}{dt} \qquad (11)$$

The term $(\partial q/\partial E)_\Gamma$ in (11) is the differential capacity of the double layer at constant Γ, *i.e.*, the differential capacity at the potential E_e. The term $(\partial q/\partial\Gamma)_E$ can be evaluated by postulating the following relationship

$$q = q_{\Gamma=0} = (q_{\Gamma=0} - q_{\Gamma=\Gamma_m})\Gamma/\Gamma_m \qquad (12)$$

which expresses that the surface charge density decreases linearly with the coverage of the electrode

(6) J. A. V. Butler, *Proc. Roy. Soc. (London)*, **122A**, 399 (1929).

(7) I. Prigogine, "Etude Thermodynamique des Phenomenes Irreversibles," Dunod, Paris, 1947; S. R. De Groot, "Thermodynamics of Irreversible Processes," Interscience Publishers, New York, N. Y., 1951.

(8) A similar method of calculation was followed by H. Gerischer (*Z. physik. Chem.*, **198**, 286 (1951)) in the study of electrode processes with coupled chemical reactions in electrolysis with superimposed alternating current.

by the adsorbed species. The q's in (12) can be calculated by integrating the differential capacity.

One deduces from (12)

$$(\partial q/\partial\Gamma)_E = (q_{\Gamma=0} - q_{\Gamma=\Gamma_m})/\Gamma_m \qquad (13)$$

The elements R_s and C_s of the series circuit equivalent to the impedance of the interface are obtained by identifying the value of the current deduced from (9) and (11) with the current i calculated from the generalized Ohm's law

$$E = R_s i + \int_0^t \frac{i}{C_s}\,dt$$

Thus

$$R_s = \frac{\frac{1}{\omega}\left(\frac{\partial q}{\partial\Gamma}\right)_E \frac{(\alpha-\beta)M}{M^2+N^2}}{\left[\left(\frac{\partial q}{\partial\Gamma}\right)_E \frac{(\alpha-\beta)M}{M^2+N^2}\right]^2 + \left[\left(\frac{\partial q}{\partial E}\right)_\Gamma + \left(\frac{\partial q}{\partial\Gamma}\right)_E \frac{(\alpha-\beta)N}{M^2+N^2}\right]^2} \qquad (14)$$

$$1/C_s = \frac{\left(\frac{\partial q}{\partial E}\right)_\Gamma + \left(\frac{\partial q}{\partial\Gamma}\right)_E \frac{(\alpha-\beta)N}{M^2+N^2}}{\left[\left(\frac{\partial q}{\partial\Gamma}\right)_E \frac{(\alpha-\beta)M}{M^2+N^2}\right]^2 + \left[\left(\frac{\partial q}{\partial E}\right)_\Gamma + \left(\frac{\partial q}{\partial\Gamma}\right)_E \frac{(\alpha-\beta)N}{M^2+N^2}\right]^2} \qquad (15)$$

with

$$M = \left(\frac{\omega}{2D}\right)^{1/2}\frac{1}{C_0} + \frac{\omega}{v_0} \qquad (16)$$

$$N = \left(\frac{\omega}{2D}\right)^{1/2}\frac{1}{C_0} + \frac{\Gamma_m}{(\Gamma_m-\Gamma_0)\Gamma_0} \qquad (17)$$

The values of $(\partial q/\partial\Gamma)_E$ and $(\partial q/\partial E)_\Gamma$ are left as such in (14) and (15) for the sake of simplicity. Equations 14 and 15 are cumbersome, and it is fruitful to calculate the quantity

$$\frac{1}{\omega R_s C_s} = \frac{(\partial q/\partial E)_\Gamma}{(\alpha-\beta)(\partial q/\partial\Gamma)_E}\frac{M^2+N^2}{M} + \frac{N}{M} \qquad (18)$$

which is equal to the tangent of the phase shift ρ between voltage and current. The quantities v_0, and $(\alpha - \beta)$ can be determined by applying (18) at two frequencies. The values of α and β can be obtained by repeating the determination for two values of E_e. Calculations are simplified if the second term on the right-hand side in (17) is dropped. This simplification is entirely justified for usual values of ω, D and C^0 when the ratio Γ/Γ_m is comprised between, say, 0.01 and 0.99. One then has $M = N + \omega/v_0$. Values of E_e which are not too different (0.1 volt or less) should be selected if α and/or β vary appreciably with potential. Another procedure is to characterize the kinetics of adsorption by the "*exchange rate*" v_0 at equilibrium (eq. 5) by analogy with the use of the exchange current in electrochemical kinetics.

The rate v_0 can be determined only if the term ω/v_0 in (16) is not negligible in comparison with $(\omega/2D)^{1/2}(1/C_0)$ and, consequently, measurements should be made at sufficiently high frequencies. However, the resistance of the cell imposes a limitation, since the impedance of the double layer should not be much smaller than the resistance of the cell. This condition is satisfied up to 0.1 to 1 megacycle according to the sensitivity of the bridge. Taking $\omega = 10^7$, $D = 10^{-5}$ cm. sec.$^{-1}$ and $C_0 = 10^{-7}$ mole cm.$^{-3}$, one concludes that values of v_0 as large as 10^{-5} mole cm.$^{-2}$ sec.$^{-1}$ can be determined by this method. This corresponds to the adsorption or desorption of a monolayer in about 10^{-4} second on the basis of an electrode area of 2×10^{-15} cm.^{2} per molecule.

It follows from (18) that the phase shift ρ approaches $\pi/2$ as the frequency increases. Adsorption can no longer follow the potential changes.

Application of this method is now being made to the study of the adsorption of a variety of organic substances on mercury, and experimental results will be reported in a subsequent paper.

Acknowledgment.—The support of the Office of Naval Research is gladly acknowledged.

Appendix

Equation 9 is derived by Laplace transformation and the use of the inversion integral. The boundary value problem in terms of the Laplace transform of the function φ is

$$d^2\bar{\varphi}/dx^2 - (s/D)\bar{\varphi} = 0 \qquad (19)$$

with the boundary condition (see (8)), as written for the particular case in which $E - E_e = \epsilon \sin \omega t$

$$(\partial\bar{\varphi}/\partial x)_{x=0} = v\left[\bar{\varphi}_{x=0} - (z/s)(\partial\bar{\varphi}/\partial x)_{x=0} + \frac{(\alpha-\beta)\epsilon\omega}{s^2+\omega^2}\right] \qquad (20)$$

There s is the variable introduced by the transformation and

$$v = \frac{v_0}{DC_0} \qquad (21)$$

$$z = \frac{\Gamma_m DC_0}{(\Gamma_m-\Gamma_0)\Gamma_0} \qquad (22)$$

Since $\bar{\varphi} \to 0$ for $x \to \infty$, the solution of (19) contains only one integration constant, which is determined by satisfying condition (20). Thus

$$\bar{\varphi} = -v\epsilon\omega D^{1/2}(\alpha-\beta)\frac{s^{1/2}\exp\left[-(s/D)^{1/2}x\right]}{(s^2+\omega^2)(s^{1/2}+A)(s^{1/2}+B)} \qquad (23)$$

with

$$A = \frac{vD^{1/2}}{2} + \left(\frac{v^2D}{4} - vz\right)^{1/2} \qquad (24)$$

and the same expression for B but with a minus sign in front of the parenthesis on the right-hand side. Since we are interested in $\int_0^t (\partial\bar{\varphi}/\partial x)_{x=0}\,dt$ rather than $\bar{\varphi}$, the value of the derivative $(\partial\bar{\varphi}/\partial x)_{x=0}$ will be calculated from (23). The resulting expression can be modified by taking into account that[9] $L\left[\int_0^t \chi(t)dt\right] = (1/s)\,\bar{\chi}(s)$. Thus

$$L\left[\int_0^t \left(\frac{\partial\varphi}{\partial x}\right)_{x=0} dt\right] = \frac{v\epsilon\omega(\alpha-\beta)}{(s^2+\omega^2)(s^{1/2}+A)(s^{1/2}+B)} \qquad (25)$$

By applying the inversion integral there results

$$\int_0^t \left(\frac{\partial\varphi}{\partial x}\right)_{x=0} dt = v\epsilon\omega(\alpha-\beta)\frac{1}{2\pi i}\int_{\gamma-i\infty}^{\gamma+i\infty}\frac{\exp(pt)}{(p^2+\omega^2)(p^{1/2}+A)(p^{1/2}+B)}\,dt \qquad (26)$$

where p, a complex variable, is written instead of s and γ is a constant which is so large that all singularities of $\bar{\varphi}(p)$ lie to the left of the lines $\gamma - i\infty$ and $\gamma + i\infty$. The integrand has simple poles at $p = \pm i\omega$ and a branch point at[10] $p = 0$. The solution for the steady state is given[11] by the

(9) See for example R. V. Churchill, "Modern Operational Mathematics in Engineering," McGraw-Hill, New York, N. Y., 1944, formula 5, p. 294.

(10) N. W. Lachlan, "Complex Variable and Operational Calculus," The Macmillan Co., New York, N. Y., 1942, p. 52.

(11) H. S. Carslaw and J. C. Jaeger, "Conduction of Heat in Solids," Oxford University Press, London, 1947, pp. 245 and 260.

product of $2\pi i$ by the sum of the residues at the poles. The residue at the pole $p = i\omega$ is

$$\frac{\exp(i\omega p)}{2i\omega[(i\omega)^{1/2} + A][(i\omega)^{1/2} + B]}$$

and the residue at the pole $p = -i\omega$ is

$$-\frac{\exp(-i\omega t)}{2i\omega[(-i\omega)^{1/2} + A][(-i\omega)^{1/2} + B]}$$

Thus, one has for the steady state

$$\int_0^t \left(\frac{\partial\varphi}{\partial x}\right)_{x=0} dt = \frac{v\epsilon(\alpha - \beta)}{2i} \left\{\frac{\exp(i\omega t)}{[(i\omega)^{1/2} + A][(i\omega)^{1/2} + B]} - \frac{\exp(-i\omega t)}{[(-i\omega)^{1/2} + A][(-i\omega)^{1/2} + B]}\right\} \quad (27)$$

This expression can be transformed into (9) after some algebra and by taking into account the relationships

$$(i)^{1/2} = (1/2^{1/2})(1 + i) = \exp(i\pi/4)$$
$$(-i)^{1/2} = (1/2^{1/2})(1 - i) = \exp(-i\pi/4)$$

DISCUSSION

MAX BENDER.—Please reconcile your capacity coefficient for your double layer with the Stern-Gouy diffuse double layer in terms of: (a) as a function of change in value with distance from electrode surface; (b) as a function of change in value with distance, from one electrolyte (concentrations) system to another; (c) the understanding that the high electrolyte concentrations considered by you are supposed to neutralize the diffuse double layer, *i.e.*, make zeta approach zero.

PAUL DELAHAY.—The double layer capacity we have to consider is the combination of the capacities for the diffuse double layer and the Helmholtz double layer. The two capacities are in series, and at concentrations of 1 molar or so the capacity for the diffuse double layer is so large that the Helmholtz double layer is determinative.

The difference of potential across the Helmholtz double layer, which can be much larger (perhaps 1 volt or more) than the zeta potential, is primarily to be considered here, and not the zeta potential.

One may expect that a change in the nature of the electrolyte causes a variation of the Helmholtz double layer, but this is unimportant here since $(\partial q/\partial\Gamma)_E$ of equation (11) is calculated from equation (13) in which experimentally accessible quantities appear. Likewise, variations in the concentrations of electrolyte are rather unimportant provided that all quantities needed in this determination of V_0 are obtained for a given concentration of electrolyte. A variation of V_0 with electrolyte concentration could be obtained especially on the anodic node.

PAUL DELAHAY.—The calculation of v_0 can be simplified if the equivalent circuit previously used is modified. Thus, from the experimental values C_s and R_s one calculates the capacity C_p and resistance R_p in parallel.

$$C_p = \frac{C_s}{1 + \omega^2 R_s^2 C_s} \quad (28)$$

$$R_p = \frac{1 + \omega^2 R_s^2 C_s^2}{\omega^2 C_s^2 R_s} \quad (29)$$

By introducing in (28) and (29) the values R_s and C_s previously derived one obtains

$$C_p = \left(\frac{\partial q}{\partial E}\right)_\Gamma + \left(\frac{\partial q}{\partial\Gamma}\right)_E \frac{(\alpha - \beta)N}{M^2 + N^2} \quad (30)$$

$$R_p = \frac{1}{\omega}\left(\frac{\partial q}{\partial\Gamma}\right)_E \frac{(\alpha - \beta)M}{M^2 + N^2} \quad (31)$$

where M and N are defined by (16) and (17).

The capacity C_p can be split into the capacity $C = (\partial q/\partial E)_\Gamma$ which corresponds to $\omega \to \infty$ and an additional capacity C'_s in series with a resistance R'_s. The elements C'_s and R'_s account for kinetic effects. Thus

$$C'_s = \left(\frac{\partial q}{\partial\Gamma}\right)_E (\alpha - \beta)\frac{1}{N} \quad (32)$$

$$R'_s = \frac{1}{\omega}\frac{M}{(\partial q/\partial\Gamma)_E(\alpha - \beta)} \quad (33)$$

It follows from (32) and (33) that

$$R'_s C'_s \omega = M/N \quad (34)$$

and, if $\Gamma_M/[(\Gamma_M - \Gamma_0)\Gamma_0]$ is negligible, *i.e.*, for coverage between, say, 0.02 and 0.98

$$R'_s C'_s \omega = 1 + (2D\omega)^{1/2}(C^0/v^0) \quad (35)$$

It is seen from (35) that a plot of $R'_s C'_s \omega$ against $\omega^{1/2}$ should give a straight line whose slope is inversely proportional to v_0.

ADSORPTION AND SILVER-SILVER ION EXCHANGE[1]

BY CECIL V. KING AND BORIS LEVY

Department of Chemistry, New York University, New York 3, N. Y.

Received February 25, 1955

The adsorption of silver sulfate on silver has been measured with S^{35} as tracer, and been shown to be dependent on both SO_4^- and Ag^+ concentrations. It was found that sodium sulfate is also adsorbed on silver. Part of each adsorption is irreversible in nature (chemisorption). Adsorption is rapid on initial immersion of the metal in solution, and the amount remaining on the surface decreases with time. Exchange was studied with Ag^{110} as tracer. Exchange is rapid on initial immersion and is greatly retarded as adsorption interferes. If reversibly adsorbed salt is washed off frequently much higher levels of exchange are obtained in a given total time of immersion. Evidence is presented that exchange between metal and adsorbed salt is faster than exchange between adsorbed salt and solution.

The adsorption of salts (or their ions) on metals is of obvious interest in several connections, notably the kinetics of corrosion and dissolution, the kinetics and mechanism of electrode processes, the interpretation of overvoltage, even the measurement of reversible potentials. Classical methods of measuring adsorption require large surface areas; methods adaptable to a few cm.^{2} are desirable. The interpretation of electrical double layer capacity, or its equivalent, for this purpose, has been explored,[2] and radioactive tracers are being widely employed.

A knowledge of the kinetics and extent of exchange of a metal with its own ions is equally important, in studying the nature of the metal and especially its surface, and in the interpretation of electrode kinetics and potentials. Exchange current at an electrode can be deduced from overpotential studies, but direct measurement is welcome. Too small exchange current makes the term "reversible potential" meaningless; mercury makes a poor hydrogen electrode, and a passive metal does not respond, in potential, to its own ions.

For these reasons it was attempted, in this research, to obtain quantitative measurements of the adsorption of silver salts on silver by tracer techniques, and to study further the exchange rate of silver with its ions. Classical adsorption measurements cannot easily distinguish between physical and chemisorption; exchange experiments, as customarily carried out, cannot distinguish between actual exchange and chemisorption. The simultaneous study of adsorption and exchange has proved helpful.

At first it was hoped to make both measurements simultaneously with Ag^{110} as tracer. If a silver coupon is immersed in an active silver nitrate solution, the amount of exchange quickly reaches a "temporary plateau" and thereafter increases very slowly.[3] It has been suspected that a portion of the activity pick-up is due to irreversible adsorption.[4] We hoped to include an estimate of reversible adsorption as well, by freeing the specimens from liquid after immersion, counting the activity, washing thoroughly and counting again.

The results of a few experiments which illustrate this method have been published.[5] Adhering liquid was removed by blotting or wiping the coupons with absorbent tissue. Since adsorption is expected to result in monolayer coverage or less, about 20×10^{-10} g. atoms/cm.,[2,6] a procedure is needed which leaves not more than 10% of this amount of unadsorbed salt, or the equivalent of a thin but reproducible liquid film. Others have dealt with this problem in various ways. Erbacher[7] allowed metal coupons to drain, cut off and discarded the lower half. Cook and Hackerman[8] estimated the liquid remaining on steel powder by weighing while moist with solvent. Smith and Allen[9] estimated the liquid necessary to wet their samples directly.

To test the blotting method of removing liquid, sodium sulfate with S^{35} as tracer was used, since it was thought that this salt would be little or not at all adsorbed. The same tracer was then used to measure both reversible and irreversible adsorption of silver sulfate, since this avoids the complication of simultaneous exchange.

Experimental

Radioactive sulfur and silver were obtained from the Oak Ridge National Laboratory. The S^{35} was in dilute hydrochloric acid, which was expelled by adding a known amount of sulfuric acid and evaporating repeatedly. The solution was then adjusted to 0.001 M H_2SO_4, and portions were added to known solutions of sodium and silver sulfates. Silver nitrate solutions were made by weighing both active and inactive salts. Silver sulfate solutions containing Ag^{110} were made by mixing active silver nitrate with slightly acid silver sulfate, warming to dryness several times to expel nitric acid, dissolving and diluting to volume.

Commercial rolled silver sheet (99.8% Ag), 0.2 mm. thick (Baker and Co., Inc.) was cut into 1 × 1″ squares. The coupons were suspended in solution from glass hooks, by means of 1/16″ drilled holes, in covered vessels. The solutions were not deaerated and were not stirred after it was found that stirring had little or no effect. Most of the experiments were at room temperature (27–32°), with one series at approximately 0° (ice- and water-bath).

It was shown that mild abrasion of the silver surface resulted in more retention of liquid on blotting and about twice as much adsorption as on the smooth surface. Most coupons were subjected to only mild cleansing as described below.

Radioactivity was measured with conventional shielding and counting equipment. With S^{35}, a weak β-emitter, the coupons were mounted as close as practical to a thin window GM tube. The counting error was usually less than 5%, but in cases of very weak adsorption as high as 12%. With

(1) Based on a Ph.D. thesis submitted by Boris Levy to the Graduate Faculty of New York University. Work done under Contract DA-30-069-ORD-1113 between the Office of Ordnance Research and New York University.

(2) R. S. Hansen and B. H. Clampitt, THIS JOURNAL, **58**, 908 (1954).

(3) H. Gerischer and W. Vielstich, *Z. Elektrochem.*, **56**, 380 (1952).

(4) A. Baerg and C. A. Winkler, *Can. J. Chem.*, **31**, 319, 521 (1953).

(5) C. V. King, *Ann. N. Y. Acad. Sci.*, **58**, 910 (1954).

(6) C. V. King and R. K. Schochet, THIS JOURNAL, **57**, 895 (1953).

(7) O. Erbacher, *Z. physik. Chem.*, **A163**, 196, 215, 231 (1933), and elsewhere.

(8) E. L. Cook and N. Hackerman, THIS JOURNAL, **55**, 549 (1951).

(9) H. A. Smith and K. A. Allen, *ibid.*, **58**, 449 (1954).

Ag^{110} the counting error was much smaller. The over-all reproducibility is shown below.

Radioactive counts were converted to amount of salt on the coupons by comparison with evaporated samples of each solution (0.5 ml. of a suitably diluted portion, spread over a silver coupon). With Ag^{110}, counts from both sides were added, or solution was evaporated on both sides and the counts averaged. Decay corrections were made by calculation or by recounting the calibration coupons.

The coupons used with sodium and silver sulfates were first washed with ether, continuously distilled for about one hour in a Soxhlet extractor. Several subsequent surface treatments were tried, on groups of six coupons. Since the differences in amount and reproducibility of adsorption were within the rather large experimental error, the following treatment was chosen: one minute in 0.1 *M* KCN, wash, one minute in 4.5% HNO_3, wash; 24 hours in inactive 0.1 *N* $AgNO_3$ (to reduce local cell action), wash one hour. Six coupons so treated were used in preliminary measurements, in which it became evident that both sodium and silver sulfates show irreversible adsorption, not removable by several hours of washing. Since a one-minute dip in 0.1 *M* KCN removes practically all of the activity, subsequent experiments included this treatment if much activity remained on the coupon. It was noticed incidentally that even a slight visible sulfide tarnish on the coupons did not measurably affect the adsorption.

Results

Adsorption of Sodium Sulfate and Adhering Liquid Correction.—Four of the coupons were used in the experiments shown in Table I. The second and fourth columns give the average amount of sulfate remaining after washing the coupons in distilled water for one hour. The third and fifth columns give the activity which was removed by washing, after blotting dry, in terms of thickness of an equivalent layer of solution. Other sodium sulfate concentrations up to nearly 1 *M* gave similar values, indicating that most of the washable salt actually comes from adhering liquid rather than being physically adsorbed. Consequently the average thickness values of Table I were used as a correction factor in subsequent measurements.

If the chemisorption of sodium sulfate is plotted as reciprocal of amount adsorbed *vs.* reciprocal of concentration, it is evident that there is no noticeable temperature effect, and linearity of the plot may indicate Langmuir-type isotherms. Unfortunately the curves cannot be extrapolated accurately to $1/c = 0$.

TABLE I

CHEMISORPTION OF SODIUM SULFATE ON SILVER, AND AMOUNT OF THE SALT REMAINING AFTER BLOTTING

Four coupons immersed 1 hr. in each solution.

	Room temp.		Ice-bath temp.	
$C_{Na_2SO_4}$, *M*	Chemisorp., moles/cm.^{2} × 10^{10}	Layer thickness, cm. × 10^5	Chemisorp., moles/cm.^{2} × 10^{10}	Layer thickness, cm. × 10^5
1.01×10^{-2}	0.418	1.77	0.450	1.13
2.06×10^{-3}	.091	1.50	.105	0.98
1.21×10^{-3}	.075	2.08	...	...
9.81×10^{-4}	.050	1.74	.053	1.11
7.12×10^{-4}	.055	2.75	055	1.65
4.43×10^{-4}	.024	1.96	.025	1.71
		av. 1.97		1.32
	av. dev., % 15			22

Adsorption of Silver Sulfate.—The same four silver coupons were now used in silver sulfate solutions, as summarized in Table II. Both silver and sulfate ion concentrations are given, since it was found that the amount of adsorption depends on both. The activity found after blotting was corrected for adhering liquid as described, and chemisorption refers to activity remaining after washing one hour.

If the chemisorption values are plotted as reciprocals, aside from a few scattered points a reasonably linear relation is found; there is no appreciable temperature effect. The physical adsorption is more erratic, partly at least because of the disparity in silver and sulfate concentrations. The values under 1.91×10^{-4} *M* Ag^+ in Table II include the effect of adding excess sulfuric acid, which increases adsorption greatly. This is not merely additive adsorption of silver and sulfate ions. The percentage average deviation column in Table II shows the degree of concordance in each group of four coupons; these deviations are typical. Duplicate runs sometimes showed greater differences than the maximum deviation in one group.

The amount of physical adsorption found changes remarkably with time of immersion of the specimen. A number of coupons were immersed in a solution containing 1.91×10^{-4} *M* Ag^+, 4.9×10^{-4} *N* $SO_4^=$ for periods from one second to 20 hours. Up to 3 minutes the physical adsorption averaged 0.85×10^{-10} equiv./cm.^{2}; after 90 minutes to 20 hours this value had fallen to about 0.30×10^{-10} equiv./cm.^{2}. Chemisorption varied between 0.2 and 0.11×10^{-10} equiv./cm.^{2} during this time and it is not sure that any change is real. Chemisorbed sodium or silver sulfates exchanged only very slowly with inactive sulfates.

Exchange and Adsorption with Silver Nitrate (Ag^{110}).—The coupons for exchange experiments were washed with acetone, acidified thiourea and water, immersed 45 hours in inactive 0.1 *N* silver nitrate to "equilibrate," then washed for one hour.

Figure 1 shows the results of exchange experiments in 0.5 *N* silver nitrate. Seven coupons were immersed for various periods of time, the first immersion periods being 10, 30 sec., 1, 5, 10, 30, 60 min. After each immersion the coupon was blotted dry, counted, washed one hour, recounted and immersed again.

The first few immersions of coupons 1 to 5 are not shown in Fig. 1. The amount of exchange is far more dependent on the number of immersions than on the time; "exchange plateaus" are found only because of the way the immersion periods are chosen. Most of the exchange of each immersion takes place in the first few seconds, although slow exchange continues indefinitely. The first dip results in exchange corresponding to equilibrium with 4.5 to 5 atomic layers, based on apparent area and considering 19.9×10^{-10} g. atoms/cm.^{2} as one layer.[5] No doubt there is an equal amount of exchange on subsequent immersion, but this amounts to only 0.5 to 1 additional layer of activity pick-up.

Chemisorption can of course not be detected in these experiments, and is very small compared to the amount of exchange. The activity which could be washed off, after blotting and counting, decreased with the number of immersions, later

TABLE II

THE ADSORPTION OF SILVER SULFATE (S^{35})

One hour immersion. Total adsorption corrected for adhering liquid.

		Room temp.			Ice-bath temp.	
		Total ads.		Chemisorp.,	Total ads.,	Chemisorp.,
		eq./cm.^{2}	av. dev.,	eq./cm.^{2}	eq./cm.^{2}	eq./cm.^{2}
C_{Ag^+}, N	$C_{SO_4^=}$, N	$\times 10^{10}$	%	$\times 10^{10}$	$\times 10^{10}$	$\times 10^{10}$
2.16×10^{-2}	2.17×10^{-2}	10.5	18	2.8	6.6	4.2
		11.4	21	3.9		
3.39×10^{-3}	3.49×10^{-3}	3.98	5	2.09	4.43	1.32
2.54×10^{-3}	2.64×10^{-3}	2.03	3	1.02	2.62	0.59
2.00×10^{-3}	2.01×10^{-3}	1.56	8	0.64	1.63	0.86
1.26×10^{-3}	1.35×10^{-3}	1.77	1	1.40	3.33	0.51
		1.92	5	1.14		
		2.03	3	0.37		
6.28×10^{-4}	6.77×10^{-4}	1.51	13	.18	1.71	0.35
		0.76	25	.24		
6.03×10^{-4}	8.03×10^{-4}	.86	4	.10	1.41	0.23
2.64×10^{-4}	3.64×10^{-4}	.40	18	.18	1.43	0.31
1.91×10^{-4}	2.91×10^{-4}	.28	15	.05	0.44	0.10
1.91×10^{-4}	4.91×10^{-4}	.61	7	.09	1.23	0.15
		.86	6	.20		
1.91×10^{-4}	1.00×10^{-3}	1.28	6	.38	1.15	0.25
8.04×10^{-5}	2.00×10^{-3}	0.96	11	.23		
2.10×10^{-5}	1.00×10^{-4}	.04	37	.01		
2.13×10^{-6}	8.2×10^{-5}	.04	15	.01		

increased again. The correction for adhering liquid, as used previously, would be 98×10^{-10} equiv./cm.^{2}, a value larger than some of the numbers actually found. This indicates that the adsorbed salt contains less active silver than the dissolved salt, at the time of washing. The decrease in washable activity and later increase with time was found in all experiments and has been noted in previous experiments.[5]

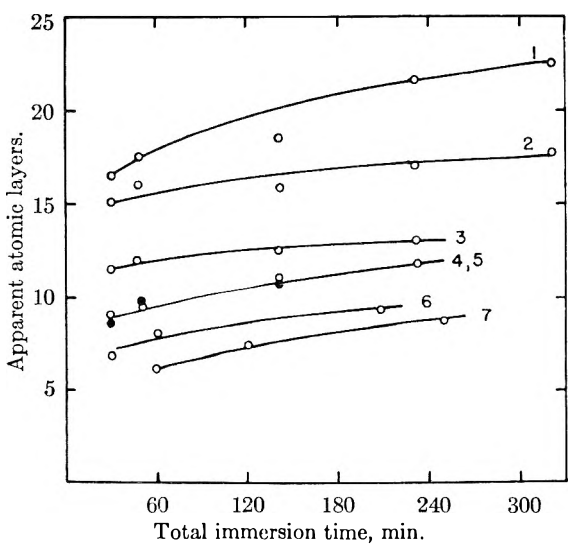

Fig. 1.—Exchange from 0.5 N silver nitrate, the effect of different immersion periods. Low number coupons had most immersions, number 7 only three.

Exchange with 0.02 M Silver Sulfate.—Since the extent of exchange depends more on the number of immersions in active solution (with washing between dips) than on the total time of immersion, coupons were given several 30 second dips, each followed by an hour's washing. Four coupons were used and the results averaged; the amount of exchange (plus chemisorption) is shown in Fig. 2.

A single coupon was given repeated 30 second dips, with only 5 minutes washing; after each five dips it was washed one hour and counted. These results are also plotted in Fig. 2. Apparently the 5 minute wash is not as effective in restoring exchange reactivity as longer washing. Mere removal from the active solution and blotting was quite ineffective in promoting exchange.

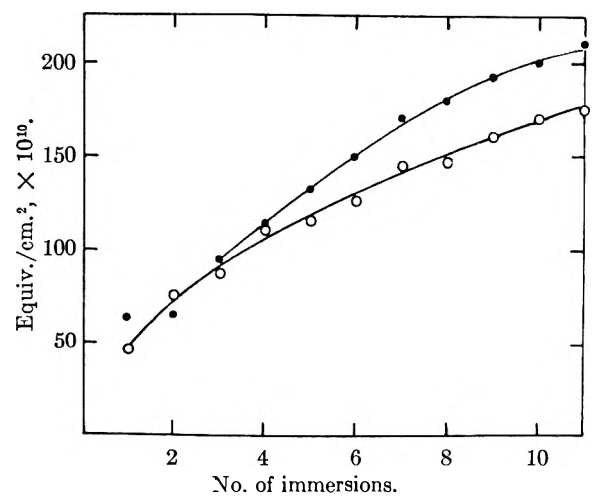

Fig. 2.—Exchange from 0.02 M silver sulfate: ○, average of 4 coupons, 30 second dips, one hour wash; ●, single coupon, each point represents five 30 second dips with 5 minute wash each dip, then one hour wash.

In these experiments stirring the solution had no effect on the exchange rate.

Discussion

The outstanding features of this research are (1) initial adsorption of silver salts is rapid and much greater in amount than equilibrium adsorption, and equilibrium is attained only slowly; (2) the rate of silver–silver ion exchange (and consequently the exchange current density at a silver

electrode) is highly dependent on the stage of the adsorption process.

Adsorption.—Rapid initial adsorption followed by slow decay to a final state has been found in other cases, namely, the adsorption of organic molecules on steel[10] and of sodium sulfate on iron.[11] However, chemisorption was referred to in these cases, and in the present system chemisorption is established quickly. In many measurements of adsorption on metals it has been customary to allow one or two hours for equilibrium to be reached[7,12] and it has been shown[13] that current flows for about two hours between a large silver electrode which has been equilibrated in silver nitrate solution and another similar electrode freshly immersed in the same solution. The anion probably has an effect; it was found that adsorption on silver powder from silver perchlorate solutions changes slowly up to 72 hours.[6]

Hackerman's explanation of the decrease with time from a maximum[10,11] is that there is a large initial pick-up of loosely held ions (or molecules), followed by a slow rearrangement to the equilibrium condition, with proper orientation and formation of chemical bonds at sites capable of forming them.

A similar explanation with regard to washable adsorption is more difficult, but this is a matter of degree, since there is no doubt every stage from very loose to very firm binding. Silver ion is probably primarily adsorbed to a much greater extent than sulfate, forming a continuation of the metal lattice. The electric charges of the adsorbed ions would not remain localized, and anions would be attracted to the entire surface. If the surface is heterogeneous with respect to adsorption sites, a smaller number of more firmly held anions could eventually take the place of a larger number more loosely held. The increased adsorption with excess sulfuric acid (Table II) resembles a solubility product effect; firm adsorption of more sulfate ions leads to more sites for the adsorption of more silver ions, and *vice versa*.

Autoradiographs of some of the coupons with adsorbed silver sulfate showed that more activity accumulates at obvious imperfections than elsewhere—along the cut edges, around the holes and along minor scratch marks. This may be a secondary effect of continuing local cell action in spite of previous "equilibration"; or it may indicate that such places are especially suitable for specific sulfate adsorption.

Silver has often been reported to behave as a "null electrode" in solutions containing about 10^{-5} N silver ion; Proskurnin and Frumkin[13] found no adsorption at this concentration, and either silver dissolution or excess anion adsorption at lower concentrations. The last two experiments of Table II show a small activity pick-up in such solutions, but of course do not show which ion is primarily adsorbed.

It was shown in previous work[6] that adsorption on silver is dependent on the anion (Ag_2SO_4 > $AgClO_4$ > $AgNO_3$). This no doubt reflects both the polarizability and the specific bond-forming tendencies of the ions. Total adsorption and its distribution must be in accordance with both the electrode potential and the double layer capacity, and the amounts actually found indicate a complex double layer.

The extent of silver sulfate adsorption found is in reasonable agreement with that found on finely divided silver,[6] for example about 0.5 monolayer, based on apparent area, in 0.02 N silver sulfate.

Exchange.—Exchange is no doubt extremely rapid at the surface of the bare metal. After a few seconds of immersion, the limiting factor in exchange kinetics is transmission of the ion through the adsorbed layer rather than diffusion in solution or diffusion within the metal. After adsorption equilibrium is reached, both desorption and new adsorption must be slow; since complete coverage is not required to make exchange very slow, adsorption may be a necessary intermediate step in exchange. The decrease in washable activity and subsequent increase with time mentioned above indicates that exchange depletes the adsorbed layer of activity, which is not replenished from solution for several hours.

Gerischer and Vielstich[3] found the time required to reach a given fraction of their "exchange plateau" to vary inversely with the solution concentration. While they do not state exactly how the experiments were performed, the behavior indicates that a definite time pattern was followed with each solution, with increasing time periods for successive immersions. If several coupons are immersed and one removed from time to time for counting, all the results are on a single (slowly rising) plateau. This was evident in previous work[5]; and in the present experiments with 0.5 N silver nitrate, the first immersion, whether for 30 seconds or one hour, always resulted in an exchange of 4.5 to 5 apparent atomic layers.

If the experiments of Fig. 2 were continued long enough, probably a much higher plateau of slowly increasing exchange would be reached, with the rate truly limited by diffusion within the metal. Exchange equivalent to several thousand atomic layers in an hour or less has been found between copper and its ions.[14] The difference may be only that adsorbed copper salt does not retard exchange. Such rapid exchange is usually ascribed to local cell reaction, but there is probably also the equivalent of a high diffusion coefficient to an unknown depth within the metal.

The effect of removing adsorbed ions was also noted by Baerg and Winkler,[4] in a somewhat different way. These authors immersed a coupon for one minute, rinsed, and transferred to dilute sulfuric acid. It was then made cathodic with a modified Bowden-Rideal technique to measure the number of coulombs required to reach the hydrogen overpotential. On repeating, an additional 0.5–1 monolayer of radioactivity was acquired per

(10) N. Hackerman and E. E. Glenn, THIS JOURNAL, **54**, 497 (1950).

(11) N. Hackerman and S. J. Stephens, *ibid.*, **58**, 904 (1954).

(12) H. von Euler and A. Hedelius, *Arkiv Kemi, Mineralogi, Geologi*, **7**, No. 31 (1920).

(13) M. Proskurnin and A. Frumkin, *Z. physik. Chem.*, **A155**, 29 (1931).

(14) M. Haïssinsky, M. Cottin and B. Varjabedian, *J. chim. phys.*, **45**, 212 (1948); M. Quintin, P. Sue and M. Bizouard, *Compt. rend.*, **226**, 1723 (1948).

immersion, and the number of coulombs passed in the charging process was in fair agreement with the activity pick-up. The authors interpret this to mean that only chemisorption takes place after the first immersion, and that the adsorbed ions are deposited as metal on electrolysis, leaving the surface again available for chemisorption.

Our experiments show, first, that far too little chemisorption occurs to account for these results, and, second, that washing is sufficient to restore the ability to exchange. To avoid any accidental electrolysis some of the coupons were handled with care to avoid any contact with other metals, etc. Further, intentional electrolysis with the silver as cathode had no observable effect. The activity pick-up found by Baerg and Winkler is similar in magnitude to exchange found in the present work after thorough washing, although the solution concentrations were quite different.

In previous work on the rate of dissolution of silver in ferric sulfate solutions,[15] it was found that slow desorption, especially of silver ions, must be a controlling factor in the kinetics. The present findings substantiate this possibility. Further, it was found that the potential of a silver electrode in ferric–ferrous perchlorate is polarized to the potential of a platinum electrode in the same solution, at a smaller silver ion concentration than would be necessary in the absence of a corrosion reaction.[16] This indicates that slow desorption of silver ion formed in the corrosion process causes the potential to correspond to a higher concentration than is present in the solution.

(15) H. Salzberg and C. V. King, *J. Electrochem. Soc.*, **97**, 290 (1950).

Discussion

Gerischer and Tischer[17] have published additional experiments on silver–silver ion exchange. Single-crystal silver gives results similar to polycrystalline silver. The difference between samples washed and reimmersed several times, compared to samples immersed for longer times, has been noted. The previous view concerning the importance of internal diffusion has been modified.

(16) C. V. King and F. Lang, *ibid.*, **99**, 295 (1952).

THE MAGNETICALLY SUSPENDED EQUILIBRIUM ULTRACENTRIFUGE[1]

BY J. W. BEAMS, H. M. DIXON, III,[2a] A. ROBESON[2b] AND N. SNIDOW

University of Virginia, Charlottesville, Virginia

Received February 25, 1955

An ultracentrifuge is described in which the rotor is magnetically suspended in a vacuum. The rotor is accelerated to operating speed by an air turbine below the vacuum chamber. A thin, flexible shaft passing through vacuum-tight oil glands connects the turbine to the rotor during the acceleration period but is disconnected during the operating period. The rotor coasts freely during the observation of the sedimentation. The rotor loses about 1 r.p.s. per 3 days when coasting freely in the vacuum chamber containing pressure of 10^{-6} mm. The sedimentation is observed with a modified type of Jamin interferometer. The rotor speed may be determined to one part in 10^6, the temperature to one part in 10^4, and the fringe shift to between 0.03 to 0.05 fringe. This gives from two to three significant figures in the precision over the entire molecular weight range above 100 when the equilibrium method is used.

Two principal methods are in general use for the measurement of molecular weights by centrifuging.[3] In the first, or rate-of-sedimentation, method the rate of settling of the substance in the centrifuge is determined, while in the second, or equilibrium, method the concentration of the substance is measured at various radial distances after equilibrium has been established between sedimentation and back diffusion. In both methods the rotor speed, the rotor temperature and the refractive index or its gradient are measured while the centrifuge rotor is spinning. The rate-of-sedimentation method employs a relatively larger centrifugal field but requires only a few hours for a molecular weight determination. On the other hand, the equilibrium method employs a relatively less intense centrifugal field but requires several days or weeks of continuous centrifuging for the determination. The theory of the rate-of-sedimentation method is based upon Stokes' law, while that of the equilibrium method is based upon thermodynamics and, therefore, is probably more reliable. Also, for the same rotor size and speed, much smaller molecular weights may be measured by the equilibrium method. Nevertheless, in the past where the molecular weights are large enough to give measurable rates of sedimentation in the centrifugal fields available, the rate-of-sedimentation method has been more widely used. The primary reason for this lack of popularity of the equilibrium method is the difficulty of maintaining the rotational speed and temperature of the centrifuge rotor sufficiently constant for long periods of time. The purpose of this paper is to describe a magnetically suspended vacuum-type ultracentrifuge which we are developing[4] principally for use with the equilibrium method, although it could equally well be used with the rate-of-sedimentation method. In this magnetically suspended centrifuge the absolute rotor temperature is maintained constant to at least one part in ten thousand; the troublesome "hunting" in the rotor speed is eliminated, and the rotor speed is measured to better than one part in a million. In the molecular weight measurements to be described it has been found advantageous to allow the rotor speed to decrease very slowly (the order of 1 r.p.s. per day) in order to reduce the centrifuging time.

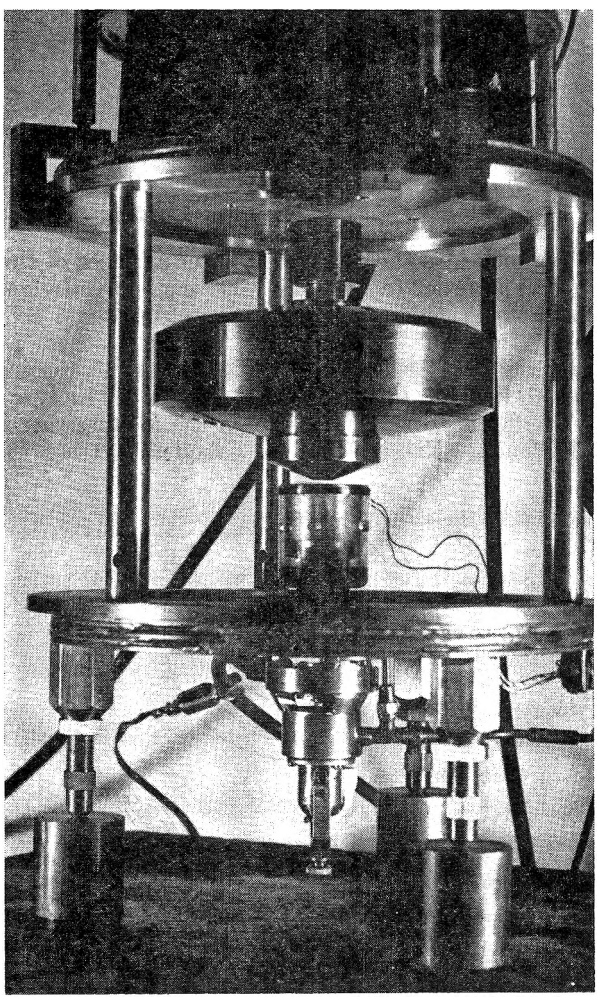

Fig. 1.—Photograph of ultracentrifuge with vacuum chamber removed.

Figure 1 shows a photograph of the apparatus with the vacuum chamber removed, and Fig. 2 is a cross-sectional diagram of the ultracentrifuge. The steel rotor is freely suspended inside of a nonmagnetic vacuum chamber by the support solenoid as indicated in Fig. 2. It is accelerated to operating speed by the air turbine situated below the vacuum chamber. A small-diameter, flexible steel shaft connects the air turbine with the rotor.

(1) Supported by Navy Bureau of Ordnance and National Science Foundation.

(2) (a) Union Carbide and Carbon Chemical Corporation fellow; (b) United States Rubber Company fellow.

(3) T. Svedberg and K. O. Pedersen, "The Ultracentrifuge," Oxford University Press, London, 1940.

(4) (a) J. W. Beams, J. D. Ross and J. F. Dillon, *Rev. Sci. Instru.*, **22**, 77 (1951); (b) J. W. Beams, *Science*, **120**, 619 (1954); *J. Wash. Acad. Sci.*, **37**, 221 (1947).

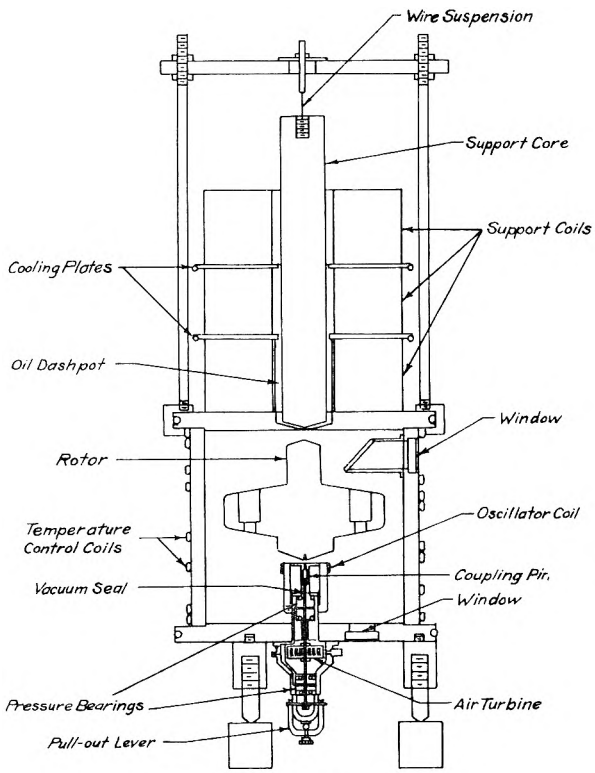

Fig. 2.—Diagram of ultracentrifuge.

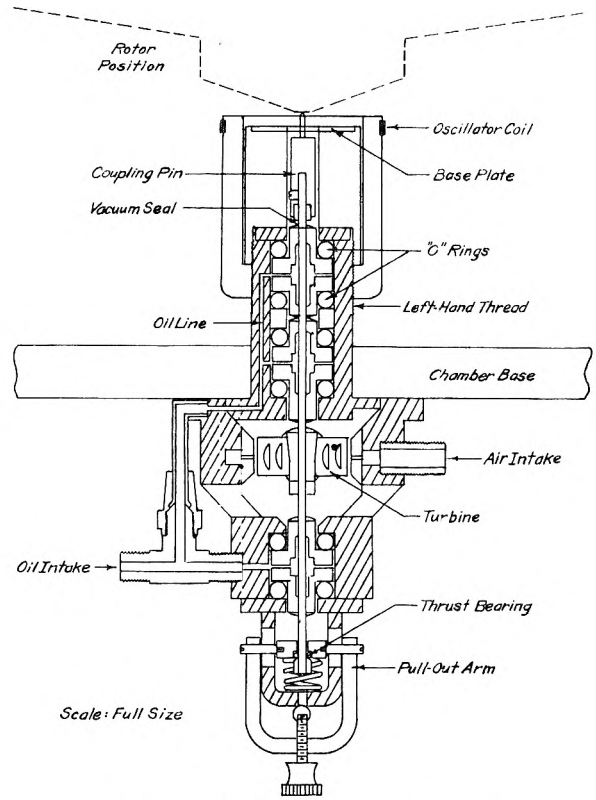

Fig. 3.—Compressed air drive system.

The shaft passes into the vacuum chamber through vacuum-tight oil glands as shown in detail in Fig. 3. During the acceleration period the shaft fits into a slot in the rotor; but, when the desired operating speed is reached, it is pulled out by a lever. This disconnects the rotor from the drive turbine and allows it to coast. The observations of the sedimentation are carried out while the rotor is coasting freely. The sedimentation is observed by passing light through the upper window, the right angle prism, down through a centrifuge cell (Fig. 6) mounted in the rotor, and out through the lower window.

The rotor shown in Figs. 1 and 2 was machined of one piece of high-strength alloy steel and weighs 13.5 kilograms. Its maximum radius is 9.4 cm., and its moment of inertia around the axis of rotation is 5×10^5 g. cm.^{2}. It has four 2.4 cm. holes drilled parallel to the axis of rotation with their centers 65 mm. from that axis. These holes carry the centrifuge cell shown in Figs. 4 and 6, a slit for chopping the light beam shown in Fig. 6, and two balancing cells. The centrifuge cell is similar to the matched double-sector type previously described.[4] Figure 4 shows a cross-sectional diagram of the cell. The cell consists of a housing internally threaded for the locking ring, washers, a double-sector spacer washer, two optically flat quartz windows with their optic axes perpendicular to their polished faces, separated by a spacer with two sectors as shown in Fig. 4. The housing and locking ring are made of duralumin ST 14, while the spacer which contains the double sectors between the windows is made of aluminum or duralumin covered with a thin coating when necessary to prevent corrosion. Grooves 0.004 cm. deep are machined into the upper and lower surfaces of this spacer in order to hold the 0.005 cm. polyethylene washers in place and seal the sector-shaped cells both from the outside and from each other. A keyway is milled into the inside wall of the housing which lines up the components of the cell and prevents them from twisting when the locking ring is tightened. Extreme care is taken in getting the

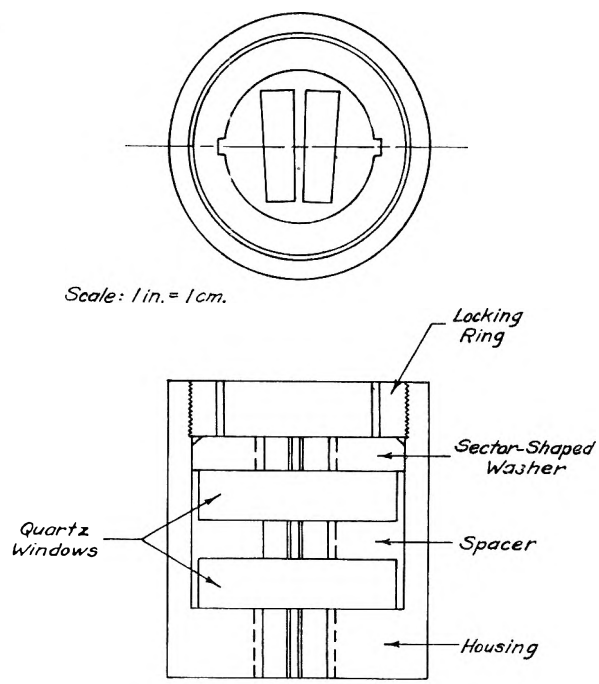

Fig. 4.—Double sector cell.

spacer flat; otherwise, leaks occur between the sectors, and the quartz windows are distorted by the pressure of the locking ring. Also, the sides of the sectors must be accurately flat. Radial lengths from 3 to 12 mm. and heights between 3 and 12 mm. have been used. The sector cells are filled, using a hypodermic syringe, through radial holes in the housing and spacers nearest the axis of rotation. These holes are sealed by threaded plugs with Teflon washers after the cells have been filled.

The cylindrical vacuum chamber is 22.2 cm. high, 23 cm. i.d., and a wall thickness of 1.76 cm. It is made of brass which is both non-magnetic and a good heat conductor. Copper cooling tubes are soldered to the vacuum chamber, and a heavy coating of glyptol is painted over the outside. The top and bottom plates of the vacuum chamber are 30 cm. in diameter and made from 1.9 cm. brass. They also have soldered copper cooling tubes (some of them in grooves for maintaining their temperature constant). Celvacene heavy vacuum wax is used to provide a vacuum seal between the end plates and the cylinder. Three heavy brass adjustable feet support the chamber and provide clearance for the air turbine assembly and parts of the optical system. Six glass windows 4.15 cm. in diameter and 1.02 cm. thick of good optical quality are arranged to provide three separate light paths through the rotor. The vacuum chamber is evacuated through a 7.6 cm. metal tube with flange connections to a Consolidated Vacuum Corporation V.M.F.-100 diffusion pump with the usual vapor traps and a "Megavac" fore pump. The pressure in the chamber is measured by a Pirani and an ionization gage. The temperature of the chamber was maintained constant to 0.03° by circulating water through the cooling coils and a thermostat bath in series.

The air turbine drive is shown in cross-section in Fig. 3. The duralumin turbine drives the rotor by a 0.25 cm. flexible steel shaft. The shaft turns in hard babbited bearings mounted in neoprene O-rings and lubricated with low vapor pressure oil ("Hy-Vac" oil freed of air and moisture). This type of bearing or gland has been described in detail previously[4] and is both slightly self-aligning and vacuum tight. The turbine is driven by compressed air admitted through small channels in the inner wall of the "air box" around the turbine. The air jets strike the turbine just above the center of the flutings and exert a slight upward force which automatically keeps the shaft engaged in the rotor while the air pressure (10 to 50 lb./in.^{2}) is applied. The brass housing is assembled in two sections. The upper section contains two bearings and extends up into the vacuum chamber. It is threaded to receive the two lucite pieces on which the oscillator coil and stainless steel base plate are mounted. Since the rotor turns counterclockwise when viewed from above, left-handed threads are used on the lucite. The base plate is of high-resistance non-magnetic 0.15 cm. stainless steel and protects the lucite if the rotor should get too low or in case of power failure. Recently Teflon has been found superior to lucite for the support of this base plate and for the base plate itself. A hardened steel "coupling pin" is attached to the upper end of the drive shaft with a set screw. The tip of the pin is hexagonally shaped to engage a modified Allen set screw located in the bottom of the rotor. A cylindrical neoprene gasket is fitted on the base of the coupling pin in such a way that, when the drive shaft is lowered to disengage the pin from the rotor, the gasket is squeezed against the top of the upper bearing and seals the vacuum chamber. This prevents oil from leaking into the vacuum chamber during the experiment. The lower section contains the turbine, lower bearing, and mechanism for disengaging the shaft from the rotor. Below the lower bearing a small knob is fastened to the end of the drive shaft and spins just below a ball-thrust bearing held up by a coil spring. The shaft is disengaged by pulling down on the pullout arm, and pressure is maintained on the chamber seal by tightening the lower thumb screw.

The support solenoid is wound in three sections or coils and contains a total of 36,000 turns of No. 22 insulated copper wire. Each section is approximately 24 cm. o.d. and 7 cm. i.d. and is separated by brass vanes cooled by water passing through copper coils soldered to the vanes. The soft iron core is 2.4 cm. diameter, 30 cm. long, and is suspended by a 0.0623 cm. piano wire inside the solenoid coil. The lower end of the core is a very flat cone (about 174°). The exact dimensions of this core are not critical. The lower end of the core is immersed in a dash pot of oil (No. 30 motor oil) and hangs about 0.15 cm. above the top of the centrifuge chamber. The top of the chamber is machined out to a thickness of 0.4 cm. just below the core as shown in Fig. 2. Any horizontal motion of the rotor is followed by the iron core, and, hence, quickly damped by the oil dash pot. The support circuit is shown in Fig. 5 and is similar to those used previously.[4a] It consists of a tuned-grid, tuned-plate oscillator operating at 3 megacycles followed by a detector from which an "error" signal and its time derivative are obtained. The time derivative serves as an anti-hunt or damping signal. The error and derivative signals are amplified separately and combined to control the current through a power stage whose load is the support solenoid. The oscillator or pickup coil is mounted on 5 cm. diameter lucite just under the rotor (Figs. 1 and 2) and consists of 10 turns of No. 22 copper wire. Leads are brought out of the chamber through Kovar seals and connected by a low-loss coaxial cable to the oscillator circuit. Vertical displacement of the rotor varies the impedance of the grid circuit which changes the amplitude of the oscillations and in turn the current through the solenoid. The current in the pickup coil is so small that no observable heating occurs. When properly adjusted, the rotor floats freely in the chamber without observable (100 power magnification) vertical or horizontal motion. In most of the experiments the rotor was supported approximately 2 mm. above the base plate and 3 mm. below the top of the chamber. To adjust the circuit, the rotor is placed upright on the base plate with the chamber removed to permit access

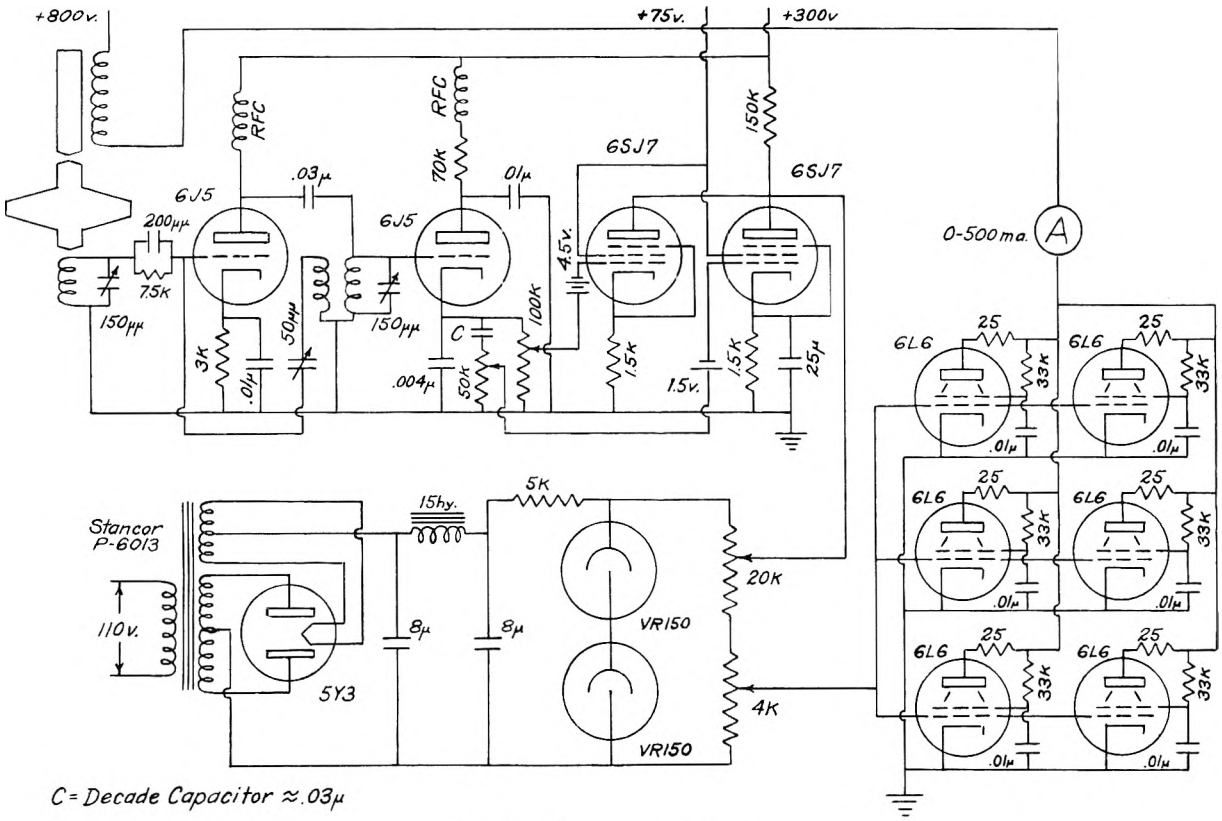

Fig. 5.—Rotor support circuit.

to the rotor. A high-resistance d.c. voltmeter is connected from cathode to ground in the 6J5 detector circuit and the grid and plate condensers tuned for a maximum output voltage (150 to 250 volts). The circuit is then neutralized to an output of about 50 volts. The rotor is next raised to the top of the chamber, and the voltage should increase to 150–200 volts. With the centrifuge completely assembled, the power supplies are turned on and the bias on the 6L6's adjusted until the rotor is picked up. The "error" potentiometer and the differentiating capacitor–potentiometer must next be adjusted until a stable support is obtained. When once adjusted for a given rotor, the circuit will remain in adjustment indefinitely. For the all steel rotor shown in Fig. 1 the support current is about 300 ma. Also the rotor friction is so small that the temperature of the rotor remains accurately equal to the surrounding vacuum chamber walls. When coasting freely at 300 r.p.s. with the vacuum chamber pressure of the order of 10^{-6} mm. of Hg, the rotor loses only about 1 r.p.s. per three days. As will be shown later, this gives sufficiently constant speed for the equilibrium experiments and, in fact, allows equilibrium to become established in a shorter time than if there were no deceleration. The rotor speed is measured by placing a photomultiplier tube in a light beam interrupted once for each rotation of the rotor (between M_2 and I_1 in Fig. 6). The resulting signal is then amplified and applied to the vertical plates of an oscilloscope. An amplified signal from the National Bureau of Standards radio station WWV or a signal from a generator calibrated and monitored with WWV is next applied to the horizontal plates of the oscilloscope. The two frequencies are compared by observation of the motion of the resulting Lissajous figures. The rotor frequency is adjusted to be near one of the broadcast frequencies

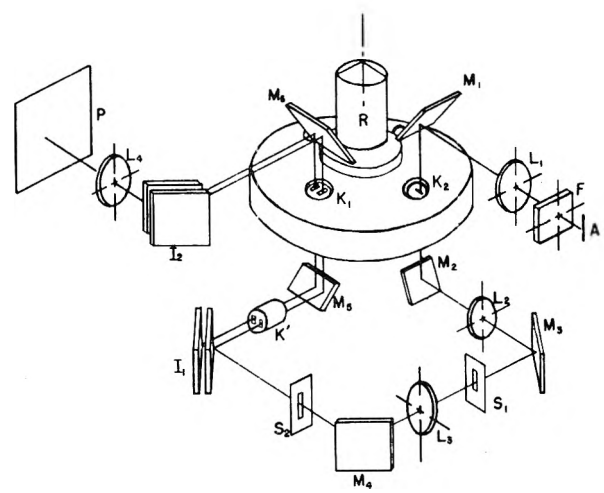

Fig. 6.—Combination light chopper and interferometer.

of WWV or one of its multiples or submultiples. The rotor speed easily may be measured to one part in 10^6. The high precision with which the temperature and the speed of the rotor can be controlled and measured makes it necessary to adapt more reliable methods to the determination of the index of refraction as a function of the rotor radius in the centrifuge cell. Fortunately, the develop-

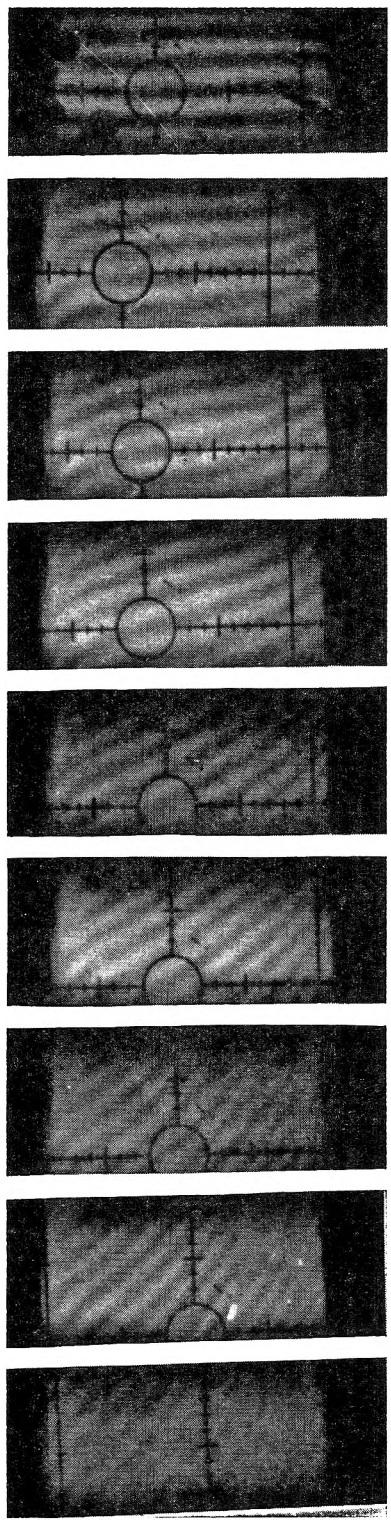

Fig. 7.—Photographs of fringes during experiment with human albumin.

ment of the double-sectored ultracentrifuge cell[5] makes it possible to use interferometer methods for these measurements. After several types of interferometer methods were tried, a modified Jamin (or Mach-Zehnder) type of interferometer was adapted to these measurements, because it not only gives precise values at various radial distances but also at all points throughout the ultracentrifuge cell (both parallel and perpendicular to the radius). The method has been described previously[6] in detail, so only a brief outline will be given. Figure 6 shows the combination light chopper and interferometer used. Light from a mercury arc is focused on the slit A and made monochromatic by the light filter F. The lens L_1 focuses the slit A on K_2 which is a radial slit in the centrifuge rotor so arranged that light can pass through only when K_2 is in the position shown. The light is next brought to focus on the slit S_1 and made parallel by the lens L_2. The width of the beam is limited by the diaphram S_2 to approximately the same as that of the sector-shaped cells in the centrifuge cell K_1. The light beam is then split by the interferometer I_1 and continues on through K^1 and K_1. The interferometer plates I_2 recombined the two beams, and the lens L_4 brings the cell K_2 to focus on the photographic plate P. The beam splitters I_1 and I_2 are each made of two optically flat glass plates. The front plate is lightly silvered so as to reflect from 25 to 35% of the light while the back plate is full silvered. If the plates in both I_1 and I_2 are accurately parallel, the interference fringes will be at infinity. However, if one of the plates in I_2 is rotated or inclined with respect to the other by a very small angle, the fringes are brought to focus on the photographic plate P. As a result both the image of K_1 and the fringes are brought sharply to focus on top of each other on P. The general theory of this type of interferometer has been given by Bennett and Kahl.[7]

The solution containing the substance to be analyzed is placed in one of the sector-shaped cells in K_1 and the solvent is placed in the other to precisely the same radial depth. The cell is then sealed and carefully aligned in the centrifuge rotor. The vacuum chamber is next evacuated to at least 10^{-5} mm. of Hg pressure, and the rotor with the drive shaft attached is magnetically supported. The rotor is then turned to the position shown in Fig. 6 by rotating the air turbine by hand. The interferometer is next adjusted so that one of the interferometer beams passes through the cell in K_1 containing the solution, while the other passes through the cell containing the solvent. Consequently, as sedimentation takes place in the solution, the interferometer fringes shift their position on the photographic plate P. The change in concentration ΔC due to a shift of one fringe is $\Delta C = \Delta n/k = \lambda/kh$ where n is the refractive index, λ is the wave length of the monochromatic light, k is the specific index of refraction increment, and h is the thickness of the cell K_1. It will be observed that, if one of the cells in the double cell K_1 is distorted with respect to the other by the effects of the centrifugal field, the fringes also will move. However, since the two cells have the same windows and housing, the effects of such distortions turn out to be negligible as shown by performing the experiments with the

(5) J. W. Beams and H. M. Dixon, III, *Rev. Sci. Instru.*, **24**, 228 (1953).

(6) J. W. Beams, N. Snidow, A. Robeson and H. M. Dixon, III, *ibid.*, **25**, 295 (1954).

(7) F. D. Bennett and G. D. Kahl, *J. Opt. Soc. Am.*, **43**, 71 (1953).

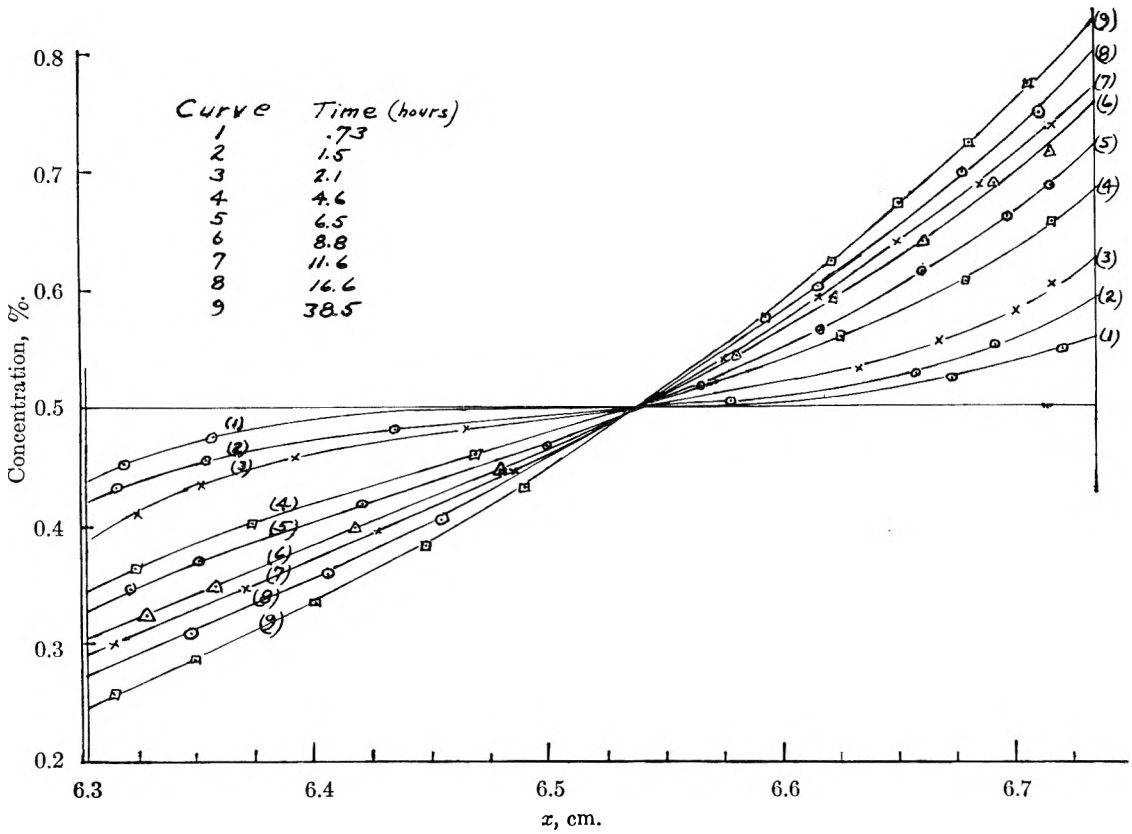

Fig. 8.—Distribution of concentration during albumin experiment.

solvent in both cells. In order to get white light fringes for reference, a cell K^1 identical to K_1 and filled in the same way is placed so that the beam which passes through the solvent in K_1 passes through the solution in K^1, while in the other beam the order is reversed. To obtain white light fringes, the filter F may be removed, or an incandescent light may be used as a source. At the beginning of the experiment white light fringes are obtained over the entire length of the cell (when they are parallel to the radius), but during sedimentation they occur only over a narrow radial region in the cell where the concentration in the sector of K_1 containing the solution is approximately the same as that at the beginning of the experiment. After the temperature of the rotor reaches a steady value, the fringes are adjusted so that they are either parallel or perpendicular to the radius of the centrifuge and are photographed in both monochromatic light and in white light. The centrifuge is then rapidly brought up to operating speed and the air turbine shaft disconnected. The fringes are again photographed both in monochromatic and white light at regular intervals until the observed concentration gradient in K_1 stops changing or until equilibrium is effectively established. As the rotor spins, light can pass the slit S_1 once each revolution and then only while the rotor turns through a small angle which is determined by the width of K_2, the properties and position of the lens L_2, and the width of S_2. In practice this angle is usually about 0.003 radian which gives sharp fringes over the entire image of K_1 on P. As a result precise values of the refractive index and, hence, the concentration are obtained for each point in the cell K_1 rather than at radial distances only.

For an ideal dilute incompressible solution, the molecular weight M_e of a mono-disperse substance obtained by the equilibrium method is given by the relation[3]

$$M_e = \frac{2RT \log_e (C_1/C_2)}{(1 - \bar{v}d)4\pi^2N^2(X_1^2 - X_2^2)}$$

where C_1 and C_2 are the concentrations at the radial distances X_1 and X_2, respectively, d is the density of the solution, $\bar{v}$ the partial specific volume, T the absolute temperature, and N the number of revolutions per second. When the solution is not ideal and dilute, the above relation must be corrected[3] as shown especially by Williams and his students.[8] In any case, the three quantities to be determined, while the centrifuge is spinning, are the rotor temperature, the rotor speed, and the concentration at various radial distances in the cell. This is also true for molecular weight distribution measurements of polydisperse substances. The other factors, such as $\bar{v}$ and d, are determined outside the centrifuge.

Figure 7 shows a series of photographs of fringes taken with monochromatic light at various times during the progress of the sedimentation of human serum albumin. Photographs, not shown in Fig. 7, taken up to 65 hours showed only a very slight change in the fringes after about 32 hours. The solution at the beginning was 0.5% albumin in 0.01 N NaCl with sodium acetyltryptophan

(8) J. W. Williams, *J. Polymer Sci.*, **12**, 351 (1954).

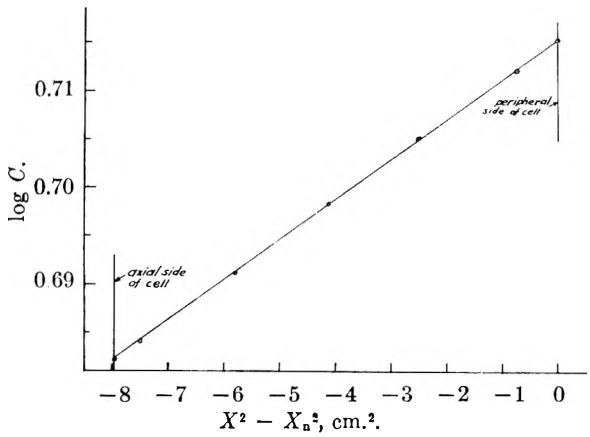

Fig. 9.—Log C *versus* $X^2 - X_r^2$ for sucrose after 58 hours centrifuging.

buffer. The rotor speed at the beginning of the experiment was 130.7 r.p.s. and at the end 129.9 r.p.s. Figure 8 shows the measured concentrations plotted as a function of the radial distance X as equilibrium is approached in a single experiment. Assuming the material to be monodisperse, the molecular weight values were found to depend upon the source, the past treatment and apparent purity of the human albumin used. Figure 9 shows the log C at radius X plotted *versus* $X^2 - X_n^2$, where X_n is the radius of the periphery of the cell for sucrose dissolved in water. The rotor speed was close to 300 r.p s. According to theory at equilibrium, this should be a straight line, the slope of which gives the molecular weight. The value obtained was 343, which agrees very well with the known value of 342.3. The curve of Fig. 9 gives the values after 58 hours of centrifuging sucrose, but after 12.5 hours the data all fall upon a straight line. All of the data taken on a number of different substances indicate that equilibrium is approached much faster than should be expected from the well known formula.[3] This results, in part at least, from the fact that the rotor speed is very slowly decreasing. Archibald[9] has shown that, if $(1/N)\ (dN/dt)/4\pi^2N^2S << 1$, where S is the sedimentation constant and N the rotor speed, then the equilibrium condition will remain once it is established in the cell.

Since the precision of the rotor speed may be obtained to about one part in 10^6 and that of the temperature to roughly one part in 10^4, the method of measuring the concentration as a function of the radius is still the factor which limits the accuracy of the results obtained at least during the centrifuging process. In practice at present a fringe shift of between 0.03 and 0.05 is about the best that can be measured with reliability. This gives a precision of about three significant figures for substances with molecular weights from about 10^2 up to the largest values known. It is usually possible to work with both relatively low or high concentrations of a substance, since the total fringe shift (and, hence, the accuracy) is increased by increasing the rotor speed. Fortunately the rotor speeds required usually are well below those obtainable with the apparatus. Nevertheless, it is highly desirable especially for measurements in extremely dilute solutions to have a more precise method of determining the concentrations in the centrifuge cell. It is well known, of course, that greater precision should be obtained if a multiple beam interferometer could be used. One of us in collaboration with Mr. D. R. Carpenter is attempting to develop this technique for the ultracentrifuge, but the results are as yet only of a preliminary nature.

We believe the centrifuge described in this paper provides an excellent equilibrium method of getting molecular weights, since it gives good precision and the data are obtained in a relatively short time. Also, it is about equally useful over the entire range of molecular weights above 100. However, there are several rather obvious improvements which we have under development that should make the apparatus more widely adaptable. For example, it is of much interest to investigate the methods of obtaining molecular weights by measuring the approach to equilibrium as suggested by Archibald.[10] This requires a very rapid acceleration of the rotor followed by an extremely constant speed. The air turbine drive described above gives the rapid acceleration without rotor heating (actually, the over-all rotor cools slightly because of stretching) but does not give the constant speed required. For some time we have been developing an electrical drive in which the rotor is essentially the armature of a synchronous motor. In order to avoid excessive heating of the rotor during the period of acceleration, the drive frequency is increased automatically at the same rate as the rotor speed. As soon as operating speed is reached, the drive frequency is controlled by a piezoelectric crystal circuit which maintains the speed contant[11] to at least one part in 10^7. The principal problem is to produce rapid acceleration without excessive rotor heating.

DISCUSSION

J. MYER (*Communicated*).—Between 1951 and 1953 a magnetically suspended centrifuge was being constructed at the University of Southern California in collaboration with Prof. K. J. Mysels, based on the earlier description (*Rev. Sci. Inst.*, **23**, 77 (1951)) given by Prof. Beams. In this connection we had to develop independently many of the improvements responsible for the good functioning of the suspension mechanism now described. There are only a few other developments worth mentioning in addition to those presented in Prof. Beams' paper:

(1) The efficiency of the magnet is greatly increased if the magnetic lines of force are guided in ferromagnetic material, not only in the core, but also above and down around the outside of the solenoid. This is achieved by suspending from the piano wire a rigid assembly of a core (of ARMCO iron), an end-plate and a coaxial cylinder surrounding the coils. (2) A further increase in lifting force is obtained by making the top of the rotor in the shape of a quite flat mushroom of ARMCO iron so that most of the lines of force are confined to the region above the body of the rotor. (3) The rotor and inside of the vacuum chamber are blackened to insure efficient radiative heat transfer. (4) The plate between the magnet and rotor supports the whole assembly and is mounted permanently on an elevator. After adjustment the assembly is lowered into the vacuum chamber (for which the plate forms a lid sealed by one O ring). (5) On the circuit side we wind the sensing coil with silver wire on glass

(9) W. J. Archibald, private communication.

(10) W. J. Archibald, THIS JOURNAL, **51**, 1204 (1947).

(11) J. W. Beams, E. C. Smith and J. M. Watkins, *J. Soc. Motion Pict. and Tele. Eng.*, **58**, 159 (1952).

for easier degassing and to improve the Q of this coil and hence the sensitivity. 5881 tubes give better power handling and reliability than 6L6's. To obtain stability, the oscillating circuit is well protected from the heat generated in the rest of the circuit. (6) Our drive mechanism (of very low power) is based on a hysteresis motor. Water-cooled field coils within the vacuum chamber drive a short sleeve of hysteresis alloy mounted on the "stem" of the mushroom above the body of the rotor.

J. W. BEAMS.—First I wish to congratulate Dr. Meyer and Dr. Mysels on their very nice magnetically supported centrifuge. It illustrates the importance of parallel development. It might be of interest to mention that Dr. A. R. Kuhlthan in our laboratory has in some unpublished work developed a reasonably precise radiation method of measuring rotor temperatures and finds that if appreciable heat is developed in the rotor blackening of the rotor and chamber walls is helpful. In our experiments the rotors and walls also were made effectively black although so little heat is generated in the rotor that this is not necessary. Incidentally if there is small comparatively short time variations in the wall or chamber temperature, as often occurs, in some thermostatic devices, it is better to make the rotor bright. The rotor temperature will then not vary as much as that of the chamber, if the vacuum is good. Also we have had some experience with guiding the magnetic flux by placing additional iron around the solenoid. In general it seems to reduce the ease of regulation. On the other hand it reduces the stray flux. The power required does not seem to be excessive without it. We have suspended masses which varied in weight from 10^{-6} g. to 5×10^{4} g. with different solenoids.

B. JIRGENSONS.—What values of molecular weight have been arrived at for such materials as serum albumins by this method? Have you studied albumins from different sources?

J. W. BEAMS.—Albumin from different sources seems to have different degrees of homogeneity. Assuming homogeneity some samples gave values as low as 60,000 while others gave values of above 70,000. A specially purified sample kindly supplied by Dr. H. Hoch gave a value of approximately 74,000.

G. KEGELES.—Is it at all serious that there is an adiabatic cooling of the rotor upon acceleration, due to stretching?

J. W. BEAMS.—There is, of course, a slight cooling of the rotor when the rotor is accelerated to operating speed. However this is very small in the equilibrium centrifuge because the rotor speed is relatively small. In any case the rotor temperature approaches very closely to that of the walls in a time which is negligible in comparison to the time for equilibrium to take place.

AN AIR-DRIVEN, AIR-FLOATED CAPILLARY TUBE ULTRACENTRIFUGE[1,2]

BY T. F. FORD, G. A. RAMSDELL AND LORAINE W. KLIPP

Eastern Utilization Research Branch, Agricultural Research Service, U. S. Department of Agriculture, Washington, D. C.

Received February 25, 1955

An air-driven, air-floated ultracentrifuge of the Henroit and Huguenard type is described. The rotor is constructed with opposed radial holes in which glass capillary cells are inserted. The rotor may be stopped at appropriate intervals during the course of centrifugation, and the tubes removed and photographed. A simple optical system utilizing a horizontally mounted research microscope is used to obtain scattered light, absorption and schlieren pictures. Sedimentation velocity results are reported on earthworm blood, snail blood, and tobacco mosaic virus protein. The agreement with results reported, using other ultracentrifuges, is good. For tobacco mosaic virus certain exaggerated dilution effects at low concentrations are noted, probably attributable to the use of non-radial cells. This is not serious and may be taken into account. Although the rotor is run in air, the temperature at the position of the cell is essentially the same as the room temperature, and effects due to temperature gradients are negligible. Diffusion constants can be calculated from photographic schlieren records, of the spreading of centrifugally produced concentration gradients, made while the tube is mounted vertically on the microscope stage. Asymptotic packing volumes of the sedimented erythrocruorin of worm blood and of the colloidal proteins of milk can be measured from photographs of the cells after centrifugation at increasing centrifugal forces. The packing volumes agree satisfactorily with the voluminosities calculated from viscosity measurements using the Einstein equation. They also agree, for the colloidal milk proteins, with voluminosities calculated from analyses of deposits compacted in bowl rotors.

Introduction

The ultracentrifuge design and technique presented are based on the fact that liquid samples confined in sufficiently small cells are so completely immobilized that the centrifuge rotor can be repeatedly stopped and the cells removed for photographing without sensibly altering the sedimentation gradients. Cylindrical cells made from ordinary glass capillary tubing are used. The technique is simple and permits the ready measurement of sedimentation constants, diffusion constants, and voluminosities, all, if desired, on a single sample. Results for erythrocruorin of earthworm blood, hemocyanin of snail blood, and tobacco mosaic virus protein are here reported.

Immobilization of liquids during centrifugation by using capillary cells seems to have been described first by Elford.[3] Most of his cells were of metal. The progress of sedimentation was followed by bacteriological and chemical analyses of the contents of the cells after centrifuging for different times. Adaptations of this basic Elford analytical technique have been described by McIntosh and Selbie,[4] who, however, used cells actually of more than capillary diameter; by Polson[5]; by Ford and Ramsdell[6]; and by Brakke, Block and Wyckoff.[7] The last-named authors used long glass capillaries,

(1) Presented at the McBain Memorial Symposium, Colloid Section of the American Chemical Society, Chicago, September, 1953. The experiments on tobacco mosaic virus have, however, been added since.

(2) The work here described was done in the U. S. Department of Agriculture and supported in part by Bankhead-Jones Special Research Funds. Preliminary work was done previously by the senior author in the laboratory of the Shell Development Company, Emeryville, California.

(3) W. J. Elford, *Brit. J. Exp. Path.*, **17**, 399, 422 (1936).

(4) J. McIntosh and F. R. Selbie, *ibid.*, **18**, 162 (1937).

(5) A. Polson, *Nature*, **148** 593 (1941).

(6) T. F. Ford and G. A. Ramsdell, "XIIth International Dairy Congress, Section II, Subject 1," Stockholm, 1950, p. 17.

(7) M. K. Brakke, L. M. Block and R. W. G. Wyckoff, *Am. J. Botany*, **38**, 332 (1951).

primarily for analysis, but they also observed the positions of concentration gradients by scattered light and calculated sedimentation constants from the data. McBain and Lewis[8] first reported optical measurements using capillary cells. They used thick-walled cells, inserted over pieces of photographic film in an air-driven spinning top type of ultracentrifuge. The rotor was run in dim light or under cover until a record was desired, whereupon the light was flashed on for one or more seconds. Ford and Ramsdell reported, but did not publish, optical measurements by the technique here described in 1946.[9] This work was referred to, and some of the pictures reproduced by McBain[10] as a part of a general discussion of ultracentrifugation. Recently Backus and Williams[11] have reported results obtained by centrifuging glass capillaries or capsules floated in a liquid of suitable density in an angle-head rotor. Subsequent to centrifugation the tubes are removed from the liquid, wiped dry, and examined by the schlieren method, making use of the optics of an electrophoresis apparatus and by differential absorption employing a spectrophotometer.

The present development has extended over many years. It has involved both improvement in operation of air-driven ultracentrifuges and development of techniques of handling and photographing capillary tubes. Our purpose has been to utilize the inherent simplicity and versatility of the air-driven spinning top. Our primary interest has been in colloids, and this is the reason for selection of the three particular test substances for which results are given in this paper.

The Centrifuge

Design of the Rotor.—A sectional sketch of a rotor is shown in Fig. 1. The outside diameter of this rotor is 8.26 cm. The rotor is supported and driven by a whirling sheet of air issuing from jets in a hollow cone stator. The principle of operation is that of the Henriot and Huguenard spinning top,[12] that of the early centrifuges built by Beams and co-workers,[13] and of the various centrifuges developed by McBain and co-workers.[10] However, the dimensions have been considerably increased over those used by these workers. In the rotor shown, the distance from the axis of rotation to the mid-point of the cell is about 3.25 cm., the same as in Svedberg's high-speed rotors.

Four pairs of holes for four diameters of tubes are equally spaced about the rotor, but only one tube is ordinarily used at a time. An opposed tube for balance is desirable. The holes are vented to the inside of the rotor to permit rapid equalization of internal air pressure as the rotor is stopped. Since air is thrown out of the rotor when spinning, a vacuum is produced, and without vents, as the centrifugal force drops to zero there is sometimes sufficient in-rush of air to blow the tubes out of the holes.

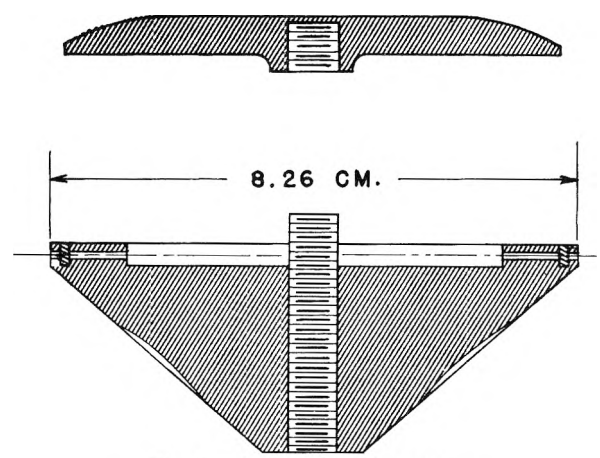

Fig. 1.—A capillary tube rotor.

Speed Control, Range and Measurement.—The speed of the rotor is determined solely by the setting of a valve at the centrifuge. The air is held in a large surge tank in the centrifuge room, and the pressure in the surge tank (usually 60 lb. per sq. in.) is controlled by a pressure regulator. The operation of the pressure regulator produces a fluctuation of about 0.4% in the r.p.s. over cycles of a few minutes, but the average speed remains constant within much closer limits for indefinite periods.

All of the sedimentation velocity experiments described in this paper were at relatively low speeds, 258 to 675 r.p.s. At these speeds, for the rotor shown in Fig. 1, the centrifugal forces at the mid-point of the cell are 8,720 and 59,700 times gravity, respectively. This rotor has been run at 960 r.p.s., giving a centrifugal force at the mid-point of the cell of 120,000 times gravity.

Below approximately 460 r.p.s. the speed is measured with an electronic tachometer and checked with a stroboscope. Above 460 r.p.s. a beat-frequency oscillator is used.

Temperature.—Experiments with thermocouples held close to the spinning rotor show the temperature at the upper surface at the mid-point of the cell to be about 0.02° below the room temperature of 258 r.p.s., 0.03° below room temperature at 480 r.p.s., and 0.03° below room temperature at 675 r.p.s. The corresponding temperature gradients along the tube in the direction of the centrifugal force are +0.11, +0.06, and −0.26°. The centrifuge is run in a temperature controlled room set at 19.5°. The normal fluctuation in room temperature is ±0.4° and the rotor temperature follows the room temperature.

The Capillary Tube Cell

The outside diameter of the capillary centrifuge tubes now regularly used is 1.59 mm., and the inside diameter about 1.10 mm. Although tubes of various lengths are used, a rotor with long holes being provided for long tubes, a good over-all length for use in the rotor shown in Fig. 1 is 13 to 14 mm. These tubes are made from selected

(8) J. W. McBain and A. H. Lewis, *Trans. Faraday Soc.*, **36**, 381 (1940); *Science*, **89**, 611 (1939).

(9) T. F. Ford and G. A. Ramsdell, paper presented before the Division of Colloid Chemistry of the 110th meeting of the American Chemical Society, Chicago, September, 1946.

(10) J. W. McBain, "Colloid Science," D. C. Heath and Company, Boston, Mass., 1950, pp. 228–230.

(11) R. C. Backus and R. C. Williams, *Arch. Biochem. Biophys.*, **49**, 434 (1954).

(12) E. Henriot and E. Huguenard, *Compt. rend.*, **180**, 1389 (1925); *J. phys. radium*, **8**, 443 (1927).

(13) J. W. Beams and E. G. Pickels, *Rev. Sci. Instru.*, **6**, 299 (1935).

micrometered sections of Pyrex capillary tubing. The tubes are always slightly tapered. The large ends are sealed in a tiny oxygen flame. Flat inside bases are produced, when desired, by inserting two or three Rose metal beads and then spinning the tubes immersed in hot lubricating oil, in special holders in a clinical centrifuge. Many tubes can be prepared in a short time. They are carefully cleaned and stored in vials. They can be re-used, and this is a desirable practice, since, in this way those with optical imperfections are gradually eliminated.

Tubes less than 1 mm. and greater than 1.59 mm. in outside diameter have been used. With large tubes, however, convection becomes a factor. Extremely small tubes are difficult to fill. The volume of liquid contained in a tube such as that described is less than 0.01 ml.

Optical Arrangements

The optical system, which need not be described in detail here, is essentially a photomicrographic apparatus. The centrifuge tube, which is mounted by means of a clip on a metal microscope slide (and on a rotatable insert for vertical alignment), replaces both the plane parallel cell and the cylindrical lens of standard schlieren systems. A good quality photographic enlarging lens mounted on the substage rack serves as the schlieren lens. The light source is an 8 v.-18 amp. tungsten ribbon filament lamp. Horizontal razor blades (for Toepler schlieren pictures), or inclined razor blades, wires, or spider webs (for Philpot schlieren pictures) are hung on a vertically adjustable crossarm just in front of the objective lens of the microscope. Wires and spider webs give well defined schlieren peaks, and razor blades give solid patterns which are easily observed visually. A collection of razor blades permanently set at various angles is provided. The apparatus is normally set to take one or another type of schlieren picture. Absorption pictures when desired require only that the razor blade be moved down, out of the light path. Scattered light pictures are obtained by switching off the schlieren light source, turning on a lamp which illuminates the tube from the side, and refocusing. Instant refocusing is secured by stops at both the schlieren and scattered light positions of the microscope tube. All of these types of pictures can be taken on the same tube in a few seconds. The enlargement used is about 6.6 times, for schlieren and absorption pictures. The image on the ground glass screen is reflected in a mirror for convenience. Cut film is used.

Operation

Filling and Sealing Tubes.—The liquid sample to be centrifuged is introduced into the tubes by means of a hypodermic syringe, and the length of the column adjusted to leave about 4 mm. of free space at the top of the tube. The filled tubes are sealed by spinning them immersed in barely molten petroleum jelly containing 0.5% sorbitan monostearate, in the clinical centrifuge, using the same holders used in melting the Rose metal beads. One or two minutes centrifuging is sufficient for this purpose. The petroleum jelly–sorbitan monostearate mixture gives an almost, though not quite, flat meniscus. Many mixtures of various substances have been tried for this purpose. The filled and petroleum jelly covered tubes are up-ended until ready for use, a practice which tends to erase any slight gradients produced by the clinical centrifugation.

Tubes have been sealed with white mineral oil also, which does not require any heating, and good results obtained despite considerable curvature of the meniscus.

Handling the Tubes.—When an experiment is to be started, the tube to be used is wiped clean, a little petroleum jelly removed from the top with a pin or sharpened toothpick to avoid overflow, and the tube again wiped clean with a soft cloth. Small metal racks are provided for tubes to be centrifuged and for those which have been centrifuged.

After the tubes are prepared, they are handled with tweezers. The rotor is marked so that when it is stopped, the tubes can be held upright during transfer to the metal microscope slide for photographing. The microscope slide is held in a vise for this operation. Although care is taken to avoid tilting the tubes during transfer, slight momentary tilting is in fact not serious. Shock does not appear to disturb the gradients, but they can be erased and homogeneous solutions again obtained by slowly up-ending, and gently rotating the tubes while they are held in a horizontal position, for about 20 minutes. Thus it is possible to rerun the same sample many times. It is found that clearer pictures and sharper gradients are often obtained on rerunning. This is partly due to clarification of the solution, and partly to further flattening of the meniscus.

Centrifugation.—The rotor with a tube in place is started by setting it on the air stream previously adjusted to the pressure desired. Acceleration is rapid. The final rotor speed is attained in about 90 seconds at 675 r.p.s., for example; in shorter times at higher speeds, and in longer times at lower speeds. The rotor is stopped by dropping the air pressure on a time schedule to 5 lb. per sq. in. and then braking with the fingers, although at low speeds it may not be necessary to reduce the air pressure. At 675 r.p.s. deceleration by dropping the air pressure requires a total of 58 seconds. For the acceleration and deceleration stages equivalent centrifuging times are calculated from speed–time plots. The combined acceleration and deceleration equivalent times may also be found by comparing results on the same sample run for different intervals.

The time elapsed in stopping the rotor, transferring the tube to the microscope slide, taking pictures, and replacing the tube in the rotor, averages about 3 minutes.

Measurements of Sedimentation Constants

The experiments on worm blood, snail blood, mixtures of worm blood and snail blood, and on tobacco mosaic virus are here reported in the chronological order in which the experiments were done. For the worm blood and snail blood experiments the rotor used was not the one shown in Figure 1, but a similar one of 7.62 cm. diameter.

Earthworm Blood.—The blood of the earthworm (*Lumbricus terrestris*) was chosen as a test substance because it is reported to contain a single respiratory protein, erythrocruorin, of moderate size[14] and because it is readily available, requires only clarification, and can be stored (at 4°) for periods up to 3 weeks or more. Total nitrogens on various lots of undiluted worm blood prepared by us were 1.53, 1.55, 1.68, 1.75, 1.86, 1.90, 1.96 and 1.97%. Of this total nitrogen, 84% is heat-coagulable, and about 87% is easily deposited by spinning at high speed in small air-driven bowl rotors. We have accordingly used the factor 0.85 for conversion of total nitrogen to pigment nitrogen. Analyses of worm blood samples variously depleted of erythrocruorin by centrifuging give the factor 5.75 for conversion of pigment nitrogen to erythrocruorin.

Figure 2 shows four types of sedimentation pictures for earthworm blood diluted with 0.9% sodium chloride solution to 0.168% total nitrogen or 0.82% erythrocruorin. These are all pictures of

(14) T. Svedberg and I. B. Eriksson, *J. Am. Chem. Soc.*, **55**, 2834 (1933).

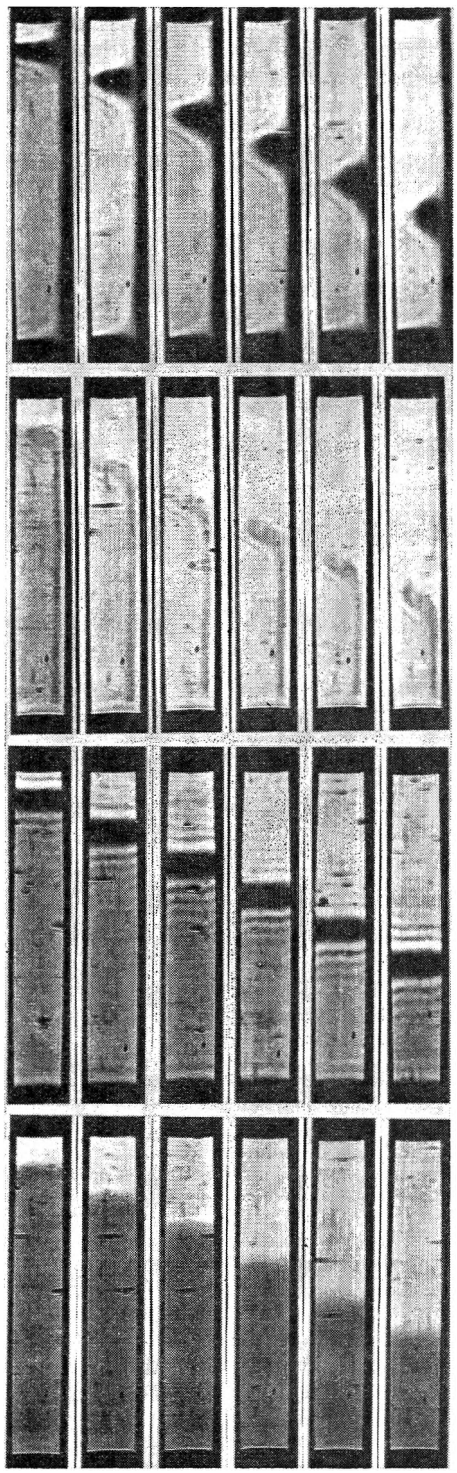

Fig. 2.—Various types of sedimentation pictures for earthworm blood. Earthworm blood diluted with 0.9% sodium chloride to 0.168% total nitrogen and 0.82% erythrocruorin; speed 485 r.p.s., centrifugal force about 27,500 times gravity; centrifuging times between pictures 8 min., equivalent to 511 sec. at 485 r.p.s. The top set of pictures was taken with an inclined razor blade (Philpot schlieren), the second set with an inclined 0.0005 inch diameter wire, the third set with a horizontal razor blade (Toeppler schlieren), and the bottom set with no razor blade (absorption). For the schlieren pictures panchromatic film was used; for the absorption pictures orthochromatic film. From top to bottom $s_{20} = 54.2$, 53.9, 55.5 and 54.0 $\times 10^{-13}$.

a single tube remixed and rerun over a period of 9 days. This particular tube was in fact rerun a total of 9 times in 20 days, with no significant change in the sedimentation constant. The tube was kept in a rack in the centrifuge room, at 19.5°, throughout this period.

Figure 3 is a plot of sedimentation constants, corrected to the standard state corresponding to water at 20°,[15] for earthworm blood at various concentrations in 0.9% sodium chloride. The effective centrifugal force in all of these experiments was about 27,500 times gravity. Eighteen runs were made at 0.168% total nitrogen (0.82% erythrocruorin), using four different tubes. The average of the 18 sedimentation constants obtained is 54.4 $\times 10^{-13}$, and the mean deviation from this average is 0.91 $\times 10^{-13}$, or 1.72%. On the main plot of Fig. 3 a median line is drawn through the value 54.4 $\times 10^{-13}$, and a deviation of $\pm 0.91 \times 10^{-13}$ is indicated by the dotted lines above and below this median line. From zero concentration to 0.210% total nitrogen the mean deviation of all the values is 1.25% of the sedimentation constant read from the median line. The intercept of the median line at zero concentration gives $s^{\circ}_{20} = 62.2 \times 10^{-13}$.

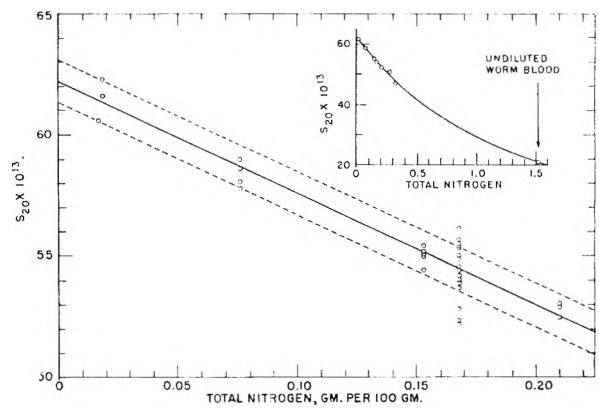

Fig. 3.—Relationship between sedimentation constant, corrected to the standard state, and total nitrogen concentration for earthworm blood diluted with 0.9% sodium chloride solution. The calculated concentrations of erythrocruorin range from 0.09 to 7.44%.

For *Lumbricus* erythrocruorin Svedberg and Eriksson[14] give $s_{20} = 60.9 \times 10^{-13}$ for worm blood diluted 25 to 30 times with 1% sodium chloride and with various buffers. The actual average of the fourteen values within the *p*H stability range used by them is, however, not 60.9 $\times 10^{-13}$ but 60.5 $\times 10^{-13}$. The mean deviation of their values from this average is 1.44 $\times 10^{-13}$, or 2.36%. They used a centrifugal force of 56,000 times gravity. Svedberg and Eriksson state that their undiluted blood contained over 4% erythrocruorin. On the basis of our analysis their diluted samples therefore contained at least 0.027–0.032% total nitrogen. Our value for s_{20} at 0.03% total nitrogen, taken from Fig. 3, is 60.8 $\times 10^{-13}$. The agreement between our values and Svedberg and Eriksson's is well within the limits of experimental error of both sets of data.

(15) T. Svedberg and K. O. Pedersen, "The Ultracentrifuge," The Clarendon Press, Oxford, 1940, pp. 34ff.

The sedimentation constants plotted in Fig. 3 are for each experiment averages of the sedimentation constants calculated for separate intervals. In most cases no effect of dilution due to centrifugation was noted, but in a few cases a definite increase in the sedimentation constant from the first interval to the last was observed. The total increase amounts to 2–3% of the mean sedimentation constant. Therefore, for strict accuracy, the various values and the final value, $s^{\circ}_{20} = 62.2 \times 10^{-13}$, should probably be diminished by about 1%.

Snail Blood (*Otala lactea*).—Figure 4 is a plot of sedimentation constants for the blood of *Otala lactea* at various concentrations at *p*H 4.26. The intercept at zero concentration gives $s^{\circ}_{20} = 91.7 \times 10^{-13}$. We know of no other published sedimentation results on the blood of this snail. The sedimentation constant obtained agrees satisfactorily with that found by Eriksson and Svedberg[16] for *Helix arbustorum*, but is lower than the values found by these authors for the hemocyanin of other snails.

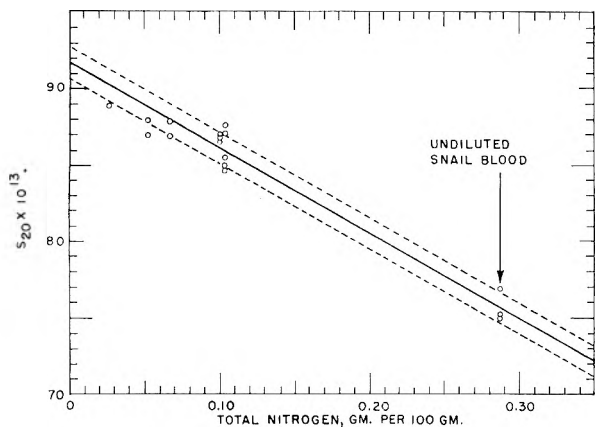

Fig. 4.—Relationship between sedimentation constant, corrected to the standard state, and total nitrogen concentration for snail blood (*otala lactea*) diluted with 0.2 *M* acetate–sodium chloride buffer at *p*H 4.26.

The blood of *Otala lactea* was also studied in buffers at *p*H 3.75, 6.63 and 8.20. In these solvents components having sedimentation constants agreeing with those of Fig. 4 were found, and in addition other components having sedimentation constants of about 50×10^{-13} and 20×10^{-13}.

Earthworm Blood–Snail Blood Mixtures.—A mixture composed of 50 parts of 0.186% total nitrogen worm blood in 0.9% sodium chloride, and 45 parts of undiluted snail blood containing 0.307% total nitrogen was prepared. Four tubes were filled with this mixture. These tubes were centrifuged on the first day and again, after standing (at 19.5°), four to five days later. The Philpot schlieren technique was used. On the first day a symmetrical lower peak and a slightly unsymmetrical upper peak were obtained in every case; on rerunning, both peaks were sharp and symmetrical (*cf.* Fig. 5). For the first day the pictures gave, for the lower peak, $s_{20} = 69.8 \pm 0.9\%$, and for the highest point of the upper peak, $s_{20} = 52.3 \pm 4\%$, $\times 10^{-13}$. The pictures obtained on rerunning the tubes gave $s_{20} = 77.0 \pm 1.4\%$ and $52.4 \pm 1.7\%$, $\times 10^{-13}$. The sedimentation constants of hemocyanin and erythrocruorin calculated for this mixture using the concentration plots of Figs. 3 and 4, are 76.9 and 52.2, $\times 10^{-13}$. Slow establishment of equilibrium is indicated. The dissymmetry of the upper peak observed the first day suggests the temporary existence of a degradation product of hemocyanin. The red color of erythrocruorin extended to the highest point of the peak.

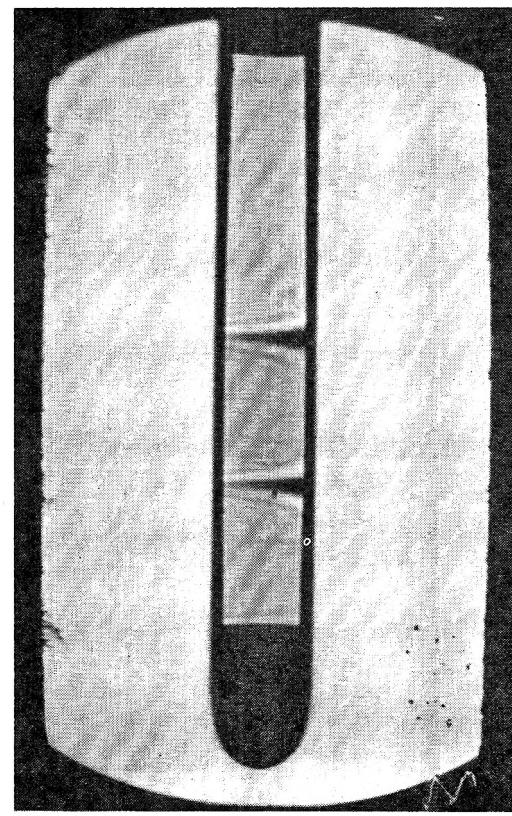

Fig. 5.—Philpot schlieren sedimentation picture for a mixture of earthworm blood and snail blood (*otala lactea*) in 0.9% sodium chloride solution for a tube rerun four days after filling. Worm blood total nitrogen, 0.098%; snail blood total nitrogen, 0.146%, speed 675 r.p.s.; centrifugal force about 56,500 times gravity; centrifuging time 24 minutes. $s_{20} = 52.0$ and 75.9×10^{-13}. This is a reproduction of the complete $2^1/_4$-inch $\times$ $3^1/_4$-inch negative.

Similar mixtures were made using undiluted worm blood, undiluted snail blood, and a 0.2 *M* phosphate buffer at *p*H 6.63. With these solutions no changes on standing for 3 to 4 days were observed. Both peaks were sharp and symmetrical, as in Fig. 5, on the first day and remained sharp. The sedimentation constants found were again in agreement with the calculated values.

Tobacco Mosaic Virus Protein.—The tobacco mosaic virus used was supplied by Prof. Max A. Lauffer. Analysis of the undiluted sample gave 0.297% nitrogen, 8.13% total solids and 1.095% phosphorus. The *p*H was 6.63. According to analyses by Best[17] tobacco mosaic virus protein contains 16.6% nitrogen and 0.52% phosphorus. Assuming all of the nitrogen in the sample received to represent tobacco mosaic virus, the concentration of virus was therefore 1.79%. The total solids

(16) I. B. Eriksson-Quensel and T. Svedberg, *Biol. Bull.*, **71**, 498 (1936).

(17) R. J. Best, *Australian J. Exp. Biol. Med. Sci.*, **26**, 65 (1948).

and phosphorus values indicate a rather high concentration of phosphate buffer probably containing some sodium or potassium chloride.

Various dilutions of this stock solution were prepared, using 0.1 M phosphate buffer at pH 6.61. Viscosities were measured, at 25°, on these solutions. These viscosities were divided by the viscosity of the 0.1 M buffer to obtain relative viscosities, η/η_0. The specific viscosities, $\eta/\eta_0 - 1$, are plotted against the concentration of virus protein in Fig. 6.

In all of the present experiments on tobacco mosaic virus except two, the centrifuge was run at 258 r.p.s., the average distance from axis to gradient was about 3.25 cm., and the average centrifugal force therefore 8,700 times gravity. The two undiluted samples centrifuged were run at 390 r.p.s. at an average centrifugal force of about 20,000 times gravity.

The results of all of the experiments on tobacco mosaic virus protein are presented graphically in Fig. 7. Some explanation of this plot is necessary. The reciprocals of the sedimentation constants are plotted against relative solution viscosities because Lauffer shows[18] that for tobacco mosaic virus, correction of observed sedimentation constants for solution viscosity tends to eliminate concentration effects. For Fig. 7 the observed sedimentation constants, at 19.5°, have been corrected to a buffer density of 1.011, the density of the 0.1 M buffer used for dilution. The density of the buffer or solvent in the original undiluted solution was taken to be 1.046. For the other solutions the densities were proportioned in accordance with the relative amounts of the original solution and added buffer. The partial specific volume used in these calculations was 0.73, which is that given by Lauffer.[18a] Some numerical error is possible as a result of these density corrections because of uncertainty as to the density of the original solvent. This error would be proportional to the concentration of virus, however, and would be zero at zero concentration.

In Fig. 7 the several sets of circles, squares and triangles represent separate experiments. For each experiment the reciprocal sedimentation constants calculated for each interval are plotted against the relative solution viscosities at the concentrations calculated to exist at the position of the gradient for the interval in question. These concentrations were found by multiplying the original concentration in each case by the square of the ratio of the distances from the center of rotation to the meniscus and to the position of the gradient. The relative viscosities were taken from the specific viscosity plot, Fig. 6. The method of calculating concentration is the same as used by Lauffer,[18b] and was for his centrifuge certainly justified since his cells were radial. To eliminate uncertainty in the squared radius relationship for cylindrical tubes, the interval s values for each set of experiments at the various calculated viscosities are connected by straight lines and extrapolated to the actual known viscosity of the solution at the original concentration. The intercepts are indicated by the arrows on the plot. These intercepts in turn define a curve which is drawn across the plot. At $\eta/\eta_0 = 1$, that is, at zero concentration of virus protein, the intercept gives $s_{obs.} = 187 \times 10^{-13}$. This is the observed sedimentation constant at zero concentration in 0.1 M phosphate buffer at 19.5°. Correcting to the standard state corresponding to water at 20° gives $s^0_{20} = 199 \times 10^{-13}$.

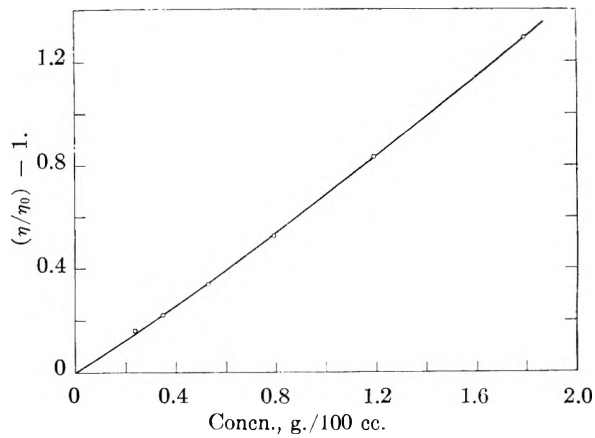

Fig. 6.—Specific viscosity plotted as a function of concentration for the tobacco mosaic virus protein preparation used in the present experiments.

Lauffer reports results of one experiment for which the effect of dilution during centrifugation was considered. In this experiment 33 pictures were taken and 32 sedimentation constants calculated. By multiplying each of these observed sedimentation constants by the corresponding relative solution viscosity Lauffer obtained a set of corrected sedimentation constants. Analysis of these values by the method of least squares gave $s_{obs.} = 215 \times 10^{-13}$. Correcting this result to the standard state corresponding to water at 20° gives $s^0_{20} = 198 \times 10^{-13}$. Since there was a drift in his set of values corrected for relative viscosity, Lauffer again corrected them, multiplying the observed sedimentation constants, not by the relative viscosities, but by hypothetical viscosities calculated by multiplying the intrinsic viscosity by the concentration. By this method he obtained $s^0_{20} = 187 \times 10^{-13}$. Lauffer reports also a set of sedimentation constants on another preparation at various dilutions. For these data the intercept of the $1/s$–concentration plot at zero concentration gives $s^0_{20} = 185 \times 10^{-13}$. These latter data were not corrected for dilution during centrifugation.

Wyckoff[19] gives sedimentation constants (s_{20} values) of 174 and 200 $\times 10^{-13}$ at 0.15% tobacco mosaic virus protein in 0.1 M phosphate buffer at pH 7. Assuming dilution according to the squared radius relationship, his actual average concentration would have been about 0.125%. At this concentration Figs. 6 and 7 give $s_{obs.} = 180 \times 10^{-13}$, and correcting this to the standard state gives $s_{20} = 192 \times 10^{-13}$. We have not observed two components in our experiments.

In Fig. 7 the straight lines through the points at the various concentrations, excepting at the lowest concentration, for which no line is drawn, were found by the method of least squares. These

(18) M. A. Lauffer, *J. Am. Chem. Soc.*, **66**, (a) 1188, (b) 1195 (1944).

(19) R. W. G. Wyckoff, *J. Biol. Chem.*, **121**, 219 (1937).

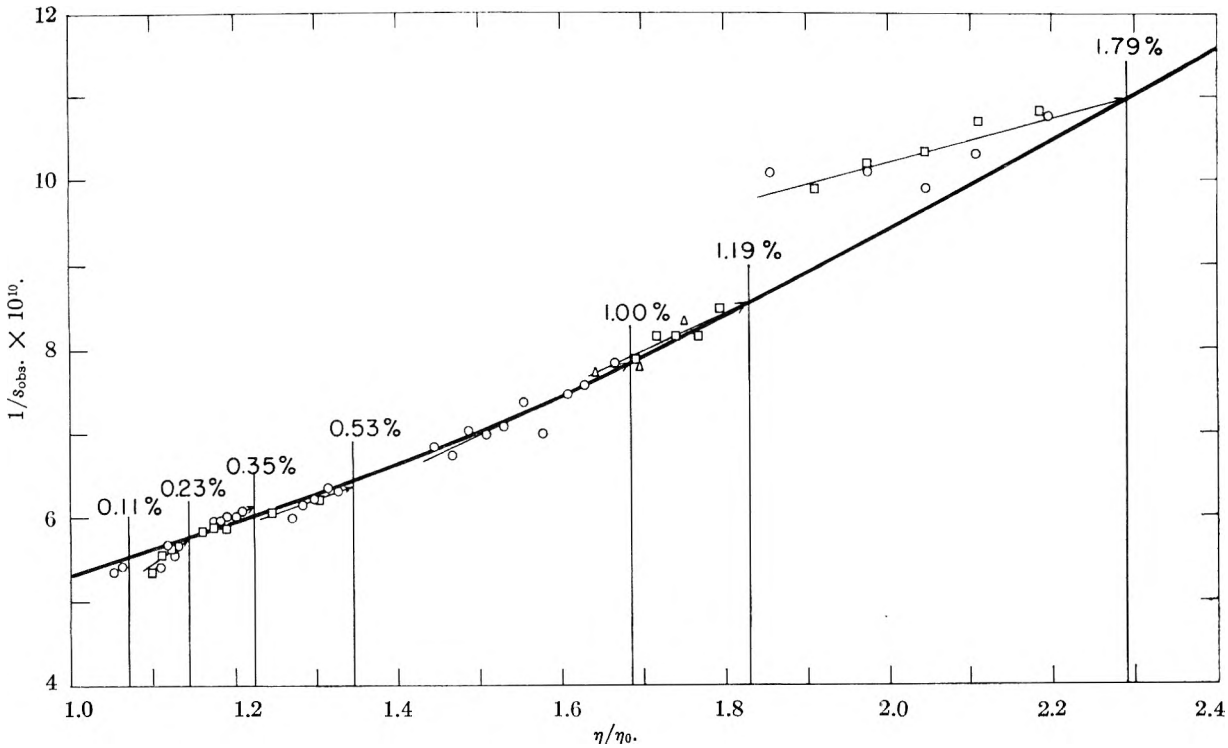

Fig. 7.—Relationship between observed reciprocal sedimentation constant at 19.5°, corrected to a buffer density of 1.011, and relative solution viscosity for tobacco mosaic virus protein.

straight lines parallel the curve through the intercepts only in the intermediate concentration range. The deviations in slope are consistent and we believe they are real. At the low concentrations they may indicate dilution in excess of that calculated using squared radius ratios. At the high concentrations the deviation is reversed and is probably here due to interference between particles during centrifugation, which would tend to neutralize the dilution effect.

The mean deviation of all of our values from the appropriate least squares values, that is, from the straight lines of Fig. 7, is 1.07%.

Measurement of Diffusion Constants

If a gradient is produced in a liquid column in a capillary cell by centrifugation, the necessary data for the calculation of the diffusion constant of the solute or dispersed substance can be obtained by taking Philpot schlieren pictures of the tube on the microscope stage at intervals as the gradient disappears. Five such sets of pictures for worm blood were taken using 0.9% sodium chloride solutions containing 0.82% erythrocruorin. These pictures gave $D_{obs.} = 2.0 \times 10^{-7} \pm 10\%$. The pictures were taken at ten-minute intervals and the experiments ran for 60 to 90 minutes. The diffusion gradient patterns were traced from enlargements of the negatives and also plotted from densitometer measurements across the negatives. Polson[20] gives $D_{20} = 1.81 \times 10^{-7}$ for *Lumbricus* erythrocruorin.

Measurement of Voluminosity

Use of the ultracentrifuge to measure the volume of sedimented influenza virus has been reported by Sharp, Beard and Beard.[21] They used a lucite cell 2 cm. long and 2 mm. in diameter in an air-driven vacuum type ultracentrifuge. The cell and the deposit or pellet in the bottom were photographed at frequent intervals over long periods at successively increased centrifugal forces. The authors note a swelling of the pellet when the centrifugal speed is quickly reduced from a high to a low value. This swelling is not rapid, however, amounting to about 8% of the volume in 15 minutes and continuing for several hours. We have made similar measurements of asymptotic packing volumes, but, as in the sedimentation experiments, photographed the tubes after stopping the rotor. For these experiments a 37 mm. diameter rotor was used. Since a rotor of this size can be stopped and the first picture taken in one minute, swelling is not great, and in any case the progress of swelling can be observed thereafter, and the volume extrapolated back to zero time. There are, moreover, advantages in being able to take schlieren, absorption or scattered light pictures at will during the swelling process.

The deposit from undiluted worm blood was compacted at gradually increasing centrifugal forces up to 240,000 times gravity over a period of 18 hours. The final volume of the deposit, corrected for swelling, divided by the weight of erythrocruorin present times its partial specific volume (0.740), gave an approximate packing volume or voluminosity of 3.0 ml. per ml. of contained dry protein. This total volume includes protein, water of hydration and solvate liquid. Ostwald viscosities were determined on various dilutions of the same blood. From a plot of these data the over-all volu-

(20) A. Polson, *Kolloid Z.*, **87**, 149 (1939).

(21) D. G. Sharp, D. Beard and J. W. Beard, *J. Biol. Chem.*, **182**, 279 (1950); D. G. Sharp, *Biochim. biophys. Acta*, **5**, 149 (1950).

minosity for the total protein calculated by use of the Einstein equation was 3.4 ml. per ml. Since the protein is about 85% erythrocruorin, the over-all voluminosity, thus calculated, cannot be far from the true Einstein voluminosity of erythrocruorin alone. Although in this case, for erythrocruorin—a small molecule compared to influenza virus—it is possible that packing was not complete even at 240,000 times gravity, the agreement between the values calculated by the two methods is nevertheless interesting. The progress of swelling of such jellies has been followed by successive schlieren pictures taken over periods of many hours. A distinct concentration gradient soon develops and moves upward until redispersion is almost or quite complete. Thus, although the swelling may be in part an effect of volume elasticity as stated by Sharp, *et al.*, diffusion processes are involved as well.

Similar compactions of the casein complex particles deposited from milk, which are very large, and for which an asymptotic volume was certainly reached, give for these particles a voluminosity of 4.3 ml. per ml. This value, for milk, is in good agreement with results of parallel compactions using an air-driven bowl rotor with which the compacted deposits could be removed for analysis, and with values calculated from viscosity measurements by ourselves and others. Since the casein complex particles are known to be spherical, the Einstein equation here certainly gives a true voluminosity, uncomplicated by shape factors. Thus, as concluded by Sharp, *et al.*, by centrifugal packing it is possible to express all the liquid not actually associated with the particles compressed. The method is therefore capable of giving a true measurement of voluminosity. For spheres the voluminosity is identical with the hydrodynamic volume.

Discussion and Summary

In the ultracentrifugal technique described the glass tubes or cells containing the material under investigation are cylindrical and of capillary diameter. The rotor into which they are inserted is air-driven and its rotation may be easily and quickly stopped at chosen time intervals for the purpose of photographing the tubes.

For the proteins used as test substances, good sensitivity and resolution are obtained and the results are reproducible. The sedimentation constants found for the erythrocruorin of earthworm blood and for tobacco mosaic virus protein agree satisfactorily with accepted values. Sedimentation constants for the hemocyanin of a snail blood not previously studied are consistent with published values for hemocyanins from other snails.

The technique provides simple optical means of measuring diffusion constants and voluminosities.

DISCUSSION

W. H. SLABAUGH.—With your equipment are you able to detect banding in the sedimentation of polydisperse systems such as observed in certain clay suspensions?

T. F. FORD.—We have observed banding with Bentonite. We have also observed banding in the casein-containing deposits from milk, and from milk containing worm blood as a reference substance. In the latter case a layer of the red worm blood erythrocruorin was deposited on top of the casein colloids.

PHYSICAL AND CHEMICAL COMPOSITION STUDIES ON THE LIPOPROTEINS OF FASTING AND HEPARINIZED HUMAN SERA[1]

BY FRANK T. LINDGREN, ALEX V. NICHOLS[2] AND NORMAN K. FREEMAN

Donner Laboratory of Medical Physica, Division of Medical Physics, Department of Physics and the Radiation Laboratory, University of California, Berkeley, California

Received February 25, 1955

Chemical studies of broad band lipoproteins isolated from fasting sera show wide ranges of lipid composition for different classes of lipoproteins, but establish relative constancy of lipid composition for lipoproteins of the same class obtained from different individuals in both health and certain disease states. Moreover, chemical studies of narrow band S_f 4–8 lipoproteins show no significant differences in lipid content when compared with the composition of broad band S_f 0–20 lipoproteins. Following intravenous heparin injection, lipid compositions of the various lipoprotein classes show some changes in unesterified cholesterol and unesterified fatty acid content. Also, nearly one-fifth of the total serum lipids are shifted, after heparin injection, into associations with proteins present in the total ultracentrifugal "residue." Studies involving the *in vitro* incubation of S_f 20–400 lipoproteins with "active fractions" obtained from heparinized plasma show similar, if not identical, lipoprotein transformations as those found to occur *in vivo*.

Introduction

Although not directly achievable, it would be desirable to know the complete chemical composition of each lipoprotein as it exists in the circulating blood stream. However, even though some alterations in the lipoproteins may occur as a consequence to the processes of blood withdrawal, serum preparation, salt solution addition and prolonged ultracentrifugation, at present no method has been found superior to the study of *in vitro* lipoproteins isolated by the ultracentrifuge. Ultracentrifugally, the serum lipoproteins can be isolated into narrow flotation or hydrated density bands.[3] However, the more detailed the isolation procedure employed, the lower the yield of lipoproteins for chemical analysis. It is primarily for this consideration of yield that most of the present lipoprotein chemical composition studies have been confined to broad bands of ultracentrifugally isolated lipoproteins.

Previous chemical studies[4] of ultracentrifugally isolated lipoproteins have established rough constituent lipid and protein composition values for the major lipoprotein classes present in human serum. However, in these studies the various lipoproteins analyzed were obtained from many different individuals, not allowing evaluation of variability of composition of particular lipoproteins from person to person. A further limitation of these studies was the unavailability of analysis for unesterified fatty acid. Also, one highly important chemical analysis was of limited reliability, namely, the glyceride analysis, which was calculated by difference of the fatty acids present as cholesteryl ester and phospholipid from the total fatty acids. Although the present study is restricted to the lipid composition of certain lipoprotein classes, it nevertheless represents an improvement over the previous study in that such highly important lipid components of lipoproteins as glycerides and unesterified fatty acids are reliably analyzed.

Intravenous sodium heparin exerts profound effects upon serum lipoproteins, particularly the low density lipoproteins.[5] Because the changes brought about by heparin strikingly resemble those transformations observed during physiologic fat absorption, there is great potential importance in understanding the basic features of the heparin transformation mechanism. For this reason, the present study includes a section dealing with physical and chemical changes in certain of the lipoprotein classes brought about by the action of heparin.

Methods

A. Isolation of Broad Band Lipoprotein Fractions.—For this fractionation all the lipids and lipoproteins present in human serum or plasma are ultracentrifugally separated into the following four density classes:

1. **Lipoproteins of Density[6] Less than 1.006 g./ml.**—Fasting serum or plasma run unaltered at 104,000 × *g* for 24 hours in a 6-ml. preparative tube (contained in a Spinco 40.3 rotor) effects flotation of all the lipoproteins of S_f 20 and higher S_f rates into the top 3-ml. fraction (S_f 20–400 low density lipoproteins[7]). The lower fraction (bottom fraction of the 1.006 g./ml. run) contains all the serum lipoproteins of density greater than 1.006 g./ml. as well as all the serum proteins.

2. **Lipoproteins of Density Higher than 1.006 g./ml. but Lower than 1.063 g./ml. (S_f 0–20 Low Density Lipoproteins Plus the HDL_1[8] Lipoprotein).**—To the bottom 3-ml. fraction from the above (1.006 g./ml.) run is added 3 ml. of a NaCl solution of density 1.115 g./ml. which is sufficient to bring the density of the protein and lipoprotein-free solution before ultracentrifugation to 1.063 g./ml. Following ultracentrifugation at 104,000 × *g* for 24 hours the S_f 0–20 and the HDL_1 lipoproteins are quantitatively isolated in the 3-ml. top fraction of the preparative tube. The 3-ml. bottom fraction contains the two high density lipoproteins as well as the other serum proteins.

3. **Major High Density Lipoproteins.**—To the 3-ml. bottom fraction of the previous (1.063 g./ml.) run is added 3 ml. of a D_2O–$NaNO_3$ solution of density 1.328 g./ml. which raises the small molecule solution density in the top milliliter of the preparative tube before ultracentrifugation to 1.200 g./ml. After ultracentrifugation of this mixture at 104,000 × *g* for 26 hours, practically all the major high density lipoproteins (HDL_2 and HDL_3) are quantitatively floated to the top fraction consisting of 1.5 ml.

(1) This work was supported (in part) by the United States Atomic Energy Commission, The National Heart Institute of the U. S. Public Health Service and the Life Insurance Medical Research Fund

(2) This work was done during the tenure of a Research Fellowship of the San Joaquin County Heart Association, an affiliate of the American Heart Association.

(3) F. T. Lindgren, H. A. Elliott and J. W. Gofman, THIS JOURNAL, **55**, 80 (1951).

(4) H. Jones, J. Gofman, F. Lindgren, T. Lyon, D. Graham and B. Strisower, *Am. J. Med.*, **11**, 358 (1951).

(5) D. Graham, T. Lyon, J. Gofman, H. Jones, A. Yankley, J. Simonton and S. White, *Circulation*, **4**, 666 (1951).

(6) All density values are given for 26°.

(7) In fasting serum no significant amounts of S_f 400–40,000 lipoproteins generally are present in the low density fraction, limiting this lipoprotein fraction almost entirely to lipoproteins of the S_f 20–400 class.

(8) HDL is an abbreviation for high density lipoprotein. Thus, HDL_1, HDL_2 and HDL_3 are abbreviations for the high density serum lipoproteins of approximate hydrated density 1.05, 1.075 and 1.145 g./ml., respectively.

TABLE I

THE LIPID CHEMICAL COMPOSITION OF ISOLATED LIPOPROTEIN FRACTIONS OBTAINED FROM FIVE FASTING HUMANS[a]

Case	Cholesteryl ester	Unesterified cholesterol	Glyceride	Phospholipid	Unesterified fatty acids
		The S_f 20–400 class[b]			
1	13	10	58	18	1
2	13	5	61	21	<1
3	9	6	64	20	<1
4	32	5	46	16	<1
5	7	12	53	23	5
Mean value	15	8	56	20	1
		The S_f 0–20 class			
1	51	10	14	24	1
2	45	11	17	26	1
3	47	12	16	24	1
4	45	12	20	22	1
5	45	16	11	26	2
Mean value	47	12	16	24	1
		The major high density lipoproteins			
1	29	5	15	46	5
2	15	7	20	51	7
3	20	6	30	39	5
4	30	5	20	41	4
5	24	8	14	47	7
Mean value	24	6	20	44	6

[a] Chemical composition data are expressed here in percentage of total lipid for each lipid constituent measured in the particular ultracentrifugal fraction. Thus the sum of all percentages for each lipoprotein fraction add up to 100%. [b] Analyses reported previously[4] indicate that lipoproteins of S_f 400–40,000 show glycerides to constitute over 75% of the total lipid, the remainder being distributed among cholesterol and phospholipid.

4. **Total Ultracentrifugal Lipoprotein "Residue."**—This fraction is the 4.5-ml. bottom fraction from the preceding (1.200 g./ml.) preparative run. In addition to all the "non-lipoproteins" of serum, this residue contains small amounts of certain lipids—particularly unesterified[9] fatty acids. Some of these lipides, such as the unesterified fatty acids, probably are bound to serum albumin. Yet, it is possible that there may exist lipoproteins in addition to fatty acid-albumin complexes of density greater than 1.200 g./ml., which because of their low abundance have not been detected and characterized. Although in normal fasting serum less than 3% of the total lipids are present in this residue, considerable increases of lipids, largely in the form of unesterified fatty acids, are observed in this fraction following the intravenous administration of heparin. Because unesterified fatty acids have been found to play such an important role in lipoprotein transformation, the total ultracentrifugal residue has been included for total chemical analysis along with the other three broad band serum lipoprotein fractions.

B. Analysis of Lipids Extracted from Lipoprotein Fractions.—The procedures for the extraction, chromatographic separation and infrared analysis of the lipids obtained from the above four ultracentrifugal fractions are described in detail elsewhere.[11] Broadly the first two procedures consist of lipid extraction with alcoholic ethyl ether, followed by lipid separation utilizing silicic acid chromatography patterned after the procedure of Borgstrom.[12] In the modified chromatographic procedure 1 g. columns, 10 ml. in diameter, consisting of a mixture of 33% Celite and 67% silicic acid by weight are employed. Before use, each column is activated by heating at 115° for 24 hr. After removal from the 115° oven, the columns are washed with 16 ml. of freshly distilled hexane. Then the lipid extract consisting of from 15–25 mg. of lipid dissolved in hexane is directly put on the column. Eluates of 64 ml. of 5% chloroform in hexane, 32 ml. of 100% chloroform and 24 ml. of 100% methyl alcohol are successively collected, allowing separation of the total lipid sample into the following three categories

Fraction I, cholesteryl esters

Fraction II, glycerides, unesterified fatty acid and unesterified cholesterol

Fraction III, phospholipids

Quantitative determination of each lipid constituent is made by measurements of infrared absorption bands characteristic of the particular lipid. Thus, glyceride, cholesteryl ester and phospholipid are measured at 5.8 μ. Unesterified fatty acid is measured at 5.9 μ and free cholesterol is determined at 9.5 μ.

In order to determine the individual lipids present in fraction II, a method[13] of three component analysis of the absorption bands is employed.

I. Lipid Composition of Lipoproteins Obtained from Fasting Sera

A. Lipid Composition of Broad Band Lipoprotein Fractions Obtained from Five Adult Individuals.—Twelve hour fasting serum samples were obtained from three normal individuals (cases 1, 2 and 3) and from two individuals exhibiting the clinical states of xanthoma tuberosum (case 4) and xanthoma tendinosum (case 5). Each serum sample was separated into the four ultracentrifugal fractions and the lipids present in each fraction were analyzed.

Table I presents in detail the chemical composition data (expressed as percentage of total lipid within the lipoprotein) for the lipoprotein fractions obtained from these five individuals. Inspection of

(9) The use of the term *unesterified* fatty acids is used in preference to "free" fatty acids. The reason for this usage is that from our studies,[10] unesterified fatty acids of human serum do not exist in the *free* (uncombined) form but are associated with either lipoproteins or proteins present in the serum. This consideration is similarly applicable to "free" cholesterol where the term unesterified again has been used.

(10) F. T. Lindgren and A. V. Nichols, to be published.

(11) N. Freeman, F. Lindgren, Y. Ng and A. Nichols, *J. Biol. Chem.*, in publication.

(12) B. Borgstrom, *Acta Phys. Scand.*, **25**, 111 (1952).

(13) N. Freeman, F. Lindgren, Y. Ng and A. Nichols, *J. Biol. Chem.*, **203**, 293 (1953).

these data permits the following generalizations to be made.

(1) The phospholipid content is significantly and markedly higher in the major high density lipoprotein group than in either the S_f 0–20 or S_f 20–400 lipoprotein classes. Phospholipid is the predominant lipid of the major high density lipoprotein group. The phospholipid content is slightly higher in the S_f 0–20 class lipoproteins than in the S_f 20–400 lipoprotein class.

(2) The cholesteryl ester content is significantly and markedly higher in the S_f 0–20 lipoproteins than in either the S_f 20–400 or the major high density lipoprotein group. Cholesteryl ester is the predominant lipid constituent of this S_f 0–20 lipoprotein class. Although the cholesteryl ester content of the major high density lipoproteins is on the average only half as abundant as in the S_f 0–20 lipoproteins, it is significantly higher in content than in the S_f 20–400 lipoprotein group.

(3) The unesterified cholesterol is approximately twice as high in content in the S_f 0–20 lipoproteins as in either the S_f 20–400 or the major high density lipoprotein group.

(4) The fraction of the total cholesterol unesterified is slightly but significantly higher in the S_f 20–400 class than in either the S_f 0–20 or the major high density lipoprotein classes.

(5) The glyceride content is much higher in the S_f 20–400 class than in either the S_f 0–20 or the major high density lipoprotein classes. Glyceride is the predominant lipid constituent of the S_f 20–400 class lipoproteins. Because of the limitations of analytical methods employed it was not possible to determine the mono-, di- and triglyceride content of the total glyceride present in the various lipoprotein classes.[14]

(6) The unesterified fatty acid content of the major high density lipoproteins is approximately 5 times higher than in either the S_f 0–20 or the S_f 20–400 lipoprotein classes. Since the ultracentrifugal lipoprotein residue contains from $^1/_3$ to $^2/_3$ of the total serum content of unesterified fatty acids (see Table II), the two major carriers of unesterified fatty acids in the serum are the high density lipoproteins and the total ultracentrifugal lipoprotein residue.

TABLE II

FRACTION OF THE TOTAL SERUM UNESTERIFIED FATTY ACID PRESENT IN THE ULTRACENTRIFUGAL LIPOPROTEIN RESIDUE

Case	Total serum unesterified fatty acids, mg. %	Unesterified fatty acids in ultracentrifugal lipoprotein residue	
		Amount, mg. %	% of Total
1	Not analyzed		
2	16	5	33
3	20	8	39
4	31	7	54
5	40	15	38

(14) The high density lipoproteins show the highest relative abundance of phospholipids and unesterified fatty acids, both being polar lipids. Mono- and diglyceride would be somewhat more polar than triglyceride because of the unesterified hydroxyl groups and hence might be relatively more concentrated in the high density lipoproteins than in either S_f 0–20 or S_f 20–400 lipoproteins. Analyses for mono- and diglycerides are needed to solve this problem.

Variability of Lipoprotein Composition.—Although data on only five individuals are available, nevertheless some comments on the degree of variability of composition among the three lipoprotein classes can be made. In this connection it is of particular interest that in addition to the three clinical normals, a xanthoma tuberosum and a xanthoma tendinosum were included in the present study. The inclusion of these two clinical states assures of having in this study individuals possessing two of the extreme types of lipoprotein distributions to be found in the population at large. Thus, where constancy in composition is found not only in the three normal individuals but also in these two clinical states as well, it may be expected that this constancy is a general feature.

Table I allows the following comments concerning lipoprotein class variability.

(1) Phospholipid shows only a low degree of variability from individual to individual within a single lipoprotein class. This holds for all three lipoprotein classes.

(2) Cholesteryl ester shows little variation, from individual to individual, within the S_f 0–20 lipoprotein class. In the major high density lipoproteins, the range of values for cholesteryl ester content does suggest *that significant variability may exist.* In the S_f 20–400 lipoprotein class the observed range of cholesteryl ester content is large, but there are reasons for considering that individual variation is less than the observed values suggest. Case 4 represents a patient with xanthoma tuberosum in whom the distribution of S_f 20–400 is much more heavily weighted toward S_f 20 than is the case for patients 1, 2 and 3. Since the lipoproteins of flotation rate near S_f 20 are higher in cholesteryl ester content than those of higher flotation rate,[4] the apparently high percentage of cholesteryl ester in the lipids of S_f 20–400 of case 4 may be largely dependent upon the weighted distribution of lipoprotein in that person. On the other hand, the low cholesteryl ester content of the S_f 20–400 in case 5 may well be related to the unreliability of this particular measurement. In case 5, a patient with xanthoma tendinosum, the yield of S_f 20–400 lipoproteins was much lower (because of the nature of the lipoprotein distribution in this disease) than was desirable for satisfactory analysis.

(3) The analytical technique for unesterified cholesterol analysis is such that within these data the apparent variability observed for any of the lipoprotein classes from individual to individual cannot be proved significant.

(4) With the single exception of case 4, the glyceride content of the S_f 20–400 lipoproteins shows little variability. In case 4, however, the same factors mentioned above which tended to raise the cholesteryl ester percentage would tend also to reduce the glyceride content. The variability of glyceride content of both the S_f 0–20 lipoprotein and the major high density lipoprotein is considered to be real variability among individuals.

(5) With the possible exception of the S_f 20–400 fraction of case 5, which was of limited reliability, the data for unesterified fatty acids are not considered to show significant variability from individual

to individual for any particular lipoprotein class.

The total ultracentrifugal lipoprotein residue was analyzed in 4 out of the 5 cases described in Table II. In these four cases, less than 3% of the total lipid content of the serum was found in the ultracentrifugal residue. Because of the very low lipid content of the residue relative to the major high density lipoprotein fraction (which would be the fraction most likely to contaminate the residue), the analysis for the lipid distribution in the residue is unreliable. This is true for such constituents as glyceryl esters, cholesteryl esters, unesterified cholesterol and phospholipid. However, because of the unusually high content of unesterified fatty acid in the lipoprotein residue, contamination (the maximum extent of which can be estimated) cannot possibly influence the value for this lipid constituent. The data for unesterified fatty acid content in the lipoprotein residue indicate that a very large part of the total serum unesterified fatty acid is present there. For the four cases analyzed, the actual fraction of the total serum unesterified fatty acid present in the residue is given in Table II.

In this study no attempt was made to determine the protein content of the various lipoprotein fractions. However, from previous determinations, we may estimate the lipids represent 85–90% of the lipoprotein for the S_f 20–400 class, 75–80% of the lipoprotein for the S_f 0–20 class and 40–50% of the lipoproteins for the major high density class. In each of the above cases, the remainder represents the approximate protein content of the lipoproteins for each class.

B. Lipid Composition of Narrow Band S_f 4–8 Lipoprotein Fractions Obtained from Two Fasting Individuals.—Twelve hour fasting blood specimens were drawn from two normal individuals, one of whom (case 2) was included in the broad band lipoprotein composition study. For case 2, however, the narrow band lipoprotein study was made on a different serum sample. In this narrow band lipoprotein study the serum samples were fractionated by differential density preparative ultracentrifugation[3] to yield S_f 4–8 class lipoproteins exhibiting a high degree of homogeneity as measured ultracentrifugally. Lipid analysis of these S_f 4–8 lipoprotein fractions presented the opportunity of comparing the lipid composition of the broad S_f 0–20 lipoprotein "spectrum" with that of the relatively narrow S_f 4–8 portion of such a "spectrum."

Table III presents the chemical composition data of the narrow band S_f 4–8 lipoprotein fractions obtained from case 2 and case 6. Comparison of the narrow band S_f 4–8 lipoprotein composition with the broad band S_f 0–20 lipoprotein composition of case 2 (Table I) reveals no significant composition differences. Thus, for this case it may be anticipated that no sudden change occurs in the lipid composition for molecules of S_f 2 to S_f 20. For case 6 the lipid composition data are also within the composition limits found for all five of the previously analyzed broad band S_f 0–20 lipoprotein fractions.

TABLE III

THE CHEMICAL COMPOSITION OF NARROW BAND S_f 4–8 LIPOPROTEINS FROM TWO FASTING INDIVIDUALS

Case	Cholesteryl ester, %	Unesterified cholesterol, %	Glyceride, %	Phospholipid, %	Unesterified fatty acid, %
2	46	11	19	24	<1
6	52	12	9	27	<1

II. The Influence of Heparin on Lipoprotein Composition and Lipoprotein Transformation

In 1943 Hahn[15] made the very important observation that the turbidity in the serum of dogs rendered lipemic by fat feeding could be *greatly* reduced by the intravenous administration of heparin. Later, in 1950 Anderson and Fawcett[16] showed that when plasma withdrawn from a heparinized animal was incubated *in vitro* with lipemic plasma, there followed similar reduction in the turbidity of the mixture. Turbidity of a solution is the result of the scattering of light by particles present in the solution. Because the serum proteins are of relatively small molecular size (molecular weights of the order of 10^5 units) they contribute insignificantly to the total serum turbidity. On the other hand, the serum lipoproteins exhibit tremendous variations of particle size, with molecular weights ranging from 10^5 all the way to 10^{11} units. Although these large sized lipoproteins may be present at relatively low concentrations, nevertheless, practically all of the serum turbidity is the result of the presence in serum of lipoproteins of the molecular weight range from 10^6 to 10^{11} (approximately S_f 2 to S_f 40,000). Since the turbidity of *lipemic* serum is primarily related to the presence of one or more of the S_f 20–40,000 lipoprotein classes, it became of prime interest to determine the effect that heparin might have on the serum lipoproteins.

Graham, *et al.*,[5] found that following the parenteral administration of heparin in the human, there followed profound changes in certain classes of the low density lipoprotein "spectrum." The typical change in the lipoprotein "spectrum" occurring *in vivo* following heparin administration is the lowering or actual elimination of lipoproteins of the S_f 20–40,000 class. At the same time there are increases in concentration of lipoprotein of the S_f 0–20 class, although not compensatory on a concentration (or weight) basis for the loss of molecules of flotation rates higher than S_f 20. These events suggest that the lipoproteins of high flotation rates are converted *in vivo* to those of lower flotation rates. This shift in lipoprotein distribution is found to occur in serum or plasma samples within a matter of minutes following the administration of heparin and persists over a period of hours. Subsequently there follows a gradual return, generally complete within 24–48 hours, to the original preheparin lipoprotein spectrum.

A. Lipid Composition of Broad Band Lipoprotein Fractions before and after Intravenous Heparin Injection.—As an approach to the study of *in vivo* heparin induced lipoprotein changes, the chemical compositions of the lipoproteins were studied in a fasting individual before and 10 minutes after the administration of 100 mg. of sodium

(15) P. Hahn, *Science*, **98**, 19 (1943).

(16) N. G. Anderson and B. Fawcett, *Proc. Soc. Exper. Biol. Med.*, **74**, 768 (1950).

TABLE IV

THE CHEMICAL DISTRIBUTION OF LIPIDS AMONG THE LIPOPROTEINS BEFORE AND AFTER THE INJECTION OF HEPARIN

Lipoprotein class[a]	Cholesteryl ester heparin		Unesterified cholesterol heparin		Glycerides heparin		Unesterified fatty acid heparin		Phospholipid heparin	
	Pre	Post	Pre	Post	Pre	Post	Pre	Post	Pre	Post
S_f 20–400	35	14	28	17	177	27	9	5	76	20
S_f 0–20	143	145	38	57	55	43	7	35	70	77
S_f major high density lipoproteins	27	32	25	23	37	27	18	35	88	95
Total ultracentrifugal lipoprotein residue	7	20	3	10	3	17	7	57	..	..[b]
Total	212	211	94	107	272	114	41	132		

[a] All chemical values in this table represent the number of milligrams of lipid constituent in that quantity of each lipoprotein class to be found in 100 ml. of serum (or plasma). [b] Phospholipid analyses are not available for this ultracentrifugal fraction.

heparin. (The individual selected for this study was characterized by appreciable fasting levels of S_f 20–400, S_f 0–20 and major high density lipoprotein). His complete analytical ultracentrifugal characterization both pre-heparin and 10′ post-heparin is given in Fig. 1. In the composition study of this individual both the pre-heparin serum and the 10′ post-heparin plasma was fractionated into the three broad band lipoprotein fractions plus the ultracentrifugal lipoprotein residue.

Table IV presents the alterations in chemical distribution of lipids among the four ultracentrifugal fractions obtained before and 10 minutes after the heparin injection.

The pertinent observations are as follows:

Changes in the Total Serum.—(1) There is a 58% drop in total serum glyceride distributed throughout all four ultracentrifugal fractions. (2) There is approximately a 3.5-fold increase in the total serum concentration of unesterified fatty acids. This rise brings the total unesterified fatty acid content of serum (or plasma) much above physiologic levels usually encountered. (3) There is no significant change in the total content of either cholesteryl ester or of unesterified cholesterol.

Changes in the Ultracentrifugal Fractions.—(1) In the S_f 20–400 class there is a marked loss of all chemical constituents with the exception of unesterified fatty acids. The glyceride loss is the most marked. (2) In the S_f 0–20 class there is a marked rise in unesterified fatty acid content, a lesser rise of unesterified cholesterol, and a fall of border line significance in the glyceride content. (3) In the major high density lipoproteins there is a very marked rise in unesterified fatty acid content and a small but significant fall in glyceride content. (4) In the ultracentrifugal lipoprotein residue all components analyzed showed increases, especially marked being the rise in both unesterified fatty acids and glycerides.

The above findings are best interpreted after consideration of the changes in percentage composition of lipids in the lipoproteins. These changes are presented in Table V.

The marked loss from the serum of glyceride during the period following heparin injection is uniformly observed in individuals possessing appreciable levels of S_f 20–400 lipoproteins. Although the increased unesterified fatty acid levels following heparin administration suggest a lipolytic mechanism for glyceryl ester removal *via* hydrolysis, the possibility of glyceride removal from the serum *as glyceride* is not ruled out considering the *in vivo* study alone. That the latter mechanism for glyceride removal is not involved has been shown by *in vitro* studies in which S_f 20–400 lipoproteins were incubated with *in vivo* heparinized plasma. In such *in vitro* experiments similar marked decreases of triglycerides occurred. However, all such glyceride decreases have been shown[18] to result from the activation of a serum hydrolytic enzyme, by heparin injection, which hydrolyzes glycerides with the

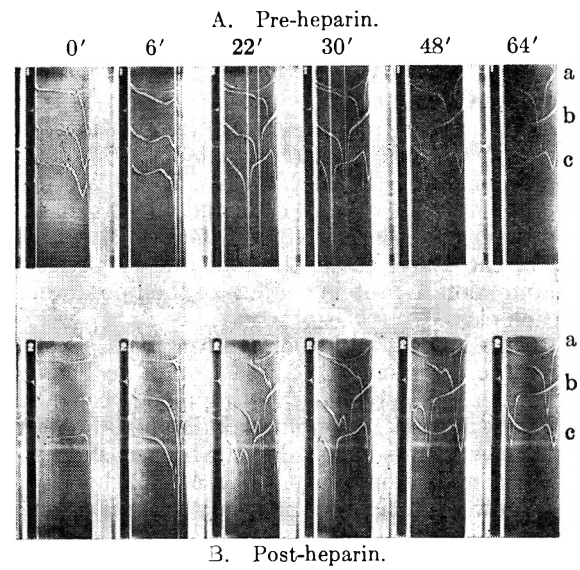

Fig. 1.—The ultracentrifugal lipoprotein photographs before (picture A) and 10 minutes after (picture B) the intravenous injection of 100 mg. of sodium heparin solution. Each picture shows 3 separate analytical ultracentrifugal runs: (a) upper pattern in all frames of both pictures represents ultracentrifugal flotation run at 1.063 g./ml.; (b) middle pattern in all frames of both pictures represents ultracentrifugal flotation run at 1.125 g./ml.; (c) lower pattern in all frames of both pictures represents ultracentrifugal flotation run at 1.200 g./ml. All runs are made at 52,640 r.p.m., 26°, distance from center of rotation to cell base = 72.5 mm., with photographic frames taken at 0, 6, 22, 30, 48 and 64 minutes after the rotor has reached full speed. (See reference 17 for further details of interpretation).

(17) O. deLalla and J. Gofman, "Methods of Biochemical Analysis," Vol. I, edited by D. Glick, Interscience Publishers, New York, N. Y., 1954.

(18) B. Shore, A. Nichols and N. Freeman, *Proc. Soc. Exper. Biol. Med.* **83**, 216 (1953).

TABLE V

THE CHEMICAL COMPOSITION OF SERUM LIPOPROTEINS BEFORE AND AFTER HEPARIN INJECTION

Lipoprotein class	Cholesteryl ester, %	Unesterified cholesterol, %	Glycerides, %	Unesterified fatty acids, %	Phospholipid, %
		S_f 20–400			
Pre-heparin	11	9	54	2	24
Post-heparin	18	20	32	6	24
		S_f 0–20			
Pre-heparin	46	12	18	2	22
Post-heparin	40	16	12	10	22
		Major high density lipoproteins			
Pre-heparin	14	13	19	9	45
Post-heparin	15	11	13	16	45

production of unesterified fatty acids. The above hydrolytic mechanism is the basis for the loss in glycerides both *in vitro* and *in vivo* together with the accompanying increase in unesterified fatty acids. Thus, in Table V the drop observed in glyceride content of S_f 20–400 lipoproteins is on this basis.

The unesterified fatty acids produced by the heparin activated hydrolysis of glycerides have become distributed largely to three ultracentrifugal fractions, namely, to S_f 0–20 class, the major high density lipoprotein class, and to the ultracentrifugal residue. However, the total unesterified fatty acids recovered from the post-heparin plasma fractions account for only 62% of the unesterified fatty acids that must have been liberated by glyceride hydrolysis. Thus, 38% of the liberated fatty acids may have attached themselves to the formed elements[19] present in the blood stream or in some way were removed entirely from the blood compartment during the 10 minutes following the heparin injection. Further study is needed to resolve the fate of this fraction of the hydrolyzed glyceride.

Table IV shows no significant change in total cholesteryl ester content. This is consistent with the findings of Shore and co-workers[18] who showed that neither phospholipid nor cholesteryl ester serves as a substrate for the heparin activated lipolytic enzyme. However, from Table IV there appears to be a shift of some cholesteryl ester from the S_f 20–400 (the lipoproteins that were largely transformed) into the lipoprotein residue. Also in the course of the heparin-induced lipoprotein transformation there appears to be a shift of some unesterified cholesterol from the S_f 20–400 lipoproteins into the ultracentrifugal lipoprotein residue. However, as might be expected the total serum content (see Table IV) of unesterified cholesterol remains unchanged.

The lipoprotein chemical composition changes accompanying the *in vivo* lipoprotein transformation can be considered from the data presented in Table V. During the 10 minutes following the heparin injection much of the S_f 20–400 lipoproteins originally present were transformed. What residual S_f 20–400 lipoproteins that were present were highly weighted toward the S_f 20 region, whereas the original S_f 20–400 lipoproteins were distributed throughout the S_f 20–400 region. Thus the shift from 11 to 18% cholesteryl ester content of S_f 20–400 lipoproteins before and after heparin injection is consistent with the chemical data of section IA which indicated that lipoproteins of flotation rate near S_f 20 are normally much higher in cholesteryl ester than those of higher flotation rates. The fall in glyceride percentage from 54% in pre-heparin S_f 20–400 to 32% in post-heparin S_f 20–400 is also consistent with the chemical data of section IA. However, the relatively high percentage of unesterified cholesterol in the post-heparin residual S_f 20–400 lipoproteins is greater than would be expected from the chemical data of IA for such lipoproteins. Lipoproteins of flotation rates well above S_f 20 have more unesterified cholesterol in relation to the cholesteryl ester content than do lipoproteins of flotation rates near S_f 20. It would therefore appear that the post-heparin residual S_f 20–400 lipoproteins have attached some of the excess available unesterified cholesterol, thus accounting for the relatively high percentage of this constituent in the post-heparin S_f 20–400 lipoproteins. In contrast to the other lipid constituents, the phospholipid composition of the post-heparin and the pre-heparin S_f 20–400 lipoproteins is not significantly altered.

The post-heparin S_f 0–20 class lipoproteins are shifted in distribution toward S_f 20 from slower flotation rates because of the influx of lipoprotein into this class as a result of the transformation of part of the S_f 20–400 into S_f 0–20 lipoproteins, especially into the S_f 10–20 region of this class. Thus, the slight fall in cholesteryl ester percentage and the rise in unesterified cholesterol percentage observed in Table V for post-heparin S_f 0–20 are consistent with the chemical composition data of IA for such lipoproteins. There appear to be no significant changes in percentage composition of phospholipid in pre-heparin *versus* post-heparin S_f 0–20 lipoproteins, which also is consistent with the chemical data of IA for such lipoproteins.

For the major high density lipoproteins the data of Table V reveal no appreciable changes in percentage composition with respect to cholesteryl ester, unesterified cholesterol or phospholipid, suggesting that no drastic alterations in these constituents of the high density lipoproteins has occurred as a result of the action of the heparin-activated lipoprotein transforming system. The slight fall in glyceride percentage of these lipoproteins, significant, suggests the possibility that some of this glyceride can serve as a substrate for the heparin-activated enzyme.

In the ultracentrifugal residue it is of great interest to note the significant accumulation of such lipids as cholesteryl ester, unesterified cholesterol, glyceride and unesterified fatty acid. Although the phospholipid fraction was lost to analysis, there is reason to suspect that phospholipid also may have

(19) Unfortunately total pre-heparin and total post-heparin *blood* unesterified fatty acid levels were not analyzed.

increased in the ultracentrifugal lipoprotein residue. For the four lipid constituents analyzed, approximately one-fifth of the total serum lipids after heparin action are to be found in the ultracentrifugal lipoprotein residue. Expressed otherwise, this represents the unusual situation where one-fifth of the serum lipids are to be found elsewhere than in the usual lipoprotein "spectrum." The physicochemical form of these lipid constituents is at present not known, although there is good reason to believe[19,20] that a large part of the unesterified fatty acids in the residue is associated chemically with albumin. Whether or not the remaining lipid constituents of the residue are in some way bound to proteins in the form of sub-structural units involved in synthesis of the usual lipoproteins remains a question for future resolution.

In the above considerations attention was focussed upon the *in vivo* effects of heparin injection upon serum lipoproteins. The concept of transformation of such lipoproteins as S_f 20–400 into S_f 0–20 lipoproteins has been directly verified by *in vitro* studies.

B. *In Vitro* Lipoprotein Transformations.—Since post-heparin plasma contains some low density lipoproteins of the S_f 0–20 and S_f 20–400 classes, it is advantageous to remove all such lipoproteins from such plasma before utilizing the heparin activity in such plasma for transformation studies. With these S_f 0–20 and S_f 20–400 lipoproteins removed, it becomes possible to study the net ultracentrifugal changes resulting from the interaction of the active constituents of post-heparin plasma with such a substrate as isolated S_f 20–400 lipoproteins. High salt concentrations destroy the activity of post-heparin plasma. Hence to allow ultracentrifugal removal of the S_f 0–400 lipoprotein, deuterium oxide (D_2O) made up to 0.9% NaCl was used to raise the solution density to 1.063 g./ml. (see Methods). The plasma so treated is then ultracentrifuged at 104,000 × *g* for 24 hours. All detectable lipoprotein-transforming activity of the original post-heparin plasma is contained in the bottom 2 ml. (out of a total preparative tube content of 6 ml.), which is hereafter referred to as the *post-heparin active fraction.* In addition to all the serum proteins, there is also present in this active fraction the two high density lipoproteins (HDL_2 and HDL_3). An isolation of S_f 20–400 lipoproteins, free of other lipoproteins and proteins, was made from a non-heparinized subject by the preparative centrifugal techniques described under Methods. This preparation served as the substrate for transformation studies. The following types of *in vitro* incubation at 37° for 2 hours were performed[21]: (a) incubation of isolated S_f 20–400 lipoproteins alone; (b) incubation of isolated S_f 20–400 lipoproteins mixed with the above-described bottom fraction obtained from *pre*-heparin serum. (c) Incubation of isolated S_f 20–400 lipoproteins mixed with the above-described bottom fraction obtained from *post*-heparin plasma.

(20) D. Robinson and J. French, *Quart. J. Exper. Physiol.*, **38**, 233 (1953).

(21) Incubations were actually performed in 6 ml. preparative centrifuge tubes to which had been added a sufficient volume of D_2O–NaCl solutions to make up a final volume of 6 ml. at a density of 1.063 g./ml.

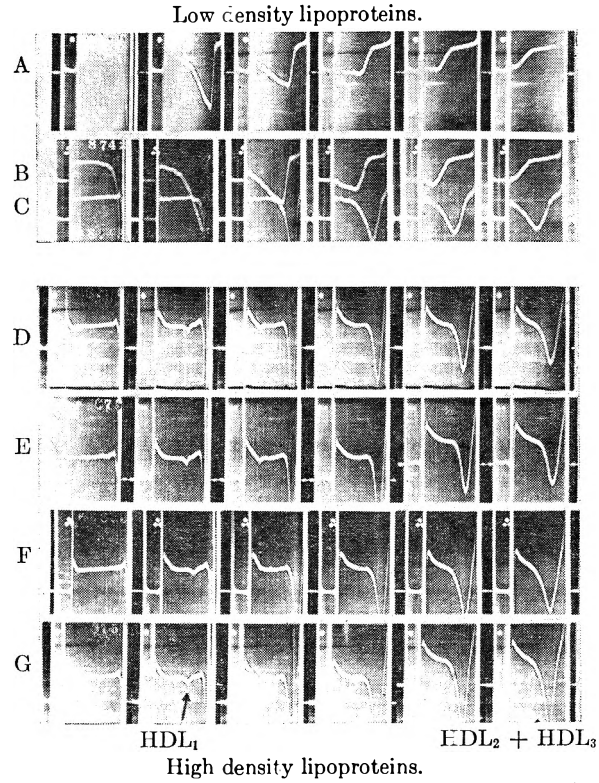

Fig. 2. Ultracentrifugal lipoprotein photographs for the incubation of isolated S_f 20–400 lipoproteins with bottom fraction from pre-heparin serum and post-heparin "active fraction." Pictures A, B and C are low density ultracentrifuge runs (density = 1.063 g./ml.) for the study of the original S_f 20–400 lipoproteins and the low density transformation products. Pictures D, E, F and G are high density ultracentrifuge runs (density = 1.24 g./ml.) for the study of high density lipoproteins in the "active fraction" before and after incubation. All runs made at 52,640 r.p.m. at 26° (center of rotor to cell base = 72.5 mm.). In pictures A, B and C, frames are taken at 2-minute intervals after full rotor speed. In pictures D, E, F and G frames are taken at 16-minute intervals after full rotor speed. In picture A is noted the original isolated S_f 20–400 lipoproteins. In picture B is noted the pattern obtained after incubation of S_f 20–400 substrate with pre-heparin bottom fraction. Note the absence of any significant alterations in the S_f 20–400 lipoproteins. In picture C is noted the pattern obtained after incubation of S_f 20–400 substrate with post-heparin "active fraction." Note the marked decrease in S_f 20–400 lipoproteins as compared with Pictures A and B, and the appearance *de novo* of S_f 0–20 lipoproteins. In picture D is noted the high density lipoprotein pattern for the HDL_1, HDL_2 and HDL_3 lipoproteins of the bottom fraction of pre-heparin serum. In picture E is noted the high density lipoprotein pattern for HDL_1, HDL_2 and HDL_3 lipoproteins of the "active" bottom fraction of post-heparin plasma. In picture F is noted the high density lipoprotein pattern after incubation of S_f 20–400 substrate with pre-heparin bottom fraction. Note absence of any significant change as compared with picture D. In picture G is noted the high density lipoprotein pattern after incubation of S_f 20–400 substrate with post-heparin "active fraction." Note that the only change in high density lipoprotein pattern is a slight increase (approximately 10%) in area (and hence concentration of the HDL_2 plus HDL_3 group of lipoproteins).

The quantitative relationships were such that the S_f 20–400 lipoprotein content of one milliliter of serum was incubated with the "active fraction" present in one milliliter of post-heparin plasma (or one milliliter of the control fraction from pre-heparin serum). Following incubation the low density and high density lipoproteins were isolated successively and separately by successive preparative ul-

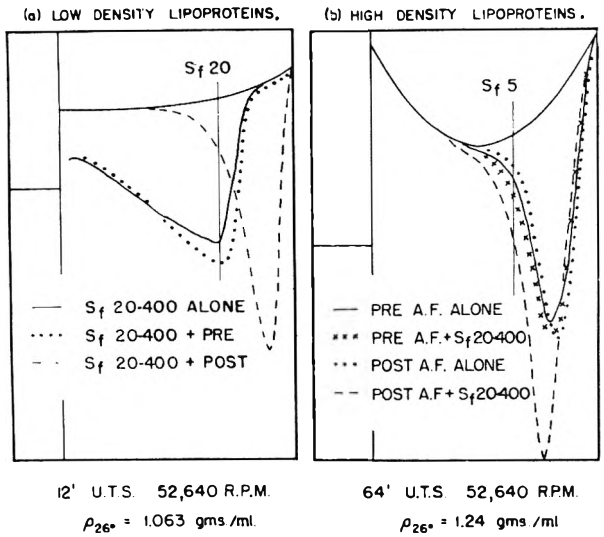

Fig. 3.—*In vitro* transformation of S_f 20–400 lipoproteins by an "active fraction" from post-heparinized plasma: (a) the low density lipoproteins; (b) the high density lipoproteins.

tracentrifugations at 1.063 and 1.24 g./ml. These separate fractions were then subjected to analytical ultracentrifugation. The analytical ultracentrifugal photographs for all incubations are presented in Fig. 2. In order to compare readily the fate of the S_f 20–400 substrate in the various incubations, tracings of Frame 3 of the low density analytical runs are superimposed in Fig. 3a.

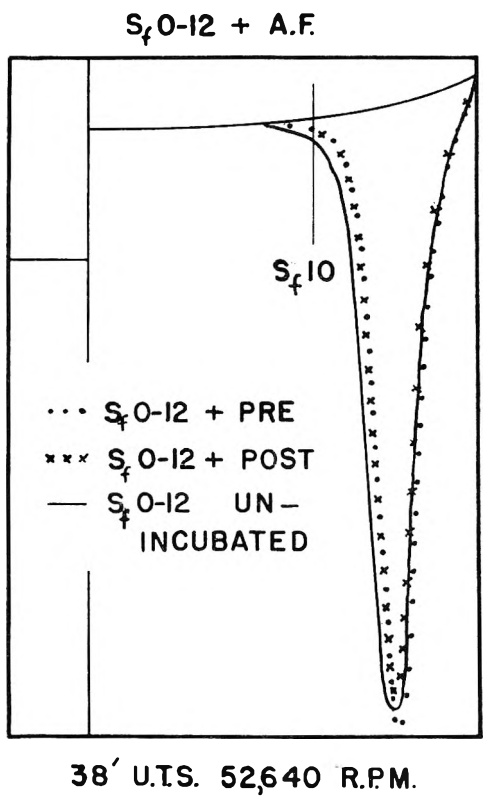

Fig. 4.—Comparison of S_f 0–12 substrate alone, after incubation with pre-heparin bottom fraction, and after incubation with post-heparin "active fraction." Note the insignificant alteration in S_f 0–12 lipoproteins, indicating that the heparin "active fraction" affects this lipoprotein flotation class minimally, if at all.

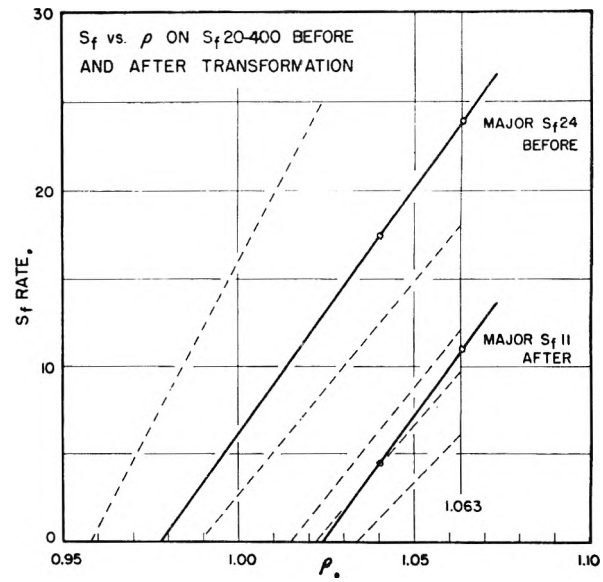

Fig. 5.—Flotation rate *versus* solution density study on pre-incubation S_f 20–400 substrate and post-incubation S_f 0–20 product. The extrapolated lines across the abscissa at the respective hydrated densities of the lipoproteins. The broken lines indicate S_f rate *versus* solution density data for isolated lipoproteins obtained without heparinization.

It is seen from inspection of Figs. 2 and 3a that the bottom fraction from pre-heparin serum has failed to influence the ultracentrifugal distribution of the S_f 20–400 substrate. In marked contrast the post-heparin "active fraction" has effected an essentially quantitative transformation of the S_f 20–400 substrate into lipoproteins of flotation rates of S_f 0–20. This directly observed *in vitro* transformation resembles strikingly the alteration in lipoproteins of this group observed *in vivo* (see Fig. 1).

With respect to high density lipoproteins, Fig. 2 shows there has been no detectable alteration in HDL_1 lipoprotein nor any appreciable production of high density lipoproteins. There is no detectable effect of incubation of preheparin bottom fraction with S_f 20–400 upon the HDL_2 and HDL_3 high density lipoproteins. However, there appears to be a small increase of approximately 10% in the concentration of (HDL_2 + HDL_3) lipoproteins as a result of the incubation of S_f 20–400 substrate with post-heparin "active fraction" (see Fig. 3b). From considerations earlier in the section on *in vivo* studies, it is anticipated that part of the fatty acid released during transformation of S_f 20–400 lipoproteins would become associated with the (HDL_2 + HDL_3) lipoproteins. The expected quantity of fatty acid released during this *in vitro* incubation might account for the ultracentrifugally observed increment in HDL_2 + HDL_3 concentration.

Similar *in vitro* transformation studies were performed utilizing isolated lipoproteins of the S_f 0–12 class as substrate. The data are presented in Fig. 4. It is seen that no significant transformation of the S_f 0–12 lipoprotein class is effected either by incubation with pre-heparin bottom fraction or post-heparin "active fraction." These findings are consistent with the experience that *in vivo* heparinization of individuals whose low density lipoprotein

patterns show no significant levels of lipoproteins above S_f 12 produces minimal, if any, lipoprotein transformation.

The question arises as to whether the *in vitro* produced S_f 0–20 lipoproteins are comparable with physiologically occurring S_f 0–20 lipoproteins. Physico-chemical studies of the hydrated density of the most abundant species of the S_f 20–400 substrate and that of the *in vitro* produced S_f 0–20 lipoproteins were determined by measurement of flotation rates *versus* solution density. By measurement of flotation rates in two solutions of different (but known) densities, the density corresponding to zero migration rate can be determined by extrapolation. This density is taken as the hydrated density of the lipoprotein under study. Figure 5 shows the S_f rate *versus* solution density determinations. The most abundant species of the S_f 20–400 substrate exhibit a hydrated density of 0.978 g./ml., whereas the most abundant species of the S_f 0–20 lipoproteins produced *in vitro* show a hydrated density of 1.024 g./ml. Comparison with data[3] on flotation rate *versus* solution density obtained for isolated human lipoproteins (obtained without heparinization) in the same S_f neighborhood indicates that the *in vitro* produced S_f 0–20 lipoproteins are closely similar to if not identical with physiologically-occurring lipoproteins of the same flotation rates.

Acknowledgment.—The authors wish to express their appreciation to Dr. John W. Gofman for his many helpful criticisms and suggestions given during the course of this investigation.

DISCUSSION

S. J. SINGER.—In a system of components in equilibrium, ultracentrifuge patterns and resolutions may depend on rates of re-equilibration reactions accompanying the separation of the components. Is there any evidence that serum. lipoproteins are in reversible equilibrium with one another?

F. T. Lindgren.—Yes. There is limited evidence that some of the lipid constituents of the serum lipoproteins are in a slow equilibrium with one another. We have some *in vitro* 37° incubation studies with in viro H^3 labelled glyceride which show that a glyceride label introduced in the S_f 20-400 lipoprotein class will migrate slowly to the higher density lipoprotein classes containing glyceride. Similarly labelled glyceride in the high density lipoprotein class will migrate into the glyceride portion of the low density lipoproteins.

We are currently evaluating the problem of equilibrium of the lipid portions of the major lipoprotein classes with one another under the actual conditions of the ultracentrifugal isolation.

L. J. MILCH.—In view of the proven instability of the lipoprotein class, it would seem that their lipid compositions would become a function of storage time prior to ultracentrifugal fractionation. Furthermore, successive analyses of the same serum sample should show varying lipid compositions. Would you care to comment?

F. T. LINDGREN.—Most of the short term "proven" instability studies on isolated lipoproteins deal with instability as the result of dialysis. Some evidence, particularly that obtained by Dr. Roger Ray, suggests this instability to be the result of an oxidative process catalized by Cu^{++} ion. Dr. Ray also has found that the small molecule background serum contains dialyzable substances which protect isolated lipoproteins against this degradation process. We generally complete our lipoprotein fractionation three or four days after the serum is obtained. During this fractionation procedure there is always present in the solution containing the lipoproteins some of this protective serum background solution.

The instability of lipoprotein, particularly isolated lipoproteins, is a very real problem. In all our studies we fractionate ultracentrifugally as soon as possible and after each lipoprotein fraction is obtained we immediately extract.

We have not yet made any specific studies of what effect prolonged serum storage may have on the chemical composition of the ultracentrifugally isolated lipoprotein classes.

STUDIES ON THE INTERACTION OF DESOXYRIBONUCLEIC ACID WITH ACRIFLAVINE[1]

BY HARRIET G. HEILWEIL AND QUENTIN VAN WINKLE

Department of Chemistry, The Ohio State University, Columbus 10, Ohio

Received February 25, 1955

The interaction of a high molecular weight sample of calf thymus desoxyribonucleic acid (DNA) with the fluorescent cationic dye acriflavine was studied in the concentration range where soluble complexes are formed and was found to be reversible. Determinations of the amount of binding were made over a wide range of equilibrium concentrations of unbound acriflavine, at several values of the experimental variables ionic strength, *p*H and temperature, by means of the partition analysis method. It was found that the binding sites for acriflavine on the DNA molecule are heterogeneous with respect to their intrinsic association constants and that the binding curves may be described in terms of a two-constant equation. The maximum number of sites available for complexing with acriflavine per DNA phosphate group is approximately 0.5 at ionic strength 0.002 at *p*H 7. A method for the treatment of fluorescence quenching data was developed which takes into account the multiple equilibria involved in macromolecular interactions. This method yields values for k_1, the equilibrium constant for the first DNA–acriflavine association, in agreement with the independent partition analysis results. As is expected for an electrostatic interaction, k_1 decreases with increasing ionic strength and with decreasing *p*H, but the evidence indicates that secondary binding forces are important. The enthalpy changes are rather large and negative. The corresponding standard entropy changes are zero within experimental error, suggesting that the macromolecular configuration of DNA does not change significantly upon interaction with acriflavine.

Introduction

It is expected that quantitative investigation of the interactions of desoxyribonucleic acid (DNA), under diverse experimental conditions, will provide information concerning the macromolecular configuration of DNA in solution and the mode of interaction of DNA in biological processes. Progress along similar lines has been made in the field of protein research,[2] and the work on protein interactions has yielded methods and concepts many of which are applicable in the study of binding by DNA. Among the more recent DNA binding studies which have been reported are a number on the complexing with inorganic cations,[3-7] with proteins,[8-12] and with small organic ions and molecules.[13-16] Several of these investigations are concerned with the interactions with DNA of certain biologically active quinoline and acridine derivatives.[13,16] Oster[13] determined that the quenching of the fluoresence of acriflavine, 3,6-diamino-10-methylacridinium chloride, by DNA is related to complex formation between the dye cation and the negatively charged phosphoric acid groups of the DNA. In the present paper fluorescence quenching data are used, in accordance with the mass law treatment of multiple equilibria,[2] to derive constants for the binding of acriflavine by a high molecular weight preparation of DNA. The results are corroborated by independent binding experiments carried out according to the partition analysis method described by Karush.[17]

Experimental

Materials.—The sodium salt of DNA used in these studies was prepared from calf thymus according to the procedure of Schwander and Signer[18] and the recommendations of Doty and Bunce.[19] The nucleate solution was diluted 1:1 with water before the first alcohol precipitation; the second alcohol precipitation was achieved by pouring one volume of aqueous nucleate into four of NaCl-saturated alcohol. The fibrous product was vacuum dried at 4°, using no drying agent, and stored at 4° in covered bottles in a desiccator over P_2O_5, care being taken to prevent contamination of the nucleate by P_2O_5 dust. The molecular weight was determined by I. J. Heilweil of this Laboratory from angular light scattering measurements in 0.2 *M* NaCl to be 1×10^7, based upon a measured refractive index increment of 0.160. In water, at 259 mμ, $E^{1\%}_{1\,cm.}$ 238, and at 231 mμ, $E^{1\%}_{1\,cm.}$ 89.4. In 0.2 *M* NaCl, at 259 mμ, $E^{1\%}_{1\,cm.}$ 204. The dry weight of nucleate samples was obtained by correcting for the moisture content after comparing, under identical humidity conditions, the sample weight with the weight of a reference sample. The dry weight of the reference sample had been determined by extrapolation to infinite time of a curve of reference sample weight, measured every few days over a month's time, *versus* reciprocal of vacuum drying time at 4°. For a particular sample, dry weight obtained in this way agreed with that determined by vacuum drying to constant weight at 100°. The DNA fibers were dissolved as needed in pre-cooled distilled water, using a magnetic stirrer at moderate speeds for 8–12 hours at 4°.

A sample of commercial acriflavine (National Aniline) was purified to remove proflavine hydrochloride by the method given by Albert.[20] Analysis for Cl gave 13.52% compared with 13.65% calculated for $C_{14}H_{14}N_3Cl$. For all extinction measurements made on acriflavine solutions, there was mounted on the Beckman DU spectrophotometer an exit filter having zero transmission for the green wave lengths of the fluorescence peak. At 452 mμ, $E^{1\%}_{1\,cm}$ 1640 in water and at *p*H 5.5, ionic strength (μ) = 0.1, 1720 at *p*H 7, μ = 0.002, and 1810 at *p*H 7, μ = 0.1 and 0.3, independent of the presence of dissolved *n*-hexanol. Deviations from Beer's law become significant at concentrations higher than 1×10^{-3}%. In *n*-hexanol saturated at 25°

(1) Taken from a dissertation submitted by H. G. Heilweil to the Graduate School of The Ohio State University in partial fulfillment of the requirements for the degree Doctor of Philosophy, 1954.

(2) I. M. Klotz in H. Neurath and K. Bailey, "The Proteins," Vol. I, Part B, Academic Press, Inc., New York, N. Y., 1953, p. 727.

(3) J. Shack, R. J. Jenkins and J. M. Thompsett, *J. Biol. Chem.*, **198**, 85 (1952), **203**, 373 (1953).

(4) A. Veis, THIS JOURNAL, **57**, 189 (1953).

(5) S. Katz, *J. Am. Chem. Soc.*, **74**, 2238 (1952).

(6) C. Neuberg and I. S. Roberts, *Arch. Biochem.*, **20**, 185 (1949).

(7) K. G. Stern and M. A. Steinberg, *Biochim. Biophys. Acta*, **11**, 553 (1953).

(8) E. P. Geiduschek and P. Doty, *ibid.*, **9**, 609 (1952).

(9) R. F. Steiner, *Arch. Biochem. Biophys.*, **46**, 291 (1953).

(10) D. P. Riley and U. W. Arndt, *Nature*, **172**, 294 (1953).

(11) P. Alexander, *Biochim. Biophys. Acta*, **10**, 595 (1953).

(12) C. F. Crampton, R. Lipshitz and E. Chargaff, *J. Biol. Chem.*, **206**, 499 (1954).

(13) G. Oster, *Trans. Faraday Soc.*, **47**, 660 (1951).

(14) L. F. Cavalieri and A. Angelos, *J. Am. Chem. Soc.*, **72**, 4686 (1950); L. F. Cavalieri, A. Angelos and M. E. Balis, *ibid.*, **73**, 4902 (1951).

(15) N. B. Kurnick, *ibid.*, **76**, 417 (1954).

(16) J. L. Irvin and E. M. Irvin, *J. Biol. Chem.*, **206**, 39 (1954).

(17) F. Karush, *J. Am. Chem. Soc.*, **73**, 1246 (1951).

(18) H. Schwander and R. Signer, *Helv. Chim. Acta*, **33**, 1521 (1950).

(19) P. Doty and B. H. Bunce, *J. Am. Chem. Soc.*, **74**, 5029 (1952).

(20) A. Albert, "The Acridines," Edward Arnold and Co., London, 1951, p. 197.

with any of the buffers employed, $E^{1\%}_{1\,cm.}$ 2340 at 470 mμ, and Beer's law is obeyed for concentrations at least as high as $5 \times 10^{-4}\%$. Since dilute acriflavine solutions were found to decrease slowly in concentration on standing, solutions were prepared fresh from the solid dye as needed, measured as soon as feasible, and kept in the dark as much as possible to minimize photooxidation.

Potassium phosphate buffers, prepared with the aid of the data of Green,[21] were used throughout.

Methods (a). Partition Analyses.—*n*-Hexanol was found to be a suitable organic solvent for the partition analysis study of the DNA-acriflavine system.[17] Eastman Kodak Technical Grade *n*-hexanol was washed with 0.01*N* NaOH, then with distilled water, and, finally, saturated with the buffer to be used in a given experiment at the temperature of the experiment. Equilibrations were carried out in pharmaceutical bottles with polyethylene snap-on caps. For each binding determination 10 ml. of washed *n*-hexanol was added to 10 ml. of aqueous solution containing DNA, acriflavine, and buffer at the desired concentrations. For each set of experimental conditions a series of blanks containing no DNA was prepared in order to determine the partition coefficients of acriflavine between the two phases over the concentration range covered in the corresponding partition experiments. The bottles were mechanically shaken at about 60 cycles per minute, for four hours, either in a cold room at 4 ± 1° or in a constant temperature room at 25 ± 1°. The free dye concentration in the organic layer was determined either spectrophotometrically in 1 cm. cells for the more concentrated solutions, or by measurement of the fluorescence intensities of the dilute ones. In the case of the blanks, both the aqueous and organic layers were analyzed.

Fluorescence measurements were made on an Aminco high sensitivity photometer designed by Oster[22] (American Instrument Co., Silver Spring, Md.) at 90° to the incident beam, with incident light of wave length 436 mμ and a yellow-green exit filter.

(b). Fluorescence Quenching Measurements.—Fluorescence quenching data were obtained by titrating a buffered acriflavine solution with a DNA solution at the same concentrations of dye and buffer. A total of about 10 ml. of the DNA–acriflavine solution was added in suitable increments, from a buret graduated to 0.02 ml., to 15 ml. of the solution containing no DNA in the square cell provided with the Aminco photometer. The solution was stirred magnetically between additions. The procedure, including the measurement of fluorescence, was carried out in the constant temperature room at 25 ± 1° or in the cold room at 4 ± 1°, as required. It should be noted that the acriflavine concentrations used in the quenching experiments fell on the essentially straight-line portion of the fluorescence–concentration curve.

Results

The partition analysis results are presented in Fig. 1, in which r, the number of moles of acriflavine bound per mole of DNA nucleotide (assuming an average nucleotide weight of 331), is plotted against r/c, c being the equilibrium molar concentration of acriflavine. The reversibility of the interaction was tested by replacing known volumes of equilibrated organic layers with fresh *n*-hexanol (Fig. 1B). In addition, binding data taken at a DNA concentration of 0.01% fall in with the results at 0.005% DNA (Fig. 1E). Although the method of equilibrium dialysis using cellophane membranes is not suited to quantitative study of acriflavine binding because of excessive membrane adsorption, the satisfactory agreement between results obtained by this technique and those from partition analysis (Fig. 1E) indicates that *n*-hexanol does not interfere in the DNA–acriflavine interaction.

The curves in Fig. 1 were calculated from the equation

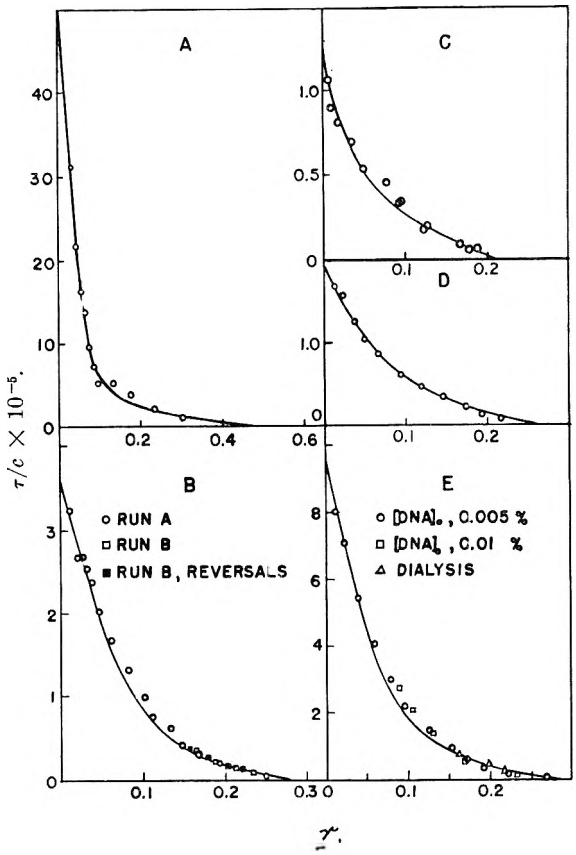

Fig. 1.—Partition analysis results for DNA–acriflavine binding; $[DNA]_0$ = 0.005% except as noted. Points correspond to experimental data. Curves calculated according to the two-constant method: curve A, μ = 0.002, *p*H 7.0, T = 25°; curve B, μ = 0.10, *p*H 7.0, T = 25°; curve C, μ = 0.30, *p*H 7.0, T = 25°; curve D, μ = 0.10, *p*H 5.5, T = 25°; curve E: μ = 0.10, *p*H 7.0, T 4°.

$$\frac{r}{c} = \frac{n_a K_a}{1 + K_a c} + \frac{n_b K_b}{1 + K_b c} \qquad (1)$$

on the assumption that the n DNA binding sites can be divided into two groups, each containing n_i sites having the same intrinsic binding constant, K_i.[23] The intercepts

$$\lim_{r/c \to 0} (r) = n_a + n_b = n \qquad (2)$$

and

$$\lim_{r \to 0} (r/c) = n_a K_a + n_b K_b = k_1 \qquad (3)$$

were selected so as to give the best fit obtainable over the whole range of r. k_1 in equation 3 is the equilibrium constant for the formation of the complex containing one molecule of acriflavine per DNA molecule. Theoretical curves of r/c *versus* r constructed on the basis of adsorption isotherms derived by Sips[24] for two continuous distributions of binding energies could not be made to fit the data. When the logarithm of the function $Q = r/(n - r)c$ is plotted against r, as recommended by Scatchard,[25] taking the value of n determined according to equation 2, the resultant straight lines yield, in accordance with $(\lim_{c \to 0,\ r \to 0} Q) = (k_1/n)$, values for k_1 in

(21) A. A. Green, *J. Am. Chem. Soc.*, **55**, 2331 (1933).
(22) G. Oster, *Anal. Chem.*, **25**, 1165 (1953).
(23) F. Karush, *J. Am. Chem. Soc.*, **72**, 2705 (1950).
(24) R. Sips, *J. Chem. Phys.*, **16**, 490 (1948); **18**, 1024 (1950).
(25) J. T. Edsall, G. Felsenfeld, D. S. Goodman and F. R. N. Gurd, *J. Am. Chem. Soc.*, **76**, 3054 (1954).

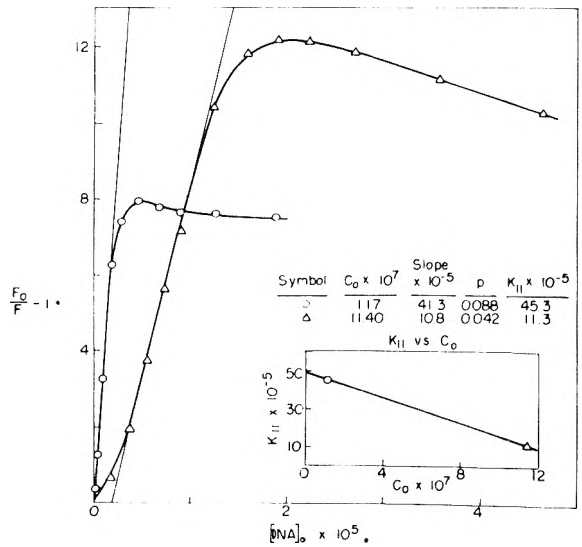

Fig. 2.—Fluorescence quenching curves at μ = 0.002, pH 7.0 and T = 25°.

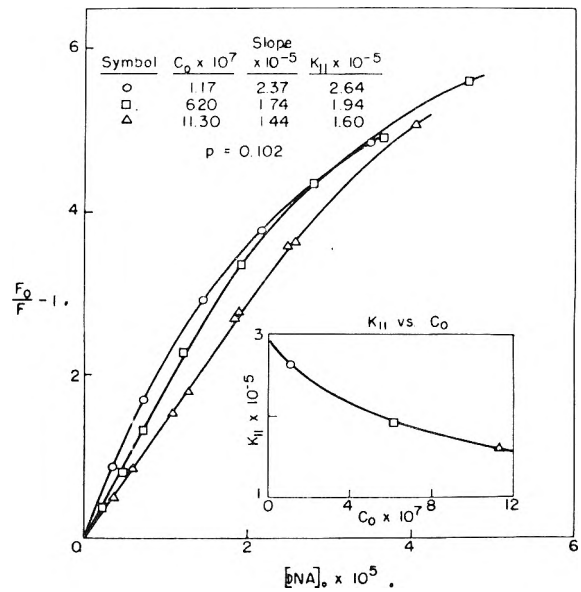

Fig. 3.—Fluorescence quenching curves at μ = 0.10, pH 7.0 and T = 25°.

satisfactory agreement with those obtained by the other extrapolation methods. The data at μ = 0.002, however, were not readily treated in this manner, perhaps because of the large effect of experimental errors. Finally, values of k_1 were calculated from the partition analysis data according to a third method, that of Steiner,[26] which requires no knowledge of n.

If it is assumed that the ratio, p, of the quantum yields of fluorescence of bound and free fluorescent molecules is the same for all bound molecules, then fluorescence quenching data may be expressed by the equation[13]

$$\frac{F_0}{F} - 1 = \frac{(1 - p)c_b}{c + pc_b} \qquad (4)$$

where F is the fluorescence intensity in the presence of quencher of a dye solution at initial concentration c_0, F_0 the fluorescence intensity without quencher, and c_b is the equilibrium concentration of bound dye. Oster[13] made the further assumption that the DNA–acriflavine interaction is represented by

$$\text{DNA} + \text{A} \rightleftharpoons \text{DNA-A}, \quad K_{11} = c_b/[\text{DNA}]c \qquad (5)$$

where A stands for acriflavine, and c_b = [DNA–A]. K_{11} was determined from the initial slope and limiting value of a quenching curve $(F_0/F) - 1$ *versus* $[\text{DNA}]_0$, the initial concentration of DNA, at constant c_0, in accordance with the relationships

$$\left[\frac{F_0}{F} - 1\right]_{\substack{[\text{DNA}]\to 0 \\ c_b \to 0}} = (1 - p)K_{11}[\text{DNA}] \qquad (6)$$

and

$$\left[\frac{F_0}{F} - 1\right]_{\substack{[\text{DNA}]\to \infty \\ c \to 0}} = (1 - p)/p \qquad (7)$$

It was necessary to assume that [DNA] $\cong$ $[\text{DNA}]_0$ at low c_0. Basic to all three of the treatments of the partition analysis data employed is the concept that a number of independent binding sites are available on the DNA molecule and that these are simultaneously in equilibrium with acriflavine.[2] This requires that the first complex, DNA–A, can exist in the absence of DNA–A_2, DNA–A_3, . . ., DNA–A_n only in solutions very dilute with respect to dye. Accordingly, Oster's quenching method should be modified: A value of the quantity denoted as K_{11} is determined from each of several quenching curves obtained at different dye concentrations c_0 (equation 6). Then, the value of K_{11} extrapolated to $c_0 = 0$ is k_1. At $c_0 = 0$, also, $[\text{DNA}]_0 = [\text{DNA}]$.

The quenching curves obtained in this investigation, contrary to the prediction of equation 4, go through a maximum, then slowly level off at high $[\text{DNA}]_0$, indicating that p is not constant for the system. This is especially evident when the amount of binding is high, as, for example, in the run at low ionic strength (Fig. 2). Since K_{11} is insensitive to the value of p, it was decided to estimate for p a value which would hold fairly well in the range of low $[\text{DNA}]_0$. This was accomplished by plotting F_0/F against $1/[\text{DNA}]_0$ and extrapolating the rising portion of the curve to $1/[\text{DNA}]_0 = 0$ (equation 7). The initial curvature in quenching curves where binding is relatively extensive (Fig. 2) is attributed to the fact that $[\text{DNA}]_0$, rather than [DNA], is plotted. In these cases, the slope of the linear portion, rather than the initial slope, was used in the calculation of K_{11}. Although the graph of K_{11} *versus* c_0 is slightly curved (Fig. 3, insert), the values of k_1 obtained by linear extrapolation to $c_0 = 0$ when quenching data were available at only two dye concentrations are in satisfactory agreement with those from partition analysis.

In Table I are listed the results for k_1 obtained by the several methods discussed under the various conditions of μ, pH, and temperature studied, together with the thermodynamic constants and the values for K_i, n_i and n. Figure 4 shows the variation of k_1 and of log k_1 with μ at 25° and at 4°. Each open symbol represents a value for k_1 estimated from quenching data at a single c_0 and from a consideration of the slopes of K_{11} *versus* c_0, assumed independent of c_0, as a function of μ.

(26) R. F. Steiner, *Arch. Biochem. Biophys.*, **47**, 56 (1953).

TABLE I

CONSTANTS FOR THE INTERACTION OF DNA WITH ACRIFLAVINE

μ		0.002	0.10	0.30	0.10	0.10
pH		7.0	7.0	7.0	5.5	7.0
T (°C.)		25	25	25	25	4
$k_1 \times 10^{-5}$	Partition Anal.:					
	Two-constant method	50.0	3.63	1.20	1.93	9.55
	Method of Scatchard	...	3.48	0.99	1.84	9.43
	Method of Steiner	49.3	3.35	1.03	1.78	9.39
$k_1 \times 10^{-5}$	Quenching-slope method	49.0	2.90	0.92	1.96	9.22
$k_{1av} \times 10^{-5}$		49	3.3	1.1	1.9	9.4
$-\Delta F_1°$, kcal./mole		9.1	7.5	6.8	7.2	7.6
$-\Delta H_1°$, kcal./mole			8.1			
$-\Delta S_1°$, cal./°K./mole			1.9			
$K_a \times 10^{-6}$		67	3.9	2.8	2.5	12
$K_b \times 10^{-5}$		4.8	1.3	1.8	1.8	3.4
n_a		0.07	0.09	0.03	0 06	0.08
n_b		0.43	0.20	0.18	0.20	0.21
n		0.50	0.285	0.208	0.262	0.285

The reversibility of the DNA–acriflavine interaction was checked by determining that the value of F for a given solution at a given temperature is independent of the temperature at which the components are mixed. Since F is time-independent in quenching titrations, equilibrium must be attained rapidly.

Qualitative experiments to determine whether DNA interacts with several cationic compounds were carried out at $\mu = 0.1$, pH 7, and 4°. While complexing with ethyl- and butylpyridinium bromides was not detected in equilibrium dialysis experiments covering a wide range of concentrations, considerable interaction was observed with the lauryl and cetyl derivatives. The doubly charged ethylene bis-quaternary pyridinium bromide[27] is bound to some extent, but, under the same conditions of concentration and μ, benzidine di-hydrochloride is not.

Discussion

The distinct curvature in the plots of r/c *versus* r (Fig. 1) indicates that there are differences among the binding sites on the DNA macromolecule with respect to their affinities for acriflavine. It was not considered that electrostatic interactions among the binding sites play a large role, first, because the dye cations replace inorganic cations at the sites,[28] and, second, because an electrostatic correction was found inadequate to account for the curvature in DNA–rosaniline binding curves.[14] Although the curves calculated on the basis of two intrinsic binding constants fit the partition analysis data fairly satisfactorily for any reasonable choice of intercepts, the values of K_a, K_b, n_a and n_b may not be interpreted too literally[14,23] but do appear to show that a small number of sites with high intrinsic affinity exists and that a considerably larger number of sites have much lower affinities. That the two-constant assumption is indeed an over-simplification is indicated by the disparity between the calculated curves and the partition analysis data in the region where the slope is changing rapidly.

As is often the case in binding studies of the kind presented here, the extrapolation to determine n is quite uncertain, and the effect of a large variation in n upon the theoretical binding curves is small, so that the values reported for n are estimates only. On the other hand, the uncertainties in extrapolating the partition analysis data to $c = 0$ by any of the three methods employed are a good deal smaller than the differences between the values of k_1 for the different environmental conditions considered. If greater accuracy were required, however, partition analyses could be carried out at lower dye concentrations by measuring the fluorescence of larger volumes of solutions than were used in these experiments.

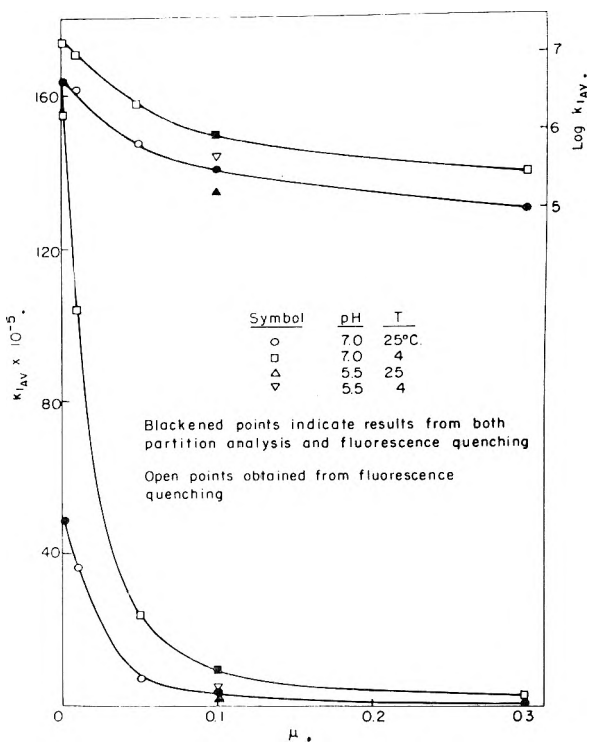

Fig. 4.—Variation of k_1 with ionic strength.

The quenching-slope procedure, despite the approximations made in applying it to the DNA–acriflavine interaction, appears to provide a relatively

(27) Kindly given by Dr. J. L. Hartwell (J. L. Hartwell and M. A. Pogorelskin, *J. Am. Chem. Soc.*, **72**, 2040 (1950)).

(28) G. Scatchard, *Ann. N. Y. Acad. Sci.*, **51**, 660 (1949).

rapid but reliable method for the determination of k_1 in interacting systems involving multiple equilibria where fluorescence quenching is appreciable and where a limiting slope at infinitely low quencher concentration can be determined. In cases where the assumption holds that p is constant, equation 4 might be used to calculate c and, hence, an entire binding curve from quenching data. If it may be assumed that the quantum yield of fluorescence for the free dye remains constant in the presence of DNA, while the yield for the bound molecules depends upon the mechanism of the binding, then the variation of p in the present instance is further indication that the binding sites are heterogeneous with respect to their affinities for acriflavine.

The values of k_1 obtained in this investigation are high relative to values reported in studies of other DNA interactions under comparable conditions of μ, pH and temperature. Because DNA binding is very often dependent to a large extent upon the degree of polymerization of the preparation,[14,15] however, comparisons between the values of binding constants determined for different DNA samples must wait until more is known concerning this additional experimental variable. The decrease in k_1 accompanying the decrease in pH from 7.0 to 5.5 may be explained on the basis of increased competition of H^+ for the DNA binding sites, the ionization of acriflavine being independent of pH in this region. While the marked dependence of k_1 upon ionic strength, especially at low ionic strengths, is expected for a basically electrostatic interaction, there is evidence, as Oster[13] pointed out, that secondary forces are very important in the DNA–acriflavine complexing. First, fluorescence quenching, such as occurs on the interaction of DNA with a number of acridines, is believed to be associated with strong van der Waals' bonding.[29] The rather large negative values found for ΔH_1^0, ΔH_a^0 and ΔH_b^0 in the present study are in accord with this hypothesis. Furthermore, the qualitative findings reported here on the interaction of DNA with several organic cations, as well as the information on DNA complexing available in the literature, indicate that binding by DNA is favored for molecules which offer opportunities for secondary interactions. The standard entropy changes calculated for the DNA–acriflavine complexing are found, within experimental error, to be zero. It appears, then, that far-reaching structural changes probably do not occur upon binding, as they are not believed to occur on nucleic acid–protein interaction.[10] For this reason, and, also, because equilibrium is reached rapidly in the DNA–acriflavine system, it would seem that a proposed configuration for the DNA macromolecule should place the charged phosphate groups so that they would be readily accessible for electrostatic interaction. Several suggested structures for DNA, that of Crick and Watson[30] included, satisfy this requirement. In addition, a structure similar to the one proposed by Crick and Watson allows that the planar hydrocarbon portion of a molecule like acriflavine slip between successive parallel planes occupied by purine and pyrimidine bases, the quaternary nitrogen oriented toward the DNA phosphate group, so as to permit strong van der Waals bonding as well as electrostatic interaction without requiring much change in the configuration of the DNA macromolecule.

The authors gratefully acknowledge support of this work by the National Institutes of Health, Public Health Service, through a grant administered by the Ohio State University Research Foundation.

(29) E. J. Bowen, *Quart. Rev.*, **1**, 1 (1947).

(30) F. H. C. Crick and J. D. Watson, *Proc. Roy. Soc.* (*London*) **A223**, 80 (1954).

ANGULAR LIGHT SCATTERING STUDIES ON THE INTERACTION BETWEEN POLY-4-VINYL-N-*n*-BUTYLPYRIDINIUM BROMIDE AND CRYSTALLINE EGG ALBUMIN[1]

BY ISRAEL J. HEILWEIL[2] AND QUENTIN VAN WINKLE

Department of Chemistry, The Ohio State University, Columbus 10, Ohio

Received February 25, 1955

Angular light scattering measurements were carried out on soluble complexes formed between poly-4-vinyl-N-*n*-butylpyridinium bromide (PVP) and crystalline egg albumin (EA), at *p*H's below the isoelectric point of the protein, as a function of ionic strength and mixing ratio. Filtration of individually prepared solutions through Millipore filters made it possible to extend the measurements to very low concentrations and low ionic strengths. Equations developed by Geiduschek and Doty were utilized to calculate δ, the weight absorption coefficient. δ increased sigmoidally with decreasing ionic strength and with increasing *p*H, showing that an electrostatic interaction occurs, probably between the cationic loci on the PVP and the carboxyl groups on the protein. The fact that δ varies linearly with weight ratio is very likely a consequence of a redistribution of EA molecules among the available PVP molecules. The variation of the osmotic virial coefficient, B, for the system as a function of ionic strength resembles the variation in simple polyelectrolyte systems. B appears to be a quadratic function of weight fraction of PVP, and there is a minimum in the plot of B *versus* *p*H near the isoelectric point of EA. Examination of the scattering function $P(\theta)$ indicates that the complex is a polydisperse coil.

Introduction

Soluble complexes formed between chemically different macromolecular species have only recently come under investigation. The angular light scattering technique is particularly suited to the study of high molecular weight materials, and, when interpreted in terms of theories of multicomponent systems,[3-5] becomes invaluable in obtaining information as to the molecular weight, binding constants, size and shape of macromolecular complexes.

Light scattering studies of macromolecular interactions reported thus far have dealt primarily with complexing between naturally occurring, structurally complicated polymers.[6-8] It was believed that it would be of value to study a model system containing at least one synthetic interactant whose structure and properties could be determined readily. This approach is exemplified in recent electrophoretic and surface film studies.[9-10] Poly-4-vinyl-N-*n*-butylpyridinium bromide (hereafter called PVP) and crystalline egg albumin (hereafter called EA) were selected for the interaction studies of this investigation since they form soluble complexes, under suitable conditions, for which configurations and molecular weights may be obtained readily by light scattering methods.

Experimental

Light Scattering Apparatus.—The light scattering photometer used in this investigation is a commercial model built according to the original design by Brice, *et al.*[11] In order to permit angular measurements down to 30°, readily interchangeable diaphragms were constructed, reducing the original limiting slits in the primary beam to 12 × 3 mm.[2]. Measurements of reduced intensity, R_θ, were carried out with a commercially available cylindrical cell after a design by Witnauer and Scherr,[12] at 27°, using unpolarized light of wave length 4360 Å., with an AH4 mercury arc as source.

The calibration of the instrument was checked by independent turbidity measurements on carefully filtered "Ludox" solutions (obtained from Dr. R. K. Iler of E. I. du Pont de Nemours and Co.) according to a procedure described by Oth, *et al.*[13] Proper corrections were applied to account for depolarization, dissymmetry and phototube sensitivity to the polarization of the incident beam. The cylindrical and dissymmetry cells were filled with identical Ludox solutions, and values of R_θ were obtained using both cells. Since the measurements with the dissymmetry cell were made using large slits, and those with the cylindrical cell using small slits, the values of R_θ obtained were the true and apparent reduced intensities, respectively. The ratio $k = R_{\theta,\text{true}}/R_{\theta,\text{apparent}}$, independent of θ, was used to obtain the absolute value of R_θ with the cylindrical cell using small slits. By using the above calibration procedure, $R_{90°,u}$ for thiophene-free benzene at 436 mμ and 25° was found to be 49.3 × 10^{-6}, in agreement with values reported in the literature.[14]

Differential Refractometer.—The refractive index increments and concentrations used in this investigation were determined on a Brice–Speiser differential refractometer.[15] The instrument constants were obtained by calibration at 25° with 0.01483 g./ml. KCl, using dn/dc = 0.1344 at 4360 Å.,[16] and with sucrose solutions ranging in concentration from 0.00500 to 0.02000 g./ml., using dn/dc = 0.1430 at 5460 Å.[17]

Materials.—Three times recrystallized egg albumin was prepared according to a procedure given by Kekwick and Cannan[18] and kept at 4° in a closed container in a desiccator over P_2O_5. The PVP used was from the batch prepared and characterized by Goodman[19] and Maio.[20]

Preparation of Solutions.—1% EA solutions by weight were dialyzed with mechanical stirring for at least six days against a total of 40 l. of distilled water at 4°, and then centrifuged at top speed for one-half hour in a Servall S1 Centrifuge. These EA solutions, kept no longer than one

(1) Taken from a dissertation submitted by I. J. Heilweil to the Graduate School of The Ohio State University in partial fulfillment of the requirements for the degree Doctor of Philosophy, 1954.

(2) Beacon Laboratories, The Texas Company, Beacon, New York.

(3) W. H. Stockmayer, *J. Chem. Phys.*, **18**, 58 (1950).

(4) W. R. Krigbaum and P. J. Flory, *ibid.*, **20**, 873 (1952).

(5) G. Scatchard, A. Gee and J. Weeks, THIS JOURNAL, **58**, 783 (1954).

(6) E. P. Geiduschek and P. Doty, *Biochim. Biophys. Acta*, **9**, 609 (1952).

(7) D. S. Yasnoff and H. B. Bull, *J. Biol. Chem.*, **200**, 619 (1953).

(8) R. F. Steiner, *Naval Medical Research Institute Report*, **11**, 579 (1953).

(9) P. F. Holt and J. E. L. Bowcott, *Biochem. J.*, **57**, 471 (1954).

(10) R. V. Rice, M. A. Stahmann and R. A. Alberty, *J. Biol. Chem.*, **209**, 105 (1954).

(11) B. A. Brice, M. Halwer and R. Speiser, *J. Opt. Soc. Am.*, **40**, 768 (1950).

(12) L. P. Witnauer and H. J. Scherr, *Rev. Sci. Instru.*, **23**, 99 (1952).

(13) A. Oth, J. Oth and V. Desreux, *J. Polymer Sci.*, **10**, 551 (1953).

(14) H. J. L. Trap and J. J. Hermans, *Rec. trav. chim.*, **73**, 167 (1954).

(15) Phoenix Precision Instrument Company, Philadelphia, Pa.

(16) A. Kruis, *Z. physik. Chem.*, **34B**, 13 (1936).

(17) H. Svenson and K. Odengrim, *Acta Chem. Scand.*, **6**, 720 (1952).

(18) R. A. Kekwick and R. K. Cannan, *Biochem. J.*, **30**, 227 (1936).

(19) P. Goodman, Doctoral Dissertation, The Ohio State University, 1952.

(20) N. J. Maio, Master's Thesis, The Ohio State University, 1953.

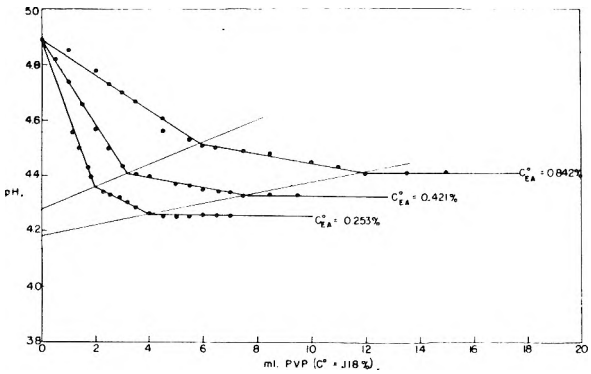

Fig. 1.—Titration of isoelectric egg albumin at various concentrations with PVP solution containing 0.118 g. PVP/100 ml. solution.

week, gave a molecular weight of 44,800 when clarified using Millipore filters by a procedure described below. PVP solutions were dialyzed against water and then stored at room temperature.

In making up the stock PVP–EA mixtures of various *p*H's, ionic strengths and weight ratios r = g. EA/g. PVP, the calculated volumes of filtered PVP solution, buffer, water and EA solution were delivered into glass-stoppered erlenmeyer flasks. In order to avoid surface denaturation, the EA was added very slowly, and care was taken always to keep the tip of the pipet below the surface of the solution. Each solution was then gently swirled and set in a refrigerator at 2° if not needed for immediate use. Dilutions of stock solutions were prepared taking the precautions described above. After the dilution, the solutions were kept at 27° for one hour prior to their use in light scattering experiments.

*p*H and ionic strength were adjusted with sodium acetate–acetic acid buffers prepared according to the data of Green.[21] Determinations of *p*H were carried out at 25° with a Beckman *p*H meter, model G, using 1190-80 external glass electrodes.

Filtration.—It was found that, at the low concentrations used, dust-free solutions could best be obtained by direct filtration into the scattering cell of individually prepared dilutions. Millipore HA filter disks,[22] properly rinsed with prefiltered water, were found to pass PVP-EA solutions without adsorption. A fresh disk was used for each dilution, and the Pyrex filter assembly, especially the fritted glass portion, was thoroughly cleaned at each change. All glassware was boiled in Haemo-Sol[23] detergent solution and rinsed with large volumes of distilled and prefiltered water.

In order to avoid EA precipitation during filtration, the stem of the Pyrex filter assembly was bent at a slight angle, so that the tip touched the wall of the scattering cell, thus permitting the filtered solution to flow down the wall in a continuous, thin, gentle stream.

Theory

Geiduschek and Doty[6] have shown that for reactions where the final concentration of one of the components, PVP in this investigation, is negligible

$$\frac{K'(c_2 + c_4)}{R_{ot}} = \frac{c_2 + c_4}{c_2 M_2(\phi_2 + \delta\phi_4)^2 + (c_4 - \delta c_2)M_4\phi_4^2} \quad (1)$$

R_{ot} is the reduced total intensity at zero degrees determined from a Zimm plot,[24] $K' = 2\pi^2 n_0^2/N\lambda^4$, $\phi_i = dn/dc_i$, and δ is the weight absorption coefficient, the weight of component 4 (EA) bound per unit weight of component 2 (PVP). The other symbols have their usual significance.

The molecular weight of the complex is given by $M_6 = M_2(1 + \delta)$, where the subscript 6 refers to the complex.

B, the second virial coefficient, and R_G, the radius of gyration for the system, are evaluated from a Zimm plot. R_G is calculated from

$$R_G = \frac{\sqrt{3}\lambda}{4\pi n_0}\left(\frac{dP^{-1}(\theta)}{d\sin^2\theta/2}\right)^{1/2}_{\theta=0} \quad (2)$$

where $P^{-1}(\theta)$ is the reciprocal particle scattering factor. Since R_G obtained from light scattering is a Z-average, R_G for the system can be taken equal to R_{G_6} when $\delta > 0.3$.

Results and Discussion

Plots of *p*H as a function of volume of salt-free PVP solution added to isoelectric EA (Fig. 1), resembling those obtained by Gibbs, *et al.*,[25] in their studies of the interactions between EA and cationic detergents, gave the first indication that complexing occurs between PVP and EA at *p*H's below the isoelectric point of EA. In these experiments, in contrast with those reported by Gibbs, *et al.*,[25] the first and second break points occurred at constant values of r (r = 22.0 and 11.2, respectively), independent of initial PVP and EA concentration.

The angular light scattering experiments reported here were carried out on PVP–EA mixtures at $r < 6.0$, where turbidity is time-independent, and under conditions of μ, the ionic strength, and *p*H such that no change in concentration upon filtration was detected. Samples of PVP–EA mixtures which had been stored up to four days at 2° or up to 72 hours at room temperature showed no change in reduced intensity at various angles, indicating that aggregation had not occurred.

The molecular weight of EA at μ = 0.001 and *p*H 4.62 was found to be 44,800. In 0.2 N NaCl the molecular weight of PVP was 620,000, in agreement with the expected value based on the molecular weight of 269,000 for the parent polymer,[19] and in agreement with molecular weight values obtained by independent sedimentation and diffusion[20] and viscosity measurements which will be reported elsewhere. Viscosity and light scattering measurements suggested further that the PVP sample studied is a heterogeneous mixture with z between 1 and 2, where z is a molecular weight distribution parameter.[26] At ionic strengths less than 0.03, molecular weights in the neighborhood of 530,000 were found for PVP, and weight average molecular weights calculated for PVP–EA mixtures using this value agree with the experimental light scattering molecular weights in cases where interaction does not occur. A similar lowering of the molecular weight of PVP with decreasing μ was found by extrapolating turbidity and dissymmetry data of Fuoss and Edelson[27] to zero concentration. Whether this decrease in molecular weight is in any way connected with bromide ion dissociation must await further investigation.

That the PVP–EA system is in equilibrium was shown by the following. The same R_θ value was obtained when a given solution was prepared directly or by dilution from a concentrated stock solution.

(21) A. A. Green, *J. Am. Chem. Soc.*, **55**, 2331 (1933).
(22) Lovell Chemical Company, Watertown, Mass.
(23) Meinecke and Company, 225 Varick Street, New York City.
(24) B. H. Zimm, *J. Chem. Phys.*, **16**, 1099 (1948).
(25) R. J. Gibbs, S. N. Timasheff and F. F. Nord, *Arch. Biochem. Biophys.*, **40**, 85 (1952).
(26) A. R. Shultz, *J. Am. Chem. Soc.*, **76**, 3422 (1954).
(27) R. M. Fuoss and D. Edelson, *J. Polymer Sci.*, **6**, 767 (1951).

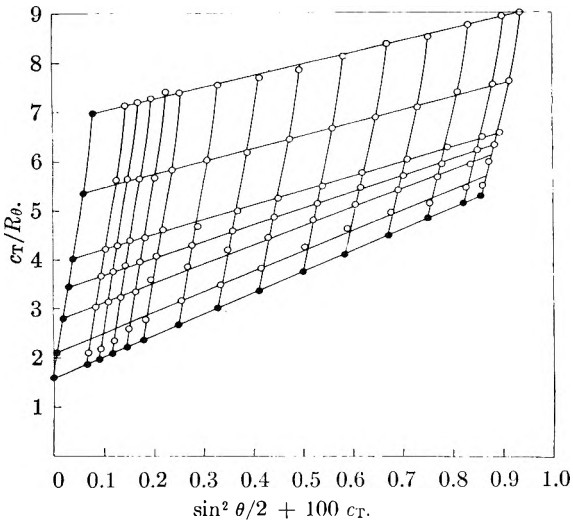

Fig. 2.—Zimm plot of reciprocal reduced scattering intensity for PVP–EA at mixing ratio, r = 1.0 g. EA/g. PVP, ionic strength, μ = 0.0025 and pH 4.60.

Furthermore, R_θ values for a solution at a total concentration $c_T = 10^{-3}$ g./ml., r = 1.0, μ = 0.01 and pH 4.60 were found to be within ±2.7% of the R_θ values obtained by adjusting to the same concentration a solution originally at $c_T = 5 \times 10^{-4}$ g./ml., r = 1.0, μ = 0.005 and pH 4.60.

In no case studied was there evidence for complex dissociation, even at a total concentration as low as 5×10^{-5} g./ml. This suggests, as does the constancy of r at the break points in the pH titration experiments, that the equilibrium constants for association must be very high.

Because ordering effects become important at low ionic strengths, and because higher virial coefficients become significant for polyelectrolyte solutions as concentration increases, it was necessary, at the ionic strengths chosen, to work at the lowest feasible polyelectrolyte concentrations. The work of Oth and Doty[28] suggests that measurements carried out in the polyelectrolyte concentration range where the dissymmetry Z decreases with increasing polyelectrolyte concentration may be used to give correct values for molecular weight and $P^{-1}(\theta)$. In all cases studied here this condition was fulfilled. Ordering phenomena were clearly indicated in a plot of Z *versus* c_T at r = 1.0, μ = 0.001 and pH 4.60. With increasing polyelectrolyte concentration, Z decreased rapidly and linearly, went through a shallow minimum to $Z < 1.0$, and then increased slowly at higher concentrations. In other runs Z decreased linearly with increasing concentration, but the minima, with the exception of a run at μ = 0.0025, were not reached.

Whereas Zimm plots for uncharged polymers usually consist of a grid system formed by two series of parallel lines, Zimm plots obtained in this investigation (Fig. 2) resembled, in many respects, those obtained by Shultz[26] and by Ehrlich and Doty[29] in their studies on other polyelectrolyte systems. It was found that curvature at high c could be eliminated when data were plotted as $(Kc/R_\theta)^{1/2}$ *versus* c

(28) A. Oth and P. Doty, THIS JOURNAL, **56**, 43 (1952).

(29) G. Ehrlich and P. Doty, *J. Am. Chem. Soc.*, **76**, 3764 (1954).

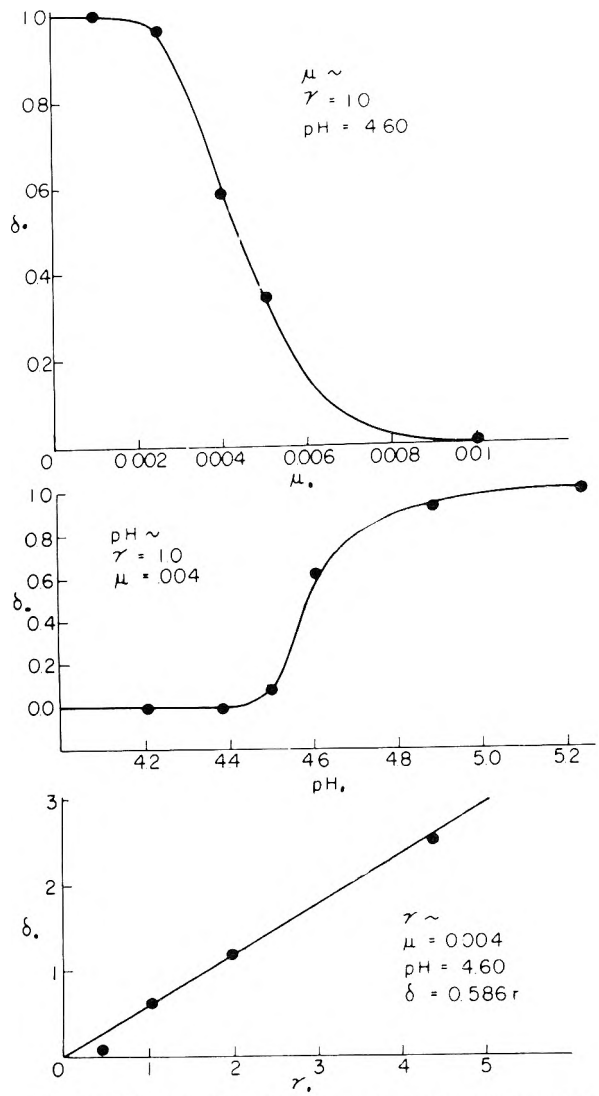

Fig. 3.—Weight absorption coefficient, δ (g. EA/g. PVP), for PVP–EA complexes *versus:* (a) ionic strength μ; (b) pH; (c) mixing ratio r (g. EA/g. PVP).

in accordance with a method suggested by Flory,[30] taking $g = 1/3$.

Equation 1 was developed for angular light scattering studies of interacting systems in which the free concentration of one of the components is negligible and in which δ is constant in the concentration region under consideration. Since the complexing between PVP and EA falls into this category, the use of equation 1 in this investigation appears to be justified, provided it is assumed that association–fluctuation coupling of the type described by Steiner[8] does not occur. It can be shown that δ, as measured by light scattering, is a Z-average weight absorption coefficient.

As Fig. 3 shows, δ increases with decreasing ionic strength, which is to be expected when interaction takes place between oppositely charged groups. As μ approaches 0, δ approaches unity, but no interaction takes place at $\mu > 0.01$. With increasing pH, the competition of hydrogen ions for the EA carboxyl groups decreases, and, therefore, the amount

(30) P. J. Flory, "Principles of Polymer Chemistry," Cornell University Press, Ithaca, N. Y., 1953, pp. 283–315.

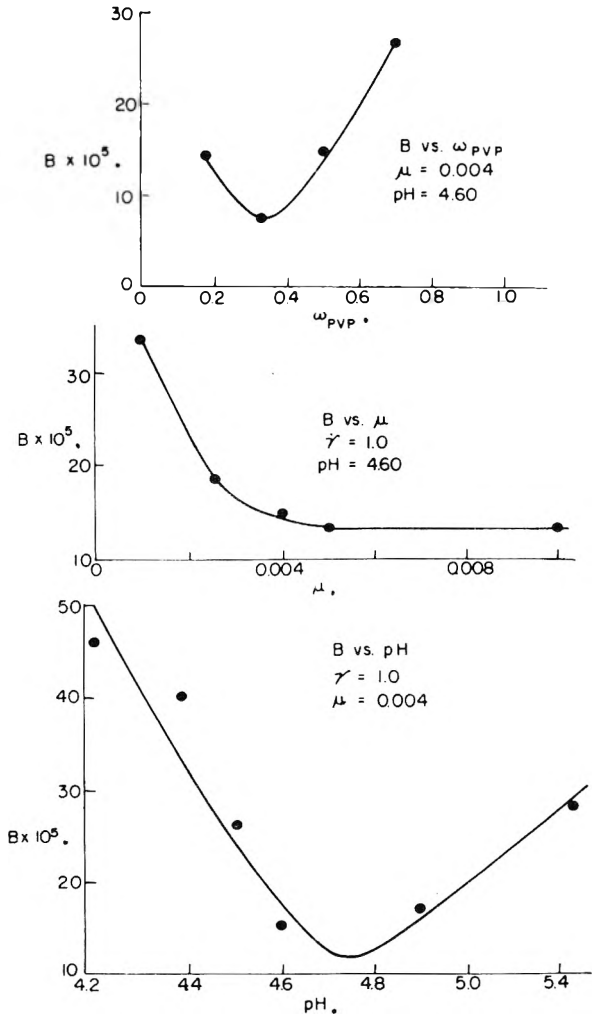

Fig. 4.—Osmotic virial coefficient, B, for PVP–EA complexes *versus:* (a) weight fraction ω, of PVP in complex; (b) ionic strength μ; (c) pH.

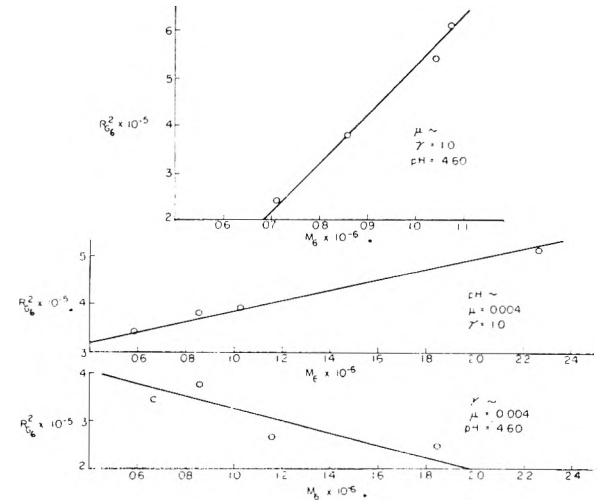

Fig. 5.—Dependency of square of radius of gyration, $(R_{G6})^2$, of PVP–EA complexes on molecular weight of complex, M_6, for variations in: (a) ionic strength μ, (b) pH; (c) mixing ratio, r.

of interaction of EA with PVP is expected to increase, if it is assumed that the interaction takes place between the carboxyl groups on the EA and cationic groups on the PVP. From Fig. 3 it is seen that no interaction takes place up to pH 4.40 and that δ reaches a value of 0.92 at pH 4.88, the isoelectric point of EA. At pH 5.23 an apparent value of about 2.0 was obtained for δ. If it is granted that at this pH, where protein and polyelectrolyte are oppositely charged, aggregation is feasible, then a value of $\delta \cong 1.0$ may be obtained by assuming that two molecules of PVP, with their bound EA, form a new molecular unit. A value of unity was assumed in plotting δ *versus* pH, but the aggregation hypothesis was not tested by means of light scattering measurements at higher pH's, because large aggregates would have been removed in the filtration procedure used in this investigation. The fact that δ varies linearly with r, for $r < 5.0$, is a consequence of a redistribution of EA molecules among the available PVP molecules as r decreases. The deviation of δ from the straight line relationship at $r = 0.429$ is in the direction predicted when the assumption, used in the development of equation 1, that no PVP molecule is bare no longer holds.

The interaction constant B for the system as a whole (Fig. 4) is high at low ionic strengths where intermolecular repulsion, of which B is a measure, is high. At high ionic strengths, where shielding of the charged groups on the polyelectrolyte is considerable, B decreases. The variation of B with pH for the system resembles the variation of B with pH for protein solutions, showing a minimum in the neighborhood of the isoelectric point of the protein. This behavior with respect to pH is expected for an electrostatic type of interaction between an ampholyte and a charged polymer which by itself is not affected by pH changes. B appears to be a quadratic function of weight fraction at constant pH and ionic strength.

Figure 5 shows how $R_{G_6}^2$ varies with the molecular weight of the complex as a consequence of variations in μ, pH and r. As the molecular weight of the complex increases, the size, and hence $R_{G_6}^2$, is expected to increase. This increase is magnified when, in addition to the growth of the complex due to increased binding, there is an extension of the flexible molecule as ionic strength decreases and repulsions between unshielded charges become increasingly important. When pH is increased at constant ionic strength, the degree of interaction increases due to the larger number of negative groups on the EA, and the complex grows in size. The rate of increase of $R_{G_6}^2$ with molecular weight is less than under variable ionic strength conditions, since the repulsive forces between PVP chain segments, which are dependent upon the concentration of simple electrolytes, are kept constant. On the other hand, neutralization of charges on the PVP molecule with complexing, caused by an increase in the number of bonds between the interacting species, might be sufficient to decrease the repulsion along the PVP backbone, so that the complex would tend to contract. It is to be noted that the amount of binding as measured by M_6 does not indicate the number of bonds formed, and a large number of bonds could explain a tendency to decrease in size even while the molecular weight of the

complex increases. If an analogy can be made with simpler systems, it is probable that, as the concentration of one of the components is increased, bonds of lower energy are more likely to form. Such a tendency seems to show up in the plot of $R_{G_6}^2$ *versus* M_6 at variable r, but the evidence is insufficient at this time to support this hypothesis.

The total reduced scattered intensity data for PVP–EA at $r = 1.0$, $\mu = 0.001$ and *p*H 4.60 are suited to the determination of the shape of the PVP–EA complex, because the dissymmetry coefficient, Z, is high, and binding appears to be complete. Values of $P(\theta)$ for various values of sin $\theta/2$ were calculated for rods, monodisperse coils, spheres and cylindrical and ellipsoidal disks from tables and graphs prepared by Doty and Steiner[31] and by Saito and Ikeda.[32] $P(\theta)$ values for polydisperse coils were calculated, assuming $z = 1$, from an equation given by Zimm[24] and were found in excellent agreement with experimentally determined $P(\theta)$ values. This leads to the conclusion that the PVP-EA complex, because of the polydisperse nature of the PVP sample, must also be polydisperse.

The authors gratefully acknowledge support of this work by the National Institutes of Health, Public Health Service, through a research grant administered by the Ohio State University Research Foundation.

(31) P. Doty and R. F. Steiner, *J. Chem. Phys.*, **18**, 1211 (1950).
(32) N. Saito and Y. Ikeda, *J. Phys. Soc. Japan*, **6**, 305 (1951).

VARIABILITY STUDIES OF THE FLOTATION TECHNIQUE OF ANALYTICAL ULTRACENTRIFUGATION

BY LAWRENCE J. MILCH, NORMAN WEINER AND LESLY G. ROBINSON

Department of Pharmacology-Biochemistry, USAF School of Aviation Medicine, Randolph Field, Texas

Received February 25, 1955

The sources of variability in the stepwise protocols for the ultracentrifugal estimation of blood plasma lipoproteins have been investigated. It was determined that most of the error in the *preparative step* can be accounted for during removal of the top fraction. It was also established that two different Model L ultracentrifuges yield almost identical results with respect to lipoprotein flotation. Reproducibility in the *analytical step* was found to be limited by the resolution capability of the optical system used in the Model E ultracentrifuge. Consequently, variability is large when low concentrations of lipoprotein are subjected to analysis. Over and above the concentration effect, there seems to be some further unaccountable difference in results obtained from the two Model E ultracentrifuges studied. The error introduced by enlargement tracing and planimetry was shown to be relatively insignificant, as was any cell assembly effect.

Introduction

In 1949, Gofman, Lindgren and Elliott[1] at the University of California, suggested the use of a flotation technique for the ultracentrifugal estimation of blood serum lipoprotein concentration. Shortly thereafter, the Gofman group established detailed protocols for the analysis, utilizing the Spinco[2] Models L and E ultracentrifuges. When these same investigators demonstrated the application of blood lipoprotein levels to human atherosclerosis, several research groups (including ours) sent representatives to California for training in the technique. Consequently, by the end of 1952, a number of institutions were subjecting blood serum to routine ultracentrifugal analysis. Nevertheless, the procedure has undergone more or less continuous revision and improvement, culminating in a recent publication of the latest protocols by De Lalla and Gofman.[3]

Routine human and animal blood lipoprotein analyses have been carried out in this Laboratory since the initial training of one of us (L.J.M.) by the Gofman group in 1950. Since early 1953, the techniques employed here have been essentially as described by De Lalla and Gofman.[3] Over the past 2-year period, therefore, a considerable body of data has been accumulated relative to the inherent variability of the multi-step procedure when the analyses are accomplished on a routine basis. Since purified, homogeneous lipoprotein fractions are not available, recovery studies of the analytical technique could not be accomplished. It was decided, therefore, to organize and expand our variability data so that even if the accuracy of a result were not known, at least the limits of comparability of successive results could be estimated.

(1) F. W. Gofman, T. T. Lindgren and H. A. Elliott, *J. Biol. Chem.*, **179**, 973 (1949).
(2) Specialized Instruments Corporation, Belmont, California.
(3) O. F. De Lalla and J. W. Gofman, "Methods of Biochemical Analysis," Interscience Publishers, Inc., New York, N. Y., 1954, p. 459.

Experimental

The analytical protocols, as practiced in this Laboratory, may be outlined as follows:

1. Dilution of the serum with salt solution to increase the density of the solvent phase.
2. Fifteen hours of preparative ultracentrifugation (Model L) to float the lipoproteins of interest within a 1-cc. volume.
3. Quantitative removal of the required 1-cc. top fraction.
4. Thirty-eight minutes of analytical ultracentrifugation (Model E) of the top fraction to obtain a photographic record of the refractive index gradient.
5. Determination of areas of planimetry from an enlarged tracing of the refractive index gradient photograph after establishing the infinite dilution boundaries of the lipoprotein classes on the basis of the straight-line relationship

$$S_{f_c} = S_{f_{c_0}}/2$$

where c = 3790 mg. % cell concentration
c_0 = infinite dilution.

The reproducibility studies to be described were carried out under the following assumptions:

1. No variability is involved due to positioning a sample in any one of the 20 holes of the preparative rotor or in either of the 2 holes of the analytical rotor.
2. No variability is involved due to temperature changes during the 38 minutes required to photograph refractive index increments in the Model E ultracentrifuge.

3. Variability due to such standard laboratory practices as *pipetting, washing of glassware and equipment*, preparation of diluting solutions, etc., was not considered.

Equipment.—Two Spinco Model E (Serial Numbers 70 and 163) and two Spinco Model L (Serial Numbers 63 and 351) ultracentrifuges were utilized for this study. All auxiliary ultracentrifuge equipment (rotors, lusteroid tubes, etc.) was standard as delivered by the manufacturer, except that the analytical cells were modified to bear two channels, as developed in this Laboratory.[4] All weighings were accomplished in 1-inch radioactivity assay metal planchets on a Fischer "Gramatic" single-pan balance.

1. **The Effects of Storage.**—When an investigation involves large-scale sampling of population segments, personnel and equipment limitations often require that blood specimens be stored for varying periods until analyses can be accomplished. In order to validate the grouping of otherwise comparable data, it was deemed necessary to establish the effects of such storage on lipoprotein concentrations. Accordingly, 700 cc. of human blood was taken and the plasma separated by low-speed centrifugation. Seventy-six aliquots of the plasma were prepared, 40 of which were immediately subjected to steps 1 through 3 of the analytical protocols. The analysis was completed at once on four of the resulting top fractions, to furnish baseline values for the storage effect. The remaining 36 top fractions were stored variously at room temperature (26°), refrigeration temperature (4°), and deep freeze temperature (−25°) for subsequent duplicate analyses at 3-day intervals up to 18 days. Thirty-six aliquots of the original plasma were also stored at the three temperatures for complete analysis, at the same intervals. The averages of duplicate analyses were taken throughout and the storage trend of the concentration of the S_f 0–12 lipoprotein class for two conditions (plasma and top fraction) and three temperatures (26, 4, and −25°) determined. The results are shown in Fig. 1.

2. **Removal of the 1-ml. Top Fraction.**—Nine aliquots of a pooled serum sample were adjusted for density with D_2O,[5] ultracentrifuged simultaneously for 15 hours, and the 1-ml. top fraction of each sample removed. The dry weight of each top fraction was determined by pipetting duplicate 0.4-ml. aliquots into separate planchets that had been dried to constant weight and the liquid phase allowed to evaporate in an oven at 37° for 24 hours. After reweighing of the planchets, the dry weight was obtained by difference and simple calculation. The data may be seen in Table IA.

3. **Run-to-Run and Machine-to-Machine Variability in the Model L Ultracentrifuge.** Forty aliquots of the same serum sample were adjusted for solvent density with D_2O. Ten samples were immediately (T_1) subjected to 15 hours of preparative ultracentrifugation in each of two Model L machines. The process was repeated with the remaining 20 samples seven days later (T_2). The dry weights of all 40 top fractions were determined and the results are shown in Table IB.

4. **Run-to-Run and Machine-to-Machine Variability in the Model E Ultracentrifuge.**—Utilizing a pooled sample of human plasma top fractions and four different analytical cells, 12 successive runs (Step Number 4 of the analytical protocols) in each of two Model E machines were accomplished over a 16-hour period. The cells were emptied, disassembled, cleaned, reassembled and refilled between successive analyses in the same machine; however, cells were transferred between machines for a duplicate analysis, with only repeated inversion to destroy boundaries. Enlargement and planimetry of the photographed refractive index increments yielded run-to-run and machine-to-machine variability for the S_f 0–12 class of lipoproteins. Similar data were collected for the S_f 20–400 class of lipoproteins by analyzing six aliquots of pooled top fraction in each Model E ultracentrifuge. In this latter instance, the cells were also emptied, disassembled, cleaned, reassembled and refilled prior to each run but not transferred between machines. Finally, in order to determine whether the routine of cleaning and cell assembly contributes to analytic variability, eight additional aliquots of the pooled top fraction were ultracentrifuged successively in the same machine after repeated inversion to destroy boundaries between runs. Results of the run-to-run and machine-to-machine testing are listed in Table II (2A and 2C).

In order to convert a photograph of refractive index increments into mg. per cent. concentration, it is necessary to make an enlarged tracing and determine "swept-out" areas by planimetry. Since all data on the Model E ultracentrifuge herein reported necessarily include such subjective manipulation, it was decided to determine how individuals differ in the tracing and area measurement. Accordingly, each of ten refractive index increment photographs were evaluated separately by two well-trained technicians. S_f 0–12 areas were enlarged, traced and measured with the K and E Polar Planimeter, used routinely in this Laboratory. The results are shown in Table II (2B).

Discussion

The data in Fig. 1 indicate a significant effect of storage on plasma lipoprotein levels. Without exception, the concentration of the S_f 0–12 lipoproteins shows a net decrease after 18 days of storage, regardless of condition (whole plasma or top fraction) or temperature. When whole plasma is stored at 4°, the decrease is found to be well within the error of measurement. Nevertheless, even in this instance, the trend of values over the period suggests some slight breakdown. The data suggest that freezing accelerates the rate of lipoprotein degradation and that this phenomenon is augmented in the presence of the high salt concentration in the top fraction. The initial and sustained rise in lipoprotein concentration when whole plasma is stored at 26° might be explained on the basis of an even more rapid breakdown of those protein molecules in plasma with densities greater than 1.063. Some of the fragments thereby produced would now have densities lower than their parent molecules and thus migrate within the S_f 0–12 envelope.

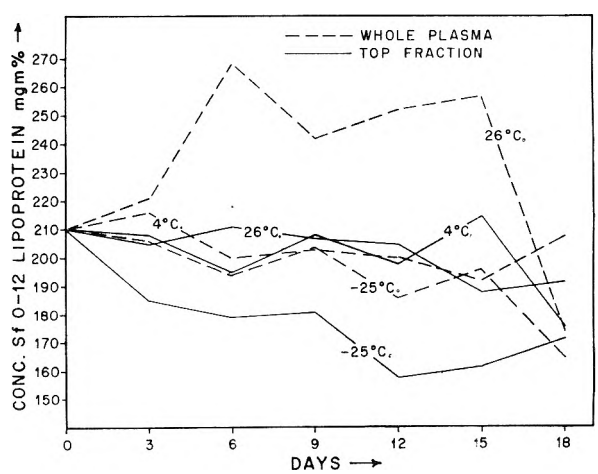

Fig. 1.—The effects of storage on the concentration of S_f 0–12 plasma lipoproteins.

The data in Table I demonstrate that the preparative step of lipoprotein analysis, as accomplished routinely in this Laboratory, is reasonably consistent. As indicated in Table IA, removal of the top fraction can be repeatedly accomplished within a range of 0.7 mg. or approximately ±6% of the solid material present. This finding is confirmed by the data listed under L_1T_1 and L_2T_1 of Table IB where ranges of 0.8 and 0.9 mg., respectively, are observed. Furthermore, the means,

(4) L. J. Milch, *Lab. Investigation*, **2**, 441 (1953).

(5) Since, in this instance, the variability was to be estimated on the basis of a weight, D_2O was substituted for NaCl solution. The presence of solid salt on the planchet after evaporation of the water might introduce an additional error.

TABLE I

PREPARATIVE VARIABILITY (MODEL L ULTRACENTRIFUGE)

Sample no.	A. Removal of the top fraction. Duplicate dry wt. determin. on 9 aliquots from the same machine at the same time: Mg. 0.4-cc. top fraction	B. Run-to-run and machine-to-machine variability. Dry wt. of the top fractions (mg.) from 10 aliquots spun in each of 2 machines (L_1 and L_2) at times T_1 and T_2: L_1T_1	L_2T_1	L_1T_2	L_2T_2
A	5.95	6.95	6.97	5.63	7.20
A_1	6.01				
B	...	7.33	7.07	6.47	6.90
B_1	...				
C	6.28	7.07	7.14	6.58	7.03
C_1	6.16				
D	6.28	7.04	6.82	6.34	6.68
D_1	6.28				
E	6.41	7.54	7.25	6.16	7.26
E_1	6.44				
F	6.39	7.37	7.38	6.50	7.04
F_1	6.36				
G	6.14	7.17	6.45	6.93	7.09
G_1	6.05				
H	6.56	6.72	7.32	6.84	5.57
H_1	6.65				
I	6.12	6.77	6.83	6.52	5.38
I_1	6.15				
J	6.49	6.77	6.94	6.23	6.23
J_1	6.51				
Mean	6.29	7.07	7.01	6.42	6.63
Range	5.95–6.65	6.72–7.54	6.45–7.38	5.63–6.93	5.38–7.26
γ	0.20	0.28	0.28	0.37	0.68

As regards run-to-run reproducibility, the data are rather inconclusive. Since 7 days elapsed between T_1 and T_2, some lipoprotein degradation could have been expected on the basis of storage effect. As a matter of fact, mean values for T_2, (Table IB) from both Model L ultracentrifuges are significantly lower than their T_1 counterparts. The fact that the results at T_2 are consistent within themselves suggests that run-to-run variability is insignificant and that the $T_1 - T_2$ change reflects a true decrease in flotable material.

Whereas the variability of the preparative step can be traced, almost *in toto*, to the subjective error of top fraction removal, the data in Table II indicate that the variability of the analytical step is almost wholly mechanical. The run-to-run portion of the results listed under 2A include the separate operations of *cell reassembly, refractive index increment photography during ultracentrifugation,* and *enlargement tracing planimetry.* It would seem that reproducibility from run-to-run in the Model E ultracentrifuge is limited to a range of approximately 12%. Since the subjective difference between trained individuals as regards enlargement tracing and planimetry (Table 2B) is essentially insignificant and successive runs without cell reassembly also yield a range of 12% (Table 2C), it could be concluded that variability in analytical ultracentrifugation is an inherent instrumental characteristic.

The significantly greater run-to-run variability recorded for the S_f 20-400 lipoprotein class (Table 2A) is readily accountable on the basis of concentration. The cylindrical lens in the Model E ultracentrifuge light path induces a marked narrowing of vertical photographic traces when superimposed on the Schlieren lens system. However, at low concentrations (small refractive index increments) the vertical component of the trace is appropriately minute and the photograph

TABLE II

ANALYTICAL VARIABILITY (MODEL E ULTRACENTRIFUGE)

2A. Run-to-run and machine-to-machine variability-cells refilled between runs in the same machine

Sample no.	S_f 0–12 lipoproteins (mg. %) E_1	E_2	Sample no.	S_f 20–400 lipoproteins (mg. %) E_1	E_2
1	268(26)[a]	259(26)	1	73(26)	90(26)
2	250(27)	259(26)	2	70(27)	73(26)
3	246(27)	268(26)	3	57(28)	127(28)
4	236(27)	249(28)	4	95(29)	93(29)
5	251(28)	271(28)	5	83(30)	100(30)
6	262(29)	249(29)	6	97(26)	87(27)
7	253(29)	241(29)			
8	236(30)	264(29)			
9	236(30)	273(30)			
10	246(25)	254(26)			
11	262(27)	270(27)			
12	243(28)	263(27)			
Mean	250	260		80	95
Range	32	32		40	54
σ	10.5	10.2		15.2	17.7

2B. Enlargement tracing and planimetry variability—2 individuals (LER and RAY) analyzing each of 10 different photographic plates

Plate no.	S_f 0–12 lipoprotein (mg. %) (LER)	(RAY)	± % Deviation
1	222	259	8
2	182	184	<1
3	244	236	2
4	101	102	<1
5	164	168	<1
6	156	155	<1
7	210	211	<1
8	180	174	2
9	185	193	2
10	187	186	<1
	183	186	<2
			<1 to 8
			2

2C. Run-to run variability cells inverted repeatedly to destroy boundaries but not refilled between runs

Sample no.	S_f 0–12 lipoprotein (mg. %)
1	274(28)
2	256(27)
3	254(27)
4	254(26)
5	254(27)
6	251(28)
7	242(28)
8	242(28)
	252
	32
	9.8

[a] Temperature of the run, °C.

ranges and standard deviations recorded for L_1T_1 and L_2T_1 indicate that the two Model L ultracentrifuges yield identical data within the measurement capability of the Gramatic balance. The range of results recorded for replicate samples ultracentrifuged in the same machine, at the same time, seems almost wholly accountable by the variability involved in removal of the top fraction.

becomes essentially a horizontal magnification of the analyzing element (0.0115 inch diameter wire). The width of the horizontal trace is further augmented by the presence of interference fringes. At low concentration, therefore, the area between the salt trace and the refractive index increment trace is often less than the combined areas of the traces themselves. Under such circumstances, slight deviations from proper alignment of either the cell rotor assembly or of some component of the optical system, become relatively important. Since the late summer of 1954, phase plates have been installed in some Model E ultracentrifuges in place of the wire analyzing element. The substitution results in a far more satisfactory photographic record at low lipoprotein concentrations. The situation should be further improved if a satisfactory method for recording Rayleigh fringes can be incorporated.

The machine-to-machine comparison recorded in Table 2A indicates a small and doubtfully significant non-uniformity. However, it has been continuously observed in this Laboratory that the Model E ultracentrifuge Number 163 (E_2) yields high results compared to instrument Number 70 (E_1). The extent of this deviation is not constant, varying in successive tests from 2–10%. The difference is observed in spite of careful and repeated determinations of machine constants.

The temperature data listed for each run in Tables 2A and 2C demonstrate that over a significant range, temperature control is insignificant. Sample Number 9, Table 2A yielded the lowest value on E_1 (236 mg. per cent.) and the highest value on E_2 (273 mg. per cent.) in spite of the fact that both analyses were done at 30°.

Acknowledgment.—The authors wish to acknowledge the technical assistance of A/3C Beulah L. Croye and A/2C Sherman S. M. Chang. We wish further to thank Doctor M. Bryan Danford, Department of Biometrics, USAF School of Aviation Medicine, for his statistical aid.

DISCUSSION

ROGER RAY.—In the storage studies, you report changes that occurred in the S_f0-12 class. Did you observe any pronounced shifts within the class itself? Also did you make any measurements on the levels of higher classes?

LAWRENCE MILCH.—We did not observe significant shifts in the position of the peak during storage. We did not determine concentrations of faster floating lipoproteins.

SIMULTANEOUS DETERMINATION OF MOLECULAR WEIGHTS AND SEDIMENTATION CONSTANTS[1]

BY STANLEY M. KLAINER[2] AND GERSON KEGELES

Contribution from the Department of Chemistry of Clark University, Worcester, Mass.

Received February 25, 1955

Within the last several years Archibald has indicated how molecular weights and sedimentation coefficients may be calculated from the ultracentrifuge data during the period of approach toward sedimentation equilibrium in a sector shaped cell. Applications of this method have been made to small molecules by Porath and by Brown, Kritchevsky and Davies. Gutfreund and Ogston, and Baldwin have devised an independent method for the determination of sedimentation coefficients based on the flow of solute past a fixed surface in the cell, and have applied this to the study of polypeptides. In the present study we have correlated the two methods so that they may be applied simultaneously to the data obtained in a single experiment. The method employs phase-contrast schlieren optics of Wolter, Armbruster, Kossel and Strohmeier and Trautman and Burns. A two-coördinate comparator is used to measure diagrams from standard ultracentrifuge cells as well as from a boundary-forming cell described by Kegeles, and used here as a refractometer. We have found that both molecular weights and sedimentation coefficients may be determined reliably within one hour of centrifugation for raffinose and for bovine plasma albumin, by the proper choice of speed.

Experimental

The method of obtaining sedimentation constants and molecular weights simultaneously is dependent upon the use of two different cell centerpieces. The first of these is the standard four degree sector 12 mm. thick centerpiece[3] which is used to measure the sedimentation constants by the Gutfreund–Ogston[4,5] method, and the molecular weight according to Archibald.[6–8] The second 12 mm. thick centerpiece is a modified two degree boundary-forming cell as proposed by Kegeles.[9] For optimum results this centerpiece, Fig. 1, is so constructed that the two side holes each have a volume of 0.07 cc. and the center of the cell is filled to 0.16 cc. In its present application, this cell is used as a refractometer to determine the concentration of the original solution.

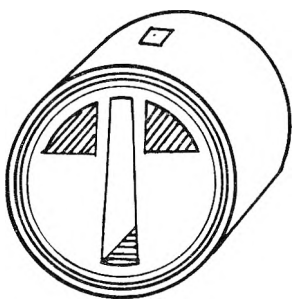

Fig. 1.—Boundary-forming cell.

To obtain results it is necessary to be able to measure the change of refractive index with time in the standard cell. This is accomplished by taking cylindrical lens schlieren[10,11] photographs of the interior of the cell at known time intervals. Experience has shown that the accuracy in determining the sedimentation constant is dependent upon how precisely the refractive index gradient curve can be measured as it approaches the baseline, while the numerical value of the molecular weight is directly related to the height of the curve at the meniscus and bottom of the cell. To make the photographs more sharply defined the schlieren optical system was equipped with a modified Wolter phase-plate[12] similar to the one suggested by Trautman and Burns.[13–15] In this case, the modification consisted of gluing a human hair across the diameter of the phase-plate along the phase border. This has the purpose of defining the baseline region of the diagram produced by light focused on the phase-plate.[13]

Fig. 2.—Sedimentation diagram from standard cell.

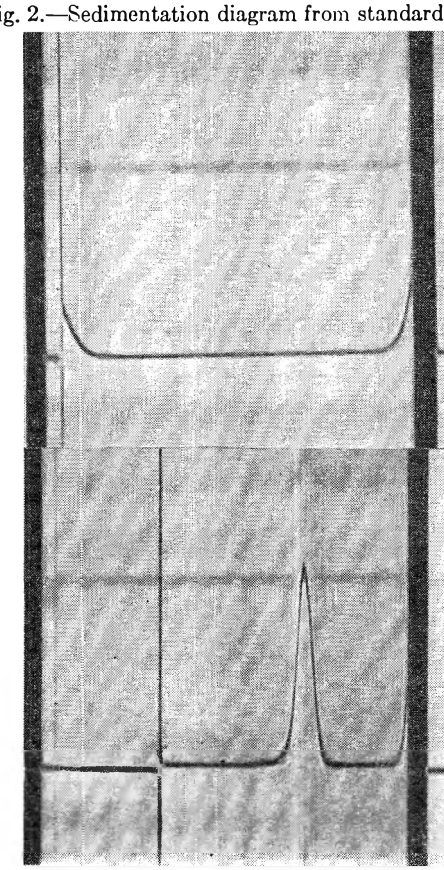

Fig. 3.—Sedimentation diagram from boundary-forming cell.

The cell with the four degree sector centerpiece gives a picture as shown in Fig. 2. While the flat portion of the curve indicates a region where the concentration is independent of the distance from the center of rotation, the curved portion is dependent upon many factors including the molecular weight of the solute and its diffusion constant, the concentration of solute, the specific volumes of the solute and solvent, the length of time the solution is centrifuged, the distance of the cell from the center of rotation, and the centrifugal velocity.[16,17] Figure 3 is representative of the type of curve obtained by use of the boundary-forming centerpiece. By measuring the area under this

(1) Presented at the 29th National Colloid Symposium, American Chemical Society, Houston, Texas, June, 1955.

(2) This material presented by Stanley M. Klainer to the faculty of Clark University in partial fulfillment of the requirements for the M.A. degree.

(3) E. G. Pickels, *Rev. Sci. Instr.*, **13**, 426 (1942).

(4) H. Gutfreund and A. G. Ogston, *Biochem. J.*, **44**, 163 (1949).

(5) R. L. Baldwin, *ibid.*, **55**, 644 (1953).

(6) W. J. Archibald, THIS JOURNAL, **51**, 1204 (1947).

(7) J. Porath, *Acta Chem. Scand.*, **6**, 1237 (1952).

(8) R. A. Brown, D. Kritchevsky and M. Davies, *J. Am. Chem. Soc.*, **76**, 3342 (1954).

(9) G. Kegeles, *ibid.*, **74**, 5532 (1952).

(10) J. St. L. Philpot, *Nature*, **141**, 283 (1938).

(11) H. Svensson, *Kolloid-Z.*, **87**, 181 (1939).

(12) H. Wolter, *Ann. Physik*, **7**, 182 (1950); O. Armbruster, W. Kossel and K. Strohmeier, *Z. Naturforschung*, **6A**, 509 (1951).

(13) R. Trautman and V. W. Burns, *Biochim. Biophys. Acta*, **14**, 26 (1954).

(14) Supplied by Specialized Instruments Corp., Belmont, Calif.

(15) We are indebted to Dr. Trautman for bringing the success of this technique to our attention prior to publication.

(16) W. J. Archibald, *Ann. N. Y. Acad. Sci.*, **43**, 211 (1942).

(17) W. J. Archibald, *Phys. Rev.*, **53**, 746 (1938).

curve it is possible to obtain a numerical value proportional to the concentration of the initial solution.

Photographs were made on Kodak 103F spectroscopic plates through a Wratten 77A filter. Measurements of the photographic plates were made with a two-coördinate microcomparator designed to read with an accuracy of one micron.[18] Care was taken to make sure the side of the plate with the emulsion was always facing the microscope. The typical refractive index gradient curves as shown in Figs. 2 and 3 are sketched in Fig. 4. These drawings aid us in describing the measurements that are made while the photographic plate is in the microcomparator. When first placed in the comparator the plate must be aligned so that the microscope cross-hair remains on the image of the liquid–air meniscus, R_0, as the plate is moved up and down. All horizontal measurements in the diagram are labeled R, and all vertical measurements are labeled Z. The first measurements are those of the reference points having horizontal coördinates, R_L and R_R; and vertical coördinates, Z_L and Z_R. Measurements are begun at R_0 and taken at intervals of 0.05 cm. until the image of the bottom of the cell, R_b is reached. All readings between R_0 and R_b are termed R_n, where $0.05n$ indicates the displacement of the horizontal coördinate beyond R_0. For each R_n there is a corresponding vertical measurement, Z_n, thus fixing each point in two coördinates. The spherical magnification factor, F, is the ratio of the horizontal dimension, Figs. 2, 3 and 4, as it appears on the photographic plate, to the corresponding dimension in the cell. The true center of the cell is 6.500 cm. from the center of rotation when the rotor is at rest. Due to slight stretching of the rotor this distance increases at higher velocities and at 59,780 r.p.m. is 6.540 cm. On the photographic plate the point R_M is equidistant from the points R_L and R_R and representative of the center of the cell. The true radius of rotation in the cell, represented by the point R_n on the diagram, is x_n cm., where $x_n = 6.540 - (R_M - R_n)/F$. The true radius of rotation of the liquid–air meniscus, x_0, and the true radius of rotation of the bottom of the cell, x_b, are calculated in the same manner.

In the ideal case Z_L and Z_R would have the same comparator measurements; but, in general, this is not so, and $\bar{Z}$, the average of the two, is used as reference. The corrected height of any point (R_n,Z_n) is $Z_n - \bar{Z}$, which is proportional to the refractive index gradient dn/dx. Since $dn/dx = k(dc/dx)$, where k is the specific refractive index increment and c is the concentration, $Z_n - \bar{Z} = Gab(\cot\phi)\cdot k(dc/dx)$. Here a is the cell thickness, b is the optical lever, G is the cylinder lens magnification, and ϕ is the inclination of the phase plate border to the vertical. When ϕ is kept constant for all measurements, the ratio of $Z_n - \bar{Z}$ to dc/dx is a proportionality factor common to all terms in the equations used for the calculations.

In general, a separate reference base line determination must be made. The reference photograph must fill two criteria. First, the R_0, R_n, and R_b of the reference picture must correspond to the values obtained for the solution. This necessitates that the cell filling for the solution and the solvent be the same. The best method of doing this accurately is by weighing the cell contents and making the necessary density corrections. Second, if the solvent contains sedimentable salts, then for each time-dependent photograph of the solution there must be a corresponding time-dependent reference picture. The reference photograph is measured at 0.05 cm. intervals between R_n and R_b and corresponding Z_n' values are obtained. The height of each specific point of the gradient for the solution above the reference base line is $(Z_n - \bar{Z}) - (Z_n' - \bar{Z}') = (Z_n - Z_n')_{cor}$. At the liquid–air meniscus, the value of $(Z_0 - Z')_{cor}$. is proportional to $(\partial c/\partial x)_{x_0}$, and at the true bottom of the cell $(Z_b - Z_b')_{cor}$ is proportional to $(\partial c/\partial x)_{x_b}$. These two quantities $(\partial c/\partial x)_{x_0}$ and $(\partial c/\partial x)_{x_b}$ are essential to the application of Archibald's method, as will be described below. The value of $(Z_n - Z_n')_{cor}$ in the region of constant concentration is zero. In the case of water as a solvent it is possible to use the flat portion of early diagrams as a reference base line.

During these experiments it was found that the true ends of the cell are not photographed. This was first noticed in measuring the picture of an empty cell spun at various speeds. The distance between the points on the diagram

(18) Supplied by David W. Mann Instruments, Lincoln, Mass.

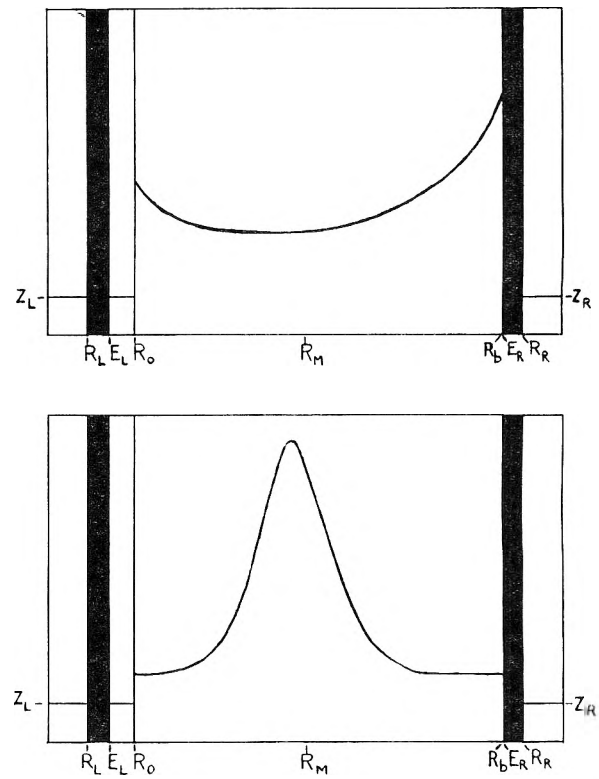

Fig. 4.—Upper figure, sedimentation diagram from standard cell; lower figure, sedimentation diagram from boundary-forming cell.

representing the top and bottom of the empty cell was less than the true height of the cell multiplied by F. This apparent foreshortening of the cell was attributed to the fact that light did not enter the cell at right angles to its windows. Under such conditions the foreshortening would be the same for each end of the cell. The true coördinate in the diagram for the top of the empty cell, E_L, is obtained by subtracting half this foreshortening from the observed coördinate. Further investigations showed that in cases where there is sedimentation of large molecules the distance from the image of the meniscus to the image of the cell bottom diminishes with time, while the distance from the image of the top of the cell to that of the meniscus remains constant. This effect concerns the bottom of the cell only and is caused by the interception at the cell window housing of light deflected by refractive index gradients near the cell bottom. This fact has no effect as far as the meniscus is concerned since the meniscus always shows. Since the apparent image of the bottom of the cell changes with time, it is necessary to calculate its actual position by reference to the image of the top of the cell and the foreshortening of an empty cell. The true coördinate, E_R, of the bottom of the cell is obtained from the corresponding quantity, E_L, for the top of the cell by adding F times the true cell height. Once E_R has been determined, values of $(Z_n - Z_n')_{cor}$ are extrapolated to this position.

Each centrifugation must be corrected for temperature change during the course of a run. To do this the filled cell is allowed to come to thermal equilibrium with the rotor, the temperature of the rotor is determined by the use of a thermocouple, the run is made, and the temperature of the rotor is again determined when it comes to rest. The initial and final temperatures are plotted against time, and a straight line drawn between these points. The plot must be corrected for heating of the rotor upon acceleration and deceleration, and also for the adiabatic cooling of the rotor during a run.[19,20] For centrifugation at 59,780 r.p.m. the heating of the rotor is 0.2° during acceleration and decelera-

(19) D. F. Waugh and D. A. Yphantis, *Rev. Sci. Instr.*, **23**, 609 (1952).

(20) A. Biancheria and G. Kegeles, *J. Am. Chem. Soc.*, **76**, 3737 (1954).

tion while the effect of adiabatic cooling is taken as 0.8°, so that 0.6° has been subtracted from the plots. For experiments performed below 10,000 r.p.m. the two effects essentially cancel each other. Temperatures have been interpolated at times corresponding to the middle of each interval of sedimentation.

The raffinose pentahydrate used in this experiment was reagent grade obtained from Distillation Products Inds., Rochester, N.Y. It was not purified, and concentrations of anhydrous material were computed assuming five moles of water per mole of raffinose hydrate.

The crystallized bovine plasma albumin, lot #370295-A, was obtained from Armour and Company, Chicago, Illinois. It was dried to constant weight in a desiccator over phosphorus pentoxide and then weighed directly into *p*H 4.40 buffer. This buffer was prepared from reagent grade sodium chloride, 0.15 *M;* sodium acetate, 0.02 *M;* and acetic acid, 0.03 *M*. The buffered bovine plasma albumin was dialyzed against several changes of buffer for 24 hours before being centrifuged. The final buffer dialysate was layered over the protein solution when the boundary-forming cell was used.

The partial specific volume of anhydrous raffinose was taken as 0.6077 cm.^{3}/g. as measured by Longsworth[21] at 25°. The densities of the solutions at various solute concentrations were calculated from the equation of McDonald and Gross.[22]

The partial specific volume of bovine plasma albumin is reported to be 0.7343 cm.^{3}/g. at 25°.[23] The density of the buffer was calculated according to the table of Svedberg and Pedersen.[24] For each solute concentration the density of the solution was recomputed from the partial specific volume.

Theory

The liquid–air meniscus and the bottom of the cell are both impervious to the flow of solute. According to Archibald,[6] this leads to the same formal equation at all times after the start of centrifugation in a sector cell, at these two radii of rotation, as the equation which holds elsewhere in the cell at sedimentation equilibrium.

$$M = RT(\partial c/\partial x)_{x_0}/(1 - V\rho)\omega^2 x_0 c_{x_0} \qquad (1)$$

$$M = RT(\partial c/\partial x)_{x_b}/(1 - V\rho)\omega^2 x_b c_{x_b} \qquad (2)$$

Here R is 8.313 (10)[7] ergs/mole/degree, T is the absolute temperature, V is the partial specific volume of the solute, ρ is the density of the solution, ω is the angular velocity, and x_0 and x_b are the radii of rotation of the meniscus and cell bottom, respectively, where the solute concentration has the corresponding values c_{x_0} and c_{x_b}.

According to Gutfreund and Ogston,[4] and Baldwin,[5] the sedimentation coefficient, s, may be computed from the combination of two alternative expressions for the flow of solute past a fixed surface, having radius of rotation X, in the cell. At X the concentration is not a function of the radius of rotation. A slight modification of Baldwin's equations[5] for the region of the cell above X yields the expression

$$-2s\omega^2 t = \ln\left[1 - \left\{\int_{x_0}^{X} x^2(dc/dx)dx - x_0^2\int_{x_0}^{X}(dc/dx)dx\right\} \Big/ c_0 x_0^2\right] \qquad (3)$$

Here t is the time of centrifugation, x is the radius of rotation where the concentration gradient of solute is dc/dx, and c_0 is the *original* solute concentration before centrifugation. By a straightforward recomputation according to the method of these authors, we find for the region of the cell below X

$$-2s\omega^2 t = \ln\left[1 + \left\{\int_{X}^{x_b} x^2(dc/dx)dx - x_b^2\int_{X}^{x_b}(dc/dx)dx\right\} \Big/ c_b x_b^2\right] \qquad (4)$$

To obtain the concentration at the meniscus, c_{x_0}, it is noted that

$$\int_{x_0}^{X}(dc/dx)dx = c_X - c_{x_0} \qquad (5)$$

The concentration c_X, in the region of the cell where $dc/dx = 0$, is a function of time according to

$$c_X = c_0 e^{-2\omega^2 st} \qquad (6)$$

Combination of equations 5 and 6 indicates that c_{x_0} is calculated according to

$$c_{x_0} = c_0 e^{-2\omega^2 st} - \int_{x_0}^{X}(dc/dx)dx \qquad (7)$$

The rearrangement of equation 3 gives

$$c_0 e^{-2\omega^2 st} = c_0 - \left\{\int_{x_0}^{X} x^2(dc/dx)dx - x_0^2\int_{x_0}^{X}(dc/dx)dx\right\} \Big/ x_0^2 \qquad (8)$$

Combination of equations 7 and 8 yields, finally

$$c_{x_0} = c_0 - \int_{x_0}^{X} x^2(dc/dx)dx/x_0^2 \qquad (9)$$

In a similar way it can be shown that

$$c_{x_b} = c_0 + \int_{X}^{x_b} x^2(dc/dx)dx/x_b^2 \qquad (10)$$

The last two equations are particularly useful in applying the Archibald method, equations 1 and 2 when refractive index gradient diagrams rather than refractive index data are available. It should be noted that the same integrals appear in equations 3 and 4 for the calculation of s by the Gutfreund–Ogston–Baldwin method. A single accumulation of two-coördinate data for dc/dx *vs.* x, therefore, serves for the application of both methods. The quantity c_0 appearing in equations 3, 4, 9 and 10 may be determined by integration of a separate refractive index gradient diagram from a boundary-forming cell, photographed prior to any appreciable sedimentation.

$$c_0 = \int_{x_0}^{x_b}(dc/dx)dx \qquad (11)$$

Calculations

A brief description will suffice to indicate how microcomparator measurements are employed in the equations developed above. In every case where an integral appears in the theory, it is replaced by the corresponding summation, *e.g.*

$$\int_{x_0}^{X} x^2(dc/dx)dx \propto (0.05/F)\sum_{n=0}^{n_X} x_n^2(Z_n - Z_n')_{cor}$$

where n_X refers to the number of increments of comparator coördinate R needed to bring $(Z_n - Z_n')_{cor}$ down to the value zero. In using such summations for integrals in equations 3 and 4, the constants of proportionality, including $0.05/F$

(21) L. G. Longsworth, *J. Am. Chem. Soc.*, **75**, 5705 (1953).

(22) E. J. McDonald and B. K. Gross, Report E, 11th Session, Int. Comm. Uniform Method Sugar Analysis, Paris, 1954. We are indebted to Dr. Andrew VanHook for calling this work to our attention.

(23) M. O. Dayhoff, G. E. Perlmann and D. A. MacInnes, *J. Am. Chem. Soc.*, **74**, 2515 (1952).

(24) T. Svedberg and K. O. Pedersen, "The Ultracentrifuge," Clarendon Press, Oxford, 1940.

derived from the comparator measurement interval and the cell magnification factor, divide out. In equations 9 and 10 the factor $0.05/F$ must be retained, because these equations appear in the denominator of the molecular weight expressions (equations 1 and 2) without corresponding summations in the numerator. All other proportionality factors cancel out.

It is convenient to make sedimentation calculations independent of uncertainties in the initial time of sedimentation. Photographs taken at times t_1 and t_2 after reaching full speed, for example, may be measured for application of equation 3. Equation 3 written for time t_1 is then subtracted from the corresponding equation written for t_2, and the sedimentation constant for an *exact* time $t_2 - t_1$ is calculated.

Results

Molecular weights for anhydrous raffinose, and sedimentation coefficients corrected to water at 20° are shown in Table I. The extrapolated value of $s^\circ_{20,w}$ at infinite dilution is estimated to be 0.31 Svedberg unit by plotting the reciprocal of the average s value for each of three concentrations against solute concentration. Recomputation of this value to 25° and combination with the known molecular weight, 504.5, in the Svedberg equation results in a calculated diffusion coefficient value of $4.3(10)^{-6}$ cm.²/sec. at 25° and infinite dilution, as compared to the value $4.339(10)^{-6}$ cm.²/sec. at a median concentration of 0.38% as given by Longsworth.[21]

TABLE I

ANHYDROUS RAFFINOSE AT 59,780 R.P.M.

Function	Time, min.	Solute, % 1.12	1.95	2.92
	Upper portion of cell			
$s_{20,w}(10)^{13}$	$t_2 - t_1 = 32$	0.25	0.24	0.23
	$t_3 - t_1 = 64$	0.25	0.25	0.23
M	$t = 32$	490	507	494
	$t = 64$	487	494	490
	Lower portion of cell			
$s_{20,w}(10)^{13}$	$t_2 - t_1 = 32$	0.29	0.26	0.21
	$t_3 - t_1 = 64$	0.29	0.27	0.22
M	$t = 32$	496	487	488
	$t = 64$	501	487	491

Molecular weights and sedimentation coefficients found from the upper region of the cell are tabulated for bovine plasma albumin in Table II. The results from the lower region of the cell were unsatisfactory, possibly due to the difficulties of extrapolation in this case. This will be investigated further. The average sedimentation coefficient in Table II, 4.0 Svedberg units, may be compared with the value 4.19 Svedberg units at 1% solute concentration recomputed from the data of Kegeles and Gutter[25] to take account of the adiabatic cooling of the rotor. The value of the diffusion coefficient of 0.5% median concentration of protein is obtained from the data of Akeley and Gosting,[26] who corrected for the presence of aggregated impurity. Their best average value appears to be $5.91(10)^{-7}$ cm.²/sec. at 20°. Combining this value with the recomputed $s^\circ_{20,w} = 4.36$ Svedberg units, we calculate for the best value of molecular weight 67,300, as compared with our present average value from Table II of 71,300.

TABLE II

BOVINE PLASMA ALBUMIN AT 8,500 R.P.M.

Function	Time, min.	Solute, % 1.004	1.088
	Upper portion of cell		
$s_{20,w}(10)^{13}$	$t_2 - t_1 = 16$	3.7	...
	$t_3 - t_1 = 32$	4.0	3.9
	$t_4 - t_1 = 48$	4.3	...
	$t_5 - t_1 = 64$	...	4.1
M	$t = 16$	71,000	...
	$t = 32$	70,000	72,000
	$t = 48$	71,000	...
	$t = 64$	72,000	72,000

Conclusions

The combined method of Archibald and of Gutfreund and Ogston permits simultaneous determination of molecular weights and sedimentation coefficients within one hour of centrifugation, for both raffinose and bovine plasma albumin. For raffinose the error in molecular weight was approximately 2% with an internal consistency of 1% in the measurements. The sedimentation constant at infinite dilution led to a calculated diffusion constant in good agreement with the literature. For bovine plasma albumin the error in the sedimentation constant seems to be about 5%, but the average molecular weight measurements are self consistent to 1% and the average agrees with a best value calculated from the literature[26] to within 6%. One of the most important factors in the reproducible results and the small internal error is the use of the modified phase-plate as previously described. The method outlined offers the distinct advantages of permitting molecular weight determinations in relatively short times of centrifugation, without resort to separate diffusion experiments, and with fairly simple calculations. Particular advantages are offered in the case of relatively unstable solutions; and in the case where small concentrations of large aggregates are being formed, complicating the interpretation of diffusion experiments.

Acknowledgment.—This work was made possible by U.S. Public Health Service Research grant RG 3449.

(25) G. Kegeles and F. J. Gutter, *J. Am. Chem. Soc.*, **73**, 3770 (1951).

(26) D. F. Akeley and L. J. Gosting, *ibid.*, **75**, 5685 (1953); see also H. Hoch, *Arch. Biochem. Biophys.*, **53**, 387 (1954), whose diffusion measurements would indicate a molecular weight over 71,000.

SEDIMENTATION IN CYLINDRICAL TUBES. EXPERIMENTS WITH A SHEARED-BOUNDARY CENTRIFUGE CELL[1]

BY B. ROGER RAY AND WALLACE R. DEASON[2]

Contribution from the Department of Chemistry and Chemical Engineering, University of Illinois, Urbana, Illinois

Received February 25, 1955

Sedimentation in a tube of circular cross-section aligned in a centrifugal field is considered for different convective and non-convective cases. Experimental results obtained with a multiple sheared-boundary cell are presented. This apparatus consists of five sections which automatically shear into alignment as the rotor slows down, thus isolating five fractions for analysis. It was found that no density gradient was necessary to stabilize the sedimentation of extremely dilute polystyrene latex. Calculated sedimentation coefficients drifted somewhat with the distance of the shear plane from the center of rotation and with the length of the run.

There are many instances in which analytical ultracentrifugation based upon an optical method of observation is not satisfactory. Diffusion may complicate the character of the boundary, the desired material may be associated with other materials and the boundaries overlap or cannot be identified and, finally, the optical method may lack the requisite selectivity or sensitivity. In contrast, the opaque or separation cell method offers advantages. In this method the concentration changes that occur within one or more portions of the solution in the cell during centrifugation are determined by analysis of the portions after completion of the run. The recent fine work of Hogeboom and Kuff[3] convincingly demonstrates some of the potentialities for determining sedimentation constants. In theory, the method could be applied to estimating heterogeneity.

Separation cells of non-convective design avoid, by use of mechanical barriers or density gradients, convection currents which would destroy the concentration effects produced by sedimentation. For instance, the Tiselius cell consists of a standard transparent sector cell fitted with a perforated metal plate and filter paper.[4] Density gradients, either normal or synthetic, have been depended upon in most cases: for example, in aligned capillaries,[5-7] in inclined tubes,[8] and most successfully in tubes in swinging-bucket rotors.[3,9,10]

The convective type of cell depends upon convection to keep all, or a known portion, of the solution at a uniform concentration (with respect to distance) during the run, except that particles which strike the end of the cell, or other immobilizing boundary, are removed irreversibly from the solution. The early work of Bechhold and Schlesinger[5] has formed the basis for many modifications in cell design. For example, the lining of the rim of the rotor with filter paper, the use of gels, and the use of metal washers and other inserts in the air driven "spinning top."[11] Elford designed a cell for the spinning top which consisted of a small horizontal capillary, in which convection did not occur, inverted into a larger cylindrical tube in which convection was assumed to occur.[12]

Valuable though opaque type cells have proved too little is known of the quantitative aspects of sedimentation in them; for instance, the difference in sectorial and cylindrical shapes, and the experimental requirements for non-convection and for convection. Our wish was to investigate further the sedimentation behavior in aligned tubes of cylindrical shape. As an aid we designed a cell with the following characteristics: sedimentation would not be complicated by a barrier; adequate volumes could be handled; isolation of portions of the solution would be positive, reproducible, and would not depend upon density gradients; all dimensions and volumes would be accurately known and reproducible. The result is a multiple sheared-boundary cell and rotor. Our first work with it has been to study the sedimentation behavior of a very dilute latex and to determine whether a stabilizing density gradient was needed.

Theoretical Considerations

Non-convective Sedimentation.—Three basic factors in the treatment of the sedimentation in separation cells are: the shape of the cell, the fact that particles tend to accelerate radially, and the effect of convective disturbances. These last can rise from non-sectorial cell shape as well as from vibration, thermal gradients, or density inversions.

Non-convective sedimentation in the sectorial cell was treated by Tiselius.[4] The Lamm equation

$$dm = s\omega^2 x_p q C\, dt \qquad (1)$$

gives the grams of material, dm, crossing a plane of area, q, in the time dt. The plane is at a distance x_p from the center of rotation, the concentration at the plane is C, and s and ω are, of course, the sedimentation coefficient and angular velocity. The plane, q, always lies somewhere within the plateau region, *i.e.*, beyond the sedimenting boundary.

(1) In part from a thesis of Wallace R. Deason submitted to the Graduate College of the University of Illinois in partial fulfillment of the requirements for the Ph.D. degree, 1953.

(2) Research Laboratories, Monsanto Chemical Company, St. Louis, Missouri.

(3) G. H. Hogeboom and E. L. Kuff, *J. Biol. Chem.*, **210**, 733 (1954).

(4) A. Tiselius, K. Pedersen and T. Svedberg, *Nature*, **140**, 849 (1937).

(5) H. Bechhold and M. Schlesinger, *Biochem. Z.*, **236**, 387 (1931).

(6) W. J. Elford and I. A. Galloway, *Brit. J. Exptl. Path.*, **18**, 155 (1937).

(7) M. Paic, *Compt. rend.*, **207**, 629 (1938).

(8) Th. P. Hughes, E. G. Pickels and F. L. Horsfall, Jr., *J. Exp. Med.*, **67**, 941 (1938).

(9) M. K. Brakke, *Arch. Biochem. Biophys.*, **45**, 275 (1953).

(10) H. Kahler and B. J. Lloyd, Jr., THIS JOURNAL, **55**, 1344 (1951).

(11) J. W. McBain and F. A. Leyda, *J. Am. Chem. Soc.*, **59**, 2998 (1937).

(12) W. J. Elford, *Brit. J. Exptl. Path.*, **17**, 399 (1936).

For the sector cell we have[13]

$$C_t/C_0 = (x_0/x_t)^2 = e^{-2\omega^2 st} \qquad (2)$$

where C_0 is the concentration at zero time, C_t is the concentration in the plateau region after time t. The particle sediments from x_0 to x_t in this interval. Substitution from eq. 2 into eq. 1, followed by integration over time t, leads to the solution for s for the separation cell.

$$s = -\frac{1}{2\omega^2 t} \ln\left[1 - \frac{2m}{C_0 q x_p}\right] \qquad (3)$$

Now an analogous treatment has been applied to the case of a cell with parallel walls such as a cylindrical or a rectangular cell. Without difficulty, one arrives at

$$C_t/C_0 = (x_0/x_t) = e^{-\omega^2 st} \qquad (4)$$

In the sector situation, two effects produce a decrease of concentration with time: an increase in velocity and an increase in cross-sectional area with distance. In the parallel case, the cross-section is constant. The simplifying assumption made is that although radial sedimentation occurs, all particles sediment parallel to the wall with a velocity given by $s\omega^2 x$. For both sector and parallel-wall cases, the plateau concentrations are uniform with distance, but they vary differently with time.

Substitution of eq. 4 into eq. 1, followed by integration, gives the solution for s in the case of idealized non-convective sedimentation in a parallel-wall tube

$$s = -\frac{1}{\omega^2 t} \ln\left[1 - \frac{m}{C_0 q x_p}\right] \qquad (5)$$

Bechhold and Schlesinger[5] were interested in non-convective sedimentation in a capillary tube with the assumption that material striking the bottom was packed irreversibly. By a circuitous route they arrived at the equivalent to eq. 5 (R, the distance of the bottom of the capillary from the center of rotation, replaces x_p). Elford[12] and Paic[7] have also treated sedimentation in capillaries, and it can readily be shown that their rather unwieldy expressions are identical and furthermore that they reduce finally to eq. 5.

Convective Sedimentation.—The case for complete convection in tubes with parallel walls has been studied by Bechhold and Schlesinger[5] and in cells of sectorial shape by McBain and co-workers.[14] The basic assumptions are, first, that particles striking the bottom or crossing some other fixed plane, are irreversibly removed, and, second, that convection produces a uniform concentration at all times throughout the column of solution undergoing convection. The correct mathematical derivations can be obtained in concise manner as follows.

Particles at the separation plane at a distance x_p from the center of rotation will have a velocity $\omega^2 s x_p$. It follows from eq. 1 that the grams per second striking will be, for the parallel-wall case

$$dm/dt = \omega^2 s x_p q C \qquad (6)$$

But $dm/qh = -dC$ where h is the height of the column of solution, and so

$$-dC = \frac{\omega^2 s x_p C\, dt}{h}$$

Integration over the time interval t, followed by substitution of C from the equality $m = qh(C_0 - C_t)$ yields

$$s = -\frac{h}{x_p \omega^2 t} \ln\left[1 - \frac{m}{C_0 q h}\right] \qquad (7)$$

Comparison with eq. 5 for the non-convective case is instructive. If, in the convective cell the column of solution is extended to the center of rotation, h becomes equal to x_p and the two equations are identical. This means that the concentration, at any given time, in the convectively stirred column which extends to the center of rotation must be the same as the concentration in the plateau region in the non-convective cell.

For the case of complete convection in the sector cell, we can write, analogously to eq. 6

$$dm/dt = (\omega^2 x_p s)(k\theta x_p)C \qquad (8)$$

in which k is the sector thickness and θ the sector angle. Let x_0 be the meniscus distance, and then the volume of solution is $k\theta/2\ (x_p^2 - x_0^2)$. Dividing eq. 8 by this quantity gives an expression for dC which can be integrated over the time interval to yield

$$\ln (C_t/C_0) = -\frac{2x_p^2 \omega^2 st}{x_p^2 - x_0^2} \qquad (9)$$

C_t can be substituted into eq. 9 from the equality $m = k\theta/2\ (C_0 - C_t)\ (x_p^2 - x_0^2)$ and the result after rearranging and writing in the logarithmic form is

$$s = -\frac{x_p^2 - x_0^2}{2x_p^2 \omega^2 t} \ln\left[1 - \frac{2m}{k\theta(x_p^2 - x_0^2)C_0}\right] \qquad (10)$$

Comparison can be made with eq. 3 for the non-convective case. When the above convective cell is extended to the center of rotation, that is, so as to give a pie-shaped column of solution, eq. 10 reduces to eq. 3 because $x_0 = 0$, and $k\theta x_p = q$. Thus, analogous to the case for parallel-wall cells, we find that the concentration at a given time in the convective sector cell which extends to the center is the same as that in the plateau region in the non-convective sector cell. It also becomes apparent that the behavior of concentration with time for pie-shaped columns of solution, with and without convection, are identical.

The earlier derivations were tedious and, in fact, dimensionally incorrect. There resulted a slightly incorrect solution for the case of the sector cell.

Partial Convection.—This situation may be expected to arise whenever the shape of the cell deviates from sectorial form, but just what contribution the wall effects make to the over-all sedimentation behavior is not clearly established. To estimate these effects in a tube of circular cross-section we derive an expression for the rate with which particles strike the walls of the tube. A particle sediments radially with a velocity $\omega^2 sx$. The component of this velocity normal to the wall will be $(\omega^2 sx)(\sin \theta/2)$. Here θ is the angle between

(13) T. Svedberg and K. Pedersen, "The Ultracentrifuge," Oxford University Press, London, 1940.

(14) J. W. McBain and F. A. Leyda, *Acta Physicochim. U.R.S.S.*, **14**, 421 (1941).

radii running from the center of the rotor to the sides of the cell at the distance x and at a vertical height n. Let $L\,dn$ be an increment of wall area of finite length L and height dn. Now the number of grams of solute, dm_w, striking this area is given by

$$dm_w = (\omega^2 sx \sin \theta/2) L\,dn\,C\,dt \qquad (11)$$

For the cell of circular cross section, θ is a function of both x and n, where n is the height level in the horizontal cell. Letting the tube radius be r we have, in the rectangular coördinate system, $r^2 = z^2 + n^2$. But at each level of height $\sin \theta/2 = z/x$; therefore

$$\sin \theta/2 = (r^2 - n^2)^{1/2}/x \qquad (12)$$

Substitution into eq. 11 for $\sin \theta/2$ and C (from eq. 2) yields an expression which can be integrated with respect to n, from $n = 0$ to $n = r$, and then integrated with respect to time. The result is for one quadrant of the circular cross-section. For the four quadrants it becomes

$$m_w = \frac{\pi r^2}{2} C_0 L(1 - e^{-2\omega^2 st}) \qquad (13)$$

Here m_w indicates the total amount that will have struck the walls of the tube over a wall length L during the elapsed time t. Interestingly enough, the rate of striking is seen to be independent of distance from the center of rotation. This is to say, at each value of n the rate is uniform at every point along a wall, changing only with time. When the wall length is given the value x_p, it can be seen that eq. 13 has a special analogy to eq. 3.

Equation 13 applies to the region of the cell beyond the sedimentation boundary, *i.e.*, to the plateau region. If the inner portion is to be included, L must decrease with time as the boundary moves outward and can be represented by $x_p - x_0 e^{\omega^2 st}$, with x_p the distance of the outer point of the cell for which m_w is to be calculated, and x_0 the meniscus distance. (Precisely, L is given by the more complicated expression $x_p - cos\ \theta/2\ x_0 e^{\omega^2 st}$). The final equation now becomes

$$m_w = \frac{\pi r^2}{2} C_0 x_p (1 - e^{-2\omega^2 st}) - \pi r^2 C_0 x_0 (1 - e^{-\omega^2 st}) \qquad (14)$$

The use of eq. 13 or 14 permits a more quantitative treatment of sedimentation in cylindrical cells. In principle, these equations might possibly be utilized to estimate the sedimentation coefficient.

For radial sedimentation in the cylindrical tube the following cases can be distinguished:

I. Upon reaching the wall the material sediments, to all intents, parallel to the wall with a velocity $\omega^2 sx$. The equations for the parallel wall cell then apply, *i.e.*, C_t/C_0 will be given by eq. 4 and m by eq. 5.

II. Upon reaching the wall the material ceases to sediment in the usual sense and behaves in one of the following ways: a. It slides along the wall essentially as a solid phase and is removed from the column of solution. b. It adheres to the wall at the point of arrival and is later removed for analysis along with the adjacent solution. c. It creates a dense layer of solution at the surface of the wall. This film flows convectively toward the bottom, where it displaces an equal volume of solution. The result is hard to predict, although certainly the concentration gradients at the bottom of the tube and in the upper region will be distorted. d. It adheres to the wall at the point of arrival and is not later removed for analysis with the adjacent solution.

Case IIa will result in a uniform concentration, C_t, throughout the "plateau" region, and C_t/C_0 will be given by the sector cell expression, eq. 2. The amount of material that will have been lost from above a given plane at distance x_p must be equal to the amount, m_r, which passed the plane by direct radial sedimentation plus the amount, m_w, which struck the walls above the plane. From eq. 1 we get the amount m_r to be

$$m_r = x_p \pi r^2 C_0 (1 - e^{-2\omega^2 st})/2 \qquad (15)$$

while eq. 14 gives us m_w. Adding, we obtain

$$m_r + m_w = \pi r^2 C_0 [x_p - x_0 - x_p e^{-2\omega^2 st} + x_0 e^{-\omega^2 st}] \qquad (16)$$

The solution for the sedimentation coefficient is

$$s = -\frac{1}{\omega^2 t} \ln \left[\frac{x_0}{2x_p} + \left(k - \frac{m}{\pi r^2 C_0 x_p} \right)^{1/2} \right] \qquad (17)$$

$$k = \frac{x_0^2}{4x_p^2} - \frac{x_0}{x_p} + 1$$

For case IIb, the concentration C_t in the "plateau region" again will be found uniform with distance. It can be obtained by adding to the final concentration that results from direct radial sedimentation ($C_0 e^{-2\omega^2 st}$), the concentration contribution due to m_w grams being redispersed into the solution. The latter is calculated from eq. 14 to be $C_0(1 - e^{-2\omega^2 st})/2$. The sum yields

$$C_t/C_0 = 1/2 + 1/2 e^{-2\omega^2 st} \qquad (18)$$

or, in other words, C_t is the arithmetical average of the original concentration and of the final concentration that results from radial sedimentation. The amount of material that will have been lost from above a given plane at a distance x_p must be equal to the amount, m_r, which passed the plane by direct radial sedimentation.

Multiple Sheared-boundary Cell and Rotor

The cell spaces in the apparatus consist of holes in five discs stacked together. Alternate discs are keyed to a shaft that can be caused to rotate 90°, thereby isolating five fractions. The acceleration of the rotor causes a pair of piston-like weights to move outward against springs, and the linear motion is transformed to rotary motion of the shaft. On deceleration the reverse procedure takes place. The major problems in design were: to achieve symmetry, balance and strength; to avoid leakage and void spaces; to reduce frictional effects.

The diagrammatic sectional views of the apparatus in Figs. 1 and 2 indicate the salient features. Figure 1 shows the Duralumin rotor in vertical cross-section through the plane of the pistons. A bearing block supports an axle A which has slots milled into each end. Two grooved wheels B fit on the axle, one of which is pressed on and pinned to the pistons E by the drive linkages G. Identical linkages pinned to the second, freely rotating, wheel are shown as dotted lines and assure balance of the assembly at all times.

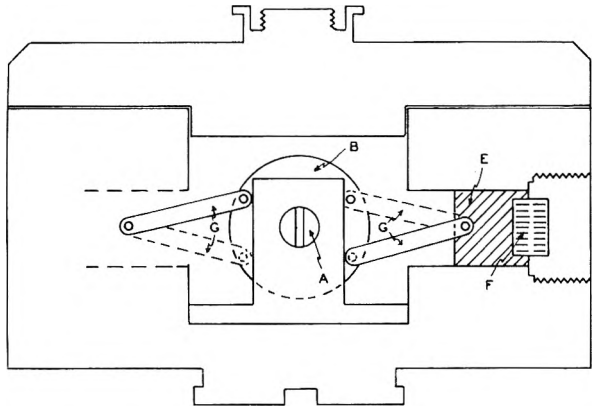

Fig. 1.—Rotor for sheared-boundary cell (shown in vertical cross-section).

Figure 2 is a view in horizontal cross-section. Here are shown the conical springs F which counteract the centrifugal masses of the pistons. One of the two identical cell assemblies is shown in place. The five discs, plus a top cover disc numbered 6, fit into the cell housing D. Discs 1, 3 and 5 are pinned into position and do not rotate. Discs 2 and 4 are attached to the shaft C by keys I. The shaft locks into the slot in the end of the axle A. The twin cell holes are shown (actually the holes should be above and below the shaft in this view). The cell holes have a radius of 0.56 cm. and the shear planes are at 4.24, 5.26, 5.77, 6.27 and 6.78 cm., respectively, from the center of rotation.

A critical requirement is that the Duralumin cell discs rotate smoothly and reproducibly. The best lubricants found were silicone DC-4 and Molycote G greases.[15] Repeated tests showed that the cells opened at 1200–1800 r.p.m. and closed at 1400–1500 r.p.m. The apparatus has been operated successfully at speeds up to 20,000 r.p.m.

To fill the cells, the five discs are assembled in the housing, aligned, and the holes filled with solution to excess. Disc 6 is dropped into position, and the excess solution forced out the screw holes assures the absence of air bubbles. Three ml. of solution is placed above disc 6 and serves to fill any void spaces around the cell parts and cell shaft.

After a run the six discs can be lifted or blown out as a unit from the housing. With the shaft removed, each cell plate is rotated in turn and the sample from each hole in each plate removed with a hypodermic syringe. Each hole is rinsed several times and the rinsings added to the sample. The usual practice was to pool the samples from the two holes of a disc.

Discussion of Results

A Spinco Model E Ultracentrifuge was used for the experiments and the customary operating procedures were followed. The average temperature was estimated from the initial and final temperatures of the rotor. The length of the run, designated as the "equivalent time," was calculated to be the sum of one-third the time to accelerate from

(15) Dow Corning Corp., Midland, Mich., and The Alpha Corp., Greenwich, Conn.

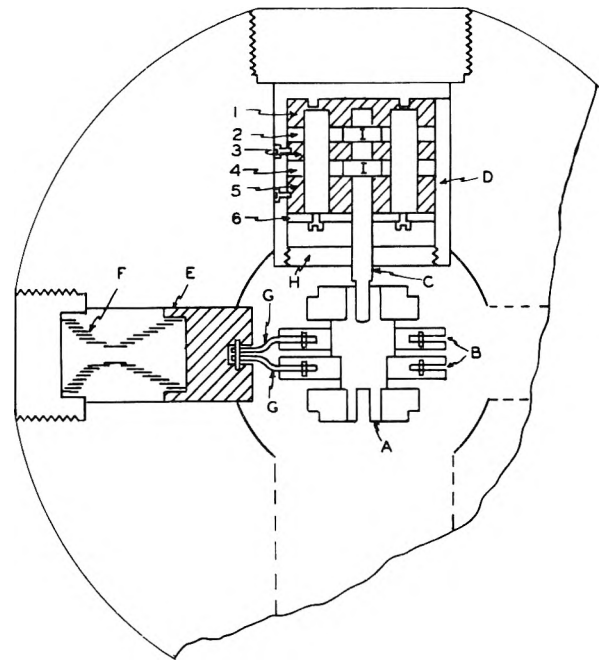

Fig. 2.—Rotor and cell assembly for sheared-boundary cell (shown in horizontal cross-section).

1000 r.p.m. to speed, the time at speed, and one-third the time to decelerate to 500 r.p.m.

The analyses of the solutions were simplified by the fact that only relative concentrations were needed. These are given as the ratio of the final to the initial concentrations. From the analytical data one could calculate what proportion of the original material in the cell was recovered. This is expressed as the recovery ratio C_0'/C_0. The values of the term m/C_0 were calculated in the following manner. (Fractions are designated according to the disc numbers in Fig. 2 and the shear planes as a, b, c and d, progressing toward the periphery.) Since $m_a = V_5(C_0 - C_f)$, where C_f is the final concentration of the solution in disc 5, then $m_a/C_0 = V_5(1 - C_f/C_0)$. Likewise for shear plane b, $m_b/C_0 = m_a/C_0 + V_4(1 - C_f/C_0)$ where C_f refers to the final concentration in disc 4.

Polystyrene Latex.—The sample was a 0.016 wt. % solution of Dow latex 580G, lot 3584, kindly supplied by Mr. Albert Vatter of our electron microscope laboratory. Table I summarizes the data for representative runs in which sedimentation was allowed to proceed to varying degrees. Run 7 was made with the 0.016% solution, the other runs at approximately 1/10 this concentration, *i.e.*, with 15 p.p.m. of latex. Concentrations were measured with a Coleman photo-nephelometer. Each concentration ratio given in Table I is the average of the values for the two cell assemblies. This was done since the concentrations of the separate assemblies agreed closely, thus giving evidence of reproducible behavior. For example, for run 3 the individual concentration ratios in the two assemblies were 0.580 and 0.582, 0.755 and 0.765, 0.745 and 0.755, 0.781 and 0.775, and 2.660 and 2.604.

The recovery ratios, given on the last line of Table I, show that essentially all of the original

Table I

Sedimentation Data on Polystyrene Latex in the Sheared-Boundary Cell

	1	2	3	4	5	6[a]	
Concn., wt. %	0.0016	0.0015	0.0015	0.0015	0.0015	0.0015	0.016
Speed, r.p.s.	73.3	74.9	74.7	74.8	74.8	74.6	73.5
Equiv. time, sec.	930	1500	2130	3300	4800	960	2135
Temp., °C.	22.0	24.7	21.5	22.9	22.1	20.0	23.6
Corr. factor, $s_{20,w}/s_t$	0.946	0.877	0.959	0.923	0.943	1.000	0.916
Concn. ratio, C_f/C_0							
Fraction 5	0.815	0.675	0.581	0.327	0.152		0.587
4	0.926	0.826	0.760	0.706	0.450		0.765
3	0.940	0.822	0.750	0.706	0.454	0.478	0.785
2	0.976	0.836	0.778	0.706	0.454	0.956	0.800
1	1.656	2.011	2.632	...[b]	4.154	1.494	2.215
Recovery ratio, C_0'/C_0	1.021	0.991	1.014	...	0.969	0.976	0.956

[a] Cell plates 1, 2 and 3 used. [b] Sample lost.

material was recovered. This fact was evidence that no material escaped or entered the individual cell holes during a run, that no material remained adhered to the walls after rinsing, that the solid layer of particles packed in the bottom of disc 1 were capable of complete redispersion, and that the calculated volumes of the individual compartments were correct. The analytical error was relatively large because the solutions were so very dilute.

Examination of the concentration ratios in Table I is instructive. In each case, the concentration in fraction 5 is smallest, the concentrations in fractions 4, 3 and 2 are about the same and represent a plateau region, and fraction 1 has accumulated the material lost from the other four. These results indicate that ordinary convection was not present in the cell column. Also, the sharp rise in concentration in going from fraction 5 to fraction 4 suggests a definite sedimentation boundary in 5 since a continuous gradient would, in longer runs at least, reach into 4. Likewise, the rise from fraction 2 to 1 suggests that the sedimented material is retained on or near the bottom surface. Although the shape and breadth of the sedimentation boundary cannot be studied by this layer analysis technique, it cannot have been too broad. In these runs the polystyrene could not have produced a density gradient to create a stabilizing action because it has a density of only 1.054, and the solutions were only 0.0016 wt. %.

Some comparison can be made with the results of other workers. Using a swinging-bucket rotor and a portion of the same lot of latex at 0.007%, Kahler and Lloyd[10] found no boundary upon analysis of the fractions unless a fairly large synthetic density gradient existed along the column of solution. Hogeboom and Kuff,[3] also using a swinging-bucket rotor, found unstable boundaries in dilute colloidal solutions, including this same latex at 0.008%, unless a synthetic gradient was introduced. The explanation may lie in the fact that during deceleration the tubes in the swinging-bucket rotor rotate from horizontal to vertical position. In addition, if the compression gradient is important then, of course, it disappears before the isolation of the fractions is accomplished.

As discussed in the preceding section, the concentration data permit the calculation of the sedimentation coefficient. To do this by "layer analysis" one calculates the value of m/C_0 for the shear plane under consideration and substitutes it into the appropriate equation along with the other experimental quantities. In Table II the sedimentation coefficients are tabulated for each of the four shear planes. The calculations[16] were carried out for the cases of the parallel cell (eq. 5), the sector cell (eq. 3), and the sector cell modified for slippage of material that impinges on the walls (eq. 17).

The sedimentation coefficient of this latex has been determined by several workers. Using the optical method, Sharp[17] reported $s_{20,w}$ as 1960 and Hogeboom and Kuff[3] 2270 at 0.008% concentration. We have likewise studied the material in the transparent cell and obtain 2075 at 0.016% and 2177 at 0.0015%. In neither case was there a refractive gradient curve, only the absorption gradient. For the runs at the latter concentration a 30 mm. deep cell was used and the photographic negatives were scanned on a Carey recording microphotometer. Using data from separation cells, values of 2155 at 0.007%[10] and 2040–2180 at 0.008%[3] are reported when stabilizing gradients were employed.

Examination of the results in Table II shows that the calculated coefficients increase as one proceeds from shear plane a through d. Furthermore, the spread in values increases with the length of the run. The calculations based upon the parallel cell equation, applicable to Case I, are always less than those based upon the sector cell equation, applicable to Case IIb. The magnitude of the difference depends upon the amounts of material transferred and the distances involved. To illustrate, for a cross-section of 1 cm.^{2} and a shear plane at 5 cm. we calculate that if 12.5% of the material has crossed the plane, then the sector-based s is 1.0% larger. We conclude that if less than 25% crosses the plane, the two calculations

(16) Some of the calculations were made using early-measured values for the distances of the shear planes. Later remeasurements were slightly less. Also, some of the concentration ratios used were corrected to C_f/C_0' so as to express the amount recovered from a compartment as a fraction of the total amount recovered from the cell after the run. Neither of these changes significantly affects the values of the coefficients; therefore recalculations to a common basis were not performed.

(17) D. G. Sharp, *J. Applied Phys.*, **21**, 71 (1950).

TABLE II

SEDIMENTATION COEFFICIENTS OF POLYSTYRENE LATEX AS DETERMINED IN THE SHEARED-BOUNDARY CELL

		1	2	3	4	5	6[a]	7
$(C_f/C_0)_5$		0.815	0.675	0.581	0.327	0.152		0.587
Sedimentation coefficient, $s_{20,w} \times 10^{13}$								
Parallel cell eq.	a	1834	1697	1780	1748	1603		1648
	b	2060	1924	2080	1952	1975		1968
	c	2169	2153	2310	2129	2275	2021	2193
	d	2186	2267	2440	2278	2507	1965	2322
Sector cell eq.	a	1872	1739	1838	1881	1770		
	b	2106	1999	2198	2132	2250		
	c	2249	2232	2510	2347	2694	2095	
	d	2240	2390	2680	2542	3007	2008	
Modified sector cell eq.	a	1435		1530		1510		
	b	1540		1715		1860		
	c	1540		1880		1985		
	d	1510		1918		2195		

[a] Cell plates 1, 2 and 3 used.

agree within experimental error. For Run 1 the difference is negligible. In effect, the difference is that the sector equation avoids the loss of any material by sedimentation from that part of the compartment which lies outside the elliptical cone with the base of area πr^2.

Calculations based upon the modified sector cell equation, referring to Case IIa, must give values considerably less than those from either of the other equations. This stems from the assumption that a part of the material has left the compartment by sedimentation and in addition some by slippage. The correction for slippage is always appreciable. In fact, it is proportionately larger for the short runs since the wall area is maximum. This can be seen by comparing Runs 1 and 5. Another feature of the modified equation is that it reduces the spread of the values as calculated for planes a through d.

It will be observed for the several runs that the coefficients calculated near the mid-point of the cell are approximately 2200 and do not seem to reflect the length of the run. The transparent cell gave 2177 at this concentration and the question might be asked as to whether or not some averaging effect is present. Hogeboom and Kuff[3] calculated the coefficient of this latex to be 2180 based upon a layer analysis of an 0.008% solution stabilized with a sucrose gradient. They cut the cell into two portions near the midpoint. In terms of C_f/C_0 their run is comparable to Run 4.

There remains a second method to evaluate the sedimentation coefficient. This is to utilize the C_f/C_0 value for the plateau region of the cell. In Table III the average C_f/C_0 ratio of fractions 3 and 4 of each run is tabulated along with the coefficient calculated according to parallel-wall eq. 4 and sector wall eq. 2. The results differ, of course, by the factor of two. Calculations are not given for eq. 18, which is applicable to Case IIb, since the values are even larger than those for the parallel case.

The plateau concentration has not been utilized by workers because it changes with time relatively slowly and it is not readily determined by the usual optical methods. In the present case the values calculated by the different equations may assist in interpreting the sedimentation behavior. Referring to Table III we find the sector equation to yield values of the right order of magnitude and therefore to suggest behavior similar to that of case IIa.

One qualitative interpretation of the results given in Tables II and III is in terms of Case IIc, in which a dense film of solution streams down the wall. This action might not seriously change the plateau concentration predicted by the sector equation. The main fluid column would be lifted slightly, and this would lead to low coefficients based upon the amounts of material that had crossed the innermost shear planes. An experiment was made to test whether streaming occurred. Cell discs 1, 2, 3 and 4 were filled with polystyrene containing 0.015 g. of sodium chloride in 15 ml., while disc 5 was filled with polystyrene containing 0.015 g. of methylene blue in 5 ml. A centrifuge run was carried out at 80 r.p.s. for 4800 sec. Colorimetric analysis of the isolated fractions showed 20% of the dye in disc 4, 0.1% in disc 3, and none whatever in discs 1 and 2. Obviously, streaming of solution did not occur in this run.

TABLE III

SEDIMENTATION COEFFICIENTS AS CALCULATED FROM THE CONCENTRATION OF THE PLATEAU REGION

Run	(C_f/C_0) av.	$s_{20,w}$ Parallel	Sector	Optical
1	0.933	3320	1660	2177
2	.824	5085	2547	
3	.755	5720	2860	
4	.706	4390	2195	
5	.452	7020	3510	
7	.775	5030	2515	2075

An additional experiment with methylene blue was performed that further substantiated the lack of convection currents. A run at 80 r.p.s. for 7500 sec. was made in which a small amount of dye had been added to the latex in disc 1. Following the run, negligible amounts of dye were found in discs 5 and 4, about 1% in disc 3, and 12% in disc 2. The amount in disc 2 was shown to be no more than

that produced by the slight turbulence accompanying the shearing motion plus that resulting from diffusion.

To this point it has been assumed that the latex is a homogeneous material with respect to sedimentation. It is true that this lot is highly homogeneous under the electron microscope, although even there a measurable distribution can be observed. A second factor exists in sedimentation: this is the particle density. In the present case, the rate is very sensitive to this because the particle density is so nearly that of the medium. In our hands this latex formed boundaries in the optical cell that had appreciable breadth. However, Hogeboom and Kuff[3] observed a sharp boundary in the optical cell but obtained a broad one in the swinging-bucket rotor even though in the second case the latex boundary was stabilized by a synthetic density gradient that would be expected to produce a sharpening effect.

A more complete understanding of the results presented here will follow from further work. We are at this time investigating the effects of slight disalignment of the cell discs, the fact that neither the meniscus nor the shear planes are curvilinear, and also the fact that a small gravitational convection is to be expected in tubes of circular cross section. Preliminary work with edestin, a very homogeneous protein with a sedimentation coefficient of around 13, indicates that its behavior in the sheared-boundary cell is quite unlike that of the latex. (The same values of the coefficients are obtained for each shear boundary, and these agree fairly well with those from optical observations.)

Acknowledgments.—We are greatly indebted to Mr. A. E. Wood for the construction of the apparatus, to Prof. D. T. Englis for assistance with some of the analytical determinations, and to Mr. R. E. Post and Dr. H. S. A. Gilmour for very helpful discussions.

DISCUSSION

JOHN SMITH.—Could not a sector-shaped cell hole be machined.

ROGER RAY.—Our machinist is now working on one. It has only three cell plates. We are decreasing the mass of the cell assemblies, decreasing the frictional areas, and using dissimilar metals for the alternate plates.

STUDIES OF THE SURFACE CHEMISTRY OF SILICATE MINERALS. III. HEATS OF IMMERSION OF BENTONITE IN WATER

BY A. C. ZETTLEMOYER, G. J. YOUNG AND J. J. CHESSICK

A Contribution from the Surface Chemistry Laboratory, Chemistry Department, Lehigh University, Bethlehem, Pa.

Received April 6, 1955

Nitrogen, ammonia and water vapor adsorption isotherms were measured on a Wyoming bentonite, a montmorillonite. In the BET range, nitrogen and water measured only the external area, whereas ammonia measured the internal area as well. The adsorption isotherms were monotonous, but heats of immersion in water of samples equilibrated at increasing water vapor pressures reflected the regions at which the first and second layers of water formed between the platelets. X-Ray data for the x-axis spacing confirmed these findings. Comparison of the heat of immersion curves for samples activated at 25 *versus* 100°, and with the adsorption isotherms, revealed high energy sites for water adsorption. These are apparently exchange ion sites.

Introduction

The first studies in this series dealt with the surface chemistry of chrysotile asbestos fibers[1,2] as revealed by gas adsorption and heat of wetting measurements. In the present paper, results of similar studies of Wyoming bentonite, a montmorillonite, are described. Future papers will deal with kaolinite, attapulgite and other silicate minerals.

Many previous workers have compared the adsorption of nitrogen and water vapor by silicate minerals. Recently, for example, Keenan, Mooney and Wood[3-5] studied a series of kaolinites and a montmorillonite by this approach. Heats of immersion of these minerals have been measured also as indicated in the summary given by Grim.[6] Unfortunately, both these techniques have not previously been used on the same samples. When the heats of immersion were measured, adsorption isotherms and surface areas were not measured, and *vice versa*.

In addition, no previous work has been reported for bentonite in which the heats of immersion were followed as the mineral was exposed to greater and greater water vapor pressures. As for asbestos, the limitations of isotherm measurements in deducing the surface properties of bentonite become apparent when the results of the heats of immersion measurements are considered. Comparison and interpretation of adsorption results on clays such as bentonite are also complicated by: (1) the number of exchange ion sites, (2) the type and number of adsorbed ions, (3) the different amounts of internal area exposed on swelling by different polar molecules, and (4) the presence of variable amounts of impurities.

Experimental

X-Ray diffraction studies of the bentonite sample employed in this investigation[7] showed it to be mainly montmorillonite

(1) G. J. Young and F. H. Healey, THIS JOURNAL, **58**, 881 (1954).

(2) F. H. Healey and G. J. Young, *ibid.*, **58**, 885 (1954).

(3) A. G. Keenan, R. W. Mooney and L. A. Wood, *ibid.*, **55**, 1462 (1951).

(4) R. W. Mooney, A. G. Keenan and L. A. Wood, *J. Am. Chem. Soc.*, **74**, 1367 (1952).

(5) R. W. Mooney, A. G. Keenan and L. A. Wood, *ibid.*, **74**, 1371 (1952).

(6) R. E. Grim, "Clay Mineralogy," McGraw-Hill Book Co., Inc., New York, N. Y., 1953, p. 184.

(7) Supplied by the American Colloid Company, Merchandise Mart Plaza, Chicago 54, Illinois. The clay is predominantly a sodium clay and is sold commercially under the trade name Veleay.

containing small amounts of feldspar, quartz, and kaolinite. The sample was extracted repeatedly with distilled water, dried at 80° and crushed in an agate mortar before adsorption and heat of wetting measurements were made.

Water vapor adsorption isotherms were determined gravimetrically at 25° for a sample degassed at 25° for 48 hours and for another sampe degassed at 100° for 24 hours. Equilibrium pressures were read on an oil manometer filled with Apiezon "B" Oil. Equilibrium was attained within 24 hours for relative pressures up to about 0.50; beyond this relative pressure much longer times were required.

A conventional volumetric adsorption apparatus was employed for the ammonia and nitrogen adsorption studies. The gases were Mathieson Pure Grade and were fractionated into storage bulbs before use. The sample bath temperature for the ammonia adsorption was held at *ca.* −32°. This temperature was maintained constant by use of an equilibrium mixture of solid and liquid bromobenzene; the presence of the solid phase was assured by a cold finger tube containing Dry Ice. The bath for nitrogen adsorption was liquid nitrogen.

The calorimeter used in the heat of immersion studies has been described.[8] Values for the heats of immersion were obtained for degassed bentonite samples and for samples equilibrated at continuously increasing amounts of adsorbed water. As for the isotherms, samples evacuated under two different conditions were studied: one series was evacuated at 25° for 48 hours, the other evacuated at 100° for 24 hours. The samples for heat of immersion studies that were exposed to water vapor were prepared on an adsorption apparatus and sealed off after the desired equilibrium pressure was attained. Care was taken to ensure that the temperature of the sample was not altered during the sealing-off process. The heat values were calculated on the basis of the dry sample weight and were corrected for the heat of breaking of the sample tubes.

X-Ray data on the exposed samples were taken with an automatic recording G.E. XRD-3 X-ray unit. The specimen holders were filled with the bentonite samples and then equilibrated in desiccators containing saturated salt solutions giving the desired relative pressure of water vapor. The specimen holders were then covered with a very thin formvar film so that there would be no change in the water content of the samples during the X-ray measurements.

Results and Discussion

Nitrogen, Ammonia and Water Vapor Adsorption Isotherms.—Bentonite is an expanding lattice type clay. The principal structural components are alternate layers of hydrated metal oxide and silicon–oxygen tetrahedron sheets. These layers are normally loosely held together by coördinately bound water molecules. When polar molecules are taken up between these layers, the familiar swelling phenomenon takes place. Thus, in the present investigation both water vapor and ammonia adsorbed on the external surface and also entered between the ultimate platelets which comprise the primary particles of the bentonite. Nitrogen, on the other hand, was only adsorbed on the external surface.[9]

The external surface of the bentonite calculated by the BET equation from nitrogen adsorption data was 34.5 m.²/g. Grinding the sample after washing and drying increased the area from an original value of 11.7 m.²/g. Mooney, *et al.*,[4] have also reported that sample preparation affected the surface area due to breaking up of some of the organized bentonite particles. The nitrogen isotherm was a typical Type II and similar to that for a nonporous solid.

The ammonia adsorption data showed that there was a much larger uptake of this gas in the BET range of relative pressure (p/p_0 0.05 to 0.35) than could be explained on the basis of the external area alone. Past this range of relative pressure the isotherm showed a very gradual increase in the amount adsorbed until a relative pressure of about 0.85 where the adsorption again increased strongly. Because of the large difference in the amount of ammonia adsorbed compared to water or nitrogen, it is evident that in the BET range of relative pressure ammonia not only adsorbs on the external bentonite surface but is also imbibed between the platelets, a number of which comprise each bentonite particle. The area calculated from the ammonia V_m amounted to 295 m.²/g. This value represents the external area and half the internal area since only one molecular layer of ammonia will be expected to adsorb between platelets in this region of relative pressure. Thus the total surface area is obtained by subtracting the nitrogen area which gives the external area from twice the ammonia monolayer area. A total area of 556 m.²/g. was estimated in this manner.

Isotherms for the adsorption of water vapor on bentonite samples evacuated at 25 and 100° are shown plotted in Fig. 1. Unlike ammonia, water

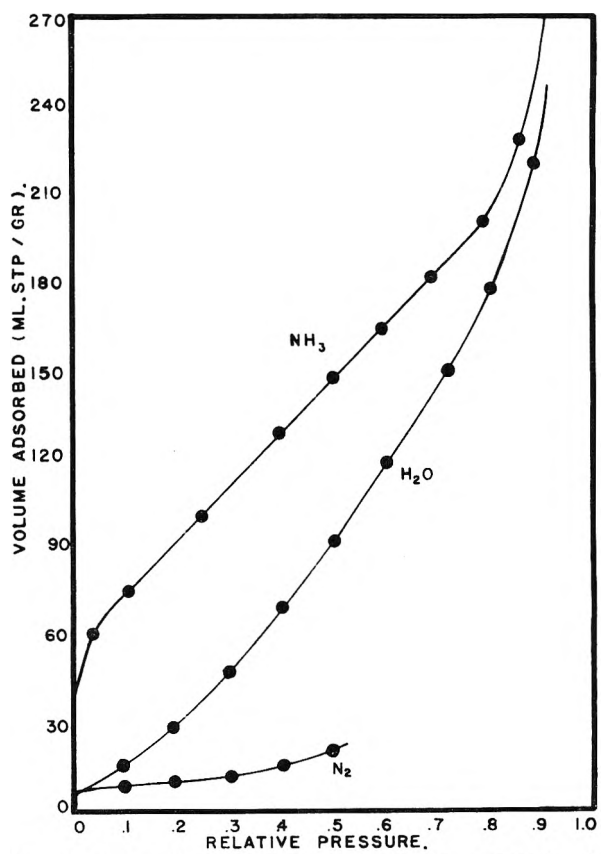

Fig. 1.—Adsorption isotherms for NH_3, N_2 and H_2O adsorbed on bentonite.

vapor was adsorbed principally on the external surface of the clay in the BET range of relative pressure. These results are contrary to those of Mooney[4] and Hendricks[10] who found that water

(8) A. C. Zettlemoyer, G. J. Young, J. J. Chessick and F. H. Healey, THIS JOURNAL, **57**, 649 (1953).

(9) S. Brunauer, "The Adsorption of Gases and Vapors," Princeton University Press, Princeton, N. J., 1945, p. 357.

(10) S. B. Hendricks, R. A. Nelson and L. T. Alexander, *J. Am. Chem. Soc.*, **62**, 1457 (1940).

vapor adsorbed on both the external and internal surfaces of their samples in this relative pressure range. The water vapor adsorption isotherms are not particularly revealing; they give no information concerning the total area nor do they indicate the swelling phenomenon which occurs when the water molecules begin to enter between the platelets.

Isosteric heats of desorption, calculated from water vapor desorption isotherms at two temperatures, reveal little further about the swelling[4] than do the isotherms. Heats of immersion at various amounts of water adsorbed, however, reveal internal adsorption quite clearly as will be indicated later.

X-Ray Diffraction Data.—The swelling of bentonite by imbibing water between the platelet structure is illustrated by the X-ray data of Fig. 2. The *c*-axis spacing (the axis perpendicular to the platelets) is shown as a function of the relative pressure at which the samples were equilibrated. As is generally found, the water uptake between platelets was not a continuous function of relative pressure but occurred at rather distinct relative pressures. Also, the water entered between the platelets in integral numbers of monomolecular layers. Thus, for the bentonite employed in this investigation, the first layer of water molecules entered at about 0.3 relative pressure and a second layer at about 0.7 relative pressure.

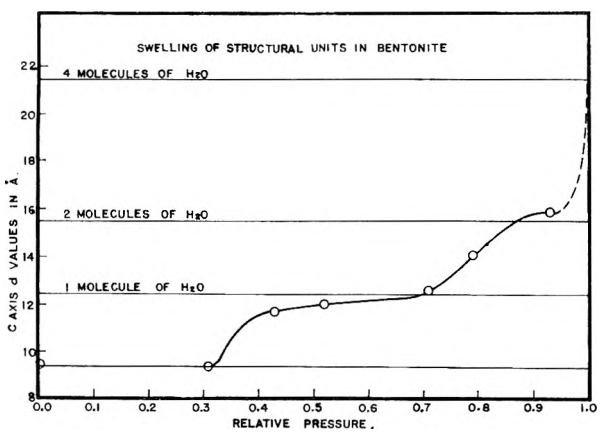

Fig. 2.—Swelling of structural units in bentonite from X-ray data.

The X-ray data supported the isotherm data that water vapor adsorption in the BET region of relative pressure was primarily on the external surface. That is to say, there was no change in the *c*-axis spacing until a relative pressure of 0.3 was reached.

The water vapor adsorption isotherms did not strongly reflect the stepwise water uptake shown by the X-ray studies. No doubt simultaneous and continuously increasing adsorption on the outer surfaces and at the edges of the platelets masked the water uptake between the layers. In addition, while the majority of platelets swelled at a rather definite pressure in each step, the imbibing of water between the platelets was probably distributed over a fairly broad relative pressure region. These processes combined to give rather smooth water vapor adsorption isotherms with only indistinct changes of slope indicating internal sorption.

It has been reported[11] that certain montmorillonite samples imbibe 4 layers of water molecules between platelets at very high relative pressures. No definite evidence of this was found in the present work up to relative pressure of 0.99. However, there did appear to be a slight increase in the *c*-axis spacing at very high relative pressures over the 15.5 Å. that represents two water layers between platelets. The finding that the imbibed water is limited to two molecular layers is in agreement with the work of Hendricks, *et al.*[10]

Heats of Immersion of Bentonite Samples in Water.—The heats of immersion of bentonite samples evacuated at 25 and 100° are plotted in Fig. 3. The heats are shown as a function of the relative pressure at which the samples were equilibrated with water vapor before the immersion measurements were made. The values of the heats of immersion are plotted on a per gram basis rather than per unit surface area because of the complication of the increase in internal area with swelling.

As indicated previously, in the case of activation at 25°, the initial adsorption of water vapor occurred primarily on the external bentonite surface. This adsorption process is reflected by the heat of immersion data for the initial portion of the lower curve for 25° activation in Fig. 3. In fact, this curve

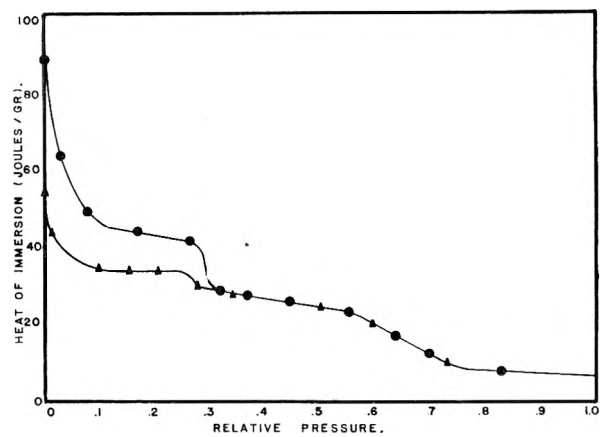

Fig. 3.—Heats of immersion of bentonite in water: ▲, degassed at 25° for 48 hr.; ●, degassed at 100° for 24 hr.

in the region from zero to 0.25 relative pressure is similar in appearance to typical heat of immersion curves for heteropolar, non-porous solids like TiO_2.[12] The initial rapid fall of the curve denotes the disappearance of the bare solid surface and the formation of a solid-adsorbed film interface as the amount preadsorbed was increased. Completion of an external monolayer of adsorbed water vapor is shown by the first plateau where further amounts of adsorbed water affected the immersion values only slightly.

When the heat of immersion values for the sample evacuated at 25° are expressed on the basis of unit area of external surface, the difference in the heat of immersion between the clean bentonite surface and the surface covered with a monolayer of water amounts to about −575 ergs/cm.^{2}. This magnitude is about 250–300 ergs/cm.^{2} higher than the

(11) W. F. Bradley, R. E. Grim and G. L. Clark, *Z. Krist.*, **97**, 216 (1937).

(12) W. D. Harkins, "Physical Chemistry of Surface Films," Reinhold Publ. Corp., New York, N. Y., 1952, p. 231.

corresponding values for other heteropolar surfaces. Therefore, either the clay surface is more energetic, adsorption wise, or another phenomenon in addition to physical adsorption such as hydration of exchange ion sites on the external surface of the clay was taking place. If hydration did occur on adsorption, it is somewhat surprising that the original water of hydration on the exchange ion sites was removed by evacuation at 25°. An absolute magnitude of the heat of immersion of the bentonite clay external surface is, of course, impossible to obtain experimentally because of the endothermic swelling process which also occurs on immersion.

The first inflection in the heat of immersion curve for activation at 25° occurred at approximately the same relative pressure as the first dimensional change shown by the X-ray data in Fig. 2. This inflection is therefore interpreted to reflect the heats of swelling and of sorption on the internal bentonite surface due to the entrance of the first monolayer of water between structural platelets. The immersion curves for the two different activations merged during this introduction of the first water layer between platelets.

The heat of immersion curve for activation at 100° (upper curve) paralleled the lower curve up to a relative pressure of about 0.25. Differences are the heat of immersion of the clean bentonite surface which was now much higher and the sharper decrease in the initial stages up to a relative pressure of *ca.* 0.05. However, the water vapor adsorption isotherms for the two different activations did not indicate large differences in the amount of water vapor adsorbed. Therefore, the initial rapid change in slope for activation at 100° represents adsorption on more energetic sites than were present after evacuation at 25°. The more energetic of these adsorption sites are presumably exchange ions on the external surface which can be hydrated; dehydration resulted from activation at 100°.

It is of considerable significance that the heat of immersion curves for the two different activations do not coincide until a relative pressure of about 0.3 is reached. Apparently, a part of the water removed by activation at 100° could not be replaced by adsorption until this relative pressure was reached. However, it will be recalled that at 0.3 relative pressure the first monolayer of water was imbibed between the platelet structure. These findings suggest that *activation at 100° not only produces highly energetic sites on the external surface but also between the platelets.* These energetic adsorption sites on the internal surface are also presumably dehydrated exchange ions.

It is of interest now to consider the magnitude of the difference in energies of adsorption for the two activation conditions. The difference in the initial heat of immersion values (at zero relative pressure) represents the wetting of additional sites uncovered by the 100° activation. Presumably these sites are exchange ion positions and were activated by removal of hydrated water. The additional amount of water desorbed from the bentonite by the 100° activation amounted to 0.0122 g. H_2O/g. clay. If this additional water removed at 100° is reversibly readsorbed, then the heat effect for readsorbing would amount to 12.6 kcal./mole H_2O.

After the heat of immersion curves for the two different activation curves merged at a relative pressure of *ca.* 0.3, they became identical up to saturation. The second plateau in the heat of immersion curve in Fig. 3 again represented primarily multilayer adsorption on the external surface. This relative pressure region of the plateau corresponded roughly to the relative pressure region in Fig. 2 where the X-ray data show little change in the *c*-axis dimensions, *i.e.*, no increased swelling of the bentonite particles. The heat of immersion curve changed only slightly in this region since the energy of adsorption for multilayer formation is nearly constant and the magnitude of the heat of immersion would be expected to change only as the fraction of water adsorbed in this region compared to the total adsorption changes.

At a relative pressure of about 0.6 the heat of immersion curves again changed slope sharply. Here multilayer formation on the external surface was still proceeding but now the second molecular layer of water molecules started to form between the platelets. Again this process was gradual for energy barriers preventing entrance of a second imbibed water layer were evidently not the same for all particles. It is probable that when one platelet pair was spread sufficiently for the entrance of the second water layer this second molecular layer formed immediately. Therefore, any endothermic heat process for the spreading of platelets was probably over-shadowed by the exothermic heat of adsorption of water molecules between the platelet pairs. This interpretation of the relative pressure region from *ca.* 0.6 to 0.8 was also supported by X-ray data which show that the c-axis changed dimension sufficiently to admit one more molecular layer of water molecules between the platelets in this region.

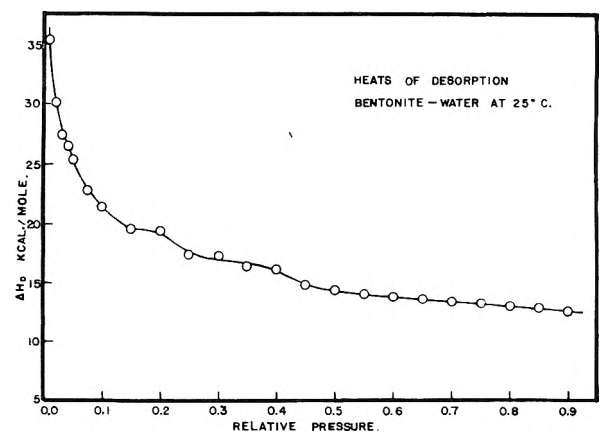

Fig. 4.—Heats of desorption of water from bentonite at 25°. Bentonite activated at 100°, 48 hr.

The final leveling of the heat of immersion curve represented primarily multilayer adsorption on the external surface. The X-ray data showed no change in *c*-axis dimensions in this relative pressure region, and no change in the internally imbibed water was to be expected. The surface area in this region calculated by the Harkins[13] absolute method was

(13) W. D. Harkins, ref. 12, p. 273.

44 m.^{2}/g. This value is about 30% larger than the nitrogen area of the dry bentonite. The reason for this difference is that the bentonite particles were now swollen and hence had a larger external area than when dry. This increase in area was also calculated on the basis of the change in the c-axis dimensions given by the data in Fig. 2; a value of 43 m.^{2}/g. was obtained, in excellent agreement with the value calculated from heat data by the Harkins absolute method.

The heat of desorption curve of water vapor from bentonite is given in Fig. 4. This curve was obtained from the heat of immersion data by dividing ($h_{SL} - h_{SfL}$) by the number of moles of water adsorbed per gram at the coverage used to obtain the h_{SfL} value and adding to this the energy of vaporization of the adsorbed water at 25°. It is significant that this curve does not reflect the changes occurring on the uptake or removal of water in such detail as the heat of immersion curves. The heat of desorption curve was based on the heat per mole of adsorbed water and since the isotherm data are reflected in this calculation the curve is smoothed out in much the same manner as the isotherms in Fig. 1.

Acknowledgment.—This work was carried out under contract N8onr-74300 with the Office of Naval Research whose support is gratefully acknowledged.

THE EFFICIENCIES OF SOME SOLIDS AS CATALYSTS FOR THE PHOTOSYNTHESIS OF HYDROGEN PEROXIDE[1]

BY RUTH E. STEPHENS, BACON KE AND DAN TRIVICH

Department of Chemistry, Wayne University, Detroit, Michigan

Received January 17, 1955

A number of solids were studied as catalysts for the photoproduction of hydrogen peroxide and of these, cadmium sulfide was found to be the most efficient. In monochromatic light, it was shown in the cases of zinc oxide, cadmium sulfide and cadmium selenide that the catalytic efficiencies extend to the absorption limit. A relation of the catalytic efficiency to the crystal structure, semiconducting and photovoltaic properties of the catalyst is indicated. It is suggested that zinc oxide and the other catalytic solids should not be abandoned as devices for capturing solar energy in a form capable of transfer to some chemical system.

Recently several investigators[2] have reported studies on the photochemical synthesis of hydrogen peroxide in systems containing water, zinc oxide and various organic additives. Our work is in general agreement with the results of these investigators and we are reporting some related work not previously published. The previous work on this reaction has been concerned largely with the mechanism of the photosynthesis of hydrogen peroxide, whereas our interest has been chiefly the role of the solid catalyst.

Experimental

Sources and Preparation of Catalysts.—In some cases the catalysts were used as obtained from chemical suppliers; for such materials the sources are listed with the experimental results in Table I. Details of preparation of the others are given here.

The active cadmium sulfide was prepared by dissolving 0.1 mole of reagent cadmium oxide in approximately 500 ml. of water containing excess nitric acid, and treating with a filtered solution of 0.2 mole of sodium sulfide. The precipitates were washed with water previously saturated with hydrogen sulfide, dried by placing first over fused sodium sulfide and finally in a vacuum desiccator over fused sodium hydroxide to remove adsorbed hydrogen sulfide. Zinc sulfides were prepared in the same manner.

Mercuric sulfide was prepared from solutions of mercuric chloride and sodium thiosulfate in the ratio described by Allen and Crenshaw[3] and added simultaneously with stirring to a large volume of water.

Gallic sulfide, Ga_2S_3, was prepared by igniting the metal in an atmosphere of dry hydrogen sulfide and also by heating the oxide to 650° in a stream of hydrogen sulfide and sulfur.

Gallium nitride was obtained by the action of dry ammonia gas on gallium metal at 800°. The oxide was obtained by the thermal decomposition of the nitrate in air above 200°.

The tellurides of zinc and cadmium were prepared by fusion of the elements in an atmosphere of nitrogen.

Powdered selenium metal (Central Scientific Co.) was converted to sodium selenosulfate by heating in aqueous sodium sulfite. The hot solution was filtered under a nitrogen atmosphere. On cooling it was treated rapidly with cold hydrochloric acid to yield a finely divided, red selenium.

Procedure for Testing Catalytic Efficiency.—The sample was irradiated in an 8-inch Pyrex test-tube, fitted with a magnetic stirrer and placed approximately 30 cm. in a horizontal direction from a water-cooled, Pyrex-jacketed General Electric A-H6 (1200 W) mercury arc lamp. Except where otherwise noted, the following standard procedure was used. A sufficient quantity (0.1 to 0.8 g.) of the powdered catalyst was added so that the suspension was opaque to light. Into the test-tube was pipetted 25 ml. of 0.04 M aqueous phenol solution, and the resulting slurry was kept continually saturated with oxygen introduced through a capillary extending almost to the bottom of the tube. The oxygen was previously washed successively with sulfuric acid, concentrated alkali solution and water. The oxygen pressure was adjusted to maintain a constant flow rate through a flowmeter placed between the purification train and the sample.

After 10-minutes irradiation the test solution was centrifuged and a 10-ml. portion was analyzed by iodimetry using a molybdate catalyst. If the catalyst was a metallic sulfide the determination was made in neutral solution to avoid interference of dissolved sulfide. To guard against errors due to oxidizing agents other than hydrogen peroxide, samples were also analyzed by adding acidic titanium sulfate and comparing the intensity of the yellow complex with standards of known peroxide content. This was done whenever a new catalyst or promoter was involved.

The light source was subject to a slow diminishing of intensity due to a gradual aging of the mercury arc lamp. For this reason, although the results given in any one series

(1) This work was supported in part by grants from the Charles F. Kettering Foundation.

(2) (a) M. C. Markham and K. J. Laidler, THIS JOURNAL, **57**, 363 (1953); (b) T. R. Rubin, J. G. Calvert, G. T. Rankin and W. M. MacNevin, *J. Am. Chem. Soc.*, **75**, 2850 (1953); (c) M. C. Markham, M. C. Hannan and S. W. Evans, *ibid.*, **76**, 820 (1954); (d) J. G. Calvert, K. Theurer, G. T. Rankin and W. M. MacNevin, *ibid.*, **76**, 2575 (1954).

(3) E. Allen and J. Crenshaw, *Z. anorg. Chem.*, **79**, 159 (1913).

are consistent within themselves, the data in one series are not necessarily comparable to those in another. In most cases the samples were irradiated with the full intensity of the A-H6 lamp as filtered by the Pyrex glass and water of the cooling jacket.

In some further tests monochromatic light was used for irradiating zinc oxide, cadmium sulfide and cadmium selenide. The various mercury arc lines were isolated by Bausch and Lomb interference filters together with supplementary solution filters. The test solutions were placed behind the filter combinations, protected from stray radiation and irradiated for 20 minutes. The relative intensities of the light used at the selected wave lengths were determined by uranyl oxalate actinometry.[4]

The solutions for the filters were chosen and adjusted in concentration to give no more than 1% transmission for any mercury line other than the desired one. The solutions used were: A, 10 g./l. $Cu(NO_3)_2$; B, 4.3 g. $CuCl_2$ and 10 ml. concd. (28%) NH_4OH per liter; C, 131 g./l. $(NH_4)_2Cr_2O_7$; and D, 31.9 g./l. V_2O_5 dissolved in dil. HNO_3. The solutions were used in cells of 1 cm. thickness. The transmittance of the solutions and the interference filters was measured in a Beckman Model D spectrophotometer. The products of the transmittances are given as percentage transmission for the principal mercury lines of interest, namely, 365, 405, 436, 546 and 578 mμ. These are: 365 + A (B. and L. interference filter for 365 mμ plus solution filter A), 27% at 365 and 1.0% at 405 mμ; 405 + B, 0.1% at 365, 23% at 405 and 0.8% at 436 mμ; 436 + B, 0.06% at 365, 1.0% at 405 and 19% at 436 mμ; 546 + C, 24% at 546 mμ; 578 + D, 25% at 578 mμ. Values for those lines not given were less than 0.01%.

Results

Investigation of Catalysts.—A search was undertaken for materials, other than zinc oxide, showing catalytic activity in the photochemical synthesis of hydrogen peroxide, in the hope that properties common to these materials would prove to be significant. The amount of peroxide formed by ten-minute irradiation was measured. Since our experiments have shown that this time lies within the range of linear yield,[5] the results are probably equivalent to a measure of initial slopes. The results of these tests are given in Table I.

The dark reaction was presumed to be negligible under the conditions of the experiment. This was verified for a number of zinc oxide and cadmium sulfide samples. Further tests were made with selenium, cadmium selenide, mercuric sulfide and zinc sulfide by bubbling oxygen for 20 minutes through suspensions in red glass vessels. No detectable amount of peroxide was formed.

As shown above it was found that cadmium sulfide precipitated from the chloride was the most effective catalyst in the group studied, being more effective than any zinc oxide sample previously tested. Heating the cadmium sulfide samples in nitrogen and sulfur atmospheres tended to reduce the activities and to lessen the difference between them. The decrease in activity may be due to a loss of sulfur atoms from the crystal with heating and the accumulation of excess cadmium as evidenced by the fact that the loss in activity is the least when the heating is done in an atmosphere containing sulfur.

The zinc sulfide samples were slightly active, the most active being those precipitated from the chloride solutions and those ignited in a sulfur atmosphere. The activity of the red cadmium selenide was not affected by heating to 600° in nitrogen.

(4) W. G. Leighton and G. S. Forbes, *Z. anorg. Chem.*, **52**, 3139 (1930).
(5) See also appropriate figures in refs. 2a and 2c.

TABLE I

YIELDS OF HYDROGEN PEROXIDE USING VARIOUS SOLID CATALYSTS

Catalyst		Treatment and source	Molarity H_2O_2 × 10^4
CdS	yellow	Pptd. from $CdCl_2$ soln.	16.75
CdS	red	Pptd. from $CdCl_2$ soln.	16.5
CdS	brown	From $CdCl_2$ soln., ignited 600° in N_2	6.25
CdS	fawn	From $CdCl_2$ soln., ignited 600° in N_2 + S_2	8.0
CdS	orange	J. T. Baker Co. Lot no. 71741	7.5
CdS	yellow	From $Cd(NO_3)_2$ soln., ignited 600° in N_2 + S_2	13.0
CdS	mustard	From $Cd(NO_3)_2$ soln., ignited 600° in N_2	5.0
CdS	yellow	Pptd. from $Cd(NO_3)_2$ soln.	14.0
CdS	red	Pptd. from $Cd(NO_3)_2$ soln.	16.0
HgS	black	From $HgCl_2$ and $Na_2S_2O_3$	0.5
HgS	red	From $HgCl_2$ and $Na_2S_2O_3$	5.0
HgS	red	Baker and Adamson, reagent Lot no. 14	0.75
GaN	gray	Burning of the metal in NH_3 at 800°	1.75
Ga_2S_3	yellow	Burning of the metal in H_2S at 600°	3.75
Ga_2S_3	cream	Heating $Ga(OH)_3$ in H_2S at 600°	3.25
CdSe	red	General Color Co., maroon no. 1027	9.75
ZnS	cream	Coleman and Bell, reagent Lot no. 490342	0.25
ZnS	white	Pptd. from $ZnCl_2$ soln.	0.75
ZnS	white	Pptd. from $Zn(NO_3)_2$ soln.	0.0
ZnS	gray	From $ZnCl_2$ soln., ignited 1100° in N_2 + S_2	1.0
ZnS	tan	From $Zn(NO_3)_2$ soln., ignited 1100° in N_2 + S_2	1.25
CdTe	black	Fusion of the elements	0.5
ZnTe	gray	Fusion of the elements	0.5
Ga_2O_3	white	Heating of $Ga(NO_3)_3$	0.5
Se	red	Treatment of $NaSeSO_3$ with acid	0.5

An interesting example of what may be a crystal structure effect was encountered in the mercuric sulfide. The sulfide first formed in solution was the black form, which on standing in the solution was transformed to a red sulfide, presumed to be cinnabar. Part of the precipitate was separated as the black form and later, part as the red form. The red precipitate was found to have several times the activity of the black.

Other materials which were tested and found not to promote the formation of peroxide are: beryllium oxide (Brush Beryllium Co., Proc. 2), tantalum nitride (Metal Hydrides, Inc.), columbium nitride (Metal Hydrides, Inc.,) red antimony trisulfide, black antimony trisulfide, titanium dioxide (du Pont No. 5496), silver oxide (Mallinckrodt Lot ZXM), stannic oxide (Fisher Scientific Co., C.P.), chromium oxide (from ammonium dichromate heated to 500°), nickel oxide (from $NiCO_3$ heated to 1100°), nickel oxide (from $Ni(NO_3)_2$ heated to 500°), cobalt oxide (from $CoCO_3$ heated to 500°), bismuth oxide (Baker and Adamson), and yellow

lead oxide (Eberbach and Son). Rankin[6] has also tested a number of solids for their catalytic activity.

Further Tests with CdS.—Because of the high activity of CdS, further tests were made with this compound. The effect of irradiation time was studied with a sample prepared by precipitation from a chloride solution and it was found that the yield rose with time at first and approached a limiting value after about 1 hr. irradiation time. The results obtained were: with 1 minute of irradiation, the yield of H_2O_2 was 2.95 in molarity $\times 10^4$; with 3 min., 8.24; 5 min., 14.3; 10 min., 21.9; 20 min., 30.3; 30 min., 32.7; and 40 min., 37.3. The yield of hydrogen peroxide was not strongly dependent upon the amount of cadmium sulfide or phenol (in the range of 0.01–0.04 *M*) as indicated by the following results obtained with a 10-min. irradiation time, (given in the order: wt. of CdS in 25-ml. sample, concentration of phenol, yield of hydrogen peroxide in molarity $\times 10^4$): 0.1 g., 0.04 *M*, 9.8; 0.2 g., 0.04 *M*, 10.1; 0.2 g., 0.0 *M*, 3.6; 0.2 g., 0.01 *M*, 11.1; 0.2 g., 0.02 *M*, 11.4; 0.2 g., 0.03 *M*, 10.0.

Catalysis with Silver Iodide.—In addition to the materials previously listed, silver iodide was found to promote the photosynthesis of hydrogen peroxide. This raises the question of the well known photolysis of the silver halides and the possibility of a quite different mechanism in this case. In Table II results are given which indicate that both zinc oxide and silver iodide require oxygen and organic additive for the photosynthesis of significant amounts of peroxide. The zinc oxide used was Mallinckrodt reagent, Lot LKT, and the silver iodide was Baker and Adamson, Lot F 120. No significant amounts of peroxide were obtained if the oxygen was rigorously excluded. However small amounts of peroxide were obtained if tank nitrogen was used or if the system was not completely flushed with purified nitrogen. No iodine was detected in the irradiated solution. The similarity of silver iodide to zinc oxide in this reaction indicates that silver iodide exhibits the same general catalytic mechanism.

TABLE II

YIELDS OF HYDROGEN PEROXIDE WITH ZnO OR AgI AS CATALYST

Experimental Conditions		Molarity $H_2O_2 \times 10^4$	
Solution	Atmosphere	ZnO (0.4 g.)	AgI (0.8 g.)
Distilled water	Oxygen	1.0	0.0
Phenol, 0.04 *M*	Oxygen	25.0	2.3
Phenol, 0.04 *M*	Nitrogen	0.0	0.0
Methyl salicylate, 0.008 *M*	Oxygen	33.0	6.5

Efficiencies of Several Catalysts at Various Wave Lengths of Light.—Previously much attention has been given zinc oxide which however is an inefficient catalyst for utilization of solar energy in that it absorbs very little of wave lengths beyond 3800 Å. Yellow cadmium sulfide and red cadmium selenide however, absorb in the visible to approximately 5200 and 5800 Å., respectively. It was of interest to know whether these longer wave lengths are effective in the photosynthesis.

Table III gives the yield of peroxide in a 0.04 *M* solution of phenol after 25-minutes irradiation at the specified wave length and in the presence of the indicated catalyst. The zinc oxide was Mallinckrodt analytical reagent, Lot LKT, the cadmium sulfide a very active sample prepared by precipitation from the chloride and the cadmium selenide was the General Color Co. sample. It should be noted that wave lengths of light far in the visible are effective providing the catalyst can absorb in this region.

TABLE III

YIELDS OF HYDROGEN PEROXIDE FOR VARIOUS CATALYSTS AT SELECTED WAVE LENGTHS OF RADIANT ENERGY

Wave length, mμ	Molarity $H_2O_2 \times 10^4$ ZnO (0.4 g.)	CdS (0.3 g.)	CdSe (0.3 g.)	Relative intensity, arbitrary units
365	3.75	4.5	1.0	2.0
405	0.25	3.0	1.1	1.5
436	0.0	4.0	1.0	2.0
546	0.0	0.8	1.0	
578	0.0	0.0	0.3	

Discussion

Since the photosynthesis of hydrogen peroxide can be brought about by such diverse materials as zinc oxide, gallium nitride, cadmium selenide and selenium, it seems probable that the catalysis is not by any particular ion or ion vacancy but rather that the crystal as a whole is a structure for the absorption and transfer of energy. The frequently reported semi-conducting and photovoltaic properties of these materials is strikingly apparent and appears to support the electrolysis mechanism of the kind first proposed by Baur[7] with the primary step being a reduction by a photoexcited electron from the crystal. It has been suggested that it is probably molecular oxygen which is reduced in the first step.[2d]

Many of the catalytic substances exhibit a light sensitivity and a tendency to darken on exposure. The darkening of zinc sulfide in this manner has been attributed by Shionoya[8] to photolysis of the crystal and the formation of reduced zinc.

It may be significant that almost all the catalysts have a common tendency to form a wurtzite crystal structure, with the exception of selenium which may have similar hexagonal symmetry. The wurtzite structure may be unique with respect to several optical properties. Schleede[9] has found the photosensitive darkening of zinc sulfide to be a property mainly of the wurtzite form. A dependence upon crystal structure has also been asserted for the photoconductivity of cadmium sulfide[10] and the phosphorescent properties of zinc sulfide.[11]

While the general properties of photoconductivity, photocatalytic activity and related phenomena may be associated with the particular crystal struc-

(6) G. T. Rankin, Ohio State University, private communication.

(7) E. Baur, *Z. Elektrochem.*, **34**, 595 (1928).

(8) S. Shionoya, *J. Chem. Soc., Japan*, **71**, 461 (1950).

(9) A. Schleede, M. Herter and W. Kordatzki, *Z. physik. Chem.*, **106**, 386 (1923).

(10) R. Frerichs, *Phys. Rev.*, **72**, 594 (1947).

(11) F. Prevet, *J. chim. phys.*, **28**, 470 (1931).

tures, it is evident that the magnitude of such photoconductivity is dependent on the manner of treatment of the individual samples. This suggests a dependence on the electronic structure of the solids and on semi-conductivity which are known to be very sensitive to impurities and to manner of preparation. This is borne out by further research in this Laboratory in which it has been shown that the photocatalytic activity of zinc oxide depends upon the amount and the kind of deliberately introduced impurities.

Part of the original interest in this research was the hope that the hydrogen peroxide photosynthesis would serve as a means of storing solar energy as chemical energy. However, the over-all reaction including the oxidation of phenol may result in a net degradation of energy as has been shown for systems containing oxalate and formate salts.[2b] Nevertheless, it is relevant to point out that the zinc oxide and other solids described here are temporary receivers of light energy in a form that can be transmitted to chemical reactants on the surface. This energy is subsequently used in supplying merely the activation energy for the hydrogen peroxide reaction so that no useful storage is obtained. This suggests the possibility of other reactions that would be upgraded in free energy by interaction with illuminated zinc oxide. If such a reaction can be found, cadmium sulfide or cadmium selenide may be still more useful than zinc oxide because of their more favorable absorption of the solar energy spectrum.

A LIGHT SCATTERING INVESTIGATION OF THE MOLECULAR WEIGHT OF PEPSIN[1,2]

BY MARTIN J. KRONMAN AND MALVIN D. STERN

A Contribution from the Department of Chemistry, Temple University, Philadelphia, Pennsylvania

Received January 21, 1955

The molecular weight of pepsin has been redetermined by the light scattering method. Dissymmetry measurements show that the enzyme is readily aggregated by mechanical agitation. Light scattering measurements were carried out at *p*H 4.50 and 5.00 at 25.6 and 14.8° in 0.200 *M* acetate buffer. The mean molecular weight of six determinations was found to be $34.8 \pm 0.87 \times 10^3$. It is believed that this value represents an upper limit for the molecular weight of pepsin. The results of this investigation indicate that pepsin solutions must be handled with extreme care in investigations where interpretation of the results involve serious consideration of the molecular weight, size and shape of pepsin.

During the course of a light scattering investigation involving the enzyme pepsin certain surface denaturation effects were observed which suggested the desirability of redetermining its molecular weight. Previous investigations of the surface inactivation of pepsin have been reported[3,4] but there appears to be little information on the effect of surface on the solution properties of the enzyme.

Experimental

Materials.—Three different preparations of crystallized pepsin were used. The first was obtained from Armour and Co.; the second was obtained from the Mann Biochemical Co.; the third was prepared by the alcohol procedure of Northrop.[5] They contained 16.5, 11.0 and 15.6%, respectively, non-protein nitrogen as per cent. of total nitrogen. Bovine serum albumin was obtained from Armour and Co. All solutions were prepared with doubly distilled water, the second distillation being made in an all Pyrex system.

Analytical Methods.—Concentrations of bovine serum albumin were determined by measuring the ultraviolet absorption at 280 mμ using a Beckman model DU spectrophotometer. We have experimentally determined a value of 6.60 ± 0.02 for $E^{1cm.}_{1\%}$ in acetate and phosphate buffers and in distilled water, in agreement with the accepted value of Cohn, Hughes and Weare.[6]

Pepsin concentrations were determined from protein nitrogen concentrations using 14.6% as the percentage of nitrogen.[7] Protein nitrogen concentration is equal to total nitrogen concentration minus non-protein nitrogen concentration. Non-protein nitrogen was determined as follows: To the aliquot of solution taken for analysis was added sufficient distilled water and 30% trichloroacetic acid to make the final concentration 0.8 *M* in trichloroacetic acid. The solution was then allowed to stand for 30 minutes with occasional mild agitation, filtered through a sintered glass fine filter to remove the coagulated protein and then analyzed for nitrogen. Nitrogen determinations were by the Kjeldahl procedure using mercuric oxide as the catalyst and following the procedure of Willits, Coe and Ogg.[8]

Proteolytic activity was considered as a possible analytical method for pepsin but was rejected because of experimental difficulties.[9]

Refractive Index Increments.—Measurement of n were carried out at 436 mμ at 25° using a Brice type differential refractometer.[10] The data of Kruis[11] on the refractive index of potassium chloride solutions is most complete at 589 mμ, and therefore calibration was carried out with a sodium vapor lamp as a light source. An aqueous solution containing 2.982×10^{-2} grams/ml. of KCl was used as a standard. The calibration constant, k, as given in reference 10 is

$$k = \cot i/2m_0(a + b/2n_0 + t/n_w) \qquad (1)$$

where i, a, b and t are related to the geometry of the refractometer and are independent of wave length. The wave length dependent parameters are m_0, the magnification of

(1) This investigation was supported in part by a grant from the Frederick Gardner Cottrell Fund of the Research Corporation.

(2) To be included in a thesis to be submitted by Martin J. Kronman to the Graduate Council of Temple University in partial fulfillment of the requirements for the Ph.D. degree in chemistry.

(3) I. Langmuir and V. J. Schaeffer, *Chem. Revs.*, **24**, 181 (1939).

(4) D. F. Cheesman and H. J. Schuller, *Colloid Sci.*, **9**, 113 (1954).

(5) J. H. Northrop, M. Kunitz and R. M. Herriott, "Crystalline Enzymes," Columbia University Press, New York, N. Y., 1948.

(6) E. J. Cohn, W. L. Hughes, Jr., and J. H. Weare, *J. Am. Chem. Soc.*, **69**, 1753 (1947).

(7) Northrop, *et al.*, ref. 5, p. 74.

(8) C. O. Willits, M. R. Coe and C. L. Ogg, *J. Assoc. Offic. Agr. Chemists*, **32**, 561 (1949).

(9) Light scattering and proteolytic activity measurements were carried out on a number of pepsin preparations in solution. Dissymmetry and 90 degree scattering measurements indicated various degrees of aggregation. Nevertheless, within the experimental error the specific activities of all these preparations were identical.

(10) B. A. Brice and M. Halwer, *J. Opt. Soc. Amer.*, **41**, 1033 (1951).

(11) A. Kruis, *Z. physik. Chem.*, **34B**, 13 (1936).

the system, n_0, the refractive index of the solvent and n_w, the refractive index of the glass of the cell. Taking the actual numerical values of k_{589}, k_{436}, m_{589} and m_{436} from reference 10, we find that within 5 parts in 10,000, for aqueous solutions, the following relationship holds true

$$\frac{k_{589}}{k_{436}} = \frac{m_{436}}{m_{589}} \qquad (2)$$

Thus, k_{436} can be obtained from k_{589} by making use of the relative magnification m_{436}/m_{589}. Magnifications were determined in the manner described by Brice and Halwer[10] for a series of slit widths, making determinations at 589 and 436 mμ without changing the slit width between successive measurements at the two wave lengths. The latter procedure was employed since only relative magnifications were desired and since the absolute slit widths were not known.

Measurements of Δn were carried out in the usual manner. Values of Δn for pepsin required a small correction for the refractive index contribution of the low molecular weight autolysis products present in all pepsin solutions. This correction was minimized by employing pepsin solutions which had been exhaustively dialyzed against the solvent and which, as a result, had a low concentration of non-protein nitrogen. Pepsin solutions were filtered through a sintered glass fine filter before measurements were made. The refractive index increment of the dialysate was determined using the combined dialysates and expressing concentrations in terms of mg. of non-protein nitrogen. This value was found to be $1.7 \pm 0.1 \times 10^{-3}$ ml./mg. N. The corrected Δn of the pepsin solutions was calculated from the following expression

$$(\Delta n)_c = \Delta n - \left(\frac{\Delta n}{\Delta c}\right) C_{NPN} \qquad (3)$$

where $(\Delta n/\Delta c)_d$ is the refractive index increment of the dialysate and C_{NPN} is the non-protein nitrogen concentration in mg./ml. of the pepsin solution.

The refractive index increments at 25° and in 0.200 molar acetate buffer at *p*H 4.50 are, respectively: Mann pepsin, 0.1905 ± 0.0040; Armour pepsin, 0.1928 ± 0.0021; Armour crystallized bovine serum albumin (not deionized to eliminate fatty acid contaminant), 0.1929 ± 0.0011. The refractive index increments at 25° and in 0.200 molar acetate buffer at *p*H 5.00 are, respectively: Mann pepsin, 0.1863 ± 0.0018; alcohol pepsin, 0.1825 ± 0.0021.

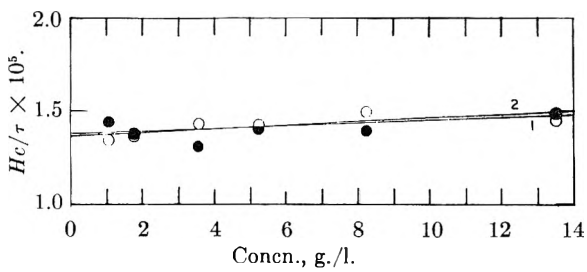

Fig. 1.—Hc/τ *vs.* *c* for bovine serum albumin in *p*H 6.44, 0.15 *M* acetate buffer: 1, as obtained on our instrument; 2, as obtained on E.U.R.P. Brice–Speiser type instrument.

Light Scattering Measurements.—"And all our yesterdays have lighted fools the way to dusty death"—after Holtzer, Benoit and Doty, from "Macbeth."[12]

The light scattering photometer used was essentially the same as that described by Brice, Halwer and Speiser.[13] It makes use of a 1P21 photomultiplier tube as a detector and uses an AH-3 mercury arc lamp as a light source. The 436 mμ line, the only wave length used in this investigation, was isolated by a suitable combination of Corning filters. Cells used in this investigation were miniature square and dissymmetry cells obtained from Phoenix Precision Instrument Co., Philadelphia, Pa. These cells were provided with hollow walled constant-temperature jackets which conform to the contours of the cell.[14]

Turbidities were measured in essentially the same way and calculated from an equation of the same form as that of Brice, Halwer and Speiser[13] as

$$\tau = Kn^2FG_{90}/G_0 \qquad (4)$$

where G_{90} and G_0 are galvanometer deflections at 90 and 0 degrees, respectively, and F is the transmittance of the neutral filter used at zero degrees. The n^2 factor is used to correct for the refraction of the scattered light at the boundary of the solution cell. Hermans and Levinson[15] have shown that the refraction correction takes this form when the receiver does not see past the edge of the primary beam. Our slit system geometry is such that this requirement is met.

The constant K was obtained by calibration with a polystyrene sample which has been used as a standard in many laboratories engaged in light scattering[16] and which was obtained from Professor P. Debye. A toluene solution containing 0.500 g. of polystyrene per 100 ml. of solution was assumed to have an apparent excess turbidity of 0.0035 ± 0.002 at 436 mμ.

The calibration was checked by making measurements on benzene, bovine serum albumin, and sample IV polystyrene fraction distributed by the Committee on Macromolecules of the International Union of Chemistry[17] and obtained through the courtesy of Professor F. R. Eirich.

Shown in Fig. 1 are the Hc/τ plots for bovine serum albumin as obtained on our instrument and on the Brice–Speiser type instrument of Dr. M. Halwer at the Eastern Utilization Research Branch of the United States Department of Agriculture. Geiduschek[18] has recently presented evidence which indicates that depolarizations of protein solutions are negligibly small. We have consequently made no correction for depolarization for either bovine serum albumin or pepsin. In Table I are shown the light scattering results, together with values taken from the literature for comparison. It is apparent from these results that the instrument employed can be used to give accurate turbidities.

Mann and Alcohol Pepsin.—Solutions were prepared for light scattering in the following manner. A freshly prepared stock solution of pepsin was filtered through a sintered glass fine filter to remove large particles and insoluble protein. In some cases the stock solution was dialyzed at 0° for a total of 100 hours against a minimum of 5 changes of buffer prior to filtration. Appropriate quantitative dilutions of the stock solutions were then made to give solutions of the desired concentration. These dilutions were then repeatedly filtered through a sintered glass ultrafine filter down a clean glass rod into the clean light scattering cell until a low constant dissymmetry was obtained; this was usually 1.05 or less. After light scattering measurements were made the entire sample was placed in the refrigerator until analyzed for protein concentration.

When measurements at more than one temperature were to be made, the following procedure was carried out. The solution which had been filtered into the cell was allowed to come to thermal equilibrium at one of the temperatures. After light scattering measurements had been made the same dilution was allowed to equilibrate at the new temperature before new light scattering measurements were made.

All three preparations of pepsin were found to be particularly susceptible to surface denaturation with subsequent aggregation to give very large particles. The existence of the latter was shown by the observation of relatively high dissymmetries in solutions which had been handled in such a manner that surface denaturation might be expected. In Table II are shown the results of an experiment carried out on a solution containing approximately 1×10^{-3} g./ml. of pepsin in *p*H 5.00, 0.200 *M* acetate buffer. The solution was filtered through a fine filter before the experiment was begun. The operations listed in the first column were carried out serially. Aeration was carried out by bubbling 20 ml. of dust-free air from a syringe through the solution. Filtrations were made through an ultrafine glass filter, conducting the solution down a rod in the cases listed and allowing it to fall freely in the other cases.

The same aggregation effect can be produced to a greater

(12) A. M. Holtzer, H. Benoit and P. M. Doty, THIS JOURNAL, **58**, 624, (1954).

(13) B. A. Brice, M. Halwer and R. Speiser, *J. Opt. Soc. Amer.*, **40**, 768 (1950).

(14) These constant temperature jackets will be described in a forthcoming publication by Wood, *et al.*, from this Laboratory.

(15) J. J. Hermans and S. J. Levinson, *J. Opt. Soc. Amer.*, **41**, 460 (1951).

(16) See reference 13 for a compilation of results obtained on this polystyrene fraction.

(17) *J. Polymer Sci.*, **10**, 129 (1953).

(18) E. P. Geiduschek, *J. Polymer Sci.*, **13**, 408 (1954).

TABLE I

COMPARISON OF LIGHT SCATTERING RESULTS WITH THOSE OBTAINED BY OTHER INVESTIGATORS

All molecular weights and slopes were obtained from a linear least squares fit of the data.

		Other Data
Polystyrene fraction IV, M	$118 \pm 6.6 \times 10^{3}$[a]	$118 \pm \times 10^{3}$[b]
dissymmetry	1.10 ± 0.01	1.11 ± 0.04[b]
2B	$8.89 \pm 0.84 \times 10^{-4}$	$9.0 \pm 0.08 \times 10^{-4}$[b]
Benzene, Rayleigh's Ratio $\times 10^{6}$	48.2 ± 1.13[c]	48.4, 48.5,[d] 48.2[e], 48.4[f], 49.7[i]
Bovine serum albumin, M	$72.5 \pm 1.6 \times 10^{3}$[h]	$73.0 \pm 1.5 \times 10^{3}$[g,h]
2B	$7.21 \pm 4.56 \times 10^{-5}$[h]	$8.99 \pm 0.02 \times 10^{-5}$[g,h]

[a] Corrected for dissymmetry and depolarization. The latter value was found to be 0.041; dn/dc was taken to be 0.110. This value is the average of two values given in reference 17. Measurements made in toluene. [b] Reference 17. [c] Obtained at 25.4°. [d] P. Outer, C. I. Carr and B. H. Zimm, *J. Chem. Phys.*, **18**, 830 (1950); C. I. Carr and B. H. Zimm, *ibid.*, **18**, 1616 (1950). [e] P. Doty and R. F. Steiner, *ibid.*, **18**, 1218 (1950). [f] Reference 12. [g] Obtained on a Brice–Speiser type instrument at the Eastern Utilization Research Branch of the United States Department of Agriculture. [h] Carried out in *p*H 6.44, 0.15 *M* acetate buffer. [i] S. H. Maron and R. L. H. Lou, *J. Polymer Sci.*, **14**, 273 (1954).

extent by agitation of the light scattering cell. In one particular case a sample in the usual buffer was found to have a turbidity which corresponds roughly to a molecular weight of 500,000.

TABLE II

	Dissymmetry		Dissymmetry
Original soln.	1.27	Filtered without rod	1.15
Aerated	1.46	Aerated	1.32
Filtered with rod	1.06	Filtered without rod	1.30
Aerated	1.24	Filtered with rod	1.06

Armour Pepsin.—The methods used for cleaning Mann and alcohol pepsin solutions failed to reduce the dissymmetry of the Armour pepsin solutions below 1.3. Filtration through the finest Schleicher and Schuell "ultrafine" filter also failed to reduce the dissymmetry as did centrifugation of individual dilutions for 5 hours at 100,000 *g* in the Spinco preparative centrifuge. The results given for the Armour preparation in the following sections were obtained using centrifugation as the cleaning technique.

Results and Discussion

Figures 2 and 3 and Table III illustrate and summarize our experimental findings on pepsin. The molecular weights and interaction constants summarized in Table IV were obtained by a linear least squares fit of the data, as were the standard errors also listed. The most apparent result is the variation in the molecular weight from 32.5×10^{3} to 42.7×10^{3} in the various experimental determinations. Our finding that pepsin is extremely susceptible to aggregation in aqueous solution as a result of mechanical shaking or contact with surfaces leads us to believe that the higher weights reported here are due to the presence of aggregates in solution. Thus, the high molecular weight obtained for the undialyzed Mann preparation at *p*H 4.50 is probably due to the presence of relatively small aggregates which make little contribution to the dissymmetry. The fact that the molecular weight is unaffected by change in temperature suggests that the disaggregation process does not readily occur. Dialysis of the same preparation at 0° for a minimum of 100 hours led to a lower molecular weight probably due to the digestion of the denatured protein by the active enzyme.

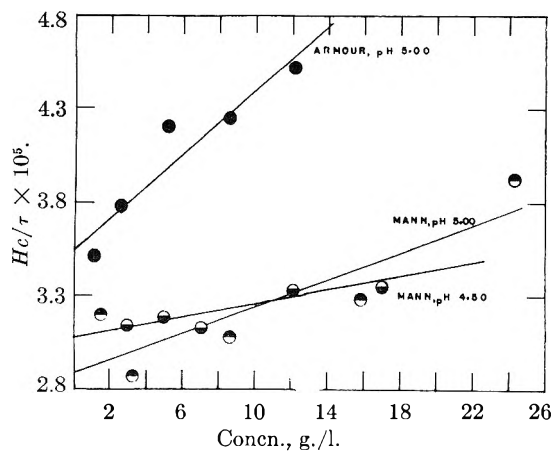

Fig. 2.—Hc/τ *vs.* *c* for various pepsin preparations in 0.200 *M* acetate buffer.

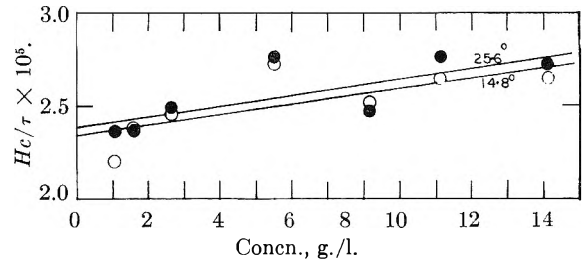

Fig. 3.—Hc/τ *vs.* *c* for an aggregated Mann pepsin sample at 25.6 and 14.8° in *p*H 4.50, 0.200 *M* acetate buffer.

TABLE III

MOLECULAR WEIGHTS AND INTERACTION CONSTANTS OF VARIOUS PEPSIN PREPARATIONS

Preparation	$M \times 10^{-3}$	$2B \times 10^{4}$
Alcohol[a]	35.1 ± 1.4	1.02 ± 1.09
Armour[a,b]	34.7 ± 0.7	8.48 ± 1.10
Mann[a]	34.7 ± 1.3	3.47 ± 0.82
Alcohol[c]	36.2 ± 0.4	-1.13 ± 0.34
Mann[c,d]	42.0 ± 1.0	2.92 ± 0.77
Mann[c,e]	42.7 ± 1.0	2.82 ± 0.78
Alcohol[c,f]	35.8 ± 0.4	-0.25 ± 0.31
Mann[c,f]	32.5 ± 0.3	1.70 ± 0.30

[a] Buffer–*p*H 5.00, 0.200 *M* acetate. [b] Measured on a Brice–Speiser type instrument at the Eastern Utilization Research Branch of the United States Department of Agriculture. Corrected for an observed dissymmetry of 1.29 from tabulated $P(\theta)$ values given by Doty and Steiner, *J. Chem. Phys.*, 18, 1211 (1950). [c] Buffer *p*H 4.50, 0.200 *M* acetate. [d] Measurement made at 25.6°. [e] Measurement made at 14.8°. [f] Dialyzed solutions.

The mean molecular weight for our measurements, excluding values greater than 40,000, is 34.8×10^{3} with an average deviation of $0.87 \times$

10^3. This average deviation is within the range of standard errors of the individual determinations.

When extreme care was taken to avoid aggregation by careful handling of well dialyzed pepsin solutions in later stages of our work, we obtained a molecular weight of 32.5×10^3. It is our belief that the mean weight average molecular weight of 34.8×10^3 may well represent an upper limit for the number average molecular weight of "pure" native pepsin. These results suggest that a careful osmotic pressure investigation of the molecular weight of pepsin is in order.

An examination of the literature on molecular weight determinations of pepsin adds little to confirm our belief in the lower molecular weight of the enzyme. Previously reported molecular weights of pepsin are, respectively, 37,624[24] by light scattering, 35,500[25] and 39,000[26] by sedimentation equilibrium, 34,400[21] by film pressure, 35,000[19] by osmotic pressure, 35,000[19] and 40,000[19] by chemical analysis, and 40,000[27] by X-ray diffraction.

Northrop's[19] osmotic pressure measurements on pepsin are subject to several criticisms. In his experiments he determined protein concentration from *total* nitrogen content. Analytical data on the preparations used in our experiments indicate that non-protein nitrogen may make up as much as 22.5% of the total nitrogen. Conn, *et al.*,[20] report non-protein contents of 10% for the preparations that they used. It might be expected therefore that the actual concentrations of protein in Northrop's solutions were lower than the values used in the calculations. The molecular weight on this account would therefore be too high. Furthermore, the osmotic pressure measurements carried out at *p*H 4.6 in a 1.0 *M* acetate buffer were made at rather high protein concentrations and were not extrapolated to zero concentration. Recent osmotic pressure measurements by Gutfreund[21] on isoelectric bovine serum albumin in 1 *M* sodium chloride indicate that the slope of the π/C *versus* C curve need not be zero, even when the net charge on the protein molecule is close to zero and the ionic strength is high. Thus, the use of unextrapolated osmotic pressure data to determine the molecular weight of pepsin is somewhat questionable. The protein concentration error and extrapolation error are in opposite directions. Since it is impossible to estimate the magnitude of each effect, the reliability of Northrop's osmotic pressure molecular weight is difficult to assess.

Dieu and Bull[22] were aware of the problem of contamination of pepsin with breakdown products and dialyzed their preparations before measurements were made. A possible objection to their method is that in view of the fact that pepsin surface denatures and aggregates so readily, it is conceivable that a significant amount of pepsin in their spread film may be in an aggregated form. Furthermore, recent work by Allen and Alexander[23] at low surface pressures indicates that molecular weight cannot be reliably estimated in the manner carried out by Dieu and Bull due to the presence of molecular cohesion at the air–liquid interface.

Yasnoff and Bull[24] apparently failed to consider the effect of degradation products both on concentration of protein and on the value of $\Delta n/\Delta c$. Their reported value of H, the light scattering optical constant, corresponds to a value of $\Delta n/\Delta c$ equal to 0.198 in contrast with our values given in Table I. Thus, the molecular weight they report is probably much too low. In addition, they do not report any measurements of dissymmetry and as a result have no indication of the presence of aggregated material.

The sedimentation equilibrium molecular weight, like the light scattering molecular weight would tend toward high values in systems containing small amounts of aggregated material.

There exists the possibility that the presence of autolysis products would tend to give a low value for the molecular weight of pepsin. Products having values of M below 10,000 would be expected to make little contribution to the intensity of the scattered light unless present in very large amounts. Since peptides in this molecular weight range are soluble in trichloroacetic acid, we may use as a measure of their concentration the non-protein nitrogen content of these solutions. These were found to range from about 20% of total nitrogen for undialyzed solutions to 2 or 3% for dialyzed solutions. These are low enough to conclude that autolysis products having molecular weights below 10,000 make little contribution to the molecular weight.

With regard to the effect of split products in the range 10,000 to 30,000, little can be said from our own experimental data since peptides in this region tend to be insoluble in trichloroacetic acid. Studies carried out on the distribution of molecular weights in peptic hydrolysates of egg albumin[28,29] β-lactoglobulin[30] and beef serum pseudoglobulin[31] indicate that little high molecular weight split product is formed. If the molecular weight distribution of autolysis products is similar to the distribution of peptic hydrolysis products, we may conclude that split products of molecular weight greater than 10,000 are present in insufficient amounts to affect the molecular weight of pepsin.

In summary, we conclude that pepsin can be readily surface denatured with subsequent aggregation, and that the presence of aggregates in various amounts is responsible for the variation in our experimentally determined molecular weights rather than any intrinsic error in light scattering measurements. Our results indicate that pepsin solutions must be handled with extreme care to prevent aggregation. This is of prime importance in

(19) J. H. Northrop, *J. Gen. Physiol.*, **13**, 739 (1929).

(20) J. B. Conn, D. C. Gregg, G. B. Kistiakowsky and R. M. Roberts, *J. Am. Chem. Soc.*, **63**, 2080 (1941).

(21) H. Gutfreund, *Trans. Faraday Soc.*, **50**, 628 (1954).

(22) A. A. Dieu and H. B. Bull, *J. Am. Chem. Soc.*, **71**, 450 (1949).

(23) A. J. G. Allan and A. E. Alexander, *Trans. Faraday Soc.*, **50**, 865 (1954).

(24) D. S. Yasnoff and H. B. Bull, *J. Biol. Chem.*, **200**, 619 (1953).

(25) J. Philpot and I. B. Ericksson-Quensel, *Nature*, **132**, 932 (1933).

(26) Quoted in "The Ultracentrifuge," Oxford University Press, 1940.

(27) J. D. Bernal and D. Crowfoot, *Nature*, **133**, 794 (1934).

(28) B. T. Currie and B. H. Bull, *J. Biol. Chem.*, **193**, 29 (1951).

(29) A. Tiselius and T. Ericksson-Quensel, *Biochem. J.*, **33**, 1752 (1939).

(30) G. Haugaard and R. M. Roberts, *J. Am. Chem. Soc.*, **64**, 2664 (1942).

(31) M. L. Petermann, THIS JOURNAL, **46**, 183 (1942).

any investigation where the size and/or molecular weight of pepsin must be considered.

Acknowledgment.—We gratefully acknowledge the generosity and help of Dr. M. Halwer and Dr. B. A. Brice of the Eastern Utilization Research Branch during various phases of this investigation, and the efforts of Mr. R. Troisi and Mr. C. Wood in their construction of the light scattering photometer, differential refractometer and associated equipment. We also wish to thank Mr. H. Levin and Mr. R. Townend for carrying out the determinations of proteolytic activity and the extinction coefficient of bovine serum albumin.

It is a pleasure to acknowledge the aid of the Research Corporation for a grant which partially supported this investigation.

THE INFLUENCE OF ULTIMATE COMPOSITION UPON THE WETTABILITY OF CARBON BLACKS[1]

BY MERTON L. STUDEBAKER AND CARL W. SNOW[2]

Phillips Chemical Company, Akron, Ohio

Received March 24, 1955

Few quantitative data have been published upon the wettability of carbon black. This is due largely to the difficulty of obtaining quantitative measurements by methods which apply to other solids. A simple method has been developed for determining contact angles of carbon black by a modification of Wolkowa's method.[3] Data are listed for a large number of carbon black samples, and the values have been correlated with their ultimate analyses.

The wetting characteristics of a finely divided solid are of considerable practical and theoretical importance. However, most methods of determining wettability have been disappointing when they were applied to carbon black.

In the work which is reported here, the procedure used was quite similar to one developed by Wolkowa.[3] This method is based on an equation derived by Washburn.[4] It can be obtained from Poiseuille's equation for viscous flow through a capillary tube and Young's equation for the determination of surface tension in a capillary. The Washburn relationship is

$$l^2 = \frac{\gamma \cos \theta \, rt}{2\eta} \qquad (1)$$

where l is the length of flow in time t seconds, and the viscosity is η, the surface tension of the liquid is γ, r is the radius of the capillary tube and θ is the contact angle. A discussion of the meaning of this contact angle, θ, is beyond the scope of this paper; it is sufficient to note that it is a measure of the wettability—the larger the contact angle the more difficult it is to wet a given solid with the particular liquid. For perfectly wetting liquids, θ is 0°, and cos θ equals one. The relative wettability of solids is frequently reported in terms of cos θ rather than in terms of the contact angle itself.

If a powder is packed into a glass tube, the resulting plug will act like a series of capillaries. The length of flow in the capillaries will be greater than the flow measured relative to the glass tube by a constant factor. If the packing is reproducible, values of r will be equal in different, identically prepared tubes. Values of l will be constant if the times of flow are measured at equal distances in the plugs, say at 0.50 cm. Now if a liquid can be found which wets the solid with a contact angle of 0°, equation 2 applies when $\theta = 0°$

$$l^2 = \gamma' r t'/2\eta' \qquad (2)$$

For the case of a liquid with a finite contact angle, we have

$$l^2 = \frac{\gamma'' \cos \theta'' r t''}{2\eta''} \qquad (3)$$

when θ is finite. Dividing (2) by (3) and transposing, equation 4 is obtained

$$\cos \theta'' = Kt'/t'' \qquad (4)$$

Hence, to determine the contact angle of any liquid against a powdered solid, we merely measure the times required to flow a given distance through the plugs by (1) a perfectly wetting liquid and (2) an imperfectly wetting liquid and substitute these values in the equation

$$\cos \theta = Kt'/t'' \qquad (5)$$

K is a constant which can be calculated from the surface tensions and viscosities of the two liquids using the formula

$$K = \frac{\gamma' \eta''}{\gamma'' \eta'} \qquad (6)$$

In this paper, the following values were used for K: toluene–water 0.653; carbon tetrachloride–water, 0.388. Within the experimental error the same values for the contact angles of water, θ_{H_2O}, against a number of different carbon blacks were obtained with either toluene or carbon tetrachloride which is justification for assuming that these liquids form zero—or at least identical—contact angles against carbon (*cf.* Table V).

Wolkowa made his measurements in a horizontal tube and listed formulas for calculating the effect of pressure and the angle at which the tube containing the sample is tilted. The maximum pressure used in these experiments was two inches of water, and under these conditions calculations show that the effects of pressure and angle of tilting of the tube are negligible, and the simple Washburn equation 1 can be used.

(1) This work was carried out prior to the middle of 1942 in the laboratories of the General Atlas Carbon Co., presently owned by Godfrey L. Cabot, Inc. Presented before the Division of Colloid Chemistry, American Chemical Society, September 16, 1952.

(2) United Carbon Company, Borger, Texas.

(3) Z. E. Wolkowa, *Kolloid-Z.*, **67**, 280 (1934).

(4) E. W. Washburn, *Phys. Rev.*, **17**, 273 (1921).

Experimental

The wettability measurements were made in thick-walled, constant bore tubes which were graduated in millimeters.[5] The samples were prepared in the following manner. A rubber stopper was inserted into the bottom end of the tube to a given mark. Enough carbon was weighed out to occupy 0.5 cm. when tightly compressed into the tube by hand. This was packed into place between tightly fitting discs of filter paper using a metal rod to exert pressure. Much more satisfactory reproducibility was obtained when a given weight of carbon was packed into a definite volume than when it was packed at a constant pressure. The packing pressure was not measured, but it is believed to be in the neighborhood of 500 p.s.i. Three such plugs were compressed, one upon the other; the top filter paper disc was carefully removed, using a needle to lift it after each plug was compressed into place. A perforated platinum disc was laid on the surface of the carbon, followed by a notched piece of glass tubing of suitable size. The whole set-up was held firmly in place by a tight-fitting, one-hole rubber stopper fitted with a glass tube, Fig. 1. Finally, the rubber stopper and filter paper disc were carefully removed from the bottom end of the tube.

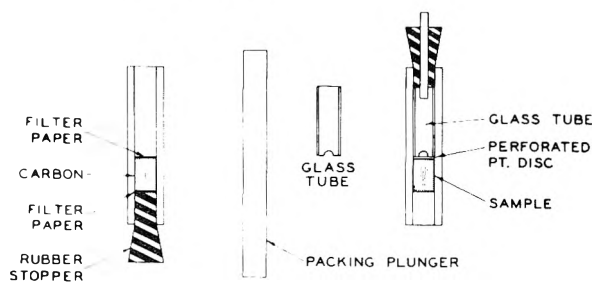

Fig. 1.—Wettability apparatus (graduations removed).

Liquid was added through the hole in the rubber stopper, and the time of flow was measured with a stop watch. The flow of liquid is observed as an advancing black front moving down the less black, unwetted plug. Strong light is essential in this observation. Finally, the time of flow was plotted against the square of the distance, and the value of time at 0.5 centimeter taken from the straight line. Non-uniformity of packing is indicated by systematic deviations from a straight line. If these are the same in all tubes, no error in determining wettability is involved. Two liquids were used and the contact angle against one of them (water) calculated from equation 5.

Duplicate samples were run in all cases, checks within the limits involved in reading the times of flow at a given distance were usually obtained, but in some cases this was not possible with the first set of tubes. When duplicate samples did not agree, two more tubes were run using the same liquid. Checks could be obtained in all cases reported. Care must be taken not to rotate the packing plunger, as this causes a smooth, shiny surface to be formed which greatly reduces the rate of flow of the liquid. With practice the values of $\cos\theta_{H_2O}$ can usually be reproduced to about 0.005. No claim to absolute accuracy of this magnitude is made, but the reproducibility is of this order. Occasionally, a sample is found which will not pack properly; wettability of these samples cannot be measured by this method. To date, we have discovered only three of these samples.

It was found necessary to exert pressure against the wetted surface (with rubber stopper, glass tube and platinum disc). When this was not done, many of the samples apparently loosened and offered very little resistance to the flow of liquid.

In the determinations reported here, the samples were all dried at approximately 150° in air before packing into the tubes. An experiment was made to determine whether moisture pick-up during the packing procedure had an effect on the results. Two sets of tubes were prepared: one in which the air-dried sample was packed into the tube in the usual manner, and another in which the carbon was first packed into the tubes and then oven-dried for an hour at 150°. Mogul, a high oxygen lithographic ink black which absorbs a considerable amount of moisture under normal atmospheric conditions, was the carbon black used in this test. Identical results for the contact angle against water, θ_{H_2O}, were obtained with the two sets of tubes.

The carbons used in this study were of three types: (1) experimental samples prepared by various heat treatments of two samples of carbon black which had quite different initial hydrogen contents, (2) commercial carbon blacks, and (3) some pilot plant samples. In this way, a series of carbons were examined which had a wide range of hydrogen and oxygen contents. It should be noted that no extractable material was present upon any of the first group of samples. The literature contains many references to the effect of oxygen content or volatile matter on the wettability of carbon black, but this is the first study reporting the effect of hydrogen content of the black upon this property.

Results

Table I lists data for a number of heat treated samples of channel black. The following empirical formula represents the data within the experimental accuracy

$$\cos\theta_{H_2O} = (0.037 \times \%\ \text{Oxygen}) - (0.185 \times \%\ \text{Hydrogen}) + 0.284 \quad (7)$$

The wettability values, $\cos\theta_{H_2O}$, calculated from the equation are compared with the experimental values in Table I, and plotted in Fig. 2. Considering the nature of the test, the correlation seems satisfactory.

TABLE I

WETTING DATA DETERMINED WITH WATER AND TOLUENE

Specially prepared samples.

Sample designation	Cos θ_{H_2O} Exptl.	Calcd.[a]	Hydrogen, %	Oxygen,[b] %
No. 6-H-1-927°	0.29	0.27	0.42	1.58
No. 6-H-2.5-927°	.26	.28	.32	1.43
No. 6-H-7.5-927°	.26	.29	.24	1.47
L.T.ch-H-2.5-440°	.33	.37	.68	5.60
L.T.ch-H-5-440°	.42	.44	.66	7.14
L.T.ch-H-16-440°	.55	.57	.60	10.84
L.T.ch-H-25-440°	.58	.67	.53	12.95
L.T.ch-H-48-400°	.64	.75	.48	15.07
L.T.ch-H-1-900°	.23	.23	.54	1.12
L.T.ch-H-4-900°	.24	.24	.42	1.01
Original L. T. Channel	.35	.28	.93	4.64
No. 6-H-16-927°-H-5-440°	.40	.37	.39	4.37
No. 6-H-16-927°-H-16-440°	.44	.50	.29	7.19
No. 6-H-16-927°-H-24-440°	.55	.55	.29	8.63
No. 6-H-16-927°-H-44-440°	.72	.65	.32	11.43

[a] Calculated from equation 7. [b] All samples were dried for one hour in a stream of dry nitrogen and were not re-exposed to air prior to analysis. No sulfur determinations were made and the oxygen values may be slightly in error. This would have only a small effect on the oxygen values for these particular samples.

Table II lists wetting data and hydrogen and oxygen values for a number of commercial samples of carbon black. These data and samples were obtained prior to the middle of 1942.

In making the ultimate analyses it is essential that the sample be treated in the neighborhood of 150° in a stream of dry, inert gas until the evolution of moisture is complete. Tests indicate that one hour is ample.[6] The sample should not be ex-

(5) These were obtained from the Ace Glass, Inc., Vineland, New Jersey.

(6) C. W. Snow, D. R. Wallace and A. L. Sweigart, "The Oxidation of Carbon Blacks," paper presented at the American Chemical Society Rubber Division, Cleveland, Ohio, May 27, 1947. Snow, *et al.*, state that "Experience has shown that this (apparently chemically combined) water is almost wholly removed from ordinary carbon blacks at 150°." They flushed their samples for one hour with helium (8 ml./min.) at 150°.

TABLE II

WETTING DATA DETERMINED WITH WATER AND WITH TOLUENE

Commercial samples for which good combustion analyses are available.

Black	Cos θ_{H_2O} Exptl.	Cos θ_{H_2O} Calcd.[a]	Hydrogen, %	Oxygen,[b] %
Elf 15	0.33	0.28	0.63	3.07
Elf 25	.36	.31	.56	3.44
Elf 30	.42	.32	.51	3.38
Elf 35	.25	.29	.73	3.68
Monarch 71	.32	.34	.35	3.18
Monarch 74	.39	.33	.37	3.14
Monarch 78	.40	.32	.48	3.23
Monarch 80	.39	.31	.53	3.26
Mogul A	.59	.51	.48	8.59
Super Carbovar	.28	.31	.51	3.26
Sterling[c]	.33	.31	.51	3.26
Vulcan[c]	.42	.37	.38	4.22
Carbolac 2	.61	.54	.41	9.05
Carbolac 3	.56	.47	.48	7.29
Std. CS-3	.28	.23	.47	1.87

[a,b] See notes following Table I. [c] These samples are no longer available commercially. They are not furnace blacks.

posed to air after the treatment! The values listed in Table III were not treated in the recommended manner. This makes very little difference with blacks containing very small quantities of oxygen. However, in this table both the hydrogen and oxygen values will be high when appreciable quantities of oxygen are present—due to re-absorption of moisture.

TABLE III

WETTING DATA DETERMINED WITH WATER AND TOLUENE

Miscellaneous commercial samples[a]

	Cos θ_{H_2O}	Hydrogen, %	Oxygen, %
Cabot's No. 6 Rubber Grade Channel Black	0.34	(0.68)	(4.72)
Elf 20	.45	(.74)	(4.72)
Mogul	.47	(.86)	(10.53)
Furnex	.10	(.33)	(.24)
Gastex (6-70)	.21	(.34)	(.12)
Standard Gastex	.09	(.31)	(.63?)
P-33—virtually unwettable—	.00	(.46)	(.37)
Thermex	.17	(.34)	(.04)
		(.27)	(.01)
Superspectra	.32	(.70)	(5.59)

[a] These samples were dried for one hour in air at 150° previous to analysis. However, the samples were weighed and handled in the laboratory air after drying and picked up some moisture. This is indicated by the parentheses. This moisture pick-up is most rapid for the samples which contain the most oxygen. It is not important for the furnace blacks, Furnex, Gastex (6–70), Standard Gastex, P-33 and Thermax.

No sulfur determinations were made. In these analyses a silver gauze was used at the outlet of the combustion tube to remove sulfur dioxide. Since the oxygen values are determined by difference, any sulfur in the sample would result in high values for oxygen content. In most cases, this error would be small and would not appreciably affect the correlation shown in Table I and Fig. 2.

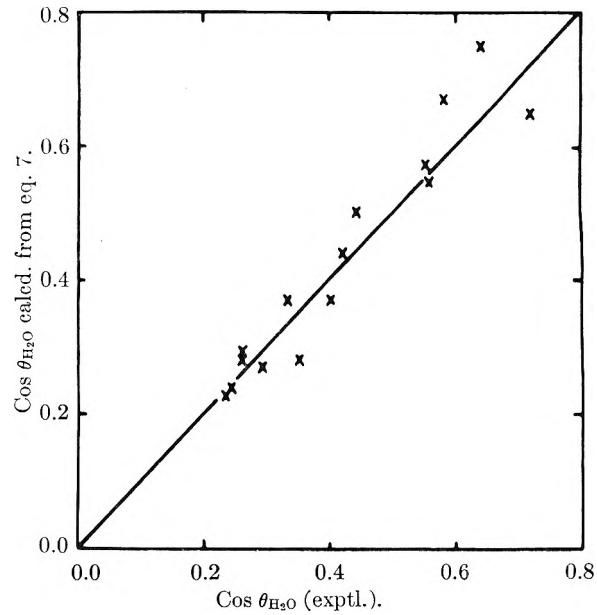

Fig. 2.—Relationship between experimental and calculated values of wettability (cos θ_{H_2O}).

When appreciable quantities by extractable matter are present, the correlation between ultimate analysis and wettability, is affected. The extractable matter decreases the wettability. This can be demonstrated by comparing the wettability of blacks of high extractable content with the values calculated from equation 7 as in Table IV. This effect is also present to some extent in the data for some of the furnace blacks in Table III.

Inorganic ash is present in varying amounts in

TABLE IV

THE EFFECT OF EXTRACTABLE MATTER ON THE WETTABILITY OF CARBON BLACK

Black	% Extractable[a]	Cos θ_{H_2O} Exptl.	Cos θ_{H_2O} Calcd.[c]	Hydrogen, %	Oxygen, %[d]
P-33	1.69	0.00	0.213	(0.46)	(0.37)
5010[b]	0.97	0.004	0.242	(0.53)	(1.51)

[a] Determined by extracting for 22 hours with benzene in a rubber extraction apparatus similar to the ASTM apparatus. [b] A furnace black deliberately produced with 0.97% extractable by benzene. [c] Equation 7. [d] See notes at bottom of Table III.

TABLE V

DATA SHOWING THAT EITHER CARBON TETRACHLORIDE OR TOLUENE MAY BE USED AS THE LIQUID WITH 0° CONTACT ANGLE IN DETERMINING THE WETTABILITY OF CARBON BLACK

All samples except the first were experimental furnace blacks.

Black	Cos θ_{H_2O} Using toluene	Cos θ_{H_2O} Carbon tetrachloride	Contact angle, θ_{H_2O} Using toluene	Contact angle, θ_{H_2O} Carbon tetrachloride
DVCB	0.263	0.260	74.8°	74.9°
288	.181	.178	79.6°	79.8°
294	.172	.175	80.1°	79.9°
301	.162	.164	80.7°	80.6°
365	.215	.216	77.6°	77.5°
283	.124	.134	82.9°	82.2°
289	.163	.176	80.6°	79.9°
298	.156	.174	81.1°	80.0°
305	.170	.180	80.1°	79.7°

carbon black. If it were present in sufficient quantity, it would be expected to make the carbon more readily wettable by water. However, the quantity of ash is usually too small to affect the correlation between wettability and ultimate analysis. With some furnace blacks, however, this effect may be significant.

It is interesting to compare values of cos θ_{H_2O} obtained with two different liquids which can be assumed to have zero contact angles against the black. Very careful tests were made using toluene and carbon tetrachloride as perfectly wetting liquids. Table V lists the results. This group of samples represents a series of pilot plant (SRF) samples obtained by varying the operating conditions. One sample of "devolatilized" channel black (DVCB) is included. It can be seen that excellent checks could be obtained for the two liquids.

Acknowledgment.—The ultimate analyses were made by Dr. E. W. D. Huffman of the Huffman Microanalytical Laboratories, Wheatridge, Colorado. Permission by Dr. C. A. Stokes, Research Director of Godfrey L. Cabot, Inc., to publish this paper is gratefully acknowledged.

THE ADSORPTION AND HEATS OF ADSORPTION OF WATER ON SPHERON 6 AND GRAPHON

BY B. MILLARD, E. G. CASWELL,[1] E. E. LEGER AND D. R. MILLS

Department of Chemistry, University of New Hampshire, Durham, N. H.

Received March 25, 1955

Adsorption isotherms and heats of immersion have been measured at 30° for the systems Spheron 6–water and Graphon–water, the Graphon having been heated in hydrogen at 1000° to remove chemisorbed oxygen. Isosteric heats of adsorption, calculated from the isotherm and heats of immersion data, show the heats of adsorption of water on Spheron to be greater than the heat of liquefaction of water, while the heats for Graphon are lower than the heat of liquefaction.

Introduction

The adsorption of water on Spheron has been measured previously by Emmett and Anderson[2] and by Pierce, Smith, Wiley and Cordes.[3] The Graphon–water system has been studied extensively by Pierce, *et al.*,[3] and by Young, Chessick, Healey and Zettlemoyer.[4]

These two surfaces are interesting since Spheron has a typical heterogeneous carbon surface which is known to be covered with a layer of chemisorbed oxygen,[5] while the more homogeneous carbon, Graphon, is essentially free from oxygen, except for about $^1/_{1500}$ of the surface which is still contaminated.[4] Pierce[3] has shown the profound influence which this small amount of residual oxygen has on the water adsorption by Graphon, the contaminated surface yielding a type III isotherm, with the clean surface giving an extreme type III isotherm with no measurable adsorption below a relative pressure of 0.9.

Zettlemoyer[4] has shown that the type II character of his isotherm is due to residual oxygen on the surface of the Graphon, application of the B.E.T. equation yielding an area which is $^1/_{1500}$ of the total surface area. Confirmation of this is given by the fact that the differential and integral entropy curves intersect at a volume adsorbed corresponding to $^1/_{1500}$ of the total surface. This criterion for monolayer completion was first pointed out by Hill, Emmett and Joyner.[6]

The data reported here are for Graphon which has been hydrogen treated at 1000° in an attempt to render the surface oxygen free.

Experimental

The calorimeter was the same as that previously reported by Harkins and Boyd[7] with several modifications. A fifty junction copper–constantan thermocouple was substituted for their thirty-six junction thermel, together with 100 ml. of water in the calorimeter instead of 650 ml.

In any stirred calorimeter of this type a constant rate of stirring is critical, since any variation will lead to erratic drifts in the time–temperature cooling curves. This difficulty was overcome by using a Raytheon constant voltage regulator in the input line to the stirring motor.

The sensitivity of the calorimeter reported here was such that the liberation of 0.1 cal. gave a deflection of 1 cm., with the galvanometer scale at 2 meters. Between electrical calibrations and heat of immersion measurements, the calorimeter was allowed to cool back to its original equilibrium temperature each time.

Sample containers were made by blowing thin-walled bulbs of volume about 10 ml. from 10 mm. Pyrex tubing. These bulbs were broken during an experiment by one half turn of a screw, which forced a metal bar down onto the bulb, thus shattering it completely. Blank runs on empty bulbs showed the crushing to evolve 0.15 ± 0.02 cal., this value being subtracted from each measurement of the heat of wetting.

Materials.—Spheron 6 and Graphon have been more widely studied than any other surface, an adequate description of them having been given by Pierce, *et al.*[3] Spheron was used as received from Dr. W. Schaeffer of the Cabot Carbon Black Co., except for out-gassing for 24 hours at 300° to a pressure of 10^{-5} mm. before use.

The original sample of Graphon was heated in a stream of hydrogen, of 99.8% purity, for 12 hours at 1000°, then in a stream of helium, of 99.8% purity, at the same temperature for a further 4 hours. The sample was cooled

(1) Submitted in partial fulfillment for the degree of Master of Science.

(2) P. H. Emmett and R. B. Anderson, *J. Am. Chem. Soc.*, **67**, 1492 (1945).

(3) C. Pierce, R. N. Smith, J. W. Wiley and H. Cordes, *ibid.*, **73**, 4551 (1951).

(4) G. J. Young, J. J. Chessick, F. H. Healey and A. C. Zettlemoyer, THIS JOURNAL, **58**, 313 (1954).

(5) R. A. Beebe, J. Biscoe, W. R. Smith and C. B. Wendell, *J. Am. Chem. Soc*, **69**, 95 (1947).

(6) T. L. Hill, P. H. Emmett and L. G. Joyner, *ibid.*, **73**, 5102 (1951).

(7) W. D. Harkins and G. Boyd, *ibid.*, **64**, 1190 (1942).

with the helium still flowing, stored in helium and finally weighed out into the sample bulb and out-gassed in the same manner as the Spheron.

The 4 hour treatment in helium at 1000° was carried out to remove hydrogen which may have been chemisorbed by the sample. Beebe[8] has shown that heating Shawinigan acetylene black at 1000° for 2 hours removes chemisorbed hydrogen.

Water vapor isotherms were obtained at 30° during the course of preparation of samples for the heat of immersion experiments. The amount of water adsorbed was determined gravimetrically, using the technique described by Pierce, *et al.*,[3] except that pressures were read on a mercury manometer with a cathetometer reading to 0.05 mm. In each case 24 hours were allowed before taking final equilibrium pressure measurements. The partially-wetted samples were then sealed off, care being taken not to affect the temperature of the sample. Our isotherms reproduce very well those obtained by Emmett and Anderson[2] for Spheron, and by Pierce[3] for Graphon.

The 2–3 gram samples used in the heat of immersion experiments were used only once, since higher values were obtained in a second run, due to partial surface oxidation after contact with water at the 300°, out-gassing temperature.

Reproducibility of heat of immersion data was good to 2–3%, except in the case of Spheron at low surface coverage where the presence of a slow heat evolution increased the error to about 5%. The data reported for the initial points on Spheron are the heats evolved after 18 minutes. These curves were reconstructed to adiabatic conditions and the calories evolved up to that time calculated. This time was selected because in the first place it was reproducible and secondly it was here that the calorimeter had actually started to cool, although much more slowly than during a calibration run.

Results and Discussion

The isotherms for both Spheron and Graphon are shown in Fig. 1. The essentially hydrophobic nature of Spheron, even though it is completely covered with oxygen complex, is well demonstrated by a comparison of nitrogen[2] and water adsorption for this surface. Whereas Spheron adsorbs a complete monolayer of nitrogen at a relative pressure of 0.1, a statistical monolayer of water is not taken up until a relative pressure of 0.7 is reached. Even though the water isotherm is of a completely different shape from those to which the B.E.T. equation normally is applied, a straight line B.E.T. plot yields a surface area of 110 sq. m. per gram compared to 114 sq. m. per gram for nitrogen.

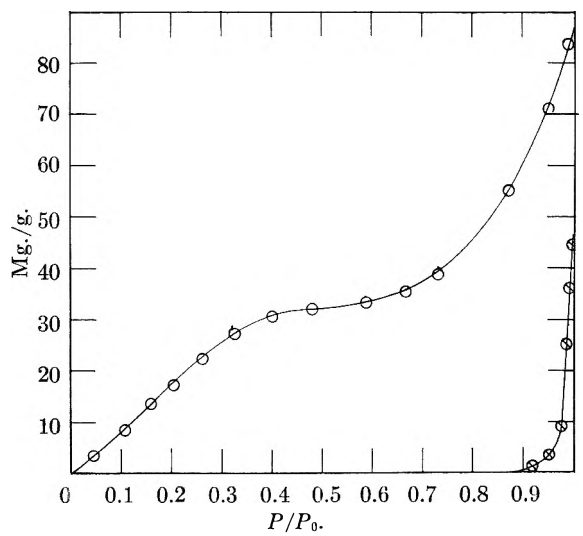

Fig. 1.—Isotherms for water at 30° on O, Spheron 6 and on ⊗ Graphon (hydrogen treated).

The heat of immersion data for Spheron are shown in Fig. 2, the value for the clean surface starting at 150 ergs per sq. cm., then falling off rapidly until a constant value of 65 ergs per sq. cm. is reached at a relative pressure of 0.4.

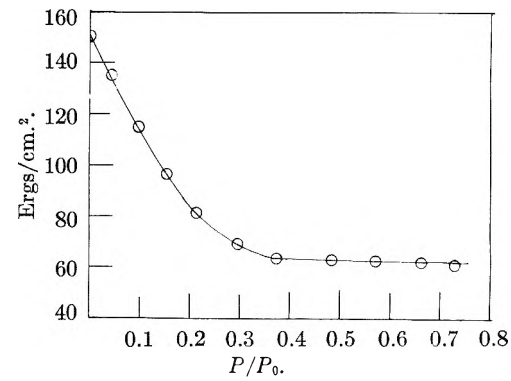

Fig. 2.—Heat of immersion, ergs/cm.², for Spheron 6 in water at 30°.

The values obtained by Harkins and Jura[9] and by Zettlemoyer[4] for the hydrophilic surfaces TiO_2 and asbestos level off at 118 ergs per sq. cm., indicating that a duplex film of water is not formed on Spheron.

The isosteric heats of adsorption of water on Spheron, calculated using the equations given by Zettlemoyer[4] and shown in Fig. 3, are typical of a heterogeneous carbon surface, starting at a value of 2.5 kcal. per mole above the heat of liquefaction of water, falling off rapidly and approaching the heat of liquefaction at a relative pressure of 0.5. It is interesting to compare our results for water on Spheron with those obtained by Beebe[10] for ammonia on the same surface, although the samples are from two different batches.

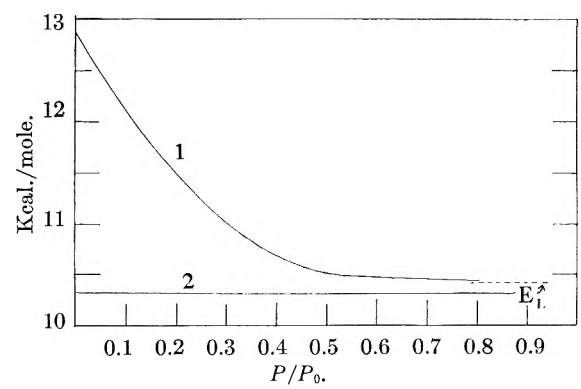

Fig. 3.—Isosteric heats of adsorption of water on Spheron 6, curve 1 and on Graphon, curve 2.

Ammonia yields a type II isotherm with the B.E.T. point "B" falling at a relative pressure of 0.15. The calorimetric heats of adsorption are high, starting at 6 kcal. per mole above the latent heat, falling very rapidly to a flat plateau at 2.4 kcal./mole and then decreasing more slowly toward

(8) R. A. Beebe, First Quarterly Progress Report, Contract No. DA 36-039-SC-56726, Signal Corps Project No. 152 B.

(9) W. D. Harkins and G. Jura, *J. Am. Chem. Soc.*, **66**, 922 (1944).

(10) R. A. Beebe and R. M. Dell, O. N. R. Technical Report No. 5, Research Contract N8-onr-66902, Project NR-358-151.

the latent heat. Beebe attributes the high heats to a reaction between the ammonia and the surface oxygen complex, rather than to simple physical adsorption on the Spheron surface. The same reasoning may also be applied to water on Spheron with the much lower heat values for water being due to the fact that water molecules are much more loosely packed than the ammonia.

Graphon shows no measurable adsorption below a relative pressure of 0.87, Fig. 1, but the heat of immersion curve, Fig. 4, starts out at a value of 25 ergs per sq. cm. increasing to 34 ergs per sq. cm. for the sample that has been equilibrated with water at a relative pressure of 0.95. These results at low surface coverages fall below those obtained by Zettlemoyer[4] but approach his curve at a relative pressure of 0.95 and run in with his results above 0.95.

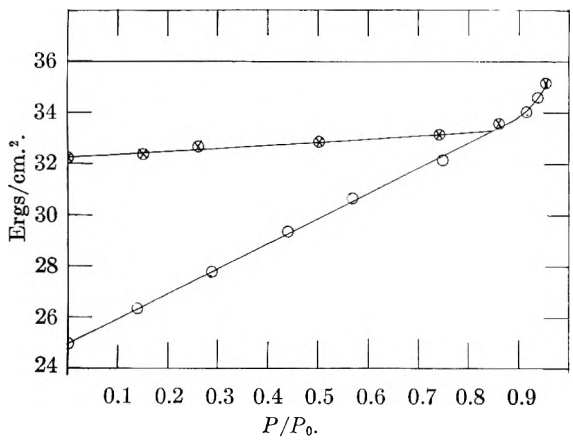

Fig. 4.—Heat of immersion, ergs/cm.², for Graphon in water at 30°: O, this research; ⊗, Zettlemoyer[4] at 25°.

Although the heat of immersion data are lower than those obtained by Zettlemoyer, the isosteric heats of adsorption, calculated from the isotherm and heats of immersion results, in exactly the same way as for Spheron, and shown in Fig. 3, lie quite markedly higher. This is brought about by the isotherms being type II for Zettlemoyer's work and type III for this research. Our heats of adsorption are constant at 78 cal. per mole below the latent heat of evaporation of water up to a relative pressure of 0.9 after which they increase toward the latent heat.

Pierce and Smith[11] found that the isotherms for water–Graphon were coincident at 0 and 28.6° up to 0.9 relative pressure. Following the suggestion of Coolidge,[12] these authors conclude that their isotherm data indicate a zero net heat of adsorption. Owing to the variation with temperature of both the heat of adsorption and heat of liquefaction Beebe[10] has pointed out that this conclusion is not necessarily true, but is good to within approximately 5%. Bartell and Suggitt[13] have also shown from heat of immersion data that the heat of adsorption of water on graphite at low surface coverage is lower than the heat of liquefaction of water.

(11) C. Pierce and R. N. Smith, THIS JOURNAL, **54**, 795 (1950).
(12) A. S. Coolidge, *J. Am. Chem. Soc.*, **49**, 709 (1927).
(13) F. E. Bartell and R. M. Suggitt, THIS JOURNAL, **58**, 36 (1954).

A plausible suggestion for the net heats of adsorption of water on Graphon being negative is that there is no lateral hydrogen bonding between adjacent molecules on the surface; this was first put forward by Beebe.[10]

Pierce and Smith[11] have suggested a cluster-wise adsorption for water on Graphon, with the first molecules going down on the chemisorbed oxygen. However, this concept is difficult to apply to the oxygen free Graphon. Rather it is felt that with water mainly being adsorbed at high relative pressures, here we have a case of capillary condensation, where the capillaries are the spaces between the granules. As Pierce[3] has pointed out, there is some evidence for vapor condensation at high relative pressures in that the particles are agglomerated and stuck together as a solid ball. This must be due to a film of liquid between the particles which acts as a binder.

That small amounts of water are adsorbed at low relative pressures, these amounts being too small to measure in our apparatus, is indicated by the steady rise in the heat of immersion curve (present work), Fig. 4. The isosteric heat curve for treated Graphon, Fig. 3, is completely flat, running at a net heat value of minus 78 cal. This flat curve indicates first that the oxygen complex has been completely removed and that secondly the surface is so sparsely populated that no lateral interaction is taking place below a relative pressure of 0.9. The adsorption of these small amounts of water, below a relative pressure of 0.9, with negative net heats of adsorption must be taking place with an increase in entropy for only then do we obtain a decrease in the free energy as required by any spontaneous process.

No evidence for a slow chemical reaction between water and Graphon was obtained in this research, the heat being liberated rapidly with no subsequent slow heat evolution, this being contrary to the findings of Pierce.[3] With the Spheron, however, the slow reaction may well have caused the slow heat evolution at low surface coverages.

That hydrogen treatment has removed chemisorbed oxygen from the Graphon is demonstrated by a comparison of the isosteric heat curves for the treated Graphon, Fig. 3, and for the untreated material.[4] Zettlemoyer's curve shows a sharp minimum at a relative pressure of 0.01 with the heats rising slowly until at a relative pressure of 0.5 the net heat is negative to the extent of approximately 2 kcal./mole. The minimum in his curve coincides with monolayer coverage of the residual oxygen complex on the surface. This work shows no such minimum.

The difference between the heats of adsorption of water on the oxygen complex on Spheron and on the oxygen complex on the untreated Graphon,[4] in the first case the net heats being positive and in the second negative to the extent of about 6 kcal./mole, can be explained by the fact that Spheron is a heterogeneous surface while Graphon is homogeneous. It would seem that in the case of Spheron lateral hydrogen bonding is operative while for the untreated Graphon no such bonding can take place.

THE MECHANISM OF THE INHIBITION OF CORROSION BY THE PERTECHNETATE ION.[1] I. THE ORIGIN AND NATURE OF REACTION PRODUCTS

BY G. H. CARTLEDGE

Contribution from the Chemistry Division of the Oak Ridge National Laboratory, Oak Ridge, Tenn.

Received March 31, 1955

In a comprehensive study of the effect of ions and molecules of the XO_4^{n-} type upon corrosion it was shown that the TcO_4^- ion is an effective inhibitor for iron and steel. Making use of the radioactivity of technetium, a study has been made of the reduction of the pertechnetate ion by the metal under inhibiting conditions, in order to determine whether inhibition is dependent upon the formation of a film of reaction products. It is shown that the reduced material follows surface activity of the metal in quantity and location, that inhibition may be achieved with far less than enough reduced technetium to form a monomolecular layer, and that the amount of beta activity does not necessarily increase over long periods of exposure (over two years). The evidence indicates that the permanently deposited activity is associated with anodic action of active sites, but that the inhibition itself is not dependent upon such action.

Of the inorganic inhibitors of the corrosion of iron and steel the chromate ion has been studied most extensively. The recent availability of radioactive Cr^{51} has permitted more detailed examination of its action to be made.[2-4] It has been shown that molybdates and tungstates also have inhibitory properties and approach the chromate ion in effectiveness when used in water at room temperature.[5,6] The study of these inhibitors has not sufficed to determine uniquely, however, whether their action necessarily depends upon chemical reaction with the ferrous substrate or on some electrical effect associated with adsorption of the unreduced inhibitor ion. Thus Hoar and Evans[7] and Pryor and Cohen[6] consider that the inhibitor oxidizes ferrous ions in the protective film and thereby maintains its integrity. The importance of the unreduced ions is argued by Uhlig[8,9] and by Powers and Hackerman.[4]

Not all ions of the XO_4^{n-} type are inhibitors, however, so it seemed possible that a careful study of the behavior of all available ions or molecules of this general formula might lead to a fuller understanding of their relation to the corrosion process. The complexity of the problem may be illustrated by the difference in behavior of the $SO_4^=$, $CrO_4^=$, $PO_4^{\equiv}$ and MnO_4^- ions. The permanganate ion reacts rapidly with iron or carbon steel and forms a visible film of reaction products, which is not ordinarily protective. The sulfate ion does not inhibit; the phosphate ion is effective only if oxygen is present. It has been shown[6] that iron (III) phosphate goes into the film under these conditions. It is also known that chromium goes into the interface when chromates are used as inhibitors, though the evidence is not entirely clear as to its chemical form. If the inhibition arose from effects due to the unreduced ion as a whole, it would be difficult to understand the extreme difference between the sulfate and chromate ions.

Such a consideration suggested the necessity of looking *within* the inhibitor particle for the property responsible for its unique action, and led to the hypothesis that a suitable degree of internal polarity might be the distinguishing feature of inhibitors of the XO_4^{n-} type. It was conceived that adsorption of an ion having such a polarity originating in a central atom of high positive charge (*e.g.*, Cr^{6+}) might provide a potential well for electrons underneath it. The induced polarization would contribute to the energy of adsorption and also render the cathodic part of the corrosion process more difficult. This hypothesis led to the expectation that, of all the elements in groups V–VIII of the periodic table, technetium in the form of the pertechnetate ion, TcO_4^-, should be the most likely one to have strong inhibitory properties. It is a transition element, like chromium, and its 7^+ valence state should compensate for the somewhat larger size of the tetrahedral ion, in comparison with the chromate ion. Its relatively low oxidation–reduction potential would also be favorable, if the unreduced ion were the important species in inhibition. The first experimental test strikingly demonstrated the validity of this expectation.

The details of the experiments on inhibition have been described elsewhere.[10,11] It was shown that a mild carbon steel (SAE 1010) was inhibited in aerated distilled water by 5×10^{-5} *f* potassium pertechnetate (5 p.p.m. of technetium element) even at 250°, which was the highest temperature investigated. It was found that a certain minimum concentration of dissolved inhibitor had to be maintained in contact with the metal, this being in the range of 5 to 50 p.p.m. of Tc for different varieties of iron or steel. The inhibition did not persist when the concentration was below such a limit, even though inhibition was first established at a higher concentration. The limiting concentration varied somewhat with the composition and

(1) This work was done for the U. S. Atomic Energy Commission and was covered in large part by official report O.R.N.L.-1833, December 30, 1954.

(2) D. M. Brasher and E. R. Stove, *Chemistry and Industry*, **8**, 171 (1952).

(3) N. Hackerman and R. A. Powers, THIS JOURNAL, **57**, 139 (1953).

(4) R. A. Powers and N. Hackerman, *J. Electrochem. Soc.*, **100**, 314 (1953).

(5) W. D. Robertson, *ibid.*, **98**, 94 (1951).

(6) M. J. Pryor and M. Cohen, *ibid.*, **100**, 203 (1953).

(7) T. P. Hoar and U. R. Evans, *ibid.*, **99**, 212 (1952).

(8) H. H. Uhlig, *ibid.*, **97**, 215C (1950).

(9) H. H. Uhlig, "Metal Interfaces, A Symposium," Am. Soc. Metals, Cleveland, Ohio, 1951, pp. 312–335.

(10) G. H. Cartledge, *J. Am. Chem. Soc.*, **77**, 2658 (1955).

(11) G. H. Cartledge, "Corrosion," to be published in 1955; presented at a Symposium conducted by the National Association of Corrosion Engineers, Chicago, Ill., March 9, 1955.

surface state of the ferrous metal, and inhibition was lost in the presence of sufficient concentrations of electrolytes. If an adequate concentration of inhibitor was maintained, the inhibition appeared to persist indefinitely, since a few experiments have been in progress for 18 to 25 months with no evidence of corrosion.

Apart from any possible practical value that technetium might have as an inhibitor, its use in studies of a theoretical nature is very advantageous. The element is produced among the fission products from nuclear reactors and is available in limited quantities. It has a half-life of approximately 2.2×10^5 years. The radiation is a 0.3 mev. beta, so that it is conveniently handled in the quantities involved without the necessity for great precautions other than the avoidance of contamination. Its specific activity of about 16 μc. per mg. of technetium gives convenient counting rates on small specimens where any precipitation occurs, and autoradiograms may be easily prepared to locate deposits when sufficient amounts are present. The oxidation–reduction potential for the reaction $TcO_2(c) + 2H_2O \rightleftarrows TcO_4^- + 4H^+ + 3e$ is -0.738 volt,[12] or about 0.6 volt less noble than the potential for the reduction of the dichromate ion in acid solution.

In the present paper, experiments will be presented which were directed toward one of the main questions regarding the detailed action of inhibitors of the type under consideration, namely, the origin and nature of any reaction film, and its relation, if any, to the corrosion process.

Experimental Materials and Procedures.—Details concerning the composition and treatment of the test metals have been given in the previous paper.[11] The metal (sample no. 102) used in most of the work in the present paper was mild steel strap containing 0.097% carbon. The potassium pertechnetate was generously supplied by Messrs. G. W. Parker and W. J. Martin of the Hot Laboratory Research Group of the Chemistry Division of this Laboratory. The crystalline salt had been prepared from fission products and was very pure. Standard solutions were prepared from crystals weighed on a microbalance. The ultraviolet absorption spectrum was redetermined on these standard solutions and was used for analytical purposes.[11] Standards for beta counting were prepared by evaporating aliquots of the same solutions on stainless steel. Calibration curves were established by counting these plates on the four shelves of the standard counting chamber of an end-window Geiger Counter and in a 2π gas-flow proportional counter.[13]

Film Formation and Inhibition.—In the inhibition experiments some beta activity always remained upon the metallic specimens after they were thoroughly washed in distilled water. The activity could arise either from irreversibly adsorbed pertechnetate ions or from insoluble technetium dioxide produced by reduction. The experiments to be described in this paper were intended to identify the source of this activity and to provide the basis for a consideration of the important question as to whether the inhibitory process itself necessarily depends upon the formation of a film of insoluble products resulting from chemical reaction between the inhibitor and substrate.

Relation to Surface Activity.—The amount of deposited technetium varied over a wide range which depended upon the composition of the ferrous material, its surface condition, the acidity of the medium, the concentration and nature of other electrolytes, etc. As an example, the following results were obtained in experiments in which stainless steel, type 347, was exposed to a solution containing 1×10^{-4} f $KTcO_4$ and 10 p.p.m. of chloride ion in 0.2 N H_2SO_4 at 85–100°. The specimens were given different pretreatments and acquired the following activities expressed in counts per minute per square cm.

Hand polished with 2/0 abrasive paper	95,000
Hand polished but pretreated in the acid–chloride mixture	14,000
Electropolished in H_3PO_4, H_2SO_4, H_2O mixture	120

It is evident that the surface was rendered less active by the preliminary pickling treatment, but not nearly so effectively as by electropolishing.

In like manner, the activities obtained on inhibited carbon steels have varied from almost nil to 10^6 counts per minute per square cm. This refers to specimens that were effectively inhibited under a variety of experimental conditions. It may be concluded, therefore, that there is no critical amount of technetium that must be deposited in a film for inhibition to be achieved.

It has been found that the technetium deposits selectively upon chemically active areas such as scratches, inclusions, pits from previous corrosion, or active areas produced by welding. Thus, Fig. 1 represents the autoradiogram obtained from a specimen previously exposed to conditions which produced a pitting type of corrosion with an intact film covering most of the specimen. The film was shown to be cathodic to the pits in such specimens by the observation that the film became plated with copper while the pits remained bright when the specimen was immersed briefly in a cupric sulfate solution of suitable concentration. Further corrosion of this specimen was prevented when it was placed in a pertechnetate solution, and the autoradiogram showed the deposition of technetium within the anodic pits previously formed. Similarly, in a study of the precipitation of technetium by welded specimens of stainless steel, a bar 7 mm. square and 15 cm. long was prepared, having the weld in the center. Beta counts were taken through a hole in a lead screen at 1-cm. intervals measured from the weld. It was found that the activity rose to a distinct maximum in the weld zone even though the surface of the specimen had been removed by machining.

The Nature and Origin of the Deposit.—There are several conceivable mechanisms by which technetium may be left on the washed specimens. There may be an essentially irreversible adsorption of the unreduced ion, or an insoluble oxide may be formed by reduction. This reduction, however, may also occur in different ways. Thus, there may be local-action cells with the cathodes and anodes separated by macroscopic distances. This was the situation during the corrosion of the

(12) G. H. Cartledge and Wm. T. Smith, Jr., THIS JOURNAL, in press.

(13) The author is indebted to Dr. A. R. Brosi and to Mrs. G. D. Gibson and Mrs. W. M. Napier for much assistance in the measurement of beta activities.

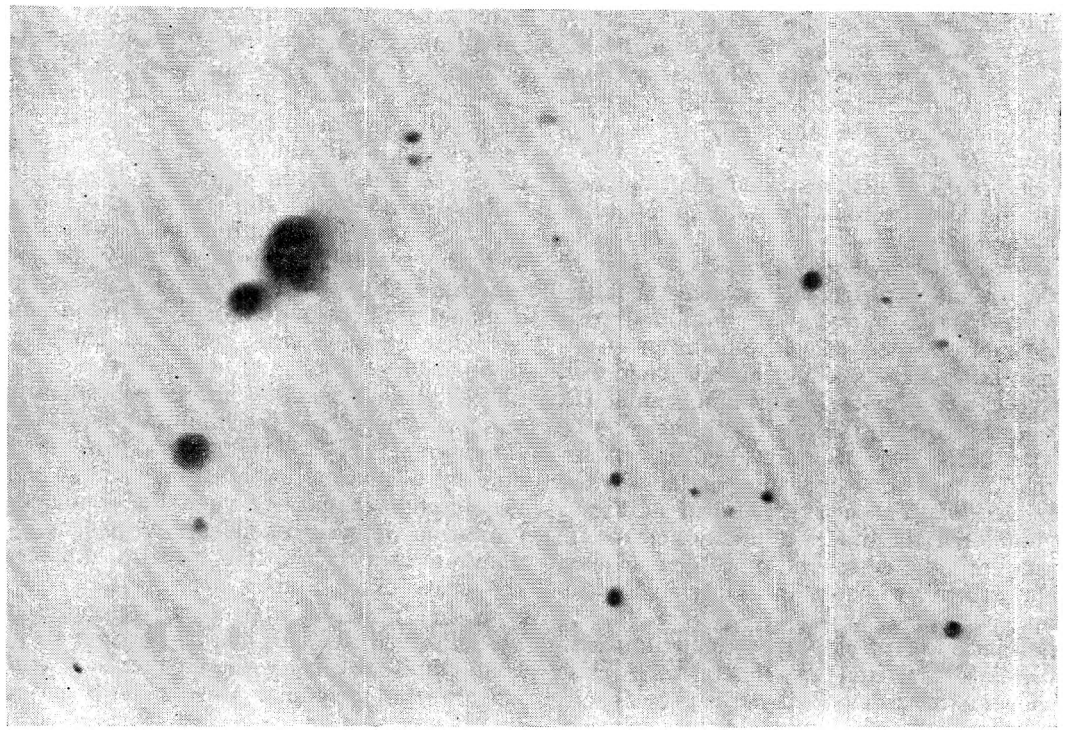

Fig. 1.—Autoradiogram of technetium activity deposited in pits in a specimen first corroded under pitting conditions and then inhibited in potassium pertechnetate.

specimen shown in Fig. 1 before it was placed in the pertechnetate solution. If the passage of current were not inhibited in the presence of the pertechnetate, then reduction to technetium dioxide should result at the cathodes. On the other hand, reduction may also occur by reaction of the pertechnetate ion with active iron areas, or with ferrous ions diffusing away from such areas. In these latter two cases, an intimate mixture of iron and technetium oxides would result, whereas cathodic reduction would give a purer technetium oxide. In order to identify the origin of the active deposit, if possible, a series of experiments was conducted to determine the electrochemical behavior of the pertechnetate ion at attackable electrodes.

One-cm. discs of cold-rolled steel bar stock 1 mm. thick were prepared. The discs were drilled and tapped to screw onto a stainless steel holding rod. The rod and one side of the disc were covered with an insulating wax. The discs were then used as electrodes in 0.1 *f* potassium sulfate containing 80 p.p.m. of Tc as potassium pertechnetate, or in potassium pertechnetate alone. After electrolysis at current densities in the range of 0.5 ma. per cm.^{2} for two to five minutes, the specimens were thoroughly washed and counted. In order to characterize the electrode deposit, advantage was taken of the fact that precipitated technetium dioxide is rapidly oxidized to the pertechnetate ion by hydrogen peroxide in ammoniacal or acid solution. It was observed that the iridescent blue cathodic deposits flashed off almost instantaneously when treated with 3% hydrogen peroxide at room temperature. The brown anodic deposits showed no visible change under similar treatment, though the beta activity was somewhat diminished. Similar electrolyses were conducted with stainless steel electrodes. The cathodic deposits were brown in these cases, but again dissolved at once in hydrogen peroxide. The stainless anodes were not visibly altered by the brief electrolysis. Table I shows the amount of activity found on the electrodes after electrolysis, expressed as mg. of technetium element, and the percentage of this remaining after two treatments with hydrogen peroxide at room temperature.

TABLE I

ELECTROLYTIC PRECIPITATION OF TECHNETIUM DIOXIDE

	Cathode		Anode	
Electrodes	Tc, mg.	% retained	Tc, mg.	% retained
Carbon steel	$1.1_5 \times 10^{-2}$	3.2	3.1×10^{-3}	68
Carbon steel	7.6×10^{-3}	7.4	2.8×10^{-3}	61
Stainless steel	1.0×10^{-2}	..	2×10^{-6}	..
Stainless steel	$1.1_5 \times 10^{-2}$	1.8	2.3×10^{-5}	39

It will be noted that very extensive deposition occurred on the anode as well as on the cathode, when carbon steel was used, but extremely little when the anode was stainless steel. Whereas the cathodic deposits were almost completely decontaminated by the peroxide treatment, the percentage removal was considerably smaller from the mixed iron and technetium oxides on the anodes. Microscopic examination of the cathodic deposits on carbon steel immediately after electrolysis disclosed a number of minute brown areas in the iridescent blue film. These brown spots remained after the peroxide treatment and doubtless represented anodic areas persisting at the low current densities employed. They no doubt were chiefly responsible for the beta activity remaining after decontamination.

Decontamination efficiencies were also determined on specimens of carbon steel that had been exposed to the pertechnetate solution without passage of external current. In three typical examples, the specimens retained 63, 46 and 51% of the initial activity, respectively.

These observations demonstrated that the pertechnetate ion may be reduced and deposited not only at cathodes but also in consequence of secondary processes associated with anodic corrosion of iron. They make it plausible to assume that the insoluble technetium found on inhibited test specimens is also associated with anodic processes occurring at limited areas of high chemical activity. Only on very active spots, however, was sufficient deposit ever formed on inhibited specimens to be visible, this being seen as an iridescent blue or bronze ring around some inclusion or flaw in the metal, as a rule. The activity shown in Fig. 1 also was found only in pits from previous corrosion. The larger cathodic areas did not have enough technetium activity to show up in any such autoradiogram.

The association of precipitated technetium with anodic dissolution of iron was demonstrated also in the following experiment. A carbon steel specimen was well inhibited in a pertechnetate solution. Its beta count corresponded to 7.4×10^{-5} mg. of technetium. A very little cupric sulfate was added, which immediately destroyed the inhibition. After reaction had proceeded for about a minute, the specimen was again washed and counted. It contained 1.6×10^{-3} mg. of technetium. After further exposure to the mixed solution an intensely active reaction product formed, which analysis showed to contain copper, iron and technetium.

It is to be noted that it is thermodynamically possible for low concentrations of the pertechnetate ion to oxidize ferrous ions to ferric hydroxide at a sufficiently high value of *p*H. The oxidation of iron(II) hydroxide is more favorable. By calculation from the standard electrode potential[12] for the half-reaction

$$TcO_2(c) + 2H_2O \rightleftarrows TcO_4^- + 4H^+ + 3e^-$$

and the free energies of Fe(II) ion and $Fe(OH)_3$ as given by Latimer[14] it may be shown that the reaction

$$3Fe^{++} + TcO_4^- + 7H_2O \longrightarrow 3Fe(OH)_3(c) + TcO_2(c) + 5H^+$$

will proceed as written in $10^{-3} f$ $KTcO_4$ if the ferrous ion concentration is $10^{-4} f$ and *p*H is above 5.6. The reaction was experimentally observed to occur slowly when the reagents were mixed in a tube from which the air was evacuated. It is possible that this process is responsible for the black smudge containing technetium dioxide that has sometimes formed *on the walls of the tube* where an inhibited specimen made contact with the glass. Such contact points might easily become anodes in a differential aeration cell and furnish current beyond the capacity of the low technetium concentration to inhibit it.

(14) W. M. Latimer, "Oxidation Potentials," Prentice–Hall, Inc., New York, N. Y., Second Ed., 1952, p. 221.

Inhibition with Minimum Deposit.—These results leave for further consideration, however, the problem as to whether anodically deposited technetium is the cause of the inhibition or merely the result of a brief and localized reaction that proceeds while inhibition is being established by some other mechanism. In examining this question, it will be recalled that the experiments have shown that there is no apparent relation between inhibition and the amount of beta activity permanently remaining on the specimen. The experiments demonstrated also that an inhibited specimen corroded at once when removed from the pertechnetate solution, or when the solution was diluted below some limiting concentration. It was also shown that the inhibition is disturbed by the presence of other ions that presumably act only by competing in the adsorption at the interface. These results leave little doubt that the inhibition depends upon current events of a dynamic nature, rather than upon a film formed in the past. Such film as actually forms wherever corrosion proceeds appears to resemble the deposits formed on an attackable anode in its physical character (porosity, weak adherence if extensive) and in the incompleteness of its reaction with hydrogen peroxide. Even an abundance of such film does not appear to stop corrosion.

It was therefore of interest to determine whether inhibition may be achieved with no beta activity at all on the washed specimen. For this purpose, solutions were prepared which contained 10 p.p.m. of chloride ion in distilled water to which was added at intervals 3% hydrogen peroxide sufficient to maintain a steady evolution of oxygen. It was presumed that the peroxide would prevent or diminish the formation of technetium dioxide, while providing a very corrosive medium with the added chloride in the absence of the inhibitor. The experiments were conducted at temperatures between 73 and 100°. In a blank containing the chloride and hydrogen peroxide, but no pertechnetate, corrosion was extremely rapid. Complete inhibition was obtained in the tubes containing 36 p.p.m. of technetium. Table II gives the results of one two-hour experiment conducted at 85° and using specimens of carbon steel SAE 1010 (sample no. 102) that had been electropolished.

TABLE II

INHIBITION BY THE PERTECHNETATE ION IN THE PRESENCE OF HYDROGEN PEROXIDE AND CHLORIDE ION

Specimen	Wt. change (mg.)	Counts per min.
(L) Control	−6 2	...
(M) Tc only	−0.0$_5$	232
(O) Tc + H_2O_2	+0.1	13
(J) Tc + H_2O_2 (dup.)	0 0	20

As shown in the table, the total activity on the two sides of specimens of O and J amounted to only 13 and 20 counts per minute above background, which corresponds to about 2×10^{-9} g. on an area of 4 cm.^{2}, or 3×10^{12} atoms of technetium per cm.^{2} By assuming a roughness factor of unity, which is, of course, considerably too low, it may be estimated that these low counts, if really signifi-

cant, correspond to no more than one or two tenths of a per cent. of a monomolecular layer. It is hardly likely that so small a fraction of the total surface of a material like carbon steel should account for its corrosion resistance by a film mechanism. The experiment, therefore, leaves little doubt that the inhibition was achieved otherwise than by deposition of reaction products. On the contrary, the corrosion of the control specimen proceeded rapidly in spite of a heavy reaction film.

Approximate Constancy of Deposit.—Another question involved in the theory of inhibitor action is whether an inhibitor of the type of chromate acts by continuously repairing defects in an otherwise protective film by reacting with any exposed metal or ferrous ions that migrate to the interface.[6,7] If such were the case, there should be a continuing increase in the beta activity of a specimen inhibited by technetium over long periods of time. Certain of the specimens used in these experiments have been under observation for periods of 18 to 25 months. Table III shows the data on two such specimens. Experiment T-29E represents a carbon steel (SAE 1010) specimen inhibited by 50 p.p.m. of technetium in a solution containing 10 p.p.m. of chloride ion as potassium chloride. For the first three months the temperature was near 100° during the daytime and 23° overnight. Subsequently the specimen was kept immersed at room temperature in a small vial. Test T-77G was a similar sample inhibited by only 5 p.p.m., first at 100°, then at room temperature. The counts shown are for the two sides of the 1 × 2 cm. specimens. The specimens remained bright and the solutions water clear for the entire period of observation, which is continuing.

TABLE III

WEIGHT AND ACTIVITY DURING PROLONGED INHIBITION OF EMERIED CARBON STEEL

Date	Weight (g.)	Counts per min. Side A	Side B
A. T-29E, 50 p.p.m. of technetium			
1-15-53	0.5728	Started	
3-17-53	.5727	873	280[a]
3-31-53	.5727	745	249
7-29-53	...	787	261
10-2-53	.5727	822	267
12-15-53	...	852	271
1-8-54	...	833	255
9-8-54	...	824	—
10-15-54	.5727	795	252
12-13-54	.5727	786	256
1-10-55	...	777	265
2-14-55	...	844	285
	Av.	813 ± 31	264 ± 9.5
	Av. dev., %	3.8	3.6
B. T-77G, 5 p.p.m. of technetium			
10-9-53	0.5581	Started	
10-14-53	...	301	134[b]
10-16-53	...	304	128
10-29-53	.5580	297	128
5-11-54	...	283	127
8-10-54	...	294	142
12-13-54	.5580	320	142
1-10-55	...	299	132
2-14-55	...	321	144
	Av.	302 ± 9	135 ± 6
	Av. dev., %	3.0	4.4

[a] 1000 counts per min. corresponds to approximately 1.3 × 10^{-4} mg. of technetium. [b] 1000 counts per minute corresponds to approximately 5 × 10^{-4} mg. of technetium.

Other specimens have been observed and counted over periods of several months with similar results even though the varying surface states of the specimens produced widely differing levels of beta activity. Thus, the higher activity of one side of specimen T-29E was associated with a minute flaw which was responsible for approximately half of the counts on that side. Because of the shape and size of the specimens originally used in these tests it was difficult to place them always in the identical position in the counter, so that the counts have a scatter of about ±3 to 4% from the average. By inserting a specimen six times into the top shelf of the counter as carefully as possible an average deviation of 2.2% was found. The observed results in Table III represent only single measurements, so the scatter is not unreasonable. In none of the specimens counted has there been a steady increase in the activity. In a few instances there have been sudden gains in activity associated with some accidental disturbance, such as a scratch, or a local deposit at contacts of the specimen with the glass walls of the container, these being ascribable to a crevice effect or differential aeration, in all probability. It is recognized that such a constancy of activity as is observed conceivably could be a balance between deposition of technetium dioxide and its reoxidation by air. It would be an extremely unlikely coincidence that such should be the case, however, considering (a) the number of experiments, (b) the different metal compositions and surfaces employed, (c) the different technetium concentrations, (d) the different levels of beta activity, and (e) the independence of temperature between 23 and 100°. It is therefore believed that the data justify the conclusion that long-continued inhibition does not necessarily involve a continuing reduction of the inhibitor.

Attempt to Measure Adsorption.—An attempt was made to determine the amount of technetium adsorbed from solution by iron specimens immersed in a solution of inhibiting concentration.[15] Fine iron wire was coiled, degreased, and immersed in 1.5 × 10^{-4} f potassium pertechnetate in narrow glass-stoppered tubes. The tubes were nearly filled by the one ml. of solution used. In one experiment, five such tubes were rotated end over end continuously for five weeks at room temperature. At intervals, 25 λ samples were removed and counted. The amount of activity removed from solution went partly into the reduced oxide deposit and partly into the adsorbed layer. It was planned to attempt to differentiate these by quantitatively rinsing the specimens and containers after equilibrium had been attained, so as to recover all reversibly removed activity. The irrecoverable portion would then represent the

(15) The author is indebted to his colleague, Dr. Walter E. Clark, for conducting this experiment.

reduced technetium, and, by difference, the adsorption could be estimated. The total amount removed, however, proved to be just beyond the counting uncertainties, so that the differentiation could not be made.

In the experiment mentioned above, the 5 coils remained bright except for a few small areas which darkened. This effect has occasionally been observed when aeration was inadequate, and especially when the technetium was near the lower limit for inhibition, as in these tests. The counting data had considerable scatter, but showed no trend either upward or downward from the counts made within one or two hours after immersion. There was consistently a slight decrease from the count of the original solution, however, and the average decrease corresponded to about 2.5×10^{14} atoms of technetium per cm.^{2} of geometrical area. Since this decrease included both adsorbed and chemically reduced technetium, it can only be concluded that the total amount of inhibitor fixed on the surface during immersion was less than a monomolecular layer by a considerable factor.

The Effect of Oxygen.—All of the inhibition tests have been made in solutions that were exposed to the air but not stirred except by the convection currents arising from the method of heating and cooling. It is proper to assume, therefore, that an oxidized surface was presented to the solution. As noted previously, there was occasionally a black smudge both on the metallic specimen and on the glass where there was contact between them. This suggested that the pertechnetate ion was locally reduced in such cases either by differential aeration currents or by direct interaction with active iron or ferrous ions, to the point that non-inhibiting concentrations were locally produced. Accordingly, a few experiments were done in which air was very largely removed from the system.

A barely inhibiting solution was placed in a small glass tube with a 1-inch piece of emeried steel wire (SAE 1030, sample no. 104) held in a constriction above the solution. The liquid was repeatedly boiled under vacuum with gentle heat and the tube was sealed while still under vacuum. The pin was then shaken into the solution. In three experiments it was observed that a dark film formed over parts of the surface, but no brown rust or turbidity was observed even after 10 weeks at 23°. The dark film contained roughly 2×10^{-3} mg. of technetium in one case.

Since at 23° corrosion of the steel hardly proceeds measurably in deaerated water even in the absence of inhibitor, the object of this experiment was not to test for inhibition but to determine whether oxygen may not be required to prevent reduction of the pertechnetate ion on active sites. The experiments appear to indicate that such is the case. The results may be reasonably interpreted by the assumption that either oxygen, if present, or the oxidizing inhibitor initially oxidizes the most anodic areas, and that thereafter the inhibitor acts on the "cleaned-up" surface by whatever specific mechanism turns out to be involved, but without further chemical reduction. This view is apparently supported by the combination of the peroxide experiments, in which the metal was at least partially "cleaned" by prior electropolishing, with the long-term observation of an essentially constant beta count on inhibited specimens.

Discussion.—The experimental results may be combined into the following argument regarding the nature and possible function of insoluble reaction products.

(a) The beta activity counted definitely follows the surface activity in quantity and location. The amount may be greatly reduced by pre-cleaning of the surface and by the presence of adequate oxygen, though these do not provide corrosion resistance in the absence of inhibitor.

(b) The abundant association of technetium activity with anodic processes was shown in the electrolysis experiments. The low decontamination efficiency of hydrogen peroxide was similar on the anodes and on the regular test specimens, suggesting that the active deposit is a secondary reaction product.

(c) Even an abundance of such deposit is not inhibitive, however, in the absence of dissolved pertechnetate. Furthermore, inhibition was achieved with as little as 3×10^{12} atoms of technetium per cm.^{2} in presence of hydrogen peroxide and 10 p.p.m. of chloride ion. This amount is to be compared with the results of Brasher and Stove,[2] who found 5.5×10^{15} atoms of chromium per cm.^{2} after three-day immersion of steel in potassium chromate. Similarly, Powers and Hackerman[4] found 5.2×10^{15} atoms of chromium per cm.^{2} on steel treated in 1×10^{-3} *f* chromate at *p*H 7.5. These workers did their experiments at 25°, whereas the technetium measurements were made at 85° and in a very corrosive medium, so that chemical attack should have been more vigorous. Yet the technetium activity found on the electropolished specimens was lower by three orders of magnitude.

(d) The inhibition process was shown to be dependent upon current events, since inhibition was quickly lost when the specimen was removed from the pertechnetate solution, or when the solution was diluted beyond a certain limit.

(e) The "current events," however, appeared not to involve continuous reduction of the inhibitor, since long exposures were not accompanied by an increase of beta activity.

(f) Although the pertechnetate ion is barely able thermodynamically to convert ferrous ions into ferric hydroxide, it is effective as an inhibitor in weakly acidic solution at a lower concentration than is required by the chromate ion, which is a considerably stronger oxidizing agent.

It therefore seems reasonable to conclude that, whereas some reaction product inevitably results when oxidizing agents (including oxygen) act on the ferrous substrate, the actual inhibition by the pertechnetate ion does not result from such products. The next paper will present evidence bearing upon the degree of reversibility of the process or state by which inhibition is determined.

NOTES

HETEROGENEOUS DECOMPOSITION OF NITROUS OXIDE AND THE THETA RULE

By Richard J. Mikovsky and Robert F. Waters

Research Department, Standard Oil Company (Indiana), Whiting, Indiana

Received April 14, 1955

The heterogeneous decomposition of nitrous oxide has been the subject of investigations resulting in a number of proposals concerning the mechanism.[1,2] Weyl suggests that the reaction proceeds by means of a transfer of electrons *from* the catalyst. If this extraction were the rate-determining step, other reactions, possessing the same rate-controlling step, should exhibit kinetics similar to the nitrous oxide decomposition over the same catalysts.

The present work was initiated to study the nitrous oxide decomposition over platinum-on-alumina catalysts which had been used for more complex hydrocarbon conversions. The experiments were carried out in a flow system in which the temperature and flow rate necessary to yield an arbitrary 30% decomposition were measured.

Experimental

Twenty-four platinum-on-alumina catalysts were studied. Fifteen contained a third component, such as MoO_3, Ru_2O_3 ZrO_2, MgO, TiO_2, Cr_2O_3 or V_2O_5. Runs with alumina alone showed that less than 10% of the measured decomposition took place on the bare alumina surface.

Nitrous oxide (Mathieson) was cooled to Dry Ice temperatures to remove water vapor and, after reheating to room temperature, was metered by a glass capillary flow meter. It was then passed upward through a reactor containing 5 to 10 g. of catalyst. Unreacted N_2O was frozen out in a constant-level liquid-oxygen trap, and the non-condensable reaction products, after reheating to room temperature, were metered by a second flow meter. The first flow meter was calibrated for N_2O flow and the second for the stoichiometric 2:1 mixture of nitrogen and oxygen. The relative readings of the flow meters indicated when 30% decomposition occurred.

In each experiment the N_2O flow rate was adjusted to a set of predetermined values between 1.2 and 4.4 liters STP/hr., and the catalyst temperature was varied by means of a manometric thermoregulator until 30% of the N_2O decomposed. The required temperatures lay between 430 and 530°. With most of the catalysts, successive runs were made until the activation energy was reproduced within 5%.

Results

A plot of the logarithm of the N_2O flow rate (log k) *versus* the reciprocal absolute temperature for 30% reaction gives the frequency factor (k_0) and the activation energy (ΔE_a) in accordance with the Arrhenius kinetic equation. In the absence of surface-area data for the platinum crystallites, the rate constants are reduced to unit weight of catalyst. The resultant dimensional units of the rate constants are liters hour^{-1} gram^{-1}.

In Fig. 1, the logarithms of the frequency factors are plotted against the energies of activation. The points define a straight line in accordance with the Theta Rule.[3] The best line, determined by the method of least squares, may be represented by

$$\log_{10} k_0 = 0.468 + 0.272\Delta E_a$$

Some of the catalysts became more active in successive runs with a corresponding drop in activation energy. The initial run for each catalyst is represented by a solid point. All of the data follow the same Theta Rule relationship.

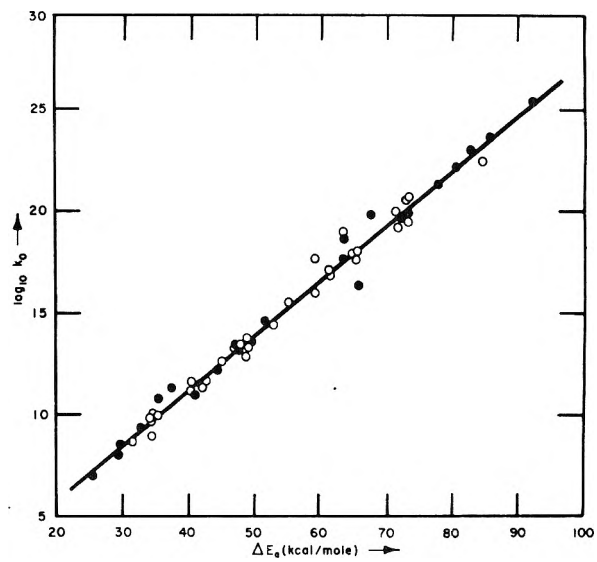

Fig. 1.—Theta rule for decomposition of N_2O over Pt–Al_2O_3 catalysts.

Discussion

Johnston[4] points out the anomalous behavior of N_2O and notes that the activation energy of the thermal decomposition ranges from 48 to 65 kcal./mole. The fact that some of our observed activation energies for the heterogeneous reaction lie outside this range focusses attention on the nature of the N–O bond. Pauling[5] reports that the N–O and N–N bonds in N_2O have properties approaching those of a double and triple bond, respectively. Briner and Karbassi[6] unexpectedly found that the threshold quantum of energy necessary for the photolytic decomposition of N_2O corresponds to 142 kcal./mole. Thus, the observed high activation energies for the heterogeneous reaction seem reasonable.

(1) C. N. Hinshelwood and C. R. Prichard, *J. Chem. Soc.*, 127, 327 (1925); G. M. Schwab, *et al.*, *Z. physik. Chem.*, **B9**, 265 (1930); **B21**, 65 (1933); **B25**, 418 (1934); E. W. R. Steacie and J. McCubbin, *J. Chem. Phys.*, **2**, 585 (1934); C. Wagner, *ibid.*, **18**, 69 (1950); M. Boudart, *ibid.*, **18**, 571 (1950); K. Hauffe, *et al.*, *Z. physik. Chem.*, **201**, 223 (1952).

(2) W. A. Weyl, "A New Approach to Surface Chemistry and to Heterogeneous Catalysis," The Pennsylvania State College Bulletin No. 57, 1951.

(3) G. M. Schwab, Proc. Intern. Congr. Pure and Appl. Chem., 11th Congr., London, 1947, Vol. I, 621 (1950); *Advances in Catalysis*, **2**, 251 (1950). E. Cremer, for reasons discussed in *Advances in Catalysis*, **7**, in press (1955), prefers to use the term "Compensation Effect (CE)" instead of Theta Rule.

(4) H. S. Johnston, *J. Chem. Phys.*, **19**, 663 (1951).

(5) L. Pauling, "The Nature of the Chemical Bond," Cornell University Press, Ithaca, N. Y., 1945, p. 124.

(6) E. Briner and H. Karbassi, *Helv. Chem. Acta*, **28**, 1204 (1945).

The slope of the line in Fig. 1 is inversely proportional to what has been termed a "preparation temperature."[3] It corresponds to the reciprocal of the absolute temperature at which the specific reaction rate constants of all the catalysts are equal. Presumably the distributions of active centers on the catalysts are all equivalent at this temperature. Hence, the slope of the line may be common to other N_2O studies and to other reaction studies involving a presumably similar electron transfer which might be rate determining. The data reported in the literature, however, give little positive support to this idea.

The authors appreciate the assistance of G. S. Marlow with the experimental work.

THE LIMITING CURRENT ON A ROTATING DISC ELECTRODE IN SILVER NITRATE–POTASSIUM NITRATE SOLUTIONS. THE DIFFUSION COEFFICIENT OF SILVER ION

By Martin B. Kraichman and Ernest A. Hogge

U.S. Naval Ordnance Laboratory, Silver Spring, Maryland

Received March 18, 1955

Equations for the steady-state rate of diffusion at a rotating disc electrode have been solved by Levich[1] for a binary electrolyte system. A previous study by the authors[2] extended these equations to the ternary system KI–KI_3 with KI as an indifferent electrolyte. Using this system with platinum electrodes, experimental data confirmed the relationships derived and yielded a value of the diffusion coefficient of the single ionic species I_3^-.

Further experimental work by the authors has confirmed the relationships of the ternary system for the case of deposition using silver electrodes and the electrolyte system $AgNO_3$–KNO_3 with the addition of small amounts of gelatin. The data also yielded a value for the diffusion coefficient of Ag^+.

Experimental

Preparation of Materials.—Boiled distilled water was used in the preparation of all solutions.

Reagent grade chemicals were used in the preparation of stock solutions of 0.2 *N* KNO_3 and 0.00602 *N* $AgNO_3$. Oxygen was removed by bubbling with tank nitrogen.

Using U.S.P. grade gelatin (Knox), 0.01% was added to the electrolyte and the system used for a single run.

Apparatus.—The silver rotating disc cathode, approximately 2 cm. in diameter, was mounted on a shaft connected to a variable speed motor. The anode consisted of silver foil whose area was about 20 times that of the cathode and was placed 5 cm. from it. A silver wire potential probe was positioned near the disc. The vessel containing the electrodes and probe held 600 ml. of electrolyte and was approximately 9 cm. in diameter. Nitrogen was led into the vessel so that a positive pressure was exerted above the electrolyte at all times.

Kinematic viscosity measurements of the 0.2 *N* KNO_3 solution at room temperature were made using an Ostwald–Fenske viscometer.

Procedure.—Current and voltage measuring apparatus, consisting of a precision d.c. milliammeter and vacuum tube voltmeter, was connected to the electrolysis cell. Known amounts of $AgNO_3$ solution were added to the supporting electrolyte, KNO_3 by means of calibrated pipets. The voltage across the diffusion boundary layer at the cathode was maintained at 0.2 volt for all readings by compensating for the ohmic drop in the solution. Limiting current values were then read for each concentration of $AgNO_3$ using various cathode speeds. All measurements were made in a temperature-controlled room.

Results and Discussion

The theory of the ternary system[2] gave the following expression for the limiting current in e.g.s. units

$$I_{\text{lim}} = \frac{n_3 D_3 e(c_3^{\circ} S^{1/2}) AN \times 10^{-3}}{0.647 \nu^{1/6}} \qquad (1)$$

where n_3 is the valence of the reacting ion species; D_3 is the diffusion coefficient of this species; e is the unit electronic charge; c_3^0 is the concentration of the reacting ion species expressed in normality; s is the rate of rotation of the rotating disc electrode in revolutions per second; A is the area of the disc electrode; N is Avogadro's number; ν is the kinematic viscosity of the electrolyte.

For fitting a regression line by the method of least squares, the product $c_3^{\circ} s^{1/2}$ may be considered as the independent variable. The regression coefficient is then given by

$$b = \frac{I_{\text{lim}}}{c_3^{\circ} S^{1/2}} = \frac{n_3 e D_3 AN}{0.647 \nu^{1/6}} \times 10^3 \qquad (2)$$

from which we can solve for the diffusion coefficient

$$D_3 = \left[\frac{0.647 \nu^{1/6} b}{n_3 eAN} \times 10^3\right]^{3/2} \qquad (3)$$

Table I shows the experimental data for various disc speeds and $AgNO_3$ concentrations. Plots of these data show a linear relationship between the limiting current and the $\sqrt{s}$ for different concentrations of $AgNO_3$. Extrapolations of these lines back to zero speed pass through the origin within experimental error.

Fitting a regression line to the data in Table I yielded a calculated value $b = 0.07495 \pm 0.00045$

Table I

Limiting Currents in Milliamperes at 0.2 v. for Various Concentrations of $AgNO_3$ and Various Cathode Speeds

$(\text{r.p.s.})^{1/2}$	Concn. of $AgNO_3$ in normality $\times 10^6$							
	2.00	3.99	5.96	7.92	9.87	33.2	54.7	74.7
1.22	0.0189	0.0377	0.0567	0.0756	0.943	0.320	0.530	0.731
1.87	.0282	.0565	.0841	.113	.141	.477	.790	1.09
2.30	.0347	.0690	.103	.140	.172	.585	.974	1.35
3.15	.0467	.0932	.140	.189	.234	.793	1.32	1.82
3.63	.0533	.108	.161	.214	.268	.905	1.52	2.08
4.28	.0627	.127	.188	.251	.312	1.08	1.80	2.43
4.73	.0693	.140	.208	.278	.347	1.20	1.98	2.68
5.31	.0776	.156	.232	.309	.385	1.35	2.20	2.97
6.22	.0898	.180	.268	.358	.452	1.57	2.55	3.37
6.66	.0960	.192	.288	.382	.482	1.67	2.72	3.66

(1) B. Levich, *Acta Physicochim. U.R.S.S.*, **17**, 257 (1942).

(2) E. A. Hogge and M. B. Kraichman, *J. Am. Chem. Soc.*, **76**, 1431 (1954).

for the regression coefficient given by equation 2, where the error is expressed to the 5% probability level.[3]

Measurement of the kinematic viscosity of the solution at room temperature (25.0°) gave $\nu^{25.0} = 0.8836 \pm 0.0028$ centistoke. The viscosity of the solution with density $\rho^{25.0} = 1.0008$ g./cm.^{3} is therefore $\eta^{25.0} = 0.8843 \pm 0.0028$ centipoise. The area of the disc electrode was measured as 3.9039 ± 0.0012 sq. cm. Calculation of the diffusion coefficient for the silver ion from equation 3 gave $D_3 = (1.416 \pm 0.013) \times 10^{-5}$ cm.^{2}/sec. All the errors indicated are expressed to the 5% probability level.[4]

Another independent experimental run at a room temperature of 25.2° gave similar linear relationships. Constants of the solution at this temperature were $\nu^{25.2} = 0.8824 \pm 0.0016$ centistoke, $\rho^{25.2} = 1.0007$ g./cm.^{3}, and $\eta^{25.2} = 0.8830 \pm 0.0016$ centipoise. The regression coefficient was calculated as $b = 0.07644 \pm 0.00033$ and the diffusion coefficient as $D_3 = (1.458 \pm 0.009) \times 10^{-5}$ cm.^{2}/sec.

The experimental values for the diffusion coefficient of Ag^+ are in good agreement with the Onsager limiting law [5,6] which predicts a value $D_{Ag} = 1.485 \times 10^{-5}$ cm.^{2}/sec. at 25°.

(3) R. A. Fisher, "Statistical Methods for Research Workers," Oliver and Boyd, London, 1946, p. 135.

(4) R. A. Fisher, ref. 3, p. 122.

(5) L. Onsager, *Ann. N. Y. Acad. Sci.*, **46**, 241 (1945).

(6) L. J. Gosting and H. S. Harned, *J. Am. Chem. Soc.*, **73**, 159 (1951).

THE INFRARED SPECTRUM OF SULFUR DICHLORIDE

BY GORDON M. BARROW

Department of Chemistry, Northwestern University, Evanston, Illinois

Received March 21, 1955

Sulfur dichloride is one of the few triatomic molecules not studied in either the Raman or infrared. Raman investigation is made difficult by the red color of the compound and the low frequencies of its fundamentals allow only an incomplete study by means of infrared. By the determination of sufficient overtone and combination bands, however, the fundamentals can be fairly definitely deduced.

The compound was prepared[1] by bubbling chlorine through sulfur monochloride containing a trace of iodine. It was distilled immediately before use and boiled at a constant value of 57.3° at 734 mm.

Figure 1 shows the spectrum of the liquid and vapor obtained on a Beckman IR2T (rock salt region) and a Perkin-Elmer Model 112 (CsBr region) instrument.

Absorptions at 460 cm.$^{-1}$ in the vapor and 445 cm.$^{-1}$ in the liquid are due to the very strong band of S_2Cl_2 contaminating the sample. None of the remaining bands can be assigned to this impurity.

Table I lists the more intense of the observed frequencies with an assignment of the overtones and combinations in terms of a set of fundamental modes. For this molecule all combinations and overtones are allowed by symmetry in the infrared. The strong band at 525 cm.$^{-1}$ in the vapor is undoubtedly a stretching fundamental. The Raman spectra[2] of Stammrich, Forneris and Sone indicate that this band is to be assigned to the symmetric stretching mode. The remaining fundamentals, reported from the Raman spectrum as 208 and 535 cm.$^{-1}$, are not observed. With these fundamentals the remaining stronger infrared bands can be satisfactorily accounted for.

Taking as gas phase fundamentals 525, 504 and approximately 200 cm.$^{-1}$, an SCl_2 angle of 103°[3] and a potential field of the form

$$2V = k[(\Delta r_1)^2 + (\Delta r_2)^2] + k\,(r_0\Delta\alpha)^2 + k_2[\Delta r_1 + \Delta r_2]r_0\Delta\alpha$$

the force constants are evaluated as $k = 2.46 \times 10^5$, $k\alpha = 0.30 \times 10^5$ and $k_2 = 0.16 \times 10^5$ dynes/cm. More detailed consideration of different force fields does not seem warranted in view of the uncertainty in the assignment of the symmetric and antisymmetric vibrations.

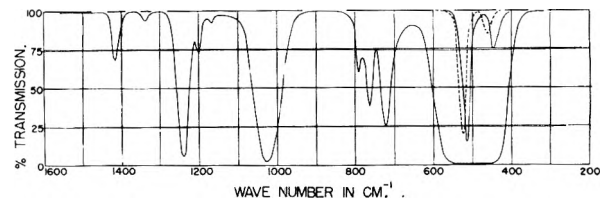

Fig. 1.—The infrared spectrum of SCl_2: ------, vapor; ———, pure liquid.

Comparison can be made, however, with the force constant of 2.42×10^5 for the SCl bond in sulfur monochloride[4] and the bending constant at 0.3×10^5. Since somewhat different force fields were used exact agreement for these molecules cannot be expected.

TABLE I

FREQUENCIES AND ASSIGNMENT OF INFRARED ABSORPTION BANDS OF SCl_2, ν(CM.$^{-1}$)

Vapor	Liquid	Assignment
	(208)	ν_2
525	514(vs)	ν_1
	(535)	ν_3
	719(m)	$\nu_1 + \nu_2$
	761 w	$\nu_1 + \nu_3$
	1027(s)	$2\nu_1$
	1237(m)	$2\nu_1$
	1416(w)	$2\nu_1 + 2\nu_2$

For a similar molecule Cl_2O and the frequencies of Hedberg[5] and of Bailey and Cassie[6] the same force field as given above gives $k = 4.75 \times 10^5$, $k = 0.46 \times 10^5$, and $k_2 = 0.32 \times 10^5$ dynes/cm. The increase in the stretching force constant and the interaction constant are to be expected for the molecule containing a first row element compared to one of the second row.

(1) N. V. Sidgwick, "The Chemical Elements and Their Compounds," Vol. II, Oxford University Press, New York, N. Y., 1950, p. 946.

(2) Since submission of this note the Raman spectrum has been reported by Stammrich, Forneris and Sone, *J. Chem. Phys.*, **23**, 972 (1955). Their reported Raman bands are used here to aid in the assignment of the infrared overtone bands.

(3) D. P. Stevenson and J. Y. Beach, *J. Am. Chem. Soc.*, **60**, 2872 (1938).

(4) H. J. Bernstein and J. Powling, *J. Chem. Phys.*, **18**, 1018 (1950).

(5) K. Hedberg, *J. Chem. Phys.*, **19**, 509 (1951).

(6) C. R. Bailey and A. B. D. Cassie, *Proc. Roy. Soc. (London)*, **142A**, 129 (1933).

Finally one can notice the variation in the frequencies of the SCl bond stretching vibrations in the set of molecules SCl_2, $OSCl_2$[7] and O_2SCl_2[8] where the average SCl frequency (for the liquid) decrease from 525 to 466 to 396 cm.$^{-1}$. Interaction with the SO frequency of the thionyl and sulfuryl chloride might be expected to increase rather than to decrease the "SCl" frequency. In this case the frequency decrease would be associated with a weakening of the S–Cl bonds in the series. This result is not readily understood in terms of the increased formal charge on the sulfur atom,[9] and a simple explanation based on the use of d orbitals by the sulfur atom follows only if it is assumed that in SCl_2 there are contributing structures involving use of the chlorine d orbitals also.

(7) C. A. McDowell, *Trans. Faraday Soc.*, **49**, 371 (1953).
(8) Vogel-Hogler, *Acta Phys. Austriaca*, **1**, 323 (1948)
(9) C. C. Price and R. G. Gillis, *J. Am. Chem. Soc.*, **75**, 4750 (1953).

A NOTE ON VISCOSITY OF MIXTURES. PART I (LIQUID–LIQUID BINARY MIXTURE)

BY R. P. SHUKLA AND R. P. BHATNAGAR

Department of Chemistry, Holkar College, Indore, India

Received March 25, 1955

A viscosity function of the form

$$(\eta_m)^{1/3} = \frac{d(x_1R_1 + x_2R_2 + \ldots\ldots\ldots + x_nR_n)}{M_m}$$

where η_m is the viscosity, M_m the mean molecular weight, "d" the density of the mixture, and "x," the mole fraction and "R" the rheochor of the component, has been tested with viscosity data on binary liquid–liquid pairs.[1,2]

The above equation for viscosity can be obtained from the equation of Smith and co-worker,[3] in the following manner.

The above authors[3] have shown that F, the additive-constitutive property

$$F = \Sigma_i x_i F_i = (x_1F_1 + x_2F_2 + \ldots\ldots\ldots + x_nF_n) \quad (1)$$

and also

$$F = f(\eta)\Sigma_i x_i M_i/d = f(\eta) \times (x_1M_1 + x_2M_2 + \ldots\ldots + x_nM_m)/d \quad (2)$$

where x_i is the mole fraction of the ith component of the mixture. Now by equating "F" in the two equations

$$f(\eta) = d\Sigma_i x_i F_i/\Sigma_i x_i M_i = \frac{(x_1F_1 + x_2F_2 + \ldots\ldots\ldots + x_nF_n) \times d}{x_1M_1 + x_2M_2 + \ldots\ldots\ldots + x_nM_n}$$

The values of F_1, F_2, etc., can be calculated from the additivity of the groups or the atomic values of the molecules and corresponds to the rheochor of the components. If R_1, R_2, etc., are the rheochor of the components 1, 2, etc., and $(x_1M_1 + X_2M_2 + x_3M_3 + \ldots\ldots) = M_m$, the mean molecular weight; η_m, the viscosity of the mixture can be obtained from the equation

$$(\eta_m)^{1/3} = \frac{(x_1R_1 + x_2R_2 + \ldots\ldots + x_nR_n) \times d}{M_m} \quad (3)$$

(1) F. W. Lima, *J. Am. Chem. Soc.*, **56**, 1052 (1952).
(2) Katz, *et al.*, *Ind. Eng. Chem.*, **35**, 1091 (1943); **35**, 239 (1943).
(3) C. P. Smith, *et al.*, *J. Am. Chem. Soc.*, **51**, 1736 (1929).

Following are the comparative results of viscosity as calculated from equation three and viscosity observed by Silawat,[4] *et al.*

TABLE I

(The detailed calculations may be published elsewhere at a later date.)

Systems	Deviations, % Maximum	Minimum
Toluene–acetic acid	3.50	0.52
Benzene–acetic acid	2.75	.03
Chloroform–acetic acid	3.12	.02
Carbon tetrachloride–acetic acid	4.40	.045
Toluene–acetone	3.57	.48

As will be seen from the table the standard deviation between the calculated and experimental viscosities is approximately 1%, while the maximum deviation being 4.4%. In the equation suggested by Lima[1] there is a maximum deviation of 15% and generally an error of 12%. Further work of binary solid–liquid and ternary liquid mixtures is being carried out.

(4) H. G. Silawat, *et al.*, *J. Ind. Chem. Soc.*, **27**, 345 (1950).

SYNTHESIS OF *n*-BUTANE-2,3-d_4 BY THE PHOTOLYSIS OF α,α'-DIETHYL KETONE-d_4

BY J. R. MCNESBY, CHARLES M. DREW AND ALVIN S. GORDON

Chemistry Division, U. S. Naval Ordnance Test Station, China Lake, California

Received April 30, 1955

In agreement with the work of Wijnen and Steacie,[1] we found that deuterium from heavy water exchanged with hydrogen in diethyl ketone exclusively in the α-positions. Nine ml. of D_2O containing 0.1 g. of K_2CO_3 was added to 10 ml. of redistilled diethyl ketone. The partially miscible system was refluxed gently at one atmosphere for 8–16 hours in a closed system. Sufficient K_2CO_3 was added to saturate the water layer. The ketone layer was separated and the procedure repeated ten times. The resulting ketone was distilled from an excess of K_2CO_3 and freed of dissolved air by repeated freezing and melting under vacuum. Mass spectrometric analysis showed about 98–99% α,α'-diethyl ketone-d_4, the remainder being the trideutero compound.

The marked ketone was photolyzed in a water cooled 200-ml. fused silica reaction vessel at 33 mm. initial pressure and at 30°, using a Hanovia Alpine burner. The photolysis was continued for about two hours or until the pressure had risen to 45 mm. The entire contents of the photolysis vessel were pumped into a 2-liter flask. This procedure was repeated 35 times. The flask containing the heavy products of the photolysis in addition to CO was sealed off.

According to the work of Kutschke, Wijnen and Steacie,[2] the main products of the photolysis in the region of room temperature are butane, ethylene, ethane and carbon monoxide. The mechanism of

(1) M. H. J. Wijnen and E. W. R. Steacie, *Can. J. Chem.*, **29**, 1092 (1951).
(2) K. O. Kutschke, M. H. J. Wijnen and E. W. R. Steacie, *J. Am. Chem. Soc.*, **74**, 714 (1952).

butane formation is probably recombination of ethyl radicals formed in the primary step

$$CH_3\text{–}CD_2 + D_2C\text{–}CH_3 \longrightarrow CH_3CD_2CD_2CH_3$$

As long as the temperature is kept low the D and H on an ethyl radical should not exchange and the indicated butane should be formed. At room temperature the ethylene and ethane should be formed almost exclusively by the disproportionation reaction *via* a head-to-tail mechanism.[1]

$$CH_3CD_2 + HCH_2CD_2 \longrightarrow CH_3CD_2H + CH_2{=}CD_2$$

The ethane, ethylene and butane were separated quantitatively by means of fractional desorption from silica gel using nitrogen as the elutant. The separation was monitored by means of a matched pair of thermal conductivity cells, one of which had pure nitrogen flowing through it at about 40 cc./min., while the other contained the desorbed gas as well as nitrogen. When the recorder indicated that a gas was being desorbed, the gas stream was directed to a refrigerated trap. In this way the material was fractionated into its component parts, each of which was contaminated only with nitrogen. The samples were then analyzed on the mass spectrometer. The ethane was 96.5% CH_3CD_2H and 3.4% CH_3CD_3, while the ethylene was principally $CH_2{=}CD_2$, 0.5% $CHD{=}CD_2$ being found in the products. It was not possible to assess the amount of $CH_2{=}CHD$ since the mass spectrum of $CH_2{=}CD_2$ is not known unequivocally.

After pumping off most of the nitrogen from the refrigerated butane trap, the butane fraction was evaporated into a 400-ml. flask equipped with a mercury cut-off valve. It was freed of residual nitrogen by successive freezing and melting under vacuum. The pumped material had a pressure of 60 mm. at room temperature. This butane gave the mass spectral pattern shown in Table I.

TABLE I

MASS SPECTRA OF $CH_3CH_2CH_2CH_3$ and $CH_3CD_2CD_2CH_3$

These spectra were measured on a Consolidated Engineering mass spectrometer, Model 21-103, ionizing current, 10.5 μa.; magnet current, 0.540 amp.; ion source T = 250°. For *n*-butane mass 58 appears at 780 v. and mass 2 appears at 3480 v. Standard sensitivity of the mass 47 peak in butane-d_4 is 48.63 compared with 50.0 for the mass 43 peak in butane.

M/e	Butane-d_4, %	*n*-Butane, %	*M/e*	Butane-d_4, %	*n*-Butane, %
2	0.2	0.1	41	6.4	30.6
3	...	...	42	4.5	12.6
4	...	...	43	10.2	100.0
12	...	...	44	17.3	3.4
13	0.1	0.1	45	14.4	...
14	0.8	0.7	46	9.6	...
15	3.3	5.0	47	100.0	...
16	0.9	0.1	48	3.4	...
17	0.8	...	49	0.1	0.2
18	0.3	...	50	0.3	1.1
26	1.1	5.5	51	0.4	1.1
27	6.7	37.5	52	0.4	0.3
28	20.8	30.7	53	0.3	0.9
29	23.8	40.9	54	0.3	0.2
30	30.7	0.9	55	0.3	1.1
31	34.9	...	56	0.2	0.8
32	4.4	...	57	0.3	2.6
33	0.3	...	58	0.6	12.1
37	0.2	0.7	59	0.4	0.5
38	0.5	1.8	60	1.3	...
39	1.6	14.0	61	0.5	...
40	4.9	1.9	62	11.0	...
			63	0.5	...

It is not possible with our present knowledge to assess the exact isotopic purity of the butane we have made. For this reason we have presented the spectrum in its entirety. Certain features of the spectrum do, however, allow us to place some limits on the purity. The fact that mass 63 is present in almost the exact amount to be expected from the natural abundance of C^{13} isotopic butane-d_4 indicates that no butane-d_5 is present. This is further confirmed by the observation of the (mass 48)/(mass 47) ratio. The fact that mass 47 is the base peak shows that we undoubtedly are dealing mainly with $CH_3CD_2CD_2CH_3$. The remaining question is, how much of the butane is $CH_3CD_2CDHCH_3$? If an appreciable percentage were present we would expect a peak at mass 61 and again at mass 46. However, these masses are also to be expected from $CH_3CD_2CD_2CH_2^+$ and $CD_2CD_2CH_2^+$, respectively. While there is no reliable method of predicting the size of the mass 61 and mass 46 peaks in pure $CH_3CD_2CD_2CH_3$ from the corresponding mass 57 and mass 42 peaks in normal butane, it is evident from a comparison of the normal butane spectrum with the heavy butane spectrum at these peaks that a very small percentage of the butane is butane-d_3. From the purity of the D_2O, we would calculate that there is a minimum impurity of 1–2% butane-d_3.

VISCOELASTIC PROPERTIES OF CRYSTALLINE POLYMERS: POLYTRIFLUOROCHLOROETHYLENE

BY A. V. TOBOLSKY AND J. R. MCLOUGHLIN

Contribution from the Frick Chemical Laboratories, Princeton University, Princeton, N. J.

Received April 13, 1955

In previous studies of the viscoelastic properties of linear amorphous polymers it was shown that certain features are common to the behavior of all of these polymers. In particular it was shown that there are four characteristic regions of viscoelastic behavior: a glassy region, a transition region, a rubbery plateau region and a flow region.[1] The existence of these regions is demonstrated in Fig. 1, showing the stress relaxation behavior of polyisobutylene. The data are plotted in the form log $E_r(t)$ *versus* log (t) where $E_r(t)$ is the stress per unit strain as a function of time in a sample maintained at constant extension.

The behavior in the transition region is particularly to be noted. In the time scale of the stress relaxation experiments (0.01 to 10 hr.), the transition region occurs in the temperature interval between −80 and −40°. In this interval the modulus changes very rapidly with time and temperature as can be seen in Fig. 1. The values of $E_r(t)$ range between a "glassy modulus" value of $10^{10.5}$ dynes/

(1) A. V. Tobolsky and J. R. McLoughlin, *J. Polymer Sci.*, **8**, 543 (1952).

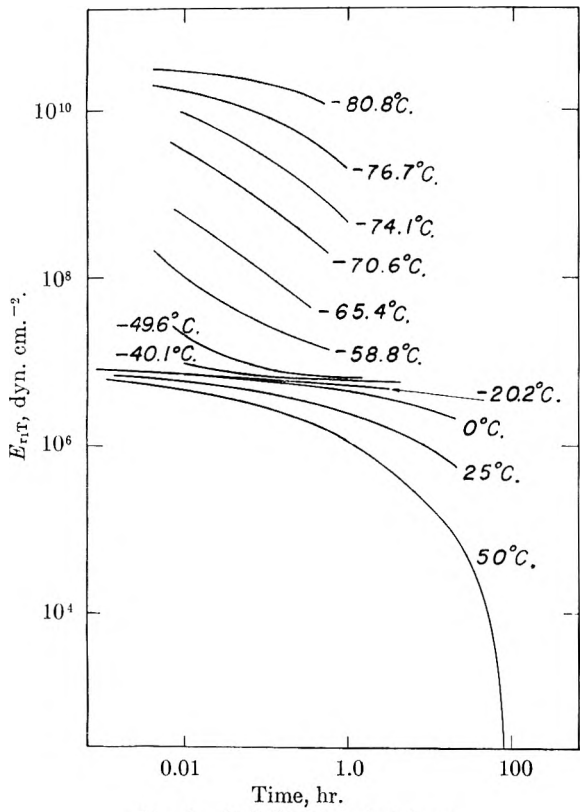

Fig. 1.—N.B.S. polyisobutylene.

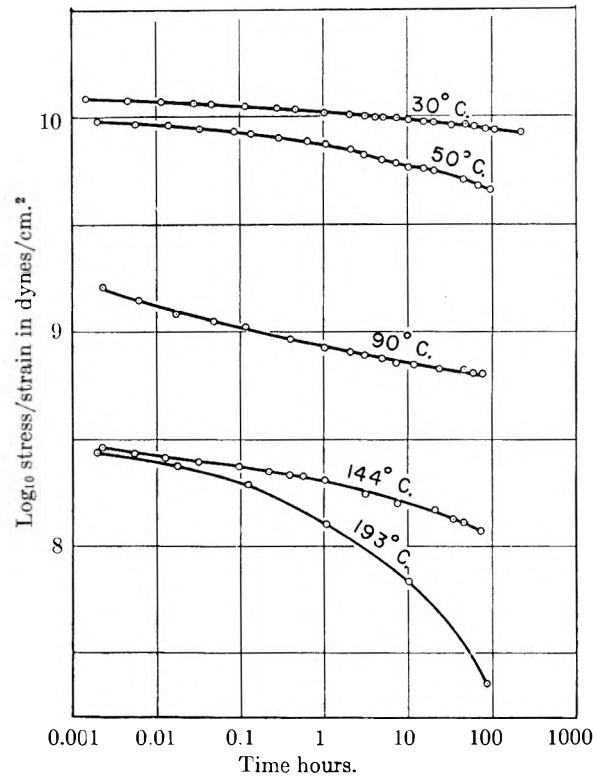

Fig. 2.—Stress relaxation of polytrifluorochloroethylene.

cm.^{2} to the rubbery modulus value of $10^{6.88}$ dynes/cm.^{2}. Stress relaxation curves at different temperatures can be superposed by a horizontal translation along the log time axis, and this principle of superposition permits the construction of a master curve that covers the complete time scale.

Polytrifluorochloroethylene is a polycrystalline polymer whose melting temperature T_m is 212°. Its glass transition temperature has not been accurately determined but should be somewhere in the neighborhood of room temperature if the approximate relation $T_g = {}^2/_3 T_m$ is valid.

Figure 2 shows stress relaxation data for polytrifluorochloroethylene in the temperature range between 30 and 193°. In this interval the modulus varies from $10^{10.1}$ dynes/cm.^{2} to $10^{7.2}$ dynes/cm.^{2}. It is particularly interesting to contrast Figs. 1 and 2. In Fig. 2 the log $E_r(t)$ *versus* log (t) curves between 30 and 144° are relatively flat; *i.e.*, the modulus change with time in the "transition region" is much less marked for the polycrystalline polymer as compared to the amorphous polymer. Also in Fig. 2 the modulus value of log $E_r(t)$ at $t = 0.01$ hr. changes from a value of $10^{10.1}$ dynes/cm.^{2} at 30° to a value of $10^{8.35}$ at 144°, a very gradual change. The "transition region," if such it can be called, for a polycrystalline polymer obviously extends over a much wider temperature range than for an amorphous polymer. The "transition region" blends into a high modulus "rubbery region," the crystallites playing the same role that entanglements or cross links do in the amorphous polymers.

The relatively rapid decay of stress at 193° is no doubt associated with a change of microcrystalline structure or texture, *i.e.*, an orientation of crystalline material.

Because there are changes with temperature in the microcrystalline structure and in the stress bearing mechanisms, it is certain that the simple time–temperature superposition that is valid for amorphous polymers in the transition region is not valid for polycrystalline polymers. There is not only a horizon displacement along the log time axis due to changing rate of molecular motions with temperature, but also an even more important vertical shift along the log $E_r(t)$ axis due to the changing structure and other factors.

METAL–POLYELECTROLYTE COMPLEXES. IV. COMPLEXES OF POLYACRYLIC ACID WITH MAGNESIUM, CALCIUM, MANGANESE, COBALT AND ZINC

BY HARRY P. GREGOR, LIONEL B. LUTTINGER[1] AND ERNST M. LOEBL

Contribution from the Department of Chemistry of the Polytechnic Institute of Brooklyn, New York

Received March 10, 1955

In the first paper in this series[2] the formation of complexes of polyacrylic acid (PAA) and copper-(II) was reported. In this paper the analogous complexes with magnesium, calcium, manganese-(II) cobalt(II) and zinc are described. The experimental procedure and the mathematical tech-

(1) A portion of this work is abstracted from the Dissertation of Lionel B. Luttinger, submitted in partial fulfillment of the requirements for the degree of Doctor of Philosophy in Chemistry, Polytechnic Institute of Brooklyn, June, 1954.

(2) H. P. Gregor, L. B. Luttinger and E. M. Loebl, THIS JOURNAL, **59**, 34 (1955).

TABLE I

COMPLEXATION CONSTANTS OF VARIOUS METALS WITH POLYACRYLIC ACID

(PAA, 0.06 N; neutral salt, 1 M potassium chloride)

Metal	$\log B_{av}$	B_2	b_1/b_2	K_2	$\frac{n_{max}}{N} =$
Mg	−3.8	2.6×10^{-8}	~0	6×10^{1}	..
Ca	−3.7	4×10^{-8}	~0	1×10^{2}	..
Mn	−3.0	9.1×10^{-7}	0.3	2.3×10^{3}	2
Co	−3.4	1.6×10^{-7}	1	4×10^{2}	2
Zn	−3.0	8.3×10^{-7}	~0	2.1×10^{3}	2

niques used to evaluate complexation constants were identical with those used before.[2]

Experiments were carried out in 1 M potassium chloride throughout. The PAA concentration was 0.06 N and the metal ion concentrations varied from 0.003 to 0.3 M; at least three different concentrations of each metal were used. In preparing standard solutions of the metal salts, magnesium and calcium were determined as the oxalate and pyrophosphate, respectively, while manganese and cobalt were titrated according to the procedure of Rosin.[3] Solutions of zinc chloride were prepared by dissolution of the electrolytic grade metal.

Results and Discussion

Figure 1 shows plots of $\bar{n}$ *vs.* p ([HA]/[H$^+$]) for 0.06 N PAA and various amounts of calcium, cobalt and zinc in the presence of 1 M KCl. Again, as was pointed out in the case of copper(II),[2] points pertaining to different concentrations of the same metal generally fall on the same curve. The curves for magnesium and manganese, which are not shown, are very similar. The data can again be represented best by a straight line over the range at $\bar{n} = 1$. The slope is large, indicating a small spreading factor.

Some of the plots show a distinct flattening out as the curves approach $\bar{n} = 2$, indicating a probable maximum coördination number of two; this flattening out is especially pronounced in the case of cobalt and zinc and is also noticeable for manganese. It may be recalled that copper did not show this phenomenon.[2]

Table I summarizes the results obtained; the notation is identical with that used previously[2]; a column indicating $\bar{n}_{max} = N$, *i.e.*, the coördination number, is included.

(3) J. Rosin, "Reagent Chemicals and Standards," D. Van Nostrand Co. Inc., New York, N. Y., 1937.

The complexity constants for the various metals with PAA are much smaller than with copper[2] ($K_2 = 6 \times 10^5$). Formation constants with the alkaline earth metals are smaller than with the transition metals, as expected.

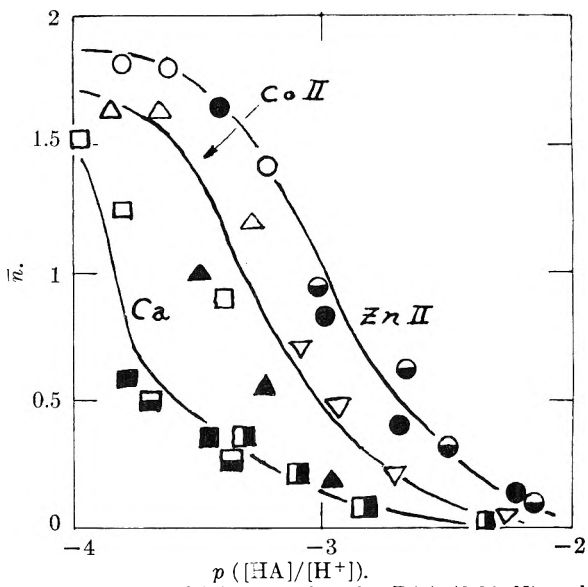

Fig. 1.—Modified Bjerrum plots for PAA (0.06 N) and calcium, cobalt and zinc in 1 M potassium chloride. With calcium: 0.00376 M (□); 0.00752 M (■); 0.01504 M (◨); 0.376 M (◧). With cobalt(II): 0.00515 M (△); 0.01287 M (▲); 0.0257 M (▽). With zinc(II): 0.00548 M (○); 0.0137 M (●); 0.0274 M (◒).

This investigation was supported in part by a research grant, RG 2934(C2) from the Division of Research Grants of the National Institutes of Health, Public Health Service. We also wish to express our gratitude to the Rohm and Haas Company which provided us with samples of the polyacrylic acid used in this investigation.

COMMUNICATION TO THE EDITOR

MONOLAYER STRUCTURE AS REVEALED BY ELECTRON MICROSCOPY

Sir:

Pankhurst[1] points out that uncovered areas in our electron micrographs of films of *n*-hexatriacontanoic acid[2] are anomalously large. He suggests that either (1) the monolayer has been disturbed during transfer from the film balance to the collodion support or (2) the islands and coherent film are multimolecular in thickness.

We recognize that the ring method of transfer may disturb the monolayer,[2] both when the ring is raised through the film and when it is lowered over the collodion support. Such strains could separate the islands and increase the uncovered area. Evaporation of water held between the monolayer and the collodion may also disturb the monolayer. Nevertheless, the *sequence* of our micrographs for samples removed at 15 dynes per cm., 25 dynes per cm., and after collapse at 58 dynes per cm., must parallel a similar *sequence* of changes during compression of the film on water.

The essential features of the micrographs obtained by the ring method have been reproduced by two more-refined techniques that effect transfer in one step. In one, a sharp-edged cup containing the collodion support is raised through the film. In the other, which may yield more quantitative results, the collodion support is raised vertically through the film at constant surface pressure as in the Langmuir-Blodgett technique. The existence of islands before transfer is further supported by Geiger-counter isotherms for radioactive stearic acid obtained by H. D. Cook in our laboratory.

The second alternative suggested—that both islands and coherent film are multimolecular—is not consistent with our data. Shadow widths for many samples removed before collapse provide direct and abundant evidence for monolayer thickness. Similarly, the "fibers" observed after collapse are two molecules thick and rest on a monolayer substrate. Our mechanism for collapse seems to account for both.[2]

Pankhurst's assumption that at 15 dynes per cm. the film area must be less than the extrapolated area does not agree with our observations. For *n*-hexatriacontanoic acid the areas are about the same. For stearic acid the film area at 15 dynes per cm. is slightly greater than the extrapolated value.[3]

Areas in these electron micrographs may not warrant quantitative treatment. Exact correspondence at each compression could hardly be expected. Transfer strains are not the only difficulty. The monolayer at low pressures may not be uniform, and the minute samples may not represent the entire surface. Furthermore, smaller islands and even individual molecules beyond the limit of detection with the electron microscope may occupy the "uncovered" areas.

RESEARCH DEPARTMENT
STANDARD OIL COMPANY (INDIANA)
WHITING, INDIANA
HERMAN E. RIES, JR.
WAYNE A. KIMBALL

RECEIVED JULY, 5 1955

(1) K. G. A. Pankhurst, *J. Phys. Chem.*, **59**, 480 (1955).

(2) H. E. Ries, Jr., and W. A. Kimball, *ibid.*, **59**, 94 (1955).

(3) H. E. Ries, Jr., and H. D. Cook, *J. Colloid Sci.*, **9**, 535 (1954).

FIRE RETARDANT PAINTS

Number nine of the ADVANCES IN CHEMISTRY SERIES

A collection of papers comprising the Symposium on Fire Retardant Paints, presented before the Division of Paint, Plastics, and Printing Ink Chemistry at the 123rd meeting of the American Chemical Society, Los Angeles, Calif., March 1953

Edited by the staff of
Industrial and Engineering Chemistry

CONTENTS

94 pages

paper bound

$2.50 per copy

Published June 1954, by American Chemical Society 1155 Sixteenth St., N. W. Washington, D. C.

Follow
the
newest
field... **NON-METALLICS**

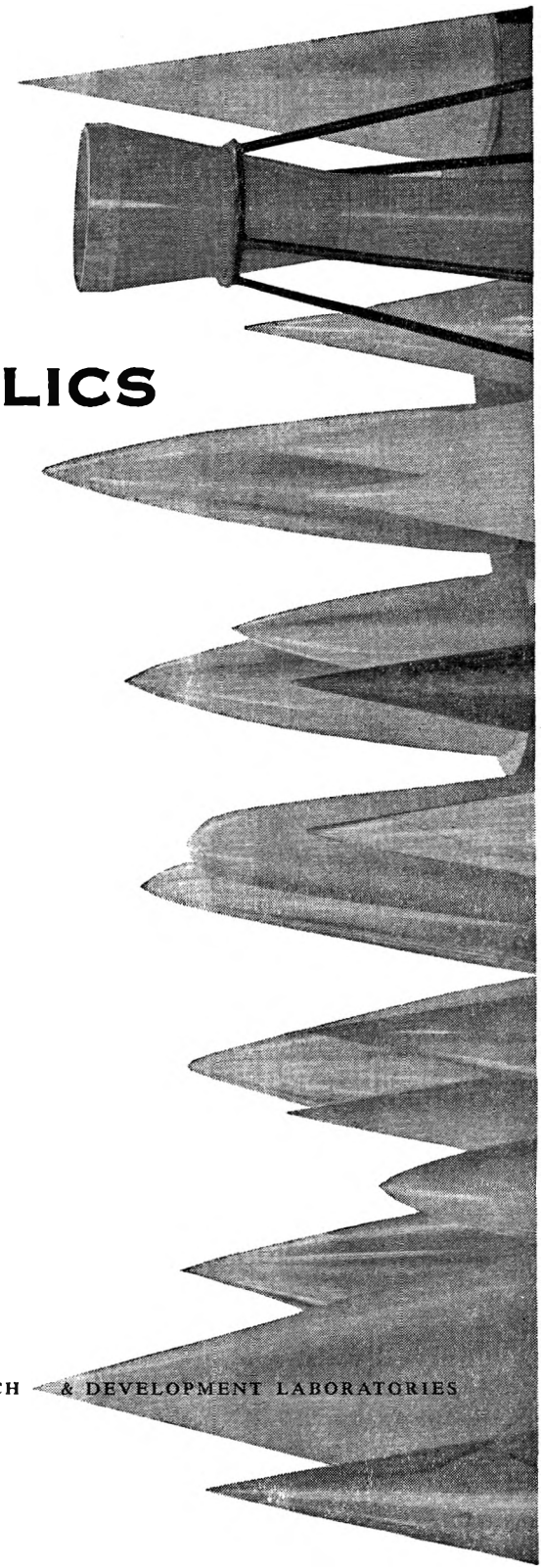

HUGHES RESEARCH AND DEVELOPMENT LABORATORIES HAVE SEVERAL OPENINGS FOR CHEMICAL AND OTHER ENGINEERS IN DEVELOPMENT LEADING TO PRODUCTION OF NEW APPLICATIONS FOR NON-METALLIC MATERIALS.

ENGINEERS AND PHYSICISTS

Hughes Laboratories are engaged in a highly advanced research, development and production program involving wide use of non-metallic materials in missile and radar components. The need is for men with experience in these materials to investigate the electrical, physical, and heat-resistant properties of plastics and other non-metallics.

ENGINEERS OR APPLIED PHYSICISTS

These men are required to plan, coordinate, and conduct special laboratory and field test programs on missile components. Experience is required in materials development, laboratory instrumentation, and design of test fixtures.

RESEARCH CHEMIST

The Plastics Department has need for an individual with a Ph.D. Degree, or equivalent experience in organic or physical chemistry, to investigate the basic properties of plastics. Work involves research into the properties of flow, mechanisms of cure, vapor transmission, and electrical and physical characteristics of plastics.

Scientific and Engineering Staff

HUGHES RESEARCH & DEVELOPMENT LABORATORIES

Culver City,
Los Angeles County, California